Investigating the Initiation & Progression of Ulcerative Colitis

Kathryn Louise Fair

Thesis submitted to The University of Nottingham for the degree of Doctor of Philosophy

3-1-2023

Dedicated to my baby, Alayna, whose unrelenting curiosity rivals my own.

My wholehearted thanks and remembrance to my late Dad and Nan for their complete and unwavering faith in me and making all I achieve possible.

Declaration

I hereby declare that the contents of this thesis are the result of my own independent work/ investigation and does not contain material previously submitted for any other thesis or dissertation submitted to this, or any other, institution.

I confirm that this thesis satisfies the University rules and regulations with respect to plagiarism and collusion.

Kathryn Louise Fair

March 2023

Acknowledgements

I would like to express my sincere gratitude to Dr Nick Hannan for his continuous supervision, support and guidance throughout the planning and execution of this research, as well as his encouragement and advice throughout all stages of the project.

Additionally, my thanks go to Tanya Monaghan who has given invaluable clinical insight and advice throughout the course of the project, helping guide research focus; Daniela Heeg and Janina Koelschbach for their assistance and support during my industrial placement with CHAIN Biotech; and my internal assessor, Abdolrahman Shams-Nateri, who's knowledge and advice was instrumental in informing the direction of the project. I would also like to thank Gordan Moran and Shellie Radford for supplying tissue samples and research advice from a clinical perspective that helped inform the best course of action at pivotal stages of this project.

A special thank you to my fellow members of the Hannan lab group who have been a pleasure to work alongside over the past few years. They are all extremely capable researchers and I wish them all the very best for their future endeavours.

Thank you to all the lab technicians, including Penny and Kasia, who have kept the labs running smoothly and have always been keen to offer help whenever needed. I extend this thank you to William Dalleywater for all his assistance and guidance through the immunostaining elements of my project.

I would like to say a heartfelt thank you to Imran Shaheem for always being there every step of the way. His endless encouragement and support has helped get me through some of the most difficult times over the past few years and for this I shall always be grateful. And finally, I would like to give my biggest thanks to my family and friends for their unending belief in me and for being my strength, through the many highs and lows, giving me the drive I needed to complete this journey.

Covid Impact Statement

The course of the project was altered due to the lasting impact of Covid-19. During this initial lockdown period, our access to laboratory facilities was halted for several months. Upon re-entry into the laboratory, difficulties continued in obtaining resources and reagents critical for sustained research. This posed numerous problems that required modifications to be made in the final stages of this project so as to ensure a timely finish from experimental work.

As a result, previously planned experimental stages had to be omitted and the scope of the project reassessed. These formerly planned research tasks included the testing of novel TLR4 inhibitors, generated as part of the industrial placement, on our colonic organoid lines. Such investigations using our patient-derived platform would have yielded greater insight into the efficacy of these novel peptides, in addition to determining whether accompanying Clostridia proteins exhibit a positive or negative impact upon the epithelium. Upon addition of our novel inhibitor, the next steps would have been to further establish the particular branch of the TLR4 pathway responsible for the disease state observed in our established lines.

Due to the premature conclusion of experimental work, the numerous organoid lines I had established were cryopreserved and the novel peptides retained with the view of building upon the findings in future research projects.

Abstract

Inflammatory bowel disease (IBD) is a significant and ever-growing problem in developed countries, with recent increased prevalence throughout Eastern countries. It is an idiopathic, progressive disease characterised by chronic GI inflammation, the aetiology of which remains largely unknown. Inflammatory phenotypes differ between healthy & IBD patients with dysregulated immune responses suspected to play a critical role in disease pathogenesis.

Toll-like receptors have been implicated in the pathogenesis of IBD, in particular TLR4. TLR4 recognises lipopolysaccharides (LPS) present on the surface of Gram-negative bacteria which appear to be in greater abundance in IBD patients. By further understanding the implications of this signalling pathway, therapeutic approaches with enhanced efficacy can be employed.

A primary 3D model generated from the colonic crypts was utilized to explore critical differences in the response of healthy tissue and that derived from ulcerative colitis patients. Once multiple patient lines were generated, a combination of analytical techniques were employed to investigate any inflammatory & fibrotic alterations that occur upon exposure to inflammatory agents, inclusive of bacterial antigens, and whether these changes are reversed following treatment with existing and novel anti-inflammatory agents.

In conclusion, a clear and substantial differential response was demonstrated between healthy & UC-derived colonic organoids, displaying a significant disease phenotype. The TLR4 inflammatory pathway, identified as being greatly responsible for many of these differences, triggers an exaggerated response to the presence of bacterial PAMPs in UC.

Table of Contents

Abbreviations

AOM	Azoxymethane
BSA	Bovine serum albumin
CAC	Colitis-Associated Cancer
CD	Crohn's Disease
CDI	*Clostridia difficile* Infection
cDNA	Complementary DNA
COPD	Chronic Obstructive Pulmonary Disease
CRC	Colorectal Cancer
DMEM	Dulbecco's Modified Eagle's Medium
DNA	Deoxyribonucleic Aacid
dNTP	Deoxynucleoside Triphosphate
DSS	Dextran Sulphate Sodium
DTT	Dithiothreitol
ECM	Extracellular Matrix
EHS	Engelbreth-Holm-Swarm
EMT	Epithelial to Mesenchymal Transition
eNOS	Endothelial Nitric Oxide Synthase
FBS	Foetal Bovine Serum
FFA	Free Fatty Acids
FMT	Faecal Microbiota Transplantation
FZDs	Frizzled Receptors
GAPDH	Glyceraldehyde-3-phosphate dehydrogenase
GLP1	Glucagon Like Peptide 1
GO	Gene Ontology
HBSS	Hanks' Balanced Salt Solution

HCC	Hepatocellular Carcinoma
HCECs	Human Corneal Epithelial Cells
Hck	Hematopoietic Cell Kinase
HDACi	Histone Deacetylase Inhibitor
hIPSCs	Human Induced Pluripotent Stem Cells
HRP	Horseradish Peroxidase
HSP	Heat Shock Proteins
IAP	Intestinal Alkaline Phosphatase
IBD	Inflammatory Bowel Disease
IEC	Intestinal Epithelial Cell
IF	Immunofluorescence
IFN	Interferon
IHC	Immunohistochemistry
IL	Interleukin
IRAK	Interleukin-1 Receptor-Associated Kinase
IRF	IFN-Regulatory Factor
ISC	Intestinal Stem Cell
JAK	Janus-Kinase
KSR	Knock-out Serum Replacement
LGR5	Leucine-Rich Repeat-Containing G-Protein Coupled Receptor 5
LPS	Lipopolysaccharide
LRR	Leucine Rich Repeat
MAMP	Microbial-Associated Molecular Pattern
MEK	Mitogen-Activated Protein Kinase Kinase
MPO	Myeloperoxidase
MUC2	Mucin-2
MyD88	Myeloid Differentiation Primary Response Protein 88
NCBI	National Center for Biotechnology Information

NETs	Neutrophil Extracellular Traps
NFκB	Nuclear Factor kappa-light-chain-enhancer of activated B cells
NIK	NFκB-Inducing Kinase
NO	Nitric Oxide
NOD2	Nucleotide-binding Oligomerization Domain-containing protein 2
OD	Optical Density
OLFM4	Olfactomedin 4
PAMP	Pathogen-Associated Molecular Pattern
PBS	Phosphate Buffered Saline
Pen/Strep	Penicillin/Streptomycin
PFA	Paraformaldehyde
PRR	Pattern Recognition Receptor
qPCR	Quantitative Polymerase Chain Reaction
RIN	RNA Integrity Value
RNA	Ribonucleic Acid
ROS	Reactive Oxygen Species
RT	Reverse Transcription
SCFA	Short Chain Fatty Acids
SDS-PAGE	Sodium Dodecyl Sulphate Polyacrylamide Gel Electrophoresis
siRNA	Small Interfering RNA
SP-A	Surfactant Protein A
SRB	Sulphate-Reducing Bacteria
STAT	Signal Transducer and activator of Transcription
TA	Transit Amplifying
TBS	Tris-Buffered Saline
TBS-T	Tris-buffered saline with Tween
TcdA	*Clostridium difficile* Toxin A
TcdB	*Clostridium difficile* Toxin B

TGF-β	Transforming Growth Factor Beta
TICAM	Toll/IL-1R Homology Domain-Containing Adaptor Molecule
TIR	Toll/IL-1 Receptor
TIRAP	Toll-Interleukin-1 Receptor (TIR) Domain-Containing Adaptor Protein
TLR	Toll-Like Receptor
TNFα	Tumour Necrosis Factor alpha
TRAF6	TNF Receptor-Associated Factor 6
TRIF	TIR-domain-containing adapter-inducing Interferon beta
UC	Ulcerative Colitis
VIL	Villin
WB	Western Blot

Table of Figures

Table of Tables

Chapter 1

Introduction

1.1 Gastrointestinal Tract Physiology

1.1.1 GI Cell Types & Structure

The gastrointestinal (GI) tract comprises all the major organs of the digestive system, including the oesophagus, stomach, small intestine, colon, and rectum. The small and large intestines are further divided into different sections which possess differing functions in the digestive process. These consist of the duodenum, jejunum and ileum of the small intestine and the cecum, ascending colon, transverse colon, descending colon, sigmoid colon, and the rectum of the large intestine.

While the GI can be divided into distinct sections it also possesses multiple layers, each with discrete structures and functions. These layers are known as the mucosa, submucosa, muscularis externa, and serosa.

The serosa is a smooth tissue membrane at the outermost layer of the GI tube. Travelling inwards, the next layer, the muscularis externa, performs the crucial role of propelling contents along the digestive tract. The 2 layers of smooth muscle that comprise the muscularis externa are the inner circular layer that works to constrict the lumen, thereby compressing the contents. While the outer layer, being longitudinal in nature, shortens the tube, hence propelling the contents down the digestive tract. The submucosa lies inwards of this muscular layer and is made up of connective tissue containing nerves, blood and lymph vessels. Finally, the mucosa is a highly specialised tissue that covers the lumen of the GI tract. It consists primarily of the epithelium and the loose connective tissue of the lamina propria. The epithelium is the focus of this study due to the complex host-microorganism interactions that aid in the control of mucosal immunity. Currently, damage to the epithelial membrane in the colon has been implicated in the development of IBD. However, the role that each epithelial cell type plays in this process remains unknown [5].

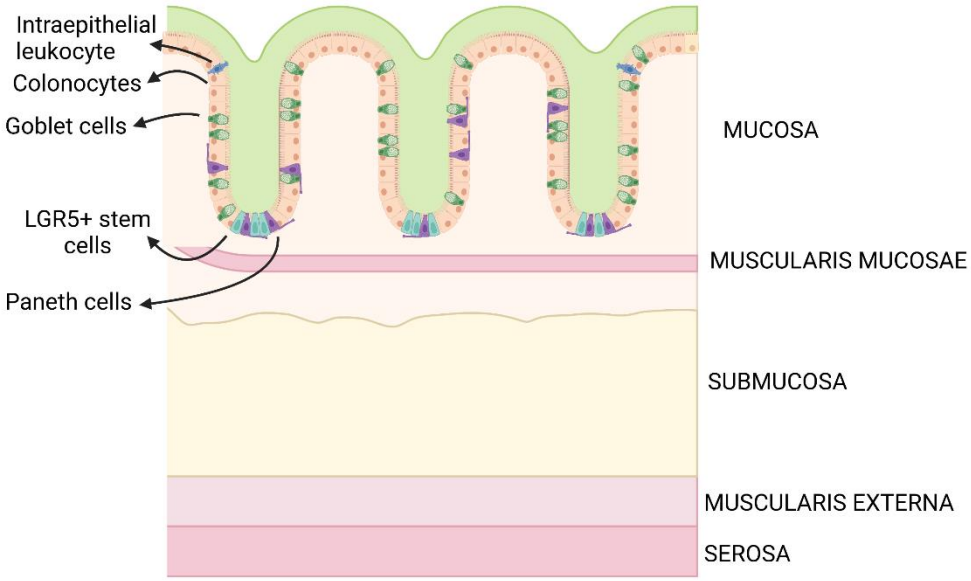

Figure 1.1: Schematic displaying tissue layers and cell types of the colon.

In this project, we shall develop a representative primary human model enabling us to more accurately explore the response of the colonic epithelium to inflammatory stressors and in particular the role of the epithelium in ulcerative colitis. Ulcerative colitis is one of the main forms of IBD, usually affecting the colon, in particular the epithelial layer. The epithelium consists of numerous cell types with specialised functions in digestion and defence.

All differentiated cell types originate from the colonic stem cells at the base of colonic crypts. These are known as the crypts of Lieberkühn which are approximately 75-110 cells deep in the human colon and 23 cells in circumference [6]. Colonic stem cells reside at the base of these crypts [7]. This stem cell population produces pluripotent daughter cells while also maintaining the population of stem cells at a steady rate [8]. In 2010, Clevers group identified a G-protein-coupled receptor, LGR5, as a specific marker for these cells [9]. A gradient between BMP and Wnt signalling pathways in the crypt determine at what stage of differentiation the cells are as they move up the crypt [10]. As the cells migrate up the walls of the crypt, they differentiate into all epithelial cell types. Cells are continually produced by this method, allowing for the continual regeneration of the epithelium, occurring in full every 5-7 days. At the end of their

cycle, differentiated epithelial cells undergo anoikis before shedding into the colonic lumen.

Located alongside these LGR5+ colonic stem cells are the Paneth cells. These are a secretory cell type that produce dense granules containing antimicrobial compounds, offering the next line of defence and regulation of the microbiota composition [11]. These granules are released into the crypt lumen upon stimulation [11]. The antimicrobial peptides released by Paneth cells include sPLA2, α-defensins and angiogenin 4 [11]. Concentrations of defensins are high within the crypt to offer increased protection towards the stem cells at the base of the crypts.

Additionally, lysozymes are secreted, however these are known to be largely effective against Gram positive bacteria, while Gram negative bacteria possess an outer membrane that protects the bacterial cell wall, rendering them comparatively resistant to breakdown by lysozyme [11].

Interestingly, there are varying numbers of Paneth cells throughout the colon with very few observed in the distal colon of healthy individuals [12]. This was not the case, however, in UC patients with Paneth cells detected in the distal colon of 85% of these patients, as well as increased numbers present in the caecum, ascending, traverse and descending colon [12]. This finding is indicative of the increased priority towards protection of stem cells during chronic inflammatory disease.

Colonocytes, comprising much of the colonic epithelium, provide absorptive functions in digestion in addition to providing a physical barrier between the luminal bacteria and systemic circulation. The cells are firmly connected by cell-cell junction proteins. Expression of these proteins has been found to be downregulated in IBD [13], thereby compromising barrier integrity. This finding was further supported by Prasad et al who reported reduced staining intensity for several claudins on the surface epithelium in UC patients [14]. This increase in permeability is further exacerbated by apoptosis of epithelial cells as well as ulceration [13].

Another key cell type yielded from colonic stem cells are enteroendocrine cells. Their main function is to produce a multitude of gut hormones, providing important roles in digestion and absorption, with enteroendocrine cells responding to detection of glucose, amino acids and short chain fatty acids (products of microbial fermentation)

[15]. Detection then triggers activation and regulation of numerous signalling pathways, informing downstream nutrient transporters and ion channels of the required functions and hence aiding in digestion. Gut hormones are then released by these cells such as glucagon-like peptide 1 (GLP1) and insulin, exerting essential roles in metabolism [16]. GLP1 has also been found to exert effects during periods of inflammation, in particular in response to LPS in triggered via the TLR4 pathway with rapid increases in plasma GLP1 reported in mice [16]. This report suggests GLP1 as an inflammatory suppressor and promoter of mucosal integrity [16]. This demonstrates colonic enteroendocrine cells as displaying great involvement in mucosal defence.

An essential differentiated cell type of the colonic epithelium, goblet cells, play a critical role in the protection of the membrane from both commensal and pathogenic microbes. Goblet cells produce multiple constituents of mucin, forming a thick mucus layer lining the GI epithelium. This mucus layer is crucial in preventing the direct contact of commensal bacteria with the epithelial surface, thereby averting passage across the membrane and ensuing unnecessary immune responses. Goblet cells in the intestine predominantly secrete MUC2. It has been found that mice lacking this mucin component developed spontaneous colitis [17]. This is due to commensal bacteria being in direct contact with the epithelium. Furthermore, ulcerative colitis patients have been reported to have thinner mucus layers than healthy individuals [18]. The distal colon is comprised of two distinct mucus layers due to the greater quantity of bacteria present. The outer layer is less dense and provides a habitat and food source for the microbiota, while the inner layer is impenetrable to commensal bacteria [19]. If this layer becomes compromised, then even the interaction of these commensal microorganisms with the epithelium can trigger an inflammatory response. Certain bacterial species have developed methods for bypassing this dense mucus layer via degradation or propelling directly through it [20]. Therefore, to offer further protection against these invading bacterial species, goblet cells also secrete antimicrobial agents to reside within this inner mucus layer. These are for the purpose of killing both commensal and pathogenic bacteria that manage to penetrate into the layer, thereby limiting microbial interaction with the epithelial cells.

The combination of cells involved in this immunoregulatory process are affected differently by each pro-inflammatory trigger. Therefore, the interaction of our model to multiple triggers shall be analysed to more effectively characterise the platform.

1.1.2 Microbiota & Commensal Bacteria Tolerance

The commensal microbiota colonises the host colon early in life, having great influence over multiple structural, functional and immune-based characteristics of the colonic epithelium. Studies have shown the impact the microbiota exhibits upon barrier integrity, PRR expression and production of antimicrobial peptides [21]. Germ-free mice have been used to confirm this hypothesis, which were found to be deficient in the production of defensin and other antimicrobial proteins [21]. Addition of certain commensal microbes have been found to induce expression of an antimicrobial peptide produced by Paneth cells, RegIIIϒ [21]. Furthermore, barrier integrity itself appears to be affected by the absence of a microbiota, with germ-free mice displaying reduced rates of epithelial cell turnover [21]. In addition to this, germ-free mice have proven more susceptible to bacterial, viral and parasitic infection due to the lack of competition against pathogens by commensal bacteria [21].

The commensal microbiota establishes tolerance to avoid activation of the immune system by multiple methods. They are thought to actively suppress epithelial pro-inflammatory signalling, with one example of this being *Bacteroides thetaiotaomicron*, known to induce the export of the NFκB p65 subunit, RelA out of the nucleus [22]. This decreases the transcription of NFκB downstream signalling genes. Interestingly, other mechanisms suggested have included the enzyme, alkaline phosphatase present in the brush border of the intestinal epithelium, possessing the ability to dephosphorylate, and hence detoxify, the lipid A compound in LPS within the lumen [23]. A mechanism such as this would likely play a further role in immune tolerance in the healthy individual. Furthermore, animal models deficient in the intestinal alkaline phosphatase (IAP) isoform appear to exhibit excessive neutrophil influx, analogous to wild-type animals upon exposure to LPS [23]. This effect was observed in zebrafish, and specifically within the segment most closely resembling the small intestine, however it is possible that this effect can be translated to the human colon.

Other important elements enhance this tolerogenic process including mucus production. The thick dual layer of mucus present in the colon act to separate the commensal bacteria from making direct contact with the epithelial surface. As commensal bacteria don't usually possess the ability to penetrate this mucus layer it avoids recognition by the innate immune system. This also acts as the first line of defence against pathogenic bacteria, many of which lack the capacity to cross the thick mucus layer when fully intact. Under less favourable conditions, the denser, inner mucus layer becomes more permeable; the luminal bacteria can then migrate from the outer to the inner layer [24].

Furthermore, specific mechanisms contributing to tolerance of the microbiota in the healthy epithelium are more immunological in nature. Some studies have shown that certain PRRs and their corresponding co-factors, including TLR4 and MD2, are expressed at very low levels in the healthy colonic epithelial cells which are, in turn, weakly responsive to LPS [25,26]. Low levels of TLR2 expression were also noted. This limited expression of integral PRRs in the healthy colonic epithelium would naturally reduce the number of PAMPs detected, thereby restricting the responsiveness to the prolific bacteria within the luminal microbiota. The findings noted in these studies were obtained from intestinal cell lines and should be researched in primary human cells for confirmation.

Additionally, a key component of microbiota tolerance in the colon is location of PRRs that detect commensal bacterial PAMPs. With non-pathogenic bacteria located in the lumen, the PRRs of the healthy colonic epithelium are orienteered on the basolateral surface of epithelial cells [27]. This is an integral factor in ensuring PRRs are not continually activated by the persistently present luminal bacteria. Hence, these PRRs will only be activated by bacteria that has managed to breach the epithelial barrier, thus preventing an overactive immune response under homeostatic conditions. This can occur for multiple reasons, including a loss of barrier integrity and a thinning of the protective mucus layer.

1.1.3 Loss of Barrier Integrity

The mechanisms driving barrier integrity in the colonic epithelium are not well understood. Given that this is a critical factor in maintaining intestinal homeostasis,

more research is required to enhance this understanding. The diversity and composition of the microbiota are suspected to heavily influence permeability of the epithelium. Certain bacterial strains promote health of the mucosa by strengthening barrier integrity and increasing mucin production [28]. Furthermore, they act to suppress pro-inflammatory responses, as well as apoptosis, to favour homeostatic conditions. Over 1000 different species appear to largely originate from five distinct phyla in the faecal microbiota of the healthy individual, with these being Bacteroidetes, Firmicutes, Actinobacteria, Proteobacteria, and Verrucomicrobia [29].

Conversely, pathogenic bacterial strains have the opposing effects upon the epithelium. Their presence in the intestinal lumen suppresses expression of tight junction proteins, increases pro-inflammatory signalling and contributes to dysregulated apoptotic and proliferative signals. This combination perturbs the host-microbiota tolerogenic crosstalk triggering an overactive immune response, resulting in substantial damage to the intestinal epithelium over time. Interestingly, this altered microbiome has also been found to be less biodiverse in nature, with a 25% decrease in the number of microbial genes present within the mucosa of IBD patients compared to healthy controls [30]. A specific reduction has also been observed in the prevalence of Bacteroidetes as well as Firmicutes phyla [31]. Moreover, a microbe typically present within the healthy microbiome, Bacteroides fragilis, has been linked to IBD, having been detected within a biofilm adhering to the epithelium of IBD patients [32]. Several phyla that are diminished in the microbiota of IBD patients are butyrate-producing. Butyrate is a necessary energy source for colonic epithelial cells, hence a lack of these bacterial species within this environment may also negatively impact barrier integrity.

Therefore, it is clear that alterations within the intestinal microbiome leading to dysbiosis strongly contribute to a loss of epithelial barrier integrity which is a major step in the development of a dysregulated immune response and, ultimately, IBD.

1.1.4 Dysbiosis

While the presence of certain bacterial strains has previously been linked with the pathogenesis of IBD, no direct evidence has been found that the presence of any of these strains is the primary cause of IBD. Instead, focus has shifted to an imbalance

in the microbiota and its subsequent interactions with the host as being more relevant as a contributory factor in the onset of IBD [33]. This imbalance is known as dysbiosis.

As mentioned in the previous section, a reduction in butyrate-producing bacteria, such as *F. prausnitzii*, has been linked with IBD pathogenesis, along with an increase in sulphate-reducing bacteria (SRB) [34,35]. SRB's are suspected to have deleterious effects upon the epithelium due to their ability to metabolise sulphate into hydrogen sulphides. This is a toxic molecule that acts to impair the oxidation of butyrate in colonocytes [36]. Hydrogen sulphide is found in excess in the faeces of ulcerative colitis patients [37]. The increase in these strains, amongst others, can lead to declining epithelial health, and hence, reduced barrier integrity. In genetically predisposed individuals, phagocytosis is impaired, preventing the killing of bacteria that passes through this permeable epithelium and into the lamina propria [38]. These factors lead to excessive stimulation of PRR including the TLRs.

Due to the link between dysbiosis and the loss of intestinal barrier integrity, bacterial PAMPs that are usually restricted to the intestinal lumen, such as LPS, are then able to translocate across the epithelium. LPS is known to be an endotoxin present in the outer membrane of gram-negative bacteria, with the role of providing protection from bile salts and certain antibiotics [36]. If LPS translocates to the bloodstream, this can lead to chronic inflammation and septic shock.

Dysbiosis has been found in conjunction with increased oxygen levels in the colonic lumen [39]. This may be a result of increased epithelial permeability or increased mucosal inflammation or a combination of both. This change naturally leads to further variations within the microbiome with a distinct reduction in the obligate anaerobe population typically present within the colon. This occurs in conjunction with an increase in facultative anaerobes such as Enterobacteriaceae [36]. This change can also lead to an increase in reactive oxygen species (ROS) within the colon. The increased presence of ROS can cause substantial damage including direct damage to the cells, DNA mutations and inflammation, all of which promote the initiation and subsequent development of cancer [40]. ROS can also play a role in the tumour microenvironment and drug resistance [40].

1.2 Inflammatory Bowel Disease

1.2.1 Background of IBD

Inflammatory bowel disease (IBD) is an idiopathic progressive, relapsing disease characterised by chronic inflammation of the mucosa occurring in the gastrointestinal tract [41]. The aetiology of IBD remains largely unknown, however several contributing factors have been identified. The pathogenesis of IBD has been linked to dysregulation of the innate and adaptive immune responses against PAMPs present in the GI tract, as a result of genetic susceptibilities [42].

Inflammatory bowel disease affects more than 5 million people worldwide with increasing prevalence each year. It has a substantial burden on the NHS with the economic impact estimated to exceed £1 billion [43].

The patient can experience a range of symptoms including severe abdominal pain, fatigue and anaemia, as well as extra-intestinal manifestations such as inflammatory arthritis and, in some cases, liver disease [44]. IBD has also been linked with an increased risk of developing colorectal cancer if inflammation is present in the colon [45].

Despite recent improvements in treatments, nearly half of Crohn's patients will require surgery within 10 years of diagnosis. Following invasive surgery, often involving resection of a large proportion of the bowel, over 1/3 of these patients will require further surgical intervention [46].

IBD is categorized into two main subtypes: ulcerative colitis (UC), which is restricted to the colon, and Crohn's disease (CD), which can affect any area of the digestive tract. During active IBD, the intestine can become highly inflamed, leading to destruction of the epithelium, deterioration in digestive functioning and chronic pain or discomfort for the sufferer.

As a multifactorial disease, IBD has a range of potential environmental and genetic factors. One of the factors implicated in the pathogenesis of IBD is dysbiosis of the gut microbiome, often affected by diet or overuse of antibiotics [47]. This is suspected to lead to disruption of immune homeostasis within the gut, resulting in chronic

inflammation. This project, therefore, focusses on the differences in the inflammatory profile, comparing inflamed and non-inflamed tissue obtained from endoscopic biopsy to determine how they respond differently to inflammatory stimuli and anti-inflammatory substances.

One of the key differences between CD and UC is the variation in the distribution of inflammation. In CD, inflammation can be present discontinuously throughout any region of the GI tract, although most commonly affecting the ileum and colon, whereas in UC inflammation is continuous and confined to the colon. Furthermore, inflammation in CD is often referred to as transmural, affecting all layers of the intestinal wall, while UC affects only the superficial mucosa. Moreover, the presence of strictures is common in CD, which is not typically the case for UC.

Here, we will be focussing on UC specifically, which we will model using a patient-derived colonic epithelial organoid platform. As UC expressly targets the colonic epithelium this model is apt for in vitro research to further our understanding of this disease.

1.2.2 Aetiology & Pathogenesis

A complex blend of environmental factors combined with host susceptibility are suspected to be crucial to the development of UC. Once these factors increase disease susceptibility, the onset of disease can be triggered by alterations to the gut microbiota, disruption of the mucosal barrier and overstimulation of the GI immune system [48]. These factors may be closely interlinked, therefore further research is required to determine the degree to which these issues contribute to disease initiation and progression.

Environmental factors include the use of antibiotics, well known for the impact they exert upon the gut microbiome. Alongside this, cessation of smoking has also been implicated in the increasing incidence of UC. This is suspected to be relevant due to the immunosuppressive nature of nicotine [49].

Depletion of 'protective' bacteria typically present within a healthy microbiome has been noted in UC patients, with faecal microbial transplantation (FMT) shown to improve inflammation in UC patients [50].

Furthermore, an abnormal innate and adaptive immune response has importantly been implicated in UC pathogenesis due to the predominant inflammatory presence responsible for the substantial damage inflicted upon the colon. There has been evidence of increased neutrophil infiltration in the intestinal tissue of UC patients. These have been found to be one of the first inflammatory cell types to be recruited in active disease [51]. They release cross-linked structures that protrude from the cellular membrane known as neutrophil extracellular traps (NETs). The role of these NETs is to trap pathogens and have been found to be overexpressed in UC [52]. Production of NETs was found to be stimulated by TNFα, IL8 and LPS [52]. Furthermore, neutrophils release myeloperoxidase (MPO), involved in catalysing hypochlorous acid (HClO) synthesis, which, in turn, can trigger formation of ROS. In healthy individuals, ROS is an important aspect of inactivating pathogens, however, with ROS production increased in UC patients, this can lead to damage of epithelial tissue and ultimately formation of ulcers [52].

Additionally, antigen-presenting cells including macrophages and dendritic cells shift their activity in UC. Dendritic cells, in particular, demonstrate increased expression of both TLR2 and TLR4, previously confirmed in biopsy samples obtained from UC patients [53]. While macrophages, typically divided into M1 (classically activated) and M2 (alternatively activated) subgroups, are activated by cytokines secreted during inflammation [53]. M1 macrophages are activated by IFN-γ, GM-CSF and LPS, which trigger them to produce and secrete a range of pro-inflammatory cytokines, including TNF-α, IL-1β, IL-12, IL-18 and IL-23, as well as ROS [53]. M2 macrophages, however, are activated by alternative cytokines such as IL4 and IL10 and, in turn, exhibit anti-inflammatory functions. During IBD, the balance between M1 and M2 macrophages appears to shift to favour the pro-inflammatory M1 type [53]. M1 macrophages also prompt the activation of Th1 cells that further enhance the pro-inflammatory environment.

While progress is being made into uncovering the processes involved in the development of UC, further research is required to give a more rounded view of the complete pathways implicated as well as the interplay of factors leading to UC pathogenesis. This can differ between patients which is evidenced by the varying presentations of the disease in addition to the fluctuating response to current treatments available.

1.2.3 Current Treatments for IBD

Treatment options available for IBD have seen an expansion in recent years, with the emergence of biologics adding to the more conventional treatments of aminosalicylates, corticosteroids and immunomodulators 54. In cases where medication has lost its efficacy or when damage is extensive at the time of diagnosis, surgical resection is performed. Aminosalicylates including sulfasalazine acts as a prodrug, which is then metabolised by colonic bacteria to produce its active constituent, 5-ASA 55. The exact mechanism of action is yet to be fully elucidated; however, it has been suggested to exhibit multiple immunomodulatory effects, including inhibition of NFκB 56. This would also have inhibitory effects upon downstream cytokines in the NFκB pathway, including TNFα. No evidence has been presented as to its ability in the induction of mucosal healing.

Immunomodulators

Oral corticosteroids have long been used as a treatment for IBD and has been found to effectively induce remission once a flare-up has occurred 57. They are specifically used for this purpose, having not displayed any efficacy in maintaining remission in IBD. The side effects of systemic oral corticosteroids are numerous, inclusive of hypertension, venous thromboembolism and osteoporosis 58.

More recently, a second generation of oral corticosteroids have become available. These have been stated to possess a more enhanced safety profile than conventional corticosteroids. Budesonide is an example of a second generation of oral corticosteroid, used as a treatment for mild to moderate IBD. Budesonide is administered as a pH-dependent capsule which acts to restrict the release of budesonide to the colon 59. This both increases efficacy within the colon and improves tolerability.

Alternatively, immunomodulators including methotrexate and thiopurines, such as azathioprine, which acts via suppression of mitogen-activated protein kinase kinase (MEK) and NF-κB via Rac1 60. Azathioprine has proved effective for many patients in maintaining remission with a 7-year remission rate of 43.9% observed in a study by Yamada et al 61. While these are favourable results in comparison to other IBD treatments that are currently available, this leaves over 50% of patients who are not benefitted to a great extent by this medication. Furthermore, side effects can be quite severe, including bone marrow suppression, liver injury and gastrointestinal intolerance 62-64. These adverse effects often occur within the first 3 months of treatment 63.

Methotrexate, however, presents a different mode of action, with low doses found to inhibit DNA synthesis, thereby downregulating various pro-inflammatory cytokines 65. This, in turn, inhibits proliferation of T-cells and the downstream inflammatory response 66. While treatment with methotrexate has shown a 65% higher remission rate when compared to control in Crohn’s disease, the same cannot be said for UC 67. Furthermore, treatment with methotrexate has been found to result in fatigue, hypoalbuminemia and atypical pneumonia 67.

Table 1.1: Mode of Action of Selected Anti-Inflammatory Drugs Tested on Patient-Derived Organoid Model.

DRUG	MODE OF ACTION
TOFACITINIB	A 2nd generation selective JAK1 & JAK3 inhibitor, thereby restricting the JAK-STAT pathway. Inhibited proliferation in CD4 + and CD8 + T cells. Corrects barrier disruption in Human Intestinal Epithelial Cells and Colonoids [54].
SULFASALAZINE	Pro-drug of 5-aminosalicylic acid, which in turn inhibits NFkB by inhibiting IκB phosphorylation. Typically acts on B cells. Also found to act on LPS & TNFα-induced rat colon cells [55].
BUDESONIDE	Binds & activates glucocorticoid receptors in cell cytoplasm to allow translocation to the nucleus. This complex activates HDAC2, which in turn reducing formation of several ILs & TNFα. Exerts anti-inflammatory effect directly upon intestinal epithelial cells.
METHOTREXATE	An anti-folate, anti-metabolite – acts to hinder adenosine and guanine metabolism

	& represses T-cell activation in addition to inhibition of IL1β binding. Particularly targets T-cells & macrophages.
AZATHIOPRINE	Converts to its active metabolites 6-MP & thioguanine, which are then incorporated into replicating DNA, thereby halting division. Co-stimulates with CD28 to induce T-cell apoptosis.

Recent advances in this field include the production of specific TNFα inhibitors which prove to be effective for a larger proportion of patients than previous conventional medications 68. Despite the increased efficacy of anti-TNFα drugs in comparison to other existing therapies, approximately 20% of patients did not respond to treatment, with a further 20-40% of patients becoming unresponsive to the drug following 1 year of treatment 69.

Furthermore, there are numerous advanced therapies that are established in the field of IBD treatment. A few to mention are anti-integrins, anti-p19/40, JAK inhibitors and S1P. I shall give a brief overview of these therapies including the mode of action in IBD.

Anti-Integrins

Anti-integrins are a class of medications that have shown promise in the treatment of IBD. Integrins are cell surface proteins that play a crucial role in the adhesion and migration of immune cells to the gut lining, contributing to the chronic inflammation seen in IBD [56]. Anti-integrin drugs work by specifically targeting and inhibiting these integrins, preventing immune cells from entering the intestinal tissue and reducing the inflammatory response [56]. Medications like vedolizumab and natalizumab have been developed to selectively block these integrins, offering a more targeted and potentially safer approach to IBD treatment, with the aim of reducing symptoms and inducing remission [56]. This targeted therapy has provided new hope for individuals living with IBD, as it helps to manage the disease and improve their quality of life.

Anti-p19/40

Anti-p19/40 therapies are a relatively newer class of medications used in the treatment of IBD. These therapies target the p19 subunit of IL-23, a cytokine involved in regulating the immune system and inflammation. By inhibiting the p19 subunit, these medications can interrupt the inflammatory processes that contribute to IBD [57]. One notable example of an anti-p19/40 therapy is ustekinumab, which is approved for IBD treatment [57]. This targeted approach provides an additional option for individuals with IBD, offering a potential alternative or complement to anti-integrin drugs and other IBD treatments, with the goal of reducing symptoms and promoting disease remission.

While the long-term efficacy and safety of anti-p19/40 therapies continue to be studied, they represent a significant advancement in the management of IBD, potentially improving the lives of those affected by these conditions.

JAK Inhibitors

Janus kinase (JAK) inhibitors are another class of medications that show promise as an IBD therapy. JAK inhibitors work by targeting specific enzymes involved in key inflammatory pathways, helping to reduce the overactive immune response seen in IBD. Medications like tofacitinib and upadacitinib are examples of JAK inhibitors used in IBD treatment [58].

JAK inhibitors offer an alternative mechanism of action compared to traditional IBD medications, such as corticosteroids or immunosuppressants. They can be effective in inducing and maintaining remission, as well as managing symptoms in patients who have not responded well to other treatments. However, their use may come with certain risks and side effects, such as increased susceptibility to infections, so careful monitoring is necessary during treatment [59].

The development of JAK inhibitors has expanded the therapeutic options for individuals with IBD, offering the potential for improved quality of life and greater control over the disease.

S1P receptor modulators

Sphingosine-1-phosphate (S1P) receptor modulators are a class of medications that have been explored for the treatment of IBD. These medications, such as fingolimod, target the S1P receptors, which are involved in regulating immune cell trafficking and inflammation [60].

S1P receptor modulators work by sequestering lymphocytes, thereby preventing their migration into the gut tissues, thus reducing the inflammatory response associated with IBD [60]. This targeted approach can help reduce symptoms and induce remission in some IBD patients.

While S1P receptor modulators show promise in IBD treatment, their use is still under investigation, and more research is needed to determine their long-term efficacy and safety. These medications may offer an alternative treatment option for individuals with IBD, especially those who have not responded well to other therapies.

However, it is critical that research continues to be carried out in the hopes of discovering alternative treatments with greater efficacy and increased reliability.

1.2.4 Emerging Technologies for the Treatment and Management of IBD

Additionally, to the medications above, there are numerous emerging therapies with varying degrees of efficacy.

Apheresis therapy is a novel IBD treatment that has been developed in Japan within the past few years. It works by isolating granulocytes, monocytes and activated lymphocytes from the peripheral blood [61]. The aim of this is to reduce the local inflammatory response. This technique has demonstrated a level of efficacy for inducing remission in both UC and Crohn's patients. The efficacy rate has been established as residing between 46% and 70% as determined by multiple studies [62,63]. Therefore, there are still a significant number of patients that are unresponsive to this treatment.

Efforts to alter intestinal microecology and reduce the degree of dysbiosis continue to be made. The methods applied thus far include the use of antibiotics, probiotics and FMT.

While antibiotic use has, naturally, been found to reduce the incidence of incisional infection in Crohn's patients [64], and has effectively treated patients with septic complications [65], a systemic review has found the efficacy of antibiotics in inducing remission to not be clinically meaningful [66]. Furthermore, antibiotics have been implicated as a risk factor for the development of IBD, with cumulative exposure associated with an increased risk of new-onset IBD [67]. This risk is greater when broad spectrum antibiotics are used. Moreover, antibiotic use within 30 days of IBD diagnosis was linked to an increased risk of *Clostridia difficile* infection (CDI) [68]. Therefore, the

application of antibiotics as a management approach for IBD may have some serious drawbacks in the long-term.

Probiotics are being utilised for the similar reason of shifting the microbial balance in the intestine, however they are instead used to deliver live microorganisms to the target site. A study by Yan et al found that administering probiotics to mice ameliorated intestinal inflammation and reduced epithelial cell apoptosis [69]. Additionally, the combination of probiotics and conventional drugs proved to be more effective than conventional drugs alone in inducing remission in UC [70]. Results however are varied with some studies demonstrating probiotics as exhibiting no benefit in inducing remission over a placebo [71].

An alternative route that has been explored over recent years for improvement in the condition of IBD patients is FMT. This therapy transplants the microbiota from the faeces of healthy donors to patients suffering from intestinal microbiome disorders such as IBD. Thus far, FMT has proved 90% effective in the treatment of CDI [72]. A study by Haifer et al published in 2020 notes the efficacy of FMT in inducing remission in UC patients with mild to moderate disease [73]. The advantage of FMT is the microbiota of patients is restored to that within healthy margins. This can aid in reversing dysbiosis to an extent. FMT has been revealed to be more effective than placebo at achieving remission in active UC [74]. This remission rate was demonstrated at 33% in UC patients receiving FMT [75]. As the microbial diversity shows great similarity to the donor, the choice of donor is very important as this will substantially affect the efficacy of the FMT. However, the fact that FMT is a time-consuming and complex process, in addition to the unknown safety profile of repeated transplants, it has not yet been advised as a routine therapy for the treatment of IBD. Encapsulation into an oral treatment may make this a more viable option in the future. Long-term studies are needed to confirm the safety and efficacy of FMT in patients with IBD as studies thus far have not exceeded a 1-year period.

1.2.5 Bacterial Delivered Therapies for Intestinal Disease

Bacterial delivery systems have gained attention as a potential therapeutic approach for ulcerative colitis by harnessing the unique properties of certain bacteria to deliver therapeutic agents directly to the inflamed gut tissue. These systems aim to enhance drug targeting,

reduce side effects, and improve treatment outcomes. Some examples of those currently in use and those being developed are outlined here.

1.2.5.1 Synthetic Biology Approaches

Probiotics are known for their importance in GI health as well as their efficacy in the treatment of GI diseases. However, in their native form they lack the stability to bypass the upper digestive tract in order to reach the site of interest (i.e., the colon). Using a genetic engineering approach, these bacterial strains can be modified to withstand these biological pressures.

Furthermore, these probiotic bacteria, including Lactobacillus and Bifidobacterium strains, have been engineered to express additional therapeutic proteins or peptides. These modified probiotics are administered orally and can deliver therapeutic agents to the gut mucosa, potentially reducing inflammation in ulcerative colitis. Certain biocontainment strategies have also been incorporated by some groups in an effort to prevent bacterial overgrowth. One approach used is to restrict bacterial replication in the absence of a particular metabolite produced.

An example of a long-used probiotic strain is Escherichia coli Nissle 1917 (EcN). Even in its unengineered form, it has been found to impede growth of pathogens including Salmonella. It has also been thought to stimulate anti-inflammatory activities [76] and aid in restoring intestinal barrier function [77]. A further benefit to using EcN in engineered biotherapeutics is the extensive knowledge and understanding of transcriptional and translational gene expression control in E. coli [78].

Mouse studies have demonstrated the development of chronic colitis in IL10-deficient mice as well as being implicated in IBD [79]. IL10 is suspected to be relevant in downregulating the Th1 response. To counteract this loss, systemic IL10 has been tested as a treatment in multicentre trials [80,81] with disappointing results. The lack of efficacy was suspected to be due to the low final concentrations of IL10 in the intestine [82]. Using this foundational knowledge, Lactobacillus lactis was engineered to secrete IL10 [83]. A study by Steidler et al, demonstrated a 50% reduction in colitis in a chronic DSS mouse model as well as preventing colitis onset in an IL-10-deficient mouse model [83]. More recently, a comprehensive study by Martin et al found oral administration of IL-10-secreting L. lactis to result in significant protective effects in DNBS-treated mice [84]. This was determined by measurement of colonic permeability, immune activation (in terms of cytokine generation: namely

TNFα, IL-4, IL-6 and IL-22) and gut-function parameters [84]. These results display clear potential for use of bioengineered bacteria in the treatment of gut diseases.

Smart Microbes

Additionally, some studies are focussed on generating "smart" bacteria that sense and respond to specific signals or conditions within the gut, releasing therapeutic agents when and where they are needed most. This approach, therefore, considerably minimises off-target effects. In the case of continuous expression of effector proteins, bacterial growth rate can consequently be reduced, however, this is not observed in the case of drug delivery utilising smart microbes [85]. The two sense-and-respond systems in place, typically include engineered bacteria that respond to physiological cues to determine the therapeutic is released at the desired anatomical site, while the other responds to disease-specific signals. These disease-specific signals can include quorum sensing molecules produced by pathogens as well as biomarkers. Due to the species-specific nature of quorum sensing molecules, these prove preferable for pathogen detection. Unlike antibiotics, which are a broad spectrum therapeutic, these engineered bacteria can more precisely target the pathogenic species of interest without inflicting harm upon the microbiome. An example of this system application is engineered EcN for the detection of N-acyl-homoserine lactone (AHL) produced by Pseudomonas aeruginosa. This is made possible by the expression of the LasR transcription factor known to bind AHL; in turn activating the PluxR promoter. Activation of this promoter would then lead to the expression of anti-biofilm enzyme, DspB, and E7 lysis protein, enabling self-lysis of EcN, and hence release of the therapeutic proteins [85].

An additional use of L. lactis is the specific targeting of Enterococcus faecalis, which has been implicated in IBD. L. lactis was, therefore, engineered to produce bacteriocins against this pathogen in the presence of the pheromone cCF10 it secretes [86].

1.3 IBD & Colorectal Cancer

Chronic inflammation is known to promote tumour growth and progression, with IBD increasing the risk of a patient developing colorectal cancer (CRC) by 2 to 6 times in comparison to healthy individuals [87]. As a result, CRC is responsible for 10-15% of deaths in IBD patients annually [87]. When CRC develops as a result of IBD it is known as colitis-associated CRC (CAC). Colitis-associated CRC displays many similarities to sporadic CRC, however some distinct molecular differences are present that are yet to be elucidated in terms of their role in CAC pathogenesis [88].

Prolonged inflammation has been shown to generate oxidative stress-induced DNA damage. Markers of oxidative damage and DNA damage have been observed to increase in the inflammation-dysplasia-carcinogenesis progression [89]. One of the key discrepancies observed endoscopically between sporadic CRC and CAC is the pattern in which the dysplastic polyps form. In CRC, these polyps typically form as clear, discrete lesions, while in CAC much larger areas of the inflamed mucosa become clearly transformed into neoplastic tissue [88].

Oxidative stress is suspected to activate tumour-promoting genes while concurrently repressing transcription of tumour-suppressor genes [90]. Some of these genes are present in both CRC and CAC, including APC, KRAS, P53, PIK3CA, SMAD4 and MYC [91]. Despite these similarities in genetic alterations, the timing of these alterations differs between sporadic CRC and CAC. For example, P53 mutations occur early in cancer development, occurring before dysplasia is observable, while loss of APC function occurs late in tumour development [92]. This is the opposite of what we see in sporadic CRC.

1.4 Pattern Recognition Receptors (PRRs)/Inflammatory Pathways

1.4.1 TNFα Pathway

Tumour necrosis factor (TNFα) has long been linked with the pathophysiology of IBD. It is a cytokine involved in the onset of systemic inflammation and is one of the key cytokines involved in the acute phase reaction. Expression of TNFα is significantly upregulated in response to various inflammatory mediators including TNFα itself, bacterial lipopolysaccharides and other bacterial products [93].

TNFα, expressed in T, B, NK, mast, endothelial and epithelial cells, is renowned for being a master cytokine significantly involved in key inflammatory pathways and the pathogenesis of IBD. This has been shown by the upregulation of TNFα mRNA in the inflamed colonic tissue of patients with CD [94], as well as inflamed and non-inflamed colonic tissue of UC patients, when compared to colonic tissue isolated from healthy individuals [95].

Expression of TNFα is dramatically increased in response to a variety of pro-inflammatory mediators, including bacterial PAMPs such as lipopolysaccharides and pro-inflammatory cytokines, IL1β. It was found that TNFα concentration was highly correlated with the level of disease activity in both the blood serum and intestinal lamina propria of CD and UC patients, in addition to the intestinal submucosa of CD patients [96].

Additionally, TNFα has been found to have effects on the intestinal epithelial barrier via mechanisms other than inducing inflammation. These are by means of disrupting the permeability of the [97]. This, in turn, can lead to the ability of many bacterial species to cross this usually intact barrier, thereby exposing the basolateral membrane and localised receptors to antigens which they do not usually encounter. This can, in turn, activate receptors involved in pro-inflammatory pathways, such as TLR4, that has been shown using immunofluorescence to be located on the basolateral surface of the colonic epithelium [98].

It has been found, using the Caco-2 cell line, that exposure of these cells to TNFα resulted in the downregulation of ZO-1 proteins, as well as altering their localisation to the basolateral membranes of intestinal epithelial cells [97]. In addition to these observations, it was found that TNFα exposure resulted in shedding of whole epithelial cells from the intestinal epithelium. The suggested mechanism in which this occurred was due to the activation of the NFκB-dependent signalling pathway by TNFα, subsequently leading to the activation of caspase-3 and other pro-apoptotic pathways [97]. This apoptosis and shedding of epithelial cells would also explain the reduced integrity of the epithelial barrier. TNF signalling also upregulated inducible nitric oxide synthase (iNOS), resulting in the increased expression of another pro-apoptotic protein, p53 [99].

A range of other pro-inflammatory cytokines involved in this pathway have functions in promoting and maintaining chronic inflammation in IBD. I have outlined some of the markers we'll be looking into below.

IL1β is a pro-inflammatory cytokine, present in various autoimmune diseases including rheumatoid arthritis and has been found to be one of the key cytokines involved in the pathogenesis of IBD. Expression levels are very high in the intestinal mucosa of

patients suffering with IBD. It is thought to promote differentiation and accumulation of Th17 and innate lymphoid cells in the intestine [100].

IL8 is a chemokine, upregulated by TNFα, produced by epithelial cells and macrophages. It primarily activates and recruits neutrophils to the site of inflammation from peripheral blood. Expression levels are significantly greater in the inflamed mucosa of CD and UC patients compared to healthy controls [101]. It is regulated at the transcriptional level by multiple transcription factors, including NFκB.

IL18 is a member of the IL1 family of cytokines, which is found to be increased in the inflamed mucosa of a subgroup of CD patients. Furthermore, polymorphisms in the IL18 gene as well as the IL18 receptor and activator genes have been found in patients with IBD [102]. It acts to promote the differentiation of T cell to the pro-inflammatory Th1 and Th17 phenotypes, in addition to stimulating expression of TNFα, IL-1β and IL8 [102]. However, it is also found to exert protective effects such as regeneration of the epithelial barrier, which offers protection against prolific microbial components.

IL23 is a cytokine known to act on immune cells of both the innate and adaptive immune system. It primarily promotes expansion of Th17 cells, which in turn secretes IL-17, a pro-inflammatory cytokine and enhances production of other pro-inflammatory cytokines, such as TNFβ, IL1β and IL8 [102]. IL23 has been shown to play a key role in the pathogenesis of many autoimmune diseases, including IBD. It has been found using a mouse model that inhibition of IL23 protects from IBD. Therefore, IL23 can be utilised as a key marker for the main inflammatory pathways prominent in IBD. IL23 was included on our panel of markers during this project to assess the role of epithelial cells in recruitment of leukocytes, including Th17 cells. While IL23 is typically found to be produced by macrophages and APCs, investigating the contribution of human colonic epithelial cells to the cytokine profile in the patient colon would further yield insight into their relevance and role in disease development.

1.4.2 NFκB Pathway

NFκB has been identified as one of the key regulators in the pro-inflammatory responses in IBD. Once activated by a range of stimuli, including TNFα, IL1β and LPS, it translocates to the nucleus, where it binds to DNA promoters or enhancers for its

target genes, including TNF-α, IL-1β, and COX-2 [103,104]. Its activation has been found to be highly induced in IBD patients, resulting in prolonged exposure of the gut to inflammation, causing destruction to the epithelium [104].

The activation of NFkB involves two main signalling pathways, known as canonical and non-canonical [104]. It has been established that the canonical pathway is involved in the rapid, transient inflammatory response, whereas the non-canonical pathway is more tightly controlled and is associated with a delayed and irreversible response involved in more chronic inflammation [104]. Both pathways are usually triggered by the same stimuli, namely via TNFR [104].

When unstimulated, the IKK complex: IKKg, IKKb, and IKKa and the NFκB heterodimer is inactive and located in the cytoplasm. The binding of a ligand to the TNF receptor, leads to the recruitment of adaptor proteins, i.e., TAK1. This, then, leads to the phosphorylation and activation of NEMO (a regulatory subunit in the IKK complex) which leads to the phosphorylation of IkBa, marking it for proteasomal degradation. This then allows for translocation of the NFκB heterodimer, i.e., RelA/p50, to the nucleus, allowing for the transcription of a range of pro-inflammatory cytokines [104].

The non-canonical NFκB pathway acts via the same TNF receptor, activating different adaptor protein complexes, composed of TRAF3, TRAF2, cIAP1 and cIAP2. This complex is then ubiquitinated and degraded, allowing NFkB-inducing kinase (NIK) to phosphorylate IKKα. This, in turn, phosphorylates P100, an inhibitory protein, cleaving it to form the active P52 subunit of NFκB. The RelB/P52 heterodimer is then able to form and translocate to the nucleus to initiate transcription of target genes, including CXCL12 and CXCL13 [104].

A role of the non-canonical pathway in the pathogenesis of IBD has been speculated. This is due to the canonical NFkB pathway being involved in the rapid, acute phase of pro-inflammatory cytokine production, whereas IBD is a chronic condition. The non-canonical pathway is required for the differentiation of T cells. Therefore, more research is being carried out to determine the role of this alternative pathway [104].

1.4.3 Toll-like Receptors Pathways

Toll-like receptors (TLRs) are a family of pattern-recognition receptors (PRRs) which recognise microbial-associated molecular patterns (MAMPs) from pathogenic and non-pathogenic bacteria. They are present in immune cells, including macrophages, neutrophils & B lymphocytes, as well as being expressed in the epithelial cells of various cell types. Stimulation of TLRs activates the innate immune response. This activation results in the increased production of various anti-microbial substances, in addition to pro-inflammatory cytokines. Activation triggers dimerization of TLRs, resulting in the activation of signal transduction pathways responsible for regulating the production of inflammatory cytokine and chemokines. This occurs via two main pathways: the canonical and non-canonical pathways. The most common mechanism for pro-inflammatory cytokine production is the and the subsequent activation of NFκB [105]. In the intestine, TLRs play a crucial role in the maintenance of homeostasis, ensuring the response to the ever-present microbiota is controlled. The exact mechanism in which TLRs perform these roles is unknown. It has been demonstrated that TLR signalling in the intestine may influence the composition of the microbial community [106]. This has been demonstrated in MyD88-knockout mice whereas the lack of MyD88 signalling notably changes the composition of the microbiota. Furthermore, the altered composition of commensal bacterial species within the gut was found to predispose the host to disease [106]. Since this class of receptors play a critical role in mediating immune responses to bacterial invasion, as well as maintaining immune tolerance from commensal bacteria in the intestinal tract, potential receptor mutations or expression changes can lead to varying levels of dysregulation in the immune response, with the potential to therefore lead to the development of IBD.

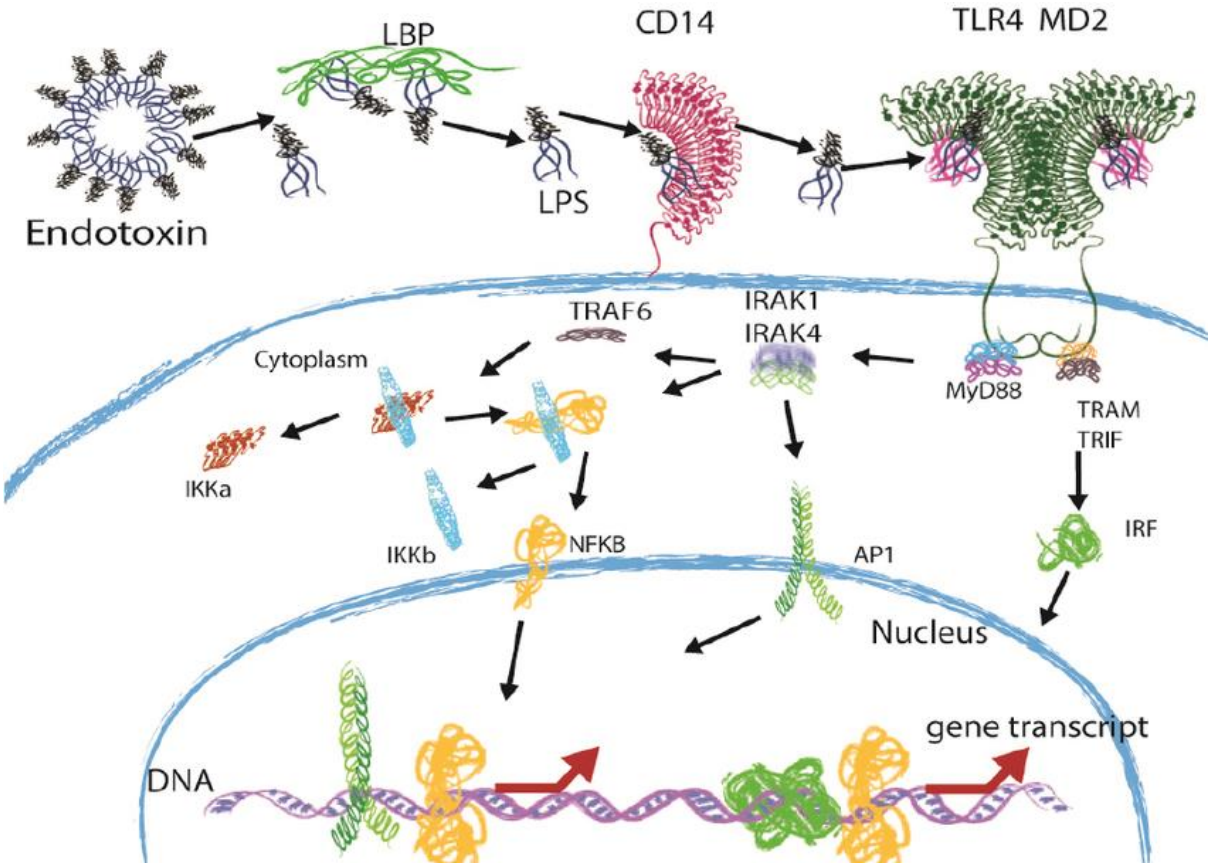

Figure 1.2: Schematic of LPS/TLR4 signalling pathway [4].

1.4.4 TLRs in Disease

In fact, TLRs have been linked to the pathogenesis of IBD. In a DSS-induced colitis mouse model, absence of TLR4, TLR2 or MyD88 was found to result in higher colitis-associated mortality than in wild-type mice [107].

TLR4 is activated by lipopolysaccharides. Lipopolysaccharides (LPS) are a major component of the outer cellular membrane of Gram-negative bacteria. LPS can be recognised by the immune system as an PAMP, and therefore induce local and systemic inflammatory responses [108]. LPS are recognised by a receptor complex, comprising the LPS-binding protein, CD14, TLR4 and MD-2 in myeloid cells as well as in intestinal epithelial cells. Recognition of LPS by this complex results in a pro-inflammatory response and subsequent inflammatory cytokine production and secretion, mediated via the IL1 signalling pathway [108]. Multiple research groups have found that intestinal epithelial cells are unresponsive to purified LPS in vitro. The reason for this was investigated and found to be due to the low levels of TLR4 and MD-2 expression in IECs. Immunohistochemical staining and qPCR techniques on human colonic biopsies and various intestinal epithelial cell lines were all found to express low levels of TLR4 [25]. This could be due to the substantially greater number of bacterial cells compared to the small intestine. The lower expression of TLRs reduces the inflammatory response initiated in the presence of innocuous bacterial cells within the microbiota. This is further supported by the lack of other TLRs present in the distal colon, with only TLR4 expressed [109].

Several years later, Vamadevan et al used T84, HT-29 and Caco-2 cell lines to model the response of IECs to LPS exposure at a concentration of 50ng/ml [110]. Using transient gene expression assays, they transfected the T84 cell line with the NFκB reporter gene, ELAM-NF-κB luciferase, co-transfected with the domains of the LPS receptor complex, TLR4 and MD-2. These cells were then grown in transwells to form an impermeable polarised monolayer. Using this method, they exposed either the apical or basolateral surface to the LPS with the aim of determining if there was a difference in response. Findings showed that only cells expressing both TLR4 and MD-2 resulted in significant NFκB activation, which was approximately 4-fold above untreated cells, when treated with LPS, on the basolateral membrane. The same effect

was not seen when the apical membrane was exposed to LPS [110]. The conclusions drawn from this data was that TLR4 and MD-2 are expressed on the polarised basolateral membrane in IECs. Since the basolateral surface of IECs is not usually exposed to the commensal bacteria, typically residing in the lumen, the location of these LPS receptor proteins would act as an appropriate mechanism to reduce the immune response to commensal bacteria and instead mount an immune response to pathogenic bacteria that is capable of crossing the epithelial barrier. Therefore, a change in the location of these receptors could be a contributing factor of IBD pathogenesis. Alternatively, if the intestinal epithelial integrity has been compromised, this would allow the crossing of both non-pathogenic and pathogenic bacteria across the epithelial membrane, therefore triggering an immune response. Previous injury or existing inflammation could result in a more permeable intestinal epithelium, further triggering immune responses, potentially leading to a destructive cycle of inflammation. It has previously been suggested that cytokines such as IFN-γ and TNFα upregulate TLR4 expression in IECs in vitro. IFN-γ has been stated to regulate expression of MD-2, the TLR4 co-receptor, through the JAK-STAT pathway [111].

TLR4 expression has previously been implicated in the pathogenesis of IBD, with expression levels of TLR4 being elevated in both IECs and lamina propria cells of both active and non-active IBD patient tissue [110]. While expression of TLR3 in IECs is reduced in CD, levels remain within a normal range in UC, as demonstrated using patient tissue sample immunohistochemistry, [112], further highlighting the vast differences in the pathogenesis of CD and UC. However, the exact mechanism in which TLR3 interacts with other proteins and its role in the regulation of pro-inflammatory cytokines is still largely unknown. Furthermore, Lu et al have found that TLR4 expression in the intestinal epithelium of UC patients was upregulated [105]. Therefore, increased TLR4 receptor expression could contribute to the uncontrolled inflammatory response and resultant ulceration in UC.

It has been shown, using the Caco-2 intestinal cell line that the presence of LPS results in an increase in intestinal epithelial permeability via a TLR4-dependent process [113]. Guo et al found that LPS caused cell death in both intestinal and immune cells, at a concentration of 50ug/ml, while the lower concentrations tested, between 0.1-1ng/ml

triggered an increase in intestinal tight junction permeability. This demonstrates that a greater presence of LPS at the TLR4 receptor is required to initiate pathogenic effects.

Furthermore, bacterial flagellin has also been found to elicit the most common antigenic response in patients with Crohn's disease. Flagellin is a protein that is the principal component of the bacterial flagellum. Bacteria require the flagellum to propel themselves in a directed manner. Bacteria readily shed flagellin monomers into their environment and as such it is a relatively ubiquitous protein found in the intestinal lumen. Flagellin is thought to contribute to dysfunction of the intestinal epithelial barrier, allowing the bacteria to pass across the epithelial barrier into systemic circulation.

It has been found that flagellin can initiate a complete pro-inflammatory response determined by pro-inflammatory gene upregulation typically induced by pathogens [114]. Likewise, the deletion of these flagellin genes abolished the ability of the bacteria to activate this gene expression. The flagellin monomers remain highly conserved across bacterial species, therefore, multiple species of bacteria, including Salmonella, are capable of inducing such a response in the gut.

Flagellin is a ligand for another of the TLR family, TLR5. TLR5 is highly expressed on colonic epithelial cells [115]. The location of this receptor also acts to control the homeostatic response to commensal bacteria, with polarisation noted on the basolateral surface, thereby only triggering an immune response when bacteria have translocated across the epithelial membrane [115]. Salmonella is capable to translocating across the epithelium due to its pathogenic nature, however most commensal bacteria is unable to breach this barrier when it is intact. In IBD, however, the epithelial membrane loses its integrity as a result of the loss of tight junction proteins, therefore, commensal bacteria are also exposed to the basolateral surface of the epithelium, triggering, an otherwise low-level, elevated inflammatory response.

1.4.5 *Clostridium difficile* Infection

Patients with IBD have been shown to be at greater risk of developing *Clostridium difficile* infection (CDI). The risk factors for developing CDI are largely unknown. Prevalence in both CD and UC patients has seen an increase in recent years, with

double the rate of CDI cases in CD patients and triple of that seen in UC over a 7-year period [116].

In a large US study, it was found that IBD patients admitted into hospital with CDI infection had a 4 times greater chance of mortality than those with either IBD or CDI alone [117]. CDI is usually hospital acquired, however for IBD patients it is often community-acquired.

The risk factors of acquiring CDI appear to be slightly different between IBD patients and non-IBD patients. Antibiotic use was shown to be a risk factor in both groups [118], however, recent antibiotic use within a 3-month period prior to CDI was seen in 69% of non-IBD patients, compared to just 40% for those with IBD [119].

Immunosuppression is suspected to increase an individual's risk of developing CDI. Immunosuppressive drugs, such as methotrexate are used as a treatment option for IBD to reduce the immune response and therefore reduce the levels of inflammation within the GI tract. However, studies have found conflicting evidence for the role immunosuppressive drugs play in the contraction of CDI in IBD patients [117].

Patients with UC appear to be at higher risk than CD patients, while CD patients with colonic disease seem to exhibit a 3-fold increased risk when compared to those with small bowel involvement [120].

CDI in IBD patients seem to have a variety of negative implications for the patient, such as symptomatic relapse, longer periods of hospitalisation and increased mortality. Even resection of large parts of the bowel does not seem to reduce the occurrence of CDI in IBD patients, where CDI will simply occur in the remaining areas of bowel, including the small intestine and ileal pouch [117]. It has also been found that IBD patients with CDI are more likely to develop extra-intestinal manifestations than those without infection, including rheumatoid arthritis, osteoporosis and chronic pancreatitis [121]. Furthermore, patients with both CDI and IBD had higher rates of both morbidity and mortality than patients with CDI alone [121].

1.5 Colonic Organoids as a Model of IBD

1.5.1 Colonic Stem Cell Niche

Due to the lack of information regarding IBD aetiology and pathogenesis alongside the severity of the disease and the critical effect it exhibits upon sufferers, further research in this field is imperative. There are multiple drawbacks to previous models of IBD including immortalised cell lines and mouse models.

The most common cell lines used as intestinal models are Caco-2 and HT-29. These were both developed in the 1970s from human colorectal adenocarcinoma [122]. The Caco-2 cell line comprises a monolayer of absorptive enterocyte cells that lack goblet-like cells [123]. While, HT-29 does in fact express mucus-secreting subpopulations, this cell line is comprised of undifferentiated cells lacking polarised organisation [124]. Both cell lines are derived from a colonic cancer and are, therefore, not representative of healthy, homeostatic tissue. HT-29 overproduces the tumour antigen p53. This could certainly skew results in a study looking into genetic changes under differing conditions. Furthermore, neither cell line contains all colonic cell types present *in vivo*, thereby preventing truly representative data to be gathered regarding the entire epithelial layer.

Mouse models are another very popular pre-clinical option for the investigation of intestinal development, disease and drug discovery. The C57BL/6J mouse model is usually subjected to external damage inflicted upon the intestine to mimic intestinal damage observed in disease. The compound, dextran sulphate sodium (DSS) is a favourite for mimicking the effects of colitis. Administration of DSS exerts very rapid effects resulting in bloody diarrhoea and weight loss over a period of several days [125]. While an acute inflammatory response is observed in this model following DSS exposure, this reaction is solely due to the non-specific damage exacted upon the colonic epithelium, as opposed to the complex interplay of factors present during the development of ulcerative colitis. The exact mechanism that DSS induces this damage is unknown, yet it is known that luminal bacteria may play a protective role for the model. Therefore, while the DSS mouse model of colitis does reveal certain responses of the colonic epithelium under times of stress, it is not a wholly accurate portrayal of the development and pathogenesis of UC. Additionally, the mouse colonic epithelium

more closely resembles that of human foetal intestine and is, consequently, less representative as a model of adult intestinal disease [126].

In recent years, the work of the Hans Clevers laboratory group has led to the production of a favourable model of GI diseases: intestinal organoids or 'miniguts' [127]. Initially, these organoids were generated from mice which display different GI anatomy to humans and, therefore, were still limited in the accuracy of the information they provided. However, this protocol has since been applied to generate human-derived intestinal organoids. These self-organising 3D structures are highly representative of the human intestinal epithelium, with structural and functional characteristics exhibited *in vivo* maintained in culture [128].

The continued culture of this model *in vivo* is possible due to the stem cell niche. The stem cell niche comprises LGR5+ stem cells present at the colonic crypt base. These stem cells continually renew as well as giving rise to all epithelial cell types. As the stem cells migrate up the sides of the crypts of Lieberkühn, they progress to become a pluripotent cell type, known as transit amplifying (TA) cells. TA cells then continue to migrate upwards while differentiating into all subsequent adult intestinal cell types [129]. Numerous niche factors allow for this balance of stem cell to differentiated cell ratio to be maintained, with the canonical Wnt and BMP pathways playing critical roles. A gradient exists along the colonic crypt axis between Wnt and BMP signals, with canonical Wnt signals existing in high concentrations at the crypt base [130]. Hence, the Wnt target gene, lgr5, has been found to be enriched in intestinal stem cells [7]. LGR5 acts as a receptor for R-Spondin-1, which, in turn, activates further Wnt signal enhancers. Conversely, BMP signals are predominant at the top of the colonic crypts. This is thought to strongly influence cellular differentiation and anoikis [131]. The shifting gradient throughout the length of the basal crypt is responsible for maintaining the hierarchy and process of tissue renewal that occurs in an orderly fashion along the crypt-axis. When this discovery is applied, it can lead to the continual culture and expansion of colonic epithelium *ex vivo* in the form of intestinal organoids.

Intestinal organoids can be generated within a culture environment favouring the Wnt signalling pathway and inhibiting BMP signals in order to support ISCs. It has been reported that addition of Wnt-3A and R-Spondin-1 was not sufficient to maintain *ex vivo* human colonic crypts for a period longer than 4 days [132]. However, when a BMP

antagonist, Noggin, and TGFβ inhibitor, A83-01, was added in conjunction, crypts were able to be maintained for a minimum of 7 days in culture [132]. At this point, the 3D matrix that supports the 3D organoid structure becomes unstable and is required to be replenished during passage. Furthermore, addition of the growth factor, EGF, was shown to promote budding in the organoid which preserves the crypt-like structure observed *in vivo* [132].

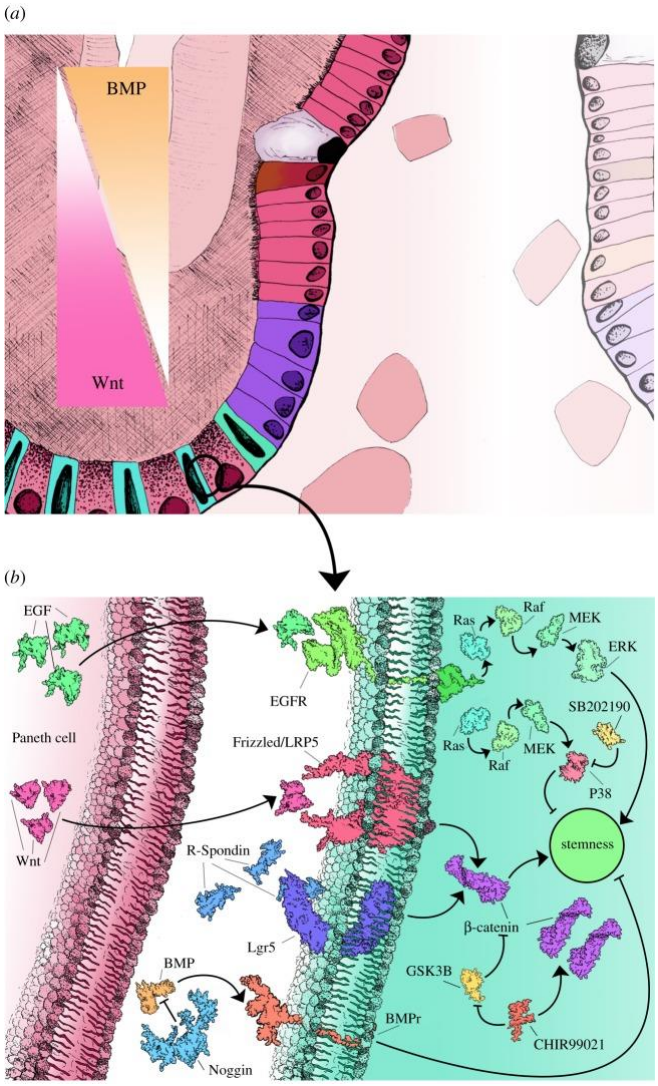

Figure 1.3: Regulation of stemness in the intestinal stem-cell niche [2].

1.5.2 Methods of Establishing Colonic Organoid Lines

There are two main approaches applied for the generation of intestinal organoids: isolation of intestinal crypts directly via surgical resection/endoscopy or via differentiation of human induced pluripotent stem cells (hIPSCs) [2].

Both methods have advantages that make them preferable in specific areas of research. The former method has certain benefits over the latter; namely the fact that biopsies can be extracted from each patient ensuring a true representation of their phenotype due to the genetic code of the patient, in conjunction with epigenetic changes, being present within the specimen. This is a useful trait as the cells are likely

to respond in the same manner as they would *in vivo* upon exposure to different treatment regimes.

Alternatively, organoids can be generated from hIPSCs derived from reprogrammed keratinocytes. Hence, the genetic background of the patient would be the same, however any variations caused by long-term inflammation or stress would not be present as the keratinocytes have not previously been exposed to an intestinal environment. Using tissue that has previously been exposed to the relevant healthy or diseased environment, means the environmental impacts upon the gene expression, including epigenetic changes, would be present, making it a more representative and relevant model. As human tissue differs in terms of response to therapies, using patient's tissue to derive organoids for use in drug and toxicity testing is desirable to allow these differences to be accounted for and studied *in vitro*.

The latter method takes longer to obtain as the differentiation process takes an additional 9 days prior to the transference of the differentiated hIPSCs into 3D culture. This method of differentiation from hIPSCs to intestinal organoids begins with the formation of the definitive endoderm induced by Activin-A. This is followed by FGF/Wnt3a to develop the posterior endoderm patterning and hindgut specification. The cells at this stage are then cultured in a pro-intestinal environment to encourage the development of specialised intestinal cells, demonstrating physiological and morphological characteristics of the intestine [133].

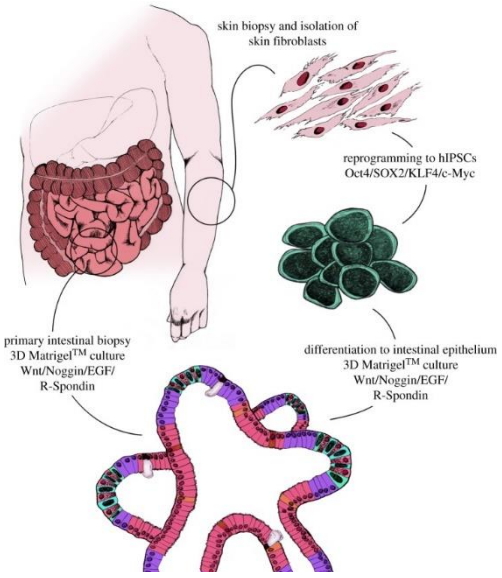

Figure 1.4: Schematic of human intestinal organoid generation [2].

The subsequent differentiated organoids have additional elements of mesenchyme. Due to the growth factors produced by the mesenchyme in the induced intestinal organoid model, this prevents differentiation, instead promoting proliferation, resulting in a less mature model than intestinal organoids derived from primary tissue. Conversely, primary-derived intestinal organoids taken either surgically or via endoscopy develop into fully mature organoids since they are isolated directly from adult epithelial tissue.

1.5.3 Prior Work on Organoids in Colitis

There have been considerable developments in the field of organoid research in colitis over the last 4 years. Stem cell-derived organoids, and to a lesser extent patient-derived primary organoids, are now widely used for the study of various scientific problems. These have replaced many studies that previously utilised animals and tumour cell lines. The ability of organoids to retain genetic alterations of the native tissue is especially useful when researching genetic-phenotypic relationships in IBD.

1.5.3.1 CRISPR-Cas9 Technology

CRISPR-Cas9 technology has become a valuable tool in colitis research, enabling scientists to explore the genetic and molecular mechanisms underlying the disease, as well as potential therapeutic approaches. There are multiple ways that CRISPR-Cas9 technology is being applied including, discovery of genes involved in cancer. Michels et al identified TGF-β receptor 2 as a tumour suppressor gene in CRC using this technique [134]. The histone lysine methyltransferase 2 A oncoprotein, KMT2A, was also revealed by CRISPR/Cas screens as a potential target of wnt/β-catenin signalling in CRC, regulating transcriptional output of β-catenin [135]. Both of these groups utilised human-derived organoids in their investigations.

Largely, CRISPR-Cas technology has been employed for the study of tumorigenesis, cystic fibrosis and refining differentiation from stem cells, with very little mention of a focus on colitis. Studies on the use of CRIPR technology on organoids to further our understanding of colitis have focused particularly on transplantation into colitis mouse models. During experimentation epithelial injury is instigated at the distal part of the colon by the administration of DSS, after which the organoids are rectally infused into the luminal space.

This assay has yielded successful results which the infused organoids binding to the injured region of intestine thereby rebuilding the epithelium [136].

There are certainly new ways that CRISPR-Cas9 can be utilised in the future of colitis research. It can be a useful tool to enhance our understanding into the genetic components at play during pathogenesis, as well as shining a light upon the root causes of variability and drug resistance in this disease.

1.5.3.2 Host-Microbe Interactions

Due to the relevance of the microbiota in IBD pathogenesis and maintenance of remission, intestinal organoids have been an important feature in researching host-microbiota interactions.

Organoid systems have been manipulated for the exploration of different aspects of IBD, including 2D culture platforms, co-culture and microfluidic-based systems.

2D culturing offers access to both the apical and basolateral membrane as well as the ability to explore diffusion of molecules and interaction of pathogens with the intestinal barrier in a more standardised fashion. Moon et al are one group who developed a 2D culture methodology from mouse colonic organoids [137]. This procedure utilised transwells that possess a permeable membrane at the bottom of the well to allow for transport of nutrients. This process requires a large quantity of cells isolated from approximately 1500 spheroids to create a monolayer in a single transwell [137]. This group confirmed, using H&E staining, that a single layer of cells had formed upon the transwell membrane. The orientation of cells was also assessed, revealing the basolateral marker, CD138, to be present on the lower surface of the well, as expected [137]. This is a very useful technique for the testing of different components and host-pathogen interactions, as the effects can easily be tested on either membrane orientation. However, a major drawback is the additional time required for the formation of a monolayer following transfer to 2D culture.

Likewise, co-culture of intestinal organoids with immunological cells has become increasingly popular in this field.

Interepithelial lymphocytes are one of the cell types previously co-cultured by Nozaki et al [138]. Previously the interaction of interepithelial lymphocytes and intestinal epithelial cells has been limited by the lack of an appropriate model. Hence, recently, intestinal organoids provide a valuable opportunity to investigate this interaction relevant to inflammatory events in the intestinal environment. The above study by Nozaki et al reported successful co-

culture, with the interepithelial lymphocytes being highly motile on and around intestinal organoids [138].

1.5.3.3 Gut-on-a-Chip

Gut-on-a-chip is an alternative approach to recreating an organ-like structure and environment with its own benefits and drawbacks. It is a microfluidic in vitro model that replicates the physiological and mechanical properties of the human GI tract, making it a valuable tool for studying GI diseases such as ulcerative colitis. "Gut-on-a-chip" systems can be used to investigate the interactions between immune cells, gut tissue, and microbiota. This allows researchers to better understand the inflammatory response in ulcerative colitis and explore potential interventions.

The monolayer structure of this platform allows simpler access to both membrane orientations removing the need for microinjection or relying on diffusion of drugs across the organoid outer cell layer. As this monolayer is cultured to cover the microfluidic surfaces of a tubular structure, this exposes the lumen enabling its exposure to bacteria, cytokines or drugs with ease. While this method has been employed for recapitulating gut function, a literature search revealed this technique only started to be utilised for the study of IBD in the past 4 years [139]. However, a key drawback to gut-on-a-chip platforms is the inherent issues with scalability and therefore rule them out for use in high-throughput experiments including drug screening.

1.5.4 Use of Organoids for Disease Modelling, Drug Screening & Personalised Medicine

Organoid technology can be utilised for the modelling of a variety of diseases. Some examples of the use of organoids in the study of disease include Short Bowel Syndrome, diverticular disease and colorectal cancer. In this project, we employ this platform as a model of IBD.

Due to the physiological similarities between organoids and the tissue from which they were derived, along with their longevity in culture, they are a desirable option for developmental and disease modelling, as well as drug screening. Furthermore, organoids provide the possibility for application into a personalised medicine

approach. This approach could include the testing of drugs on the patient's organoids prior to administering the drug directly to the patient. This will provide accurate information regarding any toxic effects the medication could exhibit, in addition to the level of efficacy for that individual.

There have been considerable developments in the field of organoid research in colitis over the last 4 years. Stem cell-derived organoids, and to a lesser extent patient-derived primary organoids, are now widely used for the study of various scientific problems. These have replaced many studies that previously utilised animals and tumour cell lines. The ability of organoids to retain genetic alterations of the native tissue is especially useful when researching genetic-phenotypic relationships in IBD.

1.5.4.1 Use of Organoids for Drug Screening

Organoids act as a more physiologically relevant platform for drug discovery than current cell lines used for this purpose, such as Caco-2. The utilisation of a more reliable cell model can aid in reducing the number of animals required for drug screening experiments. Use of an organoid system that is specific to a disease phenotype, or even a specific patient, could prove to be invaluable in the field of precision medicine [140]. This platform can then provide an accurate indication of clinical prognostic outcome without subjecting the patient to unnecessary and ineffective treatments and their subsequent side effects.

1.5.4.2 Use of Organoids in Transplantation

Furthermore, patient-derived organoids can be isolated and expanded in culture prior to being prepared for transplantation to the site of disease or tissue injury. As the organoids are immunologically compatible, this bypasses the issue of immunological rejection which is a common and serious complication of transplantation [141].

Some success has been recorded thus far with intestinal organoid transplantation in mice. Múnera et al reported morphogenesis and maturation of organoids to form tissue closely resembling that of the human intestine. The transplanted organoids also maintained regional identity, forming mature tissues that resembled either the small or large intestine, depending on *in vitro* patterning [142].

Jee et al also found that engrafted colonic organoids successfully induced regeneration in the colon of mice following damage by irradiation [143]. The grafted area was larger in mice that had received two doses of organoids at 6- and 10-days post-irradiation [143]. Cross-sections of the rectal mucosa displayed epithelial regeneration, demonstrated by crypt and villus structures at the transplant site 4 weeks post-transplantation [143]. Prior to transplantation, organoids were labelled with EGFP which enabled the final location of the grafted organoids to be determined. EGFP+ crypts were found to form in the irradiated areas [143]. A marker for proliferative cells, Ki67, was found to be expressed at the base of these crypts, whereas markers of intestinal differentiation, including villin and chromogranin A, were expressed in the upper parts of the crypts [143]. This confirms the crypt structures formed in the graft function as expected *in vivo*.

1.5.4.3 Future of Personalised Medicine

For use in the future of personalised medicine, certain elements of organoid generation must be considered. The use of retroviruses to induce pluripotency in hIPSC-derived organoids can lead to foreign DNA being integrated into the patient's genome. Furthermore, the use of oncogenes, such as Klf4, c-myc and Oct4 can lead to the formation of tumours within patients following transplant. Therefore, tissue obtained directly from intestinal epithelium could be preferable in circumventing this complication.

In this project, we generate human organoids derived directly from the colonic epithelium. This is the most relevant tissue to model in vitro due to this being the location strongly effected by ulcerative colitis. Ulcerative colitis is known to primarily affect the epithelial layer greater than any of the deeper tissue layers, hence this platform is highly applicable in the study of this disease.

1.6 Aims & Hypothesis

The main aims of this project are to validate primary colonic organoids as a model for inflammation and, specifically, IBD. Once this has been validated, the downstream pathways shall be investigated for abnormalities in the disease line compared to healthy tissue. These pathways shall then be halted with the use of synthetic inhibitors

to determine the degree of involvement of these pathways in the inflammatory response of IBD. In the final stage of the project, a novel inhibitor of a selected inflammatory pathway shall be generated using bioengineered *Clostridia*.

Aims:

- To generate an *ex vivo* colonic organoid model in long-term culture.
- To validate this platform as a model for IBD.
- To identify differential responses between healthy & UC patient-derived colonic organoids.
- To generate a novel anti-inflammatory peptide using bioengineered *Clostridia*.

Hypothesis:

- The hypothesis of this project is that an ulcerative colitis model can be successfully generated from patient-derived colonic crypts and established in culture. The response of this model to various pro-inflammatory mediators will differ from that of a healthy model.

Chapter 2

Materials & Methods

2.1 Academic Methods

2.1.1 Reagents & Solutions

Table 2.1: Components of Basal Intestinal Media.

Media component	Details	Supplier	Catalogue #
Advanced DMEM/F-12 (1X)	Reduced Serum Medium (1:1) + Non-Essential Amino Acids +110mg/L Sodium Pyruvate - L-Glutamine	Gibco	12634-010
HEPES Buffer Solution (1M)	Maintains physiological pH	Gibco	15630-56
GlutaMAX™-I (100X)	Supplement containing L-glutamine	Gibco	35050-038
Nicotinamide	Derivative of vitamin B3	Sigma	N3376
N2	Contains iron-rich human transferrin	Thermo Fisher Scientific	17502-048
B27	Supplement required for proliferation of stem cells	Thermo Fisher Scientific	17504-044
N-acetyl-cysteine	Amino acid – Precursor of L-cysteine	Sigma	A7250
Pen-Strep	Penicillin Streptomycin	Gibco	15140-122
Anti-Anti (100X)	Antibiotic-Antimycotic	Gibco	15240-062

Table 2.2: Small Molecules and Growth Factors Added to Basal Intestinal Media.

Product	Details	Supplier	Catalogue #
SB202190	p38 MAPK inhibitor	Selleckchem	S1077
A83-01	Inhibitor of TGFβ receptor, Alk5,4 & 7	Sigma	SML0788
Gastrin	Gastrin stimulates proliferation and differentiation	Sigma	G9145
Noggin	BMP antagonist	R&D	6057-NG-100
EGF	Potent mitogenic factor	R&D	236-EG
R-Spondin1	Maintains proliferation of organoid stem cells	R&D	4645-RS
CHIR 99021	Inhibitor of GSK-3	Selleckchem	S1263
ROCKi	Prevents Myc-induced apoptosis	Cayman	10005583

2.1.2 Crypt Isolation

Crypts were isolated from both healthy patients and those with a background of either active or inactive IBD. Between 4-6 crypts were taken, via biopsy during an endoscopy procedure, from the colon epithelium of the patient under local ethics approval (17/EM/0126). These were then transferred to pre-cooled Hanks' Balanced Salt Solution (HBSS) (Gibco, 14175-053) prior to culture. Each of these crypts were then further dissected using a needle and scalpel in HBSS. These smaller fragments were then transferred to a 15ml falcon tube and washed in 10ml HBSS 3 times, to remove any remaining blood and tissue debris that could interfere with the culture once in Matrigel^{TM} (Corning, 356237). Complete medium was then prepared using the formula as above. This was added in the proportion of 0.33:0.66 with Matrigel^{TM}. 30ul of this cell suspension was then carefully pipetted into the centre of each well of a 48 well Nunclon plate (Thermo Scientific, 150687). The plate was then placed at 37°C for approximately 5 minutes to allow for the polymerisation process of the Matrigel^{TM} to occur. Once the semi-solid spheres had set, 300 µl of complete medium containing all intestinal growth factors including ROCK inhibitor was added to each well. The cells were then incubated at 37°C and 5% CO2.

2.1.3 Intestinal Organoid Culture

Primary colonic organoids require a media change every 2-3 days to replenish nutrients for growth and proliferation. Organoids were cultured in intestinal basal media as outlined in table 2.1, supplemented with the small molecules and growth factors in table 2.2, in the absence of ROCK inhibitor (ROCKi).

The primary organoid lines successfully generated using this approach can be found in table 2.3, 2.4 and 2.5.

Table 2.3: Healthy Cell Lines Currently in Culture.

Cell line	Sex of patient	Age of patient (at time of biopsy)	Prognosis of patient (at time of biopsy)
COL1	F	76	Healthy
COL2	M	71	Healthy
COL3	M	53	Healthy

Table 2.4: Cell Lines Currently in Culture with an IBD Background.

Cell Line	Sex of Patient	Age of Patient (at time of biopsy)	Prognosis of Patient (at time of biopsy)	Further Information
MG015	M	24	Inactive UC	Diagnosed 13 years prior - Asacol 800 mg daily
MG020	F	22	Inactive CD Stricture present	Diagnosed 7 years prior - Humira 40mg fortnightly ICV was stenosed
MG022	M	61	Inactive UC	Diagnosed 4 years prior - Mesalazine 3.2 grams
MG025	M	36	Active UC	Diagnosed 15 years prior - Golimumab started October 2016 Azathioprine started 2003 Colazide started 2003 Ursodeoxycholic Acid started 2012

Organoid lines were derived from the biopsies of unrelated patients with either healthy, uninflamed colons derived from surgical biopsy or from those diagnosed with IBD via endoscopy. Healthy biopsies grew favourably in culture, whereas those taken from IBD patients differed in terms of survivability and growth rate. The most successful biopsies in vitro were those taken from patients with inactive disease (in a period of remission) taken from a non-inflamed section of the colon.

Table 2.5: Banked Healthy Colonoid Cell Lines.

Cell Line	Passage No.	Sex	Age (when tissue sample obtained)
MG005	7	M	58
MG006	7	F	69
MG007	7	M	78
MG008	7	M	66
MG009	7	F	58
MG010	6	F	67
COL4	7	M	65

Additional healthy cell lines were derived from colonic crypt biopsies of healthy individuals. These cell lines were expanded and cryopreserved in liquid nitrogen.

2.1.4 Intestinal Organoid Amplification and Passaging

Following 7 days of culture, colonic organoids were passaged to allow for continual expansion. Firstly, the cells in the Matrigel™ sphere were mechanically detached using the tip of a 5ml stripette. These cells were then transferred to a 15ml falcon tube (CELLSTAR®, 188261) and centrifuged at 400 *g* for 1 minute to pellet the cells. The supernatant was then aspirated. The pellet was resuspended in 10ml of cold HBSS to help break down the remaining Matrigel™. This washing process was then repeated 3 times until all Matrigel™ had been removed and only organoids remained. The cells were then resuspended in 1ml HBSS and mechanically disrupted with a p200 pipette to break the organoids into smaller fragments. These were observed under the light microscope to determine whether they required further dissociation. This suspension was then centrifuged as before and the supernatant aspirated.

The subsequent cell pellet was resuspended in the calculated volume of media, complete with intestinal growth factors, in table 2.1, in the presence of ROCKi. The appropriate amount of Matrigel™ (as calculated by the method below) was added to the cell suspension and mixed by pipetting. 30 µl of this final suspension was then pipetted into each well of a pre-heated 48-well plate. The plate was then returned to the incubator for approximately 5 minutes to allow for polymerisation of the Matrigel™. Once the Matrigel™ had set, 300ul of complete medium was then added into each well to cover the Matrigel™ sphere. The organoids were returned to the incubator (37°C and 5% CO2).

[1] Total volume of Matrigel™ & media (µl): 30µl * no. of wells of 48-well plate to seed into.

[2] Required volume of Matrigel™ (µl): Answer from [1] * 2/3

[3] Required volume of media (ul) = Answer from [1] * 1/3

Figure 2.1: Calculation of Amount of Matrigel™ and Media for Resuspension of the Cell Pellet Prior to Plating.

2.1.5 Organoid Treatment & Retrieval for Experimentation

Treatment was performed on the organoids in the 48-well plate in which they were cultured prior to experimentation. Initially, the growth medium was removed from each well and a formulation of basal media containing the relevant substance as per the experiment was added, at a volume of 300 µl per well. The treatments were added to triplicate wells to ensure a suitable quantity of cell material for harvesting, thereby yielding sufficient RNA/protein for later assays. The organoids were then cultured in this new media/treatment for the appropriate duration.

Upon completion of this incubation period, the organoids were mechanically detached from the surface of the wells with the use of a pipette tip. Once the organoids were detached, they were collected from the wells in triplicate into individual 15 ml falcon tubes and pelleted in a centrifuge set to 400 *g* for 5 minutes. The supernatant was aspirated, and the pellet resuspended in the appropriate lysis buffer before continuing with the selected assay.

2.1.6 Cryopreservation of Colonic Organoids

Colonic organoids were harvested from a 48-well plate and transferred to a 15 ml falcon tube. These were then washed three times, by centrifuging at 400 g and resuspending in 10 ml HBSS. The cell pellet was then resuspended in 1 ml 90% FBS: 10% DMSO (Sigma Aldrich). This cell suspension was transferred to cryovials (Thermo Fisher Scientific, 377267). Cells were stored in a Nalgene Cryogenic Freezing Container (Thermo Fisher Scientific, UY-44400-00) containing 100% isopropyl alcohol at -80^{o}C for a minimum of 24 hours, to allow for a gradual freezing process, before being transferred to liquid nitrogen for long-term storage.

2.1.7 RNA analysis

2.1.7.1 Primer Design

Genomic sequences were found using the National Center for Biotechnology Information (NCBI) website. The FASTA format of the sequence was input into the PrimerQuest Tool sequence search box. This search produces multiple results of potential primer sequences from which to choose the most suitable. These forward and reverse primer sequences were then be input into NCBI BLAST. Following selection of the appropriate options chosen to refine the search, this search gave the mRNA sequence that could be targeted by these primer sequences. This allows for any non-specific targets to be identified, along with further information, including the melting temperature and length of the primers, necessary to select the most suitable primer for the PCR reaction.

Table 2.6: List of primer sequences used throughout the project.

Sequence (5'-3')					
PBGD	Forward	GGAGCCATGTCTGGTAACGG	OLFM4	ACTGTCCGAATTGACATCATGG
	Reverse	CCACGCGAATCACTCTCATCT		TTCTGAGCTTCCACCAAAACTC
TNFa	Forward	GCTGCACTTTGGAGTGATCG	TLR1	CAGAGTGAATGGTGCCATTATGAAC
	Reverse	GCTTGAGGGTTTGCTACAACA		CCTTGGGCCATTCCAAATAAGTC
NFkB	Forward	CAACAGATGGCCCATACCTTC	TLR2	GAAAGCTCCCAGCAGGAACATC
	Reverse	GCTCTTTTTCCCGATCTCCCA		GAATGAAGTCCCGCTTATGAAGACA
IL1b	Forward	CCAGCTACGAATCTCCGACC	TLR3	GGACTTTGAGGCGGGTGTT
	Reverse	AGAACACCACTTGTTGCTCCA		TGTTGAACTGCATGATGTACCTTGA
IL8	Forward	CTGTGTGAAGGTGCAGTTTTGC	TLR4	GACAACCAGCCTAAAGTATT
	Reverse	CAACCCTCTGCACCCAGTTT		TGCCATTGAAAGCAACTCTG
IL18	Forward	AAAACCTGGAATCAGATTACTTTGG	TLR5	TGCCACTGTTGAGTGCAAGTC
	Reverse	GTCCGGGGTGCATTATCTCT		ACCTGGAGAAGCCGAAGGTAAG
IL23	Forward	GCAACAGTCAGTTCTGCTTGC	EGFR	CCCGCACGGTGTGAGC
	Reverse	TGGAGGCTGCGAAGGATTTT		TCGTGCCTTGGCAAACTTTC
LGR5	Forward	CTCCCAGGTCTGGTGTGTTG	COX2	CAAATTGCTGGCAGGGTTGC
	Reverse	GAGGTCTAGGTAGGAGGTGAAG		AGGGCTTCAGCATAAAGCGT
MUC2	Forward	GAGGGCAGAACCCGAAACC	HSP25	GACCCCACCCAAGTTTCCTC
	Reverse	GGCGAAGTTGTAGTCGCAGAG		TGGGATGGTGATCTCGTTGG
VIL	Forward	CTGAGCGCCCAAGTCAAAG	HSP72	AGCTGGAGCAGGTGTGTAAC
	Reverse	AGCAGTCACCATCGAAGAAGC		CAGCAATCTTGGAAAGGCCC

2.1.7.2 RNA Extraction

Following experimental treatment, cells were harvested by mechanical detachment from a 48-well plate. 10 ml HBSS was then added, along with the detached cells to a 15 ml falcon tube. The suspension was centrifuged (Eppendorf centrifuge 5702) at approximately 400 g for 1 minute to pellet the cells. The supernatant and remaining Matrigel™ was then aspirated, leaving only the cell pellet. This was then resuspended in 350 µl RLT buffer from the RNeasy Mini Kit supplied by QIAGEN (Qiagen, 74106). The suspension was pipetted several times, using a p1000, until all cells were lysed and, hence, no longer visible.

350 µl of 70% ethanol was then added to the lysed cells to precipitate the RNA present. The lysed cell suspension was then transferred to a RNeasy MinElute spin column. The column was then centrifuged at 8000 g for 15 seconds to remove the supernatant, allowing for the binding of RNA to the spin column membrane. The supernatant was discarded, 350 µl Buffer RW1 was added, then centrifuged again at 8000 g for 15 seconds. 70 µl of DNase buffer was added to 10 µl DNase, supplied by Sigma Aldrich (DNASE70-1SET), for each sample. 80 µl of this solution was then added directly to the spin column membrane and incubated for 15 minutes at room temperature.

350 µl of wash buffer, RW1, was then added and the spin column centrifuged at 8000 g for 15 seconds to wash off the remaining enzyme.

500 µl Buffer RPE was then added to each spin column and centrifuged at 8000 g for 15 seconds. A further 500 µl Buffer RPE was added before centrifuging at 8000 g for 2 minutes, discarding the supernatant after each spin.

The spin columns were then centrifuged at full speed for 1 minute to dry the membrane after the previous washes. The spin columns were then transferred to 1.5 ml Eppendorf tubes. 40 µl of nuclease-free water was then added directly to the column membrane and centrifuged at 8000 g for 1 minute to elute the attached RNA into the collection tube. The RNA yield was then quantified, as below.

2.1.7.3 RNA Quantification

The RNA yield was quantified using a NanoDrop™ 1000 spectrophotometer (Thermo Fisher Scientific). Following calibration with nuclease-free water, 2 µl of the RNA suspension was added to the NanoDrop™. To calculate the amount and purity of RNA present, the absorbance is measured at both 260 nm and 280 nm. 260 nm detects the concentration of RNA present, while other contaminants are detected at 280 nm absorbance. Therefore, the ratio of 260 over 280 determines the purity of the RNA sample. A ratio of 1.8 or greater represents a pure RNA sample, with very few or no contaminating proteins.

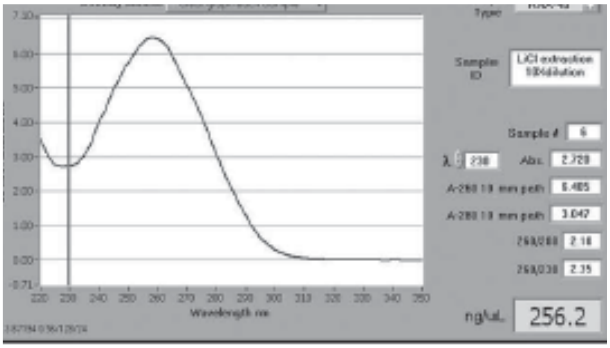

Figure 2.2: Nanodrop Data to Determine the Concentration and Purity of RNA in a Sample.

2.1.7.4 Reverse Transcription

The RNA was then converted into complementary DNA (cDNA) required for quantitative PCR (qPCR) using random primers. 500 ng of RNA from the previous step was transcribed into cDNA. A master mix of random primer and deoxyribonucleotide triphosphate (dNTPS) (taken from SuperScript ™ II kit, Thermo Fisher Scientific, 18064022) and nuclease free water was combined and 1.5 µl was added to a fresh PCR tube for each sample.

Table 2.6: Reagents required in master mix 1.

REAGENT	VOLUME REQUIRED PER REACTION (µl)
Random primer	0.5
dNTP	1

500 ng of RNA was then added to the PCR tubes. This was then incubated at 65^{o}C for 5 minutes. Following this incubation period, the suspension was snap cooled on ice to prevent the random primers and any secondary RNA structures from being formed after this denaturing step.

Table 2.7: Reagents Required in Master Mix 2.

REAGENT	VOLUME REQUIRED PER REACTION (µl)
5X 1st Strand Buffer	4
0.1M DTT	2
RNase out	0.5
Superscript II	0.125

6.625 µl of the above mastermix (taken from SuperScript ™ II kit) was then added to each tube, creating a final reaction volume of 20 µl. This was then spun down to ensure all reagents were combined, before being incubated to the below schedule.

Table 2.8: Schedule for Incubation in Reverse Transcription Reaction for Synthesis of cDNA.

Time (minutes)	Temperature (°C)	Function
10	25	Primer annealing
50	42	Extension
15	70	Inactivation of enzyme

The final cDNA product was then diluted 1:30 in nuclease-free water to a final volume of 600 µl.

2.1.7.5 Quantitative PCR

The cDNA created in the reverse transcription stage was then used in a qPCR reaction using SYBR green (Thermo Fisher Scientific, 4334973). The SYBR green emits a fluorescent signal once combined with the double stranded cDNA.

Therefore, the relative increase in this fluorescent signal can be directly correlated with the amplification of cDNA product. In the real-time qPCR process this signal is measured after each round of amplification. The threshold value is then determined, taken as the first cycle that is significantly detected above the background signal. This is known as the Ct value. The lower the Ct value, the higher the initial concentration of RNA present in the original sample. This process can thus determine the relative differences in the expression of particular genes in the sample.

Table 2.9: Reagents Required for Each qPCR Reaction.

REAGENT	VOLUME REQUIRED FOR 1 X REACTION (µl)
Forward Primer	0.6
Reverse Primer	0.6
Sensi Mix (2x)	7.5
Nuclease Free Water	1.3
cDNA	5

2.1.8 Protein Analysis

2.1.8.1 Organoid Fixing

Cells were collected from a 48-well plate and transferred into a 15 ml falcon tube. The cells were then washed in 10 ml PBS (Gibco, 14190-094) and pelleted, prior to being resuspended in 4% paraformaldehyde and left to incubate at 4oC for 20 minutes. The paraformaldehyde was then removed, and the cells washed 3 times with 10 ml PBS to eliminate any residual paraformaldehyde; completely halting the fixation process. 300 µl of PBS was then added to prevent the cells from drying and the falcon tube stored at 4oC ready for the embedding step.

2.1.8.2 Embedding & Sectioning

After fixation, the organoids are transferred to the centre of a plastic rectangular mold. 2% agarose was then heated in a Duran bottle for approximately 1 minute in the microwave (until fully melted). The liquid agarose was then added dropwise around the outside of the mold before gradually being filled until the top was reached. This was then left on ice to allow the agarose to set and, hence, hold the fixed organoids in place at the centre of the agarose block. Once the agarose was set, it was then placed

in a plastic cassette with lid, ready for embedding in paraffin wax. This step was performed by the Histopathology department. The cassette was incubated in 10% formalin for a minimum of 24 hour prior to wax embedding. Following this, the sections were cut using a microtome into 4 µm sections. These sections were then placed in the correct orientation on glass slides and left to air dry for several hours. Following the drying process, they are secured onto the glass slides by heating at 55oC for 45 minutes, ensuring the wax melts.

2.1.8.3 Antigen Retrieval

These sections, once orientated on the glass slides and secured, underwent antigen retrieval to enable accurate antibody binding. These steps must be performed in a fume cabinet.

Initially the sectioned organoids had to be dewaxed and rehydrated. This was achieved by incubating them in xylene for approximately 5 minutes. They were then transferred to fresh xylene a remaining 2 times for the same duration.

Note: Xylene solubilises and removes the paraffin, thereby dewaxing and revealing hidden epitopes prior to staining.

The slides were then transferred to a bath of IMS for a further 5 minutes before exchanging with fresh IMS for a further 5 minutes.

Note: Incubation in IMS removes residual xylene, which does not mix well with water.

All slides were then rinsed under cold water for 5 minutes to remove IMS and prevent them from drying out, which is essential once rehydration has taken place.

Next, 1L 10mM Sodium Citrate buffer (pH6.0) was prepared according to the following instructions.

Table 2.10: Reagents Comprising Sodium Citrate Buffer.

Reagent	Quantity/L
0.1M Sodium Citrate	29.41 g
0.1M Citric Acid	21.01 g

The pH was adjusted to 6.0.

This buffer was then heated by microwaving at full power until boiling. The slides were then placed in the contained containing the buffer and heated at 30% power for 20 minutes. They were then placed in slide holders for efficient washing and staining to be conducted with minimal waste of buffers and antibodies. The staining protocol was then initiated.

2.1.8.4 Staining

Immunohistochemistry Staining

The sections were washed in PBS containing 1% Donkey serum & 0.01% Triton-X. 100 µl primary antibody was added to desired concentration & incubated overnight. Following incubation, the sections were washed twice before the HRP-conjugated secondary antibody was added for 1 hour at RT. The sections were then washed twice prior to a 5-minute incubation in DAPI at RT. Upon further washing, approximately 20 µl DPX mounting medium was added to cover the section and the glass cover slip placed carefully over the section, avoiding bubbles. Once the mounting medium was set, the slides could then be imaged using the Zeiss Axio Z1 Slide Scanner.

Immunofluorescence Staining

Cells were seeded into multiple wells of a 48-well plate for each staining condition. The media was then removed from each well and the cells were then fixed with 4% paraformaldehyde for 20 minutes at 4oC. The paraformaldehyde was then removed,

and the wells washed 3 times with 300 µl PBS (Gibco, 14190-094) to remove any remaining paraformaldehyde and therefore completely halt the fixation process. 300 µl PBS was then added per well to prevent the cells from drying out. When needed, the cells were then permeabilised for 5 minutes with 0.1% Triton X-100 (Thermo Fisher Scientific, 9002-93-1) dissolved in PBS and 10% Donkey serum (Biorad, C06SB). This process is to disrupt the cellular membranes, thereby allowing for antibodies to freely enter the cell cytoplasm and nucleus to bind internally expressed proteins. The blocking and permeabilisation solution was then further diluted to 10% concentration of the original solution with 90% PBS. The desired primary antibody was then diluted in wash solution to the required concentration, to allow for maximal staining while avoiding background noise generation. This concentration varies between primary antibodies used. 100 µl of diluted primary antibody was then added to each relevant well and incubated at 4^{o}C overnight. Following this incubation period, the wells were washed with 300 µl of wash solution for 5 minutes. This was repeated 3 times, to ensure no excess primary antibody remained.

100 µl of the relevant secondary antibody was then added at a ratio of 1:1000 in Antibody/Wash solution. This was then incubated for 1 hour at room temperature, in the absence of light, to prevent deterioration of the fluorescence signal emitted from the secondary Alexa Fluor antibody. The washing process was repeated 3 times at 5 minutes each.

The primary and secondary antibody staining steps were repeated to stain for two proteins per well, preferably one internal and one external to prevent interruption of signal.

The cells were then stained with 1:1000 DAPI (Abcam, ab228549) at room temperature for 5 minutes to visibly stain the nucleus for spatial reference.

The wells were then washed twice in wash solution. 300 µl PBS was then added to each well and the plate stored at 4oC until imaging.

Images were taken using the Operetta High-Content Imaging System (Perkin Elmer, HH12000000).

Table 2.11: List of Primary Antibodies Used for Immunofluorescence Staining.

Primary Antibody	Manufacturer	Host species	Isotype	Marker Target	Catalogue #
VILLN	Abcam	Rabbit	IgG	Cytoskeletal protein present in all intestinal epithelial cells	AB130751
MUC2	Abcam	Rabbit	IgG	Constituent of inner and outer mucus layers of the colon	AB134119
CDX2-88	Abcam	Mouse	Monoclonal	Intestinal epithelial transcription factor	AB157524
CK-18	R&D	Mouse	Monoclonal IgG1	Type 1 cytokeratin	MAB7619
ZO-1	Abcam	Rabbit	Polyclonal	Tight junction protein	AB59720
EpCAM	R&D	Mouse	Monoclonal IgG2B	Epithelial cell adhesion molecule	MAB9601
E-Cadherin	R&D	Goat	Polyclonal IgG	Epithelial cell adhesion molecule	AF748

The primary antibodies in the above table were used to bind proteins of interest in our organoid model. These were then bound by secondary antibodies conjugated to a fluorescent dye to enable imaging on a confocal microscope. The microscope use was the Operetta High-Content Imaging System (Perkin Elmer, HH12000000).

Table 2.12: List of Secondary Antibodies Used for Immunofluorescence Staining.

Secondary Antibody	Manufacturer	Host species	Isotype	Catalogue #
488 Donkey Anti-Goat	Alexa Fluor®	Donkey	IgG	A11055
488 donkey anti-mouse	Alexa Fluor®	Donkey	IgG	A21202
488 donkey anti-rabbit	Alexa Fluor®	Donkey	IgG	A21206
647 donkey anti-goat	Alexa Fluor®	Donkey	IgG	A21447
647 donkey anti-mouse	Alexa Fluor®	Donkey	IgG	A21447
647 donkey anti-rabbit	Alexa Fluor®	Donkey	IgG	A31573

The secondary antibodies used the immunofluorescence protocol are outlined in table 2.13. The secondary antibodies are conjugated to an Alexa Fluor® dye, designed to emit a signal at different wavelengths.

2.1.9 RNA-Seq Protocol

2.1.9.1 Qubit Fluorometric Quantitation

Initially, the level of RNA in each sample must be accurately measured to ensure the correct amount of sample is used in the ribodepletion step. For this purpose, a Qubit® is used.

Qubit® working solution is prepared in a 1:200 ratio for each sample/standard by diluting 1µl Qubit® RNA BR/RNA HS/DNA HS reagent in 199 µl of the relevant Qubit® buffer. 1 µl of the RNA sample was then diluted in 199 µl of the above prepared solution. The standards were diluted at a ratio of 1:190.

The resultant samples/standards were then vortexed for 2-3 seconds & incubated at RT for 2 minutes. They were then run in the Qubit® Fluorometer with the appropriate setting selected.

2.1.9.2 TapeStation

The integrity of the samples was also assessed prior to ribodepletion using the TapeStation.

Note: All reagents used must be at room temperature (allow 30 minutes to warm up from 4˚C).

All reagents were vortexed and spun down before use.

For each sample, 1 µl of RNA Broad-Range (or 2 µl of sample for RNA High-Sensitivity TS) was diluted in 5 µl of RNA BR sample buffer (or 1 µl RNA HS buffer) in a tube strip.

The samples were then vortexed using an IKA vortex for 1 min and spun down in a tabletop centrifuge.

Samples were heated at 72˚C for 3 minutes to denature them, before being incubated on ice for 2 minutes. The samples were then loaded into the Agilent 4200 TapeStation instrument. The caps were removed from the tubes before inserting the RNA ScreenTape device & inputting the set-up into the Agilent TapeStation Analysis Software.

2.1.9.3 Ribodepletion

For the ribodepletion step, between 5 ng–1 µg total RNA (DNA-free) can be used made up to a total volume of 12 µl.

2.1.9.4 Hybridize the Probes to the RNA

Table 2.13: Components of Probe Hybridisation Master Mix.

Component	Volume (µl)
NEBNext rRNA Depletion Solution	1
Probe Hybridisation Buffer	2
Total Volume	**3**

To hybridize the probes to the RNA, the above master mix is added to the 12 µl volume of RNA. This is then mixed by pipetting up and down at least 10 times & spun down in a tabletop centrifuge.

The samples were then placed in a thermocycler with a heated lid set to approximately 105°C. The following program was then run:

Table 2.14: Thermocycler Program for Probe Hybridisation.

Temp	Time
95°C	2 min
95-22°C	0.1°C/sec
22°C	5 min hold

The samples were then spun down and transferred immediately to ice.

2.1.9.5 RNase H Digestion

Table 2.15: Components of Master Mix for RNase H Digestion.

Component	Volume (µl)
NEBNext RNase H	2
RNase H Reaction Buffer	2
Nuclease-free Water	1
Total Volume	**5**

The above master mix was prepared on ice & mixed thoroughly, before being added to the RNA sample & again mixed thoroughly.

The sample was then spun down & incubated at 37oC for 30 minutes in a thermocycler (with heated lid off). The samples were finally spun down & transferred immediately to ice.

2.1.9.6 DNase I Digestion

On ice, the following DNase I Digestion master mix was prepared & mixed 10 times with a pipette.

Table 2.16: Components of DNase I Master Mix.

Component	Volume (µl)
DNase I Reaction Buffer	5
DNase I (RNase-free)	2.5
Nuclease-free Water	22.5
Total Volume	**30**

This master mix was added to the RNA sample from the previous step & mixed thoroughly, prior to being spun down on a tabletop centrifuge & incubated at 37°C for 30 minutes.

Samples were then spun down & transferred immediately to ice.

2.1.9.7 RNA Purification after rRNA Depletion using NEBNext RNA Sample Purification Beads

NEBNext RNA Sample Purification Beads were vortexed thoroughly to resuspend. 110 µl (2.2X) beads were added to each RNA sample & mixed thoroughly by pipetting. Samples were incubated on ice for 15 minutes.

1.5 ml RNase-free tubes containing the samples & purification beads were transferred to a magnetic stand to separate the beads (attached to the RNA) from the supernatant. After 5 minutes, the supernatant was removed. 200 µl of 80% ethanol was added to each tube whilst in the magnetic stand. After 30 seconds the ethanol was removed.

The above step was repeated once more for a total of 2 washes.

Any traces of ethanol were removed & the beads were air-dried for 5 minutes whilst in the magnetic stand with the lid open.

The tubes were removed from the magnetic stand and the RNA eluted in 8 µl of nuclease-free water, mixed thoroughly & incubated for 2 minutes at RT. The tubes were then placed back in the magnetic stand. After 5 minutes, 7 µl was transferred to a new PCR tube.

Note: Samples can be stored at -80C until needed.

Following ribodepletion, the sample concentration & integrity were again measured on the Qubit & RNA High-Sensitivity TapeStation. A RIN (RNA Integrity) value of >7 is required for the next step.

10 ng–1 µg of DNA-free total RNA quantified by Qubit® Fluorometer and quality checked on a Bioanalyzer were then used in the library prep protocol.

The protocol is optimized for approximately 200 bp RNA inserts.

2.1.9.8 NEBNext® Ultra II Directional RNA Library Prep Kit for Illumina®

RNA Fragmentation & Priming

The following master mix was assembled on ice & mixed thoroughly:

Table 2.17: Components of Priming Master Mix.

Component	Volume (µl)
Purified mRNA or rRNA	5
NEBNext 1st Strand Synthesis Reaction Buffer	4
Random Primers	1
Total Volume	**10**

The samples were then placed in a thermocycler & incubated at 94°C for 15 minutes.

First Strand Synthesis Reaction

Table 2.18: Components of Master Mix for First Strand Synthesis Reaction.

Component	Volume (µl)
Fragmented & Primed RNA	10
NEBNext Strand Specificity Reagent	8
NEBNext 1st Strand Synthesis Enzyme Mix	2
Total Volume	**20**

The above master mix was prepared using the RNA samples from the previous step & mixed thoroughly.

The samples were incubated in a preheated thermocycler (with heated lid set to 100°C) as follows:

Table 2.19: Thermocycler Program Required for First Strand Synthesis.

Incubation Time	Temp (°C)
10 minutes	25
15 minutes	42
15 minutes	70
Hold	4

Second Strand cDNA Synthesis

The following master mix was assembled on ice:

Table 2.20: Components of Master Mix for Second Strand Synthesis Reaction.

Component	Volume (µl)
First Strand Synthesis Product	20
NEBNext 2nd Strand Synthesis Reaction Buffer with dUTP Mix (10X)	8
NEBNext 2nd Strand Synthesis Enzyme Mix	4
Nuclease-free Water	48
Total Volume	**80**

The samples were then incubated in a thermocycler for **1 hour at 16°C** without heated lid.

Purification of Double-stranded cDNA Using NEBNext Sample Purification Beads

NEBNext Sample Purification Beads were vortexed thoroughly to resuspend. 144 µl (1.8X) beads were added to the 2nd strand synthesis reaction (~80 µl) & mixed thoroughly. The samples were then incubated for 5 minutes at RT. The samples were transferred to 1.5 ml tubes, spun down & placed in a magnetic rack.

200 µl of 80% ethanol was added to each tube whilst in the magnetic stand. After 30 seconds the ethanol was removed. This step was repeated once more for a total of 2 washes. The beads were then air-dried in the magnetic rack for 5 minutes with the lid open.

The tubes were then removed from the magnetic rack and the beads eluted in 53 µl 0.1X TE Buffer & mixed well. The samples were then incubated for 2 minutes at RT, before being replaced in the magnetic rack.

Once the solution was clear, 50 µl of the supernatant was then transferred to a clean nuclease-free PCR tube.

End Prep of cDNA Library

The following master mix was prepared on ice & mixed thoroughly:

Table 2.21: Master Mix for Purification of Second Strand Synthesis Product.

Component	Volume (µl)
Second Strand Synthesis Product	50
NEBNext Ultra II End Prep Reaction Buffer	7
NEBNext Ultra II End Prep Enzyme Mix	3
Total Volume	**60**

The samples were then incubated in a thermocycler with the lid heated to 100°C for the following program:

Table 2.22: Thermocycler Program Required for Final Product Purification.

Incubation Time	Temp (°C)
30 minutes	20
30 minutes	65
Hold	4

Adaptor Ligation

The NEBNext Adaptor was diluted in Adaptor Dilution Buffer on ice. The dilution depended on the amount of RNA added at the beginning of the ribodepletion process.

Table 2.23: Instructions for Dilution of NEBNext Adapter.

Purified RNA	Dilution Required
11ng-100ng	5-fold dilution
1ng-10ng	25-fold dilution

The following master mix was assembled on ice:

Table 2.24: Components for Adaptor Ligation.

Component	Volume (µl)
End Prepped DNA	60
Diluted Adaptor	2.5
NEBNext Ligation Enhancer	1
NEBNext Ultra II Ligation Master Mix	30
Total Volume	**93.5**

The entire volume was mixed thoroughly.

The samples were incubated for **15 minutes at 20°C**. 3 µl USER Enzyme was added to the ligation mixture, resulting in a total volume of 96.5 µl. The samples were mixed thoroughly and incubated for **15 minutes at 37°C** with lid heated to 100°C.

Purification of the Ligation Reaction Using NEBNext Sample Purification Beads

87 µl (0.9X) resuspended beads were added to the sample from the previous step and mixed well. The samples were then incubated for 10 minutes at RT, before being spun down & placed in the magnetic rack.

After 5 minutes, 200 µl of 80% ethanol was added to each tube whilst in the magnetic stand. After 30 seconds the ethanol was removed. This step was repeated once more for a total of 2 washes.

The beads were then air-dried in the magnetic rack for 5 minutes with the lid open. Following this drying process, the tubes were removed from the magnetic rack. The DNA was then eluted from the beads by addition of 17 µl 0.1X TE. The suspensions were then mixed well & incubated for 2 minutes at RT.

The tubes were returned to the magnetic rack. Once the solution was clear, 16 µl of the supernatant was transferred to a clean PCR tube.

PCR Enrichment of Adaptor Ligated DNA

A PCR reaction with the Adaptor Ligated DNA was set up according to the instructions below:

Table 2.25: Components Required for PCR Enrichment of Adaptor Ligated DNA.

Component	Volume per one library (µl)
Adaptor Ligated DNA	15
NEBNext Ultra II Q5 Master Mix	25
Universal PCR Primer	5
Index (X) Primer	5
Total Volume	**50**

Note: Half reactions can also be performed.

The resultant suspensions were mixed thoroughly & quickly spun down in a tabletop centrifuge.

PCR amplification was performed using the following PCR cycling conditions:

Table 2.26: Thermocycler Program Settings for PCR Enrichment of Adaptor Ligated DNA.

Cycle Step	Temp (°C)	Time	Cycles
Initial Denaturation	98	30 seconds	1
Denaturation	98	10 seconds	6-13*
Annealing/Extension	65	75 seconds	1
Final Extension	65	5 minutes	
Hold	4	∞	

* = The number of PCR cycles varied based on the RNA input. Refer to table below.

Table 2.27: Number of Preferred PCR Cycles Depending on Quantity of rRNA-Depleted RNA.

rRNA Depleted RNA (ng)	Recommended PCR Cycles
100	6-7
50	7-8
10	9-10
1	12-13

Purification of the PCR Reaction Using NEBNext Sample Purification Beads

45 µl (0.9X) resuspended beads were added to the PCR reaction (~50 µl) & mixed well. The samples were then incubated for 5 minutes at RT, before being spun down & placed in the magnetic rack.

After 5 minutes, 200 µl of 80% ethanol was added to each tube whilst in the magnetic stand. After 30 seconds the ethanol was removed. This step was repeated once more for a total of 2 washes. The beads were then air-dried in the magnetic rack for 5 minutes with the lid open.

The DNA was then eluted from the beads by addition of 23 µl 0.1X TE. The suspensions were then mixed well & incubated for 2 minutes at RT. The tubes were returned to the magnetic rack until the solution was clear.

Once clear, 22 µl of the supernatant was transferred to a clean PCR tube & stored at -20°C. The concentration & integrity of the samples was then tested using a DNA D1000 TapeStation chip.

Note: The electropherogram should show a main peak at approximately 300bp & peaks showing the upper and lower markers.

An example of RNA library size distribution on a Bioanalyser is shown below.

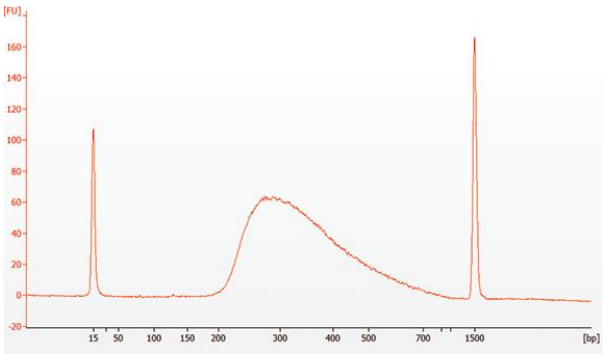

Figure 2.3: Example RNA Library Sample Distribution Plot.

2.1.10 Statistical Analysis

Statistical analyses were carried out using a two-tailed, unpaired t-test. A Bonferroni corrected p-value threshold of <0.05 divided by the number of comparisons, was used to determine significance.

2.2 Industrial Placement (Synthetic Biology) Methods

2.2.1 First Ligation

The GeneArtTM StringsTM DNA Fragments were reconstituted in ddH2O (as per instructions.

SPA4
Length: 159bp
Quantity: 400ng
Concentration: 20ug/ul

STM28
Length: 150bp
Quantity: 200ng
Concentration: 20ug/ul

Following reconstitution of DNA strands, they were incubated at RT for 1 hour.

The strands were then ligated into a pCR®-Blunt vector (Zero Blunt PCR Cloning Kit – Thermo Fisher Scientific).

Calculating amount of PCR product needed in reaction mix

To ensure a sufficient amount of reconstituted DNA fragments were added to the reaction mix, the concentration required was calculated by the following formula:

$$x \text{ ng insert} = \frac{(10)\ (y \text{ by PCR product})\ (25 \text{ ng}}{\text{linearized pCR-Blunt})}$$

A reaction mix was prepared:

Table 2.28: Components for Blunt PCR Vector Containing Desired DNA Fragments.

Component	Volume (µl)
pCR®-Blunt (25ng)	1
Blunt PCR Product*	2
5X ExpressLinkTM T4 DNA Ligase Buffer	2
Sterile water	4
ExpressLinkTM T4 DNA Ligase (5U/µl)	1

* = DNA fragments ordered from GeneArtTM StringsTM DNA Fragments (gene of interest to express desired protein)

The above ligation reaction mix was then incubated at RT for a minimum of 1 hour to ensure high efficiency of ligation into the blunt-end vector.

2.2.2 Preparation of chemically competent cells – $CaCl_2$ method – heat shock

Following ligation, the competent Top10 *E. coli* cells were prepared.

Primarily, 5 ml LB media was inoculated with a single colony & incubated overnight (at 37°C). The overnight culture was then used to inoculate 50 ml LB media at OD600 of 0.1. The culture was then grown in a baffled flask with a minimum volume of 250 ml to allow for proper aeration. This was then incubated at 37°C, until a density of 0.3-0.6 at OD600 had been reached, whilst shaking at 250 rpm on an orbital shaking heated platform.

In the meantime, 50 ml 0.1M CaCl2 with 15% glycerol was prepared & sterilised by membrane filtration. **Note: This must be kept ice-cold.**

5 ml of the above solution was then separated from the original solution & kept on ice. The centrifuge was pre-cooled to 4°C. Once desired optical density had been reached, cells were placed on ice for 10 minutes.

Cells were removed from ice & centrifuged for 10 minutes at 900 *g* (4°C). The supernatant was aseptically removed & cells resuspended by pipetting 45 ml ice-cold 0.1M CaCl2/15% glycerol. This cell suspension was incubated on ice for 30-60 minutes, before being centrifuged for 10 minutes at 900 *g* (4°C).

The supernatant was aseptically removed & cells resuspended into 2-4 ml ice-cold, filter sterilised 0.1M CaCl2/15% glycerol. (The amount resuspended in would generally be 10% of growth volume).

Note: To transform ligation mix – 50 µl cells needed to transform 5 µl ligation mix.

2.2.3 First Transformation

5 µl of ligated DNA mix was added to 50 µl competent Top10 *E. coli* cells. The cells in this suspension were then heat shocked using a water bath for 30 seconds at 42°C. The cell suspension was then snap cooled & incubated on ice for 2 minutes.

200 µl S.O.C medium was added to the cell/ligated vector mix (to ensure optimal conditions for cell recovery), before being incubated at 37°C for 1 hour on an orbital shaker. 100 µl of this competent cell/vector mix was then added to a LB plate (containing antibiotic Kanamycin to select for competent cells containing the vector) & spread evenly. They were then incubated at 37°C overnight until colonies formed.

PCR & DNA Gel Electrophoresis

Note: This step is performed to amplify colony DNA & to separate & detect the colony containing the DNA strand of interest.

Primers for the M13 marker were used for the PCR as the DNA fragment was inserted into the pCR-Blunt in the centre of the M13 gene.

Note: The DNA gel electrophoresis determines whether selected colonies have taken up the vector containing the DNA insert.

Following overnight culture, the PCR master mix was prepared:

Table 2.29: Components of PCR Master Mix.

Component	Volume for 1 reaction (i.e., 1 colony in 1 tube) (µl)
Green Taq PCR master Mix (2X)	10
Forward primer (M13)	1
Reverse primer (M13)	1
RNAse-free water	8
Total	**20**

Note: Primers used for the PCR step are listed as CH478 (forward) & CH479 (reverse) in the CHAIN Biotech database.

18 µl (of the 20 µl prepared) of the above master mix was added to each PCR tube.

8 colonies were selected & labelled from each strain. Using a p200 tip, these selected 8 colonies were picked from each strain & streaked onto another LB plate as 1cm horizontal lines labelled with the corresponding colony number & plate.

E.g., 8 colonies were picked per DNA construct (8x SPA4 & 8x STM28 = 16 colonies picked). Picking more colonies increases the chance of identifying the minimum of 2 positive colonies that are required for future experimentation. These newly streaked colonies were then incubated at 37°C overnight.

Following incubation, a small quantity of each newly streaked colony was picked using a p200 tip. This tip was then transferred to individual PCR tubes for several minutes before being resuspended using a p200 pipette.

The PCR tubes were placed in the PCR machine (Analytikjena Biometra Tone) & lid tightened. The PCR program named ‘DreamTaq’ was selected & ran for approx. 1 hour.

Note: Adjust length of annealing step depending on length of vector + inserted construct.

An agarose gel for electrophoresis was then prepared:

A 1.25% gel was prepared by dissolving 1.25g agarose in 100 ml 1X TAE buffer & microwaved until dissolved (approx. 2 minutes), before being left at RT until cooled to approx. 50°C.

10 µl SYBR Safe DNA Gel Stain was added to the bottom of the gel mould. The gel was poured into the mold & a p200 pipette tip was used to mix until the red stain was evenly spread throughout the gel. The comb was then inserted.

Once the gel had set (approx. 15 minutes) the comb was removed & the gel (contained within the mold) was placed in a horizontal gel tank. 1X TAE buffer was then poured into the tank until the gel was covered.

10 µl of ladder & 15 µl of each sample was loaded into the wells.

The gel was then run at 100V for 30 minutes.

Gel template example

1	2	3	4	5	6	7	8	9	10	11	12	13	14	15	16	17	18
Ladder	A	B	C	D	E	F	G	H	Ladder	A	B	C	D	E	F	G	H

SPA4

STM28

Once the gel had finished running, the gel was removed & placed on a blue light screen (fisherbrand).

The gel was then covered with a black box & imaged with a camera through the aperture.

Note: Positive bands should appear bright yellow.

2.2.4 Inoculation of liquid LB broth

In a 50 ml falcon tube, LB liquid media was prepared by adding 5 µl Kanamycin antibiotic to 10 ml LB stock media.

Note: Prepare as many tubes as there are colonies to be picked & sequenced.

Using a p200 pipette, 2 positive colonies from each strain with different DNA inserts were picked by puncturing solid medium and resuspending the plug containing medium & colony into relevant tubes.

The falcon tubes containing LB broth & colony suspensions were placed into a 37°C orbital shaker overnight.

DNA strands can be stored at -20°C until needed.
LB plates with remaining colonies can be stored at 4°C until needed.

Culture stocks were prepared from long-term storage at -80C

1.5 ml Nalgene tubes were labelled using white cryo-labels with construct/gene name, colony letter, initials, date, strain (i.e., Top10 *E. coli*) & letters NCH (Nottingham CHAIN) followed by allocated numerical identifier corresponding to the database.

250 µl 60% glycerol was added to each tube. 750 µl suspended Top10 *E. coli* cells were added to each relevant Nalgene tube. These tubes were then stored at -80°C.

2.2.5 Preparation of *E. coli* cells containing vector with SPA4 & STM28 DNA fragments for Sanger sequencing

Note: Sanger sequencing is a slower technique that is required due to the A-T rich sequence of the *E. coli* DNA sequence. The slower speed enables the DNA polymerase to bind more steadily to the DNA strand, hence allowing more effective & accurate sequencing.

Sequencing of the colony is required to ensure that the desired DNA insert is present & orientated in the correct position within the blunt end vector.

Extraction of plasmid for Sanger sequencing

10 ml inoculated cell suspensions were centrifuged at 1200 *g* for 5 minutes (Fisherbrand GT1R Benchtop Centrifuge). Using Promega Wizard(R) Plus SV Minipreps DNA Purification System (Cat# A1465; Lot#0000346122), the plasmid was extracted from the Top10 *E. coli* strains.

This protocol is listed below:

Production of cleared lysate

The cell pellet was resuspended in 250 ml Cell Resuspension Solution, then transferred to a 1.5 ml Eppendorf tube. 250 µl Cell Lysis Solution was added to each sample & inverted 4 times to mix thoroughly. 10 µl Alkaline Protease Solution was then added & inverted 4 times, then incubated for 5 minutes at RT. Following this, 350 µl Neutralization Solution was added, and again, inverted 4 times.

These samples were then centrifuged at top speed (21,000 g) for 10 minutes at RT.

Binding of plasmid DNA

The cleared lysate was transferred into a spin column with collection tube & centrifuged at top speed for 1 minute at RT. Flow-through was discarded.

Washing

750 µl Wash Solution (with EtoH) was added to the spin column & centrifuged at top speed for 1 minute at RT. Flow-through was discarded.

250 µl Wash Solution was added & columns were centrifuged at top speed for 1 minute at RT. The columns were then centrifuged again at top speed for 2 minutes at RT to dry the membrane.

Elution

The spin column was transferred to a sterile 1.5 ml Eppendorf tube for each sample. 50 µl NFW was added to each spin column membrane, which was then incubated at RT for 2 minutes. The tubes were then centrifuged at top speed for 1 minute to elute the plasmid contained within the membrane.

Note: DNA can be stored at -20^{o}C for several months.

Plasmid concentration measured

Using an Eppendorf Biophotometer D30 with compatible 1mm cuvette, the concentration of the isolated plasmid DNA was determined. DNA was then diluted to 50 µg/ml to be sent off for sequencing.

Sanger Sequencing Results Analysis

In Chromas, each sequencing file was opened & copied as a FASTA sequence into a word document. Next, the sequences were aligned with the designed gene sequence for each DNA fragment. For this, the online service Clustal Omega was used. To confirm these results and to create a clear graphic, the sequences were copied into another online tool, Multalin, giving you a colour coded alignment of the sequences.

Inoculation of Top10 E. coli containing desired vector backbone

Upon confirmation of the results, LB broth was inoculated with the desired vector backbone (pMTL82123) containing an unwanted DNA fragment(s) & cultured at 37°C overnight. The cell suspension was then centrifuged at 1200 *g* for 5 minutes to pellet cell debris. The supernatant was discarded.

Plasmid extraction

This step was performed using the Promega Wizard(R) Plus SV Minipreps DNA Purification System with the same protocol used above.

Plasmid concentration measured

Using an Eppendorf Biophotometer D30 with compatible 1mm cuvette, the concentration of the isolated plasmid DNA was determined.

2.2.6 Restriction Digest

The desired DNA fragment(s) contained in the pCR-Blunt vector(s) & the DNA fragment contained in the desired vector backbone was cut out of the plasmid using restriction enzymes to target the NdeI & NheI restriction sites present in the plasmid(s).

Note: Desired pCR-Blunt vector + DNA fragment samples & restriction enzymes should be stored at -20°C.

Note: A maximum of 10% enzyme can be used per overall reaction for effective activity.

500 ng of vector backbone in total was used for the reaction.

For pCR-Blunt vector containing desired DNA fragments:	For pMTL82123 vector containing desired DNA fragments:
35 µl of each DNA vector	5 µl of each DNA vector
5 µl of CutSmart(R) (NEB; Cat# B7204S) enzyme buffer	2.5 µl of CutSmart(R) (NEB; Cat# B7204S) enzyme buffer
2.5 µl NheI restriction enzyme	1 µl NheI restriction enzyme
2.5 µl NdeI restriction enzyme	1 µl NdeI restriction enzyme
5 µl NFW	15.5 µl NFW
Total = 50 µl	**Total = 25 µl**

Different concentrations were used for the pCR-Blunt & pMTL82123 vector as a surplus of the desired DNA fragment is beneficial. The tubes containing these master mixes were then incubated at 37°C for 4 hours to ensure effective binding of the restriction enzymes.

Gel electrophoresis

Gel electrophoresis was performed to isolate the desired DNA fragment and pMTL82123 vector backbone.

10% loading dye was added to each sample and mixed. 10 µl MW ladder was loaded in the 2nd column, while half of each sample was loaded in subsequent wells. The samples were run in duplicate. The gel was run at 80V for 40 minutes.

The desired gel bands were then cut out using a scalpel. These bands contained the excised DNA fragments (SPA4/STM28) & the pMTL82123 vector with the previous gene fragments removed.

Using a MinElute Gel Extraction kit (Qiagen), the DNA was purified from the surrounding agarose gel. Upon purification, the concentration of DNA in each sample

was measured using an Eppendorf Biophotometer. This gave readings for the SPA4 A, STM28 B, NCH716A & NCH716B samples.

2.2.7 Second Ligation

Desired vector pMTL82123 size = 4992 bp

SPA4 size = 159 bp **STM28 size = 150 bp**

Example calculation of amount of insert & vector required to combine:

$$10 \text{ ng insert} = \frac{5 \times 10 \text{ ng vector} \times 160 \text{ bp insert}}{4992} = \textbf{1.6 ng insert required}$$

A master mix was prepared for the ligation reaction to occur:

Table 2.30: Components Required for Ligating Desired DNA Fragment into Final Vector.

Reagent	Volume
pMTL82123 vector	1 µl
T4 buffer	2 µl
DNA insert	3 µl
T4 ligase	1 µl
Water	13 µl
Total	**20 µl**

This master mix was incubated for 1-2 hours at RT. These ligated samples were then streaked onto a Kanamycin-containing plate.

2.2.8 Second Transformation

1 µl SPA4/STM28 + pMTL82123 plasmid was added to 10 µl competent CA434 *E. coli* cells (conjugation species). The cells were heat shocked using water bath for 30 seconds at 42^{o}C, before being snap cooled & incubated on ice for 2 minutes.

150 µl S.O.C medium was added to the cell suspension (to ensure optimal conditions for cell recovery). They were then incubated at 37°C for 1 hour on an orbital shaker. 100 µl of this competent cell/vector mix was then added to a LB plate (containing antibiotic Kanamycin & Chloramphenicol to select for competent cells that have taken up the plasmid) & spread evenly. The plate was then incubated at 37°C overnight until colonies formed.

Re-streaking colonies & Colony PCR

The following master mix was prepared (for 18 samples):

Table 2.31: GreenTaq PCR Master Mix.

Component	Volume for 1 reaction (i.e., 1 colony in 1 tube) (µl)
Green Taq PCR master mix (2X)	10
Forward primer (CH22)	1
Reverse primer (CH54)	1
RNAse-free water	8
Total	**20**

After adding 18 µl of the above master mix to each PCR tube, selected colonies were picked using a p200 tip and re-streaked onto a new Kanamycin-containing plate. These plates were then incubated overnight at 37^{o}C.

The tip was then placed into the PCR tubes containing the above master mix for several minutes. The master mix was resuspended, using this tip, to detach any remaining cells present.

The PCR tubes were then run on a PCR machine using the 'DreamTaq' program, with the annealing step set to ~15 seconds (As the PCR cycle anneals the primers at around 1000 bp/ 1 minute).

Gel electrophoresis

A 1% agarose gel was prepared as described earlier.

Gel template

1	2	3	4	5	6	7	8	9	10	11	12	13	14	15	16
Ladder	1	2	3	4	5	6	7	8	Ladder	1	2	3	4	5	6

SPA4 A + STM28 B +

Once the gel had finished running, the gel was removed and placed on a blue light screen (fisherbrand) & an image was taken through the aperture.

2.2.9 Plasmid purification

Following confirmation of positive colonies, 4 colonies from each plate were picked by puncturing the LB agar gel with a p200 pipette tip. This gel plug was then resuspended in 10 ml LB broth containing 10 µl Chloramphenicol antibiotic to ensure growth of bacterial cells containing the pMTL82123 plasmid only. These 50 ml falcon tubes were then incubated at 37°C on a shaking platform overnight.

Culture stocks were then prepared from long-term storage at -80°C.

2.2.10 Preparation of E. coli cells containing vector with SPA4 & STM28 DNA fragments for Sanger sequencing

Extraction of plasmid for Sanger sequencing

The remaining cell suspensions were centrifuged at 1200 *g* for 5 minutes (Fisherbrand GT1R Benchtop Centrifuge).

Using Promega Wizard(R) Plus SV Minipreps DNA Purification System (Cat# A1465; Lot#0000346122), the plasmid was then extracted from the Top10 *E. coli* strains.

The concentration of the extracted DNA was measured using an Eppendorf Biophotometer D30. The samples were then diluted to 30 ng-100 ng/µl (i.e., 10 µl of DNA samples & 10 µl dH2O).

Note: The remaining DNA samples were stored at -20°C until sequencing confirmation.

These were then labelled with corresponding barcode following online registration with GeneWiz. The samples were then boxed & sent to GeneWiz for Sanger sequencing.

Preparation of antibiotic-containing RC plates

400 ml RC agar was melted at 30% power for 20 mins in microwave. When agar cooled down to ~55°C, 25ml 40% glucose was added to a final concentration of 2%. 500 µl thiamphenicol (1:1000) & 2.5 ml D-cycloserine (1:200) was added. 72 ml H2O was added to bring the final volume to 500 ml. This mixture was then poured into agar plate & left to cool, prior to drying in a flow cabinet & being stored at 4°C until needed.

2.2.11 Transconjugation

Both the CA434 transconjugant *E. coli* strain & the *Clostridia* NCH390 strain were inoculated in preparation for the transconjugation step. 10 ml RC broth was added to 4 x 50 ml falcon tubes. This was repeated with another 3 x 50 ml falcon tubes required later in the protocol.

In an anaerobic cabinet, 1 colony of CHAIN's NCH390 strain was added to 1 ml RC medium. 100 µl of this cell suspension was added to the first tube containing 10 ml RC broth (10^{-2}). This was gently mixed before 100 µl being added to the subsequent tube. This was repeated until a dilution of 10^{-8} was reached.

3 x 50 ml tubes containing 30 ml RC broth each were taken into the anaerobic cabinet overnight.

In conjunction with the above, 10 ml LB broth + 5 µl chloramphenicol + 5 µl Kanamycin was prepared in a 50 ml tube. A culture stock in a Nalgene tube of CA434 strain containing our engineered plasmid was taken from -80°C.

Without defrosting, a 10 µl inoculation loop was used to collect a small amount of cell material, which was then resuspended into the LB broth containing antibiotics. These tubes were then incubated on a shaking platform at 37°C overnight.

Note: 4 colonies were inoculated in total: 2 containing SPA4 (SPA4 2/1 & SPA4 2/2) and 2 containing the STM28 gene fragment (STM28 1/1 & STM28 1/2).

Following overnight incubation, the absorbance (OD600) of each bacterial species was measured to an OD 0.1.

Table 2.32: Optical Density Absorbance for Each Chosen Strain.

Bacterial Strain	Absorbance (OD_{600})
SPA4 2/2 repeat 1	0.391
SPA4 2/2 repeat 2	0.420
STM28 1/2 repeat 1	0.427
STM28 1/2 repeat 2	0.416

250 µl of the highlighted CA434 *E. coli* strains were taken & added to 10 ml LB broth + 5 µl Chloramphenicol + 5 µl Kanamycin. This was then incubated on a shaking platform at 37°C for 1 hour.

The OD of the strains was checked after this incubation period.

Table 2.33: Optical Density Absorbance for Final Selected Strains Following Incubation with Antibiotic.

Bacterial Strain	Absorbance (OD_{600}) (with 1:2 dilution for measurement)
SPA4 2/2 repeat 1	0.640 (0.341)
STM28 1/2 repeat 2	0.668 (0.363)

For the NCH390 *Clostridia* strain, 50 µl of the cell suspension from the serial dilution displaying the least visible bacterial growth was taken and incubated at the following dilutions: 1:50 (200 µl) & 1:100 (100 µl).

The OD of these strains can be found below:

Table 2.34: Optical Density Absorbance Following Serial Dilution of *Clostridia* Strain.

Bacterial Strain	Absorbance (OD_{600}) (with 1:2 dilution for measurement)
NCH390 1:50	0.722 (0.431)
NCH390 1:100	0.240

1 ml *E. coli* CA434 strain was taken & centrifuged at 500 g for 3 minutes. The supernatant was then discarded. 1.23 ml NCH390 (from the 1:50 dilution) was used to resuspend this *E. coli* pellet in an anaerobic cabinet. 20 µl of this cell suspension was then spotted onto an RC only plate until all the cell suspension was used up. This was then incubated in an anaerobic cabinet at 37°C overnight.

Following overnight incubation, a 10 µl inoculation loop was used to collect all cell material from all spots on the RC plate, before being resuspended in 500 µl RC

medium. This cell suspension was then added over 4 RC plates + thiamphenicol + D-cycloserine at volumes of 100, 100, 75 & 50 µl. A cell spreader was then used to evenly disperse the cell suspension over the plates. The plates were then incubated in an anaerobic cabinet overnight at 37°C.

The following morning, a small inoculation loop was used to collect a collect from each plate, which was then spread over 1/8th of an RC + thiamphenicol + D-cycloserine plate. This was repeated for 7 other colonies prior to incubating the plate in an anaerobic cabinet for 37°C.

DreamTaq PCR

Some cell material from each section of the plate was added to 30 mM NaOH in PCR tubes. These tubes were then boiled at 98°C for 15 minutes.

A master mix was prepared as below:

Table 2.35: DreamTaq PCR Master Mix Including Forward & Reverse Backbone Primers.

Component	Volume (µl)
DreamTaq polymerase	110
CH22/8X1XX LF/CH150	11
CH54/8X1XX RR/CH151	11
H_2O	77
Total	**209**

1 µl boiled DNA from each colony was added to the relevant tubes.

19 µl master mix + 1 µl boiled DNA (or positive/negative control) was added to each PCR tube.

The PCR program ran was listed as DreamTaq (run time ~ 1 hr 40 mins).

Table 2.36: DreamTaq PCR Program Steps.

Cycle step	Temp (°C)	Time
Denaturation	95	30 sec
Annealing	50	30 sec
Extension	72	1 min

DNA Purification

Following PCR, the amplified DNA was purified using a Qiagen PCR Purification kit following the manufacturer's instructions. The purified plasmid was eluted in 35 µl elution buffer.

The concentration was then measured using the Biophotometer. The readings are below:

Table 2.37: Concentrations of Colony DNA Following Purification.

Sample	Concentration (µg/ml)
STM28 1/2 colony 1	27.6
STM28 1/2 colony 2	29.4
STM28 1/2 colony 3	26.6
SPA4 2/2 colony 2	22.1
SPA4 2/2 colony 3	12.8

20 µl of each sample was sent off for Sanger sequencing along with 20 µl CH22 gene-specific primer. 5 µl of the remaining purified plasmid was ran on a 1% agarose DNA gel to confirm.

Note: All colonies came back positive.

2.2.12 Bacterial Growth Experiment

10 ml CGM media in 50 ml falcon tubes were taken into the anaerobic cabinet the night prior to inoculation to allow for the oxygen levels in the media to deplete. Immediately prior to inoculation 10 µl of Thiamphenicol was added to each falcon tube.

The cell material from the CGM plate was collected using a large inoculation loop before being resuspended in 10 ml CGM media with added antibiotic (1:1000). When each of the 5 strains (3x STM28 & 2x SPA4) were inoculated in broth, a dilution series was then performed from the initial suspension (10^{-2} to 10^{-8}).

This was achieved by transferring 100 µl from 10^{-2} to the next tube 10^{-4} & so on until 10^{-8} was reached. The cell suspensions were then left to incubate in the anaerobic cabinet overnight at 37°C. 3x 50 ml falcon tubes per strain (e.g., 15 tubes for 5 strains) containing 30 ml CGM without antibiotic were taken into the cabinet to equilibrate overnight.

The following morning 30 µl of Thiamphenicol was added to each 30 ml CGM broth. The last tube with visible bacterial cell growth from the dilution series was used to inoculate the 30 ml broth in triplicate. The ratio used was 1:20 to enable quicker bacterial growth as the strains grow slowly due to the p15a low copy number replicon in their plasmid.

The pH & optical density was recorded at 0 hours. Readings were then taken every subsequent hour for the following 8 hours & a final reading was taken at 24 hours. From this dataset, a bacterial growth curve was generated to determine the optimal time of bacterial growth to obtain a suitable concentration of peptide.

At each time point extra cell material was also pelleted & frozen at -20°C to preserve any peptide produced.

In conjunction with the 5 strains; 3 containing STM28 gene & 2 containing SPA4 gene; the NCH390 *Clostridia* parental bacterial strain was grown to enable naturally expressed *Clostridia* proteins to be discounted when identifying the novel proteins expressed by the engineered strain.

An *E. coli* growth experiment was run simultaneously to determine whether the TOP10 *E. coli* strains engineered at earlier stages in the project could also produce the novel peptides. As a control a parental TOP10 *E. coli* was used.

Western blot

Upon completing this bacterial growth experiment, selected samples from time point 8 & 24 hours were ran on a gel via electrophoresis (100V for 1 hour) to confirm whether a detectable amount of small peptide at the relevant size could be identified. Samples collected from time point 0 would act as a negative control for comparison. Upon transfer of the protein from the gel to the cellulose membrane, the addition of SIGMAFAST™ p-Nitrophenyl phosphate Tablets (Sigma) were used to visualise the bands without the need of a Chemiluminescent imager.

In addition to this control, an *E. coli* lysate expressing both Flag & His tags was used to confirm whether the western blot had worked.

Chapter 3

Isolation & Characterisation of Patient-Derived Colonic Organoids

3.1 Introduction

3.1.1 Intestinal Organoid Development

The identification of LGR5+ stem cells and the characterization of the intestinal stem-cell niche has led to the development of three-dimensional (3D) organoid cultures and the ability to amplify intestinal epithelium *in vitro* [127]. These primary tissue cultures can be maintained long term without any substantial changes to genetic integrity or tissue physiology.

An organoid is defined as 'an in vitro 3D cellular cluster derived exclusively from primary tissue, ESCs or IPSCs, capable of self-renewal and self-organization, and exhibiting similar organ functionality as the tissue of origin' [144].

Intestinal organoids are clusters of cells that self-organize in 3D structures that recapitulate major features of their native tissue, including a highly folded epithelium structure consisting of crypts and villi similar to native intestinal epithelium (Figure 3.1). Once embedded into Matrigel™, they self-assemble so that the luminal surface of the epithelium is directed towards the centre of the organoid and the basolateral side is in contact with the Matrigel™ and surrounding medium [127]. Analysis of the different cell types present within intestinal organoids has shown that all cell types usually found *in vivo* are present and are therefore useful for studying the complex interplay between cell types during homeostasis and disease states.

Intestinal organoids have been shown to exhibit the same absorptive and secretory functions as those that occur *in vivo*, including mucus production [128]. Intestinal organoids mimic *in vivo* epithelial regenerative capacity, with apoptotic cells being

continually released into the lumen of the organoid as new cells are differentiated from the LGR5+ cells within the crypts to replenish the epithelium [2].

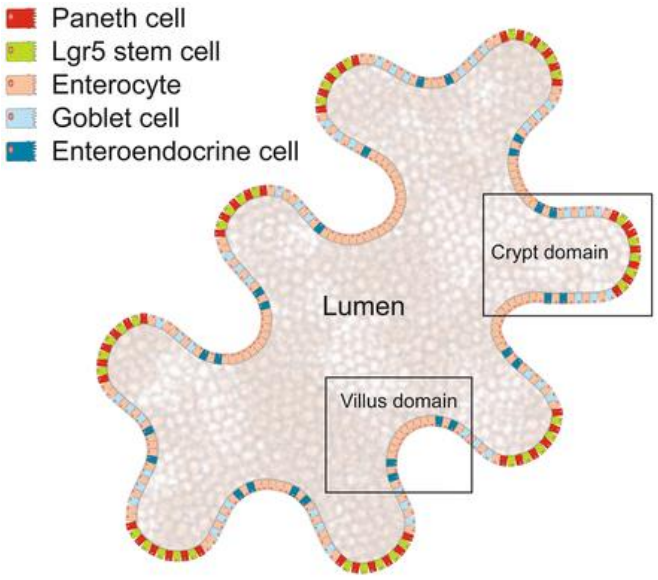

Figure 3.1. Schematic of an intestinal organoid [3].

Intestinal organoids offer an opportunity to further our understanding into the pathogenesis of IBD by investigating the effects of inflammation on the intestinal epithelium isolated from healthy patients. These results can then be used to identify differences present in the responses of intestinal organoids derived from patients with an IBD background. In this project, we aim to utilise a range of inflammatory mediators suspected to be involved in the initiation and progression of IBD and to determine the severity of the immune response. This will then be further investigated by testing the response of these organoids to common treatments. We shall then analyse key information from the patients' medical records, including age of patient, severity, location and duration of disease, as well as treatments received thus far and their response to these treatments. Patterns can then be identified between this patient information and the responses of the intestinal organoids derived from these patients. This may aid in identifying the efficacy of different IBD treatments on these patients and can contribute to a establishing a personalised medicine approach.

As described in Chapter 1, organoids are an increasingly popular platform for modelling human development and disease as well as drug testing. Organoids are also highly relevant in the field of personalised medicine. Throughout this project we focus on the use of colonic organoids for the investigation into the pathophysiology of IBD and monitor the response of existing and novel compounds aimed at the treatment of IBD. In this Chapter we demonstrate the process of the isolation and establishment of our patient-derived colonic organoid model. Once sufficient lines were established and expanded, the initial characterisation of the healthy and IBD-derived lines was performed and analysed, as will be described later. Our observations display substantial differences between healthy and IBD organoids derived from patient colonic tissue. These notable differences give crucial insight into the pathological basis for the development of IBD. This enhanced understanding of a disease that is very poorly understood and characterised can aid in the search for effective treatments and management options that can vastly improve the lives of the sufferers of this debilitating disease. This approach can be personalised to each individual patient where numerous therapeutic options can be tested for efficacy prior to being prescribed to the patient. This tactic can help prevent the patient from experiencing the many unpleasant and unnecessary side effects of the medications that would later prove ineffective. Here we have demonstrated how this method could be applied to personalised medicine by testing 5 commonly administered drugs in the treatment of IBD on 3 organoid lines.

3.1.2 Aims & Hypothesis

Aim: To isolate colonic epithelial biopsies for the purpose of generating primary colonic organoids.

Hypothesis: Multiple organoid lines will be generated from IBD patients and healthy individuals for comparison of any potential differences.

3.2 Results

3.2.1 Generation of Patient-Derived Colonic Organoids

Colonic organoids were generated from crypts via surgical resection and endoscopy procedures. For the successful establishment of sufficient organoids to expand into a patient line, between 4-6 crypt biopsies were required. To amplify the chances of viability, the isolated crypts were washed and stored in a balanced salt solution (HBSS) until prepared for culture. The crypts were sectioned into multiple fragments prior to being transitioned into Matrigel and decanted into a multi-well plate as drops. The crypts then develop into organoids over a period of several days before being passaged and continually expanded. Once established, we generated a biobank of 10 healthy lines, in addition to 3 UC and 3 Crohn's disease lines for future use and data comparisons. Additionally, we established 2 lines isolated from adenocarcinoma patients.

Upon embedding isolated crypts in culture, the crypts grow and expand to form spheroids. Within 48 hours the epithelium thickens. A few days later they fully develop into organoid structures. These structures become more complex when left for longer in culture, resulting in multiple crypt-like protrusions orientated outwards towards the surrounding Matrigel^{TM} complex. This displayed orientation demonstrates the interior of the organoid corresponding to the apical domain present in the gut lumen *in vivo* [145]. These crypt-like structures have been found to contain LGR5+ cells, responsible for continued proliferation and differentiation into all other intestinal cell types present *in vivo*. including colonocytes, goblet cells, Paneth cells, and enteroendocrine cells.

The process of epithelial renewal is continuous, as can be observed *in vivo*, the apoptotic cells are sloughed off into the lumen of the organoids. Here the cells collect and remain until the structures are manually dissociated in the passaging process [146]. These structures exhibit proliferation and multilineage differentiation that can continue these functions for years when cultured in the presence of GFs favouring Wnt & Notch Signals [146].

We noted that organoids generated from UC & Crohn's tissue developed and grow slower, perhaps due to a slower rate of epithelial renewal (data not shown). Conversely, those generated from adenocarcinoma grew very quickly and displayed a much lower degree of sensitivity in respect to the conditions in which they were being cultured. While healthy & IBD organoid lines required CHIR99021 to maintain intestinal stem cells in a self-renewing and undifferentiated state, adenocarcinoma lines showed no reliance of CHIR in the culture environment. This is due to the adenocarcinoma being able to produce its own wnt, thereby enabling it to thrive in the absence of exogenous input from the rest of the system. It has been reported that CHIR can even restrict the growth of adenocarcinoma organoids due to an overall excess of wnt being present [147]. This excess of wnt would result in the imbalance of the wnt gradient present in the intestinal stem cell niche.

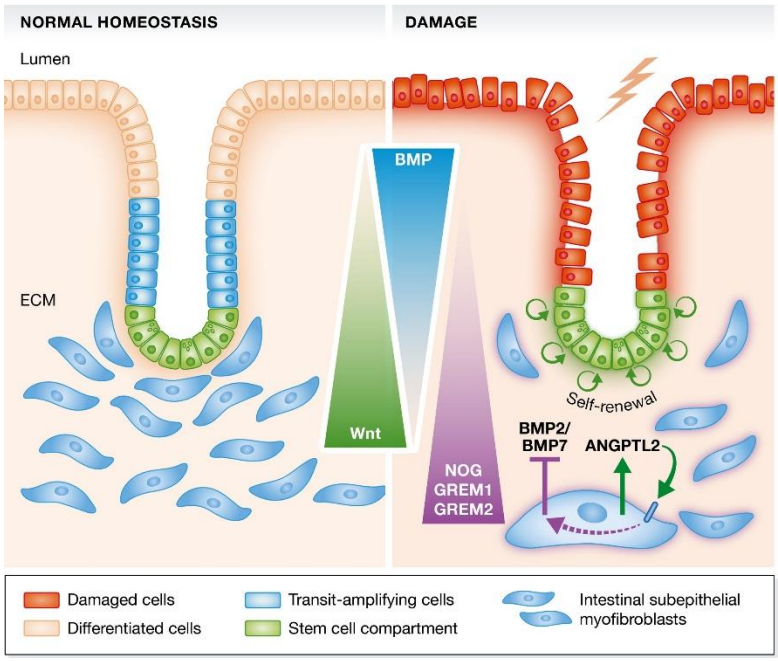

Figure 3.2: Balancing signals in the intestinal niche, [1].

3.2.1.1 Development of Healthy & IBD Organoid Lines from Biopsy to Establishment.

The below figures demonstrate the stages from biopsy to establishment of healthy & UC organoid lines. Crypts begin to form spheroids with a thin epithelium and simple round structure. This process typically occurs during the first 24 hours in culture. Over the course of several days, the spheroids then begin to expand, and the epithelium thickens. 48-72 hours later budding occurs, resembling the crypt-like structure observed *in vivo*. The lumen of the organoids begun to contain apoptotic cells due to regeneration of the epithelium. These remain in the lumen until they are released when the organoids are passaged (figure 3.3).

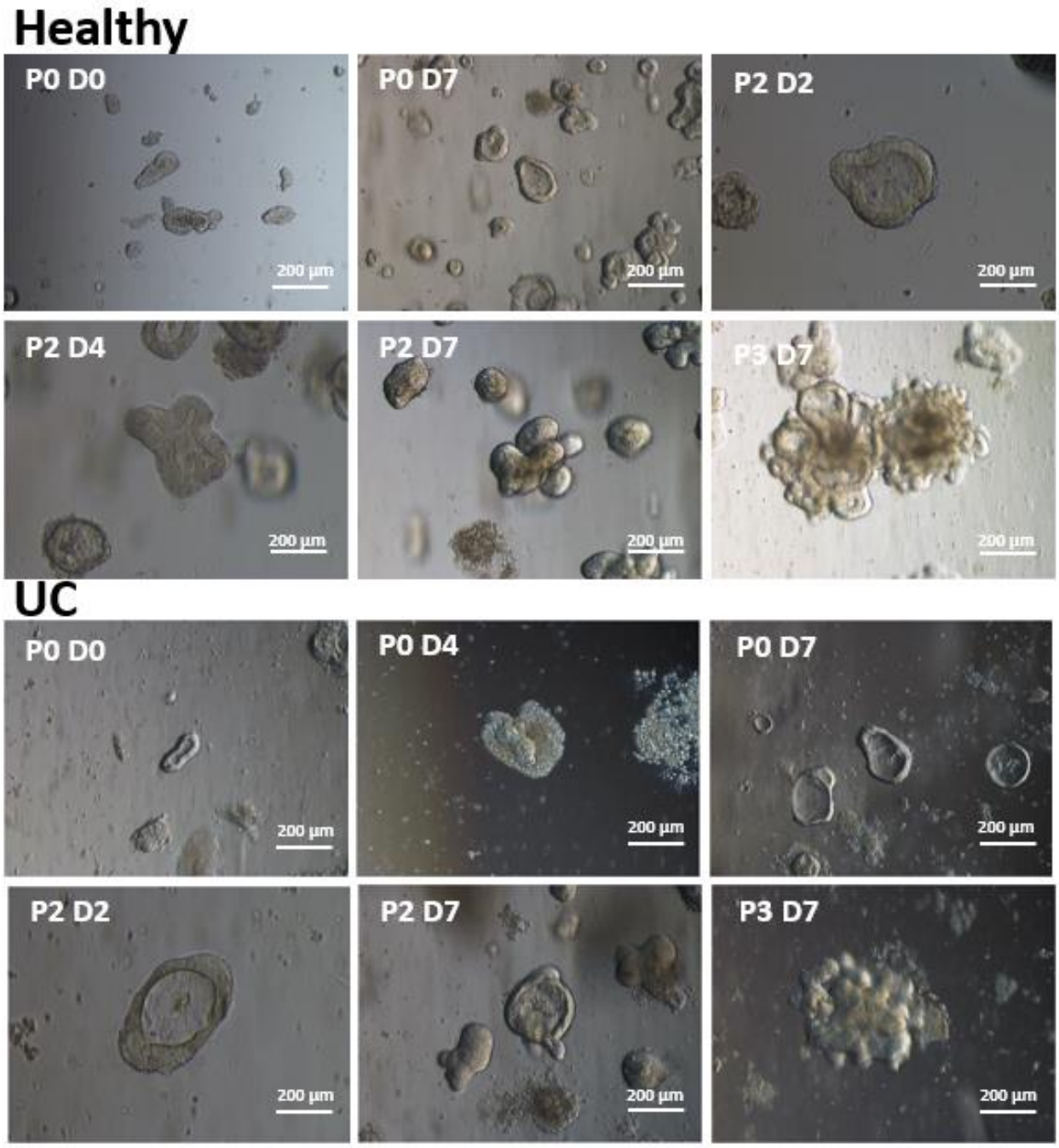

Figure 3.3: From Crypt Biopsy to Organoid: Step-by-Step of Organoid Development Following Washing & Embedding of Crypts into Matrigel™. The same process can be observed for healthy and UC-derived organoids alike.

Once the organoids had fully developed, after 7-10 days, they were passaged. During the passaging process, the organoids were manually dissociated to break each organoid to release the trapped apoptotic cells and to encourage expansion of the line. Following dissociation, each organoid is broken into approximately 2-3 fragments which then form individual organoid structures. This leads to expansion of the line over time. Due to this process and the slow growth rate of patient-derived colonic organoids, the expansion of the organoid cultures occurs at a much slower rate than that of monolayer cell lines.

3.2.1.2 Patient-Derived Colonic Epithelium Isolated Distal from Inflammation Increased Culture Success

We reported a significant discrepancy in the survivability between crypts isolated from healthy, IBD & adenocarcinoma colonic tissue. The establishment of healthy intestinal organoid lines from samples extracted via endoscopy demonstrated a high success rate. This can be observed in figure 3.4 displaying 83% of those samples received via endoscopy survived and thrived in 3D *in vitro* culture. Loss was defined by the appearance of necrosis in the tissue samples within 48 hours of plating. Organoid integrity and viability were assessed visually by brightfield microscopy; however other methods available include a trypan blue dye exclusion assay; ATP or LDH release detection and CellTox™ Green Assays to allow for a more accurate, less subjective approach.

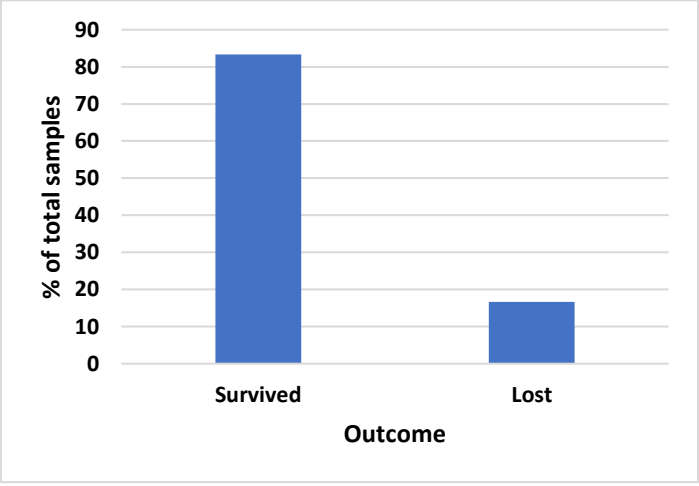

Figure 3.4: Success Rate of Long-Term Culture of Organoids Isolated from Healthy Tissue. N=14 (Biological replicates)

Conversely, tissue taken from areas of high inflammation in the UC colon showed very minimal survivability (figure 3.5), often unviable within an hour of extraction via endoscopy. Following the culture of healthy organoids from surgical resected tissue, as outlined in the materials & methods section, organoid models were generated from tissue isolated from patients with UC & Crohn's disease. Initially over 80% of IBD samples isolated from inflamed regions of the colon failed to survive the transition into 3D culture, with complete necrosis observed after 1-3 days. This hastened tissue necrosis could be as a result of the heightened state of inflammation.

While we observed loss of cell viability morphologically, with necrosis being very clear under a confocal microscope, further analysis could be performed using an LDH colorimetric assay or propidium iodide staining via flow cytometry.

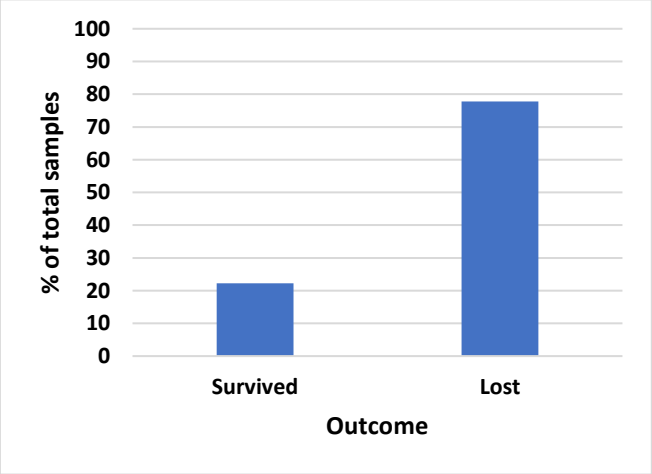

Figure 3.5 Success Rate of Long-Term Culture of Organoids Isolated from IBD tissue. N=27 (Biological replicates)

Different methods were attempted to improve crypt survival, including transferring crypts immediately to cold HBSS to slow degradation of the tissue. The tissue was transported from Queens Medical Centre to Biodiscovery Institute in the cold HBSS, helping maintain neutral pH and osmotic pressure on the sample as HBSS mimics the salinity of the human body. The time between sample extraction from the body and processing for culture was also reduced to improve chances. These changes did confer some improvement although the majority of samples received were still unviable. This was discussed between the lab and clinical teams where it was decided that future samples would be taken from a section more distal to the observable

inflammation within the patient's colon. This had a much more favourable effect on the rate of sample survival of UC patients' tissue, with this method of acquiring samples was shown to increase survivability of IBD tissue resections by 10%.

This is a successful but modest increase in tissue survival upon extraction and embedding into 3D culture (figure 3.6). Therefore, the genetic background of the numerous IBD patients that have donated tissue to this project confer effects on to the chances of survival even when the tissue is not visibly inflamed. Despite there being no visible inflammation, the minimal improvement in survival of samples suggests that LGR5+ stem cells are likely affected leading to failure of the crypts to grow and thrive in culture. This gives an important insight to the remaining, seemingly viable, gut tissue in IBD sufferers. The substantially muted success of tissue survival points to a very dominant genetic or epigenetic factor presenting a prominent and immediate difference between healthy and IBD colonic tissue prior to appearance of phenotypic changes.

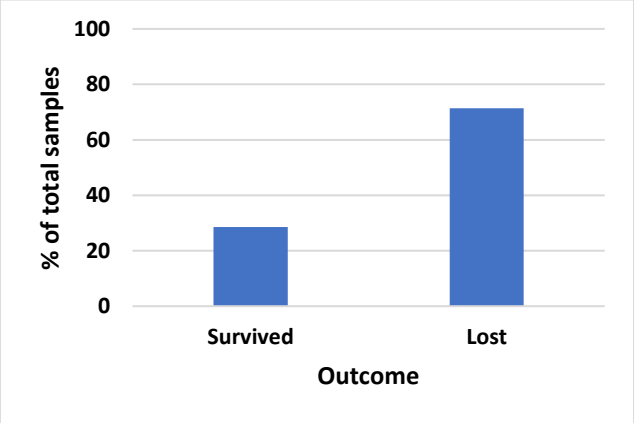

Figure 3.6. Success Rate of Inflammation-Adjacent Tissue in Culture. N=5 (Biological replicates)

Those samples that survived the transfer into 3D culture displayed differing rates of growth, and thus ability to establish into an ongoing organoid line. These differences depended on the condition of the patient, location sampled within the colon and current level of inflammation. Age appeared to exert little difference on crypt survival *ex vivo* (table 3.1).

Table 3.1: Patient Details at Time of Biopsy from first 3 successfully generated lines from healthy & UC samples.

Sample ID	Gender	Age At Time Of Biopsy	Diagnosis
COL1	F	76	No intestinal issues
COL2	M	71	No intestinal issues
COL3	M	53	No intestinal issues
MG015	M	24	Inactive UC
MG020	M	61	Inactive UC
MG022	M	36	Active UC

3.2.2 Transferring Patient-Derived Organoids From 3D to 2D Culture

3D culture offers many great benefits for intestinal organoid culture as it recapitulates *in vivo* tissue architecture contributing to increased maturity of intestinal cell types and is therefore a more favourable model for intestinal disease research. As this 3D culture environment more closely resembles *in vivo* physiology it is a more useful tool for understanding disease progression, drug discovery and personalised medicine. While 3D culture has greatly improved the reliability and impact of the in vitro study of the intestinal epithelium, this culture system still lacks features required to fully mimic the *in vivo* gastrointestinal environment. As a result of this, other methods have been investigated to support this 3D method. One of the most prominent methods utilised over the past few years has been transferring 3D organoids to a 2D environment with an air-liquid interface. A primary issue encountered in 3D culture during experimentation is the lack of convenient access to the lumen of the organoid. When drugs are tested using this model, on some occasions these therapies are preferentially tested on the luminal space as this is the location of *in vivo* exposure when the treatment is given to the patient via the oral route. Likewise, pathogenic interactions within the gut are required to be tested on the luminal membrane as this is the location of these interactions in their native environment. In an attempt to overcome some of these limitations, the 2D culture method of dissociated organoids has been established.

In this 2D culture method, Matrigel^{TM} is still required to aid in the formation of an adherent monolayer, as well as to act as a feeder layer for the cells (figure 3.7). The

Matrigel is coated to the surface of well inserts (Thermo Fisher Scientific, cat no. # 140620) which possess varying pore sizes to allow transportation of nutrients and drugs between the growth medium in the well and the cultured cells. The inserts utilised in our experiments had a pore size of 4µm and were added to the wells of a 48-well plate. Media was then added to the base well. This creates the air-liquid interface more reminiscent of the *in vivo* intestinal environment.

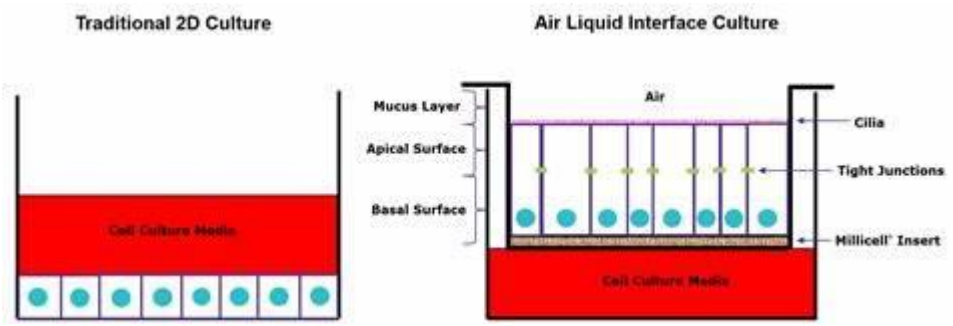

Figure 3.7: Comparison of 2D culture methods in 48-well plates.

Once plated onto this set-up, the basal surface of the cells then orientates to media below and the apical surface to the air. To effectively recapitulate the *in vivo* intestinal epithelium, a complete monolayer must be formed on the insert. We found during our experimentation that a large number of cells, isolated from a minimum of 6-8 wells, was required to form a monolayer (figure 3.8). If multiple conditions are required, this could require an entire 48-well plate of organoids. Due to the time taken to culture and expand this model, this method was neither efficient nor sustainable. Furthermore, we recorded a substantial amount of cell death, due to a lack of attachment upon seeding. This meant an even greater number of organoids were required for this process. Another significant drawback of 2D culturing of the intestinal epithelium as a monolayer is the inability to culture using this method for a prolonged period of time. This is due to the loss of ISCs and increased apoptosis that has been observed. Hence, each time 2D culture is required it is necessary to transfer organoids from 3D. It was therefore decided that compounds tested throughout the project would be tested on the basal surface of the organoids in 3D culture. This technique would still be representative of the conditions we are attempting to recapitulate since the

compounds being tested are produced by bacteria present in the colon. In IBD patients, the integrity of the colonic epithelium has been compromised, and hence, the basolateral membrane would also be exposed to these compounds *in vivo*, which has been suggested as one of the triggers for the pathogenesis of IBD.

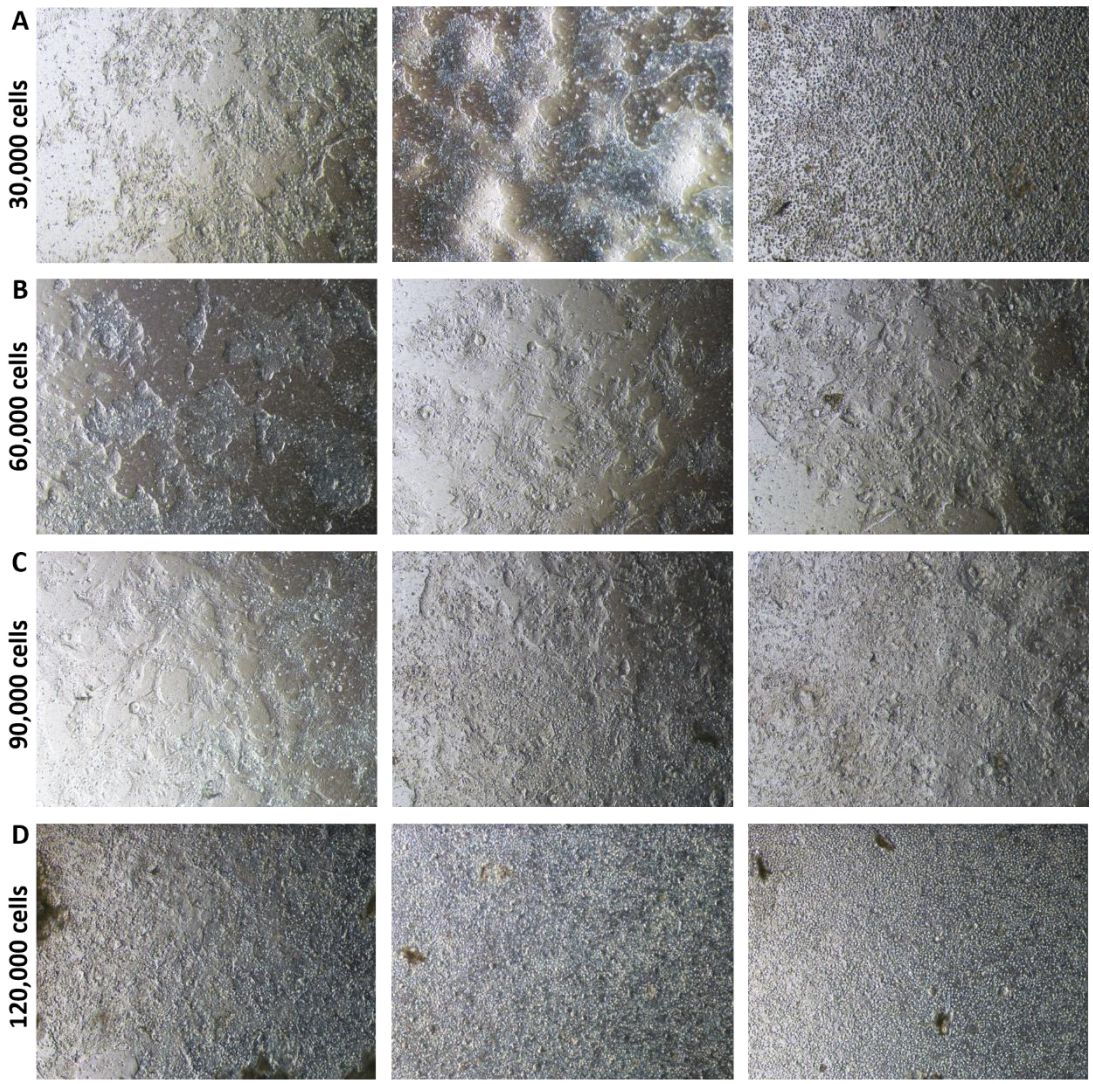

Figure 3.8: Cells from dissociated organoids were plated onto transwells coated with Matrigel™. (A) 30,000 cells plated initially attached to the 2D surface before spreading out. Prior to a monolayer being formed, cells began to die and detach. **(B)** 60,000 cells were plated onto transwells. Cells promptly attached to the surface, before proliferating and spreading out. Too few cells were plated to form a monolayer prior to senescence. **(C)** Over the course of 5 days, 90,000 cells successfully formed a monolayer on the surface of 2D transwells. **(D)** 120,000 cells initially attached to the 2D surface prior to spreading out. Before a monolayer could be formed, cells began to die and detach suggesting too many cells were plated. Imaged on Zeiss Axio light microscope at 10X magnification.

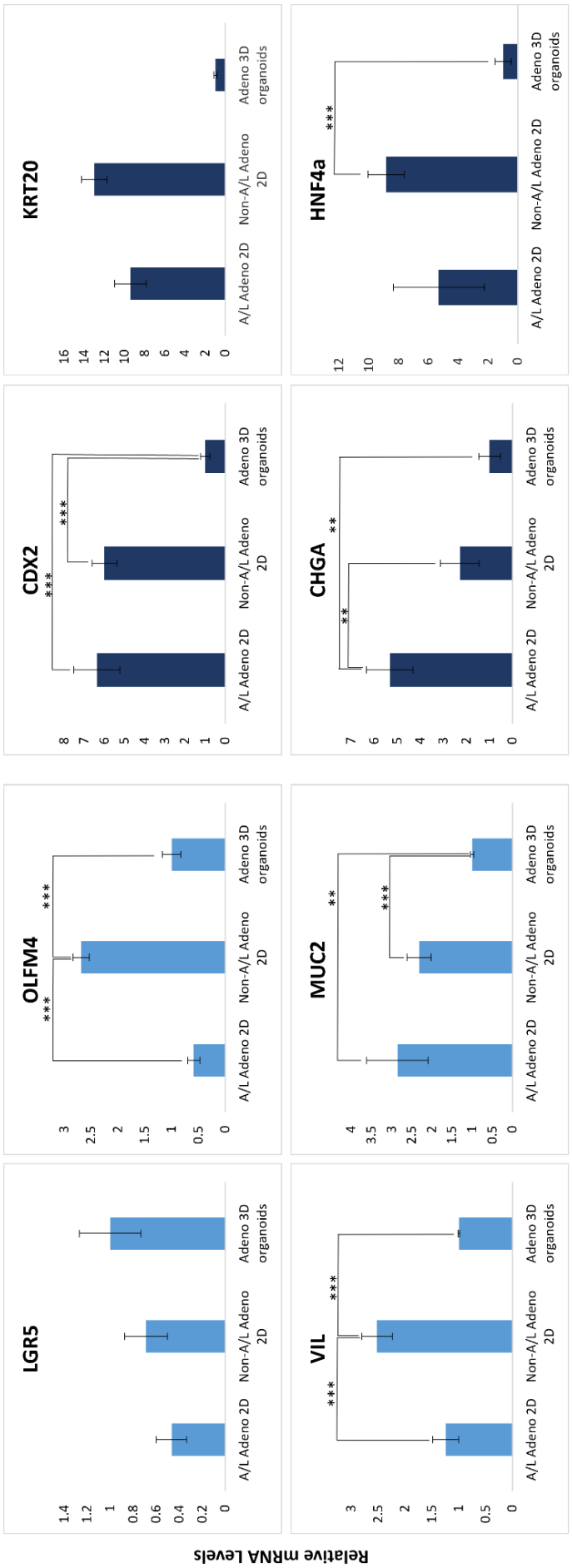

Figure 3.9: Transcriptional data demonstrating the effects of both 2D & 3D culture conditions on patient-derived colonic epithelial organoids. The most substantial differences observed across the panel were between 2D non-air-liquid and 3D culture conditions. Statistical analyses were performed by two-sided students t-test. Data are expressed as mean ± SD of each group. *P < .05; **P < .001; ***P < .0001. N=2 (Technical replicates)

As can be observed in the above graphs, intestinal stem cells are, as expected, negatively impacted following transfer to a 2D culture environment (figure 3.9). This is evidenced by the substantial drop in the reliable ISC marker, LGR5. The second marker tested for in this context was OLFM4. These results, while similar with regards to the drop in expression between 3D and 2C culture, this effect can only be found in the A/L interface condition, Conversely, an increase occurs in the non-A/L interface. As OLFM4 has also been proven to be a marker for inflammation [148], it is likely that this increase is indicative of a rise in inflammation in this platform. However, since no other markers of inflammation were examined, as this was not the aim of in this experiment, accurate conclusions cannot be drawn in this regard. Moreover, an increase in differentiated cell marker expression can clearly be noted across the board. This is expected due to the lack of stem cell niche structures in the 2D environment. This fact results in the inability of intestinal organoids, when cultured as a 2D monolayer, to continually regenerate as they can in the 3D environment.

3.2.3 Testing Response of Patient-Derived Organoids to Commonly Prescribed IBD Medications

Once our 3D culture system and healthy patient-derived colonic organoid lines were established and expanded sufficiently, we used the platform to test the efficacy of a range of medications used regularly in the treatment of IBD.

Upon testing 5 commonly used IBD medications in the presence of TNFα, it was evident that necrosis was still observed to a great extent in the azathioprine-treated condition. While the other drugs tested had some necrosis occur, however to a lesser extent (figure 3.10).

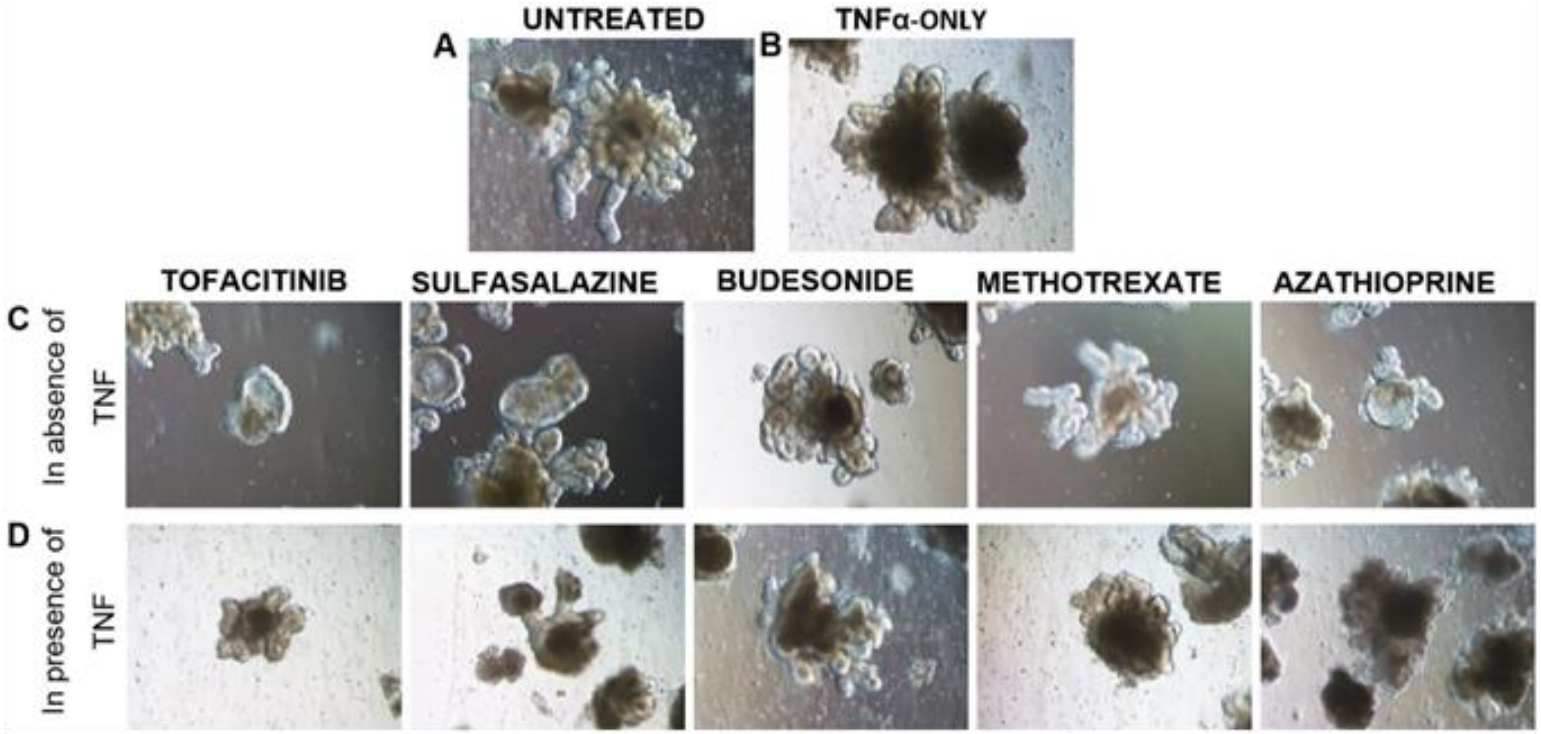

Figure 3.10: Morphology images of healthy organoids comparing the effects of several commonly used anti-inflammatory drugs with those untreated. (A) Untreated healthy organoid. **(B)** Treated with TNFα only. **(C)** Healthy organoids treated with 5 anti-inflammatory medications in the absence of TNFα. **(D)** Healthy organoids treated with 5 anti-inflammatory medications under inflamed conditions, in the presence of TNFα. Imaged on Zeiss Axio light microscope at 20X magnification.

CP Citrate 690550 (Tofacitinib), known to inhibit the JAK pathway, was the first to be tested on the model. It is commonly used to treat autoimmune diseases including rheumatoid arthritis and ulcerative colitis. As this therapy targets the family of JAKs, it can dampen immune cell function, thereby reducing the overactive inflammatory response that occurs in UC. Since this drug targets immune function in ulcerative colitis, a condition primarily affecting intestinal epithelium, testing the response on our model would reveal relevant data. However, as can be seen from the below graphs the effects of CP Citrate on this organoid model demonstrated this compound having undesirable effects on the colonic epithelium in conjunction with TNFα. In fact, the effects of TNFα seem to be worsened by the addition of CP Citrate as are shown by the exaggerated increase in IL8 expression and reduction in MUC2. If these combined effects are translated to the protein level this could cause substantial adverse effects on the epithelium. The less mucin produced by the goblet cells the less protective mechanisms in place to counteract the effects of the increased inflammatory response (figure 3.11).

Sulfasalazine was also on the panel of drugs tested on our epithelial-based platform. This treatment, however, is often used to relieve symptoms in Crohn's patients. Its mode of action is suspected to lie in its alteration of metabolic breakdown of 5-aminosalicyclic acid (5-ASA) in the colon. While it has been stated to also be used as the treatment for ulcerative colitis, it has been reported to have a higher affinity for connective tissue. This may mean that Sulfasalazine has a greater therapeutic effect in Crohn's disease as a disease that affects the connective tissue to a greater extent. The true effects of Sulfasalazine *in vivo* may not be transferable to an in vitro model due to the lack of connective tissue present to act upon. Furthermore, this platform is unable to metabolise the parent drug into 5-ASA, therefore it is likely that the desired effects of the drug were not realised in this experiment. This can be seen in the results below which demonstrate a muted response. A more exaggerated response to these drugs may be observed in our IBD patient-derived model, whereas in this experiment the drugs were tested on our healthy lines as these had been established primarily (figure 3.11).

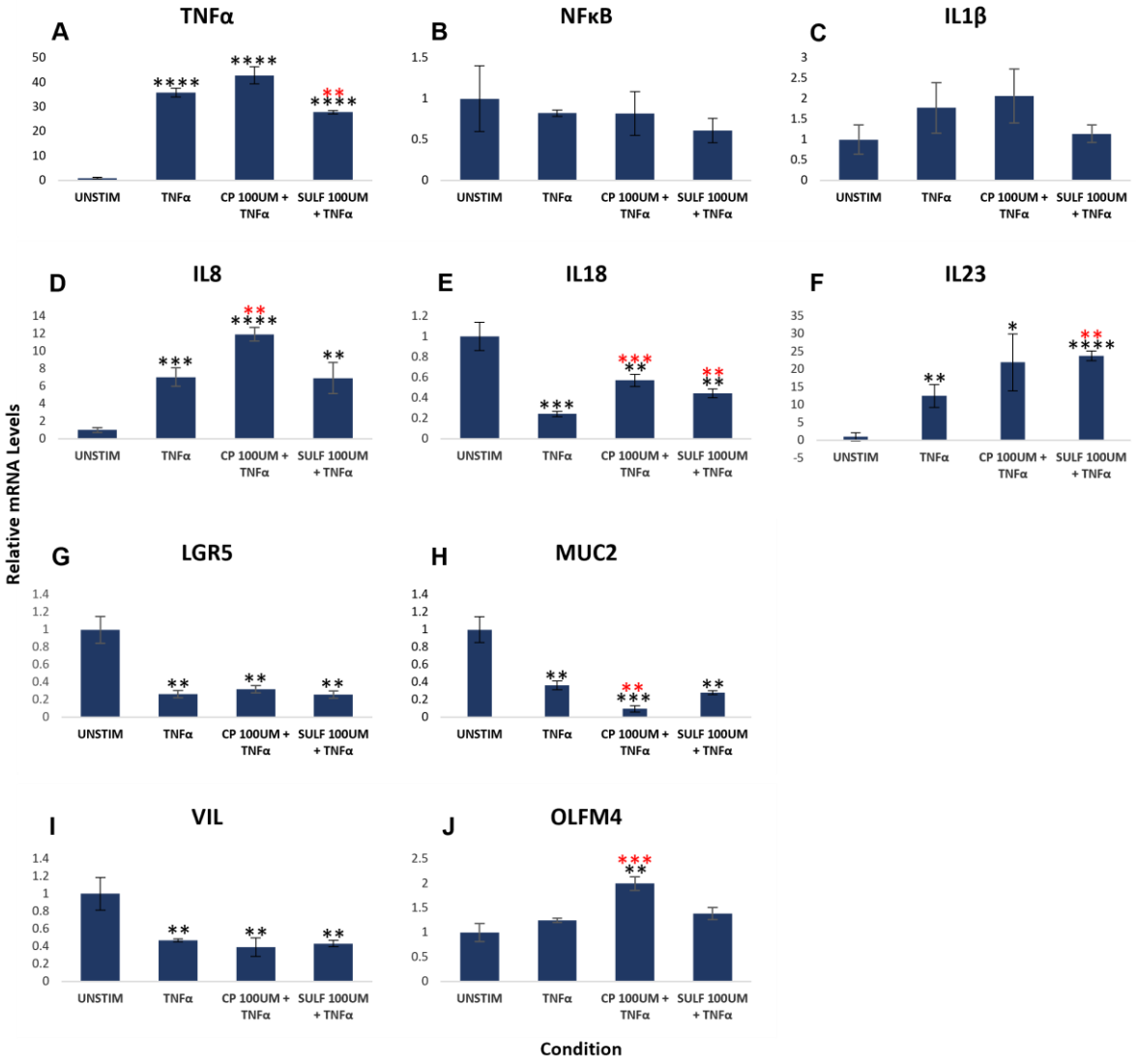

Figure 3.11: Transcriptional data depicting the response of healthy patient-derived colonic organoids to treatment with clinical IBD medications; CP Citrate (100 μM) & Sulfasalazine (100 μM) following exposure to TNFα (40 ng/ml). A-F Effects of CP Citrate & Sulfasalazine on pro-inflammatory marker expression after 48-hour treatment. G-J Neither drug successfully resolved the negative impact upon intestinal gene expression. 4 wells were collated from each treatment condition into individual Eppendorf tubes. The RNA concentration was then assessed prior to qPCR sample preparation. Statistical analyses were performed by two-sided students t-test. Data are expressed as mean ± SD of each group. *P < .05; **P < .001; ***P < .0001. N=1 (Technical replicates)

Budesonide is a glucocorticosteroid drug, typically used for the long-term management of autoimmune disorders such as asthma and chronic obstructive pulmonary disease (COPD). It has also recently been utilised as a treatment for mild to moderate Crohn's disease and ulcerative colitis. For the treatment of these intestinal inflammatory disorders, Budesonide is typically administered as an extended-release capsule, or as a rectal foam for distal colitis [149]. There are various effects of corticosteroids in the reduction of inflammation. A notable effect they exert at a systemic level is to decrease vasodilation and reduce permeability of capillaries. This decreases leukocyte migration to the sites of inflammation. As you can see from the results, budesonide causes a minor decrease in the pro-inflammatory cytokines, TNFα, IL8 & IL23 (figure 3.12). This could have an important impact *in vivo* as it would indeed decrease vasodilation as stated in what is understood of the mode of action. A decrease in vasodilation would prevent the migration of inflammatory cells involved in the progression of IBD including Th2 cells. While these effects weren't statistically significant, we could expect to see an exaggerated effect in one of our IBD lines due to the differential response we have noted between healthy and IBD lines, both in the absence and presence of inflammatory triggers.

Methotrexate is typically used for the treatment of a variety of cancers, in addition to severe psoriasis and rheumatoid arthritis. Its mode of action focusses on inhibition of multiple enzymes involved in nucleotide synthesis. This action leads to both prevention of cell division which therefore inhibits tumour growth and suppression of inflammation, useful in the treatment of autoimmune disorders. Due to the severity of methotrexate's toxicity and subsequent side effects including mouth sores, seizures and skin blistering, it is often only used once all first line treatments have failed. This experiment yielded some interesting results with Methotrexate exhibiting the most overall positive and significant results. A reduction in the critical pro-inflammatory cytokines, TNFα and IL23 would substantially reduce overall inflammation in the gut. Furthermore, there was no recorded reduction in the ISC marker, LGR5, conversely to what was observed following Azathioprine treatment. We also observed an increase in MUC2 expression following the deleterious effects exhibited by TNFα. TNFα alone inhibited MUC2 expression by 60% which would cause significant damage to the *in vivo* epithelium as MUC2 is a major component of Mucin (figure 3.12). Mucin is a vital factor in the first line defence against both pathogenic and native bacteria in the gastrointestinal tract.

In the colon, a thick mucin layer is paramount to protect from the high concentration of bacteria translocating across the epithelium resulting in a sudden increase in surrounding inflammation, potentially leading to systemic infection and sepsis. It appears that Methotrexate is the only drug tested that reverses the detrimental effect of TNFα. This is an important finding that helps us learn more of the beneficial impact of Methotrexate on Crohn's & UC patients.

The final drug tested was Azathioprine, a prodrug of 6-mercaptopurine. It functions through suppression of Rac1 target gene activation. Rac1 target genes include mitogen-activated protein kinase kinase (MEK) and NF-κB. This results in apoptotic stimulation of T cells and hence a reduction in downstream inflammation. As can be seen in the morphological images above, Azathioprine causes noteworthy substantial damage to the epithelium. This data is supported by the transcriptomic data below. While treatment appears to cause a reduction in IL23 expression following the initial increase from TNFα exposure, the finding is not significant. The visible epithelial damage, evident in figure 3.10, is supported by the substantial reduction in LGR5 expression. It is clear this reduction is not as a result of the TNFα alone, as a further drop was observed in the Azathioprine-treated + TNFα condition, that was measured as statistically significant (figure 3.12).

However, one positive effect that Azathioprine exhibits is a reduction in TNFα, that has found to be significant. As TNFα is a prominent cytokine in various critical pro-inflammatory pathways, a reduction in this cytokine *in vivo* could have widespread effects, reducing overall inflammation and therefore improving the patient's condition. It is yet unclear whether this beneficial effect of Azathioprine treatment would counteract the numerous adverse effects we observe from the data. In addition, Azathioprine reversed the effects on OLFM4 expression to below control. OLFM4 is another marker of ISC's and has been found to be highly expressed in crypt base columnar cells in both the human small intestine and colon [150]. Therefore, decreasing the expression of this marker may seem detrimental to the health and integrity of the epithelium. However, OLFM4 has also been closely linked with the early stages of neoplastic formation in this subset of cells and thus the development of CRC [151]. High levels of OLFM4 have also been found in *ex vivo* colonic biopsies from patients with UC [151]. In these biopsies, it was also found that while LGR5 expression would fall in

response to an inflammatory stimulus, OLFM4 would rise accordingly [151]. This corroborates our data, indicating that while TNFα would trigger an inflammatory response observed in a chronic inflammatory condition such as UC, Azathioprine reverses this effect. This reversal could prevent the development of CRC in UC patients, who's risk is significantly increased.

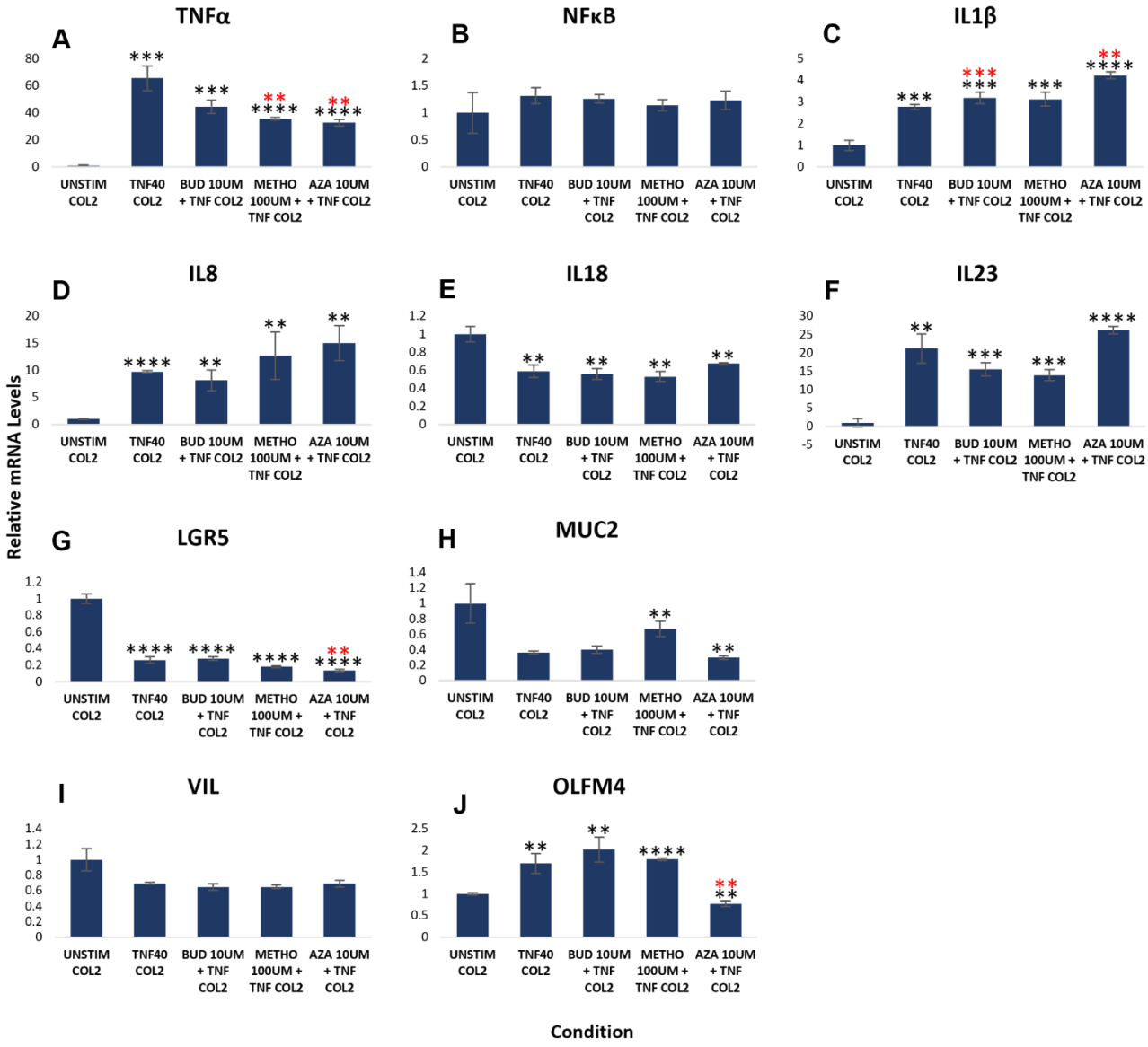

Figure 3.12: Transcriptional data depicting the response of healthy patient-derived colonic organoids to treatment with clinical IBD medications; Budesonide (10 μM), Methotrexate (100 μM) & Azathioprine (10 μM) following exposure to TNFα (40 ng/ml). A-F Inconsistent effects were observed between Budesonide, Methotrexate & Azathioprine on pro-inflammatory marker expression after 48-hour treatment. **G-J** IBD medications tested had mixed effects upon intestinal gene expression. Cell material collected from 4 wells per condition. Statistical analyses were performed by two-sided students t-test. Data are expressed as mean ± SD of each group. N=1 (Technical replicates) *P < .05; **P < .001; ***P < .0001.

3.2.4 Testing Response of Patient-Derived Colonic Organoids to Bacterial Metabolites

Butyrate & its derivate 3-hydroxybutyrate have notable substantial anti-inflammatory effects on the colonic epithelium, with the expression of multiple genetic markers being significantly altered following treatment. Conditions were tested in the presence and absence of TNFα. As TNFα is a key pro-inflammatory mediator that is also present in autoimmune diseases, such as UC, it is essential to determine the effects of SCFAs in an inflammatory environment. NFκB rose suddenly upon exposure to TNFα alone (Figure 3.13A). This initial increase dropped substantially to 50% below control with butyrate treatment. While a drop in expression was observed with 3HB treatment, this drop was muted and hence not statistically significant. The combination of both butyrate and 3HB produced similar results to butyrate only which points to butyrate being the active ingredient in this mix.

As can be seen in figure 3.13B, TNFα triggered a considerable reaction on the expression of IL8. Both butyrate and 3HB alone did not trigger any change to IL8 expression. In conjunction with TNFα, butyrate reduced IL8 gene expression with a greater than 50% reduction which would drastically reduce the abundant inflammation triggered by TNFα. It's also clear that it's derivative 3HB, conversely, has no positive effect on this marker.

The IL18 expression profile appears to be atypical in comparison to the other inflammatory marker profiles (Figure 3.13C). As is evident in this figure, TNFα shows no effect, while butyrate alone triggered a three-fold increase.

As with IL8, IL23 expression also displayed favourable effects to butyrate treatment (Figure 3.13D). Following a 25-fold increase triggered by TNFα, the most substantial effect observed on any of the markers thus far, the addition of butyrate in conjunction with TNF yielded very promising results. Under these conditions, IL23 expression had dropped from 25-fold to 2-fold above control. This is a substantial effect that further demonstrates the efficacy of butyrate as an anti-inflammatory treatment option.

Furthermore, butyrate exhibited effects upon the colonic epithelium. The markers measured in this instance were the stem cell marker, LGR5; goblet cell marker, MUC2

& cytoskeletal marker Villin. The impact of butyrate upon LGR5 was surprisingly negative in this experiment with the result being a greater reduction in expression than elicited by TNFα itself (Figure 3.13E). This reduction lowered LGR5 expression by 80% below control. Incidentally, 3HB had the same effects to a similar extent. Interestingly, when butyrate is combined with TNFα, the impact on the stem cell niche is significantly less severe. Intriguingly, the combination of TNFα with 3HB halted the detrimental effects on the ISCs. The results on OLFM4, another marker of ISCs, are identical, thereby confirming that the effects seen are a genuine effect on the ISCs themselves (Figure 3.13F). In addition to reducing inflammation, this suggests that the SCFAs tested here are effective in protecting the regenerative capacity of the colonic epithelium, when in a pro-inflammatory environment.

Villin is an important marker in determining the condition of the intestinal epithelium. Here we found no detrimental effects exhibited by neither butyrate nor 3HB (Figure 3.13G). This is an important finding to affirm the possibility of using SCFAs for the treatment of UC. MUC2 displayed similar positive results, ensuring protection of the mucus layer (Figure 3.13H).

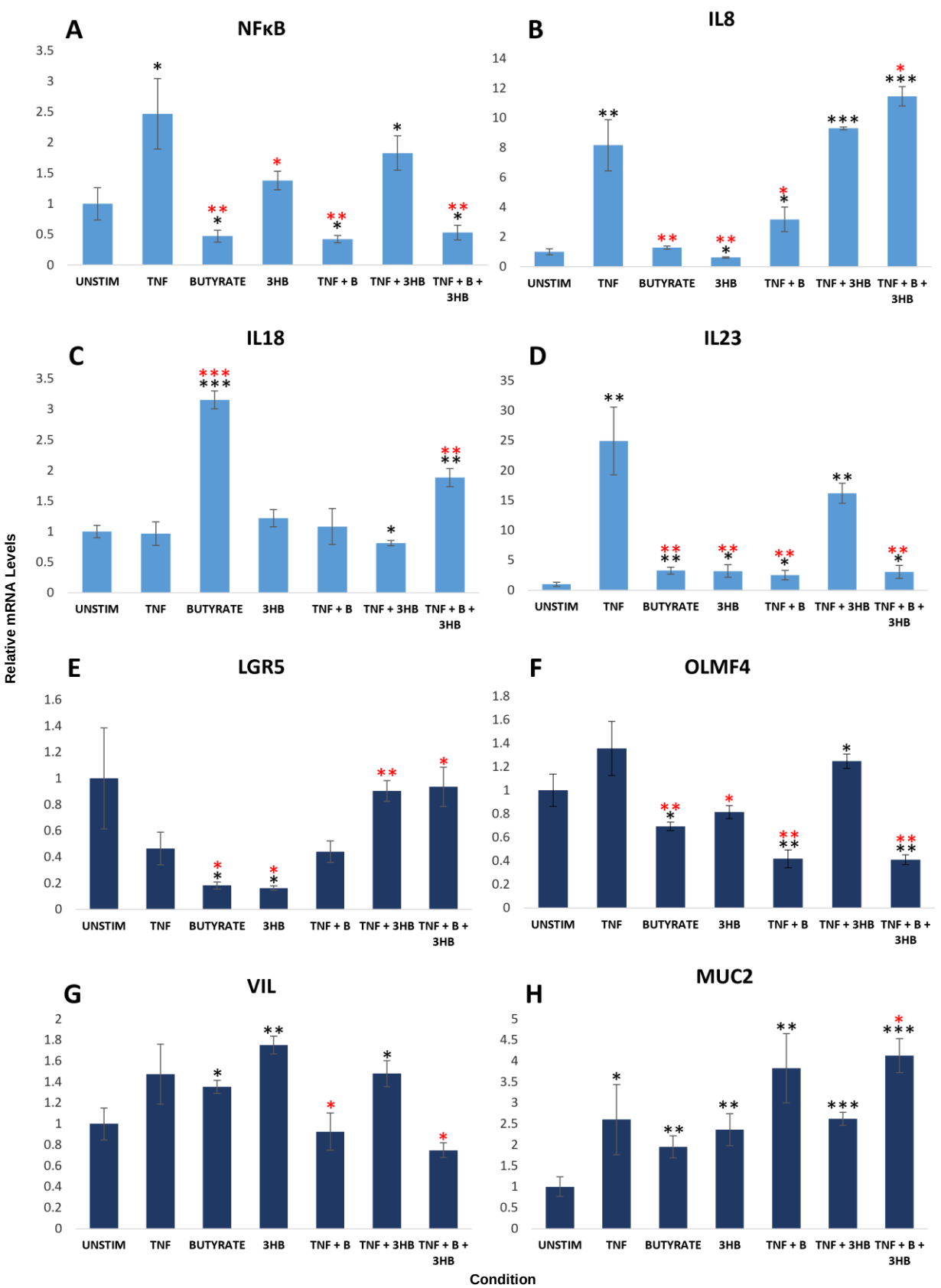

Figure 3.13: Healthy Colonic Organoids were treated with short chain fatty acid (SCFA), butyrate (1 mM), and it's derivative 3-hydroxybutyrate (3HB) (1mM) over a period of 48 hours in the presence of absence of TNFα (40 ng/ml). A-D Butyrate appeared to have a greater anti-inflammatory effect as made evident by the response of pro-inflammatory markers; NFκB, IL8 and IL18 and IL23. **E-H** Butyrate and 3HB appear to have a less consistent effect directly upon the epithelium itself. Statistical analyses were performed by two-sided students t-test. Data are expressed as mean ± SD of each group. *P < .05; **P < .001; ***P < .0001. N=2 (Technical replicates)

3.2.5 Banking of Patient-Derived Colonic Organoid Lines

Our established patient-derived colonic organoid platform was initially stored long-term in liquid nitrogen. Over the course of the project each line has been banked for future use. This banking process involved multiple washing steps to remove any residual MatrigelTM that could interfere with the freezing of the organoids. For the first year of the project, KSR media was used as a freezing medium for all organoid lines. To prepare this media, 10% DMSO was added to defined Knock-out Serum Replacement (KSR) solution. DMSO is used as a cytoprotectant to lower the freezing point of the medium thereby protecting the cells. This process, in the absence of a cytoprotectant, can be lethal to the cells due to the formation of crystals, leading to irreparable cell damage and subsequent death. Once this solution was prepared the washed and pelleted organoids were resuspended thoroughly in the KSR+DMSO solution and aliquoted into a cryovial. The vial was then transferred to a Mr. Frosty freezing container (Thermo Fisher Scientific, # 5100-0001) before being stored at -80^{o}C overnight. The use of the Mr. Frosty further aids in the gradual cooling process at a rate of -1°C/minute. After overnight storage at -80^{o}C, the vials could then be transferred into long-term storage in a liquid nitrogen dewer.

After the first year of the project, the lab group changed freezing medium to Foetal Bovine Serum (FBS) (Thermo Fisher Scientific, #10437-028). This was prepared in the same way as the previous KSR medium. FBS is a more enriched medium that improves the chances of cell survival during long-term storage.

There was a high percentage of survival for organoids frozen in the KSR media in this first year after having been stored for a short period of time. However, we have observed a lower survival rate of organoids in the latter stages of the project with 25% of those thawed surviving past the first 48 hours of thawing into continuous culture. There are various reasons that this could have occurred including fluctuations in the temperature of the liquid nitrogen dewers over time. The vials had changed dewers multiple times prior to issues in the thawing process being encountered. Other factors that have varied in this time include a decrease in the size of the cryovials for storage from 1.7 ml to 0.7 ml in addition to the freezing medium used. These latter factors are

unlikely to have caused an issue in the wellbeing of the organoids during long-term storage however it is worth noting to determine the cause of any future issues.

3.2.6 Comparison of Dissociation Methods

In the initial stages of organoid model establishment, multiple methods of dissociation were trialled during the passaging and expansion of each of the lines. Initially, the organoids were incubated for 5 minutes in TrypLE™ Select Enzyme (Gibco™ 12563029) to cleave the peptide bonds present between the individual cells comprising the organoid complex. After this incubation, the organoids were gently agitated to ensure fragmentation prior to removal of the TrypLE™ and subsequent washes. The results of this were effective in dissociating the organoid. However, incubating organoids for the recommended time in TrypLE™ led to a significant degree on fragmentation, with some being disintegrated into single cells. The very small fragments produced by this enzymatic dissociation method would often fail to thrive after passage, increasing the amount of cell death. This finding is likely due to the lack of LGR5+ ISCs remaining in the smaller fragments, halting the ability of these fragments to survive for more than a few days prior to cell renewal occurring. As the differentiated cells perish in the renewal process there are no ISCs present to replace those that are removed.

Once the increased amount of cell death was noted, an alternative method of dissociation was attempted. This involved resuspension of the organoid pellet in 1ml HBSS and manual dissociation with a P200 pipette. The organoids were first aspirated up into the tip and ejected against the bottom of the 15 ml falcon tube. This shear force was sufficient to fragment the larger organoids into 2-3 pieces. Each of these larger pieces is more likely to possess at least one ISC allowing for regeneration of the organoid. We observed this to be the case, with the frequency of cell death much lower after alternating to this method of dissociation during passaging. Therefore, manual dissociation has been the method consistently used for the duration of the project.

3.3 Discussion

In this chapter, I have described our method for the establishment and banking of patient-derived colonic epithelial organoids. The process of acquiring the colonic crypts has been explained and each stage leading to the generation of mature organoids has been described.

3.3.1 Current Disease Models

Immortalized cells and animal models have delivered important but limited insight into the mechanisms that initiate and propagate these diseases. Human-specific models of intestinal development and disease are more relevant and representative when investigating the mechanisms involved in the pathogenesis of IBD, as these can more closely recapitulate the structure and function of the human gut in vitro. Advances in pluripotent stem cells and primary tissue culture techniques have made it possible to culture intestinal epithelial cells in three dimensions, such cells will self-assemble to form ‘intestinal organoids'. These organoids allow for new, human-specific models that can be used to gain insight into IBD and potentially deliver new and more effective therapies [2].

Colonic organoids, also referred to as ‘miniguts’, have become increasingly popular for use in the investigation of various intestinal diseases in addition to furthering our understanding of GI epithelial development and function. This system is suitable for developmental research due to the focussed platform it provides with the absence of extraneous variables such as the surrounding microbiome. This enables a more directed approach which offers a clearer picture of the events that occur during healthy development and ongoing functioning of the GI tract. The microbiome has been suspected to play an extensive role in the healthy development and functioning of the intestinal tract. Intestinal organoids can also be used to model these interactions and further understand the necessity of the microbiome for normal homeostasis and how dysbiosis can lead to substantial damage to the epithelium and connecting tissues as well as the patient’s overall health. To study this, bacteria can be added directly to the model and the subsequent effects observed, or alternatively, specific compounds

isolated from commensal and pathogenic bacteria can be added to determine a more exact cause for these observations.

A further benefit of utilising ‘miniguts’ in developmental and disease research is the ability to link findings to the genetic background of the donor. This is of increased importance in IBD due to the vast array of genes associated with the onset of this disease, with 163 loci suggested to contribute to susceptibility. Many of these genes are not fully understood therefore patient-derived organoids offer a chance to further understand the function these genes play in IBD, as well as the interplay between them. The differences between patient presentations and severity of disease can be further understood by assessing and comparing organoids donated by a variety of patients.

The comparison of morphology, structure, growth patterns and response to drug testing can provide insight into the differential features and responses that are essential to enhance our understanding into the characteristics of diseased tissue in different environments. This could then be compared to tissue isolated from visibly healthy colonic epithelium in patients without inflammatory disease. Our 3D patient-derived colonic organoid model is able to highlight some of these characteristics and differences and hence further investigate the root causes of these differences as well as methods to target them for the benefit of IBD sufferers. This model effectively recapitulates *in vivo* functionality and structural organisation and possession of all intestinal epithelial cell types. This accurate model therefore preserves the whole genetic, transcriptomic and proteomic profile of the patient’s tissue even after long-term culture. This is of great importance to enable the data acquired from this research to yield reliable, relevant and translatable findings on a broad, as well as specific, case.

3.3.2 Characterisation of Patient-Derived Colonic Organoids

In this chapter, you will find evidence of the generation of these patient-derived colonoids from 9 healthy donors in addition to 4 Crohn’s & 3 UC patients. The process is outlined from retrieval of 5-6 crypts to embedding into 3D Matrigel™ domes and subsequent expansion. This method is in contrast to the alternative way of 3D colonic organoid generation. This approach utilises iPSCs generated from patient skin

fibroblasts which undergo retroviral reprogramming in vitro. This method of 'minigut' generation is more time-consuming to obtain as the differentiation protocol can take several weeks until an established organoid culture is obtained. It has also been found that 'miniguts' developed via this method can be maintained in culture for a limited number of passages in contrast to patient-derived colonic organoids, which have been found to be passaged and maintained in culture for many years without genotypic changes observed [152]. Furthermore, they have been found to possess a more immature, foetal phenotype, that, while being applicable in the research of gut development, is detrimental to the validity of adult chronic disease research such as IBD [152]. Maturity of iPSC-derived organoids can be improved by transplantation into immunocompromised mice. This evidently further lengthens the process of obtaining mature organoids and requires use of animal models which should be avoided at all costs as our research follows the 3R's principal. Hence, use of patient-derived organoid models bypasses these additional steps and complexity in the generation of a relevant and applicable platform for the study of IBD.

3.3.3 Transferring Patient-Derived Organoids From 3D to 2D Culture

Multiple groups have preferred to use the complex and well differentiated model of 3D intestinal organoids while attempting to mimic the transfusion of nutrients and compounds via an air-liquid interface. A further advantage to this method is improved access to the apical membrane for the purpose of host-pathogen interactions. Initially, the 3D structures must be lysed into single cells to be able to form a complete, intact monolayer on the transwell surface. Once added to the transwell pre-coated in MatrigelTM, the single cells reorientate with the apical surface orientated to the air and the basolateral surface towards the liquid interface (i.e., growth medium). This self-orientation means a range of compounds and pathogens that would typically be exposed to the apical intestinal membrane can easily be administered to the desired location, negating the need for microinjection which proves to be a time-consuming and intricate process.

Here, we look at the major intestinal markers of regeneration as well as differentiation. The results from this study display the favourable environment for the LGR5+ stem

cell niche in the 3D environment when compared to 2D culture. This is as expected as outlined in the previous section. MUC2 expression was also lower in 3D conditions. This finding alone is ambiguous due to an increase in this key mucin constituent being both beneficial in certain situations, such as to enhance the protective effects during periods of infection. Conversely, this increase in 2D culture could be representative of a strain put upon the epithelial cells following complete dissociation and removal from their natural structure. The same conclusions can also be drawn from the villin results, which demonstrate no change in expression between 3D and 2D A/L interface conditions, while being doubled in non-A/L. This doubling is suggestive of a substantial boost in epithelial differentiation. Coupled with the reduction in LGR5+ in like conditions, this further substantiates this finding. This is beneficial if interests lie only in the response of the differentiated adult epithelium to future experimental conditions, whereas it is much less relevant if a more representative picture of the regenerative epithelium is required. An enrichment for differentiation in this 2D system is further supported by the 6-fold increase observed in CDX2 expression: a nuclear marker for differentiated adult intestinal epithelial cells. Findings that are further validated by the expression patterns of HNF4α and KRT20.

As touched upon previously in this report there are several disadvantages to transferring organoids from 3D to 2D culture. One of these issues being the inability to maintain this 2D culture monolayer while avoiding stem cell loss and subsequent rapid apoptosis. Stem cell loss occurs due to the lack of the intestinal crypt structures within the 2D environment. This crypt structure ensures the correct Noggin and Wnt gradient to control the maintenance and gradual differentiation of LGR5+ stem cells. Therefore, the process of transfer from 3D to 2D is required each time an experiment is conducted. It was therefore decided against in this case due to the drawbacks of this system and its time-consuming nature in a project where time is limited.

3.3.4 Testing Response of Patient-Derived Organoids to Commonly Prescribed IBD Medications

The 3D culture method was used in our next experimental investigation testing current clinically relevant IBD medications that are widely prescribed to patients. Colonic

organoids were treated with 5 major medications in the presence and absence of TNFα.

The results as shown in this chapter, demonstrate varied responses on this model which is very much expected as each of the drugs tested all have different mechanisms of action. This isolated platform has given insight into the effects the drugs play directly on the epithelium and less so in a systemic capacity. For example, Methotrexate exhibited the most profound effect on our model as it typically acts by inhibition of enzymes in the process of nucleotide synthesis. This evidently has a strong effect that we measured on our *ex vivo* colonic epithelial cell platform.

Conversely, Sulfasalazine has very limited observable effects on this platform which could be due to the nature of action being on a more systemic level. Interestingly, Azathioprine has a significant detrimental effect on this epithelial model which is an important observation that could inform clinical decisions for IBD patients.

A study by Khare et al has reported the response of T-84 cells and primary human colon epithelial cells HCEC-1CT cells to azathioprine, confirming our cultures to be an appropriate platform for the testing of this drug. However, differences were found between the epithelial response in the study by Khare and the results observed in this experiment. Khare et al reports a decrease in paracellular permeability via the rearrangement of various junctional proteins including E-cadherin [153]. Interestingly, this group further reported the inhibitor effect of azathioprine on cell proliferation, putting a limitation on wound healing. The proposed mechanism resulting in this effect is the inhibition of Rho-GTPases and DNA synthesis in S phase (via suppression of the RR1 enzyme and stabilisation of cyclin D1) [153]. This halting of cell proliferation would undoubtedly result in the eventual necrosis of our primary colonic organoid model due to the inability to replenish lost cells following anoikis.

3.3.5 Testing Response of Patient-Derived Colonic Organoids to Bacterial Metabolites

As evidenced by our data, SCFAs produced by colonic bacteria in the microbiome confer protective effects against the pro-inflammatory response. This was

demonstrated by both the reduction of TNFα expression by butyrate and 3HB individually, while this finding was further enhanced with combined treatment.

As is further revealed by the results of this experiment, multiple central markers of inflammation dropped considerably, to a significant degree, following treatment with butyrate. The effects of 3HB were much more variable.

Butyrate, when added alone, had a striking effect upon IL18 expression, commencing a 3-fold increase. This finding is supported by Kalina et al following experimentation upon the HT-29 cell line[154]. While mixed results have been reported with respect to the role IL18 plays in inflammation, the contribution of IL18 in colon cancer is much less ambiguous. Loss of IL18 synthesis has been previously linked with colon adenocarcinoma when compared to healthy colon mucosa [155]. Hence, it's possible that this increase in IL18 expression is indicative of protection being conferred by butyrate against colitis-associated cancer development.

Another key aspect worth investigating was the impact of butyrate upon the epithelium itself. This has been indicated by the effects it has upon goblet cells and mucus production, demonstrated by MUC2 activity, as well as colonocytes and regenerative cells in the stem cell niche, VIL & LGR5, respectively. The overall effect observed, as outlined in the previous section shows no negative effect upon the differentiated epithelium. Conversely, detrimental effects were exerted on the stem cell niche when exposed to both butyrate & 3HB in isolation. On the contrary, when treated in conjunction with TNFα, these damaging effects were no longer evident. 3HB appeared to rectify the initial drop instigated by TNFα. This is a very intriguing and relevant result due to the nature of the condition. As patients will have profuse inflammation present in their lower GI tracts, the destructive effects presented by butyrate alone, are unlikely to occur when inflammation is prolific. These are promising findings that would require further exploration to determine the future of butyrate as a restorative compound in the treatment of UC.

A recent paper has corroborated this finding, demonstrating the butyrate metabolic pathway to be key in improving symptomatic UC. This group explored the hypothesis by inducing a colitis-like condition in mouse models using Dextran Sulphate Sodium (DSS). They found, via bioinformatic analysis, butyrate metabolism to be the

exclusively down-regulated pathway present in both adult and paediatric models of DSS-induced UC in mice. To further confirm this finding, Zhou et al reintroduced butyrate into the models, where they found it suppressed inflammation [156]. As of yet, this group has done no further work to carry up on this finding. Our study has added to this research by demonstrating that the reported effects of butyrate translate to human tissue and its effects during periods of inflammation. This is a promising area of investigation in which more research should be conducted into harnessing the advantageous impact of butyrate on the inflamed colon.

Furthermore, relevant data has been reported on the efficacy of butyrate inhibiting the development of colorectal cancer. Due to the relationship between UC and prevalence of CRC, this result is unsurprising. Interestingly, these effects are suspected to be as a result of butyrate's role as a histone deacetylase inhibitor (HDACi). However, the molecular mechanisms and pathways triggered by the treatment of butyrate in an inflammatory environment need to be more deeply explored to better facilitate the development of more highly effective therapeutics for both UC and CRC [157].

A recent clinical trial exploring the effects that butyrate exhibits upon the microbiota of IBD patients has been conducted to determine the underlying mechanism by which butyrate acts to alleviate symptoms in the individual. Researchers administered a microcapsule containing sodium butyrate, which facilitates slow release of its contents. Sodium butyrate was demonstrated to alter the composition of microbiota in IBD patients over a period of 12 weeks. In particular, an increase in the growth of SCFA-producing bacteria (Lachnospiraceae spp.) was revealed in UC patients [158]. Fecal calprotectin levels, used to measure the extent of intestinal inflammation, were decreased in line with these alterations to the microbiota [158]. Further investigations are next to be conducted into the clinical impact of this treatment.

In conclusion, the use of SCFAs in the treatment of UC is a very promising field to study further. The use of our model confirms the positive effects two of these compounds bestow upon the inflamed epithelium.

3.3.6 Conclusion

In conclusion, we have outlined the generation, characterisation and banking of patient-derived colonic organoids and methods to overcome common challenges arising during these stages. In addition to using this as a physiologically relevant platform for studying the fundamental effects of well-known commonly used IBD medications, the beneficial effects of SCFAs have been validated, further directing the future of IBD therapeutics. These studies gave insightful findings that help us further understand the interactions between the colonic epithelium and surrounding microbiome in addition to the efficacy of drug compounds.

Due to time constraints during this project, exacerbated by limited laboratory access and delays in reagent shipping throughout the Covid-19 pandemic, additional investigations including assessment of epithelial permeability were not able to be performed. If the project were to be continued this would be an important aspect to explore, both at the 3D organoid and 2D monolayer level. A FITC-dextran assay could be applied for this purpose, with the addition of 4 kDa FITC-dextran. The permeability could then be monitored using luminal absorption under a fluorescent microscope.

Further investigations to ensure all cell types present were, in fact, epithelial would also offer confirmation that the findings recorded here are solely due to the effects upon the epithelium, without the input of influence of mesenchymal cell types. Flow cytometry could be performed for this purpose to identify mesenchymal markers, including CD44, CD90, CD166 and fibroblast marker, FSP1. Moreover, qPCR could determine the possible presence of myofibroblast marker, α-SMA (typically upregulated in response to inflammation).

Furthermore, while changes to mucin production were determined indirectly by measurement of its primary constituent, MUC2, at a transcriptomic level, direct measurement of mucin production was not performed during this experimental time frame. One method that could have been employed in determining the thickness of mucin in the organoid lumen is histological analysis of snap frozen organoid tissue after treatment. Another would be the use of a mucin-specific ELISA which would offer more accurate quantification of histology alone. These methods were not utilised due to time constraints; however, this is an important next step for clarification in the

differential response we have observed here between healthy and UC organoid lines that would be highly relevant if the project was to continue.

Chapter 4

Investigating the effects of inflammatory mediators on Patient-Derived Colonic Organoids

4.1 Introduction

4.1.1 Inflammatory Pathways

4.1.1.1 TNFα Pathway

TNFα is a cytokine implicated in many inflammatory pathways and has been proven to be prolific in IBD [159]. Increased TNFα levels were found in serum, stool and mucosal biopsies taken from IBD patients [160-162]. However, the contributory factor to these persistently elevated TNFα levels was not known. This link between TNFα and IBD was further strengthened by demonstration of the efficacy of anti-TNF drugs, such as infliximab, in the treatment of Crohn's disease [163]. Once such a strong link was established, further research was performed into the role of TNFα in IBD. More recently, a TNFΔARE/ΔARE mouse model was generated to shed light onto this connection. This mouse model was produced to chronically overexpress TNFα specifically within the intestinal epithelium [164]. These mice were found to have increased mucosal, as well as, systemic, TNFα levels, in addition to severe chronic ileitis aggravated by increased neutrophil infiltration [164]. There was also a greater presence of $CD69^{(+)}$ and $CD4^{(+)}CD62L^{(-)}$ lymphocytes [164]. However, these effects were isolated to the intestine, demonstrating that the persistent presence of TNFα in the intestine is sufficient to induce severe Crohn's-like ileitis. While this demonstrates the importance of TNFα in intestinal disease development, ulcerative colitis is a complex disease that demonstrates other factors to be dysregulated that should also be taken into consideration. This is supported by the variable response of patients to anti-TNF medication in clinical practise, with 30% of IBD patients displaying no clinical benefit

[165]. These findings suggest that other factors contribute to UC pathogenesis and each patient has a different inflammatory phenotype that leads to disease development.

4.1.1.2Lipopolysaccharides

Therefore, we went then went on to explore another largely implicated factor in IBD pathogenesis and tested the response of our model. Lipopolysaccharides are a main constituent of Gram-negative bacterial membranes, and therefore inevitably have an impact upon the epithelium of the colon which contains approximately 10^{11}/ml of colonic content [166], with the proportion of these being Gram-negative bacteria varying between individuals. This proportion varies widely due to factors such as diet, smoking and antibiotic use. LPS has been linked with systemic inflammation and sepsis when entered into circulation [167].

Research has been conducted into the response of various immune cells, including monocytes, to LPS. van der Bruggen et al found that such cells secreted 3 times greater levels of TNFα in response to LPS as determined by ELISA [168]. While 10 ng/ml of LPS was added in this experiment, we shall be adding a range of doses starting at 1 ng/ml and reaching 1 µg/ml. This will inform whether the responses we observe are, in fact, due to the addition of the LPS alone, as well as identifying the concentration that elicits the greatest inflammatory effect for characterisation and future comparison with other cell lines.

IL8 secretion has also been reported to be upregulated in response to LPS, induced by IFNϒ [169]. This effect proved to be more prevalent in immature crypt cells than mature villous cells [169]. Our model encompasses all colonic epithelial cell types that can be studied for their response to LPS. Therefore, we could measure crypt cell and colonocyte-specific markers to determine the cell type that exhibited the greatest effect in a dose response experiment.

While LPS triggers a greater inflammatory response in immune cells, intestinal epithelial cells are typically considered hyporesponsive to LPS [169]. This is to ensure careful regulation of the immune response to the ubiquitous bacteria present in the colonic tract throughout an individual's life. This is essential in maintaining homeostasis under normal conditions. This careful regulation, however, is suspected

to be lacking in IBD. While TLR4 has been implicated in this increased response to LPS, the exact role it plays, and other mechanisms involved, are not fully understood.

4.1.1.3Flagellin

A component of motile bacteria, flagellin, also triggers the sensitised immune system via another TLR receptor, TLR5. TLR5 is also expressed in epithelial cells, as well as monocytes and immature dendritic cells of the innate immune system [170]. While TLR5 has been found to be expressed on the apical surface of respiratory epithelium, expression can be found specifically on the basolateral surface of intestinal epithelium cells [171]. This basolateral location is to ensure an immune response is only initiated following activation by pathogenic bacteria that has successfully crossed the epithelial membrane. However, this mechanism does not confer the intended regulatory effect when membrane permeability is increased, allowing a much higher proportion of bacteria to cross this barrier and, thereby, trigger this widespread immune response. This exaggerated response of TLR5 can lead to a further change in the composition of the gut microbiota [172]. Once the immune response targets commensal bacteria in the colon, pathogenic bacteria are better able to colonise, becoming more prominent than the non-pathogenic bacteria of the microbiota.

Interestingly, when activated, TLR5 relies on MyD88, an adaptor protein which has also been found to be required in the canonical TLR4 response to LPS [173]. This has been further demonstrated in MyD88 -/- mice, who possess wild-type levels of TLR5. These mice proved to be unable to eliminate P. aeruginosa upon exposure [174].

During this chapter, we shall explore the downstream effects of TLR5/MyD88 activation in healthy organoids in a dose dependent manner. This can aid in characterising our platform in terms of its inflammatory profile. This will inform us to the relevance of the platform, demonstrating whether this *ex vivo* primary model is representative of the *in vivo* effects we see under pathogenic conditions.

4.1.1.4*Clostridium difficile* Infection

C. difficile Infection (CDI) is found more commonly in IBD patients than in the general population and can exert severe effects, which can, in turn, lead to hospitalisation. CDI is known to trigger flare-ups in these patients [117]. Contraction of CDI can also lower

the efficacy of certain drugs, such as metronidazole, in addition to increasing the duration of hospitalisation, colectomy rates and mortality [175]. Therefore, it is a very serious disease, that should be further explored to improve current therapeutic options. Present treatment consists of immunosuppressive agents and antibiotic use. However, both immunosuppressive drugs and prior use of antibiotics contribute to an individual's risk of acquiring CDI. Therefore, further understanding as to the increased propensity of IBD patients to contract this disease could aid in preventing initial infection and improving therapeutics.

In this project, toxins isolated from *C. difficile* would be added to our platform in a dose dependent manner and the subsequent inflammatory and epithelial response monitored. This experiment allows us to further characterise the inflammatory response of the model in addition to providing further information as the effects that *C. difficile* toxins exert on the healthy epithelium. Once this data is obtained, the findings can be extrapolated to CDI infection in the healthy individual allowing the differential characteristics of the UC colonic epithelium to be identified in further research.

4.1.2 Prior Research into IBD

Mouse models have, thus far, being used to investigate the roles of theses pathway in IBD, however, this is an insufficient method to accurately portray this disease in humans due to the biological discrepancies in cell expression and colonic architecture. Numerous differences exist between the colon of a human and mouse. Human colon consists of a series of small pockets, known as haustra. This macroscopic characteristic is not present in the mouse colon which gives the possibility of altering function. These differences extend to the cellular level, with goblet cells differential distributed along the colonic epithelium [176]. Furthermore, Paneth cells, essential for the production of anti-microbial peptides, are wholly absent in the colonic mucosa [176]. These difference signal differences in the mucosal immune system that can result in profound discrepancies in the colonic response to infection, and hence, the pathogenesis of IBD.

Due to these discrepancies between the mouse and human colon, this limits the relevance of data acquired from host-pathogen interaction studies and the study of

mucosal immune response. We have, therefore, utilised a platform derived from human samples as a more representative model of the colonic involvement in IBD.

4.1.3 Aim & Hypothesis

Aim: We aim to determine the response of primary colonic organoids to various pro-inflammatory stimuli.

Hypothesis: We hypothesise that primary human-derived colonic organoids will respond to inflammatory and anti-inflammatory stimuli in a predictable way that can be quantified.

4.2 Results

4.2.1 Response of Patient-Derived Colonic Organoids to TNFα

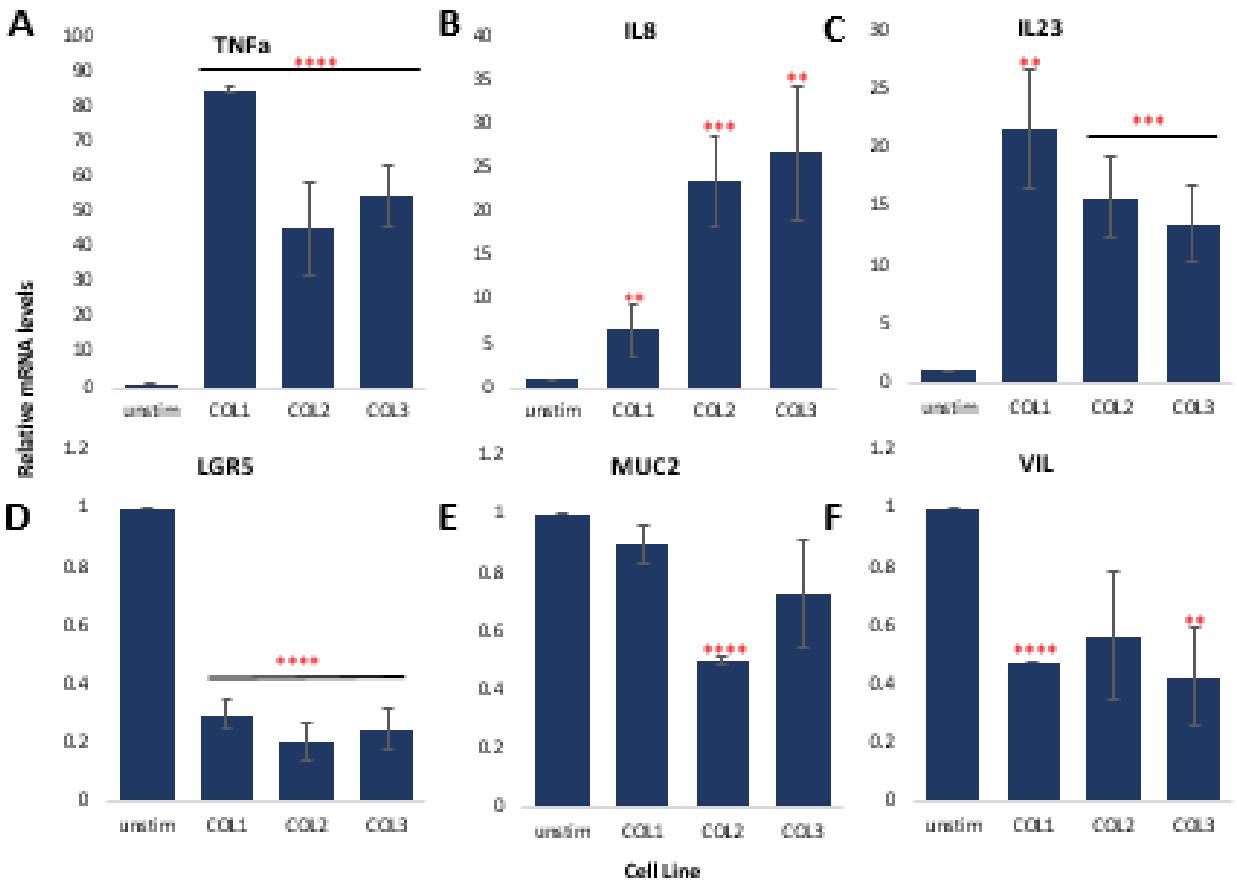

Figure 4.1: Effect of TNFα (40 ng/ml) on the inflammatory profile & intestinal cell expression of healthy colonic organoids. (A-C) Inflammatory profile of healthy colonic organoids following 48-hour treatment with TNFα measured by qPCR. Pro-inflammatory markers, TNFα, IL8 & IL23, were elevated across all 3 healthy lines. **(D-F)** Expression of intestinal stem cell marker, LGR5, decreased upon TNFα treatment. Component of mucin & goblet cell marker, MUC2, had variable expression between cell lines, although all showed a downward trend. Structural protein, Villin, decreased evenly across all 3 lines. Statistical analyses were performed by two-sided students t-test. Data are expressed as mean ± SD of each group. *P < .05; **P < .001; ***P < .0001. N=3 (Technical replicates)

To begin this work, we were interested to assess how our intestinal organoids would respond to a variety of extracellular inflammatory signals. The overall capacity for an inflammatory response in our healthy model was initially determined by incubating three healthy patient-derived colonic organoid lines with 40 ng/ml TNFα over a 48-hour period.

In this experiment, TNFα stimulation resulted in increased TNFα mRNA expression in a positive feedback mechanism with a considerable rise in production with 40-80 times that produced at baseline (Figure 4.1). Similar inflated responses to chronic TNFα exposure can be seen in IL8 and IL23 expression profiles. We have clearly demonstrated in this study that IL23 is produced significantly by colonic epithelial cells in response to TNFα, with expression of between 12-22-fold higher than unstimulated control.

After examining the effect of TNFα on expression of other inflammatory cytokines we next decided to assess how this might affect expression for genes responsible for controlling stem cell behaviour and defining the stem cell niche. TNFα appeared to have an effect on the stem cell compartment as well as epithelial cell function by decreasing LGR5, villin and MUC5a mRNA levels. Suggesting that TNFα may reduce the stemness of LGR5+ cells or potentially cause their depletion from the crypt.

Overall, the response of this model to TNFα is very strong across all lines tested. However, COL2 appears to have a more consistent response when considering both inflammatory and epithelial changes to expression. Therefore, COL2 was selected as the most reliable line to carry forward to future experimentation to give a profound, yet consistent and representative response inclusive of all the major measures considered in our inflammatory and epithelial panel.

4.2.2 Response of Healthy Patient-Derived Colonic Epithelium to Lipopolysaccharides

After determining the effects of pro-inflammatory stimulation by the prolific cytokine TNFα, the next aim of this study was to explore the effects of TLR ligands. This avenue of investigation would help garner further information into the widespread effects that receptor activation by an antigen can trigger. Antigenic exposure typically

results in an activation cascade encompassing multiple pathways. To determine the specific effects of bacterial dysbiosis in the colon, we exposed each line to bacterial LPS, acquired commercially, from 2 different species of gram-negative bacteria, *Salmonella enterica* serotype *typhimurium* (cat. no. # L6143) & *Escherichia coli* O127:B8 (cat. no. # L5024). These are both non-spore-forming, rod-shaped bacteria belonging to the *Enterobacteriaceae* family [76].

4.2.2.1 Effects of *S. typhimurium*-isolated LPS

A recent study has reported that chronic infection with *Salmonella enterica* serotype *typhimurium* leads to severe and enduring intestinal fibrosis in 129Sv/J mice [177]. Upon further analysis, similarities in site-specific protease staining profiles were identified between intestinal fibrotic tissue obtained from infected mice and tissue from human IBD patients [177]. This was determined by immunohistochemical staining. Interestingly, it was confirmed that this onset of fibrosis was a result of overall increased protease expression in macrophages and epithelial cells, whereas no enhanced activity was found in fibroblasts. This result clearly demonstrates the potential role for this bacterial species to initiate chronic disease in the colon. This effect peaked at 21 days post infection [177]. Therefore, it would be interesting to examine the inflammatory process that occurred on the lead up to visible fibrosis in the colon. They reported that the crypt architecture was severely damaged and large numbers of inflammatory cells were observed in the underlying tissues of the mucosa and submucosa [177]. However, the inflammatory profile was not measured in this study, therefore, further work into this area would add substantially to knowledge of the earlier pathophysiological stages of intestinal fibrosis and IBD. Hence, with prior reports on its impact upon the colon, as well as further knowledge into the mechanisms of the preceding inflammatory response being needed, this is one of the main LPS species include in this project.

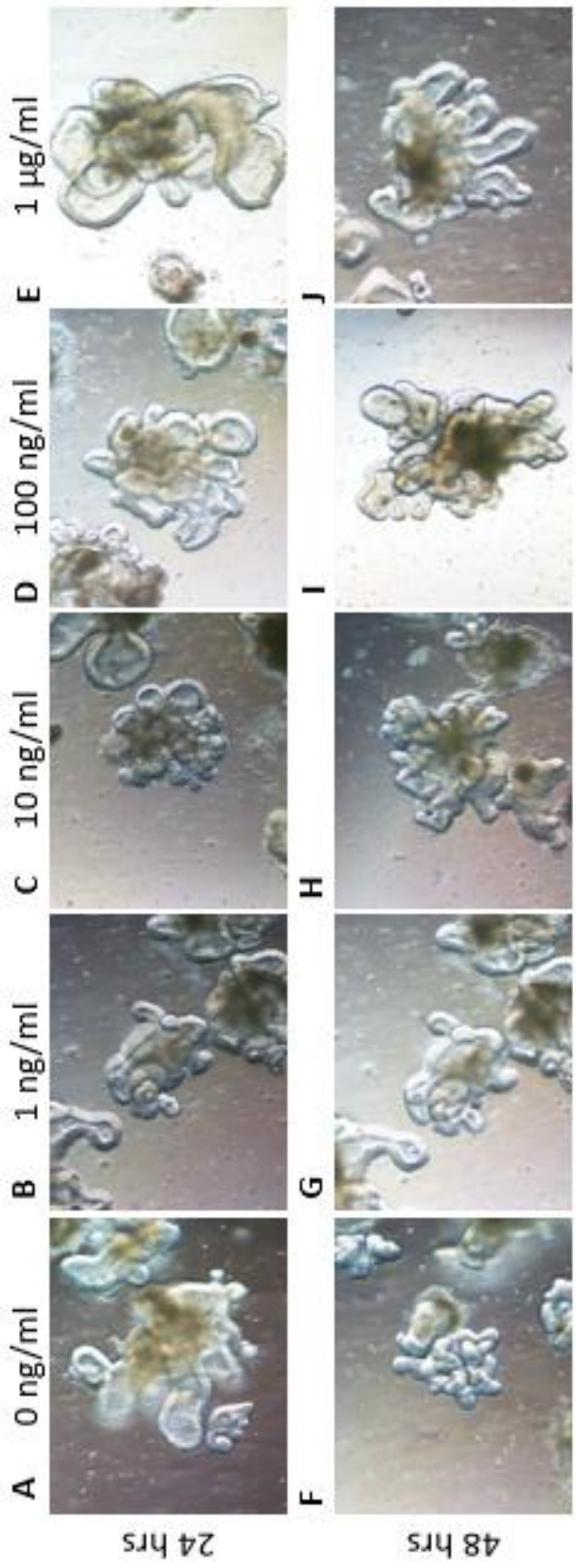

Figure 4.2: Healthy organoids infected with LPS isolated from *S. typhimurium* in a dose response experiment at concentrations 0-1 µg/ml. A-E were treated over a 24-hour period, while **F-J** were treated for 48 hours. Some necrotic tissue can be found in the lumen of organoids infected with 100 ng & 1ug/ml LPS at 48 hours. Imaged on Zeiss Axio light microscope at 20X

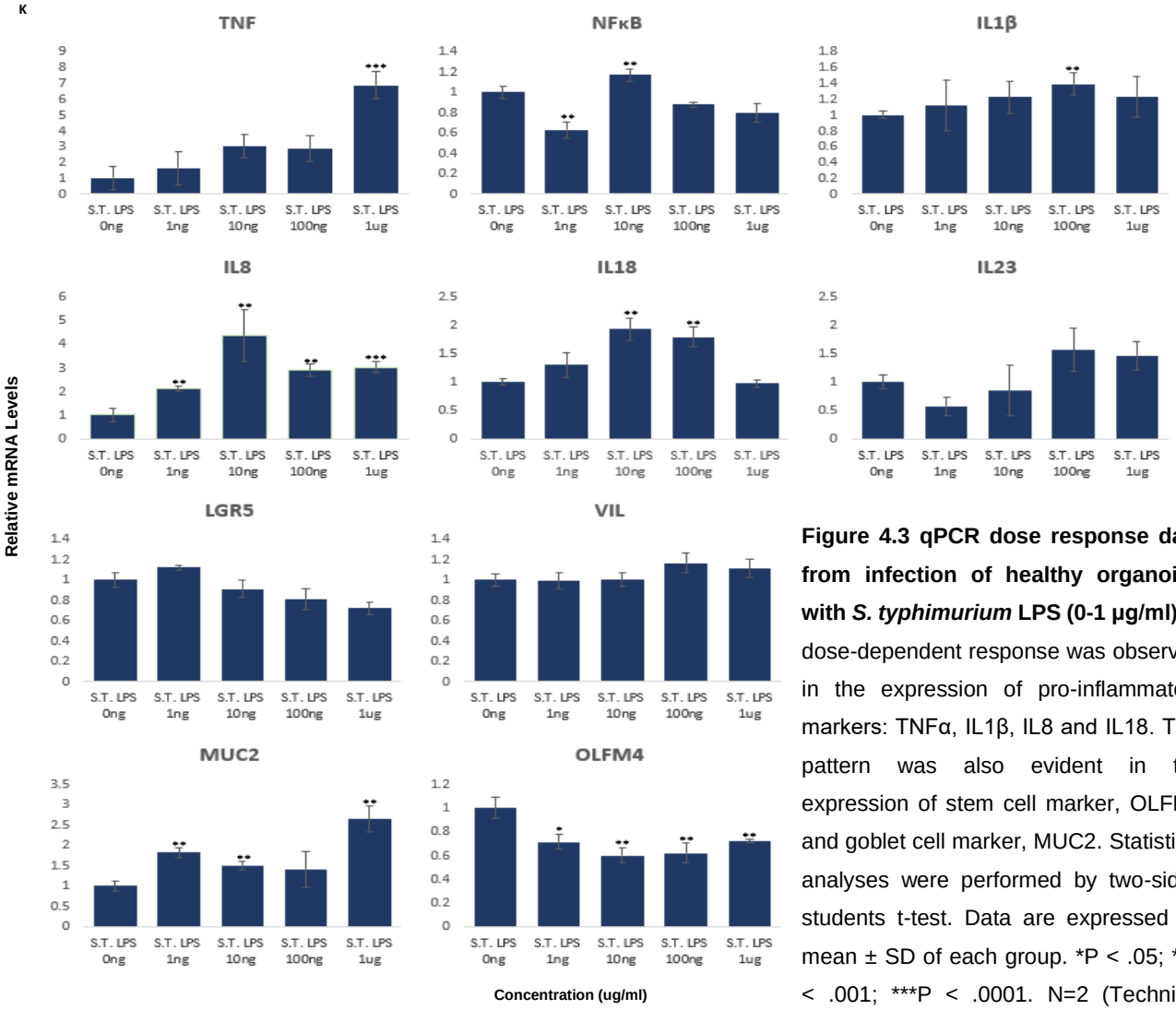

Figure 4.3 qPCR dose response data from infection of healthy organoids with *S. typhimurium* LPS (0-1 µg/ml). A dose-dependent response was observed in the expression of pro-inflammatory markers: TNFα, IL1β, IL8 and IL18. This pattern was also evident in the expression of stem cell marker, OLFM4 and goblet cell marker, MUC2. Statistical analyses were performed by two-sided students t-test. Data are expressed as mean ± SD of each group. *P < .05; **P < .001; ***P < .0001. N=2 (Technical replicates)

To assess the response of our primary intestinal organoids to LPS we chose a dose range of between 0-1 µg. Morphological analysis suggested that the organoids did not respond to the LPS, with no detectible change in organoid morphology or cytotoxic effects over the dose range chosen (figure 4.2). To confirm this, we assessed the response of numerous pro-inflammatory and epithelial genes via qPCR (figure 4.3). There is a definite dose response demonstrated by significant dose-dependent increases in TNFα, IL1β, IL8 and IL18 expression. However, this response was muted, with minimal alterations to epithelial marker expression. This combined with the morphological images displaying healthy, intact organoids present in all conditions, including the maximal dose administered, it was decided to increase the upper concentration used from 1 µg/ml to 100 µg/ml. This dramatic increase would be sure to reach the upper limit of epithelial organoid tolerance. The effects of this heightened concentration are reflected in both morphological and genetic data seen in figures 4.4 and 4.5.

Initially, inflammatory markers were investigated to determine the pro-inflammatory effects we expected to find upon exposure to LPS. This experiment was performed on healthy organoids to establish the baseline response to this inflammatory mediator which can then be used as a reliable comparison to our disease line response. As can clearly be seen in this data, TNFα and IL18 present an obvious dose-dependent response indicating that it is the factor being controlled for that is causing this effect. IL1β also demonstrates this trend, however to a lesser extent, although significant at 100 ng/ml.

To confirm this outcome could also translate to the epithelium directly, further analysis was performed on a range of intestinal cell markers. The intestinal stem cell markers, LGR5 and OLFM4, can be seen steadily decreasing in conjunction with rising *S. typhimurium* LPS concentration. While a promising result showing LPS does, in fact, exhibit a deleterious effect upon the epithelium itself in addition to the increase in gut inflammation it initiates, the decrease at 1 µg/ml still only demonstrates a reduction of 25% below control. This finding can be corroborated by Li et al, who found the same response in mouse intestine [178]. As greater reductions in stem cell expression have been observed previously with TNFα exposure alone, it was worth verifying whether a greater effect would be exhibited by exposure to an increased LPS concentration.

Expression of mucin constituent, MUC2, was increased 2.5-fold above untreated control at the upper treatment range. This significant increase reveals the response of goblet cells to the increased presence of LPS, which provides one of the most important protective mechanisms in the colon.

Villin expression appeared to remain stable throughout this dose response, suggesting that while the stem cell niche suffers damage under these conditions, the differentiated colonocytes remain relatively unaffected.

This data, therefore, reveals that LPS has the greatest impact upon the renewability of the epithelium. Since the colonic epithelium must renew every 3-5 days to retain its integrity and function, [179], this effect would have considerable consequences for the gut health of the patient. During acute flares of inflammation in the colon, this effect can be compensated for by reprogramming differentiated cells into stem cells with the aid of R-spondin-3 [180]. This research was conducted following data indicating that stem cells in the niche are selectively lost during a bout of colitis [180]. This report supports the data obtained in our experiment, whereas a bout of inflammation appears to most greatly affect that stem cell compartment, demonstrated by a great reduction to LGR5 & OLFM4 markers.

In this absence of R-Spondin-3 however, this regeneration is no longer possible, despite the injury being severe or mild. While this is an important finding to note, this paper goes on to demonstrate that this innate protective mechanism that occurs upon injury is only beneficial in response to acute injury. Under conditions of severe chronic colitis, however, these differentiated cells also perished resulting in collapse of epithelial crypts and, hence, reduced to epithelial integrity [180].

Expression of these key inflammatory cytokines continued to trend upwards in this initial dose response experiment, while stem cell marker expression continued downwards. It was decided to further assess whether this trend would resume with higher concentrations. It would then be possible to establish which concentration would exhibit the most heightened response by this model prior to toxicity occurring. Therefore, the experiment was repeated using a greater concentration span, ranging from 1-100 µg/ml.

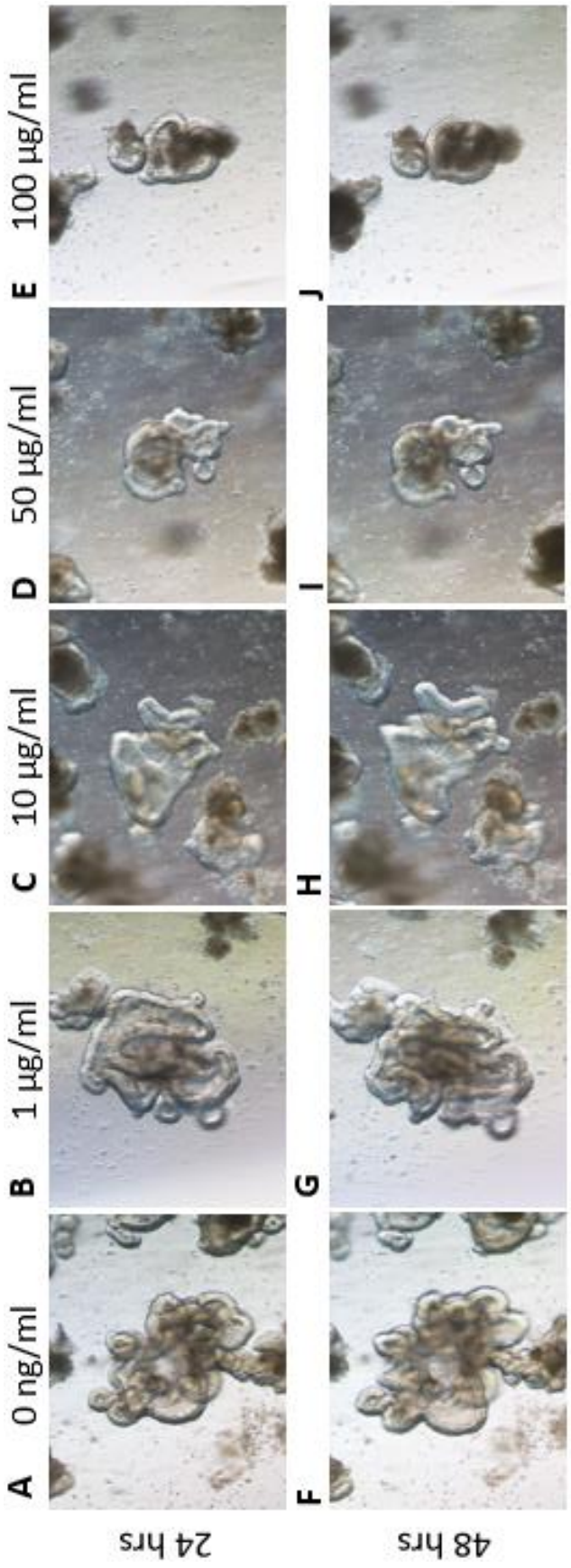

Figure 4.4: Healthy organoids infected with LPS isolated from *S. typhimurium* in a dose response experiment at concentrations 0-100 µg/ml. A-E were treated over a 24-hour period, while **F-J** were treated for 48 hours. Some necrotic tissue can be found in the lumen of organoids infected with 100 ug/ml LPS at 24 & 48 hours, however this damage has not caused complete organoid death. Imaged on Zeiss Axio light microscope at 20X magnification.

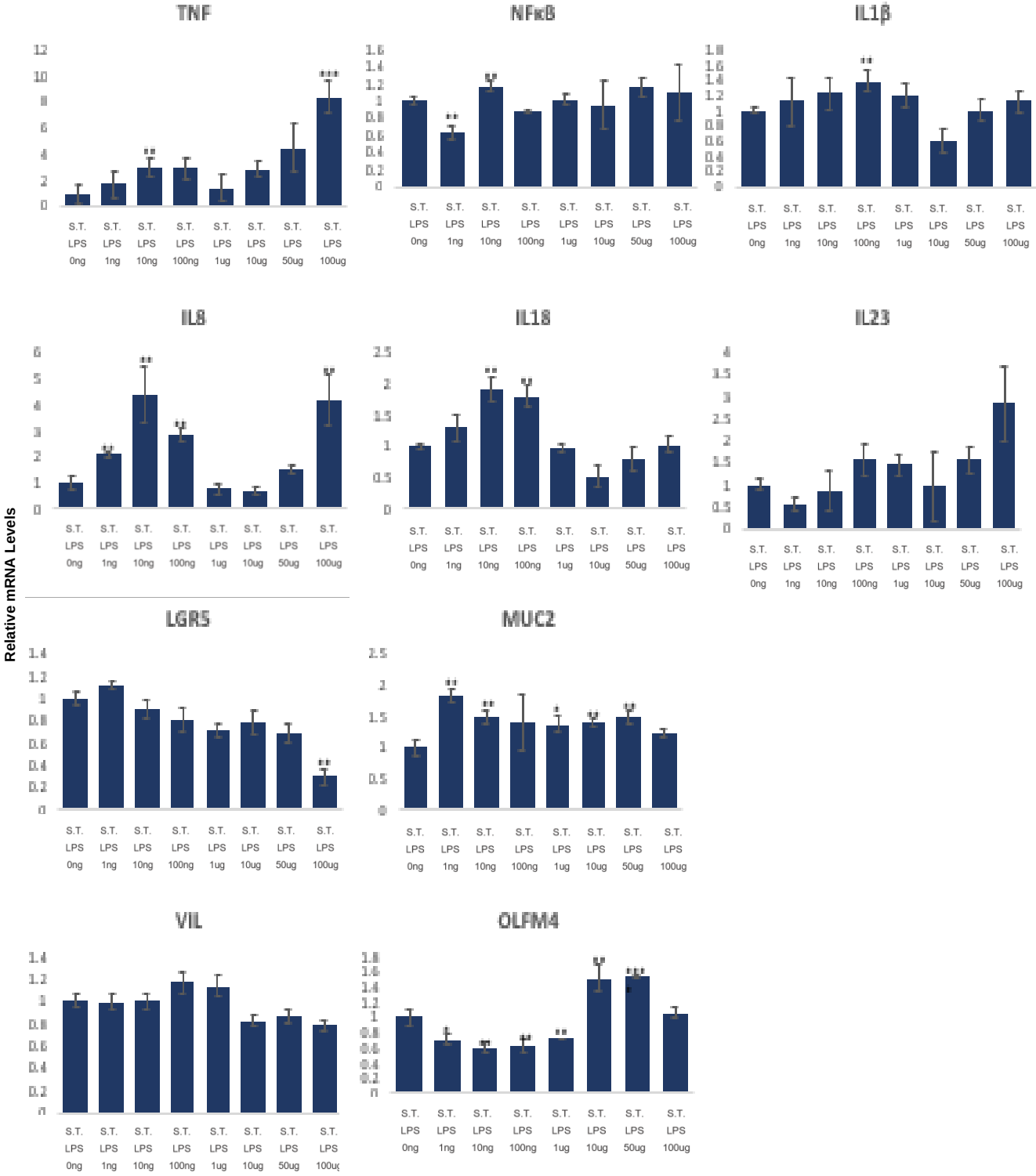

Figure 4.5: qPCR dose response data from infection of COL2 with *Salmonella typhimurium* LPS at concentrations between 0-100 µg/ml over a 48-hour period. TNFα expression continued to rise in a dose-dependent manner. Other pro-inflammatory cytokines, IL1β, IL8 and IL18 increased steadily to between 10-100 ng/ml before declining. This could be due to cell loss. In line with the necrosis observed morphologically, loss of colonic cell marker expression was evident with increasing doses of LPS. Statistical analyses were performed by two-sided students t-test. Data are expressed as mean ± SD of each group. *P < .05; **P < .001; ***P < .0001. N=3 (Technical replicates)

As we can see in these morphological images, the higher concentration range yielded a much stronger reaction to LPS with widespread toxicity being apparent at 100 µg/ml (figure 4.4). Once this had been determined, RT-PCR analysis was performed to establish if these results were concurrent with what could be visually evaluated.

It was made evident by the following data that 100 µg/ml of *S. typhimurium*-derived LPS caused a substantially greater level of inflammation that the highest concentration, of 1 µg/ml, previously used. TNFα expression was increased dramatically by 8-fold above both untreated and 1 µg/ml, in this experimental repeat (Figure 4.5).

NFκB had a rather muted response across all concentrations tested. TLR4 does, in fact, activate NFκB via both MyD88- and TRIF-dependent pathways, [181]. It is clear that this is a key transcription factor playing an important role in the activation of the inflammatory response we observe in this experiment. However, as the levels of mRNA expression do not change throughout the dose response, it is likely the changes initiated in this pathway are a result of changes to translocation from cytoplasm to nucleus rather than to expression itself.

The pro-inflammatory cytokine, IL8, increased in expression 4-fold above control, while IL23 raised 2.5-fold. These are crucial cytokines in the TNFα pathway and therefore this further demonstrates the increased activity we have already seen by the significant boost in TNFα expression directly. IL18, however, begun rising steadily, doubling expression in response to stimulation with 10 ng/ml, before dropping at higher concentrations. IL18 is not mentioned in the literature in terms of its role in the TLR4 pathway upon activation by LPS, therefore the response of this cytokine is less relevant to be considered in respect to this experiment.

Alterations to intestinal epithelial integrity following exposure is, however, relevant as this can have a vast impact on the progress and advancement of this disease, amplifying symptoms in the patient over time.

Figure 4.5 shows a gradual decline in LGR5 expression as LPS concentration increased, culminating in expression reaching 70% below control following simulation with 100 µg/ml. A 70% drop in stem cell presence in the intestinal niche is critical and can result in severe damage to the ability of the epithelium to regenerate in response

to further damage. The effects of this would be evident very quickly due to high cell turnover in colonic regeneration.

Conversely to the last dose response experiment performed, Villin expression dropped at 10 µg/ml, continuing to the maximum dose. As this response was not observed at the lower concentrations, this likely indicates the increased toxic effect of LPS on colonocytes as concentrations increase. This data confirms observations made from morphological changes (Figure 4.5). These findings combined, point to the detrimental effects that high concentrations of LPS have upon epithelial integrity and regenerative capacity.

This experiment was repeated in another healthy line generated from another patient to confirm whether these findings were, in fact, consistent and representative of other healthy tissue. This experiment confirmed this to be the case (data not shown).

4.2.2.2Effects of *E. coli* O127:B8 on colonic organoids

Secondly, it was decided that *E. coli* O127:B8 would be appropriate to test alongside this, with reports suggesting that LPS isolated from this species induces inflammation in the ileum. This experimental repeat could help confirm whether the species expressing the LPS has a distinguishable effect on epithelial response. Differences have previously been reported on the response of rabbit ileum to different serotypes [182]. In this specific study, *E. coli* O127:B8 was found to induce inflammatory response and changes to contractility more effectively than the *E. coli* serotype, O111:B4. The former is therefore the serotype being investigated in this project.

Once the serotype most relevant for use in our study had been determined, we went on to perform an experiment to investigate its downstream effects. Unlike the study published by Grasa et al, LPS was added for a 48-hour period. This method would more closely emulate chronic exposure that is found in the colon during times of dysbiosis, thereby giving a clearer indication of the inflammatory profile present after prolonged contact. As this approach had not previously been reported using our model, it was necessary to generate an initial dose response curve.

As can be seen in figure 4.6, an upward trend can be observed across all markers, with the exception of IL18. This upward trend, in line with rising concentration, is the

expected response to stimulation by LPS. While IL18 is also a pro-inflammatory cytokine involved in numerous inflammatory pathways, interestingly, it is also linked with tumour suppression [183]. It can therefore be speculated that a reduction in IL18 expression, in response to LPS, could be increasing the risk of tumour development in these patients. As IBD has been very closely linked with CRC development, this finding could point to another factor directing this outcome in IBD patients. This would be an interesting field to explore further.

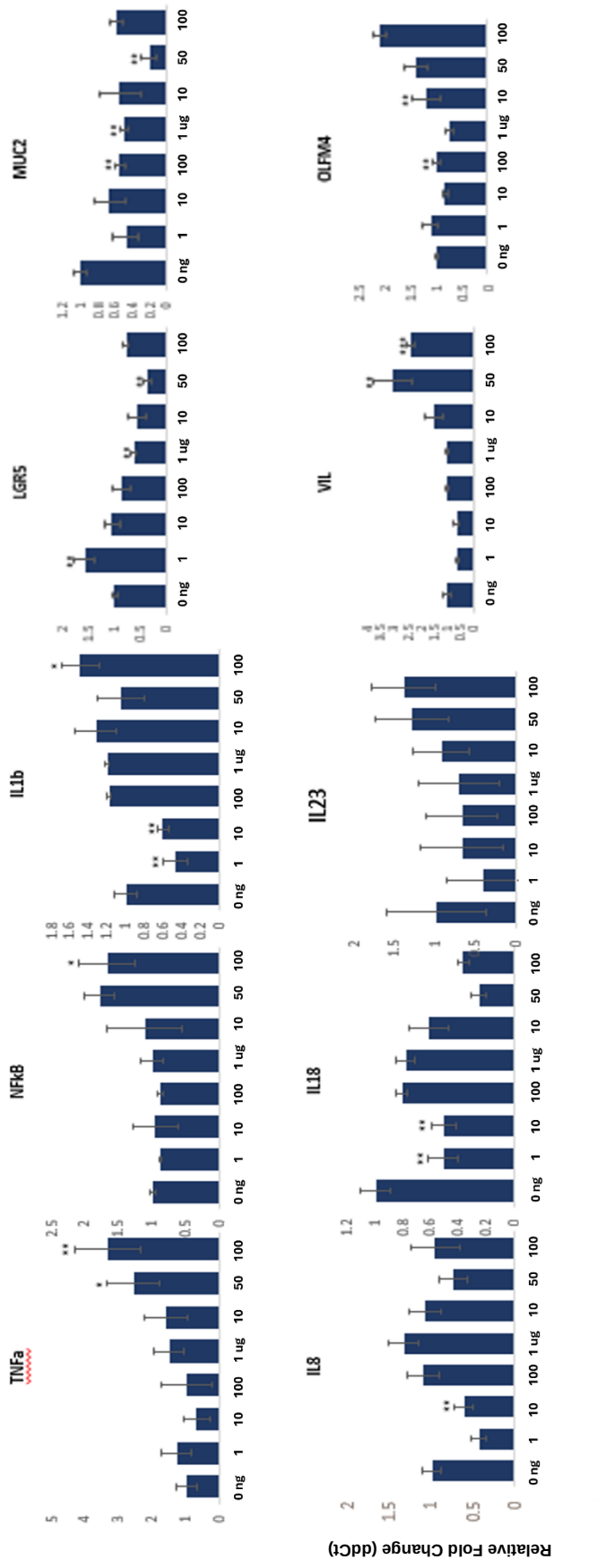

Figure 4.6: qPCR dose response data from infection of COL2 with Escherichia coli LPS at concentrations between 0-100 µg/ml over a 48-hour period. Similar effects were observed from those seen following exposure to LPS from *S. typhimurium*, although IL1β expression increased in a more dose-dependent manner. Statistical analyses were performed by two-sided students t-test. Data are expressed as mean ± SD of each group. *P < .05; **P < .001; ***P < .0001. N=3 (Technical replicates)

Response of this representative healthy line to *E. coli* LPS generated an almost identical intestinal marker expression profile to that observed following stimulation with LPS isolated from *S. typhimurium*.

This was made evident in the continuous decline of LGR5 and increase in OLFM4, consistent with the rise in LPS concentration. Slight differences can be seen in MUC2 expression, with a drop of 40% marked at the highest concentration. As this marks a reduction in goblet cell prolificacy in the epithelium, it is possible that *E. coli* LPS triggers a greater effect upon the epithelium itself. This effect is supported by data showing increased Villin; a response that wasn't present in the previous experiment. An increase in Villin, under these conditions, suggests a compensatory mechanism to increase differentiation in the epithelium in response to a perceived bacterial threat. This would assist in enhancing epithelial integrity. However, this is likely to be a short-term correction prior to worsening toxicity resulting in widespread cell death. The beginnings of this can potentially be seen at 100 µg/ml with a drop from 3-fold above control at 10 µg/ml to 2.5-fold (figure 4.6).

Treatment with *E. coli* O127:B8 LPS appeared to yield a much more consistent response across all other major inflammatory cytokines tested. Therefore, it was decided that LPS isolated from *E. coli* would generate the most reliable data for interpretation of future experiments.

To further explore the varied effects LPS initiates upon this model, it's influence on the fibrotic response in healthy epithelium was measured. Collagen-1, in particular, is strongly associated with inflammation [184]. Collagen-1 is produced by mesenchymal fibroblasts, however the lung epithelial cell line, BEAS-2B, has also been reported as expressing COL1A1 [185]. Therefore, it was deemed applicable to add this marker to the panel profile. To further assess the role the epithelium might play in ECM remodelling, these investigations could have been followed up by transferring the organoids to a 3D hydrogel to limit the influence ECM proteins, present in Matrigel™, exhibit upon this fibrotic response.

Two critical markers of fibrosis, TGFβ & Collagen-1, produced a clear dose response curve displaying increased expression in conjunction with increase LPS-mediated inflammation.

This evident increase in expression reveals the early stages of fibrosis are initiated promptly after the commencement of severe inflammation triggered by the overgrowth of gram-negative bacteria in the colon. With such an obvious and sudden increase of pro-fibrotic cytokines during a chronic illness such as UC, it is easy to see how fibrosis is occurring at a fast pace from the very beginnings of the disease. Hence, it is important to ensure that the progression of fibrosis is carefully monitored from early disease development and preferably a treatment regime is introduced prior to any macroscopic fibrotic presence to prevent uncontrolled collagen deposition and reduced colonic function as a result.

4.2.3 Response of Healthy Patient-Derived Colonic Epithelium to Flagellin

After testing LPS, a commonly known bacterial PAMP, this model was used to test another antigen, flagellin. Flagellin, beneficial for bacterial motility, are largely expressed by gram-negative bacteria. It has, in recent years, emerged as a potent immune activator [186]. It operates via TLR5, which has been shown earlier in this thesis to be increased significantly in expression upon the addition of TNFα. As TLR5 is expressed on intestinal epithelial cells *in vivo*, it can be triggered by the presence of flagellin in this model [115]. Following this TLR5 activation, the downstream inflammatory and epithelial effects were then assessed.

The flagellin used in this experiment was isolated from *Salmonella typhimurium* (cat. no SRP8029). A representative healthy line was utilised to model a dose-dependent response with a concentration range of 0-200 ng/ml. The highest concentration, 200 ng/ml, resulted in a high degree of necrotic cell death originating from the organoid lumen (figure 4.7). This impact could be observed from 24 hours onwards. For all other concentrations in this dose response experiment, there was some degree of cell death, however, there was a great deal of viable cell material remaining. This was isolated, prepared and analysed. The data from which can be seen in figure 4.8.

Many of the inflammatory cytokine markers responded in a dose-dependent manner, including TNFα, which peaked at 11-fold above untreated control at the 48-hour time point. Interestingly, NFκB expression also increased by 40%, however this response was only measured at 25 ng/ml. Since other inflammatory effects continue to present at higher doses of flagellin, despite the lack of NFκB response, it is possible that there are also NFκB-independent inflammatory mechanisms at play. Gao et al suggest an NFκB-independent protective mechanism when human corneal epithelial cells (HCECs) were primed with low-dose flagellin aiding in wound healing [187]. Therefore, it is also likely this NFκB-independent mechanism can occur at higher pro-inflammatory doses.

IL1β had a similar pattern of expression, with the peak occurring at 25 ng/ml, suggesting IL1β to be involved in this NFκB-mediated response.

Following TNFα, the next most notable response was recorded from IL8, with expression peaking 6 times greater than control at 200 ng/ml flagellin. This steady dose-dependent increase is consistent and comparable to TNFα (figure 4.8).

Kinnebrew et al found IL23 subunits to be maximally expressed within 60 minutes of flagellin exposure in mouse intestine [188]. We did not test at such an early time point in this experiment as we are interested in more chronic effects. However, it is evident that IL23 expression remained high even after 48 hours of flagellin administration (figure 4.8).

Once this clear inflammatory profile had been established, the impact of flagellin upon intestinal cell expression was evaluated. Both differentiated and stem cell markers showed an overall decline in expression. LGR5+ positive cells appear to have reduced considerably, by 50%, at both 25 and 50 ng/ml which would elicit serious consequences for cell turnover within the crypt and subsequently the entire epithelium. The effect appears to be less severe upon administration of 100 and 200 ng/ml over the 48-hour period. This seems to be in line with the trend evident in both NFκB and IL1β expression. As expression of these inflammatory markers reduces, the effect upon the LGR5+ stem cells lessen. This occurrence is worth further exploring to determine whether there is a divergence of pathways following flagellin exposure in the colonic epithelium.

Differentiated colonocyte marker, Villin, drops expression below 50% across all concentrations in this range, signalling critical consequences for the integrity of the epithelium. A similar response is apparent by MUC2, with an initial increase at 25 ng/ml, expression is substantially reduced by approximately 50% below untreated control. This initial resurgence is indicative of the compensatory response initiated by goblet cells in response to bacterial invasion, in an effort to prevent further increase in microbial load. This occurs at the lowest tested concentration, indicating that sufficient viable goblet cells remained in order to commence this response. However, with rising concentrations the goblet cells would sustain increased damage which appears to have resulted in overall mucin reduction.

OLFM4, a dual marker, represents the expression of both ISCs in some instances, while highlighting the increase in prevalent inflammation in others. Due to the opposing

trend of OLFM4 with LGR5; a specific ISC marker; it is likely that OLFM4 is representative of the substantial inflammatory reaction of colonic organoids to flagellin. Interestingly, an almost identical pattern of expression is apparent between OLFM4 and IL8 (figure 4.8).

To further establish the response of this patient-derived model to flagellin, major fibrotic markers, TGFβ1 and Collagen-1, were measured. The findings show a reduction in fibrotic response upon exposure to flagellin (Figure 4.8). Inflammation-mediated fibrosis in UC is TLR4 pathways [189]. However, less literature is available on the initiation of fibrotic response via TLR5 in the colon, therefore it may be a less of an issue when this pathway alone is activated. Likewise, a fibrotic response could indeed be triggered at a later time point.

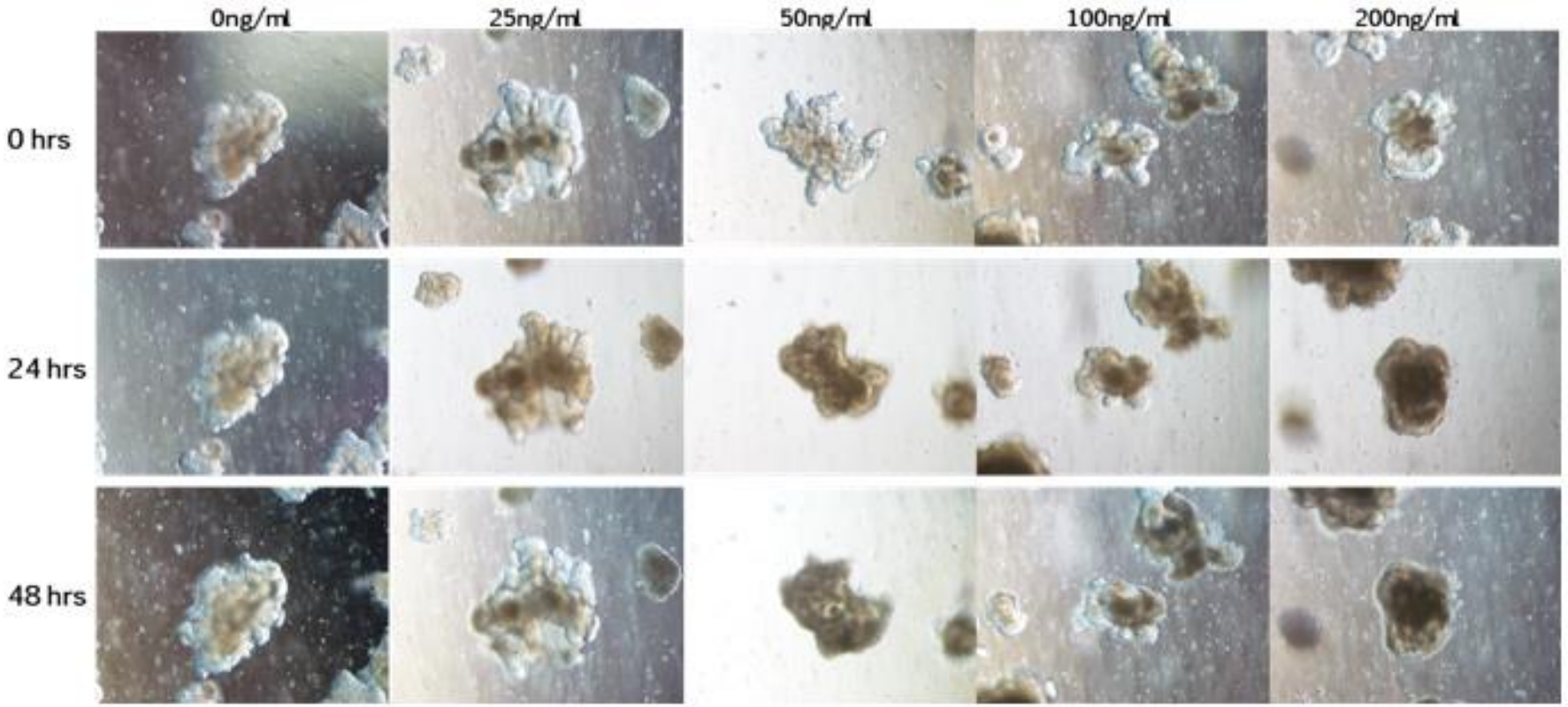

Figure 4.7: Morphology images of healthy organoids infected with flagellin at a range of concentrations between 0-200 ng/ml over a 48-hour period. In a dose response experiment. Necrosis worsened as LPS dose increased. Imaged on Zeiss Axio light microscope at 20X magnification.

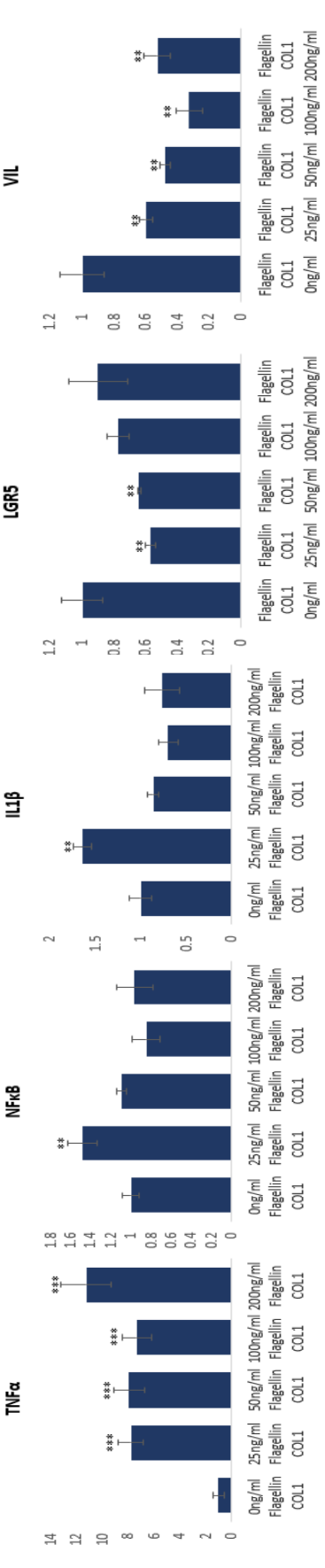

Figure 4.8. qPCR dose response data from infection of healthy organoids with flagellin at a range of concentrations between 0-200 ng/ml over a 48-hour period. While LPS induced a pro-inflammatory response, it also decreased expression of differentiated epithelial cells. Marker of fibrosis were also reduced in a dose-dependent manner. Statistical analyses were performed by two-sided students t-test. Data are expressed as mean ± SD of each group. *P < .05; **P < .001; ***P <0.0001. N=1 (Technical replicates)

4.2.4 Infection of Healthy Patient-Derived Colonic Organoids with *Clostridium difficile* Toxins

To further validate this platform, toxins isolated from *Clostridium difficile*, were added at increasing concentrations in a time course experiment.

Unlike LPS*, C. difficile* is a gram-positive bacterial species that, alone, does not cause any adverse effects in the colon. However, it does produce two toxins that cause a range of symptoms including diarrhoea accompanied with a fever, loss of appetite and abdominal pain [190]. In severe cases, serious damage to the colon can arise, resulting in partial or complete removal.

C. difficile infection (CDI) often colonises the colon of patients following antibiotic use, causing dysbiosis in the gut, allowing this pathogenic species to take a stronghold [191].

CDI has been linked with worsening of UC and has been found in between 2-6% of UC patients admitted to hospital [190]. In these patients, CDI infection increases the risk for colectomy as well as increasing the likelihood of fatality. A combination of treatment with antibiotics and immunosuppressants have also been associated with a fatal outcome in 12% of cases after just a 3-month period [192]. This is, therefore, a serious connection to UC that deserves further attention in an attempt to limit or mitigate these risks.

Due to the relevance and severity of CDI in combination with UC in the colon, we further explored the effects on our patient-derived colonic platform.

As is evident in figure 4.9, widespread toxicity was observed at all concentrations tested at both the 24- and 48-hour time points. While exposure to toxin A (TcdA) (cat no. # SML1154) and toxin B (TcdB) (cat no. # SML1153) independently, resulted in the development of necrosis originating from the centre of the organoids, there was some viable tissue remaining around the crypt region. It is likely these organoids would largely not have recovered from this extensive damage anyway, however, if passaged and dissociated it is possible that some new organoids could be generated from any remaining healthy crypts. *In vivo* this would be promising if the prompt removal of

toxins from the patient's system could allow for some level of regeneration in the epithelium.

Conversely, a combination of both toxins resulted in global necrosis with exposure to TcdA at 50 ng/ml in addition to TcdB at 50 ng/ml.

This concentration range was selected as reports have suggested a wide range of sensitivity of different tissue types, ranging from 1-5 ng/ml to 500 ng/ml on a range of cell lines including those taken from pancreatic and colon carcinomas [193].

Another study reported the results of a dose response experiment using TcdA only. They tested concentrations of 10, 100 and 1000 ng/ml on colonic lamina propria cells. While 10 ng/ml had minimal effect upon this cell line, 100 ng/ml exhibited a significant effect upon the inflammatory response; measured by the proportion of CD25+ T-cells; and subsequently the cell viability [194]. Viability begun to drop at 24 hours, however no significant response was determined until 72 hours. The cellular inflammatory response did, however, demonstrate an increase at 24 hours a 3.5% increase above control, with a significant spike to 12% above control at 48 hours [194]. As a result, the experiment conducted in this project used a spread of concentrations within the ranges seen in this study. The concentrations being 25 ng/ml, 50 ng/ml and 100 ng/ml all tested as individual toxins or in combination over a 48-hour period.

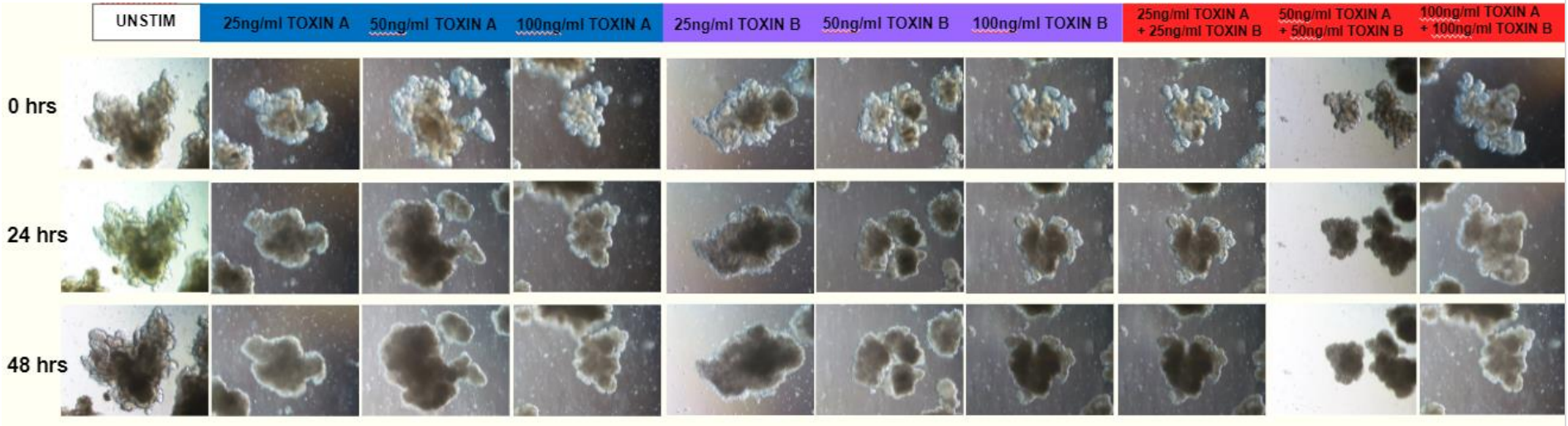

Figure 4.9: Morphology images of healthy organoids infected with *Clostridium difficile* toxins A, B and A+B at a range of concentrations between 0-100ng/ml in a dose response experiment over a 48-hour period. Widespread necrosis is evident from the lowest dose: 25 ng/ml after 24 hours. Imaged on Zeiss Axio light microscope at 20X magnification.

This severe effect upon the epithelium was too great to obtain accurate measurements as to the inflammatory profile in response to either toxin (Figure 4.9). This demonstrates evidence that primary cells are much more sensitive than carcinoma cell lines previously tested. Therefore, the results of this study yield a more accurate representation as to the response of colonic epithelium *in vivo*.

This experiment was then repeated at concentrations substantially lower; 1, 5 and 10 ng/ml, with the aim of initiating a measurable and significant inflammatory profile in response to exposure without inducing overwhelming toxicity within the organoids. The morphological data from this experiment can be found in figure 4.10.

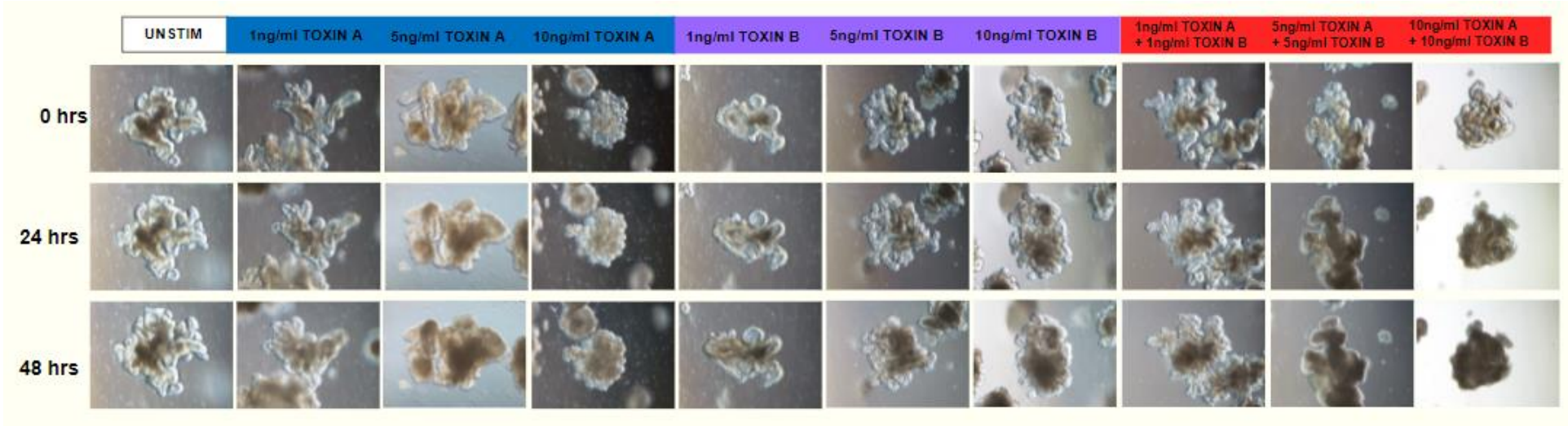

Figure 4.10: Morphology images of healthy organoids infected with *Clostridium difficile* toxins A, B and A+B at a range of concentrations between 0-10 ng/ml in a dose response experiment over a 48-hour period. Organoids survived the lower doses tested of singular toxins, however the combination of both toxins at 5 and 10 ng/ml resulted in complete necrosis. Imaged on Zeiss Axio light microscope at 20X magnification.

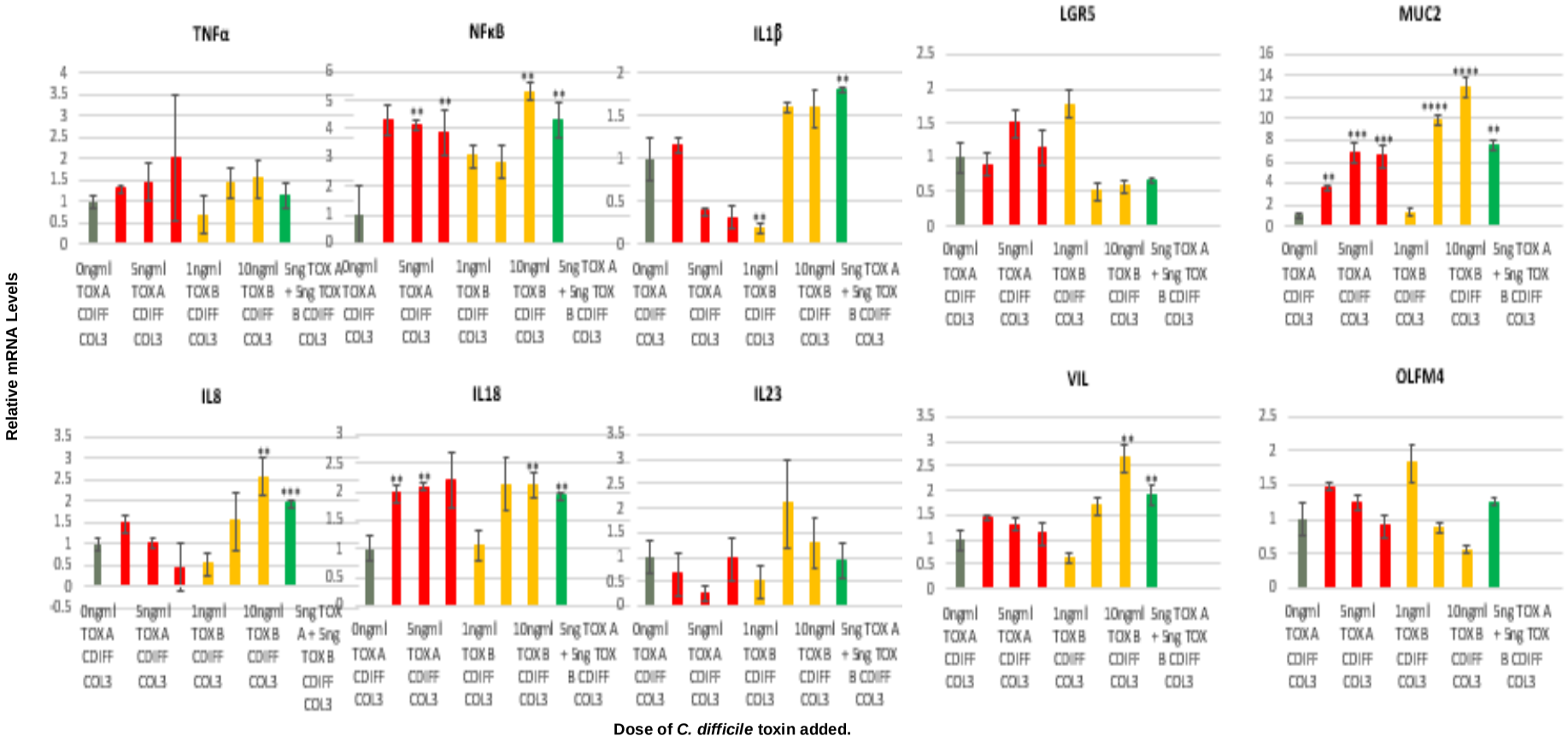

Figure 4.11: qPCR dose response data from a 48-hour infection of healthy organoids with *C. difficile* toxins at a range of concentrations between 0-10ng/ml. Expression of NFκB and IL18 rose considerably with the addition of toxins A & B, both alone and in combination, while other pro-inflammatory markers displayed opposing responses to toxin A & toxin B. Goblet cell marker, MUC2, responded dramatically to both toxins. Statistical analyses were performed by two-sided students t-test. Data are expressed as mean ± SD of each group. *P < .05; **P < .001; ***P < .0001. N=1 (Technical replicates)

It is clear that TcdA and TcdB combined induced necrosis at both 5 and 10 ng/ml (figure 4.10). This demonstrates the potency of these toxins and the subsequent deleterious effects they exert on the colonic epithelium. Even at low concentrations such as these, the epithelial layer can be irreparably damaged. This would lead to loss of digestive function in addition to increased bacterial translocation out of the colon and into circulation.

Despite this reaction at the upper limit of those tested, organoids in all other conditions remained largely viable. This allowed for material to be gathered and analysed. Samples were prepared and RT-PCR was performed. Data shown above.

NFκB expression increased considerably compared to treatment with previous inflammatory inducers, signifying NFκB is heavily involved in this toxin-induced inflammatory response compared to effects seen in previous experiments following exposure to specific pro-inflammatory cytokines or bacterial PAMPs. This response occurs following treatment in all conditions across all concentrations tested with a significant rise at 10 ng/ml of TcdB.

IL18 follows a similar trend of expression to that of NFκB. This is another interesting difference in comparison to responses noted previously as IL18 had very limited involvement in previous inflammatory responses (figure 4.11). These findings suggest that a different set of signalling pathways are triggered by gram-positive bacterial toxins than gram-negative bacteria in colonic epithelial cells. This is an interesting result that, with further research, could inform a preferential treatment plan in patients with combined UC flare-ups and CDI.

It appears TcdB and a combination of toxins were associated with the most substantial cellular response. IL1β & IL8 expression increased ~2-fold upon exposure to toxin B & A+B.

A combination of TcdA and TcdB at 1 ng/ml generated a similar level response to those triggered by the individual toxins alone at 10 ng/ml. As stated earlier, it was not possible to obtain data on combined toxin exposure at 5 and 10 ng/ml due to substantial necrosis (figure 4.11).

TcdB also had the most severe effect on intestinal stem cells, with LGR5 & OLFM4 expression dropping ~50%. Meanwhile, Villin and MUC2 expression increased considerably, potentially in response to the greater cell death, with increased differentiation into mature epithelial cell types to reinforce the epithelial integrity (figure 4.11). This is important to note the distinction in the response to each toxin separately as TcdB generates an all-round more severe response and subsequent damage to the epithelium.

4.3 Discussion

The data described in this chapter demonstrates the varied response of patient-derived colonic organoids to a range of inflammatory mediators commonly found in the colon *in vivo*, under normal conditions. These cytokines, bacterial PAMPs and toxins are present in greater quantities when dysbiosis is present. While these are kept in check by a healthy functioning immune system, in individuals with heightened susceptibility to UC this can cause a continual, uncontrolled inflammatory response leading to potentially serious systemic effects.

The inflammatory mediators tested on this platform either initiate an inflammatory and fibrotic response via an individual toll-like receptor or a combination of receptors. We have also reported in this chapter, the impact upon the epithelium directly. This is important to analyse to determine the overall severity of exposure to these agents, which will reveal the origin for patient symptoms, aiding in improving treatment based on the level of a patients dysbiosis and the pathways most greatly affected.

Once the inflammatory profiles of healthy lines can be ascertained, this leads to a greater understanding of this representative platform. This serves as a good foundation for the comparison of differential responses between healthy tissue and tissue predisposed to UC in a pro-inflammatory environment.

4.3.1 Response of Patient-Derived Colonic Organoids to TNFα

TNFα was the first inflammatory agent to be tested on this platform as it is well-known that TNFα plays a critical role in the induction of inflammation in many different diseases and disorders and has been closely linked to UC [195]. This response can be produced by both immune cells and epithelial cells. It has been reported that epithelial TNFα overexpression leads to early activation of intestinal myofibroblasts which confound the inflammatory cascade [196]. While TNFα is heavily involved in many downstream pathways, the relationship and interactions of many are incompletely understood. Hence, TNFα gives a robust foundational response of our model,

triggering substantial inflammatory reactions in the epithelium which would offer a suitable comparison to other pro-inflammatory agents.

In this study, TNFα was found to initiate the most significantly heightened response observed on this platform with an increase in expression of over 40-times expression across all 3 lines tested. This demonstrates the sensitivity of healthy patient-derived colonic organoids to TNFα exposure, which was tested over a 48-hour period at 40 ng/ml. These results all proved to be highly significant with a threshold of $p<0.0001$. The remaining cytokines, prevalent in the TNFα pathway; IL8 and IL23, also elicited a substantial response significantly above the corresponding untreated control. These cytokines are closely linked with TNFα, activated downstream in this pathway [197]. IL23 has also been linked with multiple autoimmune diseases and has been suggested to also initiate an auto- and paracrine response resulting in production of IL-1, TNFα and IL23 itself [198]. Schmidt et al found IL23 to be present in large numbers in Crohn's disease tissue, reporting main expression by macrophages and dendritic cells [199].

While variability was observed between the response of each line, even the smallest increase measured would have profound effects on the activation of the immune system and recruitment of macrophages and T-cells to the epithelium. Due to the positive feedback observed, this inflammatory response could certainly lead to substantial and ongoing tissue damage if measures are not in place to mute this response when required. In healthy tissue, this response is closely regulated, however in autoimmune diseases such as UC, these regulatory mechanisms can be dysfunctional or muted.

Furthermore, intestinal cell markers were analysed to determine the effect TNFα had directly upon the epithelium. The response of LGR5 was severe in response to TNFα, with an 80% reduction in expression, indicating an overwhelming loss of viable LGR5+ stem cells in the stem cell niche. This data combined with the drop in differentiated epithelial cell expression is indicative of the critical impairment of the colonic epithelium in an inflammatory environment, initiated within just 48 hours of initial exposure. This effect was substantiated by Lee et al, stating that a similar concentration of TNFα (30 ng/ml) increased necrosis of differentiated intestinal cells and caused stem cell dysfunction [200]. While this group conducted their study on enteroids isolated from

Crohn's disease patients, the data published in this thesis clearly displays a similar response in UC.

This significant upregulation of TNFα, upon TNFα exposure, gives insight into a positive feedback mechanism. This dysregulated response *in vivo* would lead to an excessive, uncontrolled inflammatory reaction within the intestinal epithelium. Over a prolonged period, this chronically exaggerated inflammatory response would result in the destruction of the epithelium and loss of function. This increased sensitivity in conjunction with positive feedback mechanisms would certainly play a role in the continual progression of disease.

Once this foundational response had been analysed, the differential responses between healthy and UC could be investigated. This will be addressed in the upcoming thesis chapter.

4.3.2 Response of Healthy Patient-Derived Colonic Epithelium to Lipopolysaccharides

LPS, a bacterial PAMP, expressed by gram-negative bacteria, is abundant in the colon under normal conditions. In patients with a healthy functioning immune system and intact epithelial barrier, LPS, prolific in the gut lumen, do not penetrate across the intestinal epithelium [201]. However, in instances of increased epithelial permeability, LPS can translocate to the basolateral membrane of the epithelium and trigger an intensified immune response [113]. In healthy individuals this effect is suspected to be short-term and resolve once the initial cause has been determined and treated. Conversely, in patients with UC, this inflammation transcends into an ongoing cyclical response that is difficult to control even with the intervention of medications. Disturbances in the TLR4 receptor pathway, activated by LPS, are proposed to be one of the potential mechanisms responsible for UC development. Therefore, LPS is an important focus of this project, to better understand the differences in UC and further elucidate the mechanisms and pathways involved.

In this chapter, we explore the effects of LPS on healthy patient-derived colonic organoids, first conducting a dose-response experiment to determine the dose which initiates the most significant response prior to toxicity. LPS isolated from two species

were investigated, both of which can be found in abundance in the colon. While the initial dose-response yielded significant results across numerous inflammatory and intestinal cell markers, there was no evidence of a reaching a maximally effective dose in the range 0-1 µg/ml. Therefore, this experiment was repeated using a broader range of LPS concentrations, reaching 100 µg/ml. Here, an increase in necrosis was evident morphologically following exposure to 100 µg/ml, indicating the maximum dose this healthy model can endure had been reached. The data showed a notable inflammatory response and decline in health of ISCs and goblet cells.

NFκB, although largely involved in the TLR4 pathway, exhibited a muted response at all concentrations across the board. The lack of change to expression can be explained and corroborated by literature in this area of study. A key explanation that has been reported is that the translocation of NFκB from the cytoplasm to the nucleus is responsible for the instigation of inflammation via either one of the TLR4-dependent pathways. This occurs following activation of NFκB via degradation of its inhibitor, IκB via ubiquitination. A study by Sakai et al, confirms this finding using reporter macrophages expressing EGFP-tagged p65 and a TNFα promoter-driven mCherry combined with live-cell imaging [202]. This group reported that NFκB translocation occurred following stimulation with LPS, (isolated from *E. coli* serotype O55:B5 supplied by Enzo Life Sciences), despite cells lacking TRIF [202]. However, in cells lacking MyD88, there was strongly reduced translocation of NFκB to the nucleus following LPS stimulation. This study confirms the findings reported in this project that, while NFκB expression remains stable this pathway requires the translocation of NFκB to initiate downstream responses. This data is backed by a study by Pang et al published in 2018 [202]. This would be confirmed by immunostaining that shall be outlined in upcoming chapters.

Additionally, direct changes to the epithelium proved evident with decreases to stem cell expression and elevated production of mucin. This increased production has also been reported by Li et al, who described a similar effect in mice following administration of a low dose of LPS, increasing the thickness of the whole mucus layer. While a small number of gram-negative bacteria still manage to successfully cross this barrier to interact with the epithelium itself, a significant number are kept at bay. Furthermore, after prolonged exposure of this mouse model to a high dose of LPS, a

substantial number of lysosomes in goblet cells exhibited reduced function, and hence, the mucus layer thickness was significantly decreased. However, this response was recorded after a very protracted period of exposure; 32 days [178]. It is, therefore, interesting to note that despite the initial increase in protective mechanisms successfully initiated by the intestinal epithelium, these begin to fail after a more extended period of time. As prolonged inflammatory presence is a key characteristic of UC, it is relevant to note this decline in mucus barrier protection over time can result in a sudden increase of bacterial translocation and systemic inflammation.

In response to these findings, the concentration that would be used in future experimentation is 100 µg/ml as this elicited a significant and notable response without compromising organoid viability beyond what is required for analysis.

As touched upon earlier, this dose response experiment was repeated with LPS isolated from a second species, *E. coli* O127:B8. Grasa et al aimed at assessing these effects on TLR4 [182]. They then measured the subsequent changes to mRNA expression and localisation of TLR4 in the muscular and mucosal tissues of the ileum following addition of *E. coli* LPS over a 2-hour period. Their findings showed a decrease in mRNA expression of TLR4, increased inflammatory presence and altered the normal contractile functioning of the ileum [182] Though the group made this claim, they have not made clear the results displaying increased inflammation. As this study utilised a rabbit model and focussed their research on the ileum, it was relevant to conduct investigation into these effects on the human colon.

Treatment with LPS isolated from *E. coli* O127:B8 appeared to generate a much more consistent response across all major inflammatory cytokines tested. This was, therefore, the species of LPS that would be carried forward in this study due to the greater level of reliability of the data for interpretation and comparison.

These investigations brought important aspects to light of the colonic response to LPS which can inform future experiments and comparisons made within this project.

4.3.3 Response of Healthy Patient-Derived Colonic Epithelium to Flagellin

After testing LPS, a commonly known bacterial PAMP, this model was used to test another PAMP, flagellin. This, too, is often expressed by commensal and invasive gram-negative bacteria and is prolific in the human colon.

Flagellin, which activates TLR5, instigated a significant and considerable reaction, with the greatest response observed in TNFα and IL8 expression.

NFκB displayed a change in expression at the lowest concentration of 25 ng/ml. Since other inflammatory effects continue to present at higher doses of flagellin, despite the lack of NFκB response, it is possible that there are also NFκB-independent inflammatory mechanisms at play. Gao et al suggest an NFκB-independent protective mechanism when human corneal epithelial cells (HCECs) were primed with low-dose flagellin aiding in wound healing [187]. Therefore, it is also likely this NFκB-independent mechanism can occur at higher pro-inflammatory doses.

IL1β displayed a similar trend in response to flagellin at this concentration, suggesting a link between the pathways driving this reaction. Datta De et al report a link between IL1β and NFκB affecting acid secretion in the gut [203]. They claim IL1β is the initiator of NFκB-mediated downregulation of gastrin. Therefore, this initial increase in IL1β expression could have driven the rise in NFκB we observe here. It seems this mechanism occurs at a 1:1 ratio, with expression of both increasing by 50% above control.

Flagellin has been found to stimulate production of IL8 in human colonic mucosa samples in addition to worsening colonic inflammation in DSS-treated mice [115]. This effect occurred only when inflammation was already present, and the epithelial integrity was compromised. It was established that this finding was due to basolateral exposure to flagellin instigating this response, a phenomenon that does not occur upon apical stimulation alone [115]. Rhee et al exposed colonic mucosa samples to 100 ng/ml flagellin for 2 and 4 hours. They reported an increase in IL8 expression of 3-fold and 4-fold, respectively. While this was a significant increase, we noted a much larger response with an increase of 6-fold that above control ($P<0.001$) at 200 ng/ml.

As stated in this chapter, in addition to the extensive inflammatory effects outlined, flagellin also had a profound detrimental impact upon the epithelium with significant effects observed across all cell markers. Limited research has been conducted into the more direct impact flagellin has upon the colonic epithelium itself, therefore this data is of significance to increase the awareness of these isolated effects, distinct from the wider cellular inflammatory response *in vivo*.

4.3.4 Infection of Healthy Patient-Derived Colonic Organoids with *Clostridium difficile* Toxins

To further validate the inflammatory profile of this platform, the response to *Clostridium difficile* toxins were determined. This experiment was conducted as a dose response experiment to best determine the concentration at which the toxins had the greatest effect while maintaining viability.

C. difficile is a gram-positive anaerobe linked with a range of disorders ranging in severity [204]. *C. difficile* typically colonises a patient's GI tract following disruption of the microbiota [204]. This could be due to antibiotic use or in patients with pre-existing dysbiosis and disease including UC.

While *C. difficile* itself doesn't directly cause inflammation in the colon, the two toxins it produces, TcdA and TcdB, trigger a severe inflammatory response. These toxins are glucosyltransferases, which are known to play a role in the inactivation of Rho, Rac, and Cdc42 in its target cells [191]. This mechanism of action has been found to disrupt the cytoskeleton, thereby expediting epithelial barrier loss of function [204]. TcdA is reported to primarily effect the intestinal epithelium, while TcdB has broader cell targets [191].

During this experiment, patient-derived colonic organoids were found to be highly sensitive to both *C. difficile* toxins A and B. In the first dose response conducted necrosis could be observed across all conditions and time points. This was evident morphologically with no viable tissue remaining for analysis. This experiment was therefore repeated with a much more conservative dose range; 10% of those tested previously. Upon repeating, the outcome was much more favourable with the majority of conditions remaining viable, with the exception of combined toxin exposure at 5 and

10 ng/ml. This highlights the potency of these toxins and the considerable damage that can be done to the colon, even at low concentrations. A previous study by Lyerly et al reported TcdB caused death in hamsters only if intestinal damage was already present or if TcdA was co-administered [205]. This suggests that both toxins may act in a coordinated fashion to elicit a much stronger and more lethal response. It has been proposed that TcdA acts initially to disrupt epithelial integrity enabling TcdB to enter epithelial cells and instigate a toxic inflammatory response [205]. This would explain why toxin A and B combined exhibited toxic effects at relatively low doses. Furthermore, TcdB alone provoked the strongest immune response which could be due to it acting more significantly when access has been gained within the cell, as suggested.

The rest of the conditions yielded interesting data, with increased expression found across all markers, especially after exposure to TcdB. The primary effects observed were as changes to NFκB and IL18 production. This is an interesting finding, indicating that toxins, while exerting a highly inflammatory response on the epithelium, target distinct pathways than previous PAMPs tested.

As evident in figure 4.10, TcdB also exerts the most severe effects upon the epithelium, with a critical drop in ISC markers and an indisputable increase in differentiated cell markers. MUC2 increased to a greater extent than in any other experiment performed previously, with a rise of 12-fold above control upon exposure to 10 ng/ml TcdB. This would result in considerable thickening of the mucus layer offering protection to the underlying epithelium. This enhanced level of protection would slow down the progression of this infection by preventing the binding of *C. difficile* to epithelial cells and subsequent invasion.

Research is still being undertaken into how these toxins enter host cells. One group investigating these mechanisms is looking further into Frizzed proteins (FZDs) and chondroitin sulphate proteoglycan 4 (CSPG4) as two major host receptors involved. Hence, once the bacteria have penetrated the mucus barrier, *C. difficile* can easily enter epithelial cells via this mechanism exposing the epithelium to a much greater bacterial load. More research is needed into these mechanisms so improved targeted therapeutics could be discovered rather than use of broad-spectrum antibiotics which, in some cases, exacerbate the issue further and lead to continued dysbiosis in the gut.

4.3.5 Conclusion

In conclusion, this chapter covers the differential responses of healthy patient-derived colonic organoids to a range of inflammatory mediators, commonly implicated or linked with UC. This has given us a clear foundational understanding of the similarities this model has to *in vivo* colonic epithelium. It is evident that these responses are largely representative of those reported *in vivo*, confirming the benefit of using this platform in the investigation of UC pathogenesis. A further benefit of a reductionist approach is that this allows the impact upon the epithelium to be better understood as well as the critical role the epithelium alone plays in the initiation of the early inflammatory and fibrotic response to be more accurately studied. The results of these experiments have informed future directions this project would take and areas that are most relevant to focus further research upon.

Chapter 5

UC Derived Colonoids Display Exaggerated Inflammatory Responses to Inflammatory Stimuli

5.1 Introduction

5.1.1 Effect of TNFα on UC colonic epithelium

TNFα is a critical pro-inflammatory mediator that has been implicated in the pathogenesis of IBD [206]. TNF is also a key cytokine produced in response to stimuli with numerous different inflammatory mediators. These include stimulation with bacteria, viruses and tumours [122]. In turn, TNFα then circulates, activating several other downstream pathways, including NFκB and MAPK [207,208]. Initiation of these pathways can then cause further production of TNFα in a positive feedback response [208]. Hence, TNFα acts upstream and downstream of these pathways, increasing the importance of research into the response of this primary cell line to TNFα and how this differs in disease.

It was therefore of great interest that our patient-derived UC colonic organoids are treated with TNFα in the same manner as the healthy counterpart as reported in the previous chapter. In line with the literature, we would expect to find greater feedback from our UC line due to the link between TNFα and IBD [209]. Our primary model derived directly from human colonic epithelial samples can provide a relevant and accurate insight into the effect of pro-inflammatory mediators directly upon the epithelium. Performing this experiment in isolation from additional factors, such as the mesenchyme and immune cells, gives a clearer understanding as to the role of each element in the pathogenesis of disease and the degree to which each contributes.

5.1.2 Differential Response to Lipopolysaccharides

Lipopolysaccharides act on a member of the TLR family; TLR4. Stimulation of TLR4 instigates receptor dimerisation and subsequent triggering of a signalling cascade promoting activation of NFκB, MAPKs and promotion of pro-inflammatory responses. This typically occurs in response to invading pathogens in the immune cells and mucosal tissue of healthy individuals. MD2 is a crucial adaptor protein required for the TLR4 response to LPS. MD2 is also known to associate with TLR2, however the bond is weaker. The TLR4 pathway diverges into 2 distinct signalling cascades; these involving separate adaptor proteins: TRIF and MyD88. These mutually exclusive pathways are known as are MyD88-dependent (TLR4/MyD88/NF-kB) and MyD88-independent or TRIF-dependent (TLR4/TRIF/IRF3).

As stated in the previous chapter, prolific LPS has been associated with the pathogenesis of IBD. Increased TLR4 expression in the intestinal epithelium of UC patients has also been reported which would have profound effects in the magnitude of the downstream immune response [110].

The differences in receptor expression, in addition to receptor localisation, are crucial to further confirm and investigate in our model. This will also provide insight into whether these differences remain following removal and ongoing culture of this tissue in a non-inflammatory environment prior to experimentation. Using this set-up, we can explore whether receptor upregulation and a shift in receptor location are present under homeostatic conditions or whether LPS alone triggers these changes. This is harder to explore in a typical *ex vivo* tissue resection as a clear picture cannot be acquired as to the state of the tissue prior to initiation of inflammation.

In this chapter we shall explore the response of UC patient-derived colonic organoids to TNFα and LPS, before drawing comparisons to that of their healthy counterparts. The alterations to downstream cytokine production shall first be investigated. The impact of pre-treatment with a TLR4 inhibitor shall then be studied to confirm that any LPS-mediated effects are instigated via the TLR4 receptor and not another independent mechanism. The localisation of the TLR4 receptor, and related proteins in this signalling pathway, shall then be determined using immunohistochemistry and immunofluorescence. To further measure the effects of LPS on this system, the

expression in the absence or presence of LPS shall then be studied to determine whether any notable differences exist which are contributing to the characteristics of UC we see both in vitro and in the patient.

5.1.3 RNA-Sequencing

RNA-Sequencing (RNA-Seq) is a high-throughput sequencing method that has become increasingly popular in recent years, largely replacing microarray techniques. RNA-Seq gives a large amount of information into the transcriptome of the cell. This technique can, therefore, provide a greater range of detail when comparing different treatment regimens or culture conditions. For this reason, it is considered a type of deep sequencing that is rapidly becoming the preferred tool for gene expression studies.

RNA-sequencing gives a sizable output with many gigabytes of data. This can be analysed using different methods. The sequences detected by this technique are then able to be recognised by pairing RNA-Seq output to gene databases that have previously been gathered from thousands of transcriptomics studies. This can generate an accurate list of the genes measured and determine whether the levels expressed are considered significant. A popular method of initial analysis includes the grouping of related genes that are reported to be linked through involvement in the same pathway or are found to be highly expressed in the same stage of development of disease. This is known as Gene Ontology (GO) analysis [210]. This type of analysis aids in focussing the analysis of such a large dataset by highlighting biological processes relevant to the experimental project. This can concentrate research on the categories with the known biology.

While, we have focussed on a distinct profile of inflammatory and intestinal markers to indicate critical differences between healthy and UC-derived colonic organoids, it was decided to utilise RNA-seq in this project to enable the identification of any other proteins and pathways potentially involved in UC development affecting the epithelium.

For the purpose of this study, focus was on multiple groups containing genes involved in important pathways of interest. These groups included genes involved in regulation

of inflammation, which are the main interest in this study for investigating the development of UC and TLR4/LPS signalling pathways. Additional groups included in this analysis comprised of those involving stress response pathways.

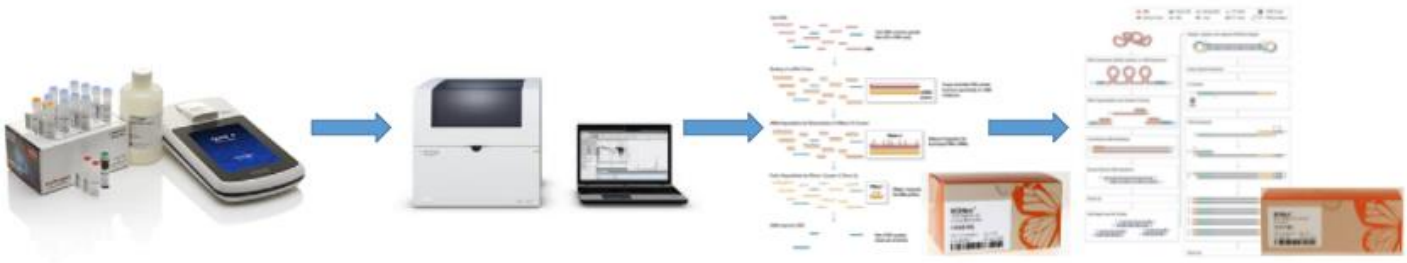

Figure 5.1: Workflow of sample preparation for RNA-Sequencing.

5.1.4 Aim & Hypothesis

Aim: We aim to investigate differences in the response between healthy and UC patient-derived colonic organoids upon stimulation with pro-inflammatory mediators, TNFα and bacterial PAMP, LPS.

Hypothesis: We hypothesise that a significant differential response will be observed between healthy and UC human-derived colonic organoids, when subjected to TNFα and LPS, that can be quantified.

5.2 Results

5.2.1 Differential Response of Healthy & UC-Derived Colonic Organoids to TNFα

Data in Chapter 4 demonstrated that exposure to TNFα elicits a strong inflammatory response in healthy colonoids, while simultaneously resulting in the loss of colonic stem and differentiated cell types. Once data had been acquired with regards to the response of healthy colonic organoids to universal pro-inflammatory mediator, TNFα, the experiment was then repeated on UC organoids. Once the healthy response to TNFα had been ascertained, the inflammatory and intestinal profiles could then be compared to UC and any differences indicated.

Hence, both healthy & UC-derived lines were treated with 40 ng/ml TNFα over a 48-hour period via addition directly to the media. All cell material was gathered, lysed and analysed. In healthy organoids TNFα was previously found to initiate a significant rise in TNFα expression of 40-80-fold, however the effects upon our UC organoids were much more considerable. An average increase of approximately 500-fold above the untreated UC control was recorded (Figure 5.2A). This is highly indicative of UC organoids being hyper-sensitive to stimulation with TNFα.

This result suggests that, like the clinical observation, UC derived colonoids initiate an exaggerated inflammatory response when exposed to inflammatory mediators, with TNFα being such a critical cytokine, essential for mounting an immune response across multiple pathways. This increased TNFα mRNA expression in UC organoids to TNFα itself, suggest our platform could provide important insight into the pathological effects we observe in UC. Despite UC patient-derived organoids being cultured long-term in favourable non-inflammatory conditions, it appears there is an underlying genetic predisposition exhibiting a tremendous effect on their response when transferred to a pro-inflammatory environment. This is despite having been removed from the inflamed *in vivo* environment months prior. Due to time constraints, the samples were not sent for whole sequence or SNP genotyping, therefore it is of course not possible to resolutely conclude the response observed in our lines is due to a genetic predisposition. However, it's well known that polymorphisms in genes relating to TNFα expression are present in IBD patients [211]. Hence, while it is reasonable to

assume these differences between our organoid lines are a result of these mutations, further genomic analysis would be required to make firm conclusions based on these findings.

This inflammatory profile pattern was then observed in several other genes implicated in the inflammatory response. UC organoids further showed a muted response of both NFκB (Figure 5.2B) and IL8 (Figure 5.2D) mRNA expression and a tremendously heightened response from the UC line. While similarities to this trend can be observed in IL1β and IL23 expression (Figure 5.2C & E), the response of healthy organoids was more intensified than in other markers, demonstrating a significant difference between TNFα-treated and control. Despite this, a clear differential response remained evident between healthy and UC-derived samples. IL1β displayed a 2.5 times greater UC response when compared to the healthy treated control and a 10 times increase was measured in IL23 expression.

The data demonstrates the response of colonic epithelial cells to be more variable. As can be observed in figure 5.2, both healthy and UC organoids exhibit opposing reactions to TNFα exposure, with a sudden drop of 80% below control observed in our healthy condition while UC-derived organoids present a 4-fold rise in crypt stem cell marker expression, LGR5 (Figure 5.2F). To further support this finding, OLFM4 also displayed a relatively muted response in our healthy organoids, while an increase of 150 times was measured in our UC-derived line. This is likely a projection of the increased inflammation, in line with the pattern of expression observed in TNFα, NFκB and IL8. These responses differ entirely, affecting the overall quantity of ISCs present within the epithelium and is therefore an important differential response to consider.

Considering the interesting results observed so far, we decided to extend our characterisation of genes into those that are important for epithelium maintenance/homeostasis and functionality. Interestingly, very little change in villin mRNA expression was observed in either organoid line (Figure 5.2H), with any shift in expression proving insignificant. This data suggests that the main effect of TNFα on the colonic epithelium is to induce an inflammatory response and influence colonic stem cell activity. Conversely, significant alteration was displayed in MUC2 expression (Figure 5.2G). This could be indicative of a change to the overall number of goblet cells or to mucin expression specifically. The data shows the negative impact TNFα

inflicts upon the healthy colonic epithelium's ability to produce a defensive layer of mucus, essential for protection against bacterial invasion. Reduced mRNA expression of mucus constituent, MUC2, was observed with a considerable drop of 50%. Undoubtedly, this reduction could potentially halve the protective benefits of the dual-layered mucus barrier. However, the impact upon organoids derived from UC patients was much greater, dropping to below 10% that of control. This fall in mRNA expression, if translated to the proteomic level, could affect the barrier functionality of the epithelium and may result in additional exposure of epithelial cells to inflammatory stimuli such as bacteria and bacterial PAMPs. The fact that a disease such as UC is compounded by prolonged and exaggerated inflammation, this finding would result in serious detrimental effects to colonic health and the ability to regenerate in periods of reduced inflammatory presence.

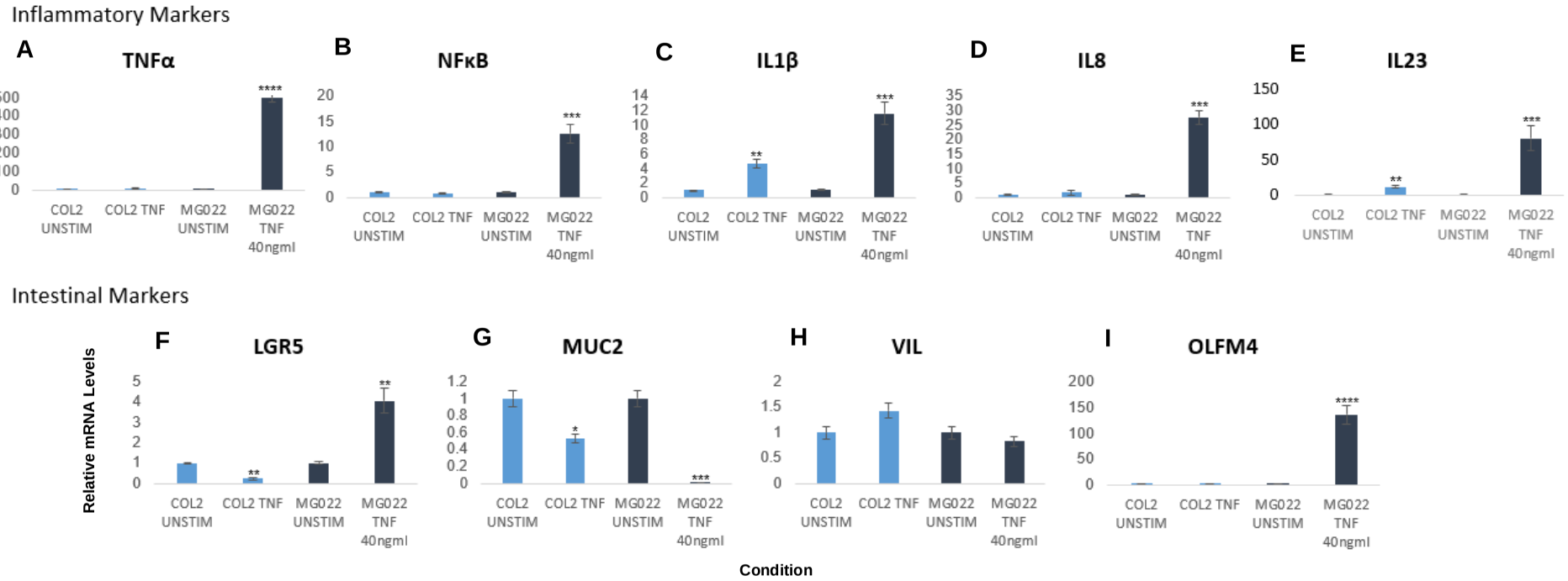

Figure 5.2: Effect of TNFα (40 ng/ml) on the inflammatory profile & intestinal cell expression of healthy & UC patient-derived colonic organoids. Cell material collected from 3 wells per condition. Statistical analyses were performed by two-sided students t-test. Data are expressed as mean ± SD of each group. *P < .05; **P < .001; ***P < .0001. N=3 (Technical replicates)

The effect on mucin expression was an interesting observation and suggests a potential mechanism whereby an initial inflammatory stimulus may expose the colonic epithelium to pathogens in the colon. The main receptors responsible for sensing viral and bacterial PAMPs in the body are the Toll-like receptors (TLRs). Therefore, we were interested in assessing expression of TLR mRNA in colonic epithelium following exposure to TNFα.

Further qPCR analysis was performed to assess baseline and inflammation induced expression of prolific PPRs, TLRs 1-5.

There was a clear differential response to TNFα in UC across all TLRs measured, with very different TLR expression compared to control (Figure 5.3). Expression of TLRs 1, 2, 4, & 5 were elevated in TNFα-treated UC organoids (Figure 5.3 A, B, D & E), responsible for sensing TNFα, lipopeptides, LPS & flagellin, respectively. However, TLR3 expression, responsible for viral recognition, was decreased (Figure 5.3C). The mRNA expression levels of several TLRs are significantly higher in UC with the largest increases in expression recorded for TLR2 & TLR4 (Figure 5.3B & D), with a 28-fold and 9-fold increase, respectively.

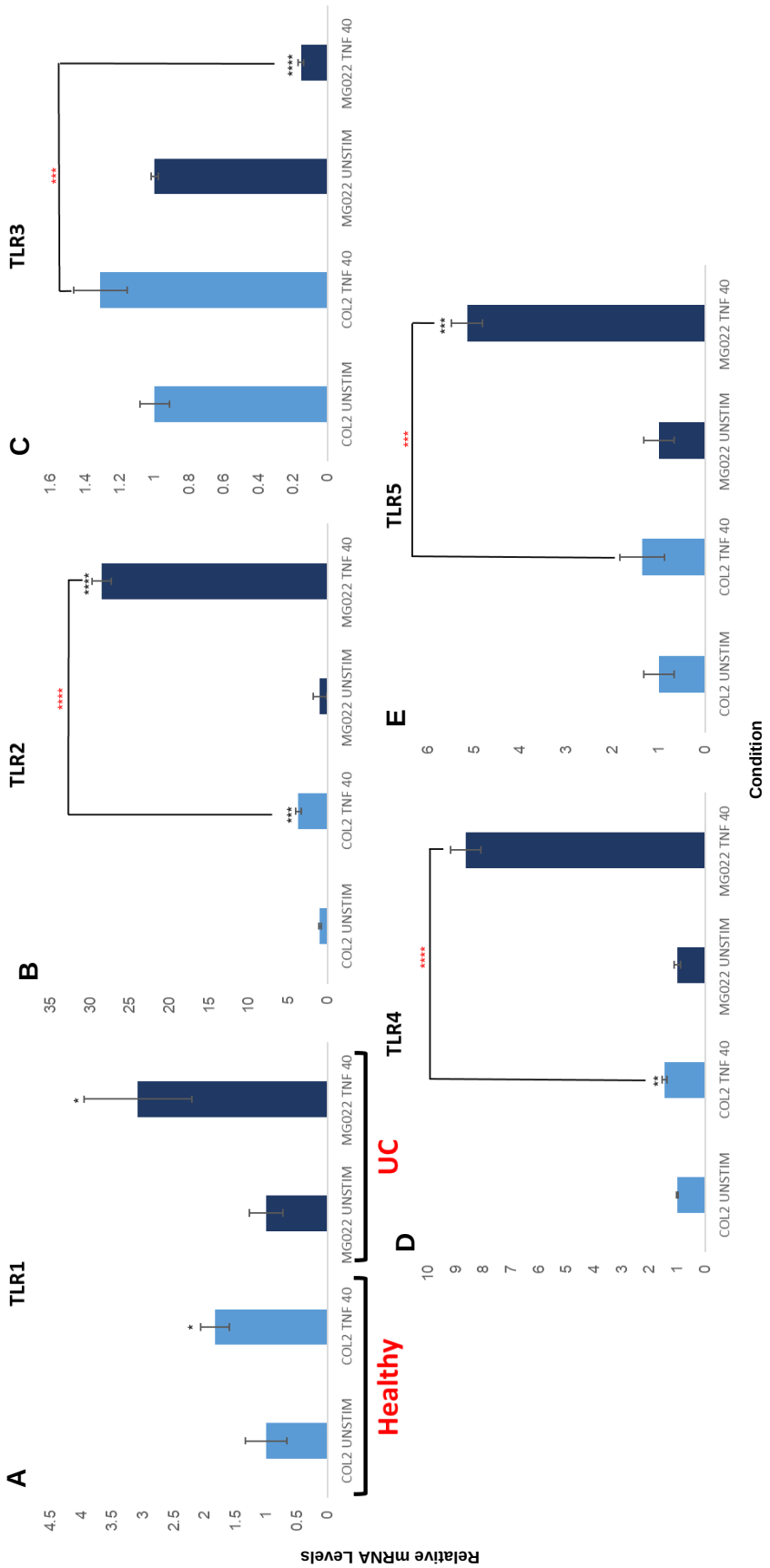

Figure 5.3: TNFα (40 ng/ml) induction of TLRs in healthy & UC organoids shows clear disease phenotype. UC organoids respond to a significantly greater degree to TNFα induction with expression of TLR1, 2, 4 & 5 all rising substantially above treated healthy organoids after a 48-hour treatment period, as demonstrated by qPCR. Statistical analyses were performed by two-sided students t-test. Data are expressed as mean ± SD of each group. *P < .05; **P < .001; ***P < .0001. N=3 (Technical replicates)

5.2.2 Differential Response to Lipopolysaccharides

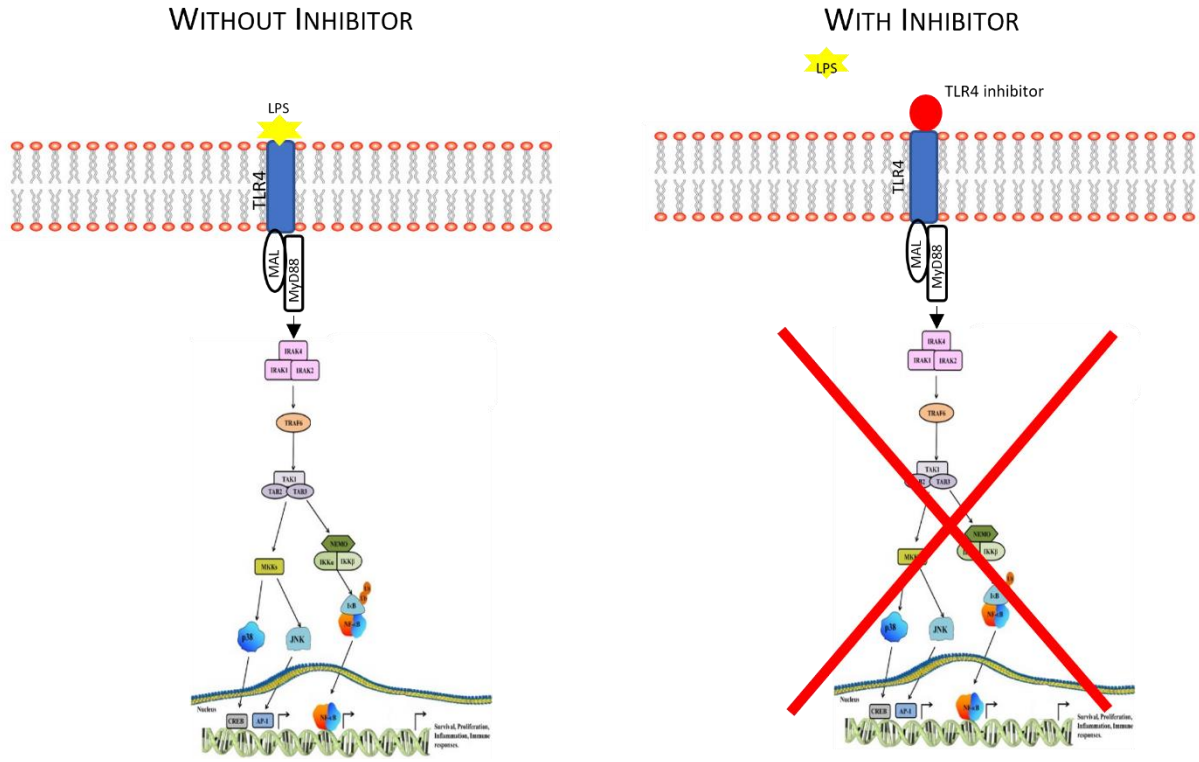

Figure 5.4: Schematic outlining the TLR4/LPS signalling pathway and the effects of TLR4 inhibition.

Our results suggest an inflammatory stimulus not only induces increased expression of pro-inflammatory cytokines in UC organoids compared to healthy, but also induces up-regulation of TLRs. To test if this increased expression in TLR mRNA levels translates to an increased sensitivity to pathogens found in the colon, intestinal organoids were exposed to flagellum and LPS.

The morphological images below reveal the visible changes that are apparent following treatment with LPS (Figure 5.5). The highest concentration found to exhibit a reaction in the previous experiment, 100 µg/ml was utilised in future experiments, as this was found to elicit the most significant effect in the absence of toxicity. As figure 5.5 displays, chronic exposure of organoids to 100 µg/ml LPS triggered a necrotic response that generated visible changes to the epithelial organoids signalling destruction (5.5B & D). Enough viable material remained for each condition to be isolated and prepared for RNA extraction, cDNA synthesis and RT-PCR. This data would reveal whether this effect could be extrapolated to the cellular level in terms of an inflammatory outcome. These results are presented in figure 5.5.

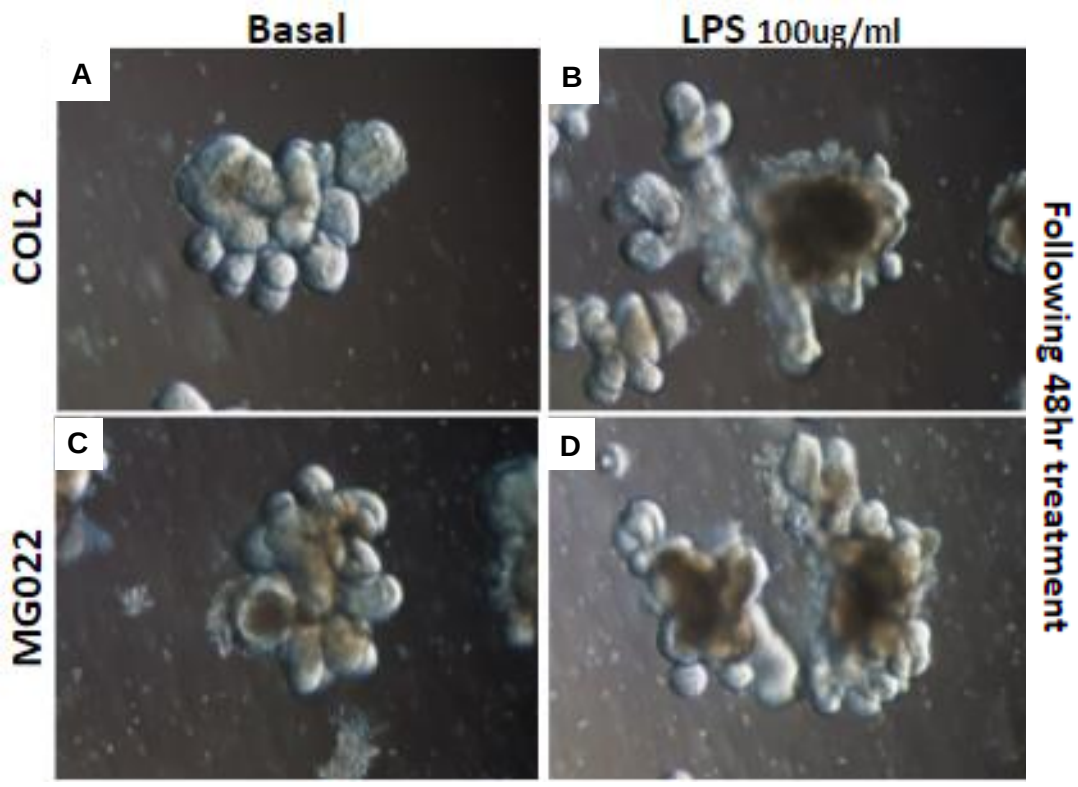

Figure 5.5: Morphology images of healthy & UC-derived organoids infected with LPS at a concentration of 100 µg/ml over a 48-hour period. Both lines appear to be substantially affected by this prolonged exposure with necrosis visible, suggesting a detrimental impact that was to be further investigated later in depth. Imaged on Zeiss Axio light microscope at 20X magnification.

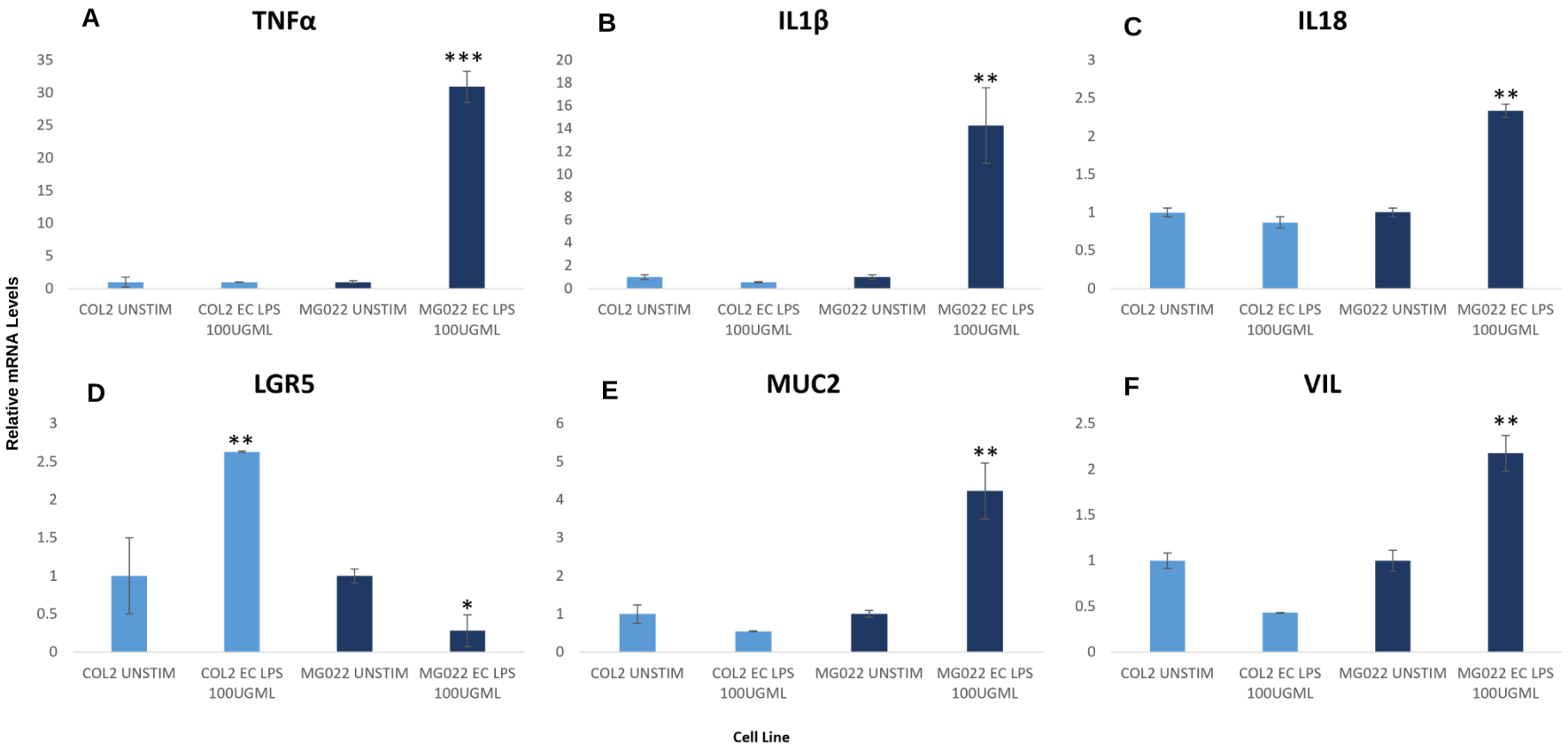

Figure 5.6: Effect of LPS isolated from *E. coli* 0127:B8 (100 µg/ml) on the inflammatory profile & intestinal cell expression of healthy & UC patient-derived colonic organoids. Cell material was obtained following 48-hour treatment time from wells in triplicate. Statistical analyses were performed by two-sided students t-test. Data are expressed as mean ± SD of each group. *P < .05; **P < .001; ***P < .0001. N=3 (Technical replicates)

This experiment was inclusive of 4 conditions: untreated healthy; treated healthy; untreated disease and treated disease. All treated were performed in conjunction over a 48-hour period. Initial treatment involved exposure to 100 µg/ml LPS, isolated from *E. coli*, in the absence of any inhibitor. This would highlight the fundamental differences between the healthy and UC epithelial response to the most prolific PAMP in the colon.

A significant discrepancy between the response of healthy and UC lines is clearly visible and considerable across all inflammatory markers. The most marked differences were observed in TNFα and IL1β production (Figure 5.6A & B), with a 30-fold increase in expression of the former, in our UC-treated condition and a 15-fold increase of the latter. This response is even more remarkable due to the stark contrast to the muted healthy response to LPS, seen here and in the previous dose response experiments reported in Chapter 4.

Furthermore, IL18 expression displayed a significant rise of 2.5 times greater than the equivalent untreated control in our UC line only (Figure 5.6C). Interestingly, we found in the healthy line a slight drop in IL18 expression of approximately 20%. This result shows a distinct similarity to the changes observed to IL18 expression in the initial dose response experiment. However, the decrease in expression was more prominent, with a drop of 70%, following exposure to 100 µg/ml LPS. This replicable result suggests the healthy colonic epithelium possesses a negative feedback response at high concentrations of LPS, possibly inclusive of IL18. This effect appears not to be present in UC tissue.

The effects of LPS extend to the epithelium, with LGR5 significantly affected in both healthy and UC organoid lines (Figure 5.6D). However, the data depicts opposing influences between the two. LGR5 expression was increased 2.5-fold above untreated control in healthy tissue-derived organoids, whereas a detrimental decrease was measured in our UC line, displaying a 70% decrease. This data suggests that while healthy tissue retains the ability to increase stem cells in an attempt to counteract the damage inflicted by pathogenic bacteria, this initial protective measure is not present in UC. The immediate drop detected in ISC expression in UC would have a notably disadvantageous effect, even in the occurrence of a short-term infection.

This differential response also extended to villin, with virtually no alteration in expression following addition of LPS in COL2 (Figure 5.6F). Conversely, a significant 3-fold increase was observed in the UC line, MG022. This data displays the vast disparity in the sensitivity of healthy- and UC-derived epithelial tissue to LPS. This disparity wasn't observed in MUC2 expression as both patient-derived lines displayed the same reduction of approximately 20% (Figure 5.6E). However, this change in expression proved to be insignificant, signifying LPS as having a greater effect on colonic stem cells and colonocytes than goblet cells.

Once this differential response had been established, the experiment was then repeated, inclusive of a commercial TLR4 inhibitor (Figure 5.7 & 5.8). Addition of a TLR4 inhibitor would primarily confirm whether the response we have previously reported, (Figure 5.6), was generated as a result of LPS activating the TLR4 signalling pathway via the TLR4 receptor. If this was the primary pathway activated, then addition of a specific inhibitor would prevent many of the extreme effects observed.

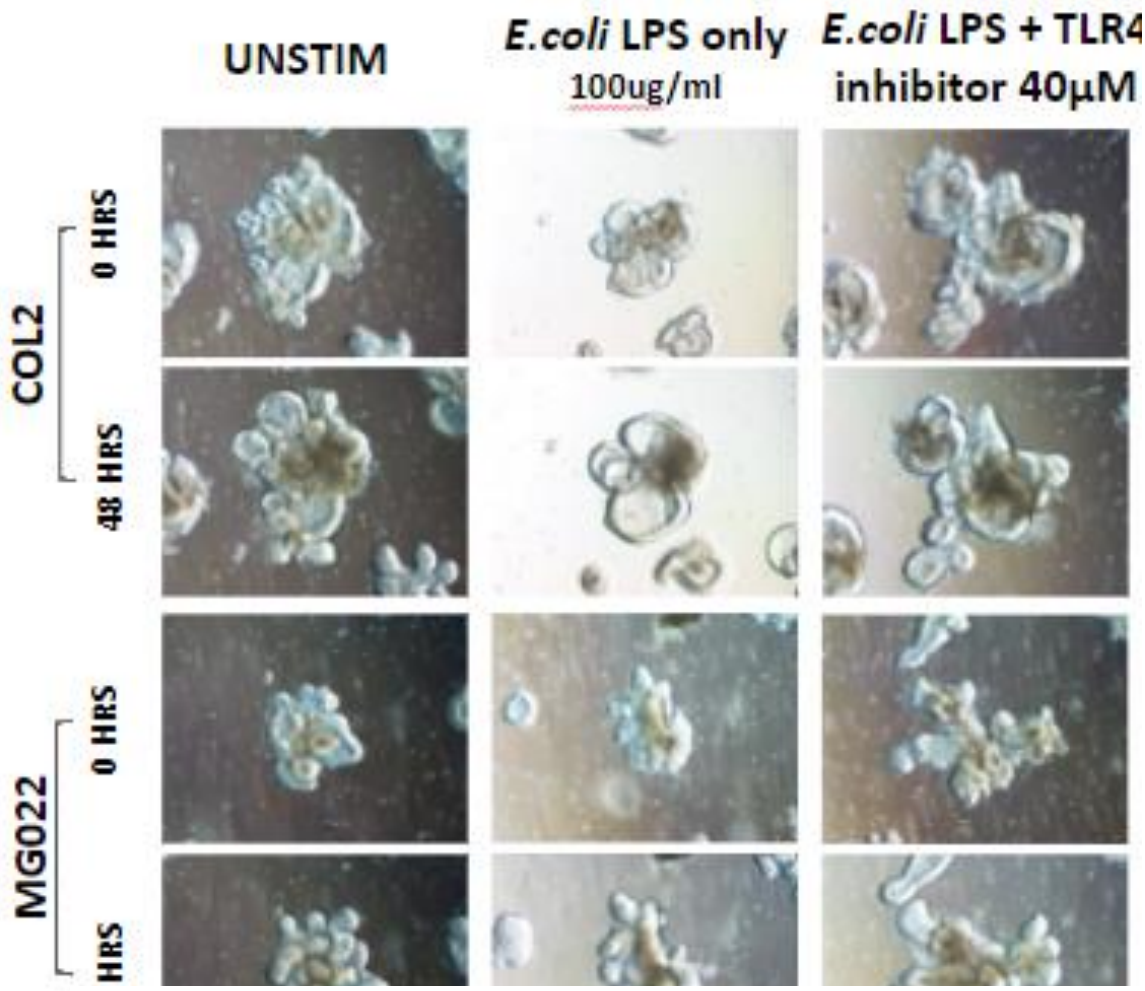

Figure 5.7: Morphology images of healthy & UC-derived organoids infected with LPS only (100 µg/ml) or LPS combined with TLR4 inhibitor (40 µM) over a 48-hour period. These images reveal little as to the effects of these conditions upon the patient-derived organoids, therefore more experimentation was required. Imaged on Zeiss Axio light microscope at 20X magnification.

Images were taken prior to a treatment, displaying a healthy intact folded epithelium. A commercial TLR4 inhibitor (cat no. # SML0832) was then added to the culture medium for 48 hours to maximise the competitive binding time of the inhibitor to the TLR4 receptors. After this treatment period, *E. coli* LPS was administered in conjunction with the TLR4 inhibitor for a further 48 hours.

Figure 5.7 displays the morphological state of the organoids prior to any treatment which can then be compared to the effects following 48 hours of LPS + TLR4 inhibitor treatment. 48 hours labelled in this figure represents 48 hours of combined treatment, however this is 96 hours after the first images were taken due to the additional 48-hour pre-treatment period.

While there was some debris build-up in the lumen of the organoids following completion of the experiment, this is likely due to the natural sloughing of cells during epithelial turnover as a result of the prolonged experimental period.

Organoids remained viable during this period across all conditions therefore cell material could be gathered and analysed. No other visible changes could be identified following incubation with TLR4 (Figure 5.7). The effects were further investigated to determine whether any fluctuations would be evident at a genetic level.

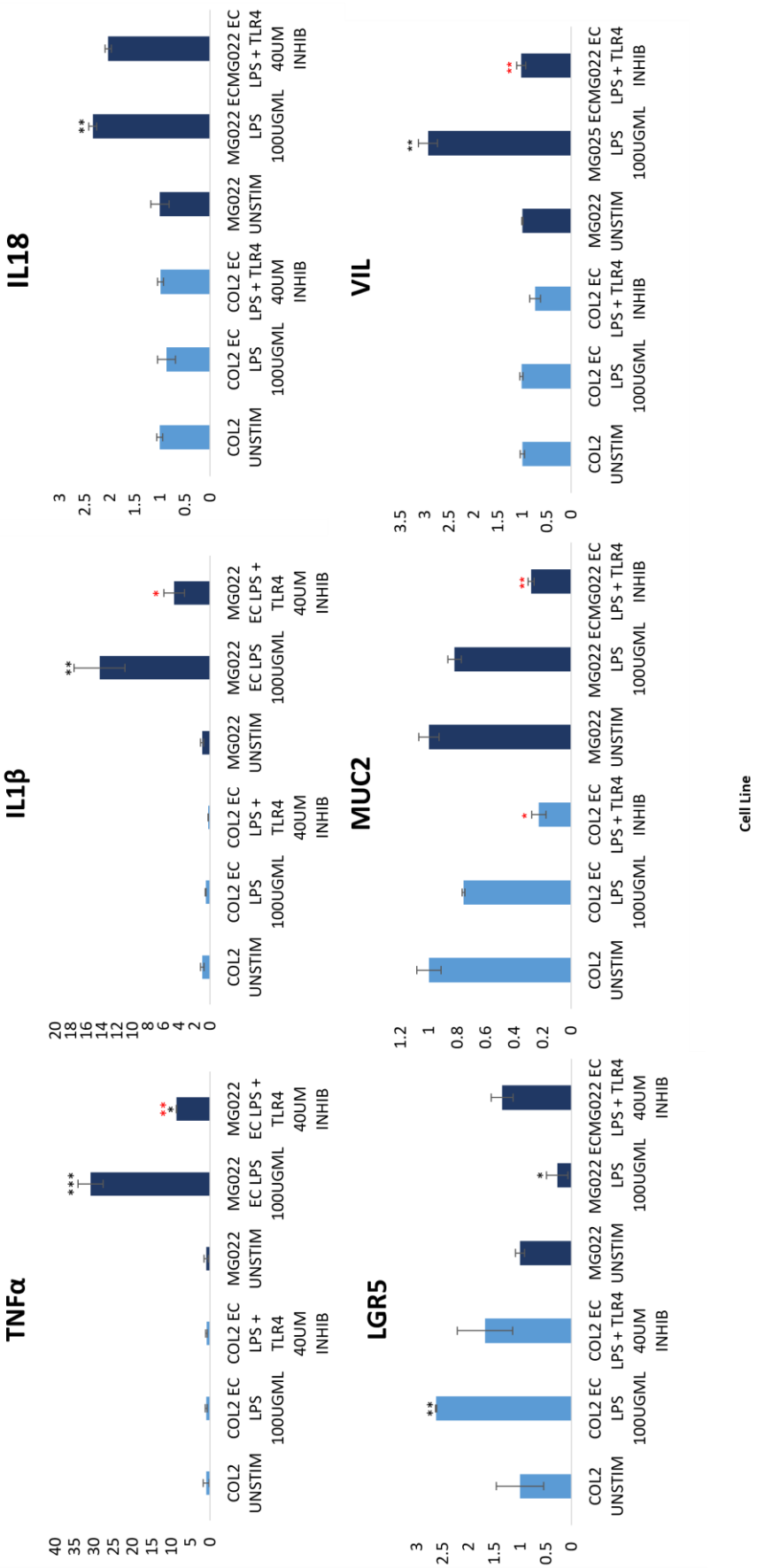

Figure 5.8: *E. coli* LPS (100 µg/ml) induces inflammatory response, altering expression of key inflammatory and intestinal cell markers. This effect is then reversed by TLR4 inhibition (40µM). Statistical analyses were performed by two-sided students t-test. Data are expressed as mean ± SD of each group. *P < .05; **P < .001; ***P < .0001 relative to unstimulated. N=3 (Technical replicates)

As observed in the initial experiment, exposure of healthy organoids to LPS, in the absence of a TLR4 inhibitor, elicited a very muted response. While in our UC organoid line the same increase of 30-fold expression is evident. This was a highly significant finding, with a clear differential response between tissue isolated from healthy and UC-diagnosed individuals. However, pre-treatment with a TLR4 inhibitor, instigated a very notable reduction in TNFα expression, with a drop of 70% measured below those exposed to LPS alone (Figure 5.8A). This is a very strong indication that LPS is acting via the TLR4 pathway specifically.

Furthermore, we find that TLR4 inhibition reduces IL1β expression, in healthy organoids, even dropping below baseline levels. Following a 15-fold increase in IL1β in the UC-derived line, TLR4 inhibition displayed a similar effect to that observed on TNFα, with a reduction of 60% below the LPS-only-treated condition (Figure 5.8B).

In healthy tissue, when LPS elicits no or minimal response, such as is the case with IL18, TLR4 inhibitor has no significant effect upon expression. This signifies that TLR4 inhibitor only yields a measurable response when inflammation is present, further substantiating that it is acting to inhibit LPS only. Therefore, if no inflammatory response is elicited by LPS then, while TLR4 inhibitor is still bound to its relevant receptors, no change is detected. Although LPS raised IL18 expression in our UC line by 2.5-times basal levels, TLR4 inhibition had a rather subdued effect under these conditions, with a minimal reduction in expression (Figure 5.8C). This result implies that the IL18 response under inflammatory conditions may be partially driven via the TLR4 pathway and possibly another inflammatory pathway.

We then turned our focus to the intestinal profile, to determine whether the TLR4 inhibitor can mitigate some of the effects we had reported earlier in the chapter. As previously mentioned, LPS appears to have a stimulatory effect on ISC proliferation in healthy organoids, with an increase of 2.5-fold above control. TLR4 inhibitor reversed this effect to some extent, however this reduction didn't appear to be significant. While the opposing effect was observed in UC, with a 70% drop in expression caused by LPS exposure. This negative impact upon LGR5+ cell expression was entirely reversed by pre-treatment with the TLR4 inhibitor (Figure 5.8D). This is a very promising result as reversal of this effect could limit the damage inflicted upon the epithelium and its ability to regenerate following a dysregulated response to LPS.

As we observed earlier, MUC2 expression was similarly affected by chronic LPS exposure, with a 25% dip in expression compared to each untreated control. Interestingly, TLR4 inhibitor also exhibited similar effects upon each line, however this resulted in a further 50% decrease (Figure 5.8E). While, this result is consistent across healthy and UC organoids, the further reduction is an unexpected finding.

According to the trend we observed in the other pro-inflammatory marker profile, villin remained relatively unaffected in the healthy line following addition of LPS alone. Due to the lack of effect by LPS, addition of TLR4 inhibitor had little effect on the expression of villin when added in combination. Conversely, LPS initiated a 3-fold increase in villin production in UC-derived organoids, which was entirely reversed by the pre-treatment with TLR4 inhibitor competitively binding to LPS receptors (Figure 5.8F). This is a noticeably strong effect exhibited by the TLR4 inhibitor, signifying that any change to villin transcriptomic expression, in addition to the other intestinal markers, is due to LPS binding to and activating TLR4 receptors and its subsequent downstream pathway.

5.2.3 Confirmation of Differential Response in Healthy & UC Patient-Derived Organoids by Immunohistochemistry and Immunofluorescence

Once an initial expression profile had been ascertained, the next step was to establish whether these differential responses are, in fact, translated to the proteomic level. Primarily, immunohistochemistry and immunofluorescence techniques were applied for this purpose. Immunohistochemical staining, as displayed in figure 5.9, demonstrates is clear expression of both pro-inflammatory and intestine-specific markers. The expression of CDX2 demonstrates the presence of differentiated colonocytes within these organoids. Other proteins present displayed positive expression and correct localisation, with MUC2 expressing selective intermittent expression, thereby depicting the spread of goblet cells throughout the epithelium. Additionally, villin displays specific apical localisation as is present in the *in vivo* colonic epithelium. This data, therefore, demonstrates that the tissue-derived organoids generated in this project have retained their intestine-specific structural features and functional properties *ex vivo*.

Once expression of structural, functional and inflammatory proteins had been accounted for, thereby confirming the validity of this platform for disease modelling, the differences between these healthy and UC tissue-derived organoids, could then be established. Initial findings show CDX2 to remain largely stable in the healthy organoid model, in response to LPS, with all nuclei displaying comparable strength staining between conditions. E-cadherin, a protein expressed on the cell surface of most epithelial cells; vital in maintaining cell-cell adhesion and epithelial integrity; appears to be unaffected by LPS exposure in the healthy epithelium. This result was also observed in another protein responsible for structural integrity of the epithelium, villin. Conversely, the presence of MUC2 showed a distinct increase in an inflammatory environment, while being essentially restored to an extent upon culture with a TLR4 inhibitor. Still, greater levels of MUC2 protein remained in comparison to basal conditions.

Changes to levels of inflammatory-related proteins were greater as demonstrated by TLR4 expression, in conjunction with that of MD2, increasing in response to LPS.

TLR4 is clearly restricted to the basolateral membrane under basal conditions in healthy organoids, whereas this appears to differ upon induction of inflammation with both basolateral and apical expression present. This effect is reversed with TLR4 inhibition.

As expected, under basal conditions, NFκB is diffuse within the cytoplasm due to it being in its inactive state. While there is some potential nuclei-based expression upon induction of inflammation, NFκB remains largely located in the cytoplasm of healthy epithelial cells.

These findings diverge widely from those depicting the UC inflammatory response at the proteomic level. LPS exposure appears to exhibit a much more substantial effect on both intestinal and inflammatory proteins alike. While all intestinal proteins were present in UC organoids with the correct localisation, changes to their expression levels were noted (Figure 5.10).

One instance of this was a drop in homeobox transcription factor, CDX2, upon LPS induction. This is observed concurrently with a dramatic increase in villin, in concordance with previous findings from transcriptomic data. Furthermore, TLR4 inhibition reversed this effect. TLR4 and MD2 staining can disclose whether the numerous changes recorded are due to alterations in the quantity of receptors expressed or the orientation of these receptors within the cell. The staining reveals a noticeable change in TLR4 presence within the organoids upon 48-hour LPS exposure. Of note, the majority of these TLR4 receptors appears to be localised on the apical membrane in all treatment conditions, while the expression returns to basal levels with the addition of a TLR4 inhibitor. Similar findings were uncovered for MD2, with a rise observed under inflammatory conditions, followed by a return to normal expression following inhibition. The initial rise was, however, to a lesser extent to that seen in TLR4 staining. The expression profile matched that of TLR4 with largely apical expression. Interestingly, TLR4 expression in unstimulated UC organoids was lower than that of our healthy line, followed by an excessive increase upon LPS stimulus, thereby corresponding with our later RT-PCR data.

Contrary to healthy data, NFκB localisation did differ under inflammatory conditions, with widespread translocation to the nucleus, signalling its activation. It is this

translocation that then enables transcription of various pro-inflammatory genes and the initiation of subsequent events.

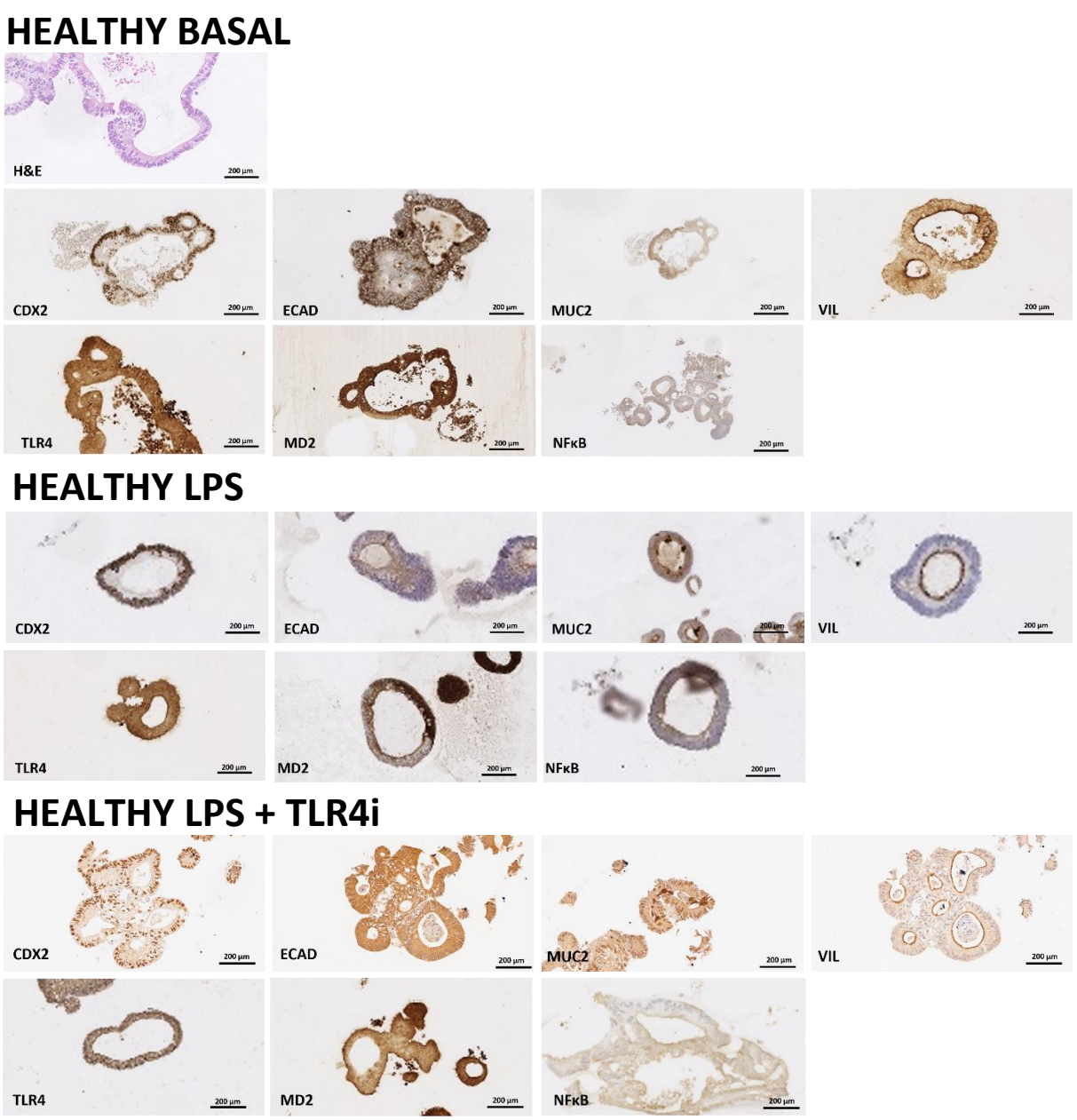

Figure 5.9: Images obtained via immunohistochemistry representing intestinal and inflammatory proteins expressed in healthy organoids following 48-hour treatment. These images present clear differences in the same line upon exposure to LPS (100 µg/ml) at the protein level, which appears to be rectified by the 48-hour pre-treatment of a TLR4 inhibitor (40 µM). Imaged on Zeiss Slide Scanner microscope at 20X magnification. Resolution = 2240 x 1600 pixels

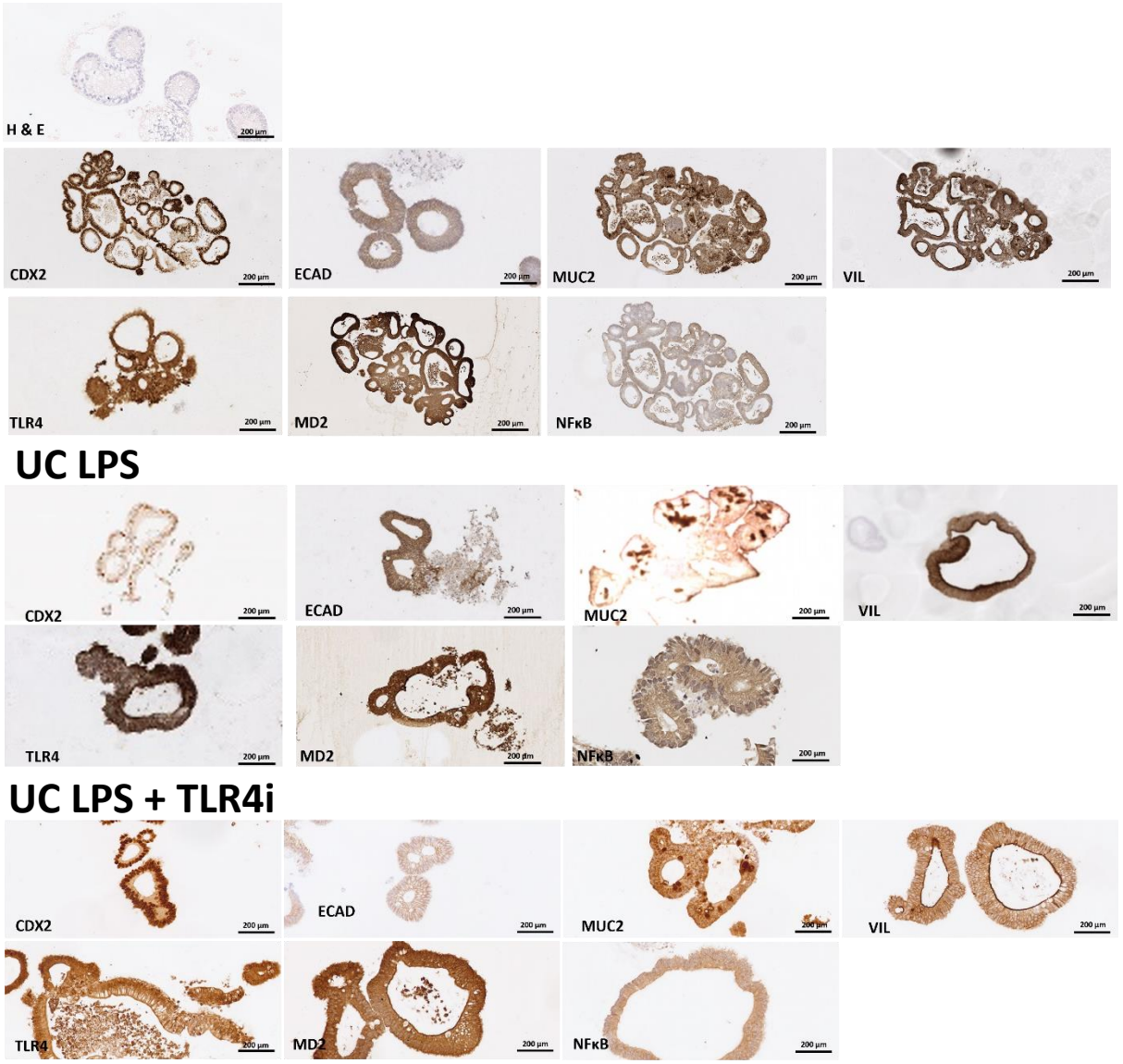

Figure 5.10: LPS (100 µg/ml) triggers a strong change in expression across both intestinal and inflammatory proteins in UC patient-derived organoids. These images support previous transcriptomic data with regards to the fluctuations we see in each protein in the panel. Imaged on Zeiss Slide Scanner microscope at 20X magnification. Resolution = 2240 x 1600 pixels

Whilst immunohistochemistry revealed important information into the relative expression of various proteins-of-interest, immunofluorescence was then performed to garner insight into their relative locations to one another. Proteins stained for in this experiment capture both structural and inflammatory elements, revealing differences between lines, as well as between conditions.

Epithelial-specific proteins, villin and CDX2, were initially co-stained to give a clear indication as to their relative location within the 3D structure (figure 5.11). Further to providing insight into the apical-basolateral orientation of the organoid, any changes to the structural and functional dynamic can be ascertained upon exposure to LPS. Structural protein, villin, is distinctly expressed in these organoid lines, however, there appeared to be a lower level of baseline expression in healthy organoids. LPS-treated UC organoids clearly display the highest level of expression amongst the sample conditions, consistent with transcriptomic findings. Moreover, the same pattern of expression was observed in CDX2 with LPS-treated UC organoids exhibiting the greatest level of expression. Levels of adhesion protein, ECAD, however, are highly expressed in inflamed healthy organoids and remain constant in those incubated in the presence of LPS. On the other hand, ECAD levels appear to drop in UC organoids upon LPS exposure.

TLR4 staining does not present as clear as in immunohistochemistry, with staining appearing diffuse and non-specific. While, a precise idea of location is not provided, the overall expression levels of TLR4 does differ between conditions. Changes to Mucin-2 are also evident between basal and LPS-treated conditions with mucin production greater in an inflamed environment (figure 5.12).

Co-staining of villin and TLR4 was performed to determine whether the localisation of TLR4 could be ascertained as being apical or basolateral. Very clear and specific villin staining can be seen in figure 5.13. In healthy organoids, the levels of villin expression appears to be comparable between basal LPS conditions, consistent with previous findings. Alternatively, the signal is substantially stronger for LPS-treated UC organoids. TLR4 receptor expression remains low level in our healthy organoid model with apparent basolateral orientation evident. Expression is greater in LPS-treated UC organoids, which supports our transcriptomic data. The localisation, however, is much

less specific and appears to be diffuse, with neither apical nor basolateral positioning obvious.

MD2 staining gives a clearer picture with noticeable basolateral orientation in healthy organoids, while appearing lowly expressed. This positioning acts to minimise exposure to bacteria present in the colonic lumen *in vivo*. On the contrary, UC-derived organoids express MD2 to a much higher degree, with both apical and basolateral expression evident (figure 5.14).

Densitometry was performed on these images using ImageJ for relative quantifiable comparison between protein expression changes. This data is provided in Appendix 3.

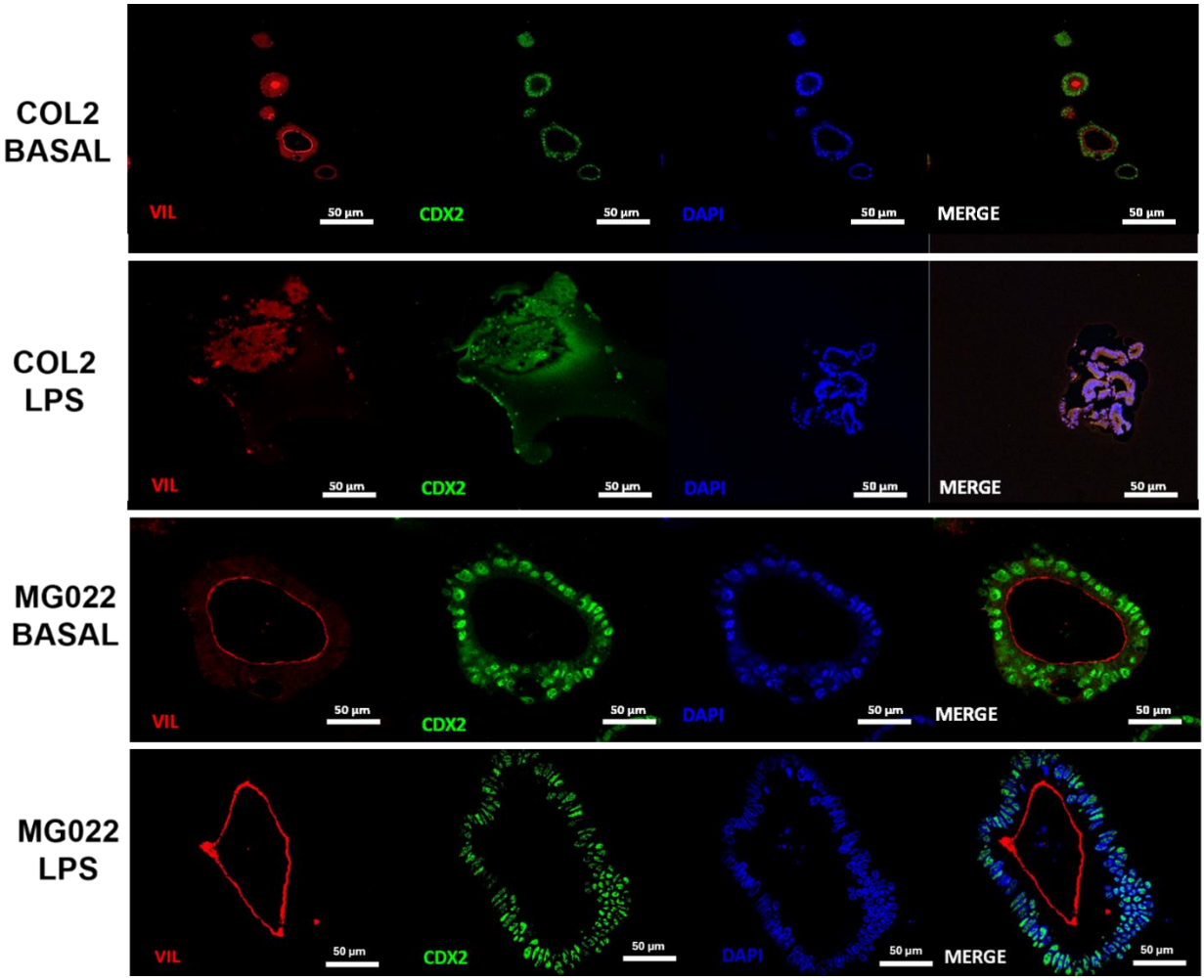

Figure 5.11: Detection of Villin and CDX2 protein in healthy and UC patient-derived colonic organoids in the absence and presence of LPS (100 µg/ml) over a 48-hour period. Healthy organoids display a muted response to LPS, while UC organoids display an increase the presence of both proteins. Imaged on Zeiss Elyra Super Resolution Microscope at 20X magnification. Resolution = 2049 x 2049 pixels (72 DPI)

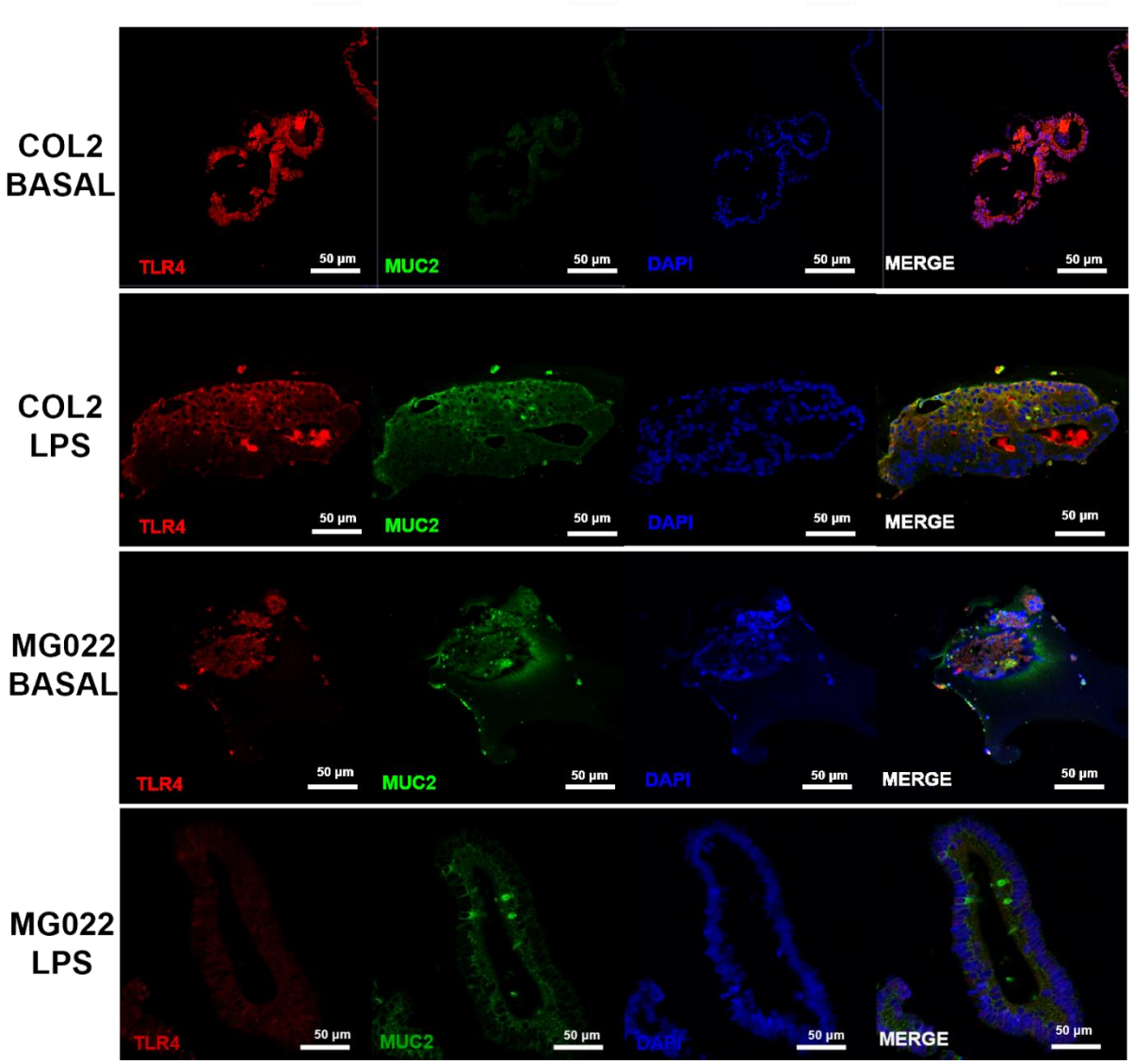

Figure 5.12: Detection of MUC2 and receptor, TLR4, via immunofluorescence staining in the absence and presence of LPS (100 µg/ml). Mucin production is higher in UC organoids under inflammatory conditions in comparison to inflamed healthy organoids. Imaged on Zeiss Elyra Super Resolution Microscope at 20X magnification. Resolution = 2049 x 2049 pixels (72 DPI)

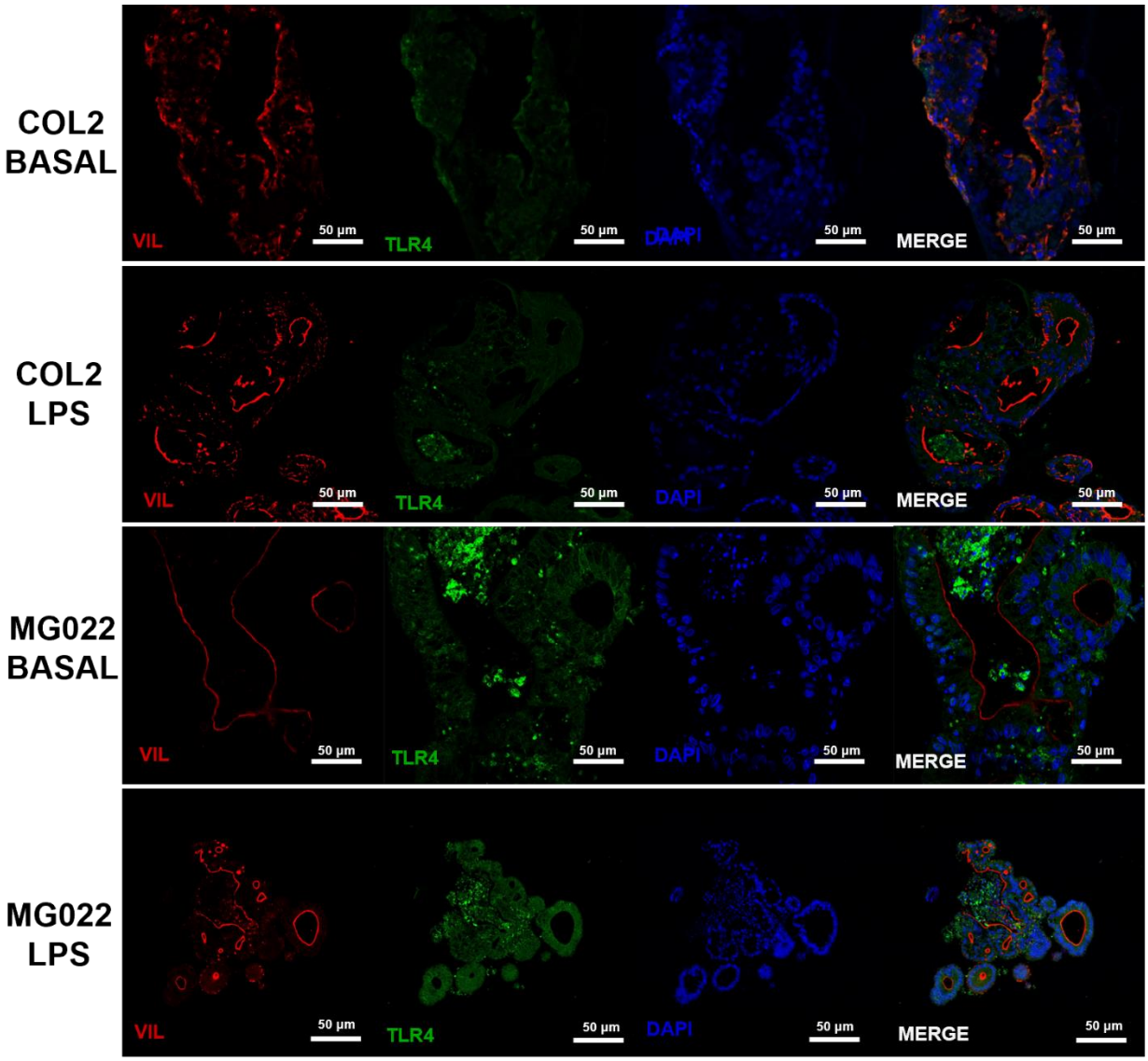

Figure 5.13: Co-staining of villin and TLR4 in healthy and UC epithelial tissue-derived colonic organoids in the absence and presence of LPS (100 µg/ml). Villin remained consistently expressed in healthy organoids with fluctuations noted in UC organoids. Basolateral expression of TLR4 can be seen in healthy organoids, while UC tissue appears to be located apically. Imaged on Zeiss Elyra Super Resolution Microscope at 20X magnification. Resolution = 2049 x 2049 pixels (72 DPI)

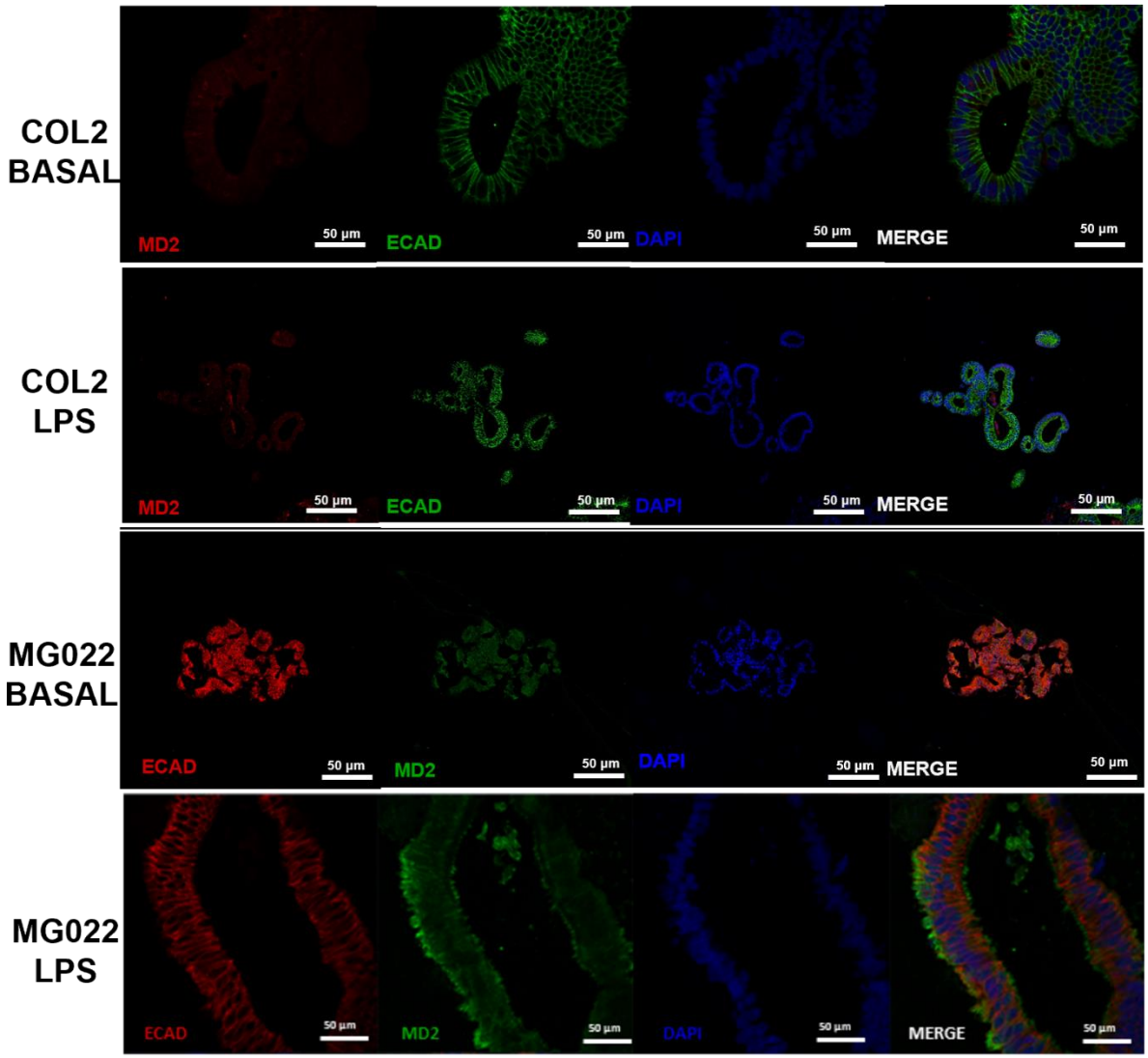

Figure 5.14: Co-staining of E-cadherin and MD2 under basal and inflamed conditions. ECAD expression remained stable in healthy organoids with basolateral MD2 expression greater than in the basal condition. Conversely, UC organoids display lesser ECAD availability upon LPS exposure and greater MD2 expression located at both the apical and basolateral surface. Imaged on Zeiss Elyra Super Resolution Microscope at 20X magnification. Resolution = 2049 x 2049 pixels (72 DPI)

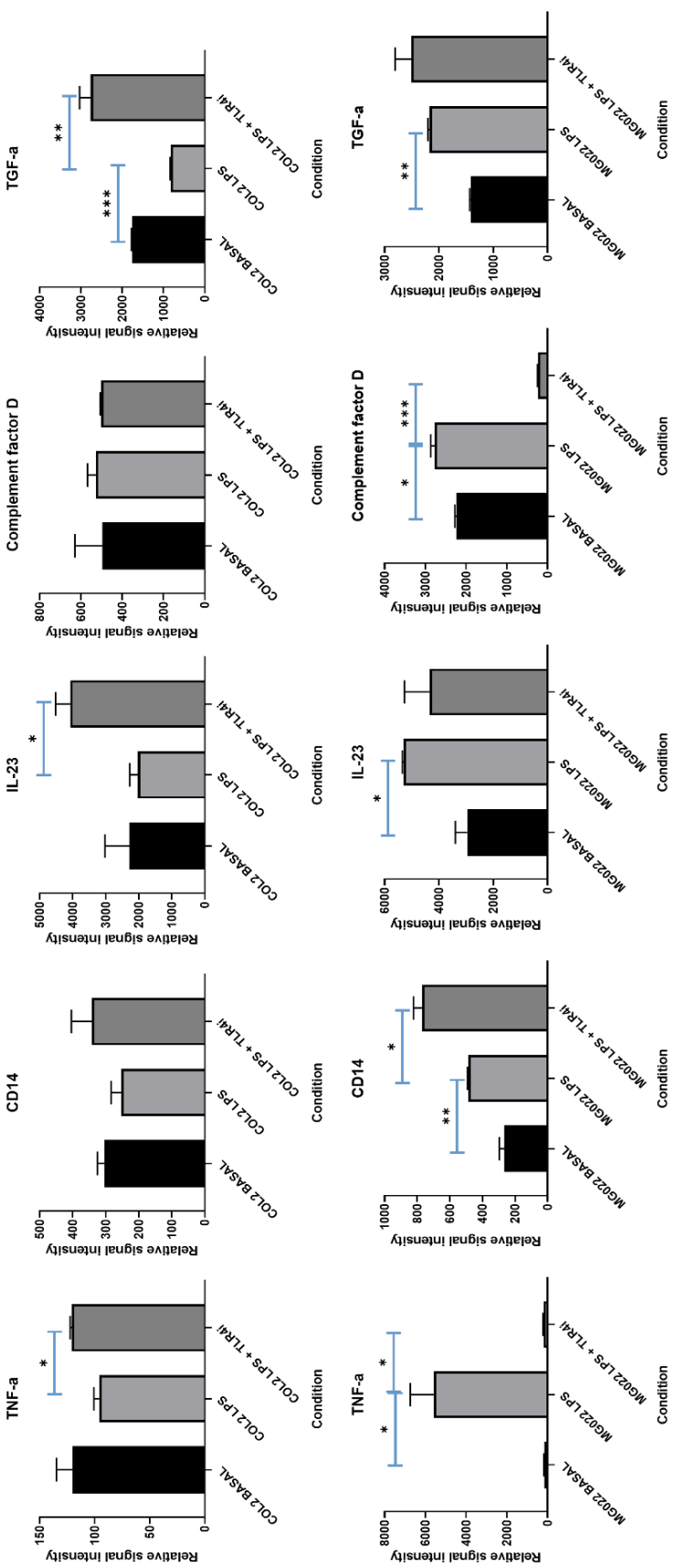

Figure 5.15: Cytokine Array data reveals substantial differential response in UC as supported by transcriptomic datasets after treatment with LPS (100 µg/ml) over a 48-hour period. Data acquired from Biotechne Proteome NFκB Array. Statistical analyses were performed by two-sided students t-test. Data are expressed as mean ± SD of each group. *P < .05; **P < .001; ***P < .0001 relative to unstimulated. N=2 (Technical replicates)

Proteomic Arrays Further Confirm the Differential Response Observed in Patient-Derived Colonic Organoids

To supplement all other datasets obtained during this project, proteomic arrays were performed (Methods in Appendix 1). These arrays offer a more accurate quantification of marker expression than immunostaining techniques which provide more information regarding localisation of proteins within the cell (Raw data found in Appendix 2). A wider range of markers can also be easily measured across numerous signalling pathways. Here, we report numerous hits revealed by these arrays that demonstrate the highest significance and are part of relevant inflammatory response signalling pathways.

Primarily, a secretome assay was performed (Biotechne Proteome Profiler Human XL Cytokine Array Kit; cat no. # ARY022B) to inform as to whether the trend observed at the transcriptomic level could be translated to the proteomic level. Some of the top hits can be seen in figure 5.15.

Initially, levels of TNFα protein demonstrated a lack of significant change in the LPS-treated sample of healthy organoids compared to untreated. This muted response is in line with literature, in addition to previous findings acquired in this project. In contrast, a highly exaggerated response was measured in UC-derived organoids with a 40-fold increase in expression levels determined by relative signal intensity (measured using a chemiluminescence imaging system). This intense differential response in TNFα levels is, therefore, clear at both the transcriptomic and proteomic level.

This differential response is further evidenced by changes to CD14 expression. Again, no notable differences occurred in healthy organoids upon exposure to LPS at the 48-hour time point, while CD14 expression doubles in our UC model upon stimulation with LPS. Interestingly, these levels continue to increase in conjunction with TLR4 inhibition, suggesting that CD14 expression may be influenced by multiple pathways.

IL23 is a major cytokine implicated in IBD that we have found to be disproportionately upregulated in our UC-derived model at the transcriptomic level. LPS exposure instigates a significant increase in IL23 expression in UC organoids, while an opposing response is exhibited in healthy organoids (Figure 5.15).

Furthermore, Complement Factor D was significantly differentially expressed between organoid lines, with a notable increase in expression of approximately 25% in treated disease organoids compared to the slight drop observed in our corresponding healthy line. Interestingly, inhibition of TLR4 appears to have a drastic effect upon Complement Factor D expression in UC, with a sharp drop in expression below untreated control.

An additional pro-inflammatory cytokine investigated in this array, TGFα, displayed interesting results, with a 50% drop in expression occurring in LPS-stimulated healthy organoids. This drop was rectified by the presence of a TLR4 inhibitor, which raised levels substantially, even rising above basal levels. In our UC model, however, TGFα expression increased by 40% upon addition of LPS over the 48-hour period. This suggests an increase in inflammation that was not present in the healthy tissue-derived line. However, TLR4 inhibition demonstrated little influence in reversing this effect. Therefore, perhaps the sensitivity of the TGFα response is great enough that the dose of TLR4 inhibitor was too low to effectively halt this LPS-mediated effect. Alternatively, this effect could have occurred as a result of multiple pathway activation, possibly amplified downstream of TLR4.

These findings confirm the trends observed previously in this project, further implicating LPS and the TLR4 pathway in the pathogenesis of UC. The results obtained from our healthy model clearly display the negative feedback response to LPS stimulation, designed to prevent a sudden and exaggerated inflammatory response in the healthy individual, protecting from unnecessary inflammatory-induced damage.

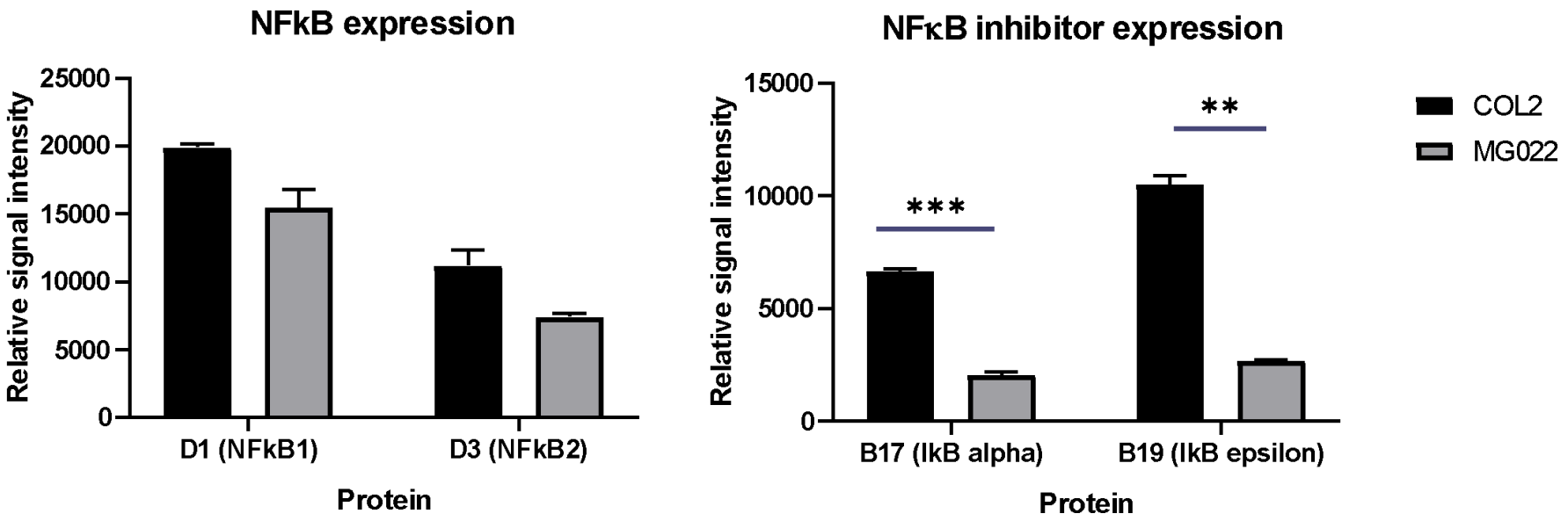

Figure 5.16: NFκB inhibitor expression plays a critical role in the establishment of downstream pro-inflammatory response in UC colonic tissue. Data acquired from Biotechne Proteome NFκB Array. Statistical analyses were performed by two-sided students t-test. Data are expressed as mean ± SD of each group. *P < .05; **P < .001; ***P < .0001 relative to unstimulated. N=2 (Technical replicates)

Further to the initial investigations conducted into the upstream differential responses to LPS, additional analyses were performed on these samples for the identification of alterations further upstream in the signalling pathway.

An important factor in the TLR4 signalling pathway is the transcription factor, NFκB. TLR4 is known to be a significant inducer of the NFκB pathway, influencing the subsequent inflammatory reaction. Hence, a NFκB pathway array was utilised to identify some of the key proteins that may be of interest in this pathway (Biotechne Proteome Profiler Human NFkB Pathway Array; cat no. # ARY029).

Initial analysis strengthened transcriptomic findings showing comparable expression levels of NFκB components, p50 and p51, between lines. While NFκB is known to be overexpressed in IBD, [212], we have shown conclusively that this is not an occurrence in our representative UC patient-derived line. This demonstrates the variations occurring in the pathogenesis of UC between individual patients, thereby supporting the relevance of a personalised approach for the treatment of this disease. Despite analogous NFκB levels between healthy and UC samples, a differential response in this pathway was still measured. In UC organoids, expression of an important inhibitor of NFκB, IκBα, was half that measured in our healthy lines (figure 5.16). This is a crucial difference between healthy and UC colonic models, displaying differences present even in the unstimulated state. This result was further compounded by the 80% disparity in the expression levels of inhibitor, IκBε. Together, this data confirms the downstream responses we observe are largely due to key differences at the NFκB inhibitor level.

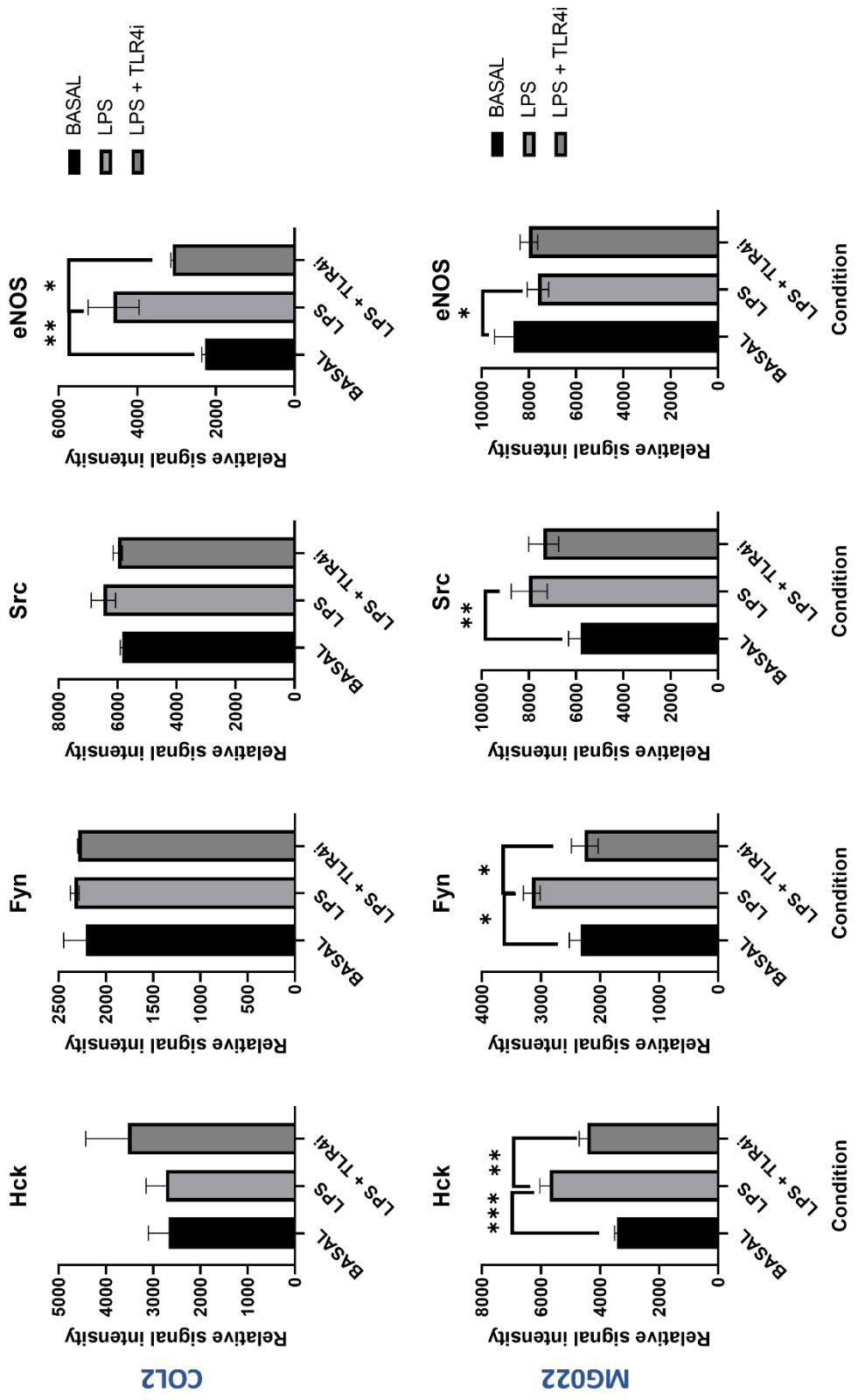

Figure 5.17: Relative expression of important kinases (and interacting proteins) demonstrated opposing responses to acute exposure to LPS (100 µg/ml) (1 hour). Data acquired from Biotechne Proteome Kinase Array. Statistical analyses were performed by two-sided students t-test. Data are expressed as mean ± SD of each group. *P < .05; **P < .001; ***P < .0001 relative to unstimulated. N=2 (Technical replicates)

Once the above datasets confirmed our existing findings, and uncovered new findings, in regard to the upstream and downstream pathway responses, intermediary proteins within this pathway were then analysed. Samples were measured using a phospho-kinase array (Biotechne Proteome Profiler Human Phospho-Kinase Array Kit; cat no. # ARY003C). A selection of the top hits are displayed in figure 5.17. These are inclusive of several members of the Src kinase family: Hck, Fyn and Src.

The expression of Hck and Fyn follow the same expression profile in response to LPS with highly significant increases recorded in UC organoids only. This response is completely absent in healthy organoids, revealing a crucial differential response capable of far-reaching effects into downstream inflammatory signalling. These kinases are further implicated in the TLR4 signalling pathway due to the successful reversal of these effects by TLR4 inhibition. The final member of this family demonstrating a response to LPS treatment is Src, with a substantial 25% increase in Src protein production upon exposure to LPS.

Another critical protein which typically functions to regulate endothelial homeostasis was observed to be downregulated in UC organoids in response to LPS treatment. Furthermore, expression was doubled in healthy organoids, occurring prior to a subsequent return to basal levels following 48-hour pre-treatment with a TLR4 inhibitor. These opposing responses establish a role for eNOS in LPS-mediated TLR4 signalling.

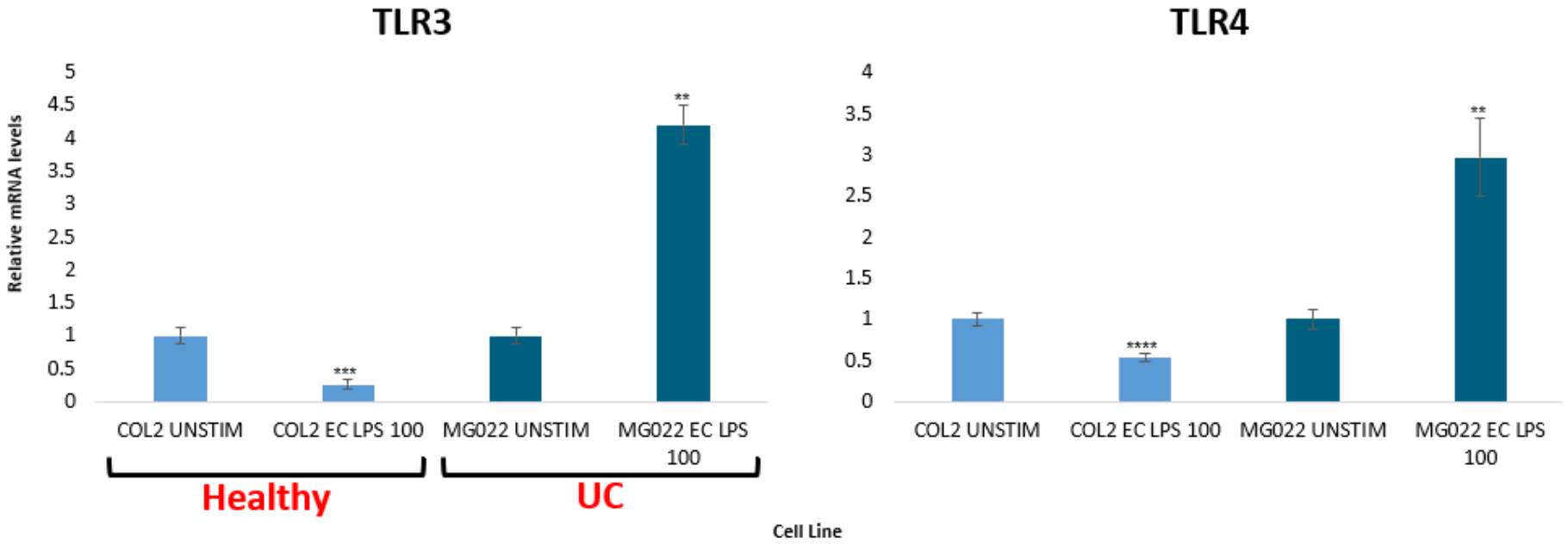

Figure 5.18: TLR3 & -4 expression in healthy v UC organoids post-treatment with LPS (100 µg/ml. All values compared to unstimulated condition of own cell line. TLR3 and TLR4 both have opposing expression profiles between COL2 and MG022, demonstrating a clear disease phenotype in response to these inflammatory mediators. Statistical analyses were performed by two-sided students t-test. Data are expressed as mean ± SD of each group. *P < .05; **P < .001; ***P < .0001. N=3 (Technical replicates)

.

The expression of the PPR responsible for the detection of LPS was measured for potential differences occurring upon exposure to this PAMP. LPS, demonstrated a typical response with a definite disease phenotype present in UC.

We then set about investigating the reasons for this discrepancy in response to TNFα and LPS. Initially, we explored whether the expression of the TLR4 receptor could be attributed to the changes we are measuring in this clear differential response. As figure 5.18 clearly shows, the level of TLR4 receptor expression is significantly altered by exposure to LPS over this time period, with distinct divergences in the response of healthy & UC organoids. The effects we can see are completely opposing with TLR4 receptor expression dropping 45% after 48 hours. This is in contrast to the substantial 3-fold increase measured in our UC-derived organoids. The evident differences in TLR4 expression, alongside the degree of significance, highlight this avenue of research as especially relevant and important to explore.

TLR3 is another receptor shown to exhibit a potential cross-talk with TLR4, hence TLR3 expression was also measured and analysed. Interestingly, the same profile was recorded as found in TLR4, with a prominent drop of 70% in healthy organoids, compared to a major rise in expression of 4.2-fold in UC (figure 5.18).

Therefore, while the expression of both TLR3 & TLR4 were downregulated in a negative feedback mechanism in response to LPS in healthy tissue, these receptors underwent significant upregulation in the UC-derived organoids. This insinuates a dysregulated response of UC epithelial cells to the presence of bacterial LPS is, at least partially, responsible for the substantial inflammatory presence in this disease.

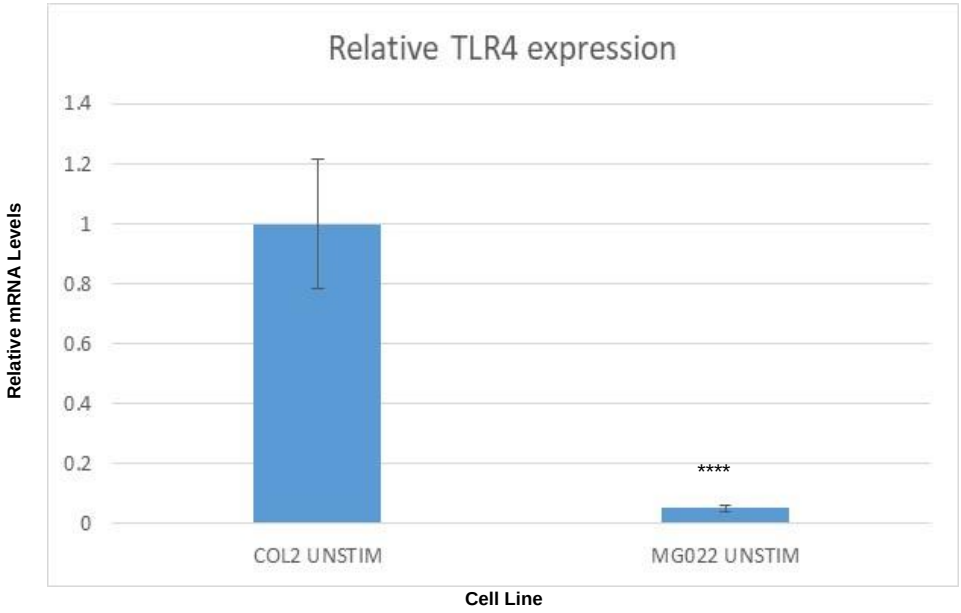

Figure 5.19: Basal TLR4 expression is lower UC organoids. Raw baseline values demonstrate baseline TLR4 expression is substantially lower in disease epithelium compared to healthy epithelium. Data acquired by RT-PCR; expressed as mean ± SD of each group. *P < .05; **P < .001; ***P < .0001; ****P < .00001. N=3 (Technical replicates)

Once the differential response between patient-derived healthy & UC organoids had been established at both the inflammatory level and that of receptor expression, we then set out to determine whether there were any discrepancies in basal expression. To determine this, TLR4 expression was measured in a basal, untreated state. This would inform us as to whether the exaggerated rise in TLR4 expression in UC observed previously was accompanied by a greater basal expression. We expected that this basal expression might be higher when compared to healthy tissue. Interestingly, the data shows a large discrepancy of 95%, in the basal expression levels of healthy and UC-derived lines. However, it is our UC line that exhibited substantially lower basal TLR4 levels which was found to be highly significant ($P<0.0001$). This data confirms that there are considerable differences between healthy and UC epithelial tissue even under basal, non-inflammatory conditions when no morphological discrepancies are present (figure 5.19).

We can conclude from this data that colonic epithelial tissue isolated from UC patients does not continually express high levels of TLR4 prior to stimulation. It does, however, upregulate TLR4 expression by approximately 60 times upon LPS stimulation, whereas healthy tissue downregulates TLR4 by ~50%. This provides supporting evidence of TLR4 involvement in the elevated immune response of UC.

5.2.4 The Relationship between Ulcerative Colitis & Colorectal Cancer

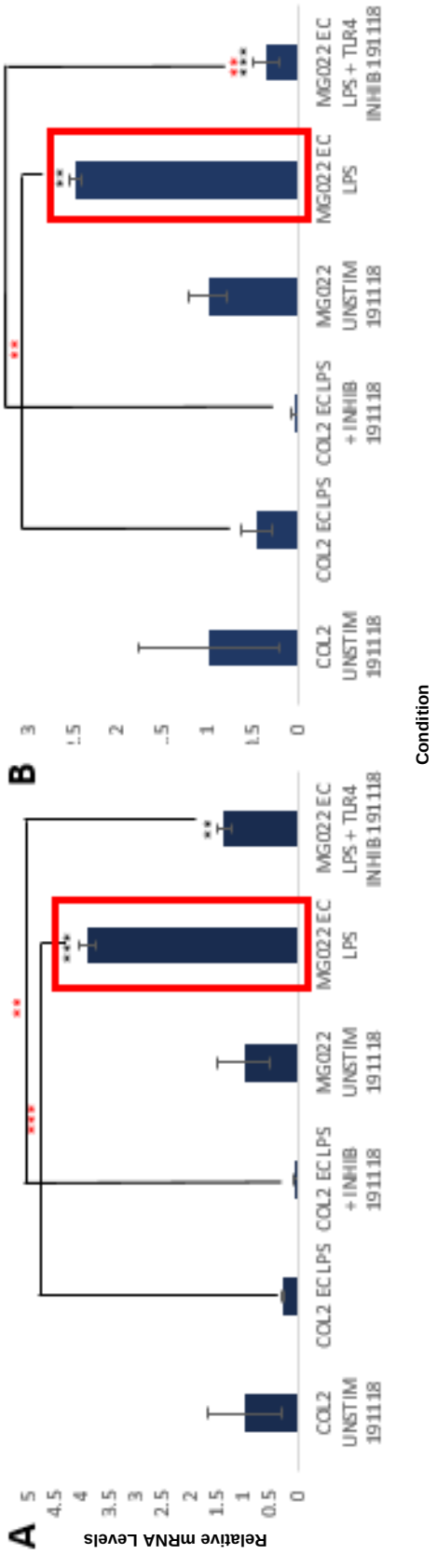

Figure 5.20: Colorectal cancer markers show differential expression between healthy & UC organoids. (A) EGFR expression drops by 70% upon LPS **(100** (µg/ml) exposure in the healthy line, while a contradictory effect is observed in the UC line, where expression is increased by 4-fold. TLR4 inhibitor (40µM) rectified this increase reducing expression by approximately 70%. **(B)** COX2 expression mirrors the expression profile of EGFR in the absence and presence of TLR4 inhibitor. Statistical analyses were performed by two-sided students t-test. Data are expressed as mean ± SD of each group. *$P < .05$; **$P < .001$; ***$P < .0001$. N=3 (Technical replicates)

It has previously been reported that prolonged UC can lead to the development of colorectal cancer, known as colitis-associated cancer (CAC) when diagnosed in UC patients. As we had established LPS to have such an amplified and significant pro-inflammatory and epithelial response when compared to our healthy organoids, it was decided that our model would be relevant and suitable for the study of LPS and its link with CAC.

To do this we first examined two major markers reported to be upregulated in CRC: EGFR and COX2. If a differential response in the way these two markers responded to treatment, this is very indicative of the connection between LPS, UC and CAC.

EGFR plays a regulatory role in the TLR4 signalling pathway, with activation of EGFR participating in TLR4 activation. Therefore, the role of EGFR in the TLR4 pathway and regulation was investigated. This experiment compared the effects and differential responses of both healthy & UC-derived organoids. As the data shows, LPS instigates opposing effects on both EGFR and COX2 expression between the healthy & UC organoid lines. Upon administering LPS to each line, expression had dropped by 70% and 55%, respectively. This trend was further exacerbated by combining TLR4 inhibitor (figure 5.20).

Furthermore, the activation of TLR4, in this manner, also results in an increase in EGFR, which is dampened by TLR4 inhibition. TLR4 inhibition has such a profound effect as to reduce the initial increase back to within unstimulated levels. This is an optimal response demonstrating the efficacy of TLR4 inhibition and hence the impact LPS has upon EGFR expression via the TLR4 pathway. EGFR is found to be upregulated in CRC. This response is, therefore, significant in linking EGFR with inflammatory-related cancer development (figure 5.20).

A similar expression profile is evident in the COX2 response to LPS, with a drop in COX2 expression in healthy organoids following 48-hour incubation. Expression was then further reduced by inhibition of TLR4. COX2 expression was also significantly raised by *E. coli* derived LPS, despite being to a lesser degree. This impact was further determined to be directly related to LPS acting via the TLR4 pathway. This was confirmed by the reduction of COX2 following the pre-treatment with TLR4 inhibitor. In fact, expression dropped below unstimulated levels, suggesting there may have been

a degree of background inflammation that was additionally blocked by this inhibition method (figure 5.20).

While UC is more receptive to LPS-induced inflammatory changes, we also find that CAC markers closely associated with CAC are highly induced in this this inflammatory model. Raised COX2 expression is also found in most CRC tissue and is associated with poor survival in CRC patients. Reduction of COX2 expression, by treatment with NSAIDs, has been found to reduce the risk of the patient developing tumours [213]. Here, we found that TLR4 inhibition did, in fact, have this same effect of reducing COX2 expression, therefore exhibiting anti-inflammatory, anti-tumour effects.

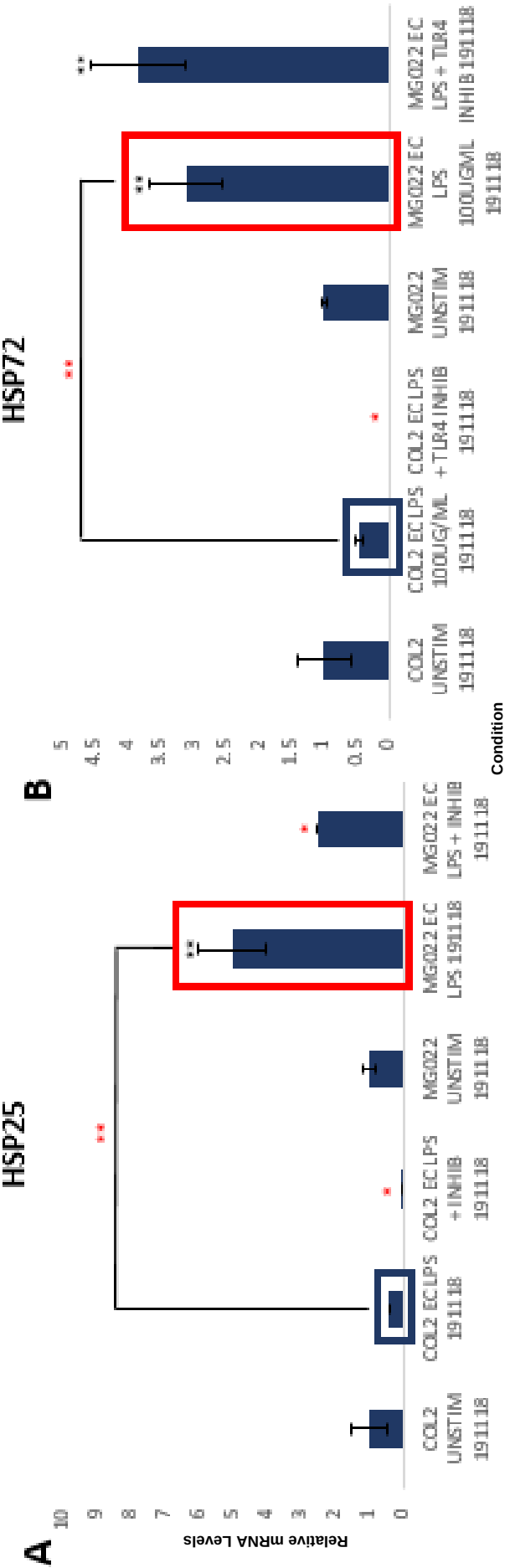

Figure 5.21: Heat shock proteins may play a role in UC pathogenesis and potential escalation of CAC. (A & B) Heat shock protein (HSP) expression shows substantial upregulation in UC epithelium following *E. coli* (EC) LPS treatment, while healthy tissue downregulated HSPs under inflammatory conditions (in a possible compensatory response). This demonstrates a clear disease phenotypic difference in the response of HSPs in colonic epithelial tissue. **(A)** TLR4 inhibition (40μM) reverse this effect in HSP25 expression. Statistical analyses were performed by two-sided students t-test. Data are expressed as mean ± SD of each group. *P < .05; **P < .001; ***P < .0001. N=3 (Technical replicates)

The next step in the study of the UC/LPS/CAC connection was to investigate the response of heat shock proteins (HSPs). HSPs have been reported to play a decisive role in the progression and metastasis of CRC and have very recently been proposed as a therapeutic target in cancers such as CRC.

It was decided, therefore, that these important proteins; typically involved in protection of cells against oxidative stress; were a good avenue to explore using this platform and experimental set-up. As a potential contributor to UC pathogenesis, it is possible that LPS can also trigger changes in HSP expression along with other colorectal cancer-related markers and increase the risk of CAC development.

Two HSPs, in particular, were selected to focus this initial experiment on as they have both been previously reported to be expressed in higher levels in tissue isolated from CRC, when comparing with normal mucosa or of that adjacent to the tumour.

As is shown by figure 5.21, an expression profile was recorded that is remarkably similar to that of EGFR and COX2. Due to the reputation of all these proteins to be involved in the pathogenesis of CRC, this is a very interesting finding to note.

This initial drop in expression of approximately 50%, for both HSP25 and HSP72 was observed in COL2 which further declined in response to TLR4 inhibition. On the contrary, HSP expression rose considerably in the UC line upon stimulation with LPS to 5-fold and 3-fold, respectively. The difference occurs between HSP25 and HSP72 when the former demonstrates a substantial reduction in expression upon co-culture with TLR4 inhibitor, by 50%, while the latter appears to be largely unaffected by the presence of this inhibitor.

This data combined suggests that chronically LPS-stimulated UC tissue is more susceptible to CAC progression. TLR4 inhibition did prevent this increase of HSP25, conferring a potential protective effect, while HSP72 was largely unaffected.

5.2.5 Analysis of Transcriptomics Obtained from RNA-Sequencing

Once initial experiments had been conducted and the preferred dose and treatment time had been established, the experiment was repeated using these parameters. Previous experiments reported here had concentrated on a focussed marker profile for both inflammatory and epithelial proteins most relevant to UC. Following this focussed approach, we set about performing RNA-sequencing on a larger scale to identify any potential markers of interest. These markers could then expand our area of research to involve other proteins also related to UC progression and/or CAC development.

Once, the LPS + TLR4 inhibitor experiment had been optimised; yielding promising and statistically significant data; it was decided that samples from this experiment would be sent off for RNA-Seq analysis.

As in RT-PCR, RNA was initially isolated from the samples. As samples used for RNA-Seq must be generated from high quality, pure RNA, the samples were analysed using a Qubit fluorometer to confirm this was the case. Once these accurate results had been obtained, the samples were further analysed on the TapeStation. The results can be found in figures 5.22 and 5.23. The samples then underwent further steps, as follows: ribodepletion; probe hybridisation; RNase H digestion, followed by DNase I digestion. Once the rRNA depletion steps had been performed RNA purification was conducted using NEBNext RNA sample purification beads (cat no. # E7767S). These purified samples were then prepared using the NEBNext® Ultra II Directional RNA Library Prep Kit for Illumina® (cat no. # E7775).

Initially, samples were prepared in the same manner as before with a basal, unstimulated acting as a negative control; an LPS-only treated condition with 48-hour exposure at 100 µg/ml and lastly a condition that underwent pre-treatment with TLR4 inhibitor over a 48-hour period prior to the addition of LPS for a further 48 hours. In this latter 48-hour treatment period, fresh TLR4 inhibitor was added to the media to ensure the concentration didn't wane at this timepoint. The samples from both healthy

& UC-derived organoids were then isolated and lysed as previously mentioned using the Qiagen RNA Extraction kit.

However, during this experiment, the method for RNA measurement had to be more accurate for the purposes of RNA-sequencing. Hence, the samples were measured using a Qubit. The steps for this protocol are outlined in the Materials & Methods section. This is to ensure the correct amount of sample is used at the ribodepletion step.

Once the RNA concentration had been ascertained, the integrity of the samples was analysed using a TapeStation. This system uses an electrophoresis that gives an output in both a gel image and a Trace format. The Trace shows different peaks as can be seen in figure 5.23. This demonstrates the presence of any contaminants within the RNA sample that would interfere with the latter stages of cDNA library preparation.

As can be seen in this figure, the upper and lower limits are marked. The expected library range is then determined, with any peaks present outside the expected range, likely due to primer dimers or adapter dimers. A DNA Integrity Number is then assigned to determine the level of DNA degradation. A DIN of 10 is indicative of a high level of DNA Integrity while a value of 1 indicates severe degradation. The samples prepared for this project had a very good level of integrity and were therefore sent off for RNA-sequencing at the Babraham Institute.

Samples from the 6 conditions were prepared in duplicate, each with a different index added to the end of the sequence. The index added to each RNA sample generated from each condition is outlined in table 5.1. This index acts as a type of barcode to enable accurate identification of the condition the sample originated from following amplification and sequencing. This step of indexing is required due to the process of RNA sequencing often involving the pooling of samples to the same flow cell.

Table 5.1: Sample details and corresponding index sequences.

Sample	Description	Index
COL2 UNSTIM	Healthy intestinal organoids (basal media only)	ATCACG
COL2 LPS	Healthy intestinal organoids treated with 100ug/ml lipopolysaccharides	CGATGT
COL2 LPS + TLR4i	Healthy intestinal organoids treated with 100ug/ml lipopolysaccharides in the presence of TLR4 inhibitor	TTAGGC
MG022 UNSTIM	Ulcerative colitis organoids (basal media only)	TGACCA
MG022 LPS	Ulcerative colitis organoids treated with 100ug/ml lipopolysaccharides	ACAGTG
MG022 LPS + TLR4i	Ulcerative colitis organoids treated with 100ug/ml lipopolysaccharides in the presence of TLR4 inhibitor	GCCAAT
COL2 UNSTIM	Healthy intestinal organoids (basal media only)	CAGATC
COL2 LPS	Healthy intestinal organoids treated with 100ug/ml lipopolysaccharides	ACTTGA
COL2 LPS + TLR4i	Healthy intestinal organoids treated with 100ug/ml lipopolysaccharides in the presence of TLR4 inhibitor	GATCAG
MG022 UNSTIM	Ulcerative colitis organoids (basal media only)	TAGCTT
MG022 LPS	Ulcerative colitis organoids treated with 100ug/ml lipopolysaccharides	GGCTAC
MG022 LPS + TLR4i	Ulcerative colitis organoids treated with 100ug/ml lipopolysaccharides in the presence of TLR4 inhibitor	CTTGTA

Table 5.2 displays the readings recorded from Qubit and TapeStation for all samples at each stage of sample preparation for RNA-Seq. Two samples needed to be repeated at the ribodepletion stage due to unfavourable trace readouts. The results for these are present in the centre of the table following repeat.

		Initial RNA sample measurements			Measurements taken following ribodepletion				2ul OF RIBO-DEPLETED RNA ADDED TO LIBRARY PREP				
	Sample name	Qubit (ng/ul)	RNA BR TS (ng/ul)	RIN Value	Concentration following ribodepletion (pg/ul)	Comments	Post-ribodepletion (RNA HS TS)	Concentration (Repeated ribo on 2 samples (RNA HS TS)) (pg/ul)	RIN Value (Repeat of ribo on 2 samples (RNA HS TS))	Number of PCR cycles ran per sample	Post-Library prep (DNA1000 TS) concentration (ng/ul)	Qubit (ng/ul or ug/ml)	DNA peak size	Index (Primer) number used for each sample
First set of library preps (Pink tubes)	COL2 BASAL	51.8	50.2	8.6	1670	Questionable peak (but decided not to repeat)	1			12	7.22	12.7	284	1
	COL2 EC LPS 100UGML	64.1	38	9.3	5890	Too large a peak	1.5	1370	1.6	12	16	20.2	289	2
	COL2 EC LPS + TLR4 INHIB 40UM	100	38.1	8.4	974		1.7			12	12.5	18	280	3
	MG022 BASAL	225	194	9.7	793	Ideal peaks	1.6			12	1.71	5.44	259	4
	MG022 EC LPS 100UGML	89.7	60.9	9.7	697		1.2			12	6.6	30.7	270	5
	MG022 EC LPS + TLR4 INHIB 40UM	98.9	36	7.3	246	Too low a concentration	1	987	1.7	12	6.22	13.7	276	6
Second set of library preps from same ribodepleted samples as above (Purple tubes)	COL2 BASAL									12	8.66	10.1	272	7
	COL2 EC LPS 100UGML									12	6.47	21.4	265	8
	COL2 EC LPS + TLR4 INHIB 40UM									12	8.22	10	271	9
	MG022 BASAL									12	8.97	12.2	274	10
	MG022 EC LPS 100UGML									12	7.8	10.5	274	11
	MG022 EC LPS + TLR4 INHIB 40UM									12	17	23.2	266	12

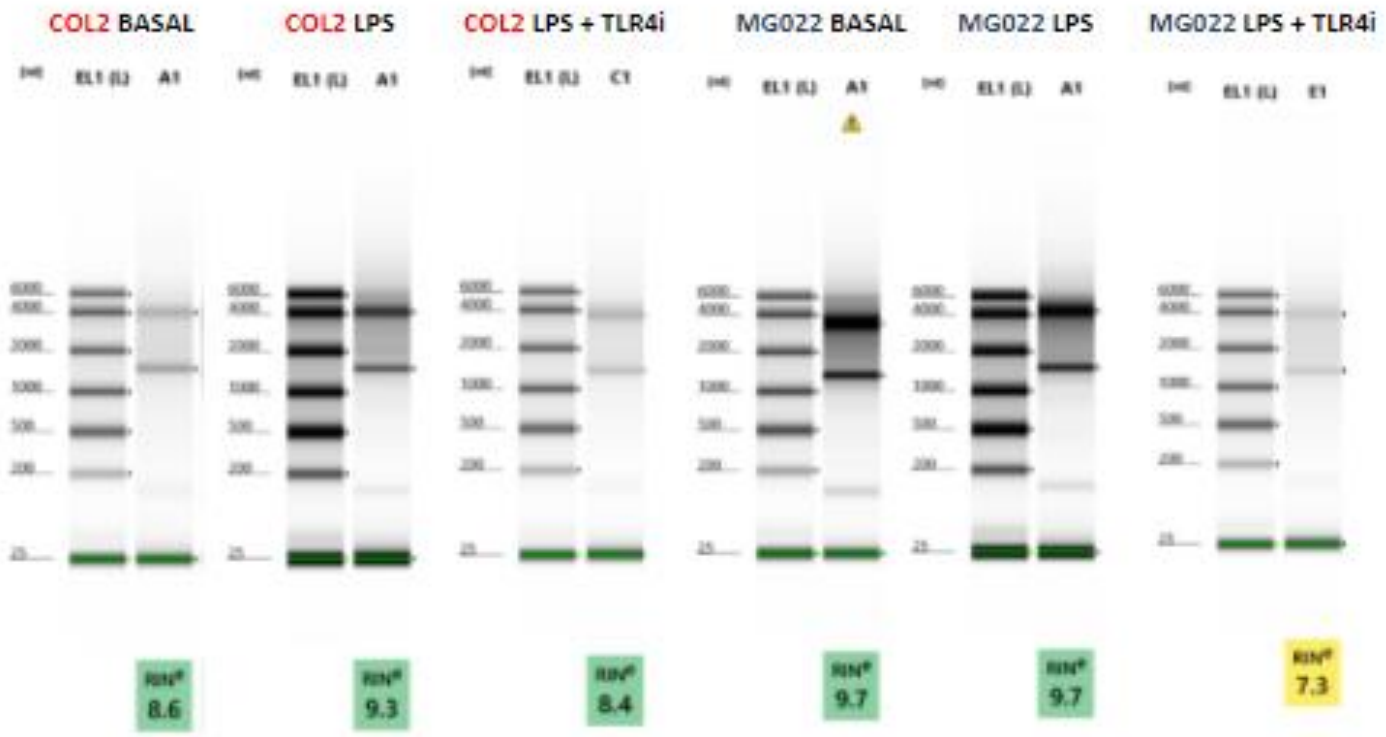

Figure 5.22: TapeStation electrophoretic gel images and subsequent RIN values. RIN values signal purity level of RNA present within the samples prior to library prep.

The electrophoresis data above demonstrates the results of the TapeStation following the initial RNA isolation. TapeStation can reliably perform electrophoretic separation of RNA in a sample down to 5 ng/µl. The RIN values are displayed beneath the gel images for each sample, all of which are representative of excellent quality RNA with the exception of the last sample. After seeking advice on this from employees at Babraham, the integrity of this sample was deemed sufficient to continue with the next steps of sequencing preparation.

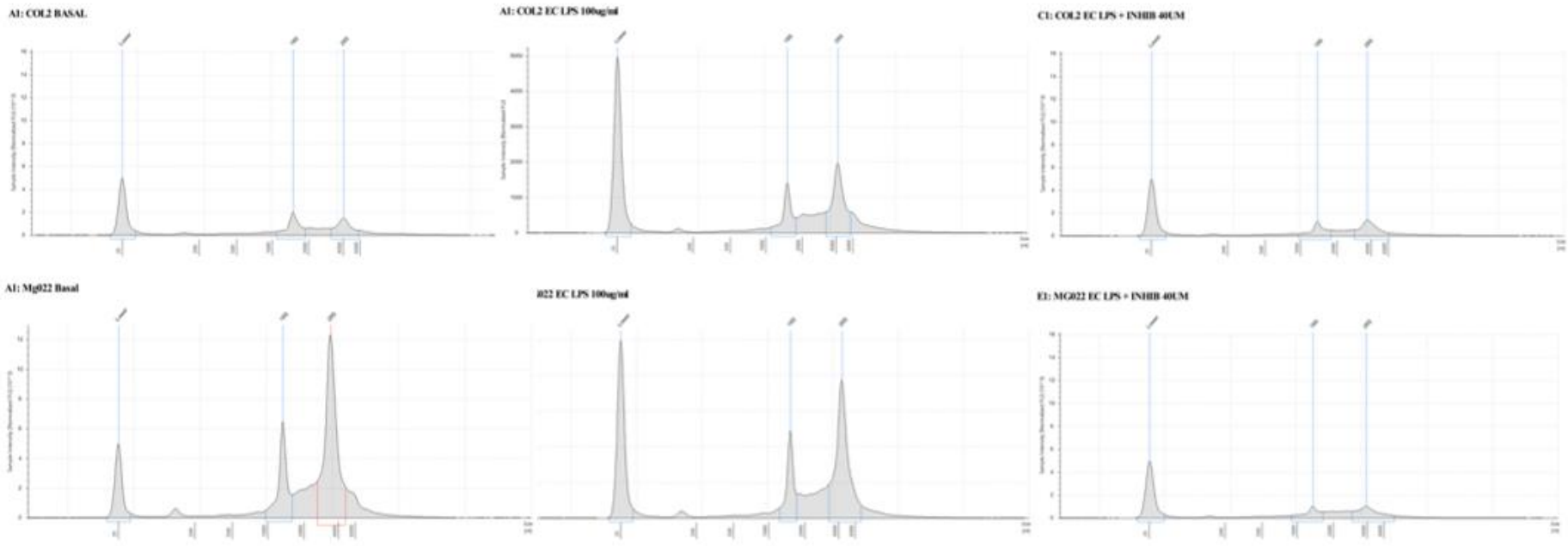

Figure 5.23: Broad Range TapeStation electrophoretic traces with key peaks indicated. The quantity of the RNA at each size is represented by the area of each peak.

The TapeStation also provides this data in the form of a trace for each sample displaying the size of the fragments in nucleotides across the X axis. The quantity of the RNA at each size is represented by the area of each peak.

The trace also demonstrates the existence of any primer dimers or adapter dimers that could interfere with the sequencing output.

Following ribodepletion, the samples were then run on the RNA High Sensitivity TapeStation. This step was to confirm rRNA had been successfully removed during the ribodepletion process. The trace data from the RNA High Sensitivity TapeStation can be seen in figure 5.24 (below). The RIN values were lower, as expected, as a result of the rRNA being effectively removed in the ribodepletion stage of sample preparation.

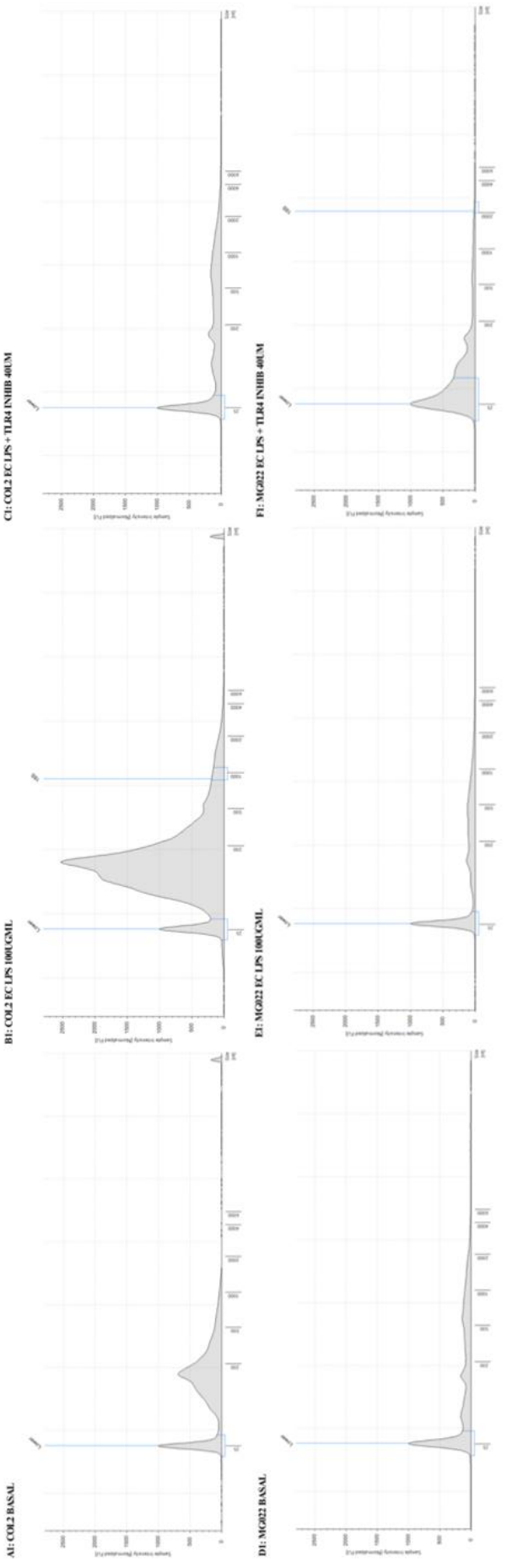

Figure 5.24: High Sensitivity TapeStation electrophoretic traces with key peaks indicated for each sample following ribodepletion. The quantity of the RNA at each size is represented by the area of each peak post-ribodepletion.

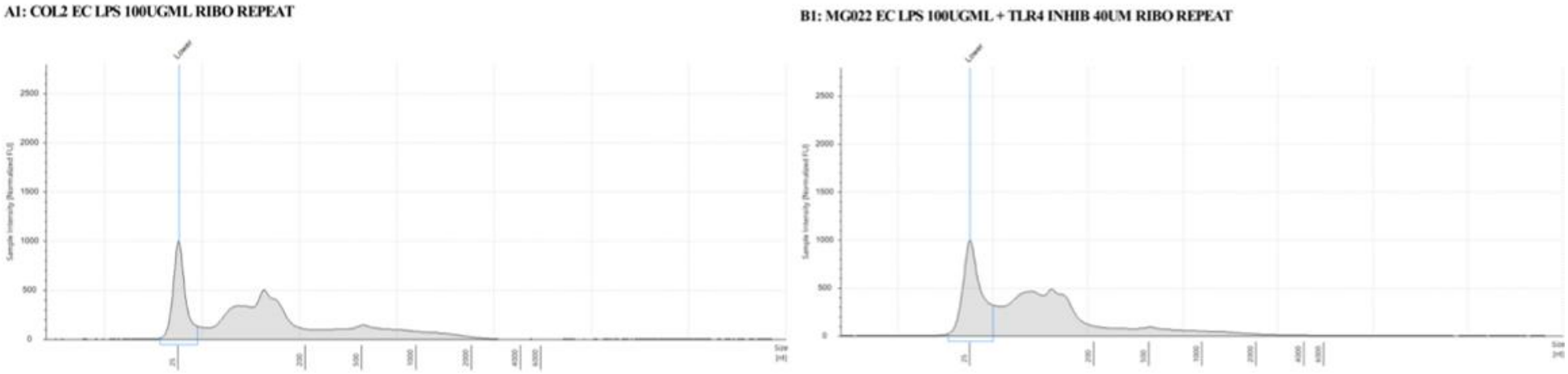

Figure 5.25: High Sensitivity TapeStation electrophoretic traces for two samples following repeat ribodepletion step due to substandard trace results in previous figure.

Two of the samples demonstrated an unfavourable trace and were therefore repeated. The peaks were much smaller and distinguishable from the lower marker which wasn't evident previously.

Following the repeat, it appeared that the ribodepletion was much more effective than the initial attempt. These samples were then combined with the previous and further prepared for sequencing.

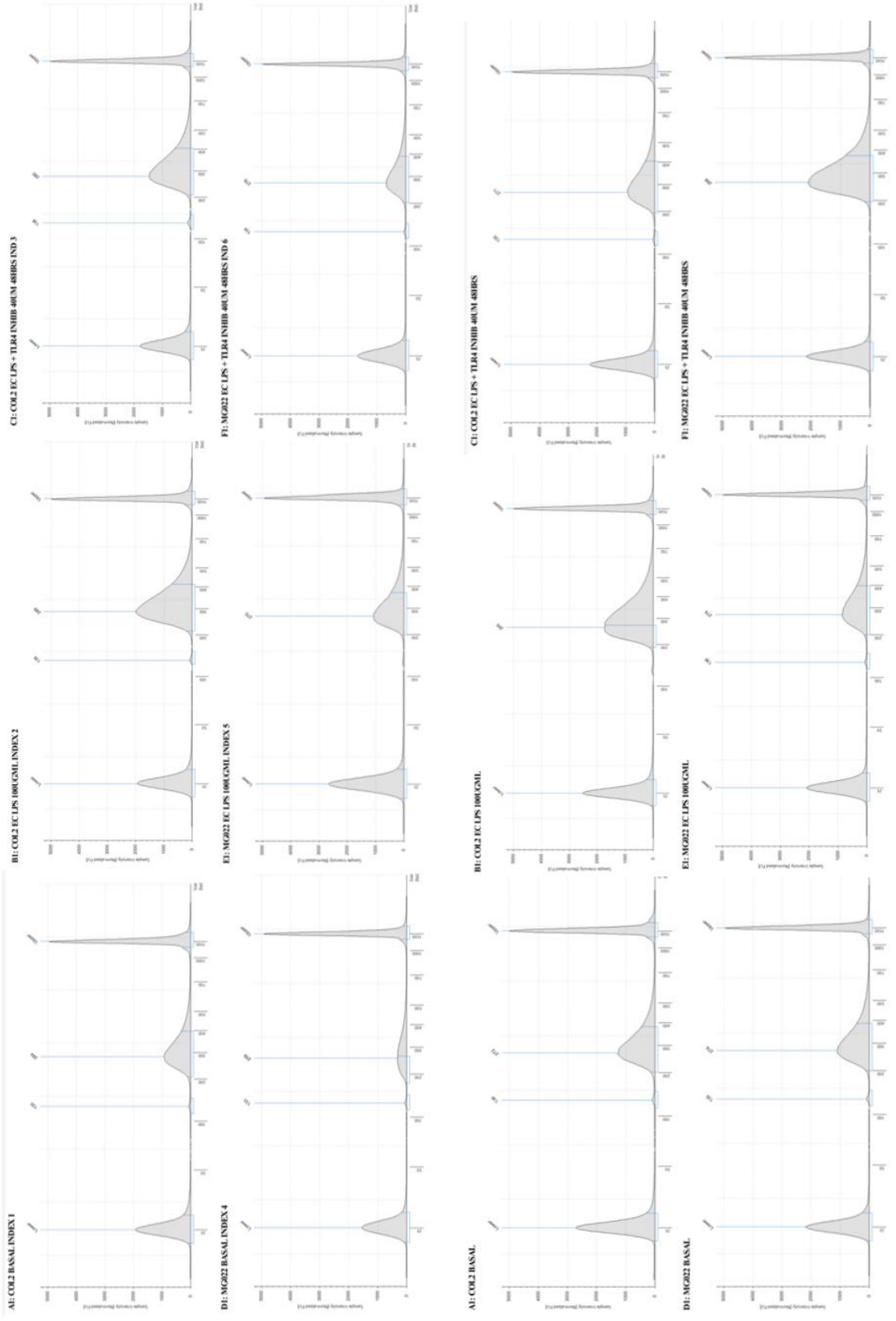

Figure 5.26: DNA D1000 TapeStation electrophoretic trace data for each sample following library preparation.

The concentration & integrity of the samples was then tested again using a D1000 TapeStation chip. The traces for these are displayed in figure 5.26. These peaks are preferable, and the concentrations are within acceptable ranges. The electropherogram should reveal a main peak at approximately 300 bp in addition to the upper and lower peaks. As we can see in this figure, this is the case for all 12 samples. This indicated that the samples were ready to be sent off for RNA-Sequencing.

After several weeks, we received the raw data that was then analysed with the help of the team at Babraham Institute. The analysis was focussed by the parameters of the project to ensure any analysis completed was most relevant to the hypothesis we were intending to answer. The process for analysis is outlined below.

From a GO database, a list of genes of interest was compiled and sent to Babraham to assist with this analysis. These genes were stored in groups within the database; therefore, we would include the entire group to determine if any genes we had not yet considered were, in fact, relevant. These groups can be found in the table below:

Table 5.3: GO database name and code with number of genes contained within group.

Gene List from GO Database	GO Code	Number of genes
Inflammatory Regulatory Genes	GO:0050727	538
TLR4 Signalling Pathway	GO:0034142	52
Intestinal Epithelial Structure Maintenance	GO:0060729	6
Response to ER Stress	GO:0034976	667
Cellular Response to ROS	GO:0034614	156
Epithelial to Mesenchymal Transition (EMT)	GO:0060231	215
Apoptotic Signalling Pathway	GO:0097193	433
Heat Shock Protein Binding	GO:0031072	240

All these gene ontology groups had potential relevance in this study and highlight new areas to expand our research focus. Although there are a substantial number of genes in certain ontology groups, these genes are often repeated within the same or different groups and are referred to using different GO identifying codes.

I shall outline some of the sample quality analysis required prior to interpretation of the RNA-Seq data.

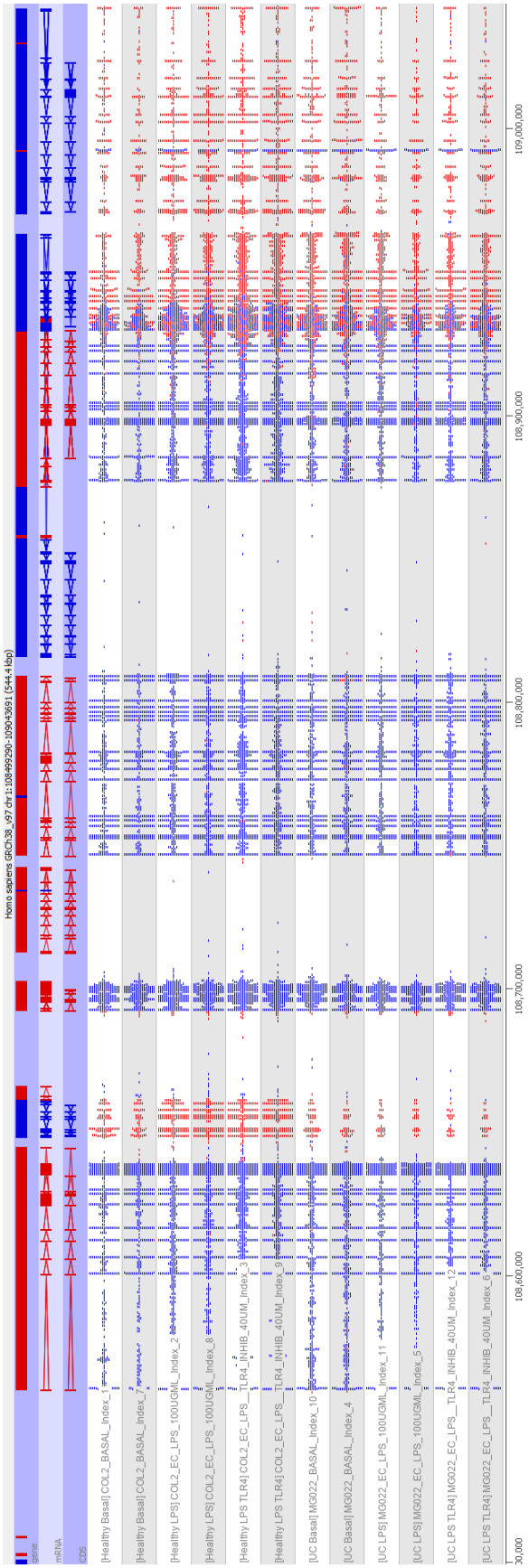

Figure 5.27: Snapshot of raw sequencing data to determine any obvious differences among samples.

Figure 5.27 shows a snapshot of the raw sequencing data that demonstrates the sequencing is very clean with no evidence of duplication. The samples replicates appear to have comparative results which is what we would hope for as evidence that the samples were correctly matched, and no alterations were introduced during the library preparation process.

The following RNA-Seq QC plot demonstrates an increase in the percentage of rRNA detected in the COL2 Basal sample replicates. This suggests the presence of some level of rRNA contamination. It's possible that the questionable peak discussed earlier (refer to table 5.2) regarding COL2 Basal TapeStation results following ribodepletion had a greater impact upon the sequencing of this sample than anticipated. Hence, there was a big drop in the total data size, as can be seen in the 'Percentage of max data size' section of the figure. This is due to much of the rRNA not being mappable and was therefore excluded from the final mapped data.

However, this occurrence did not interfere with the ability to analyse this data.

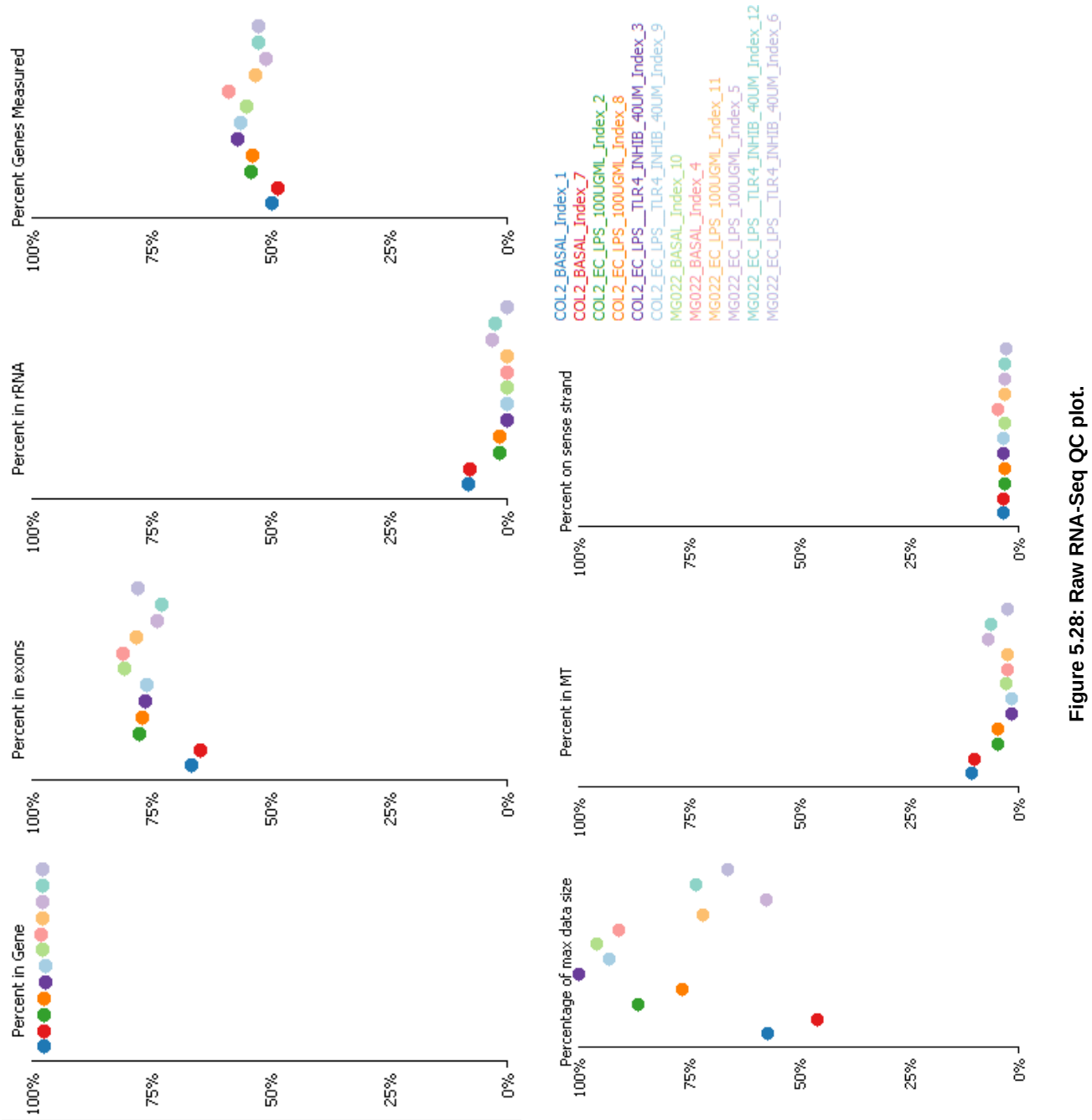

Figure 5.28: Raw RNA-Seq QC plot.

Following these sample QC checks, the raw data provided by the sequencing could then begin to be analysed. The data comparisons conducted initially concentrated on the differences in gene expression between basal and LPS-treated samples for both healthy and UC organoid lines.

A high level of consistency was found between sample replicates which provides a lot of power to detect genuine changes in gene expression between the samples and treatment groups.

Initially, the untreated basal and LPS-treated conditions were compared for both healthy and UC samples. A list of the top hits for both upregulated and downregulated genes were prepared for each GO list. This gives an indication of the genes most significantly affected by LPS in these models according to this RNA-Seq data using DESeq analysis. This data can be seen collated in tables 5.4 – 5.18.

HEALTHY BASAL V LPS DESEQ GO HITS

GO0097193_Intrinsic Apoptotic Signalling Pathway

Table 5.4: Log2 fold change of genes contained within the Intrinsic Apoptotic Signalling Pathway GO database between basal and LPS-treated samples in healthy colonic organoids.

Gene	Description	Log2 Fold Change	P-Value
PTGS2	Prostaglandin-endoperoxide synthase 2 (Also known as COX2)	5.246848	0.004093
DDIAS	Anti-apoptotic protein involved in DNA repair or cell survival	1.779047	0.001376
IFI6	Negatively regulating the intrinsic apoptotic signalling pathway	1.707513	2.8804544E-4
HELLS	Plays role in stem cell proliferation	1.628206	2.4197198E-16
IKBKE	Regulates inflammatory responses via NFκB, STAT, TNFα and IL1	1.477497	5.3778547E-7
TP53	Tumour protein p53	1.413544	1.0232996E-13
BRCA2	DNA repair associated	1.346389	1.0496441E-9
CD44	Cell-surface glycoprotein involved in cell–cell interactions & cell adhesion	1.304282	1.4E-45
BRCA1	DNA repair associated	1.277293	9.8165016E-5
TRIAP1	Transcriptionally activated by p53 to inhibit apoptosis	1.231806	5.509915E-5
MUC1	Membrane-tethered mucin	1.202507	2.64274E-5
TRAP1	Mitochondrial Hsp90 family chaperone	1.046511	3.691725E-11
FIGNL1	Promotes cell proliferation	1.029776	4.7450543E-5
ATAD5	Increases post-transcriptionally in response to DNA damage	1.002486	0.001167701
PTTG1IP	Interacts with Proto-oncogene, PTTG1	-0.53314	3.0275374E-15
HMOX1	Heme oxygenase 1 (exhibits anti-inflammatory, antioxidant, and antiproliferative effects)	-0.53979	1.4373803E-5
PRKCD	Inhibition of PRKCD reduced expression of E-selectin and ICAM-1	-0.57107	7.219704E-10
BCL2L1	Apoptosis inhibitor gene	-0.58761	3.5941408E-12
PINK1	Protein kinase protecting cells from stress-induced mitochondrial dysfunction	-0.59018	8.29256E-12
MAPK7	Regulates ERK5 localization and activity	-0.61213	1.9820462E-5
CDKN2D	Inhibits proliferation	-0.68824	0.004359997
CIDEB	Enhances apoptosis	-0.69937	8.655743E-4
BMF	Activated by TGFβ - Induces apoptosis via Smad4 pathway	-0.73817	0.001093672
BAD	Pro-apoptotic member of the Bcl-2 gene family	-0.73963	4.384354E-9
DAPK2	Downregulation limits apoptosis	-0.89256	3.9632272E-14
TRIB3	Downregulation significantly inhibits proliferation, invasion, & migration of ovarian cancer cells	-0.91041	2.1011125E-24
DDIT3	Activated by endoplasmic reticulum stress, and promotes apoptosis	-0.932	5.8777528E-6
NUPR1	Inhibits iron-dependent oxidative damage	-1.3084	9.2896744E-7
NFATC4	Downregulation induces oxidative damage	-2.13431	3.6759313E-9

In these tables we can see a lighter blue, these are the genes found to be upregulated following the 48-hour addition of *E. coli*-derived LPS at 100 µg/ml. The differential response of these genes is substantially significant with p-values of less than 0.001.

The change in gene expression between basal and LPS-treated samples is presented as a log2 fold change. The data displayed this way demonstrates the proportional, rather than exact, changes in gene expression which can then easily be compared.

The hits have been separated into their individual GO databases and, hence, some hits are repeated between groups. The initial GO database we applied to our analysis contained genes that fell into the category of the Intrinsic Apoptotic Signalling Pathway (GO0097193).

Table 5.4 displays the top 15 upregulated and top 15 downregulated gene hits in this GO category and the corresponding gene expression change in our healthy line between untreated and LPS-exposed samples.

In this data, we can see some important trends stand out, including the upregulation of anti-apoptotic genes (DDIAS; IFI6; TRIAP1) and those encouraging proliferation (HELLS & FIGNL1). In conjunction with this finding, the data shows the downregulation of pro-apoptotic genes (CIDEB; BMF; BAD; DDIT3).

GO0060729 Intestinal Epithelial Structure Maintenance

Table 5.5: Log2 fold change of genes contained within the Intestinal Epithelial Structure Maintenance GO database between basal and LPS-treated samples in healthy colonic organoids.

Gene	Description	Log2 Fold Change	P-Value
TLR4	Toll like receptor 4	0.458709	0.007078902
INAVA	Loss of INAVA reduces the intestinal cells ability to detect bacteria	-0.36062	5.1487907E-5
SLC22A5	Encodes OCTN2. Downregulation of OCTN2 plays a role in progression of IBD	-0.47315	1.3361314E-6

Analysis revealed much fewer genes to be statistically significant in the GO category focussing on Intestinal Epithelial Structure Maintenance (GO0060729) (table 5.5). However, these genes are highly relevant with TLR4 showing a significant increase in expression compared to basal. This response is expected due to the colonic epithelium increasing available TLR4 to ensure the increased bacterial levels are detected and kept in check.

Nevertheless, to compensate for this increased TLR4 in response to prolonged LPS exposure, INAVA expression was reduced to a similar degree. This effectively reduces the ability of the epithelial cells to detect, and subsequently, clear bacteria which is likely to be a protective mechanism to ensure the pro-inflammatory response is carefully regulated.

Downregulated SLC22A5 expression is also closely linked with pro-inflammatory cytokines generated by bacterial infection. It is likely this is, therefore, a temporary decrease in expression which would return to normal once the threat had been removed. It would be interesting to investigate this in a further study.

GO0060231 Epithelial to Mesenchymal Transition

Table 5.6: Log2 fold change of genes contained within the Epithelial to Mesenchymal Transition GO database between basal and LPS-treated samples in healthy colonic organoids.

Gene	Description	Log2 Fold Change	P-Value
STAT1	STAT1 has a key role in many gene expressions that cause survival of the cell, viability or pathogen response	0.426907	1.5767555E-4

As is made evident by table 5.6, there proved to be a very limited number of EMT-related genes impacted by this experiment. This demonstrates a limited chance for distinct cellular alterations and the possible development of fibrosis in response to inflammatory challenge.

Whilst included in this GO group, STAT1 does, in fact, play an integral role in numerous pro-inflammatory pathways.

GO0050727 Regulation of Inflammatory Response

Table 5.7: Log2 fold change of genes contained within the Regulation of Inflammatory Response GO database between basal and LPS-treated samples in healthy colonic organoids.

Gene	Description	Log2 Fold Change	P-Value
SLC7A2	Confers protective effect from CAC in chronic colitis	3.295544	2.6524282E-5
CX3CL1	Multifunctional inflammatory chemokine	1.970818	4.9789464E-6
C2CD4A	Involved in inflammatory processes & regulation of cell adhesion.	1.625529	3.657223E-4
FANCD2	Overexpression associated with upregulation of proliferation-related genes	1.603397	9.360069E-10
LPL	Regulates both inflammatory and anti-inflammatory gene expression in cultured macrophages.	1.452442	9.067671E-8
PBK	Increased expression of PBK has been linked to poor prognosis in ovarian cancer patients	1.217253	3.1996613E-5
GPRC5B	Increases inflammatory and fibrotic signaling	1.181753	0.009519308
FANCA	Correlated with upregulation of E2F3. E2F3 involved in cellular proliferation.	1.119474	3.7156653E-6
IL1R1	Interleukin 1 receptor type 1	1.110783	3.7156357E-4
BIRC3	Promotes EMT, cell migration, and metastasis via upregulating MAP3K7, and, hence, induction of ERK1/2 phosphorylation	0.896348	3.6151844E-22
ATM	Initiates activation of DNA damage checkpoints, leading to cell cycle arrest, DNA repair or apoptosis.	0.893242	1.2496108E-6
TNFAIP3	Induced by TNF-mediated NFκB activation. Associated with inflammatory carcinogenesis	0.824237	5.554085E-10
CHID1	High expression of CHID1 is a marker of good prognosis for adenocarcinoma	0.613455	4.5407785E-4
IL33	Promotes inflammation and fibrosis	0.599257	1.0074195E-5
NAPEPLD	Enzyme that synthesizes endocannabinoids (triggers inflammation)	0.565456	7.730869E-10
TNIP1	Key repressor of inflammatory signalling	-0.56188	7.049061E-13
PRKCD	Inhibition of PRKCD reduced expression of E-selectin and ICAM-1	-0.57107	7.219704E-10
MAPK7	Regulates ERK5 localization and activity	-0.61213	1.9820462E-5
DUOXA2	Upregulated during bacterial infection and, specifically, during IBD	-0.62957	5.3055084E-4
TRADD	Mediates programmed cell death signalling	-0.64019	1.080773E-4
ENPP3	Decreases ATP concentration & suppresses basophil and mast cell activity.	-0.65305	6.562222E-14
PPARD	Regulates cell metabolism, proliferation, and inflammation	-0.66556	4.984964E-14
GPX4	Downregulation of GPX4 increases lipid ROS level	-0.71979	3.5301408E-11
LDLR	Downregulation of LDLR mediates the endocytosis of LDL cholesterol, increasing the risk of human HCC.	-0.79254	1.328664E-30
DUOXA1	Reduced expression in metastatic breast cancer cell lines	-0.8234	5.803085E-5
BCL6	Transcription factor for regulation of T helper cell proliferation	-0.88928	3.680713E-12
ADAM8	Inhibition of ADAM8 in leukocytes suppresses migration, integrin upregulation & adhesion	-1.0466	1.7798055E-8
APOD	Inverse correlations of ApoD linked with tumour growth	-1.29116	0.008493234
NUPR1	Inhibits iron-dependent oxidative damage	-1.3084	9.2896744E-7
TLR9	Toll like receptor 9	-2.6088	4.941861E-5

As expected, the ‘Regulation of Inflammatory Response’ gene database has the largest number of hits returned from this experiment.

This data demonstrates a balance of genes involved in protection from CAC to initiation of pro-inflammatory pathways and regulation of cell adhesion. While those downregulated are inclusive of repressors of inflammatory signalling (TNIP1; MAPK7; PPARD) (table 5.7).

The relevance of these expression changes will be explored in further detail in the next section of this Chapter.

GO0034976_Response to Endoplasmic Reticulum Stress

Table 5.8: Log2 fold change of genes contained within the Response to Endoplasmic Reticulum Stress GO database between basal and LPS-treated samples in healthy colonic organoids.

Gene	Description	Log2 Fold Change	P-Value
CXCL8	Also known as IL8	2.16485	4.450875E-8
USP13	stabilizes STAT1 & promotes IFN-induced signalling	1.486142	8.4532244E-4
FOXRED2	Involved in Aβ-induced cell death and the ER stress response	1.443969	1.0771776E-4
TP53	Tumour protein p53	1.413544	1.0232996E-13
PMAIP1	Encodes pro-apoptotic protein within the BCL-2 protein family	0.94588	0.005693525
MBTPS2	Membrane bound protease that activates signalling proteins involved in ER stress	0.746873	6.106982E-5
THBS1	Directly binds and activates TGFβ1	0.736214	1.2345042E-18
SRPRB	Upregulation suspected to increase cell apoptosis & decrease the expression and phosphorylation of NF-κB	0.622434	2.1118856E-4
AIFM1	Induces apoptosis	0.590372	1.7711716E-6
DNAJC10	Encodes ER co-chaperone	0.567667	1.3101443E-7
EIF2AK4	Involved in signalling pathway in IECs following infection with *E. coli*, activating autophagy to & inhibiting *E. coli*-induced inflammation	0.507449	4.8065383E-4
ASNS	High expression of ASNS associated with increased inflammation & damage to hepatocytes	0.49961	8.958177E-6
UGGT1	A key ER protein involved in UPR	0.494955	9.495906E-8
STC2	Encodes glycoprotein playing a role in inflammation, ER & oxidative stress, cell proliferation, & apoptosis	0.482601	2.0074984E-4
ATF3	Induced by IL-1β	0.477483	1.3642588E-6
NPLOC4	Involved in G2/M checkpoint signaling	-0.62119	5.046019E-15
SHC1	Promoted cell cycle progression and inhibition of apoptosis	-0.62542	5.2720562E-12
FLOT1	Erk1/2, p38, JNK, and NF-κB pathways were inactivated by FLOT1 downregulation	-0.63825	3.3613848E-13
ANKZF1	Mutations found in ANKZF1 in infantile-onset IBD	-0.65803	1.5500205E-10
CTDSP2	Induces cyclin-dependent kinase inhibitor, p21, via increase of Ras.	-0.7607	7.950532E-28
DDX11	Facilitates cell progression in gastric cancer	-0.78194	2.107135E-9
PLA2G4B	Plays role in cell proliferation and survival in some cancers	-0.80006	0.001654514
ARFGAP1	Represses cell growth through mTORC1	-0.82245	5.255708E-10
CDK5RAP3	Tumour suppressor gene	-0.8337	4.958635E-15
YOD1	Controls cell cycle progression, transcriptional activation, & signal transduction.	-0.90703	1.9457364E-21
FBXO2	Regulates the EMT signalling pathway in CRC	-0.90911	1.5503899E-9
TRIB3	Downregulation significantly inhibits proliferation, invasion, & migration of ovarian cancer cells	-0.91041	2.1011125E-24
DDIT3	Pro-apoptotic transcription factor	-0.932	5.8777528E-6
NUPR1	Inhibits iron-dependent oxidative damage	-1.3084	9.2896744E-7
PDIA2	Upstream regulator of UPR pathway	-2.11496	9.779724E-12

The GO0034976 group encompasses genes related to the response of ER stress, amongst those more generally involved in pro-inflammatory and cell cycle regulatory pathways.

Here, we can clearly see an increase in pro-inflammatory cytokines; IL8 and IL1β; in response to LPS. Further inflammatory-related genes important in the initiation and control of the innate immune response include USP13, encoding a ubiquitin hydrolase enzyme, responsible for promoting interferon signalling. Furthermore, genes more specifically related to ER stress found to be significantly upregulated include FOXRED2, MBTPS2 and DNAJC10, amongst others.

Additionally, there were some interesting results in the top downregulated hits we can see here. This comprises the inactivation of several major pro-inflammatory pathways: NFκB; JNK and Erk1/2, which are all affected by the downregulation of FLOT1. Other gene hits found to be downregulated have key functions surrounding cell cycle regulation and cancer progression (table 5.8).

GO0034614 Cellular Response to Reactive Oxygen Species

Table 5.9: Log2 fold change of genes contained within the Cellular Response to Reactive Oxygen Species GO database between basal and LPS-treated samples in healthy colonic organoids.

Gene	Description	Log2 Fold Change	P-Value
LCN2	Elevated LCN2 levels associated with severe inflammation in IBD	3.465764	2.6524282E-5
CCNA2	High CCNA2 expression associated with poor overall survival in ovarian cancer	1.241577	9.977536E-9
CDK1	Plays key role in cell cycle regulation	1.171485	4.910933E-7
TRAP1	Mitochondrial Hsp90 family chaperone	1.046511	3.691725E-11
TNFAIP3	Induced by TNF-mediated NFκB activation. Associated with inflammatory carcinogenesis	0.824237	5.554085E-10
PCNA	Upregulated in CRC	0.757874	7.999863E-10
MYB	Proto-oncogene	0.686008	1.3901753E-8
PPARGC1B	Increases NLRP3 inflammasome activity & IL-1β production		1.5819223E-6
BMP7	Binds TGFβ receptors leading to recruitment & activation of SMAD family TFs	0.652655	5.299788E-4
APEX1	Promotes inflammation by orchestrating the NFκB pathway	0.636687	3.131204E-7
DHFR	Key enzyme in folate metabolism. Increased in IBD.	0.605173	0.002222847
AIFM1	Induces apoptosis	0.590372	1.7711716E-6
IMPACT	Contributes to GCN2-dependent mechanisms - A stress response kinase that regulates the immune system & survival of tumour cells	0.582531	2.6434005E-4
HNRNPD	RNA binding protein involved in post-transcriptional regulation of carcinogenesis mediators	0.561461	8.149641E-9
PPIF	Found to be overexpressed in endometrial cancer	0.545817	1.8044043E-4
MAPK13	Activated by proinflammatory cytokines and cellular stress	-0.41684	3.328935E-8
RELA	NF-κB p65 subunit & proto-oncogene	-0.41915	1.8354847E-5
PSAP	Important for neuron survival during oxidative stress	-0.47124	1.2057498E-12
SZT2	Negative regulator of mTORC1	-0.50453	3.9159704E-6
STAT6	STAT6 activation detected in inflamed colonic epithelium of active IBD patients	-0.51245	7.149174E-10
KLF4	Regulates cellular processes including cell growth, proliferation & differentiation	-0.55851	2.884699E-12
PRKCD	Lack of PRKCD causes immunodeficiency with B-cell deficiency and severe autoimmunity	-0.57107	7.219704E-10
PINK1	Protein kinase protecting cells from stress-induced mitochondrial dysfunction	-0.59018	8.29256E-12
SMPD3	Downregulation may contribute to cancer progression	-0.60041	1.8420831E-8
MAPK7	Regulates ERK5 localization and activity	-0.61213	1.9820462E-5
HDAC6	Regulates mitochondrial metabolism	-0.64269	2.5723267E-8
MAPK3	Also known as ERK1.	-0.65768	5.014104E-12
ANKZF1	Mutations found in ANKZF1 in infantile-onset IBD	-0.65803	1.5500205E-10
DNM2	Downregulation by siRNA or drug in hepatocellular carcinoma cell lines aids migration & invasion of tumour cells	-0.75001	4.428124E-23
RNF112	Rnf112 functions to downregulate TLR4	-2.16963	0.001033838

Interestingly, the group comprising genes involved in the Cellular Response to Reactive Oxygen Species (GO0034614) also primarily encompass pro-inflammatory genes (LCN2; PPARGC1B; DHFR) and those orchestrating carcinogenesis (CCNA2; TNFAIP3; PCNA).

Conversely, a large selection of the genes downregulated in response to LPS stimulation also encompass those with roles in initiation of inflammation and carcinogenesis. These results demonstrate the careful balance the healthy colonic epithelium has in place to modulate and regulate the response to bacterial threats (table 5.9).

While this data displays a snapshot of the epithelial response to LPS after 48 hours, the expression of these genes likely to continue to fluctuate at different time points. It would be interesting to investigate these fluxes and the timeframe in which these genes return to normal basal levels following exposure.

GO0034142 Toll-like Receptor 4 Signalling Pathway

Table 5.10: Log2 fold change of genes contained within the Toll-like Receptor 4 Signalling Pathway GO database between basal and LPS-treated samples in healthy colonic organoids.

Gene	Description	Log2 Fold Change	P-Value
TNFAIP3	Induced by TNF-mediated NFκB activation. Associated with inflammatory carcinogenesis	0.824237	5.554085E-10
LYN	Proto-oncogene	0.556418	2.4696243E-5
MFHAS1	Upregulated via Raf/MEK/ERK pathway	0.544759	4.861749E-7
TLR4	Toll like receptor 4	0.458709	0.007078902
APPL1	Shown to regulate LPS-induced pro-inflammatory response in RAW264.7 cells	0.343835	0.001218241
NFKBIA	NFκB inhibitor	-0.24255	0.007394155
F2RL1	A TGF-β target gene	-0.37225	1.2639423E-6
APPL2	Positive regulator of Wnt/β-catenin pathway	-0.404	1.8507586E-7
NR1D1	Downregulation induces a pro-inflammatory phenotype in astrocyte cell lines	-0.49628	6.845148E-4
S100A14	Downregulation correlates with poor differentiation & poor prognosis in oral cancer	-0.56809	2.3552996E-15
TICAM2	Reduced expression prevents neutrophil exhaustion upon LPS challenge in neutrophils	-0.87907	7.682633E-6

The GO group, GO0034142, comprises genes revolving around the TLR4 signalling pathway. Since this is a core pathway in LPS signalling and of great interest in this study, the variation in these genes is important to highlight any further expression variations that may be important and relevant for further examination.

As we have seen previously, TNFAIP3 is raised a sizeable amount in response to LPS in this line. This confirms our previous data as it is a gene rapidly induced by TNF, which is a cytokine we have reported to be elevated in this experiment. Importantly, this gene has been found to encode deubiquitinating enzyme which exhibits a regulatory effect upon the innate immune response. Critically, this regulatory effect incorporates inhibition of NFκB, in addition to apoptosis (figure 5.10).

Conversely, another NFκB inhibitor, NFKBIA, is downregulated. This may minimise the effect of TNFIAP3 upregulation, however, to fully understand the extent as to which this regulates NFκB activity would have to be further studied with knockdown and inhibitor studies.

Interestingly, TICAM2, which has been found to prevent neutrophil exhaustion when downregulated may offer an additional regulatory step preventing overburden of both the innate and adaptive immune systems.

Furthermore, we have found a gene found to be involved in the regulation of the LPS-mediated inflammatory response in RAW264.7 cells, a macrophage cell line, to be raised in response to LPS in this epithelial platform. This finding indicates that APPL1 may be an important gene in the LPS-mediate response in multiple different cell types.

GO0031072 Heat Shock Protein Binding

Table 5.11: Log2 fold change of genes contained within the Heat Shock Protein Binding GO database between basal and LPS-treated samples in healthy colonic organoids.

Gene	Description	Log2 Fold Change	P-Value
GBP1	Highly induced by IFN-γ	1.585405	4.8175032E-5
CDK1	Key player in cell cycle regulation	1.171485	4.910933E-7
SACS	Hsp70 Co-chaperone	1.166588	0.00146127
BAG2	Binds Hsp70 ATPase domain and promotes substrate release	1.159999	8.5100004E-7
CHORDC1	Encodes gene product Morgana, a component of the IKK complex	0.809143	7.161138E-8
HSPA8	heat shock protein family A (Hsp70) member	0.793269	3.4550151E-22
TOMM34	Forms complex with HSP70 & HSP90	0.752752	1.12320035E-4
DNAJC9	DnaJ heat shock protein family (Hsp40) member	0.742832	1.0122632E-5
TFAM	Plays a dominant role in the mtDNA stress-mediated inflammatory response	0.677759	3.7330265E-6
HSPA9	heat shock protein family A (Hsp70) member	0.663898	2.5436532E-13
DNAJC10	DnaJ heat shock protein family (Hsp40) member	0.567667	1.3101443E-7
HIF1A	Critical to the initiation of acute inflammation	0.563547	4.2236648E-11
DNAJA1	DnaJ heat shock protein family (Hsp40) member	0.547592	2.937405E-8
FAF1	Mediates apoptosis	0.504152	0.00114702
FKBP5	Promotes inflammation by activating NFκB	0.500926	0.002013072
AHSA1	Activator of HSP90 ATPase activity	0.302223	0.009302199
HTT	Maintains ZO1 at tight junctions	0.301744	5.424278E-4
FKBP4	Promotes cell proliferation, migration & invasion via Akt/mTOR signalling pathway	0.282431	0.004381645
TPR	Involved in cell cycle regulation	0.277978	0.004543831
HSP90AB1	heat shock protein 90 alpha family	0.26916	6.390391E-4
DNAJB1	DnaJ heat shock protein family (Hsp40) member	0.218769	0.008670006
ZFP36	Deficiency leads to increased tissue inflammation	-0.26035	0.007405405
ARHGDIA	Downregulation contributes to human glioma progression via activation of Rho GTPase signalling pathway	-0.30265	0.002471133
EIF2AK3	Cells lacking EIF2AK3 are more sensitive to ER stress	-0.32948	0.002560799
HSF1	Heat shock transcription factor	-0.36024	0.003944419
CSNK2A1	Encodes CK2. Downregulation of CK2 leads to ROS activation	-0.37811	3.1841334E-6
CDKN1B	Controls the cell cycle progression at G1	-0.49363	1.9953959E-5
NPAS2	Promotes fibrosis. NPAS2-deficient fibroblasts expedite skin wound healing	-0.62989	2.418373E-13
HDAC6	Regulates mitochondrial metabolism	-0.64269	2.5723267E-8
MVD	Also known as CD34.	-0.74312	3.2248114E-13

In table 5.11, we see a number of HSP proteins and co-chaperones upregulated to a substantial degree upon LPS stimulation. This increase in HSPs offers a protective effect against stress and damage exerted by the abundance of LPS. This can induce tolerance to the prolific LPS by lessening the expression or activity of downstream pro-inflammatory cytokines.

Among the top downregulated hits is HTT, a gene typically functioning to maintain ZO1 expression at tight junctions. Downregulation of this gene could lead to increased epithelial permeability thereby enabling crossing of bacteria across the epithelial barrier, potentiating inflammation (table 5.11).

Downregulation of genes such as NPAS2 protects against the progression of fibrosis under these inflammatory conditions, which would confer a protective effect for the individual by avoiding the further, longer-lasting, issue of fibrosis following infection.

UC BASAL V LPS DESEQ GO HITS

GO2000353_Positive Regulation of Endothelial Cell Apoptotic Process

Table 5.12: Log2 fold change of genes contained within the Positive Regulation of Endothelial Cell Apoptotic Process GO database between basal and LPS-treated samples in UC-derived colonic organoids.

Gene	Description	Log2 Fold Change	P-Value
AKR1C3	Associated with increased PGF2α production	0.583761	2.4046046e-11
THBS1	Mediates cell-to-cell & cell-to-matrix interactions	-0.35947	2.1061149e-5

For comparison, the most significant gene hits in our UC samples were analysed and put into a table format. Table 5.12 displays hits in the GO2000353 group that emphasise genes influencing the apoptotic process.

Initially, we can see that there were few results from this group, however the hits that were returned as highly significant are relevant and important to consider. AKR1C3 encodes an aldo/keto reductase enzyme that catalyses the activation of prostaglandins, which are an important aspect of inflammation and increased in IBD.

THBS1 is downregulated compared to control which leads to a loss of cell-cell and cell-matrix interactions. This would have serious ramifications in the health and functioning of the epithelium in addition to further exacerbating the bacterial infection and subsequent inflammatory response.

GO0060231 Epithelial to Mesenchymal Transition

Table 5.13: Log2 fold change of genes contained within the Epithelial to Mesenchymal Transition GO database between basal and LPS-treated samples in UC-derived colonic organoids.

Gene	Description	Log2 Fold Change	P-Value
FZD7	Wnt pathway receptor	0.567097	3.29626e-4

While there has been no clear reporting of FZD7 upregulation in IBD, it can be conjectured that such an increase could progress to the development of carcinogenesis with uncontrolled proliferation initiated via the Wnt-β-catenin pathway (table 5.13).

GO0050727 Regulation of Inflammatory Response

Table 5.14: Log2 fold change of genes contained within the Regulation of Inflammatory Response GO database between basal and LPS-treated samples in UC-derived colonic organoids.

Gene	Description	Log2 Fold Change	P-Value
IL1B	Interleukin 1 beta	2.027469	2.2882004e-6
BIRC3	Promotes EMT, cell migration, and metastasis via upregulating MAP3K7, and, hence, induction of ERK1/2 phosphorylation	1.5850106	2.3872004e-6
ZC3H12A	TLR-inducible gene & immune response regulator	1.4874555	5.021319e-28
NFKBIZ	NFκB inhibitor	1.4369951	2.8296903e-26
ADAM8	Involved in migration, integrin upregulation & adhesion	1.3051387	3.5511693e-25
NUPR1	Inhibits iron-dependent oxidative damage	1.2531737	9.7349885e-26
TNFAIP3	Induced by TNF-mediated NFκB activation. Associated with inflammatory carcinogenesis	1.1309117	2.8149884e-22
DUOXA2	Upregulated during bacterial infection and, specifically, during IBD	1.0727342	5.147369e-25
DNASE1	Endonuclease	0.727912	9.853918e-6
NFKBIA	NFκB inhibitor	0.65850973	2.4939932e-11
TLR3	Toll like receptor 3	0.6355063	1.0283593e-6
PTGER4	Prostaglandin E receptor	0.58963346	5.582718e-5
ACE2	Attached to the membrane of IECs. Serves as an anchor for viral homing	0.5887516	3.92139e-6
ENPP3	Highly expressed in renal cell carcinoma	0.516281	1.9168718e-7
SMAD3	TGFβ receptor-associated signalling molecule	0.47210145	2.3948557e-8
BIRC2	Inhibits apoptosis by binding to TNF receptor-associated factors: TRAF1 & TRAF2	0.4716982	1.1688521e-6
BCL6	Transcription factor for regulation of T helper cell proliferation	0.4559781	5.474048e-4
NAPEPLD	Enzyme that synthesizes endocannabinoids (triggers inflammation)	0.40952885	5.578191e-4
MAPK14	Encodes p38 MAPK (stress-activated kinase)	0.26996166	5.578191e-4
CEBPA	Facilitates cell apoptosis	-0.41543633	3.0344914e-5
MVK	Deficiency linked to autoimmune disorders	-0.448644	8.6241047e-4
IL17RA	Interleukin 17 receptor	-0.56775147	5.1552095e-5
FFAR4	Also known as GPR120. Mediates anti-inflammatory effects.	-0.7590038	7.361986e-11
PYCARD	Also known as ASC. Implicated in tumour suppression	-0.90139896	6.8404697e-6

The GO group, GO0050727, returned a large number of hits as seen in our healthy samples. The majority of these hits, however, were upregulated genes with very few downregulated genes when comparing LPS-treated to basal conditions.

Amongst those upregulated are those directly involved in inflammation such as IL1β, BCL6 and NAPEPLD. In addition to these genes, it is evident that exposure to LPS sensitises UC-derived organoid lines to viral infection with data demonstrating increased TLR3 (receptor for double-stranded RNA) and ACE2 (encoding an enzyme assisting in viral homing). This increased expression and subsequent sensitisation leads to a highly exaggerated immune response in the event of a viral presence. This data confirms our previous data showing a significant increased expression of TLR3 in UC organoids upon LPS-mediated immune challenge.

Aspects promoting carcinogenesis including EMT and cell migration appear to be favoured by increased expression of BIRC3 and ADAM8. While not reported in CRC, another cancer-associated gene, ENPP3, is found to be upregulated in these samples when compared to control. It is, therefore, of interest to further research the possible role of ENPP3 in CRC as this may be a new finding linking LPS stimulation, UC and CRC.

The downregulation of several gene hits listed in table 5.14, could indicate interesting ramifications, including CEBPA which typically facilitates apoptosis, however, when downregulated, apoptosis will be restricted, favouring unchecked cell proliferation. Interestingly, MVK deficiency, which we see in these LPS-treated samples, has been linked to autoimmune disorders. It is therefore possible that reduced MVK expression also plays an important role in UC pathogenesis. FFAR4 is known to mediate anti-inflammatory effects and hence, when downregulated, these effects are substantially limited. Another gene hit that is very relevant in linking UC and CRC is ASC. This gene is implicated in tumour suppression and is downregulated to a significant degree in this experiment. This could lead to tumour progression.

GO0034976_Response to Endoplasmic Reticulum Stress

Table 5.15: Log2 fold change of genes contained within the Response to Endoplasmic Reticulum Stress GO database between basal and LPS-treated samples in UC-derived colonic organoids.

Gene	Description	Log2 Fold Change	P-Value
NUPR1	Inhibits iron-dependent oxidative damage	1.2531737	9.7349885e-26
PMAIP1	Determines whether a cell commits to apoptosis	1.2341281	6.7178007e-7
CXCL8	Also known as IL8	1.1598135	1.151877e-6
KDELR3	Involved in metastasis	1.1348472	7.119348e-15
ERO1A	Contributor to cellular oxidative stress & ROS production	0.8245975	1.569006600000000001e-027
BBC3	Also known as p53 upregulated modulator of apoptosis	0.8089645	2.2637103e-6
PML	Senses ROS, then activating p53 during oxidative stress	0.6492798	3.8325135e-5
ATF3	Induced by IL-1β	0.61732876	2.705977e-9
TNFRSF10B	Binds TRAIL and mediates apoptosis	0.5897953	4.6134896e-10
ANKZF1	Mutations found in ANKZF1 in infantile-onset IBD	0.5794915	6.1623666e-8
DNAJB9	DnaJ heat shock protein family (Hsp40) member	0.5747797	7.7135956e-5
PDIA2	Upstream regulator of UPR pathway	0.5666675	5.807429e-4
NCK1	Elevation promotes migration of breast cancer cells via regulation of ERK1/2 signalling	0.5337522	1.6977308e-4
ERN1	Triggers UPR process in response to ER stress	0.5293869	1.0253137e-6
CDK5RAP3	Co-factor for the oncogenic transcription factor STAT3	0.4880996	2.6508857e-5
UGGT1	A key ER protein involved in UPR	-0.31588992	7.0605206e-4
FLOT1	Erk1/2, p38, JNK, and NF-κB pathways were inactivated by FLOT1 downregulation	-0.35228667	1.3245913e-4
THBS1	Adhesive glycoprotein that mediates cell-to-cell & cell-to-matrix interactions	-0.35946628	2.1061149e-5
ATP6V0D1	Deficiency enhanced inflammasome activation	-0.36225134	0.001439433
DCTN1	Binds to microtubules.. Involved with ER-to-Golgi transport	-0.3937077	4.212129e-5
TLN1	Critical for reinforcement of integrin-cytoskeleton bond	-0.41974953	3.0270546e-6
DNAJB12	DnaJ heat shock protein family (Hsp40) member	-0.44686416	0.001217236
BCL2L1	Apoptosis inhibitor gene	-0.50237864	4.777302e-7
AIFM1	Induces apoptosis	-0.5137814	1.7580489e-5
ERN2	Encodes a pro-apoptotic protein	-0.52306956	1.2208334e-5
TOR1A	TorsinA aids in the movement of membranes within the ER.	-0.53085965	0.002637021
CFTR	Downregulation of CFTR in bronchial epithelial cells found to lead to activation of MAPK & NFκB pathways, excessive COX-2/PGE 2 & IL8 production	-0.72542757	4.263413e-14
SESN2	Knockdown of SESN2 results in LPS-mediated NFκB phosphorylation & increased secretion of pro-inflammatory cytokines	-0.8059524	1.5318856e-10
CHAC1	CHAC1 degrades intracellular antioxident	-0.89111215	2.3696879e-7
SCAMP5	Knockdown severely impairs vesicle endocytosis	-1.0509659	3.3180788e-6

As previously reported in our healthy line, the GO group, GO0034976, revealed interesting data, especially in the top 30 hits listed in table 5.15.

Multiple increases in genes relating to oxidative stress, inflammation and tumour progression were observed in this data. These findings are concurrent with the effects of chronic exposure to LPS in predisposed tissue.

Genes displaying reduced expression encode proteins relating to inflammatory activity and cell-to-cell adhesion. Often the downregulation of these genes, such as ATP6VOD1, CFTR and SESN2, enhances the inflammatory response. Whereas deficiency of the THBS1 gene is likely to be detrimental to cell-cell and cell-matrix interactions, leading to enhanced permeability of the epithelium (figure 5.15).

GO0034614 Cellular Response to Reactive Oxygen Species

Table 5.16: Log2 fold change of genes contained within the Cellular Response to Reactive Oxygen Species GO database between basal and LPS-treated samples in UC-derived colonic organoids.

Gene	Description	Log2 Fold Change	P-Value
LCN2	Elevated LCN2 levels associated with severe inflammation in IBD	3.429006	6.160004e-8
AXL	A receptor tyrosine kinase implicated in fibrogenic pathways	1.352049	1.2758415e-8
TNFAIP3	Induced by TNF-mediated NFκB activation. Associated with inflammatory carcinogenesis	1.130912	2.8149884e-22
BMP7	Acts via the TLR4-NLRP3 inflammasome complex	0.884866	1.342179e-12
CDK1	Key player in cell cycle regulation	0.716131	6.807173e-4
AKR1C3	Associated with increased PGF2α production	0.583761	2.4046046e-11
ANKZF1	An independent factor of poor survival in CRC	0.579492	6.1623666e-8
PYCR1	An enzyme involved in cell metabolism - shown to be up-regulated in cancers	0.443407	1.7951248e-4
PSAP	Closely related with mTOR signalling	0.2963	6.0779555e-5
JUN	Proto-oncogene	0.284186	7.0356595e-4
GCH1	Induces immunosuppression through metabolic reprogramming	-0.49316	2.550698e-4
AIFM1	Induces apoptosis	-0.51378	1.7580489e-5
RHOB	Controls endothelial barrier integrity during inflammation	-0.55218	2.72606e-7
PPARGC1B	Increases NLRP3 inflammasome activity & IL-1β production	-0.66435	1.9947551e-7
FABP1	Downregulation predicts invasive progression of bladder cancer	-0.69233	5.289609e-4

While the previous group comprised a few genes related to stress response and ROS production, this GO database was more specified in this area of biological processes. Included within this group are genes contributing to the generation of ROS, namely BMP7 and PSAP, which hold critical implications in the stress response pathways.

Additionally, inflammatory-specific genes including LCN2, TNFAIP3 and AKR1C3, are found to be upregulated in this dataset. Conversely, immunosuppressive genes, such as GCH1, have been downregulated. RHOB encodes a member of the Rho GTP-binding protein family, which controls endothelial barrier integrity during periods of

inflammation via regulation of Rac1. This downregulation could also lead to loss of epithelial integrity in cases of UC (table 5.16).

GO0034142 Toll-like Receptor 4 Signalling Pathway

Table 5.17: Log2 fold change of genes contained within the Toll-like Receptor 4 Signalling Pathway GO database between basal and LPS-treated samples in UC-derived colonic organoids.

Gene	Description	Log2 Fold Change	P-Value
TNFAIP3	Induced by TNF-mediated NFκB activation. Associated with inflammatory carcinogenesis	1.130912	2.8149884e-22
TICAM2	Toll like receptor adaptor molecule	0.754464	8.3983736e-4
NFKBIA	NFκB inhibitor	0.65851	2.4939932e-11
PELI1	Regulates TLR and T cell receptor signalling. Upregulated in several cancers	0.399573	8.4142994e-5
S100A14	Downregulation correlates with poor differentiation & poor prognosis in oral cancer	-0.29973	1.5388975e-4

TNFAIP3 was found to be much further upregulated in our UC samples in comparison with the healthy control. Moreover, TICAM2 was found to be significantly increased in UC samples, whereas we have observed this gene to be highly downregulated in our healthy samples. This is an integral factor differing between healthy and UC patient-derived organoid platforms as TICAM2 plays a critical role in the TLR4 pathway. In addition to this finding, PELI1 expression was also raised, this gene has been linked with regulation of TLR and T-cell signalling also.

The NFκB inhibitor, NFKBIA, was also found to be upregulated; in indicating that much of the response we can see in this experiment is not due to a high degree of NFκB activity (table 5.17).

GO0031072_Heat Shock Protein Binding

Table 5.18: Log2 fold change of genes contained within the Heat Shock Protein Binding GO database between basal and LPS-treated samples in UC-derived colonic organoids.

Gene	Description	Log2 Fold Change	P-Value
GBP1	Facilitates caspase-4 recruitment	1.0823895	0.001117016
CHORDC1	Encodes gene product Morgana, a component of the IKK complex	0.99614745	1.1231004e-7
HSPA1B	Heat shock protein family A (Hsp70) member	0.95358884	3.0596115e-28
DNAJA1	DnaJ heat shock protein family (Hsp40)	0.77123517	1.5161974e-11
HSPA8	Heat shock protein family A (Hsp70) member	0.7671301	1.7492522e-19
CDK1	Drives cell division	0.7161311	6.807173e-4
DNAJA4	DnaJ heat shock protein family (Hsp40) member	0.594179	3.2765195e-9
DNAJB9	DnaJ heat shock protein family (Hsp40) member	0.5747797	7.7135956e-5
DNAJB1	DnaJ heat shock protein family (Hsp40) member	0.55472517	0.001217236
ERN1	Triggers UPR process in response to ER stress	0.5293869	1.0253137e-6
HSPA1A	heat shock protein family A (Hsp70) member	0.47485197	0.001858028
HSP90AB1	heat shock protein 90 family member	0.42274854	5.4788774e-7
CDKN1B	Controls the cell cycle progression at G1	0.4144371	7.3467054e-5
FKBP4	Promotes cell proliferation, migration & invasion via Akt/mTOR signalling pathway	0.40048072	3.7493734e-5
BCOR	An oncogenic mechanism has been suggested – not yet fully understood	0.35860115	0.002034554
CSNK2A1	Encodes CK2. Downregulation of CK2 leads to ROS activation	0.35562167	8.67465e-6
PTGES3	Encodes p23 – Co-chaperone for the Hsp90 pathway	0.3123688	1.5608732e-4
HTT	Maintains ZO1 at tight junctions	-0.29498923	7.201291e-4

Table 5.18 demonstrates upregulated gene hits such as GBP1, CHORDC1 and FKBP4 that are directly involved in formation of complexes and activation of pro-inflammatory pathways. The other upregulated hits in this list are, for the most part, genes encoding heat shock proteins and those involved with the response to ER stress.

The gene encoding the protein kinase, CK2, is downregulated, which has been reported to contribute to ROS activation. While HTT downregulation leads to a loss of ZO1 at epithelial tight junctions resulting in increased barrier permeability.

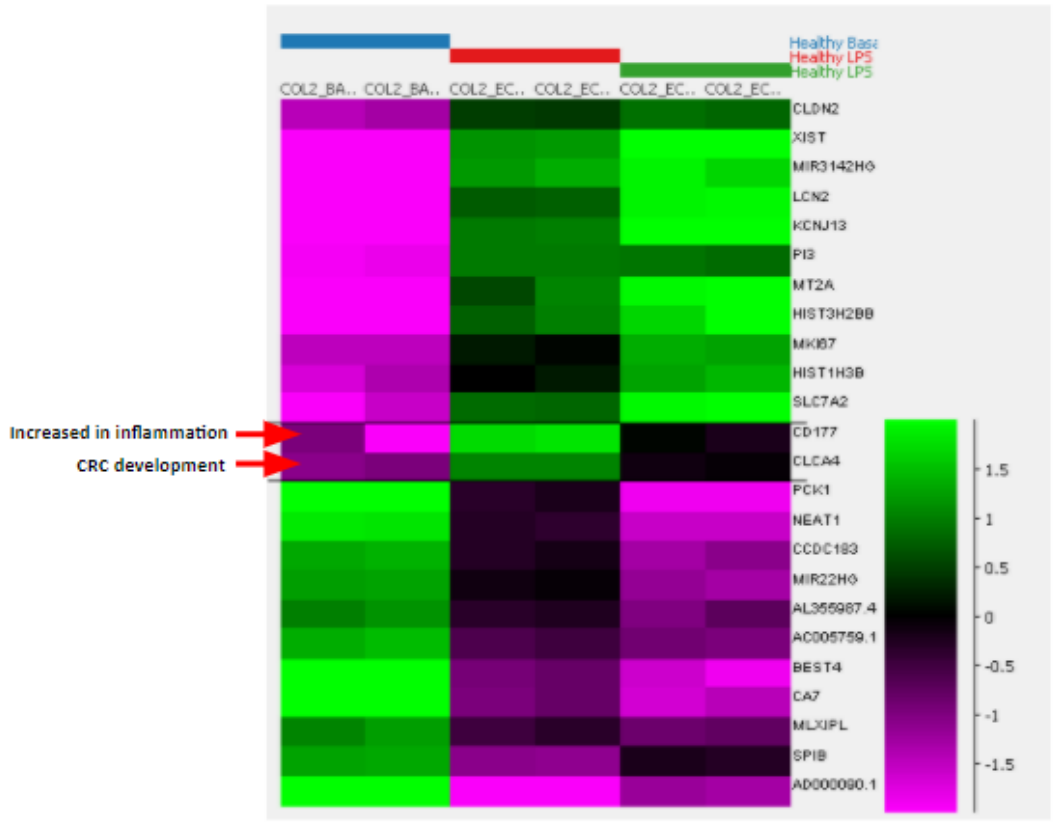

Figure 5.29: Heatmap comparing the data from basal, LPS-treated and LPS + TLR4 inhibitor samples isolated from healthy colonic organoids.

The top hits in terms of the most significant alterations to gene expression were then converted into a heatmap format to allow for clearer visualisation. Original representation by scatter plots is provided in Appendix 4. Figure 5.29 presents the data comparisons between the 3 conditions of our healthy organoid line.

Green represents the genes that were upregulated in each condition compared to control. While purple suggests the gene has been downregulated and black signifies no change. While there are 24 genes that are listed as the most statistically significant in this analysis, two, in particular, demonstrate an increase following administration of LPS which is then reduced upon the addition of the TLR4 inhibitor. Very low expression can be observed in the basal condition, displayed in purple. These genes, CD177 and CLCA4, have not been measured in these previous experiments and were therefore interesting to investigate further. CD177 is a gene encoding the antigen present on neutrophils and is therefore this gene is naturally increased under inflammatory conditions. This is supported by the data we see from this experiment, with a substantial increase in the LPS-treated condition in comparison to basal levels. To further demonstrate that this protein is expressed at increased levels due to acting via the TLR4 pathway, the data clearly shows that expression was reduced considerably upon the inclusion of the TLR4 inhibitor. The same expression profile was recorded for CLCA4, a gene encoding the chloride channel. Increased expression of this gene has also been suggested to be a biomarker of IBD. The remaining genes included in this heatmap are divided into upregulated genes, in the top half of the figure, and downregulated genes. These results indicate the number of genes impacted by activation of the LPS/TLR4 pathway.

This range of genes includes: Claudin-2, a tight junction protein associated with colonic inflammation; Lipocalin-2, an innate immune protein; the nuclear-restricted lncRNA, NEAT1, involved in IL1β production and CA7, another example of a lncRNA usually found to be expressed in the colon, with decreased expression previously found in CRC tissue.

These are very interesting results that shall be further reflected upon later in this chapter.

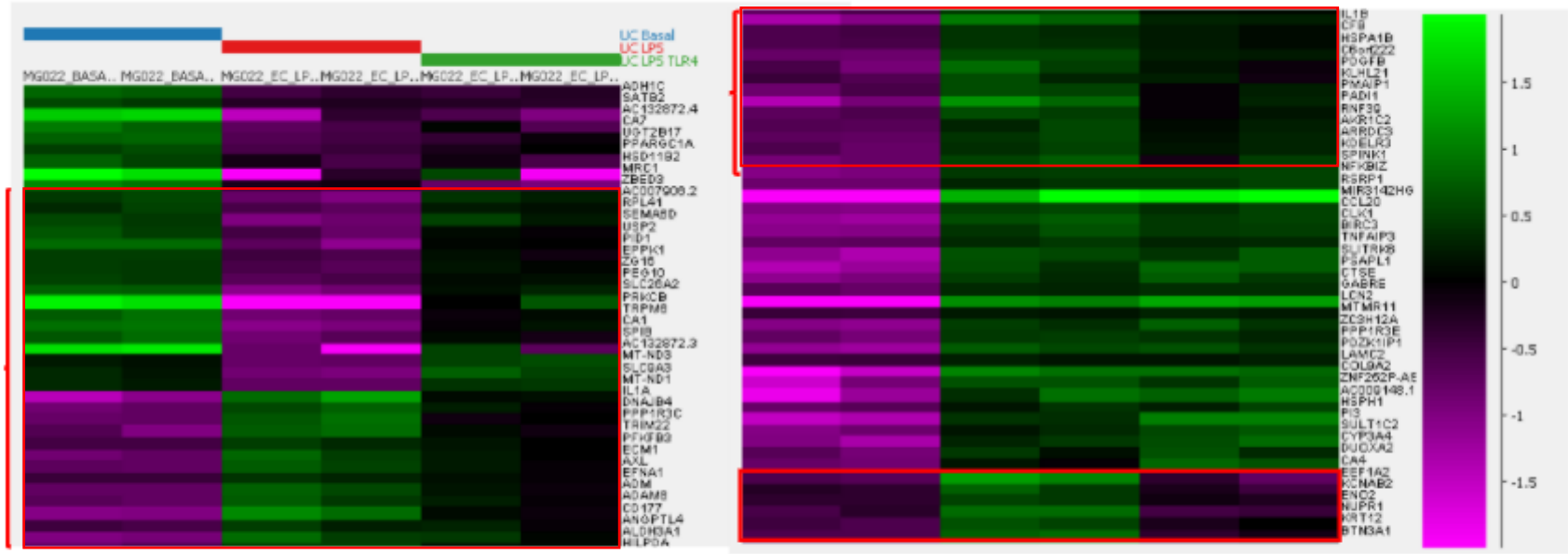

EFNA1 – Required for CRC tumour growth
ADAM8 – Overexpressed in CRC. Associated with worse disease outcome.
CD177 – Increased in inflammation
ALDH3A1 – Confers chemoresistance
HILPDA – Positive modulator of malignant progression in colonic epithelial cells.

EEA1A2 – Oncogene
ENO2 – Upregulated in metastatic CRC
NUPR1 – Early stress response gene (induced by ATF4)
KRT12 –
BTN3A1 – Detected on epithelial cells at CRC tumour site

Figure 5.30: Heatmap comparing the data from basal, LPS-treated and LPS + TLR4 inhibitor samples isolated from UC-derived colonic organoids.

A separate heatmap was then generated for UC colonic organoids, comparing all 3 treatment conditions after the 48-hour treatment period (figure 5.30). Here we can initially see the difference in the number of hits in comparison to those in the previous figure focussing on healthy organoids only. The difference is almost double with 45 hits compared to 24. This is suggestive of the greater impact LPS has upon UC tissue, reflecting the enhanced response we have found across all previous experiments conducted comparing UC-derived models with healthy controls.

While all these hits are the most significant of all the genes ran from the GO database groups, the genes highlighted by the red boxes demonstrate the greatest effect of the TLR4 inhibitor following the effects instigated by LPS alone.

A selection of these genes were present in the COL2 data, including CA7 which is also downregulated in this UC model. Also evident in this dataset are that a large proportion of the genes in this list, are associated with CRC development. This is a very interesting finding and relevant to this project as it further corroborates our data suggesting that UC-derived tissue is positioned towards CRC development prior to any observable indications. A list of oncogenes upregulated by LPS in this model are listed in the table below:

Table 5.19: Selection of genes reversed by pre-treatment with TLR4 inhibitor.

GENE	FEATURE
EFNA1	Required for CRC tumour growth.
ADAM8	Overexpressed in CRC. Associated with worse prognosis.
ALDH3A1	Confers chemoresistance.
HILPDA	Positive modulator of malignant progression in colonic epithelial cells.
EEA1A2	Oncogene.
ENO2	Upregulated in metastatic CRC.
BTN3A1	Detected at CRC tumour site of epithelial cells.

Hits info:

JUN – Forms complex with AP-1 contributing to inflammation.
CCL20 – Enhanced expression in UC. Binds with CCR6.
PXK –
MECOM –
BCL6 – Restrains IRF6 transcription. Negative regulator for interferon IFN-β production.
RBPJ – Transcription factor that mediates signalling through Notch receptors.
TLR3 – Microbial recognition receptor.
TICAM2 (aka TRAM) – Recruited by TLR4. Leads to IRF3 activation.
NDST1 – Upregulated in inflammation in macrophages.
MAPK14 – In TNF pathway.
ENPP3 – Knockdown increases granulocyte infiltration.
TNFAIP3 – Inhibitor of NFκB activation.
NAPEPLD – mRNA levels decreased in UC.
FFAR4 (aka GPR120) – Attenuates NFκB activation.
ADAM8 – Overexpressed in CRC.
MVK –
NFKBIA – Associated with risk of UC.
PNMA1 –
THBS1 – Activates TGFβ1. Decreased expression increased pro-inflammatory cytokine production.
DUOXA2 – Upregulated in UC. Involved in H_2O_2 production.
NUPR1 –
CD68 – Macrophage surface marker. Inflammatory antigen.
IFNGR2 – A major cytokine in IBD pathogenesis.

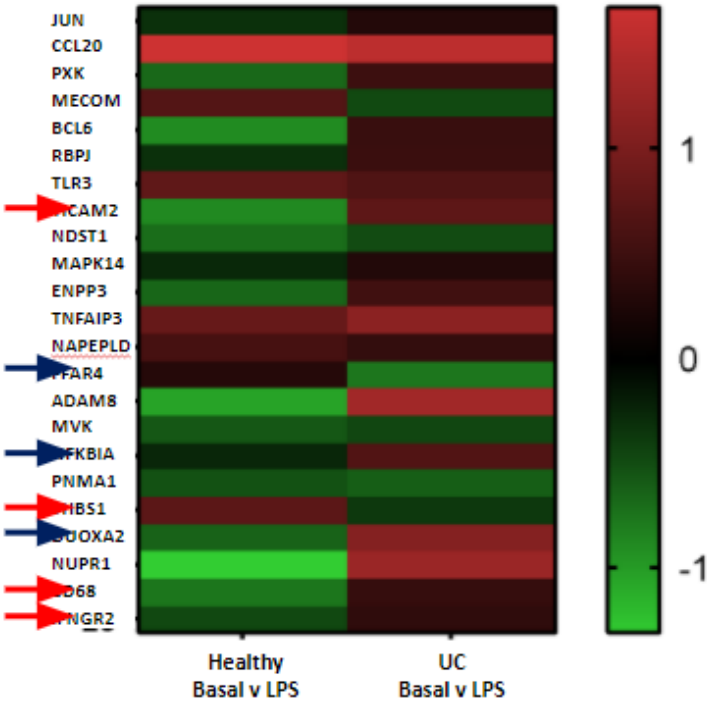

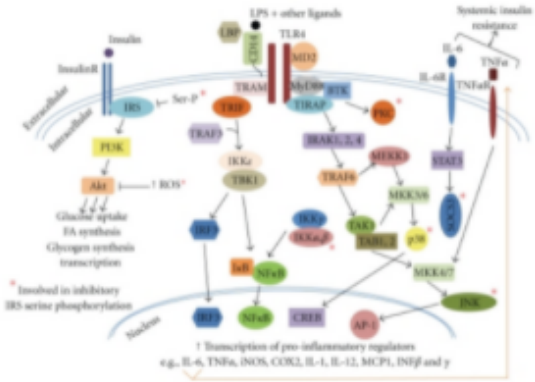

Figure 5.31: Inflammatory genes - Heatmap comparing the differential responses of samples under basal & LPS-treated conditions isolated from both Healthy & UC-derived colonic organoids.

Following the comparison of basal, LPS-treated and TLR4 inhibitor-pre-treated conditions for both healthy and UC organoid platforms, the basal and LPS conditions were focussed on, and direct comparisons made between the two models. This data displays more depth around the genes that are differentially expressed between the lines. Of these 23 hits, the most significant are TICAM2 (otherwise known as TRAM); FFAR4; NFKBIA; THBS1; DUOXA2; CD68 and IFNGR2. These genes are all of interest and are heavily involved in the TLR4 pathway or overall inflammatory response (figure 5.31).

Hits info:

TINAGL1 – Inhibits EGFR activation.
LEPR – Phosphorylates STAT1, -3 & Smad7.
HIST2H2BE – Associated with colitis & CRC.
QSOX1 – Involved in ROS production.
LAMC2 – Regulated by CDK2 & TNFα.
LYPD8 – Exp lower in active UC lesions.
TFPI – Higher expression in UC.
IHH – Anti-inflammatory modulator.
SERPINE2 – Promotes ECM production. Upregulated in human CRC.
CCL20 – Increased in IBD.
PROS1 – Decreased in IBD. Increasing risk of thrombosis.
FGFBP1 – Upregulated in cancers.
EGF – Upregulation favours colitis-associated carcinogenesis.
SLC9A3 – Downregulated in patients with UC.
SELENOP –
CCL28 – mucosae-associated epithelial chemokine.
HBEGF – inhibits expression of inflammatory cytokines.
SPINK1 – Promotes IBD & CRC development.
HIST1H2BC – Associated with colitis & CRC.
VEGFA – promotes intestinal angiogenesis & inflammation.
SMPDL3A – Co-purified with TLR4.
AGR2 – Deletion increases inflammation.
IGFBP3 – Upregulation increases IGF-independent apoptosis.
HILPDA – HILPDA transcripts are highly expressed in CRC. Upregulated in inflammation.

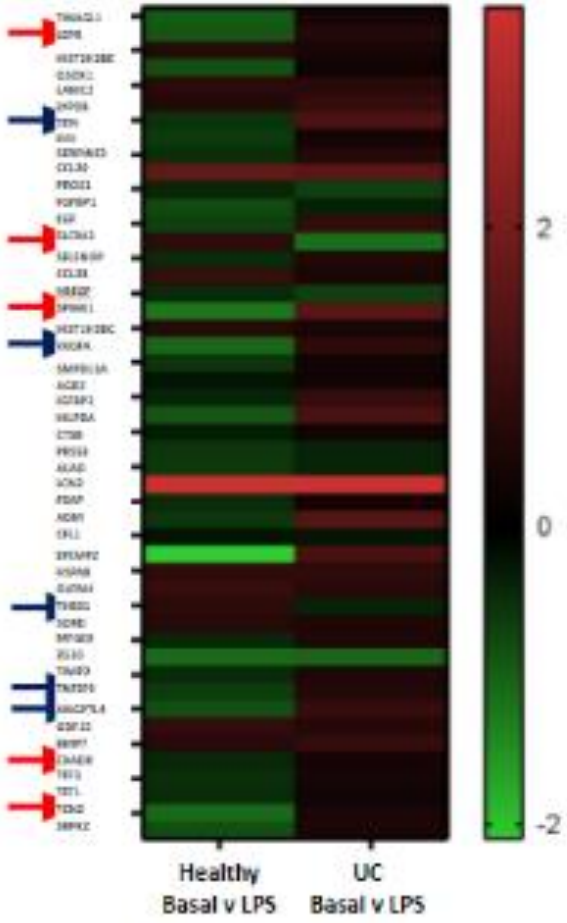

CTSB – Cathepsin B.
PRSS3 – Encodes trypsinogen-3.
ALAD – Involved in heme synthesis.
LCN2 – an anti-microbial peptide.
PSAP – regulator of lysosomal function.
ADM – Reduces inflammatory indices. Activates HIF signalling pathway.
CFL1 – promotes cytoskeletal dynamics.
EFEMP2 –Induces EMT via the PI3K/AKT/mTOR pathway.
HSPA8 – to induce TNF-α, IL-1β & IL-6 via activation of TLR4.
OLFM4 – Glycoprotein present in mucus. Overexpressed in IBD.
THBS1 – Anti-inflammatory & anti-angiogenic.
SORD – sorbitol dehydrogenase.
MFGE8 – Attenuates inflammation.
ZG16 – mucus-secreting cell marker.
TIMP2 – Usually inhibited by LPS.
TNFSF9 – Promotes inflammation.
ANGPTL – Downregulation attenuates inflammation.
GDF15 – Induced exp in inflammatory conditions.
BMP7 – Reduces inflammation and oxidative stress.
CXADR – Promotes inflammation.
TFF3 – couples with MUC2.
TFF1 – couples with MUC5AC.
TCN2 – binds vitamin B12.
SRPX2 – Promotes cell adhesion.

Figure 5.32 Secretory genes - Heatmap comparing the differential responses of samples under basal & LPS-treated conditions isolated from both Healthy & UC-derived colonic organoids.

Once the inflammatory genes had been assessed and the differences between healthy and UC-derived organoids were further evaluated, the expression profiles were then compared for secretory genes specifically. The top 48 hits with the highest level of significance were presented in this heatmap (figure 5.32). All these highly significant hits appear to be linked to IBD and the development of CRC, with functions focussed on ECM production, cell adhesion and oxidative stress. The genes revealed in this data will further uncover the link between the TLR4 pathway, UC pathogenesis and CRC development and the mechanisms involved in the epithelial tissue.

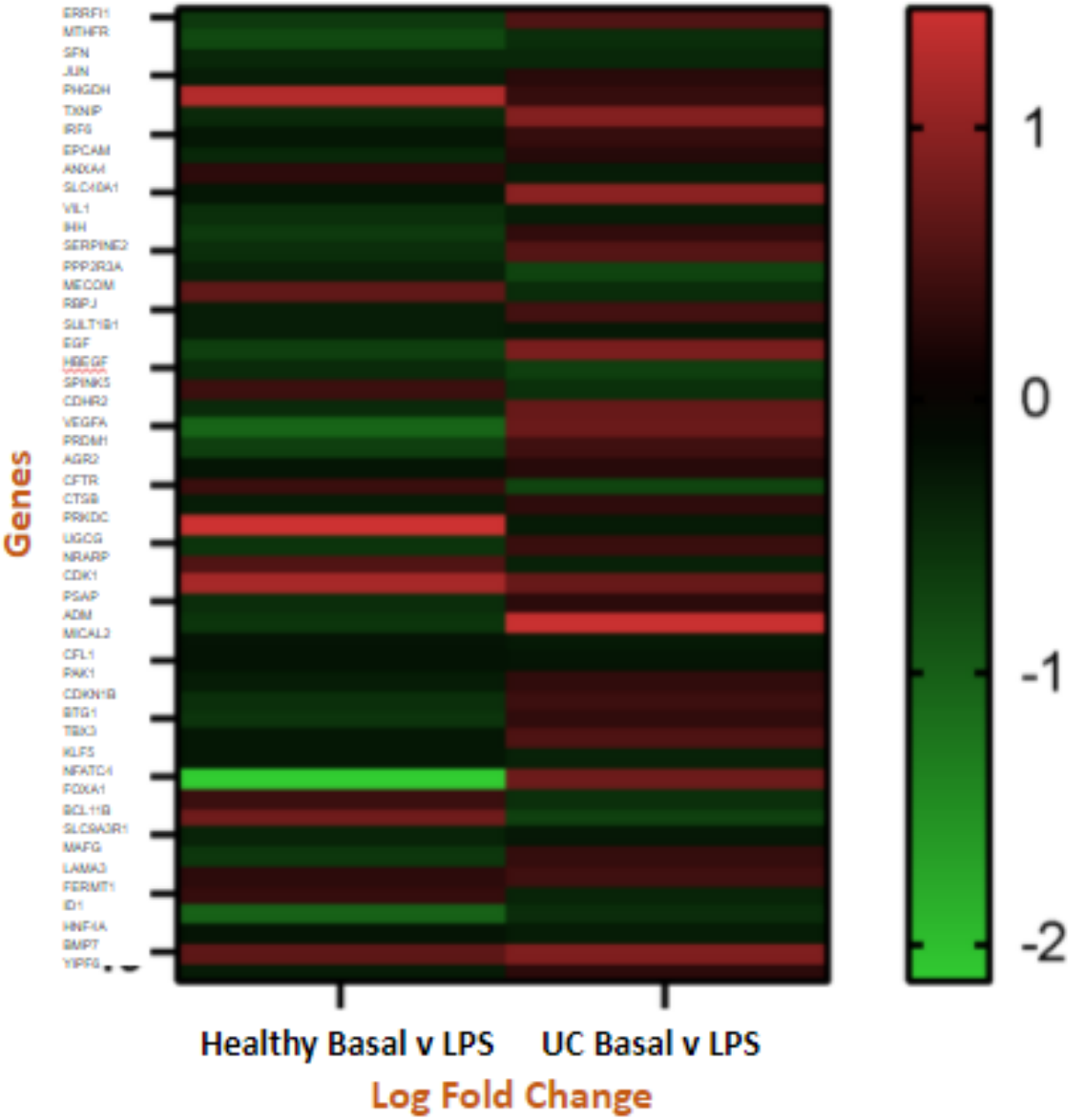

Table 5.33: Top hits with greatest Log2 fold change between healthy and UC-derived lines under basal and LPS-induced conditions.

Once a clearer idea of the processes triggered by activation of the TLR4 pathway was garnered, analysis was then focussed on epithelial genes to illustrate the impact more directly upon the epithelium. The genes highlighted in this group include VILLIN, which we have explored by RT-PCR; SERPINE2; SPINK5; VEGFA and NFATC1 (figure 5.33). These genes, along with others on this list, have important implications in UC and CRC that has been found in immune cell lines but never reported in a patient-derived colonic epithelial model. The importance of these results shall be further explored in the discussion section.

5.3 Discussion

5.3.1 Differential Response of Healthy & UC-Derived Colonic Organoids to TNFα

TNFα is a critical factor heavily involved in inflammation in infection and disease, including UC [195].

Further to our initial testing and optimisation performed on our healthy lines, in which we saw considerable increases in expression of over 40-fold above control, the next step was to continue experimentation on both healthy and UC-derived organoid lines simultaneously to determine whether a differential response is present and to what degree.

We expect to see a much greater surge of pro-inflammatory cytokines in response to a pro-inflammatory stimulus, such as TNFα, in UC tissues when compared to healthy epithelial tissue. This is due to the exaggerated immune activity present in the GI tract of UC patients during a flare-up.

While TNFα is an essential factor in the functioning healthy immune system, it has been established as having clear involvement in IBD pathogenesis, with increased levels detected in serum, stool and mucosal biopsy specimens of IBD patients [160,161]. Furthermore, it has also been demonstrated that persistent TNF overproduction in the intestinal epithelium can lead to chronic intestinal inflammation demonstrated by mouse studies [214]. These changes were detected as early as 16 weeks after gestation [214]. Therefore, TNF is an important component to research in regard to UC and to analyse the comparisons that can be made with healthy epithelial tissue.

As we have previously demonstrated in our study, stimulation with TNFα triggers a positive feedback response, enhancing the production of TNFα itself, along with other pro-inflammatory cytokines and chemokines in the TNF signalling pathway, including IL8 and IL23. Furthermore, we have investigated the effect upon the colonic epithelium directly through the measurement of expression changes related to LGR5+ stem cells, colonocytes and goblet cells, all crucial to the healthy functioning of the colon and its capacity to continually regenerate.

The data acquired from the simultaneous treatment of our healthy & UC-derived organoid platform with 40 ng/ml TNFα clearly shows the distinct differential response between the representative lines. The pro-inflammatory response was much stronger in our UC line when compared to the healthy control as evidenced by the substantial raised expression of TNFα itself, NFκB, IL1β, IL8 and IL23. Expression of TNFα was upregulated 500-fold compared to the untreated control. In comparison to the treated healthy response, this was over 10 times greater which demonstrates an overwhelming sensitivity to TNFα that is not present in healthy colonic organoids. This significantly heightened positive feedback response to one of the most prolific pro-inflammatory cytokines is highly likely to contribute to a considerable uncontrolled immune response leading to substantial damage of local tissues following recruitment of numerous immune cell types.

This exaggerated inflammatory profile was observed across all markers tested, with IL23 displaying the next most prominent response to TNFα with expression in UC-derived organoids almost 10 times higher than that initiated in healthy organoids. As well as TNFα inducing raised IL23 expression, this effect has also been reported to occur in reverse, with IL23 promoting the expansion of CD4+ cells which in turn produce TNFα, amongst other inflammatory chemokines [215]. This cyclical effect following initial stimulation with TNFα would lead to persistent chronic inflammation that builds exponentially. Hence, it is easy to see how the inflated elevation of these cytokines seen here in UC organoids could easily lead to tissue destruction in a relatively short period of time.

Expression of IL8 in our UC line was found to be elevated 6 times above the corresponding healthy treated sample. IL8 is a neutrophil chemoattractant found to be correlated with the levels of inflammation in colonic biopsies from UC patients [216]. IL8 expression levels have also been linked with increased IL1β and TNFα which we have confirmed in this experiment [216].

The NFκB pathway has been proposed as a mechanism linking TNFα and IL8 production. IL8 production has been found by Wang et al to be increased in a time-dependent and a dose-dependent manner in response to TNFα. In conjunction with this response, phosphorylation of p38 MAPK and translocation of the NFκB p65 protein to the nucleus was observed in immunofluorescence staining [217].

However, this study utilised the human hepatocellular carcinoma cell line, MHCC-97H, only and had not tested this pathway resumed in non-cancerous cells. Our data also demonstrates that this pathway and correlation between TNFα, NFκB and IL8 does exist under inflammatory conditions in non-cancerous primary cells.

In addition to the overwhelming pro-inflammatory response of UC to TNFα stimulation, the epithelium-specific effect was also analysed in this experiment. This data was more variable, however LGR5 shows very distinct opposing responses to TNFα. LGR5 expression dropped substantially in healthy organoids which complements data presented in the previous chapter showing healthy cells alone treated with TNFα. Interestingly, we see a 4-fold increase in LGR5 expression in our UC line. Under normal conditions, this increase would lead to a positive impact and aid in restoring the epithelium in the wake of damage. However, in the case of UC it is likely this response could be due to a short-lived compensatory mechanism in order to protect the epithelium, or, more likely, it could be an indicator of predisposition to CAC. Several recent studies have found increased LGR5 expression to be correlated CAC progression, p53 expression and to be associated with poor prognosis of patients with CAC [178,218]. This may explain the data we can see in this experiment with the discrepancy between the two lines.

This profile is replicated in OLFM4 expression to a much greater extent, with a 130-fold increase in comparison to healthy lines. OLFM4 can jointly act as a marker for ISCs as well as a marker for inflammation. OLFM4 is a glycoprotein regulated by multiple signalling pathways including NFκB, Wnt and NOTCH [140]. Inhibition of OLFM4 has been found to interfere with NFκB pathway activity which is closely linking these proteins in the inflammatory response [140]. Our data supports this finding by demonstrating the substantial elevated expression of both NFκB and OLFM4 in UC colonic organoids in response to TNFα.

The drop in MUC2 expression we can see in figure 5.2 is evidence of the reduced protection of the colonic epithelium under these conditions. When the thicker, inner layer of mucus is reduced bacteria is able to reach and penetrate colonic epithelial cells, further exacerbating inflammation. This, in itself, can intensify IBD in patients [219]. Furthermore, MUC2 has been found to play a suppressive role in inflammation by inhibiting β-catenin and subsequently NFκB [220]. Therefore, this loss of MUC2 we have

observed and reported here would have a much greater effect upon the progression of IBD in the presence of any additional inflammatory stimulation (i.e., TNFα) than allowing bacterial translocation alone. Further investigation could help determine whether these findings are as a result of changes to the overall number of goblet cells or to a reduction in the production of mucin by these cells. Immunofluorescence or flow cytometry would offer greater confirmation.

This data, together, suggests a genetic predisposition of colonic tissue in UC patients demonstrated by an overwhelming dysregulated immune response. This is made evident by the disproportionately greater inflammatory response to TNFα following long-term culture in non-inflammatory basal conditions. This finding would mean any colonic tissue in a patient with UC could undergo such a response at any time, under pro-inflammatory conditions, suffering severe damage despite there being no obvious visible tissue changes previously. Therefore, any treatment should target both visually inflamed and non-inflamed tissue to prevent further spread of the disease and subsequent damage. While there is no doubt to the extensive differences in phenotypic response of healthy & UC-derived epithelial tissue, sequencing would be required for confirmation of the possible genetic predisposition.

Once the comparisons between healthy and UC patient-derived organoids were made in terms of stimulation with a broad range pro-inflammatory cytokine such as TNFα, and the differential response analysed, the next step was to determine whether such a differential response would be observed in response to emulated bacterial stimulation by exposure to LPS over a prolonged period.

Toll-like receptors are responsible for the binding of viral and bacterial PAMPs, resulting in the activation of many downstream inflammatory signalling pathways. Hence, mRNA expression of the 5 most abundant TLRs were analysed for the purpose of ascertaining whether TNFα has any impact upon antigen sensing following exposure. Priming of TLRs has been suggested to increase sensitivity to subsequent microbial presence, leading to an elevated systemic inflammatory response. In UC, subsequent infections can cause severe damage to the colon of the patient. The mechanism responsible for this priming effect is not yet well understood.

5.3.2 Differential Response to Lipopolysaccharides

Ulcerative colitis was largely considered a disorder solely mediated by leukocytes, and hence, the role other cell types play in this pathogenesis have largely remained unexplored until recently. During this time, evidence was uncovered that implicated an inflated immune response to the microbiota in UC pathogenesis [221]. Further understanding of the mechanisms involved in this dysregulated response to microbial compounds are, therefore, a key area of interest.

This chapter reveals the effects of LPS exposure on UC patient-derived organoids. The experiment was conducted in conjunction with healthy isolated colonic organoids to be able to more accurately compare and assess the differences and discrepancies between the responses of each. This can further inform as to the deviations of UC epithelial tissue under inflammatory circumstances and to what extent the predisposition towards UC affects tissue response.

Once the most effective dose found to induce the greatest inflammatory response had been ascertained using healthy organoids, this was carried through to subsequent experiments. Furthermore, it was decided in prior experimentation that LPS isolated from *E. coli* O127:B8 would be selected for continued use in this study, as it instigated a more consistent response by our platform, proving to be more reliable for future comparisons.

The relevance of LPS in IBD pathogenesis was first speculated in 2000 when Caradonna et al reported that LPS had been detected in the plasma of IBD patients [222]. In addition to this finding, the group described the presence of ‘abnormal microflora’ [222], suggesting dysbiosis which links into the increased presence of LPS within the gut, however, this does not reveal the reasoning for elevated levels of LPS within patient plasma. The occurrence of increased permeability of the intestinal mucosa was also present and is likely caused by the increased presence of LPS.

Other studies have since researched this involvement of LPS, also finding the alterations in intestinal permeability in conjunction with the increased presence of gram-negative bacteria expressing LPS [223]. However, the exact mechanisms and pathways involved have not yet been ascertained and the root causes for the

discrepancy to healthy epithelial response have not been closely investigated. Several studies have involved primary patient tissue, with which the current inflammatory state was measured immediately upon tissue removal [224-226]. This method gives insight into the inflammatory state of the tissue at the moment of extraction, however the tissue cannot then be further manipulated and analysed to determine factors that can alter this state using a more specific experimental approach. Alternatively, other groups have conducted their research on LPS and IBD in mouse models or using immortalised cell lines [227,228]; [223], both of which have their limits and disadvantages in the modelling of a human disease such as IBD.

5.3.2.1 Transcriptomic Techniques Identified Differences Between Healthy & UC Colonic Organoid Response to LPS

In our study exploring the differential response between healthy and UC patient-derived colonic epithelial organoids, the data we acquire can be relied upon to give a simplified, but representative, view of possible epithelial response *in vivo*. This experimental set up included the use of a TLR4 inhibitor to further investigate the extent to which the effects being measured are in fact mediated via the TLR4 signalling pathway. Both morphological, transcriptomic and proteomic data establish LPS as having a substantial negative effect on this platform with necrotic tissue present in both lines after 48 hours of exposure. The data displayed in figure 5.6 clearly depicts a highly inflated response on the part of our UC organoids in comparison to their healthy counterpart. TNFα reached 30-fold above control while healthy organoids maintained a rather muted response. Understandably, this response isn't as strong as exposing the platform to TNFα directly, however this is substantially heightened and capable of instigating an inflated and persistent inflammatory presence within the epithelium.

IL1β supports this effect with an increase of 14-fold above untreated control, being the second most substantial response in this experiment. This finding is supported by research demonstrating IL1β to be upregulated in UC mouse models, possibly acting as further clarification of the link between LPS and UC development [229].

Consistent with previous data acquired from experiments conducted on healthy organoids alone, IL18 sees a dip in expression, while UC tissue responds by

increasing expression by almost 2.5-fold. This is a highly differential response between healthy and UC-derived organoids treated under matched conditions.

Plasma concentration of IL18 was found to be correlated with the visible degree of mucosal damage as determined via endoscopy [230]. This level of IL18 expression was higher in the plasma of UC patients with more severe disease than those with mild disease [230]. This increase in IL18 plasma concentration was also found in mucosal tissues, however to a much lesser extent, which was not found to be significant [230].

An extreme differential response still holds for ISC expression, as demonstrated by LGR5, with a distinct drop measured in UC organoids of approximately 75%. Contrary to this, healthy epithelial organoids demonstrate a 2.5-fold increase. This increase we observe would be favourable in the defence against further bacterial invasion, with increased barrier integrity and regenerative capacity in the epithelium. This response would decrease the ability for bacteria to penetrate and invade systemically, while also promoting recovery following inflammation-inflicted damage.

This emphasised difference between lines was also present in villin with a subdued response in healthy organoids and 3 times higher expression in UC. These findings, in conjunction with the LGR5 data points, depicts an image of increased differentiation of ISCs to colonocytes. Alternatively, villin has been suggested to act as an anti-apoptotic protein. This has been demonstrated by villin-deficient mice which were more prone to the development of DSS-induced colitis due to the increased occurrence of apoptosis [231]. This lack of villin resulted in severe epithelial damage and increased infiltration of inflammatory cells [231]. The increase observed in this experiment could be as a result of initial compensation of the epithelium under these conditions or an indicator of predisposition of these samples to CRC development.

5.3.2.2 Immunohistochemistry & Immunofluorescence Techniques Reveal Spatial Information Regarding Intestinal & Inflammatory Proteins

Our transcriptomic findings were further corroborated by proteomic methods including immunofluorescence, immunohistochemistry and proteome arrays. In addition to

offering confirmation of transcriptomic data, these techniques gave insight into pathway differences, both at the receptor level and downstream.

Responses of healthy organoids to LPS, as measured by intestinal protein (CDX2, MUC2, VIL, ECAD) and inflammatory protein (NFκB, TLR4, MD2) expression, remained muted across the board, with the exception of MUC2. MUC2 displayed a minor increase in response to heightened inflammation, as observed by immunohistochemistry.

Under normal conditions, pro-inflammatory receptor, TLR4, is reported to be lowly expressed within the healthy epithelium, where it is located on the basolateral surface of colonic epithelial cells [112]. This basolateral presentation limits exposure to the plethora of bacterial antigens present in the colonic lumen, thereby controlling the necessity for an immune response to the microbiome. Staining in this project has confirmed the basolateral orientation of TLR4 in healthy colonic-derived epithelial organoids.

Transcriptomic data has revealed the minimal impact of LPS over 48 hours on healthy tissue. NFκB localisation, as demonstrated by staining, depicts this to be the reason for the lack of pro-inflammatory cytokines generated. NFκB is clearly localised in the cytoplasm of epithelial cells under basal conditions, as expected. However, this remains the case upon LPS exposure with this no visible transfer to the nucleus.

Vastly different results are realised in respect to our UC-derived epithelial model, with a strong, exaggerated response to an inflammatory culture environment. Of these, a drop in CDX2 was observed as the expression other pro-inflammatory markers rose. CDX2 is a transcription factor playing an important role in the balance between proliferation and differentiation, critical for maintaining epithelial barrier integrity. This finding is in agreement with Coskun et al who report CDX2 downregulation in ulcerative colitis biopsies [232].

Conversely, villin expression saw an increase upon LPS-mediated inflammatory induction. This is in line with our previous transcriptomic data that revealed an initial increase as a result of LPS exposure.

Once these intestinal changes were unveiled, focus was shifted to changes at the inflammatory protein level that could highlight the cause of these effects. Unlike in healthy organoids, TLR4 and MD2 expression showed substantial differences between conditions, with exposure to LPS resulting in a considerable increase for both proteins. These raises were rectified with 48-hour pre-treatment of tissue with a TLR4 inhibitor. Expression of both proteins were found to be largely apical, differing from findings in healthy tissue. Apical expression of these receptors leads to unavoidable, continuous activation of their downstream pro-inflammatory pathways, in response to the ongoing presence of commensal bacteria in the colonic lumen. Over time, this heightened level of inflammation causes extensive damage to the surrounding tissues.

A key factor in the downstream TLR4-mediated inflammatory pathway is the transcription factor, NFκB. NFκB is known to initiate transcription of processes controlling cytokine production. In our UC organoid platform, there was very clear NFκB translocation to the nucleus upon LPS exposure, signalling subsequent transcription of multiple pro-inflammatory genes including IL1β and IL18.

5.3.2.3 Proteomic Arrays Provide Further Insights into TLR4-Related Signalling Proteins

A range of hits from our array data was selected for analysis based on the significance and scale of the differential response measured between our two representative lines. While the relevance of the protein to the specific downstream signalling was taken into account, additional discrepancies in proteomic expression were also noted as possible future disease markers.

Proteomic array analysis into the downstream effects of NFκB activation confirmed TNFα to be considerably overexpressed at the protein level with an increase of 600-fold over basal levels. Hence, the 30-fold increase observed at the mRNA level is amplified to a substantial degree.

Furthermore, a significant 1.5 times increase in the expression of IL23 was measured. IL23 has been found to be a critical cytokine overexpressed in ulcerative colitis as demonstrated in ulcerative colitis plasma samples [233]. Here, we have demonstrated that the presence of LPS triggers such a response in this UC patient-derived model.

Another difference highlighted in proteomic array data was that of CD14. CD14 participates in the activation of TLR4, subsequently leading to the activation of both the MyD88 and TRIF-dependent downstream pathways. Our data reveals the absence of change in healthy organoids in response to LPS. Conversely, CD14 expression doubled in UC organoids. This change would result in greater availability and, potentially, increased activation of TLR4. The difference triggering this change could go some way to explaining the presence of an exaggerated immune response in UC colonic tissue, while the same conditions do not elicit similar tissue damage in healthy tissue.

As a continuation of our transcriptomic data set, expression of NFκB and related proteins was measured at the proteomic level. While NFκB expression showed no significant difference at the genomic level in our representative UC line, further exploration into the possible role of this transcription factor in UC revealed altered expression of its inhibitors. NFκB is comprised of subunits that combine to form dimers. Two of the most prolific class I subunits are NFκB1 (p50) and NFκB2 (p52) - [234]. Here, we have measured expression of these subunits at the basal level. Levels of p50 were higher in both lines when compared to p52 although not to a significant degree. This supports our transcriptomic findings, indicating that direct changes to NFκB expression are not responsible for the differential inflammatory responses that occur.

Subsequently, further investigations were conducted to determine if regulators of NFκB differed in response to LPS, thereby driving the discrepancies we observe between healthy tissue and UC. There are many inhibitors of NFκB that regulate signalling activity, therefore the expression of several of these inhibitors was assessed to determine any disparities of interest. Two members of the NFκB inhibitor family did, in fact, display substantial differences in expression that proved to be highly significant. One of these inhibitors was IκBα; one of the major NFκB inhibiting proteins. The expression of IκBα was found to be 70% less in UC organoids than in our healthy counterpart. This is a notable finding that points to a major cause of inflammatory dysregulation in UC. The same trend was found to an even greater extent in another NFκB inhibitor family member, IκBε. Expression in our UC model was found to be 80% lower in comparison to healthy levels. These are considerable differences that can

help provide an explanation as to the role of NFκB in UC pathogenesis in the absence of direct NFκB expression alterations.

The next step to round out the picture was to explore the differential responses occurring at the mid-level in this pathway. Multiple non-receptor tyrosine kinases were highlighted in the top hits obtained from this array: Hck, Fyn and Src. Interestingly, these kinases have been associated with the regulation of TLR4 in other tissue types, however a literature search revealed no link reported in IBD. Our data reveals the possible link between these tyrosine kinases and UC pathogenesis is worth further exploring.

The kinase demonstrating the greatest, and most significant, difference between the healthy and UC response is hematopoietic cell kinase (Hck). Hck are mainly expressed in macrophages, however, here we've demonstrated the important role they play in epithelial cells of the colon. Smolinska et al found Hck to have a prominent role in the production of TNF and IL6 in macrophages, as induced by TLR4 via transcription factor, AP-1 [235]. Our data reveals a distinct differential response with a complete lack of Hck response upon LPS stimulation in healthy epithelial organoids and, conversely, a significant 60% increase ensuing in our UC-derived organoid model. The successful reversal by TLR4 inhibition supports the involvement of TLR4 in this response.

Co-localisation of TLR4 and proto-oncogene tyrosine-protein kinase, Fyn, has been reported following LPS treatment in astrocytes [236]. This interaction was halted with the addition of a Src kinase inhibitor (PP2), inhibiting phosphorylation of the TLR4 tyrosine residue [236]. A very clear differential response was observed in our array data, with healthy organoids displaying the absence of any change to Fyn expression and significant elevated expression in UC organoids. TLR4 inhibition brings this increase down to basal levels with complete efficacy. This leaves little doubt for the involvement of TLR4 in this initial Fyn expression increase.

Another proto-oncogene tyrosine-protein kinase, Src, displays an even greater increase in expression to that observed of Fyn in UC organoids with a 25% increase above control. TLR4 inhibition does also exhibit a reduction in Src levels, however not to a significant degree. This effect would have a cyclical influence, while TLR4

activation is required for increasing Src production, activated Src is required for tyrosine phosphorylation of the TIR domain of TLR4. Phosphorylation of TLR4 is necessary for TLR4 signalling. This interplay goes for all members of the Src family.

Furthermore, EGFR, that this project has observed to be substantially increased in UC samples is an activator of Src kinases, further uncovering the pathway connections leading to UC development.

While not a kinase, an additional noteworthy difference in the expression profile between healthy and UC epithelial tissue is the enzyme endothelial nitric oxide synthase (eNOS). Knockdown of eNOS is associated with the enhancement of LPS-mediated changes to IL6 production and endothelial permeability [237]. Therefore, loss of eNOS enhances TLR4 signalling in human microvascular endothelial cells. Our data demonstrates this correlation to also be present in human colonic epithelial cells with a significant drop in eNOS expression detected in UC organoids and a substantial rise occurring in their healthy counterparts; rectified by TLR4 inhibition. In addition, oxidative stress has been found to result in a loss of eNOS [238]. Hence, the loss observed in this dataset could be indicative of elevated oxidative stress in UC-derived epithelial organoids in response to LPS.

These novel findings markedly reveal the role between TLR4, and multiple principal kinases/enzymes found downstream in the TLR4 signalling pathway in colonic epithelial cells. This information promotes TLR4 as a promising target for the improvement of UC-related inflammation as well as uncovering new potential targets for genetic or drug-based management of this disease. The convincing involvement of these proteins in epithelial cells is worth further investigating to confirm the link with other kinases partaking in this signalling cascade that could additionally be targeted.

5.3.2.4TLR4 inhibition significantly reverses LPS-mediated inflammatory response

Additionally, this response was further investigated to ensure that this effect was largely mediated by the TLR4 signalling pathway. To determine this, we pre-treated each line with 40 µM TLR4 inhibitor to favour competitive binding onto TLR4 receptors, thereby inhibiting attachment and activation by LPS.

While morphological images seen in figure 5.7 reveal little change between each condition, the cell material was gathered and prepared for RT-PCR. This data unveils the effects of TLR4 on both healthy and UC-derived organoids. As we can see in figure 5.8, TLR4 inhibitor clearly demonstrates a significant response across the board in both inflammatory and epithelial gene expression profiles. A prominent effect can be witnessed on TNFα expression, with a reduction of approximately 60% in those samples that had been pre-treated with inhibitor prior to the addition of LPS. This pattern was also observed to the same degree in IL1β expression, confirming these are involved to a similar extent in this pathway. TNF and IL1 have been found to exhibit interdependent activities with each being able to induce production of the other [239]. This interdependency could explain the highly comparable expression profiles in response to LPS and the similar efficacy exhibited by the TLR4 inhibitor.

IL18, however, did not show as great a reduction in the presence of the TLR4 inhibitor. The initial increase could be explained by the presence of residual TNFα and IL1β as IL18 is triggered downstream of this pathway. Furthermore, the minor presence of IL18 may trigger an inflammatory cascade via activation of MyD88 directly as IL18R is capable of instigating this [240]. Therefore, further inhibition of MyD88, in conjunction with the use of a TLR4 inhibitor, may further halt the inflammatory cascade under conditions of bacterial invasion.

The presence of the TLR4 inhibitor appears to have exerted a greater effect upon epithelial marker expression, with LGR5 expression returned to basal levels in both healthy & UC organoids. This is a highly promising result as restoration of LGR5+ ISC expression would offer increased barrier protection.

Conversely, MUC2 expression was not altered to a significant degree by LPS alone in this experiment with only a minor reduction of approximately 20%. Nevertheless, inhibition of the TLR4 receptor seemed to reduce MUC2 production further. This effect is supported by other groups researching into the effects of bacteria on the biliary epithelium [241].

The effects of TLR4 inhibition upon villin, however, demonstrated the most favourable results with expression remaining at basal levels in the pre-treated condition of UC organoids, while LPS alone instigated a 3-fold increase in expression. Furthermore,

there was no reduction or other deleterious effect of TLR4 inhibition on villin in the healthy organoids where expression remained constant. This result was corroborated with immunohistochemical and immunofluorescence staining displaying the reversal of increased villin with TLR4 inhibition.

This data is highly indicative of LPS acting via the TLR4 receptor and activation of the subsequent pathway. These inhibitive effects could potentially be increased with prolonged pre-treatment or a combination of TLR4 inhibitors to more effectively bind all TLR4 receptors prior to exposure to inflammatory stimulus.

5.3.2.5Upregulation of TLR4 receptor expression could contribute to heightened UC epithelial response

Due to the affects we observe here, along with the confirmation that these effects are mediated via the TLR4 pathway, we next investigated whether the heightened response of UC epithelial colonic organoids was as a result of upregulation of the TLR4 receptor directly.

To confirm this, TLR4 was measured following the experimental set up with untreated and LPS-exposed healthy and UC organoids we had seen previously. TLR4 was reduced in our healthy organoid model, implying a negative feedback mechanism with the activation of TLR4 by LPS triggering a reduction in the expression of TLR4 to regulate the inflammatory response. This would ensure a controlled inflammatory response in the presence of LPS. In other inflammatory cell types, this effect of LPS-tolerance has also been recorded. Nomura et al found TLR4 mRNA expression was downregulated in mouse peritoneal macrophages following stimulation with LPS [242]. To corroborate these findings, the group also found reduced activation of the LPS-signalling cascade, including reduced activation of NFκB and IRAK [242]. This group treated macrophages with the same concentration used in our study of 100ng/ml over a 3- and 24-hour period. They found that TLR4 expression began to decrease within the first hour of LPS stimulation and remained suppressed over the 24-hour time period [242]. As this study was carried out on macrophages isolated from the healthy C57BL/6J mouse model, this response is indicative of the healthy response upon LPS stimulation.

Conversely, a clear disease phenotype was observed with a notable increase in TLR4 expression in response to 48-hour LPS stimulation in our UC organoids alone. This is corroborated by Hausmann et al who reports upregulation of TLR4 found in inflammatory tissue from UC patients and not that of healthy controls [243]. This would amplify the immune response leading to greater epithelial damage over prolonged infection. This points to a dysregulated negative feedback response upon LPS stimulation, which could go some way to explaining the heightened and prolonged inflammatory response observed in ulcerative colitis patients.

As TLR4 is the receptor through which LPS signals, initiating a pro-inflammatory response, it is of particular interest that the TLR4 expression levels upon LPS treatment differ so considerably. This data therefore suggests the differing responses between healthy and UC tissue is, at least in part, mediated by discrepancies in TLR4 response or sensitivity.

In conjunction with this, TLR3 was also measured to determine whether expression of this receptor was also affected by exposure to LPS due to the cross-talk reported between these two receptors [244]. This synergistic effect has only been reported in alveolar macrophages isolated from C57BL/6 mice, therefore, we have now demonstrated this mechanism to also occur in human colonic epithelial cells. This is an important finding that indicates sensitisation to viral infections occurring as a result of activation of the TLR4-MyD88-NFκB pathway.

Hence, patients with an existing bacterial infection and LPS-induced inflammatory response, could have an escalated immune presence at the site of infection upon viral invasion. This immune over-activation could severely hamper immune homeostasis. This could lead to severe damage to the intestinal epithelium, exacerbating disease severity.

Furthermore, TLR3 has also proved capable of responding to necrotic cell material [245]. Therefore, any necrotic damage occurring as a result of inflammatory mediators or infectious agents can trigger a TLR3-mediated immune response.

5.3.2.6 Basal TLR4 expression is lower in UC compared to healthy organoids

Once a clear differential response between patient-derived healthy & UC organoids had been recognised with the inflammatory, epithelial and receptor profile being established, it was then decided that the basal, untreated expression levels should be analysed. This would give us insight into whether the elevated expression levels of TLR4 in UC are higher under homeostatic conditions prior to applying a pro-inflammatory trigger.

While we might expect to find higher baseline levels of TLR4 receptor expression in untreated UC samples, we in fact measured UC levels as being 95% lower than in healthy organoids ($P<0.0001$). This is a very interesting result demonstrating that a substantial discrepancy exists in TLR4 expression levels between healthy and UC-derived lines even under homeostatic conditions. Additionally, this suggests that the exaggerated response to LPS observed in our previous experiments are not as a result of continually elevated TLR4 receptor presence in UC tissue. The dramatic increase in TLR4 expression therefore occurs as a result of LPS stimulation, resulting in considerable changes throughout the epithelium.

Comparing this data with our previous findings indicates that TLR4 expression is increased over 60 times as a result of LPS stimulation in UC tissue and is downregulated by approximately 50% in healthy epithelial tissue. This remarkable response to LPS strongly indicates involvement of TLR4 in the elevated immune response in UC.

5.3.3 CRC Markers Increased in LPS-treated UC Organoids

As well as playing a substantial and significant role in inflammation & the pathogenesis of IBD, TLRs have also been implicated as a major player in the development of cancers, including CRC. Further to the upregulation of TLRs in the IECs of IBD patients, various TLRs, including TLR4, have been found to be upregulated in CRC tissues [246]. This supports the association between TLRs and the progression of CRC from chronic inflammatory disorders.

Studies in mice have shown the effect of pro- and anti-inflammatory mediators on CRC progression. An azoxymethane (AOM)-treated IL10-knockout mouse model was found to have an increased risk of both CRC & colitis development while a wild-type mouse model treated with AOM showed no development of colitis and much lower occurrence of tumour development [247]. Since, AOM is used as colonic carcinogen, the reduced prevalence of colorectal tumour development in the presence of the anti-inflammatory cytokine, IL10, demonstrates the role inflammation plays in tumour development.

Furthermore, following AOM treatment, MyD88-deficient mice expressed lower transcription of the IL12 & IL23 subunit IL12p40, as well as TNFα, with the mice remaining tumour-free [247].

With this link established, further research is being conducted into the potential signalling pathways involved in the initiation & progression of this process. As TLRs play a vital role in inflammation, there is increasing interest in the role they play in dysregulated immune responses & the subsequent effects throughout the body.

In addition to the effect upon pro-inflammatory cytokine expression, the TLR4 signalling pathway also triggers a cascade that results in increased production of prostaglandin E2, COX2 and EGFR in chronic colitis [248]. It is via this pathway that TLR4 overexpression can result in deterioration of the patient's condition.

Use of anti-inflammatory or anti-oxidative agents, therefore, offer the potential for cancer prevention. The expression of several known markers of CAC were measured following LPS treatment in the absence or presence of a TLR4 inhibitor.

5.3.3.1IBD, CRC & COX2

COX2 upregulation has been found in many colorectal cancer tissues and is associated with worse prognosis for CRC patients [213]. Fukata et al states that COX2 is regulated by the TLR4 signalling pathway in response to tissue injury [249]. This was demonstrated in mice deficient in either TLR4 or MyD88. Upregulation of COX2 in this model is dependent on these signalling proteins, showing that it is via the canonical pathway that this mechanism is initiated. Use of COX2 inhibitors blocked downstream production of the prostaglandin, PGE2, following stimulation by LPS. Gene silencing by small interfering RNA (siRNA) against MyD88 produced the same results [249]. It was reported in TLR4 -/- mice a significantly reduced rate of proliferation and an increased rate of apoptosis following injury by DSS compared to WT mice. Though this would impair tissue repair processes, this effect could also reduce the risk of development of CAC. This is an important effect to note as COX2 is a major marker in CRC, with over 80% of colorectal tumours expressing upregulation of COX2 [250]. Furthermore, a previous study found, that COX2 inhibition suppressed colonic tumour development in an AOM/DSS mouse model [251].

Our findings also show a significant upregulation of COX2 upon LPS treatment in UC organoids. This showed the opposite trend to that observed in healthy organoids, which showed a reduction in expression. Therefore, the disease phenotype is clearly demonstrated, along with a link to LPS induction of inflammation. Interestingly, TLR4 inhibition substantially reduced this effect, suggesting that the impact upon COX2 expression is mediated by the TLR4 signalling pathway.

Therefore, the clear link between COX2 & the TLR4 pathway ought to be further explored, with its inhibition preferentially reducing colonic inflammation as well as reducing the imminent risk of inflammation-associated CRC.

5.3.3.2TLR4 & EGFR in cancer

EGFR, a tyrosine kinase receptor, can be activated by a wide range of ligands, including infectious and non-infectious stimuli. Activation of EGFR leads to phosphorylation and activation of several important kinases, namely ERK and PI3K/Akt. These kinases play critical roles in a plethora of cellular processes, such as

the regulation of cell proliferation, differentiation, & migration in both normal and pathological states, explicitly cancer [220].

EGFR plays an important role in the development of UC and has been linked to the progression of CAC. Mutations are suspected to lead to this overexpression and result in its continued persistent activation [252].

The EGFR initiates a signal from the cell membrane which is transmitted to the nucleus via the downstream pathway. Multiple family members of EGFR such as HER2, HER3 & truncated HER4 have all been detected in the nucleus of tissue isolated from numerous cancer biopsies.

As it has been revealed that the EGFR family of receptors lack a DNA binding region. Therefore, it is likely that these receptors will then interact with specific DNA binding transcription factors, such as STAT3, capable of signal transduction [253].

However, there are other methods of signal transduction proposed. These include, upon EGFR receptors translocation to the nucleus they potentially bind to an AT-rich sequence of the target gene's promoter [253].

As a result of these findings, a number of EGFR inhibitors have been taken to clinical use for the treatment of cancers caused by EGFR upregulation [253] Among these are lung cancer, pancreatic cancer & colon cancer. Several therapies targeting EGFR in cancer are monoclonal antibodies and tyrosine kinase inhibitors. However, treatments that act on EGFR inhibition have several harsh GI side effects that would not suit a patient with existing GI complaints.

It is suspected that activation of EGFR by LPS in macrophages inhibits the anti-inflammatory cytokine, IL10, thereby accelerating colitis [246]. In particular, EGFR has been shown to be required for LPS-mediated production of interferons triggered by the TLR4 signalling cascade [254]. EGFR inhibition, in a mouse model, prevents LPS-induced expression of the pro-inflammatory cytokines, TNFα & IL6 [255]. Furthermore, NFκB activation is reduced by EGFR inhibition. This informs a link between TLR4, NFκB & EGFR expression.

Our findings corroborate this data with substantially increased expression of EGFR in the UC model compared to our healthy control, demonstrating this effect is also present in intestinal epithelial cells in addition to immune cells. A study investigating the effects of EGFR inhibition discovered that inhibition of the intracellular EGFR signalling pathway reduced the development of colitis-associated dysplasia [256].

Therefore, a reduction in EGFR signalling could ameliorate the progression from ulcerative colitis to CAC. TLR4 inhibition reduced the expression of EGFR in UC line to within normal levels. This demonstrates that inhibition of the TLR4 signalling pathway reduces the risk of CAC development as well as inflammatory progression.

5.3.3.3The role of ROS in IBD & CRC

Reactive oxygen species (ROS) are formed as a by-product of metabolism. Under normal conditions, concentrations of ROS are low. They then act as signalling molecules involved in the defence against infectious agents. Under stress conditions, however, greater levels of ROS are generated, leading to an exaggerated inflammatory response, DNA damage and increased apoptosis [257]. Due to DNA damage and other uncontrolled effects of ROS, increased ROS production can also increase risk of cancer development.

Nitric oxide (NO) has been tagged as being a key molecule involved in the pathogenesis of experimental colitis induced by DSS in mice [258]. The mechanism in which it produces these detrimental effects in the colonic mucosa remain largely unknown. It has, however, been suggested that NO increases expression of TNFα, which in turn leads to induction of P-selectin and ICAM-1. These adhesion molecules are then capable of promoting the infiltration of neutrophils, thereby damaging colonic tissue [258].

5.3.3.4Heat shock proteins in UC and CRC

Heat shock proteins (HSPs) facilitate protein folding, maintaining protein structure and function. They are usually triggered under stress conditions, playing an important role in the regulation of various cellular mechanisms including proliferation, apoptosis and metastasis.

Expression of multiple HSPs is increased in various cancers and therefore they have the potential to act as biomarkers as well as therapeutic targets. HSPs are also claimed to be responsible for resistance to certain anti-cancer drugs [259]

Our findings show opposing expression levels in healthy & UC organoids. In normal mucosa, the reduction in HSP expression upon pathogenic stimulation is expected to play a role in the resistance of the colonic epithelium to continual exposure to inducible signals from bacterial surface ligands [260]. Therefore, the reduction observed in our study would support this idea of microbial resistance in healthy epithelium. This evident differential response between healthy and disease epithelium points towards the possible link between LPS/TLR overactivation and the increased likelihood of developing CAC. As HSP expression often informs cancer prognosis and tumour differentiation state, these are important markers to note [261]

HSP25, a homologue to HSP27, is a small HSP that traps partially folded proteins to prevent aggregation. These proteins are then shuttled to ATP-dependent HSPs to refold or send for destruction [262]. TLR4 inhibition has demonstrated to be effective in reversing this increase, with HSP25 expression returning to normal levels. This data suggests that HSP25 expression could be modulated via the TLR4 pathway and therefore linked with inflammatory activity.

While, TLR4 inhibition had notable effect on HSP72 expression in a healthy model, this was not observed in UC organoids. This could be due to a delayed response of HSP72, compared to HSP25, or HSP72 expression could also be promoted via other receptors, including TLR2 [263].

5.3.4 Analysis of Transcriptomics Data Obtained from RNA-Sequencing

To expand the analysis of the differential response between healthy and UC-derived colonic organoids that we've uncovered in previous experiments, RNA-sequencing was performed on samples treated according to the LPS/TLR4 inhibitor assay. RNA-

sequencing gives a more expansive insight into the genes affected by activation of the TLR4 signalling pathway that have not previously been explored.

To begin this process, the samples were first prepared for sequencing. This process and the subsequent results are outlined in the results section of this chapter. Once the quality of the samples had been established, they were then sent to the Babraham Institute for sequencing.

The raw data was then processed to compare untreated and LPS-treated samples from both healthy and UC organoids, in addition to further investigating the more widespread effects of TLR4 inhibition.

To efficiently investigate the responses of relevant genes that we may be interested in for this project, multiple GO databases were utilised and the genes within each employed to compare against the log2 processed data. These data comparisons are presented in tables 5.4 to 5.18. and display many crucial differences between the responses of healthy and UC patient-derived colonic organoids.

Some of the findings demonstrated in this data, concerning the differential response of healthy and UC epithelium, include the increase in several genes responsible for the induction of inflammation. A few of these genes have been previously reported as being involved in IBD development, however we have discovered multiple genes that have not been linked with IBD and the potential for cancer development.

This data set provides further evidence of TLR4-TLR3 cross talk, with both TLR3 and ACE2, an enzyme involved in viral homing, upregulated substantially in LPS-treated UC organoids. This further confirms the sensitisation we have previously described and has been reported by other groups also [244].

Other pro-inflammatory factors activated downstream were confirmed to be upregulated in UC lines following LPS exposure, such as IL1β, LCN2, TNFAIP3 and AKR1C3. While immunosuppressive genes, such as GCH1, were downregulated. This is highly indicative of these genes been associated with IBD development via chronic LPS exposure in predisposed patients. Furthermore, TNFAIP3 was found to be upregulated to a much greater extent in UC than in our healthy organoid line. This finding is supported by Overstreet et al reporting upregulation of TNFAIP3 in IECs to

result in increased susceptibility to bacterial invasion and colitis in a IL10 -/- mouse model [264].

Another of the key genes that are differentially expressed between healthy and UC-derived organoids is TICAM2 (Toll Like Receptor Adaptor Molecule 2). It was found to be highly upregulated in UC organoids, while being downregulated in our healthy model. This is an integral factor differing between healthy and UC patient-derived organoid platforms as TICAM2 plays a critical role in the TLR4 pathway. Once activated, TLR4 interacts with TICAM2 via its TIR domain [265]. TICAM2 then activates TICAM1 (also known as TRIF). This pathway then leads to production of pro-inflammatory cytokines including type 1 interferons [265] Additionally, PELI1, a gene associated with TLR and T-cell signalling regulation, was also increased.

Genes promoting carcinogenesis were also favoured with BIRC3 and ADAM8, with roles in EMT and cell migration [266]. Microarray analysis has shown BIRC3 overexpression to be implicated in tumour proliferation and metastasis in hepatocellular carcinoma (HCC) via upregulation of MAP3K7 and, hence, ERK 1/2 phosphorylation [266]. Liu et al discovered that silencing of ADAM8 reduced cellular migration and invasion. This also resulted in dephosphorylation of IκBα and p65 and subsequent reduction in signalling of the NFκB pathway and reduced MMP13 expression. Therefore, ADAM8 is thought to promote ECM degradation, enabling tumour metastasis [267].

Furthermore, other findings demonstrate the potential for serious ramifications including the loss of genes encoding adhesion molecules resulting in the loss of cell-cell and cell-matrix interactions, which are key for epithelial integrity as a first line defence against pathogenic bacteria. An example of these genes includes RHOB, encoding a member of the Rho GTP-binding protein family. RHOB controls endothelial barrier integrity under pro-inflammatory conditions via regulation of Rac1 [268]. The downregulation observed in this data is indicative of a loss of epithelial integrity in certain cases of UC. The downregulation of HTT we witness in treated UC samples also signals loss of ZO1 at tight junctions and subsequent increase in epithelial permeability [269]. Alternatively, we found HTT to be upregulated in healthy-derived organoids. This clear differential response offers an interesting insight into the healthy and disease response to bacterial invasion, with healthy tissue

increasing availability of ZO1 at epithelial tight junctions. Hence, reducing the penetrability of the protective barrier against pathogenic bacteria. THSB1, an adhesive glycoprotein also known to mediate cell-cell and cell-matrix adhesion [270], was found to be downregulated in UC, while increased in our healthy line. This further confirms the differential response of the colonic epithelium under the same pro-inflammatory conditions.

Furthermore, LPS-treated healthy organoids demonstrated downregulation of multiple genes involved in the pro-inflammatory pathways; NFκB, JNK and ERK 1/2, all of which are critical players in the LPS-mediated pathway, amongst others. These are all impacted by the downregulation of FLOT1. Genes encompassing functions in cell cycle regulation and cancer progression are also downregulated. This finding further suggests that protective mechanisms are in place in the healthy epithelium to ensure that the inflammatory response remains closely regulated. These mechanisms appear to be lacking in the UC epithelium.

Together, this data provides novel markers to further research that can provide more information regarding IBD pathogenesis in particular patients as well as highlighting possible therapeutic targets that could modulate and control IBD development and progression.

5.3.5Conclusion

In conclusion, the aim of this Chapter has been fulfilled and the hypothesis has been proven true. A substantial and significant difference has been reported in the response of UC-derived colonic organoids to bacterial PAMP, LPS, when compared to their healthy counterpart. A spike in inflammation was observed upon induction with both TNFα and LPS in UC epithelium across several pro-inflammatory markers. A deleterious effect directly upon the colonic cells was also apparent. This would strongly impact healing required to rectify any inflammatory-related damage. These findings were confirmed using multiple techniques at the genomic and proteomic level. Further investigations revealed possible links between UC and development of colitis-associated colorectal cancer in our representative model with elevated expression of key cancer markers. This data gives important insight into the pathways that lead to CAC which can be further explored using this platform.

The techniques employed in this chapter have limitations in drawing accurate conclusions regarding the involvement of SNPs or other mutations that may be contributing to this observable effect, therefore further genomic analysis would be required for confirmation.

Furthermore, some of the cytokines and kinases released by the epithelial cells in this reductionist model, in response to LPS, influence the behaviour of other cell types in the colon. It is therefore necessary to introduce other cell types to the platform to augment our understanding of their role in IBD.

Chapter 6

Applying Synthetic Biology Techniques for the Generation of a Novel Anti-Inflammatory Peptide

6.1 Introduction

6.1.1 Inhibition of TLR4

TLR4 is a receptor consisting of three distant segments: a leucine rich repeat (LRR) domain localised on the outer membrane; a transmembrane domain and a Toll/IL-1 receptor (TIR) domain located intracellularly [271]. The domain responsible for recognition of ligand, LPS, is the LRR domain, while the transmembrane domain secures TLR4 to the membrane, and lastly the TIR domain emits signals into the cell [271]. The TIR domain is also responsible for dimersation of TLR4 receptors upon activation. Once dimersation has occurred, the downstream cascade of proteins bind to create a complex. These proteins include TIRAP/TRAM; MyD88/TRIF; IRAK-1 and -4 and TRAF6. Upon the formation of this aggregated structure the kinase, TAK1, then binds to TRAF6. This kinase plays the role of phosphorylating the NFκB inhibitor complex, IKK [272]. IKK then phosphorylates the another of the NFκB inhibitors known for preventing binding of NFκB to DNA, IκBα. This marks IκBα for degradation. The NFκB is then able to enter the nucleus where transcription of genes encoding pro-inflammatory cytokines and chemokines can take place, including that of TNFα, IL1β and COX2 [273,274]. Additionally, TAK1 phosphorylates MKK 3/6, which in turn phosphorylates p38 MAPKs and, hence, results in activation of the downstream MAPK signalling pathway [275].

TLR4 inhibitors can be sub-divided into glycolipid-based and non-glycolipid-based. These act by binding to distinct domains on TLR4 to prevent activation of this pathway.

Synthetic glycolipids FP7 and FP12; have been generated from glucosamine with two phosphate groups and two fatty acid chains. They act via direct competition with LPS for the MD2 binding site, as well as preventing internalisation of CD14. The latter mechanism alone would not be enough to prevent activation of the downstream MyD88-dependent and TRIF-dependent pathways due to the ability for TLR4 activation to occur in the absence of CD14 in response to other ligands. However, in combination with direct TLR4 inhibition, this may increase efficacy.

Caffeic acid is a phenolic compound and an example of a non-glycolipid-based inhibitor that has been found to possess anti-inflammatory, anti-tumour and anti-oxidative properties [271]. A compound based on this structure was found to inhibit TNFα and NO production in LPS-stimulated microglia cells [276]. Furthermore, dimerization of the TLR4-MD2 complex is prevented when macrophages were treated 10 μM of caffeic acid [277]. Use of molecular simulation techniques have revealed that the 4-hydroxyphenyl group of this compound forms a hydrogen bond with Glu439 of TLR4 at the interface of TLR4/MD2 binding [277].

All TLR4 inhibitors demonstrate a different mechanism of action, some of act to inhibit the formation of the TLR4/MD2 complex whilst others inhibit binding of LPS directly. Alternative compounds are being explored that display enhanced efficacy and pharmacokinetic properties. Our aim in this project is to generate a novel anti-inflammatory peptide that acts via inhibition of TLR4 specifically. The activity of this peptide can then be tested on our primary colonic organoid platform and the exact mechanism of action can also be explored.

6.1.2 Novel TLR4 Inhibiting Peptides

During a literature search, we found several novel peptides that reportedly target the prolific toll-like receptor, TLR4 [278]. Only peptides that appeared to have a high level of success at inhibiting TLR4-induced responses and did not currently have any patents pending were selected for continuation to the next step of the project. SPA4 & STM28 were both found to directly inhibit the TLR4 receptor itself rather than any downstream or indirect targets [279,280].

These two peptides, SPA4 & STM28, were chosen for generation by the *Clostridia* system developed by CHAIN Biotech.

6.1.2.1SPA4

SPA4 is a small peptide suspected to bind directly to the TLR4 receptor. This direct binding prevents the downstream phosphorylation of NFκB subunit, p65, typically induced by LPS. The inhibition of NFκB activation thereby limits the production of subsequent pro-inflammatory cytokines associated with this pathway, including TNFα, IL-1β and IL-6.

SPA4 is derived from the C-terminal region of a larger peptide, surfactant protein A (SP-A), a natural endogenous defence protein [281]. SP-A is a protein usually expressed in the epithelial cells of the lung; however, they have also been identified at other mucosal sites, including the intestine [279]. As these sites have regular contact with commensal bacteria, as well as pathogens, the presence of this protein suggests it plays a role in maintenance of immune homeostasis *in vivo*.

Furthermore, SPA4 has been found to decrease the expression of TLR4 itself [279]. We have previously found TLR4 expression increases upon activation of the TLR4 signalling pathway in response to stimulation with LPS via a positive feedback mechanism. The decrease initiated by SPA4 would prevent this uncontrolled immune response, thereby limiting the amount of inflammatory-induced damage to the intestinal epithelium. This would greatly improve control of an auto-immune disease such as ulcerative colitis. Reducing the inflammatory environment would also help foster healing from previous epithelial damage.

A previous study has reported the maximum inhibitory effect of SPA4 on the human colon cancer cell line, SW480, to occur 5 hours after treatment [279]. This was determined by measurement of NFκB activity, demonstrated by phosphorylation of the p65 subunit. The following concentrations were tested in this study: 10 and 50 μM. The upstream mechanism of action was explored with the use of MYD88DN-transfected cells. While these cells exhibited reduced NFκB activity upon LPS stimulation, SPA4 did not further reduce this inflammatory activity. Therefore, it was assumed that SPA4 acts via the MyD88-dependent signalling pathway [279]. While

expression levels of NFκB-related signalling proteins only exhibited a slight change following treatment with SPA4, further investigation revealed there was a substantial decrease in the phosphorylation of NFκB [279]. This decreased phosphorylation occurred after LPS-challenged SW480 cells were treated with SPA4 peptide for 1 hour [279]. This effect could be observed up until 5 hours after initiating treatment [279]. Furthermore, while observing the downstream effects of SPA4 treatment on these cells, it was found to inhibit the pro-inflammatory cytokines: IL-1β & IL-6.

6.1.2.2 STM28

STM28 has been found to completely abrogate the response initiated by LPS in the human monocyte cell line, THP-1 [280]. Upon testing multiple TLR4-binding peptides, Sugiyama et al found a peptide, which they named STM28, significantly and substantially inhibited LPS-mediated NF-κB activation [280]. This effect was observed following the treatment of THP-1 with a concentration of 40 μM [280]. All other peptides tested had no, or very little, ability to reduce LPS-induced effects in this cell line.

The response to other TLR ligands was tested to ascertain whether this response is specific to TLR4 or is common to multiple TLRs. It is important that any peptide used for therapeutic purposes possesses a high level of specificity that is well understood to enable the response in patients to be more carefully controlled.

The downstream response of STM28 was investigated to ensure the pro-inflammatory response induced by LPS was entirely abrogated upon the inactivation of NF-κB. A dose-dependent effect upon TNFα production was also reported, confirming this effect is not isolated to NF-κB [280]. However, only 2 doses of STM28 were tested in this experiment: 10 & 40μM. To draw accurate conclusions that this response is dose-dependent it would be more satisfactory to test a wider array of concentrations.

The effect of STM28 has also been tested in a mouse model. This gives us useful information as to any adverse effects it may have on a whole organism and whether the *in vitro* effects still occur. It was found that treatment of an endotoxin shock mouse model improved survivability when treated with a final concentration of 20 μg, completely inhibiting LPS-induced lethality [280]. These are very promising results that suggest STM28 to be an encouraging novel peptide with the potential to be adapted

for clinical use upon additional testing in both *in vitro* & *in vivo* models. A preferable model to demonstrate the effects upon human tissue would be patient-derived human primary intestinal organoids. The direct response of human tissue is more representative of patient response than the effects observed in animal tissue.

6.1.3 CHAIN Biotech's Clostridia-based Drug Delivery System

CHAIN Biotech have developed a state-of-the-art system known as the *Clostridium* Assisted Drug Development (CADD™) platform. This platform offers the ability to engineer *Clostridia* strains for the production of novel therapeutic agents. These can then be delivered successfully to the colon, avoiding destruction by stomach acid once in their sporulated form. This enables therapeutics to effectively reach the target site, thereby reducing the risk of side effects by acting on off-site tissues in addition to improving the therapeutic potential of the drug. Upon reaching the anaerobic environment of the colon the *Clostridia* spores then begin to germinate and thrive. Within this preferential environment they shall begin to secrete the novel peptide they have been engineered to produce. This approach offers a host of benefits over other drug delivery systems, either oral or rectal, as it enables the full-length of the colon to be targeted. This is particularly beneficial in the treatment of inflammatory diseases known to specifically affect the colon, including ulcerative colitis.

Generation of novel therapeutics for the treatment of ulcerative colitis is the main focus of this project. Therefore, CHAIN's innovative delivery system combined with recently discovered novel peptides can pave the way for a vastly improved therapeutic option for millions of ulcerative colitis patients in the future.

Patient-derived intestinal organoids offer an insight into the epithelial response to inflammatory and fibrotic conditions, as well as acting as an excellent drug testing platform. The results of which offer a more representative human response than many *in vitro* and animal models currently used. It is this platform we intend to use for the purpose of testing the novel anti-inflammatory peptides generated by CHAIN Biotech's engineered *Clostridia* bacterial species.

6.1.4 Aim & Hypothesis

Aim: The aims of this project are to engineer CHAIN Biotech's unique *Clostridia*-based system to express two carefully selected novel peptides. The novel peptides we intend to generate have been shown to exhibit anti-inflammatory properties. If successful, these novel peptides shall then be tested on a patient-derived colonic organoid platform to determine the downstream effects on *in vitro* colonic epithelial tissue.

Hypothesis: A strain of *C. butyricum* can be successfully generated to express a small novel peptide with possible TLR4-inhibitory effects, extending to a reduction in downstream pro-inflammatory signalling compounds.

6.2 Results

The initial step, successfully completed, was to convert the peptide sequences discovered in the literature for SPA4 & STM28 into DNA sequences prior to designing a vector backbone with the appropriate features for aiding in expression of these peptides.

The relevant promoter & replicon sequences, as well as NheI & NdeI restriction sites, were then added to the plasmid design. In addition, a flag tag sequence was added for detection via western blot at the end of the project to determine whether the engineered strains produced the selected peptides (figure 6.1).

FLAG for detection only

SPA4:
5′
GTGTAATTTTTAAGGAGGTGTGTTACATATGgattacaaggatgacgacgataag**GGCGACTTCAGGTACAGCGA**
CGGCACCCCCGTGAACTACACCAACTGGTACAGGGGCGAGTAAGCTAGCggcgcgccgttctgaatccttagcta
atggttcaa 3′

STM28:
5′
GTGTAATTTTTAAGGAGGTGTGTTACATATGgattacaaggatgacgacgataag**CCCGGCCTGGCCAGCAGGAA**
GGTGGTGGTGCTGCTGGTGTGGGGCAGCAGGTAAGCTAGCggcgcgccgttctgaatccttagctaatggttcaa

Figure 6.1: SPA4/STM28 DNA Sequences with inserted promoter, replicon sequences and NheI & NdeI restriction sites.

3′

The promoter would be part of the plasmid backbone pMTL82123 and therefore is not added to the gene sequence to be manufactured.

Once designed these DNA fragments were then sent to GeneArt™ Strings™ (Thermo Fisher Scientific) to be generated.

Following the arrival of the designed DNA fragments, they were reconstituted in RO-H2O according to supplier instructions before being ligated into a pCR-Blunt vector and transformed into a TOP10 *E. coli* strain.

Following cell recovery and overnight incubation after transformation, a colony PCR of 8 *E. coli* colonies was performed. Although the colonies that formed are likely to be positive for the plasmid due to the antibiotic selective pressure by culture on the antibiotic-containing agar, it was still necessary to confirm this by colony PCR. The results of this colony PCR can be found in figure 6.2.

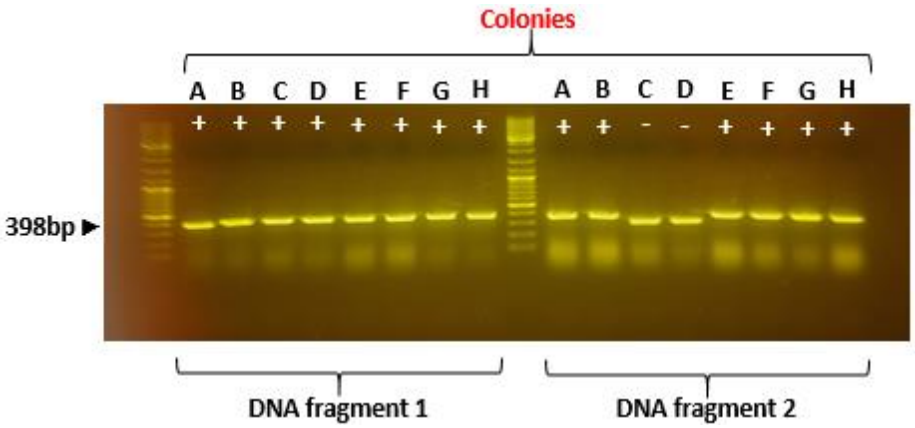

Figure 6.2: Colony PCR results displaying all 8 positive colonies containing SPA4 & 6 out of 8 colonies positive for STM28 DNA fragments contained within pCR-Blunt vector.

The extracted DNA, from the above colonies confirmed as positive, in the PCR was then sent off for further confirmation by Sanger sequencing.

As the plasmid sequence is A-T rich this makes it difficult to sequence, therefore Sanger sequencing is used for this purpose as it is a slower process allowing the DNA polymerase greater time to attach to the DNA strand for amplification. This is necessary as the polymerase complex does not securely attach to A-T rich sequences which can, in some cases, lead to partially sequenced strands.

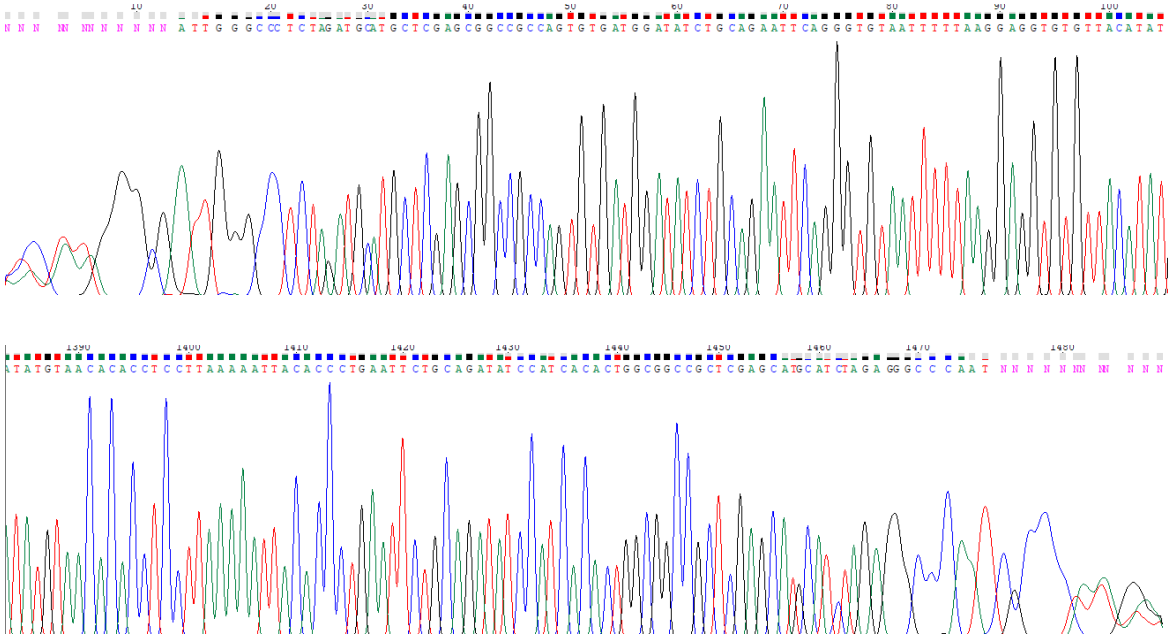

Figure 6.3: Forward & Reverse Chromatogram Sequences of SPA4-Colony A. Sanger sequencing results displayed by Chromas software showing forward and reverse sequences of SPA4 pCR-Blunt plasmid.

Once the Sanger sequencing results were received, the files were opened in Chromas software (by Technelysium Pty Ltd). Both the forward and reverse sequences were then copied in FASTA format before being imported into Clustal Omega (software by EMBL-EBI) (figure 6.3). These sequences were individually compared to the original DNA fragment design containing all additional promoter, replicon & restriction site sequences. The alignment was then checked using the Multalin tool to further confirm sequence alignment (figure 6.4). This is to determine whether any insertions or deletions have occurred following transformation by the bacteria. It also confirms whether the DNA fragments have been inserted in the correct orientation into the pCR-Blunt vector.

Multalin

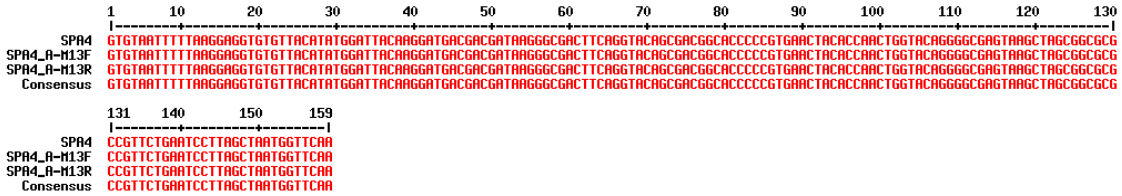

Figure 6.4: Sequence alignment of SPA4 colony A confirmed by Multalign.

Once the sequences were confirmed the positive colonies were then inoculated in conjunction with another *E. coli* strain possessing the relevant plasmid backbone required for the project. This plasmid is designed by CHAIN Biotech as part of the pMTL80000 modular plasmid series under the name pMTL_82123. The features of this plasmid backbone can be found on the ClosTron website.

Following the growth of the 2 Top10 *E. coli* strains, the plasmids from each strain were extracted & purified using the Promega Wizard(R) Plus SV Minipreps DNA Purification System. Using NdeI & NheI restriction enzymes the desired gene fragments were spliced from the pCR-Blunt plasmid backbone. Likewise, the pMTL82123 backbone was spliced from a previously inserted DNA fragment. This was confirmed by DNA electrophoresis (figure 6.5).

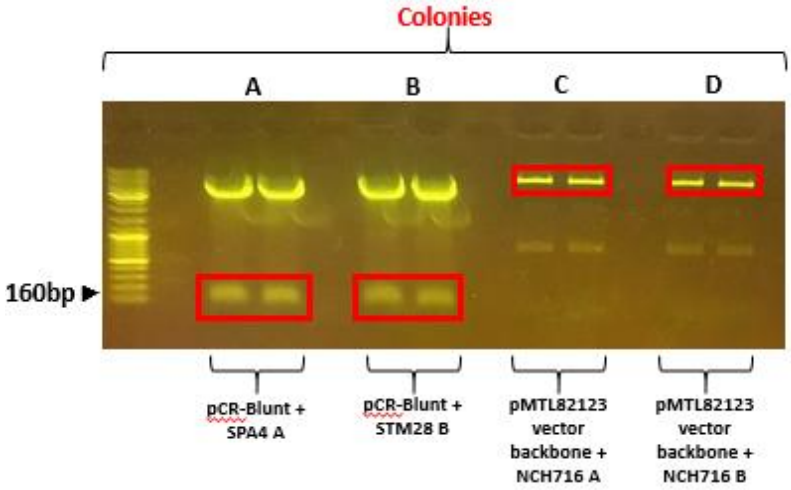

Figure 6.5: Gel electrophoresis using 1% agarose gel. (A) SPA4 DNA fragment in duplicate is highlighted in red. **(B)** STM28 DNA fragment in duplicate highlight in red. A & B are the desired gene fragments, SPA4 & STM28 that have been cut out of the pCR-Blunt vector backbone. **(C & D)** pMTL82123 vector backbone with gene fragment excised in duplicate rea highlighted in red. This is the desired backbone with the correct replicons, antibiotic resistance gene & Pfdx promoter. The previous gene has been removed to enable insertion of the new gene fragments.

The desired gene fragments and plasmid backbone were cut from the gel with a scalpel before being purified from the surrounding gel matrix. The gene fragments were then ligated to the plasmid backbone resulting in the final complete plasmid. This plasmid was then transformed into TOP10 *E. coli* cells. Following overnight incubation, the colonies were tested to determine whether they had in fact taken up the plasmid, as confirmed by colony PCR. The primers used for the PCR step are specific to the pMTL82123 backbone.

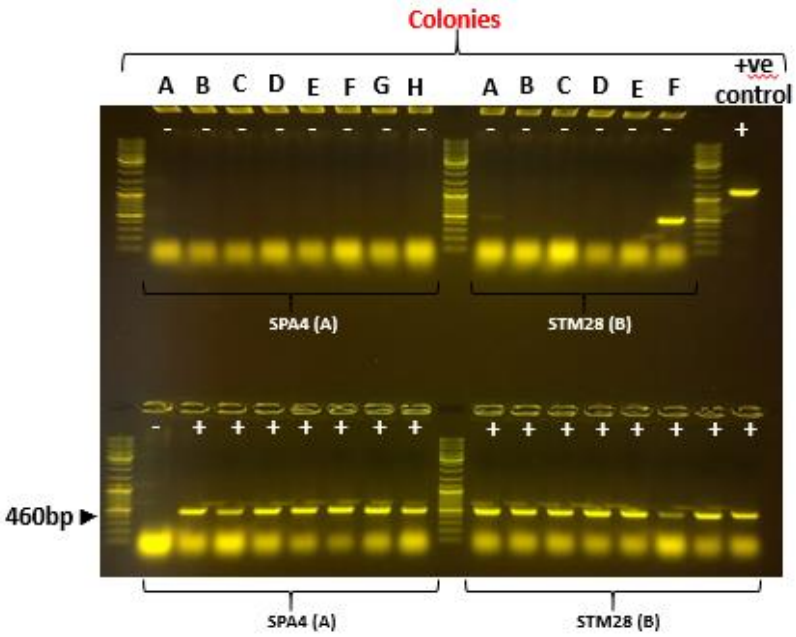

Figure 6.6: Colony 1% gel electrophoresis shows initial Top10 competent *E. coli* colonies picked are negative for either DNA fragment (top panel). While 7 of the 8 colonies picked (lower left panel) contain SPA4 & all 8 colonies picked (lower right panel) contain STM28 fragment. 4 selected colonies containing each of the DNA fragments were sent off for Sanger sequencing to confirm this positive result using the C55 primer supplied by CHAIN Biotech.

As the above figure shows, the initial colonies that grew on the Kanamycin-containing plate were negative for the complete plasmid (figure 6.6). The reason for this is unknown as the antibiotic should have prevented the growth of any bacteria lacking this plasmid. However, the plate was returned to incubate for a further 24 hours. Following this incubation period many more colonies had formed. The colony PCR was then repeated with these newly formed colonies. 15 out of 16 colonies tested came back positive.

The plasmid was then extracted from the positive colonies and the process repeated for transforming the plasmid into the conjugative *E. coli* strain, CA434.

The CA434 conjugative *E. coli* species was then cultured in line with the *Clostridia butyricum* species that would later uptake the novel peptide. The results of the transconjugation were confirmed by colony PCR. As we can see from the results below, 2 out of the 3 final colonies tested positive for the plasmid (figure 6.7).

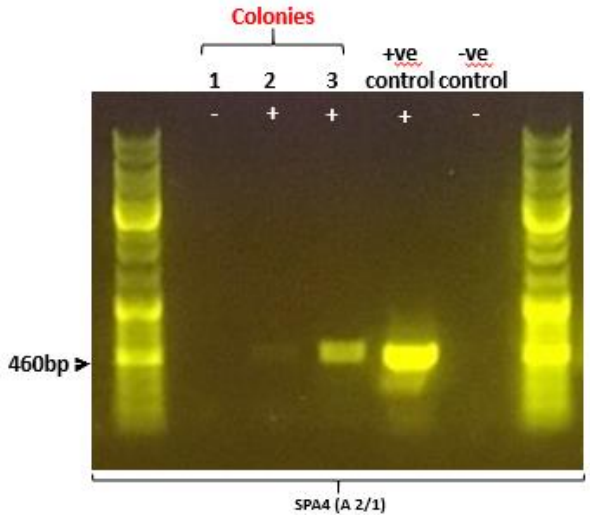

Figure 6.7: The resultant transconjugant DNA was then measured by PCR to determine which of the 3 colonies were positive. Colonies 2 & 3 were positive for this plasmid.

The transconjugation of *E. coli* and *C. butyricum* was repeated with the next peptide-encoding plasmid for STM28. The process of PCR & electrophoresis was then repeated with all samples using multiple primer sets. These primers used were specific for the backbone upstream of the gene fragment, the plasmid backbone and for the specific *Clostridia* strain.

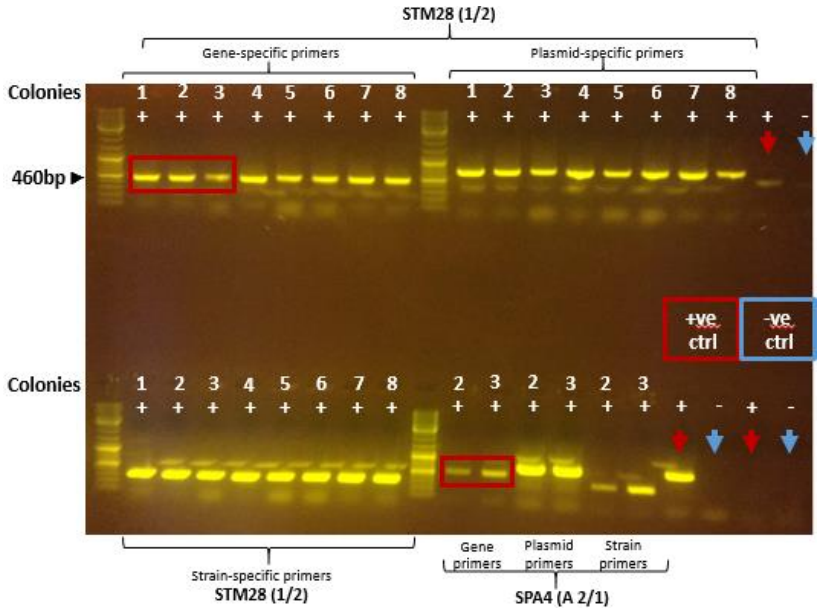

Figure 6.8: The resultant transconjugant DNA was then measured by PCR. All STM28 colonies tested positive for DNA fragment backbone, plasmid backbone and the *Clostridia* strain. Colonies 1, 2 & 3 were selected for the growth experiment, while colonies 1 & 2 containing the SPA4 sequence re-tested as positive with all 3 primer sets.

The above results show all colonies picked to be positive, including the 2 picked previously. From these positive colonies, 2 colonies containing SPA4 gene & 3 containing STM28 were chosen for the bacterial growth experiment (figure 6.8).

Upon confirmation, these positive plasmid-containing colonies were grown over a 24-hour period in broth to enable a growth curve to be completed. Cell lysates were taken every hour throughout the growth experiment. A selection of these samples were then later tested to determine whether the novel peptide(s) was produced. This was confirmed via western blot.

A western blot determined whether the flag tagged protein encoded by the engineered plasmid was expressed in these samples and, if so, at what stage during the *Clostridia* growth cycle.

As the below western blot displays, one of these samples expressed sufficient peptide detectable by western blot (figure 6.10). This could be confirmed as the novel peptide as it was not present in the blot of any other samples, or in either of the controls. This level of protein was evident after 24 hours. There would be less protein detected via blot than was originally produced in culture due to degradation by proteases produced by the *Clostridia*.

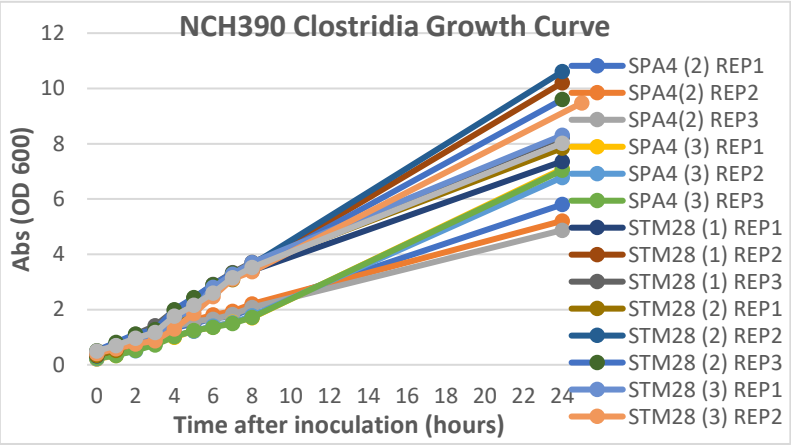

Figure 6.9: Bacterial growth curve from Clostridia growth experiment over a 24-hour period. As this growth curve demonstrates the engineered Clostridia strains possessing one of two final peptide-encoding plasmids we slow to initiate growth, potentially due to the p15A low copy number plasmid. However, the growth continued exponentially over the 24-hour period.

Each optical density (OD) measurement taken over the course of the 24-hour experiment was plotted on a graph for each of the 5 strains grown simultaneously (figure 6.9). This gives an indication of the growth rate for each engineered strain. Typically, bacteria produce the greatest quantity of peptides when they are in the exponential phase of their growth. Therefore, the bacterial growth plot demonstrates the time point that these bacteria are most likely to produce the peptides. It is at these time points that cell lysates can then be taken and tested for the presence of the novel peptide.

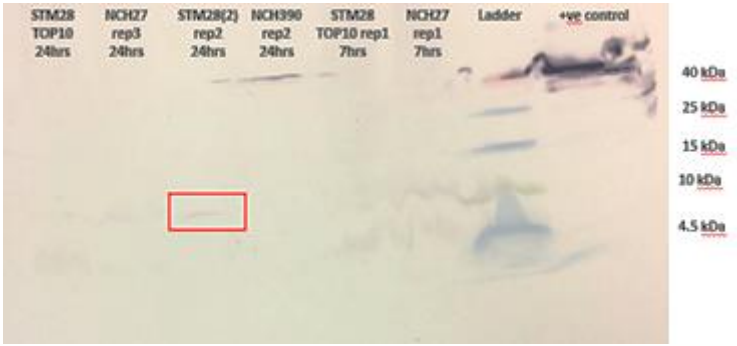

Figure 6.10: Western blot membrane of final growth experiment. A seemingly positive result is observed in the STM28-encoding *Clostridia* strain after 24 hours growth.

6.3 Discussion

Ulcerative colitis is a chronic debilitating condition characterised by prolonged & exaggerated inflammation of the colon. The pathogenesis of this disease is multifactorial involving genetic predisposition, loss of epithelial integrity & dysregulated immune responses. However, the more precise factors contributing to the pathogenesis of this disease are not fully understood. With the incidence of inflammatory diseases, including ulcerative colitis, rising in recent years it is imperative to improve the therapeutic potential & prognostic outlook for these patients.

During the course of this project, we have applied innovative technologies to address this issue. Using CHAIN Biotech's new technology, CADD, it is possible to combine targeted drug delivery with novel & improved anti-inflammatory therapeutic molecules delivered directly to the colon.

The initial aims of this project have been successfully fulfilled with a strain of *Clostridia butyricum* genetically engineered to express a novel small molecule, STM28. Several steps were required to achieve this, beginning with the design of DNA fragments that could then be initially inserted into a chemically competent TOP10 *E. coli* bacterial strain. *E. coli* is a preferred host for gene cloning due to the high efficiency of introducing DNA molecules into cells. The complete plasmid could then be transferred to the final strain capable of expressing these peptides.

6.3.1 TLR4 signalling pathway: (& how SPA4 & STM28 acts on this pathway)

The anti-inflammatory molecules that we have selected for generation by this *Clostridia* based system act via inhibition of a critical innate inflammatory pathway involved in the pathogenesis of several autoimmune diseases, driven by activation of TLR4.

Inhibition of this pathway reduces the abundance of pro-inflammatory cytokines and chemokines in circulation. This, in turn, reduces the recruitment of innate immune cells including monocytes, neutrophils & eosinophils [282]. In ulcerative colitis, recruitment of these immune cells to the site of cytokine production (i.e., the gut epithelium) results

in increased production of reactive oxygen species and proteases. This can lead to the disruption of epithelial barrier integrity and epithelial apoptosis, resulting in severe epithelial damage and potential fibrotic accumulation. This disrupted epithelial barrier can allow increased passage of bacterial cells into circulation, triggering a further consequential prolonged cycle of inflammation.

Halting or reducing this vicious cycle of inflammation can allow for epithelial regeneration and, hence, recovery of epithelial integrity along with improved colonic function.

Our aim was to generate a novel anti-inflammatory peptide that can later be tested using our human colonic organoid platform to determine if anti-inflammatory effects are elicited.

6.3.2 Production of Small Peptide

Two peptides were selected for trial in CHAIN Biotech's delivery system to increase chances of one of them being successfully expressed.

Following generation of the plasmids containing SPA4 and STM28-encoding genes, the plasmids were transferred to CHAIN's host *Clostridia* strain via transconjugation from the CA434 *E. coli* conjugative strain. The bacteria were then amplified to encourage peptide production and verify if our target peptides can be identified and subsequently isolated.

During the bacterial growth experiment 5 strains were cultured: 3 containing the STM28-encoding gene and 2 containing the SPA4 gene. The NCH390 *Clostridia* parental bacterial strain was grown concurrently to identify, and thus rule out, any naturally expressed *Clostridia* proteins. As observed in the final western blot, many larger bands were produced across all samples with an approximate weight of 14 kDa, suggesting these are continually expressed proteins specific to *Clostridia* and unlikely to be the small peptide engineered into the strain.

It was decided following the first run of this experiment to also run an *E. coli* growth experiment simultaneously to determine whether the TOP10 *E. coli* strains engineered at earlier stages of the project could also produce the desired novel peptides.

However, it was found that the *E. coli* did not produce a sufficient amount of peptide to be visible on the final western blot.

There was one engineered strain, however, that appeared to express a peptide displayed at the approximate weight of 4 kDa that was specific to that sample. This strain was engineered to express the STM28 peptide. The peptide was expressed & detectable at 24 hours of growth, suggesting this to be the most beneficial time point to harvest the novel peptide prior to declining growth rate or peptide degradation by naturally expressed proteases.

STM28 was discovered in a screen conducted for the purpose of identifying peptides that associate with TLR4 in macrophage cells. This peptide was found to inhibit NFκB activation upon stimulation by LPS [280]. Receptor specificity was confirmed by the addition of TLR1/2, TLR3 and TLR9 ligands in the mouse macrophage cell line, RAW 264, however no inhibitory effects on NFκB activation were observed. Furthermore, this small peptide suppressed TNFα production in another immune cell line, THP-1 [280]. This is a human line established from a monocyte isolated from the peripheral blood of an acute monocytic leukaemia patient and may, therefore, be more representative than the mouse line used for the majority of their experiments.

The RAW 264 cell line was pre-treated with a range of STM28 concentrations for just one hour prior to exposure with LPS for 6 hours [280], whereas our study has pre-treated for a much longer period, of 48 hours, with a commercial TLR4 inhibitor. This was to ensure maximal binding to the inhibitor to TLR4 prior to culture with LPS. As this study reported clear inhibitory effects downstream after a much shorter period of time, it is possible STM28 exhibits greater potency. However, a greater time period of pre-treatment may be required in organoid experimentation due to the diffusion process required for the inhibitor to reach all the cells with the organoid's 3D structure. It is also important to note that the lowest concentration demonstrated to be effective was 10 μM, therefore this would be a suitable concentration to test on our organoid platform.

Clostridia is a bacterial species known to produce a large quantity of proteolytic enzymes that would rapidly degrade any small peptide soon after it being produced [283]. This would reduce the peptide yield during our bacterial growth experiment.

Proteolytic activity begins to peak at around 6 hours into bacterial growth [283], hence, it would be beneficial to add protease inhibitors to the growth medium to slow this degradation process. This would result in an increased yield of the desired small peptide.

6.3.3 Conclusion & Future Directions

In conclusion, the initial aims of this project have been fulfilled. We have successfully generated a *Clostridia* strain possessing an engineered plasmid with a DNA sequence encoding a novel anti-inflammatory peptide. A wide range of techniques were utilised throughout this project to achieve these final aims, including the design of plasmid DNA constructs, ligation, transformation, PCR and transconjugation, amongst others. These techniques can assist in a range of projects that can combine microbiology, synthetic biology & cell culture. The next steps of this project are to test the peptides produced by these engineered *Clostridia* strains on healthy & disease organoids with the aim of verifying the response of human-derived colonic epithelium to these novel peptides. Additionally, the organoid response to the presence of other compounds expressed by *Clostridia butyricum* can also be investigated.

There are various challenges in the production of small peptides. These challenges encompass the destruction of peptides by proteases present in bacterial cell culture. This degradation occurs to a greater extent during the exponential phase of bacterial growth. Small peptides (typically between 2-50 amino acids) are degraded rapidly, therefore, during the time it takes to acquire a sufficient concentration of the desired small peptide, a large proportion of it may have already been degraded. This degradation process could be the main cause for the remaining 4 out of 5 strains not producing a detectable quantity of our target small peptide. This is an issue when large quantities of peptide are required to have a medicinal effect on the patient.

If this experiment was repeated, there are various amendments that could be made to combat this issue. These improvements would increase the likelihood of success in the generation of small peptide fragments.

A method to limit proteolytic degradation of small peptides in a repeat of this experiment would be to engineer the *Clostridia* to produce linked units of the target

peptide. As the degradation occurs at the ends of the peptide, the centre unit would likely be more protected. Upon completion of the bacterial growth experiment the peptides can be purified and digested at the linking peptide sites. Following the bacterial growth stages there is likely to be an increased quantity of peptide remaining for purification & future applications.

Additionally, the use of protease inhibitors will aid in slowing the degradation process during the bacterial growth experiments, allowing for sufficient accumulation of the desired peptide throughout these bacterial growth stages.

The next stage for this project will be to test the STM28 peptide on the patient-derived colonic organoid platform. Firstly, the colonic organoids will be pre-treated with STM28 over a 48-hour period to allow for any competitive inhibition of TLR4 to occur. Following this treatment, the colonic organoids shall be exposed to a high concentration of lipopolysaccharides for another 48 hours to activate the TLR4 inflammatory pathway. The organoids shall then be harvested for transcriptomic and proteomic analysis to determine the anti-inflammatory effects of this novel peptide and to determine its therapeutic potential.

Chapter 7

Discussion

7.1 Inflammatory Bowel Disease

Inflammatory bowel disease is a debilitating and incurable condition with millions of sufferers worldwide, while numbers continue to rise. The effects of this disease expand further than inflammation in the GI tract with numerous complications reported (i.e., colorectal cancer). While a link has been made to various risk factors, the aetiology of this disease and its progression is not yet understood.

While there has been significant advancements in the treatment of IBD over recent years, including the introduction of biologics, current therapies vary in their efficacy with the risk of relapse high in many patients undergoing treatment. Many of these treatments also exhibit unpleasant side effects, further impacting the patient's quality of life. Hence, a better understanding of IBD pathogenesis may contribute to the discovery of more focussed treatment plans with a greater level of efficacy.

Ulcerative colitis causes extensive damage to the colon, primarily of the mucosal and epithelial layers. At the base of epithelial crypts resides the stem cell niche, comprising of intestinal stem cells and mesenchymal cells. These crypt-based cells are critical to the restoration of the epithelium following injury. An inflammatory cascade within the colon involving both the innate and adaptive immune response is responsible for this epithelial damage. The infiltration of immune cells into the colonic mucosa result in histopathological changes due to a loss of epithelial integrity, disrupted crypt architecture and ulceration These factors cause disturbed colonic function and ongoing pain for the patient, in addition to the increased risk of sepsis and long-term complications.

Factors suspected to be implicated in the pathogenesis of ulcerative colitis are considered genetic, environmental or immune-related. The interplay of multiple factors from these groups are thought to contribute to disease development. Gut dysbiosis is considered to occur as a result of environmental factors including diet and the use of

antibiotics [47]. This altered microbiome is suspected to lead to immune dysregulation. Some of the possible mechanisms involved in immune dysregulation were explored during this project. This was achieved by modelling ulcerative colitis on our patient-derived organoid platform, with multiple lines isolated from healthy individuals and UC patients.

The aim of this project was to determine the interplay of the colonic epithelium to possible environmental triggers under inflammatory conditions. This could then shed insight into the underlying processes involved in the inflammatory cascade leading to the pathological damage observed as the disease progresses.

Our approach was to initially generate a patient-derived model of the human colonic epithelium that can accurately depict the innermost layer of the colonic wall. Following the establishment of this model, the cell type expressed were determined by identification of key markers, namely MUC2, VIL, LGR5, CDX2 and CHGA. Once the presence of these proteins was confirmed, the responses of this 3D model under varying conditions were established. We stimulated this patient-derived model with a range of common inflammatory mediators and the subsequent response was measured by the alterations to downstream inflammatory pathways. Once a more focussed approach revealed insight into the innate and adaptive immune response, further analysis was conducted to confirm these findings in addition to identifying any novel markers that differ between the healthy and UC inflammatory responses.

Of particular interest were a prolific family of pattern recognition receptor known as toll-like receptors, as these have been reported to play a crucial role in the innate immune response to pathogens. Multiple cell types that are typically exposed to microorganisms are known to express TLRs including leukocytes, endothelial cells and epithelial cells [284]. These receptors bind to highly conserved microbe-associated molecular pattern (MAMPs) expressed by the majority of microbes. MAMPS are expressed by commensal and pathogenic bacteria alike. TLRs are indispensable in maintaining homeostasis in the mucosal environment, however disproportionate receptor signalling results in chronic intestinal inflammation, which, in predisposed people, leads to conditions such as IBD and colorectal cancer (CRC). The exact mechanisms of this process were investigated throughout this project.

IBD patients are up to 6 times more likely to develop CRC [87], with CRC being responsible for up to 15% of deaths in IBD patients [87]. Hence, markers of CRC (and related contributory factors, including oxidative stress) were measured to determine whether these factors are present to a greater extent in ulcerative colitis tissue, thereby demonstrating at which stage this increased risk begins during the course of the disease.

7.2 Profiling Organoid Model

With this in mind, the project was begun by generating our healthy and IBD models before characterising them by exploring their response to different inflammatory environments. Our model was generated from colonic crypts isolated via surgical resection during exploratory surgery in addition to endoscopy. Multiple samples were cultured from individuals differing in age and sex as well as the severity of disease. Once expanded in culture, initial investigations were conducted to determine the response of each before choosing the most representative lines for effective comparison.

Immediate differences were noted in the growth of healthy and UC organoids, with the latter taking several days longer to become established in culture. Furthermore, a substantial discrepancy was found in the survivability of samples. These factors already display the impact that inflammation has upon the health of the UC epithelium. To limit this effect samples had to be taken more distally to the site of observable inflammation. This improved survivability, however, only to a marginal extent. This finding demonstrates the decreased tissue health in UC patients throughout the colonic epithelium prior to visible damage.

While it would have revealed some interesting insights, no histological comparison was made between the distal and proximal sites of the colon due to the ethical limitations of biopsy quantity taken from the patient as well as time restrictions during the project.

To explore whether these discrepancies continue; further investigations were performed at a transcriptomic and proteomic level. A divergence in the response between healthy and UC lines was observed immediately upon exposure to pro-

inflammatory cytokine, TNFα, across a panel of markers. A self-perpetuating cycle of inflammation ensued in our ulcerative colitis model with an overwhelming increase in expression of pro-inflammatory markers across the board, including TNFα, NFκB, IL1β, IL8 and IL23.

Conversely, while there is an increase in the expression of these markers in our healthy line, this was to a very modest degree. These results indicate a clear differential response between healthy and UC tissue. Furthermore, intestinal health was determined by a change in the expression of LGR5, amongst mature intestinal cell markers, villin and mucin2. Stem cell marker expression was substantially higher in UC, indicated by increased LGR5 and OLFM4 expression. This is an interesting result as it might be expected that in the event of epithelial damage occurring a reduction in intestinal cell markers, including stem cells, may occur. However, this result is indicative of a compensatory mechanism in the initial stages of inflammation. Alternatively, increased LGR5 expression is present in cases of CAC.

Markers of inflammation were analysed next to markers of both mature intestinal cells and colonic stem cells to give a more well-rounded idea as to the effects of inflammatory stimuli on our primary model. The results gained from in this experiment very clearly showed an extreme response to TNFα, triggering a cycle of inflammation demonstrated by numerous prolific pro-inflammatory cytokines and chemokines. An increase in these signalling proteins initiates downstream recruitment of T cells, B cells and macrophages, amongst others. Therefore, the effects observed here are accurate indications of the level of immune response initiated.

Intestinal cell markers further confirmed the discrepancy between the effects upon UC and healthy epithelium. MUC2, an important component in the protection against bacteria, therefore an immense drop in expression, as observed in our UC model, would prove detrimental to epithelial health and, hence, the health of the patient. A drop of 90% was observed in Chapter 5 which would have disastrous effect on the epithelial layer *in vivo*. This can be compared against the drop in MUC2 expression in healthy organoids which occurs to a much lesser extent, of 50% below control.

In recent years, a breakthrough in stem cell biology has led to the successful isolation of primary tissue stem cells that can then be continually cultured *in vitro* [285]. In the

presence of a cocktail of growth factors and other constituents, stem cells present in the tissue, such as isolated intestinal crypts, are able to proliferate and differentiate into the myriad of cell types witnessed *in vivo*. Isolated intestinal crypts close to form a sphere with the apical cell surface arranged towards the lumen [286].

While numerous studies have employed healthy intestinal organoids for their investigations, much fewer have explored the possibility of culturing IBD patient-derived crypts. Transcriptional and methylation differences have been reported between UC organoids and controls [287,288]. The transcriptional signature that is acquired during disease progression was found to be maintained long after acute inflammation was alleviated [289]. These differences include the overexpression of lysozyme C (LYZ), an enzyme involved in the degradation of multiple Gram-positive bacteria [290]. This dysregulated expression of lysozyme C has also been associated with metaplastic Paneth-like cells [291]. Furthermore, ectopic expression of Claudin-18 (CLDN18) was reported, typically linked with experimental colitis and UC in humans [292]. Additionally, a correlation has also been drawn to the CRC developmental pathway [293]. Additionally, a reduction in MUC2 has been reported in organoids isolated from IBD patients [294], corroborating our data. The permanent changes observed in the UC colonic epithelium are suspected to be elicited by alterations in the stem cell compartment, thereby translating these alterations *ex vivo* [287]. These findings validate discoveries made during this project.

Our initial findings prompted further investigation into the expression levels of critical PRRs that play a key role in the cell response to TNFα. TNFα is known to bind to TLR2, therefore, TLR2 expression was measured along with 4 additional key TLRs involved in MAMP recognition. The TLR2 data uncovered from this experiment correlated with existing literature stating TLR2 as being highly expressed in IBD tissue samples [295]. However, contradictory to findings displayed in the IBD samples obtained by Cantó et al, we observed a 4 times greater increase in TLR2 levels than this group recorded. In contrast, healthy epithelial organoids revealed a modest 50% increase above control following TNFα-stimulation. This data points to a more inflammatory phenotype in the samples being cultured in this project than has been recorded in other projects.

Dysregulated TLR2 expression itself was, therefore, confirmed as being responsible for the surge in pro-inflammatory cytokine production in our UC platform in response to TNFα. Following this confirmation, the next step was to determine whether there were any cross-reactions or multiple TLR receptors involved in this heightened immune response. TLRs 1, 4 and 5 displayed significant increased expression in response to TNFα. This data was compared against the response of healthy organoids to this treatment regime, which demonstrated a modest increase in expression that proved to be insignificant. These findings clearly indicate heightened sensitivity in UC epithelium to other inflammatory mediators when primed with TNFα.

Together with the significantly raised expression of downstream pro-inflammatory cytokines and chemokines, this is indicative of an ongoing and uncontrolled cycle of inflammation in UC epithelium initiated by TNFα, that is absent in healthy epithelium. This is an important finding to note and suggests that inhibition of multiple TLRs could provide a more effective route in targeting the unchecked succession of inflammation present in UC.

Following investigations into the downstream effects of TNFα stimulation in our model, an upstream inflammatory activator of the TNFα signalling pathway was studied, LPS. LPS has previously been detected in the plasma of IBD patients pointing to microbial dysbiosis, thereby playing an integral role in IBD pathogenesis. Various studies have demonstrated this, including a study by Tulkens et al who verified the presence of LPS-containing extracellular vesicles in the plasma of patients diagnosed with either IBD or chemotherapy-induced intestinal mucositis [296]. Furthermore, LPS from various species has been shown to exhibit an impact upon tight junctions in the Caco-2 cell monolayer line, thereby increasing permeability [223]. Since these findings were reported in this 2D cell line alone, it is necessary to further establish these effects in a 3D model and more representative environment. It is also important to investigate the subsequent influence of systemic LPS following passage through this highly permeable intestinal epithelium.

Therefore, LPS was selected as an important upstream inflammatory trigger to further explore using our platform. LPS isolated from two bacterial species was tested to determine whether there are subtle differences in the response they elicit in this platform.

The first LPS tested was isolated from *Escherichia coli* 0127:B8. LPS from this strain was reported as activating TNFα production in PBMCs to a statistically significant degree. It was found that *Escherichia coli* 0127:B8-derived LPS was more potent in instigating an inflammatory response than that isolated from *Salmonella typhimurium*. *Salmonella typhimurium* is typically an enteric pathogen that, interestingly, requires intestinal inflammation to sustain its replication within the intestinal tract [297]. Hence, to support its own replicative abilities it releases effector proteins to instigate an immune response in the host, while avoiding destruction by the innate immune system [298]. TLRs are the first to detect *Salmonella* and are critical in mounting an immune response, while at the same time appear to be required by *Salmonella* to induce its SPI-2 virulence genes. This was displayed by the lack of sensitivity of mouse models lacking TLRs 2, 4 and 9 to *Salmonella* infection [299]. LPS from this species was therefore selected for comparison to that of *E. coli*.

Definitive differences between cell lines were immediately noted with clear visual distinctions following 48-hour LPS exposure. These differences were confirmed by transcriptomic data, with TNFα expression overwhelmingly elevated 35 times above control in UC organoids. In contrast, the healthy line displayed a negligible change in response to LPS. While to a lesser extent, IL1β and IL18 followed this same pattern of expression, confirming the dysregulated inflammatory response observed in response to TNFα also occurs in response to LPS. These findings offer further clarity into the contributory factors involved in the progression of UC. The overwhelming rise of inflammation in response to this prolific bacterial PAMP is further compounded by the destructive alterations occurring in epithelial cell expression. Expression of LGR5-expressing cells increases in healthy organoids following exposure to LPS, pointing to a protective mechanism in place acting to increase turnover in the epithelium for the replacement of damaged cells. This process of enhancing ISC expression under inflammatory conditions offers crucial protection by increasing compromised epithelial integrity, thereby limiting further bacterial invasion. This safeguard was not found to be present in UC organoids, and moreover, LGR5 expression decreased considerably. This finding alone demonstrates the tremendous extent with which UC differs to healthy functioning. To further investigate whether these discrepancies extended to differentiated epithelial cells, villin and MUC2 expression was also measured. Unexpectedly, while villin remained unaffected by LPS in our healthy model,

expression was, in fact, doubled in our UC line. This is contradictory to the effect we observed on stem cell expression, however, indicating that the presence of inflammation triggered a differentiation cascade. This effect would impact epithelial integrity by enabling an initial increase in the structural integrity as there is a greater presence of adult intestinal cells to plug the openings made by previous epithelial damage. This would offer an initial benefit of delaying further bacterial translocation, however, the reduced stem cell presence in the colonic crypts would prevent a long-term solution to this problem once the differentiated cells have undergone damage and/or anoikis and no cells are available for replacement.

Once the inflammatory response had been determined in these representative human-derived lines, the effect of a TLR4 inhibitor upon this response was then investigated. If the responses observed were, indeed, due to LPS acting via the TLR4 receptor then a competitive inhibitor would largely reverse this effect. The chosen inhibitor, TLR4-IN-C34, is an aminomonosaccharide that works to block TLR4 activity by binding to the hydrophobic pocket of MD-2. This prevents activation of the downstream TLR4 signalling pathway. The efficacy of this compound to inhibition of the LPS-induced immune response has been displayed in BV2 microglia cells [300].

The findings from this experiment demonstrated this to be the case, with significant reversals across several key inflammatory and intestinal markers when treated in conjunction with LPS over a 48-hour period. This data demonstrates that the organoid responses we observed are due to activation of the TLR4 signalling pathway.

Having obtained confirmation of the involvement of the TLR4 pathway in the inflammatory and cellular response, the next step was to determine the factors contributing to the differences we observe between healthy and UC organoids when placed under identical conditions over the same time period. To ascertain whether the level of receptor expression itself was a critical factor, TLR4 expression was measured under basal conditions and compared with the response to chronic LPS exposure. Findings very clearly show a substantial difference between the reaction of healthy and UC organoids in terms of TLR4 mRNA expression similarly to that we reported following TNFα exposure. However, we observed a further exaggerated response here with a reduction in TLR4 occurring in healthy organoids in the presence of LPS. This is likely to limit the perpetual overstimulation of abundant LPS, thereby preventing

further damage to the epithelium. This negative feedback response has been identified in the lung and the RAW 264.7 macrophage cell line. This group have reported a role for microRNAs in this protective downregulation in lung cells. Jiang et al found that miR-181a overexpression was linked with reduced production of inflammatory cytokines, in addition to a reduction in NFκB activation and ROS. The pathway found to be targeted by this miRNA is TLR4, which was bound by miR-181a directly via the 3′-UTR. [301]. Furthermore, this miRNA was recorded as suppressing TLR4 expression itself in response to LPS, demonstrating the existence of a negative regulation following initiation by abundant bacterial PAMPs. This mechanism may be aberrant in UC epithelial cells as a reduction in this miRNA can lead to a substantial increase in these markers, hence, the link between TLR4 pathway and miRNAs may be worth investigating in this model.

To further assess whether the differences are enhanced by a change in the expression of other TLRs, we decided to measure the expression levels of 4 other TLRs before and after LPS exposure, thereby determining whether there was any referred effect as we previously discovered after the addition of TNFα. Significant differential expression was found in the TLR3 expression between healthy & UC organoids in both basal and inflammatory conditions. However, unlike the results observed upon the addition of TNFα, TLR3 expression follows the same trend as TLR4 following LPS exposure. Hence, the negative regulatory mechanism identified in TLR4 also impacts TLR3. The dysregulated expression of TLR3 noted in our UC model would result in further amplification of the inflammatory response *in vivo*, sensitising the colonic epithelium to any potential viral presence. This is an important finding that would inform the treatment of UC with greater awareness of the risk that a further viral infection could exert on the patient's condition.

Following this interesting finding, it was decided to measure the basal expression levels to identify if this dysregulation occurs upon stimulation or differences exist under homeostatic conditions. As we've reported in Chapter 5, basal expression levels of TLR4 do, indeed, differ between healthy and UC-derived epithelial tissue with 95% less TLR4 being encoded in UC. If there was a difference between healthy and UC tissue expression under inflamed conditions, we might expect UC organoids to be expressing a greater amount of TLR4 at basal levels also. No other studies were

discovered during the literature review that investigated the differences in TLR expression under basal conditions. This is, therefore, an unexpected discovery, which highlights the considerable reaction to LPS in UC with a 60 times upregulation of TLR4. This level of upregulation would, in turn, lead to a chronic cycle of inflammation. This data clearly demonstrates that while LPS induces an overwhelming increase in TLR4, the UC colonic epithelium does not continually express TLR4 at a heightened level in comparison to healthy controls. Hence, colonic tissue in patients suffering with UC remains sensitive to LPS despite residing in basal, non-inflamed conditions for weeks prior.

7.3 Colitis-associated Colorectal Cancer

Once the link between UC, LPS & TLR4 had been displayed using our model, the next step was to investigate a connection to colitis-associated colorectal cancer. While the association between UC and colorectal cancer has previously been reported, the path from UC to CRC development has not been fully elucidated.

The incidence of UC-CRC is up to ten times higher than sporadic CRC, with the age of onset being 20 years earlier [302]. There are certain mutations found in sporadic CRC including *p53* that are also present in UC-CRC. A key difference being that mutated *p53* has been detected early on in the adenoma-carcinoma progression of UC-CRC but doesn't occur until much later in sporadic CRC development [303]. Several other discrepancies in genetic characteristics have been reported including expression of a number of microRNAs. An example of this is miRNA-124a, a gene encouraging tumour suppression, is methylated during CAC development [304]. It has been suggested that inflammatory stresses present in UC contribute to the occurrence of these genetic changes, however there is yet much understanding of the mechanisms of CAC development lacking.

To determine if LPS activation of TLR4 and the subsequent signalling pathway plays a role in the development of this serious condition, several critical markers of CAC were analysed in this project. The platform was treated in accordance with the previous experimental conditions over the same time period. Of these markers, two responded to a particularly significant degree, displaying a strong differential response between healthy and UC tissue.

EGFR was found to be highly overexpressed in our UC model when LPS was applied to the culture environment. The opposite effect was noticed in our healthy model, with an overwhelming 70% decline in expression. This is an interesting divergence in epithelial response between a healthy and disease epithelial platform. These opposing reactions suggest the negative feedback mechanism apparent in the healthy colonic epithelium confers a protective effect for maintaining homeostatic conditions. The EGFR pathway is one of the most important pathways for the control and orchestration of growth, proliferation, differentiation and migration in most cells in the human body. Hence, if this pathway becomes imbalanced and dysregulated at any juncture, the downstream effects can be catastrophic for the functioning of numerous organs and, therefore, for the health of the individual. TLR4 has very recently been found to promote EGFR phosphorylation which, in turn, promotes inflammation within the cell [305]. EGFR effects the IFN branch of the TLR4 signalling pathway, with the downstream ramifications being recruitment of natural killer cells and cytotoxic T lymphocytes. When EGFR is inhibited in mice, IFN-β is also effectively inhibited, whereas TNFα expression is enhanced. This effect is due to EGFR being required for IFN-regulatory factor (IRF) activation via the PI3 kinase/AKT pathway. following stimulation of TLR4. Inhibition of EGFR has been shown to halt LPS-induced septic shock in mice by occluding the IFN branch of the TLR4 pathway [254].

As we know, chronic inflammation can contribute to the development of cancer and augment progression. One of the suspected factors contributing to this synergistic effect between inflammation and cancer is the role immune cells such as macrophages play in the evolution of cancer from a few erroneous cells to large tumours. In cancer mouse models, these immune cells are recruited by cancer cells, which, in turn, secrete a range of cytokines to create an ongoing cycle of inflammation. Furthermore, macrophages emit pro-angiogenic factors such as VEGFA, CXCL8 and CXCL12 [306].

EGFR has also been found to be linked to macrophage activation in human and mouse macrophage cell lines during a *H. pylori* infection [252]. Increased levels of phosphorylated EGFR were reported by Hardbower et al in murine gastric tissues. EGFR deficiency in mice led to dysregulated macrophage activation, thereby reducing pro-inflammatory cytokine and chemokine production.

Macrophage count was also significantly greater in EGFR-positive tumours, linking EGFR with immune response and tumour development. In a cyclical fashion, EGFR expression also boosts cell surface expression of TLR4 as demonstrated in macrophages, [307], leading to continuous worsening of inflammation and exacerbation of cancer progression. This cycle has so far been reported in lung and breast cancer; however, no connection has yet been found in colitis-associated cancer. Our data demonstrates that this pathway is prominent in a human-derived colitis platform, which is a likely signal of the early stages of cancer development.

In our study, EGFR expression was downregulated when UC organoids were cultured in conjunction with a TLR4 inhibitor, suggesting that LPS-induced activation of the TLR4 signalling pathway was responsible for the raised EGFR levels, enhancing the progression from colitis to cancer. Therefore, inhibition of TLR4 itself or a downstream adapter could aid in protecting against this development.

This same negative feedback response in healthy organoids and the exaggerated response in UC was observed for COX2 transcriptomic expression. Expression was also reduced below initial baseline levels following pre-treatment and ongoing culture with TLR4 inhibitor over a 48-hour period.

Until very recently, COX2 remained unexplored in the context of UC. A study by Li et al published in 2018 sought to identify the role COX2 signalling plays in intestinal epithelial regeneration [308]. However, these effects were only investigated upon activation of the TNFα pathway alone. TNFα was found to induce COX2 expression in monocytes isolated from patients who were responsive to TNF inhibitors, whereas those isolated from non-responders displayed consistently high, non-inducible COX2 expression [308]. This finding is of great interest to determine the patients who are more likely to respond effectively to therapy.

COX2 has been found to be released by fibroblasts, M2 macrophages and some cancer cells, however, expression of this enzyme has not yet been reported in colitis-associated cancer linked to the TLR4 pathway. Here, we demonstrate this link, further elucidating the pathway critical for cancer pathogenesis in UC patients.

Once this link had been revealed from the data, the downstream effects were further explored. One of the avenues investigated was that of heat shock proteins. Heat shock

proteins are stress-responsive molecules that play a major role in numerous biological processes, including cellular proliferation and differentiation. They also strongly promote carcinogenesis and are therefore found to be overexpressed in a wide range of cancers.

Heat shock proteins are continually expressed in the colonic epithelium due to the prolific presences of bacterial PAMPs, including LPS and SCFAs [309]. HSF1, a transcriptional regulator of the HSP response, has been found to exhibit dual roles in the different stages of UC and CAC development. Some of the ways it contributes to tumour progression is by regulating of ECM remodelling, as shown in mouse colon fibroblasts, via the upregulation of genes encoding for matrix remodelling enzymes including MMP7 and MMP9 [310].

Furthermore, HSP25 was found to be highly expressed in tumours with a low level of cell death following cancer treatment (i.e., sarcomas). Furthermore, the overexpression of this protein repressed proteosome function, antigen presentation and, hence, increase occurrence of tumours [311]. This overexpression was also observed using our colonic model for inflammation, with opposing effects detected between healthy and UC-derived organoids. Five times the level of expression was recorded in our UC line under pro-inflammatory conditions, again clearly demonstrating a link between UC, chronic inflammation and colorectal cancer. These effects were reversed by TLR4 inhibition, providing evidence for the strong involvement of this signalling pathway.

These findings are reciprocated to some extent by another heat shock protein, HSP72. Expression of HSP72 is often induced under stressful conditions and is otherwise very lowly expressed. However, in the cells of various tumours, including breast, renal and endometrial cancer, they are often constitutively overexpressed [312]. Additionally, overexpression of HSP72 is evidence of a poor therapeutic outcome. It has been found using depletion of HSP72 by siRNA that this protein promotes cancer progression by repressing senescence via the p53-dependent pathway.

It appears this risk is mitigated in healthy tissue by a downregulation upon inflammatory stimulation. On the other hand, HSP72 expression climbs markedly in

UC tissue in the presence of LPS. This suggests LPS stimulation in UC colonic epithelium increases the risk of colorectal cancer in UC patients.

This cumulative data demonstrates similar expression profiles for multiple markers linked with various cancers. These findings therefore show evidence of a pre-disposition to cancer in our UC organoid platform. This is indicative of the development of colitis-associated cancer, however, the timescale for this occurrence is unknown. Upon future comparison of this data with the patient prognosis would reveal further information. This information would expose the timeframe in which these markers become detectable prior to the development of cancer.

This experimental data displays the involvement of the TLR4 signalling pathway in colitis-associated carcinogenesis, demonstrated by the considerable effect of suppression by TLR4 inhibition.

7.4 Genomic Sequencing

The data from our experiments throughout the first stages of the project informed us as to the best experimental set-up to reveal important and relevant information. Following on from these investigations, a more comprehensive transcriptomic review was conducted. RNA-seq was utilised for employing a broader approach for the identification of novel markers that could be targeted and exploited in UC and CAC diagnosis.

Genes were analysed from several gene ontology groups including inflammatory regulation, TLR4 signalling, ER stress, EMT, apoptotic signalling and heat shock protein binding.

The data obtained from this experiment corroborates data acquired previously from RT-PCR, this includes the TLR3-TLR4 crosstalk evident in our colonic epithelial model. Several markers downstream of TLR4 were also shown to be upregulated, while immunosuppressive genes were downregulated.

This data confirms that TLR4 itself is strongly and significantly upregulated upon LPS exposure. Interestingly, additional hits revealed the impact LPS can have on the epithelial ability to sense bacterial presence, with the loss of INAVA. This inability to

effectively sense, and hence clear, bacteria can leave someone susceptible to IBD progression [313].

New genes hits were also discovered by RNA-seq that were not in our previous panel of markers. Several of these genes include those that transcribe those proteins that interact with TLR4 including TICAM2, providing further evidence of the TLR4 involvement in UC pathogenesis.

In addition to evidence confirming a TLR4-associated differential response in UC, numerous hits further signalled the link between UC and cancer. These genes favoured carcinogenesis, promoting EMT, cellular proliferation and cell migration. Many of these genes have been found to be associated with other types of cancer, however they haven't been reported for their role in colorectal carcinogenesis. The overexpression of these genes in UC organoids signals the propensity of this tissue to form tumours in the future and could act as markers to determine a patient's risk. This allows vigilant measures to be put in place with regular testing for any change in these markers prior to macroscopic changes occurring.

A notable marker favouring inflammatory carcinogenesis is TNFAIP3. This has been reported as being activated by TNF-induced NFκB activation. Overexpression of this gene has been linked to poor survival in oesophageal squamous cell carcinoma patients [314]. However, no studies have found this association in CAC, therefore this result is worth further investigation.

Loss of TRADD, associated in mediation of programmed cell death, is another marker suggesting a transcriptomic leaning towards pro-carcinogenesis. Additionally, loss of genes involved in cell growth cycle checkpoints and tumour suppression, including NPLOC4 and CDK5RAP3 respectively and upregulation of protooncogenes such as Lyn, would further support this hypothesis.

Moreover, changes in genes relating to cell adhesion, inclusive of THBS1, were also shown to be altered. As well as likely encouraging UC progression by allowing greater translocation of luminal bacteria across the epithelium, loss of this gene has been linked to increased susceptibility to cancers in mice [315]. Intriguingly, loss of expression of this marker is not linked with deletion of mutation but is rather due to epigenetic

silencing via hypermethylation, as reported in human neuroblastoma [316] but not yet CAC.

The subsequent effects of this would result in the loss of membrane integrity and increase the potential for crossing of bacteria across the barrier and eventually into circulation. The discovery of these genes' aids in the understanding of the genetic differences contributing to the pathogenesis of UC. Once the genes responsible have been pinpointed they can then be targeted by novel medications or by genetic editing once these technologies have been better adapted for clinical use.

7.5 Manufacturing a Novel TLR4 Inhibitor

As many of the genes uncovered in our data were related to the TLR4 signalling pathway, the next steps were to develop a novel inhibitor of this pathway using cutting-edge technology in synthetic biology designed by CHAIN Biotechnology.

Following the selection of a novel short peptide found to bind TLR4, a plasmid was designed containing the genetic sequence of this peptide with the relevant promoters and restriction sites compatible with the final Clostridium species chosen for its production. These steps were completed over a period of several months culminating in the successful development of a *C. butyricum* strain able to express STM28 and another to express SPA4.

C. butyricum is naturally found in the healthy human gut, and therefore has a proven safety profile. In its non-toxigenic form, it is also used as a probiotic in some countries. Therefore, it is an excellent contender as a biotherapeutic. CHAIN Biotech have formulated this sporulating strain into capsule form for effective delivery to the colon. The spores can successfully avoid degradation in the stomach and only germinate once conditions are favourable for anaerobic strains (i.e., the colon). A further advantage of the use of this strain as a therapeutic is its release of a by-product of fermentation: butyric acid. Butyric acid is a short-chain fatty acid (SCFA) with powerful anti-inflammatory and anti-oxidative effects demonstrated in multiple cell lines [317]. It has been shown to act by reducing the expression of TNFα, IL-6 and FFAs, amongst other inflammatory mediators [318]. Furthermore, it has been shown to decrease NFκB activation which is a key mediator in the TLR4 pathway [317]. This can provide additional

benefits for the use of *C. butyricum* to transport our anti-inflammatory peptide to the site of inflammation in the colon.

The novel peptides selected were very recently reported as exhibiting anti-inflammatory effects via TLR4 inhibition. SPA4 is a region of the surfactant protein-A (SP-A) present in alveoli. It was reported as being effective in suppressing the pro-inflammatory cytokine, TNFα in the murine dendritic cell line, JAWS II, upon LPS challenge by Awasthi et al [319]. This group also found the next region, SPA5 to be productive in inhibiting the effect of LPS, however to a lesser degree. SPA4 has also been shown to remedy endotoxic shock symptoms in a mouse model [320]. This peptide has not been tested in a primary model and the effects within the colonic epithelium have not yet been considered. Therefore, the small peptide region was therefore chosen as an effective inhibitor to express in our system.

A second peptide, STM28 formed of 17 amino acids, was selected to determine which provides the most effective inhibition of this pathway. In a study investigating the role of TLR4 in multiorgan failure triggered by acetaminophen, STM28 was found to attenuate livery injury [321]. Pre-treatment with STM28 also delayed time of coma onset. This peptide was therefore demonstrated as being an effective TLR4 antagonist with efficacy in the prevention of the inflammatory cascade contributing towards multiple organ failure.

These peptides were, therefore chosen for generation using synthetic biology techniques for subsequent testing on our platform. Following the engineering of two Clostridia strains containing plasmids with the genetic sequences to encode each of these peptides, a growth experiment was then conducted to expand each strain and collect lysates at regular intervals throughout the growth experiment. The lysates were then tested for the presence of these peptides within the bacterial cells. STM28 was identified after 24 hours of growth, as demonstrated by western blot, while no production of SPA4 was detected. This could be due to the quantity produced being too minimal to detect or due to the engineered strain being unable to express this peptide.

The identification of STM28 proves the protocol conducted to be successful with a TLR4 antagonist produced via bioengineering. This is a promising avenue to further

explore with the potential for an oral medication to be engineered on a larger scale for the treatment of inflammation within the colon of UC patients.

For this potential to be realised, there needs to be some refinement of the strain. These include the ability to secrete the peptide for ease of isolation. The peptide can then be purified from other sugars and peptides in the surrounding medium. STM28 can then be tested on numerous patient samples in organoid culture to demonstrate the efficacy of treating UC of varying severities. It is possible the age of the patient as well as the location of ulceration could affect the efficacy of the compound, therefore, it would be beneficial to test STM28 on samples from patients with varied degrees of disease.

7.6 Study Limitations

7.6.1 Limitations of Model

Despite the numerous advantages to using our primary organoid model for the study of ulcerative colitis, there are, of course, also limitations to take into consideration. Current organoid culture depends on the use of Matrigel^{TM}, a gel-like extracellular matrix (ECM) produced by the Engelbreth-Holm-Swarm (EHS) mouse sarcoma. It is rich in various proteins including laminin, collagen IV and heparin sulfate proteoglycans. Matrigel^{TM} is required to mimic the 3D conditions that are found *in vivo*, necessary for producing a characteristic model of the *in vivo* intestinal epithelium. Certain small molecule screening experiments can be hindered by the surrounding ECM, interfering with the availability of the full dose to reach each organoid. Therefore, changes to the ECM, during experimentation, could allow for alterations to be made in the permeability of the ECM, thereby allowing more uniform exposure.

Additionally, due to Matrigel^{TM} being a biologically generated product, the levels of ECM are poorly defined with a high degree of variability between batches. This variation holds certain disadvantages for experimentation where analysis of fibrosis using intestinal organoids is required, due to the large number of fibrotic elements present in the culture environment. Hence, the surrounding ECM proteins can impact the production of fibrotic markers.

Moreover, due to the production of Matrigel^{TM} being dependent on mouse sarcoma, this prohibits the use of organoids for transplantation into humans. Therefore, a more

well-defined environment is needed, with fewer variations, which does not interfere with organoid behaviour and that will, in the future, comply with health regulations for transplantation into humans.

An additional factor that may contribute towards variability between organoid lines, as well as impacting upon the ability to generalise our findings to the *in vivo* system is the variations in their size and shape. This will undoubtedly influence the response of individual organoids to different treatments. However, when all the organoids are measured and analysed together this will present us with the average organoid response. Alternatively, individual organoids can be tracked using live imaging techniques to determine the changes in a particular organoid.

7.6.2 Limitations of Study

While invaluable insight was gained in this study, there are other important points to consider that may affect the ability to entirely extrapolate these findings to other individuals suffering with UC.

There is great variability in the location, severity and prognosis of this disease observed between patients, in addition to differences in age at onset and potential triggers all differing greatly. Furthermore, the response to treatment of each individual is highly unpredictable, requiring each patient to receive an array of medications prior to successful induction of remission. These factors indicate the polygenic nature of this disease suggesting the results from this study may not necessarily be representative of all cases of UC. Expanding this study to a greater number of patient lines could reveal whether our findings hold true for the majority of UC sufferers, despite variations in disease presentation. A personalised medicine approach would also offer a solution to this variability, confirming whether their colonic tissue mimics the response found in our study, prior to administering treatment.

The lack of other cell types in our model offers a reductionist approach that can focus the study to the interaction between epithelial cells and the alterable immune environment. However, this reductionist system removes the key elements that influence the immune response *in vivo*, including the mesenchyme and immune cells typically residing in the colon. Hence, following initial investigations conducted on this

epithelial system, a preferable solution would be to then add in additional missing elements until a more extensive representative understanding is developed.

Furthermore, certain conclusions were made as to the viability of the organoids during experimentation using morphological assessment alone. While this method clearly displays whether the organoid is in the early or late stages of necrosis, it would be more accurate to use a more quantifiable assessment of organoid viability, such as an ATP assay, to exclude cell toxicity during the dose response assays. The lack of such assessment could lead to misinterpretation of transcriptional data as to the effects of substances at the extreme ends of the dose response range. It would be unclear as to whether any drop in marker expression levels is due to a reduction in expression by the epithelial cells within the organoid or as a result of a reduced viable cell count.

7.7 Conclusion & Future Directions

The project presented in this thesis has built upon existing research in this field, including investigation into the response of receptors, expressed in intestinal organoids, to their respective ligands. Additionally, the differential response between healthy tissue of the colonic epithelium, and that found in UC, were analysed and yielded important findings that homed in on crucial factors contributing to UC pathogenesis and subsequent complications. Furthermore, a potential novel peptide was produced using a synthetic engineering approach that could hold potential as a therapeutic for the relief of inflammation in UC.

Future studies in this line of work should focus on further exploring the linked pathways connecting LPS, TLR4, UC and CAC. This work should aim to investigate in greater depth the proteins within the TLR4 pathway that can be targeted for inhibition to effectively reduce the exaggerated inflammation we observe in UC induced by abundant LPS. As the immune system is so important in maintaining homeostasis and promoting commensal over pathogenic bacteria in the gut, this focussed inhibition should not cause detrimental effects in the functioning of the immune system to real invasive threats. Following on from identification of the multiple cancer-associated markers we exhibited as being present in UC, further research should be performed to further explore the timing of their expression during the course of disease. This

would inform us as to the stage of disease when greater surveillance is required as well as the timing of treatments for the prevention of life-threatening complications.

These investigations are likely to be of significance in other mucosal-related diseases beyond UC, thereby improving the fate on many individuals silently suffering with chronic life-altering mucosal diseases with a phenotype of an inflated inflammatory presence.

References

1. Horiguchi, H.*, et al.* ANGPTL2 expression in the intestinal stem cell niche controls epithelial regeneration and homeostasis. *EMBO J* **36**, 409-424 (2017).

2. Fair, K.L., Colquhoun, J. & Hannan, N.R.F. Intestinal organoids for modelling intestinal development and disease. *Philos Trans R Soc Lond B Biol Sci* **373**(2018).

3. Lukovac, S. & Roeselers, G. Intestinal Crypt Organoids as Experimental Models. in *The Impact of Food Bioactives on Health: in vitro and ex vivo models* (eds. Verhoeckx, K.*, et al.*) 245-253 (Cham (CH), 2015).

4. Nijland, R., Hofland, T. & van Strijp, J.A. Recognition of LPS by TLR4: potential for anti-inflammatory therapies. *Mar Drugs* **12**, 4260-4273 (2014).

5. Parikh, K.*, et al.* Colonic epithelial cell diversity in health and inflammatory bowel disease. *Nature* **567**, 49-55 (2019).

6. Baker, A.M.*, et al.* Quantification of crypt and stem cell evolution in the normal and neoplastic human colon. *Cell Rep* **8**, 940-947 (2014).

7. Barker, N.*, et al.* Identification of stem cells in small intestine and colon by marker gene Lgr5. *Nature* **449**, 1003-1007 (2007).

8. Marshman, E., Booth, C. & Potten, C.S. The intestinal epithelial stem cell. *Bioessays* **24**, 91-98 (2002).

9. Barker, N. & Clevers, H. Leucine-rich repeat-containing G-protein-coupled receptors as markers of adult stem cells. *Gastroenterology* **138**, 1681-1696 (2010).

10. Li, Y.*, et al.* A growth factor-free culture system underscores the coordination between Wnt and BMP signaling in Lgr5(+) intestinal stem cell maintenance. *Cell Discov* **4**, 49 (2018).

11. Elphick, D.A. & Mahida, Y.R. Paneth cells: their role in innate immunity and inflammatory disease. *Gut* **54**, 1802-1809 (2005).

12. Simmonds, N., Furman, M., Karanika, E., Phillips, A. & Bates, A.W. Paneth cell metaplasia in newly diagnosed inflammatory bowel disease in children. *BMC Gastroenterol* **14**, 93 (2014).

13. Landy, J.*, et al.* Tight junctions in inflammatory bowel diseases and inflammatory bowel disease associated colorectal cancer. *World J Gastroenterol* **22**, 3117-3126 (2016).

14. Prasad, S.*, et al.* Inflammatory processes have differential effects on claudins 2, 3 and 4 in colonic epithelial cells. *Lab Invest* **85**, 1139-1162 (2005).

15. Gribble, F.M. & Reimann, F. Function and mechanisms of enteroendocrine cells and gut hormones in metabolism. *Nat Rev Endocrinol* **15**, 226-237 (2019).

16. Lebrun, L.J.*, et al.* Enteroendocrine L Cells Sense LPS after Gut Barrier Injury to Enhance GLP-1 Secretion. *Cell Rep* **21**, 1160-1168 (2017).

17. Van der Sluis, M.*, et al.* Muc2-deficient mice spontaneously develop colitis, indicating that MUC2 is critical for colonic protection. *Gastroenterology* **131**, 117-129 (2006).

18. Johansson, M.E. Mucus layers in inflammatory bowel disease. *Inflamm Bowel Dis* **20**, 2124-2131 (2014).

19. Johansson, M.E., Larsson, J.M. & Hansson, G.C. The two mucus layers of colon are organized by the MUC2 mucin, whereas the outer layer is a legislator of host-microbial interactions. *Proc Natl Acad Sci U S A* **108 Suppl 1**, 4659-4665 (2011).

20. Desai, M.S.*, et al.* A Dietary Fiber-Deprived Gut Microbiota Degrades the Colonic Mucus Barrier and Enhances Pathogen Susceptibility. *Cell* **167**, 1339-1353 e1321 (2016).

21. Round, J.L. & Mazmanian, S.K. The gut microbiota shapes intestinal immune responses during health and disease. *Nat Rev Immunol* **9**, 313-323 (2009).

22. Kelly, D.*, et al.* Commensal anaerobic gut bacteria attenuate inflammation by regulating nuclear-cytoplasmic shuttling of PPAR-gamma and RelA. *Nat Immunol* **5**, 104-112 (2004).

23. Bates, J.M., Akerlund, J., Mittge, E. & Guillemin, K. Intestinal alkaline phosphatase detoxifies lipopolysaccharide and prevents inflammation in zebrafish in response to the gut microbiota. *Cell Host Microbe* **2**, 371-382 (2007).

24. Cai, R.*, et al.* Interactions of commensal and pathogenic microorganisms with the mucus layer in the colon. *Gut Microbes* **11**, 680-690 (2020).

25. Abreu, M.T.*, et al.* Decreased expression of Toll-like receptor-4 and MD-2 correlates with intestinal epithelial cell protection against dysregulated proinflammatory gene expression in response to bacterial lipopolysaccharide. *J Immunol* **167**, 1609-1616 (2001).

26. Naik, S., Kelly, E.J., Meijer, L., Pettersson, S. & Sanderson, I.R. Absence of Toll-like receptor 4 explains endotoxin hyporesponsiveness in human intestinal epithelium. *J Pediatr Gastroenterol Nutr* **32**, 449-453 (2001).

27. Fusunyan, R.D., Nanthakumar, N.N., Baldeon, M.E. & Walker, W.A. Evidence for an innate immune response in the immature human intestine: toll-like receptors on fetal enterocytes. *Pediatr Res* **49**, 589-593 (2001).

28. Jergens, A.E., Parvinroo, S., Kopper, J. & Wannemuehler, M.J. Rules of Engagement: Epithelial-Microbe Interactions and Inflammatory Bowel Disease. *Front Med (Lausanne)* **8**, 669913 (2021).

29. Rinninella, E.*, et al.* What is the Healthy Gut Microbiota Composition? A Changing Ecosystem across Age, Environment, Diet, and Diseases. *Microorganisms* **7**(2019).

30. Qin, J.*, et al.* A human gut microbial gene catalogue established by metagenomic sequencing. *Nature* **464**, 59-65 (2010).

31. Frank, D.N.*, et al.* Molecular-phylogenetic characterization of microbial community imbalances in human inflammatory bowel diseases. *Proc Natl Acad Sci U S A* **104**, 13780-13785 (2007).

32. Swidsinski, A.*, et al.* Mucosal flora in inflammatory bowel disease. *Gastroenterology* **122**, 44-54 (2002).

33. Shanahan, F. & Bernstein, C.N. The evolving epidemiology of inflammatory bowel disease. *Curr Opin Gastroenterol* **25**, 301-305 (2009).

34. Li, J., Butcher, J., Mack, D. & Stintzi, A. Functional impacts of the intestinal microbiome in the pathogenesis of inflammatory bowel disease. *Inflamm Bowel Dis* **21**, 139-153 (2015).

35. Sokol, H.*, et al.* Faecalibacterium prausnitzii is an anti-inflammatory commensal bacterium identified by gut microbiota analysis of Crohn disease patients. *Proc Natl Acad Sci U S A* **105**, 16731-16736 (2008).

36. DeGruttola, A.K., Low, D., Mizoguchi, A. & Mizoguchi, E. Current Understanding of Dysbiosis in Disease in Human and Animal Models. *Inflamm Bowel Dis* **22**, 1137-1150 (2016).

37. Jorgensen, J. & Mortensen, P.B. Hydrogen sulfide and colonic epithelial metabolism: implications for ulcerative colitis. *Dig Dis Sci* **46**, 1722-1732 (2001).

38. Fava, F. & Danese, S. Intestinal microbiota in inflammatory bowel disease: friend of foe? *World J Gastroenterol* **17**, 557-566 (2011).

39. Rigottier-Gois, L. Dysbiosis in inflammatory bowel diseases: the oxygen hypothesis. *ISME J* **7**, 1256-1261 (2013).

40. Lin, S., Li, Y., Zamyatnin, A.A., Jr., Werner, J. & Bazhin, A.V. Reactive oxygen species and colorectal cancer. *J Cell Physiol* **233**, 5119-5132 (2018).

41. Kim, D.H. & Cheon, J.H. Pathogenesis of Inflammatory Bowel Disease and Recent Advances in Biologic Therapies. *Immune Netw* **17**, 25-40 (2017).

42. Xu, X.R., Liu, C.Q., Feng, B.S. & Liu, Z.J. Dysregulation of mucosal immune response in pathogenesis of inflammatory bowel disease. *World J Gastroenterol* **20**, 3255-3264 (2014).

43. Ghosh, N. & Premchand, P. A UK cost of care model for inflammatory bowel disease. *Frontline Gastroenterol* **6**, 169-174 (2015).

44. Danese, S.*, et al.* Extraintestinal manifestations in inflammatory bowel disease. *World J Gastroenterol* **11**, 7227-7236 (2005).

45. Kim, E.R. & Chang, D.K. Colorectal cancer in inflammatory bowel disease: the risk, pathogenesis, prevention and diagnosis. *World J Gastroenterol* **20**, 9872-9881 (2014).

46. Burisch, J., Jess, T., Martinato, M., Lakatos, P.L. & EpiCom, E. The burden of inflammatory bowel disease in Europe. *J Crohns Colitis* **7**, 322-337 (2013).

47. Francino, M.P. Antibiotics and the Human Gut Microbiome: Dysbioses and Accumulation of Resistances. *Front Microbiol* **6**, 1543 (2015).

48. Porter, R.J., Kalla, R. & Ho, G.T. Ulcerative colitis: Recent advances in the understanding of disease pathogenesis. *F1000Res* **9**(2020).

49. Sheikh, M.N., Hanif, S., Zia, M. & Qayyum, Z. Effects of nicotine on an in vitro reconstituted model oral mucosa in terms of cytokine production. *J Ayub Med Coll Abbottabad* **23**, 80-84 (2011).

50. Costello, S.P.*, et al.* Effect of Fecal Microbiota Transplantation on 8-Week Remission in Patients With Ulcerative Colitis: A Randomized Clinical Trial. *JAMA* **321**, 156-164 (2019).

51. Pavlidis, P.*, et al.* Interleukin-22 regulates neutrophil recruitment in ulcerative colitis and is associated with resistance to ustekinumab therapy. *Nat Commun* **13**, 5820 (2022).

52. Dinallo, V.*, et al.* Neutrophil Extracellular Traps Sustain Inflammatory Signals in Ulcerative Colitis. *J Crohns Colitis* **13**, 772-784 (2019).

53. Kaluzna, A., Olczyk, P. & Komosinska-Vassev, K. The Role of Innate and Adaptive Immune Cells in the Pathogenesis and Development of the Inflammatory Response in Ulcerative Colitis. *J Clin Med* **11**(2022).

54. Sayoc-Becerra, A.*, et al.* The JAK-Inhibitor Tofacitinib Rescues Human Intestinal Epithelial Cells and Colonoids from Cytokine-Induced Barrier Dysfunction. *Inflamm Bowel Dis* **26**, 407-422 (2020).

55. Dik, B., Sonmez, G., Faki, H.E. & Bahcivan, E. Sulfasalazine treatment can cause a positive effect on LPS-induced endotoxic rats. *Experimental Animals* **67**, 403-412 (2018).

56. Gubatan, J.*, et al.* Anti-Integrins for the Treatment of Inflammatory Bowel Disease: Current Evidence and Perspectives. *Clin Exp Gastroenterol* **14**, 333-342 (2021).

57. Verstockt, B.*, et al.* IL-12 and IL-23 pathway inhibition in inflammatory bowel disease. *Nature Reviews Gastroenterology & Hepatology* **20**, 433-446 (2023).

58. Honap, S.*, et al.* Anogenital Crohn's Disease and Granulomatosis: A Systematic Review of Epidemiology, Clinical Manifestations, and Treatment. *J Crohns Colitis* **16**, 822-834 (2022).

59. Samuel, C., Cornman, H., Kambala, A. & Kwatra, S.G. A Review on the Safety of Using JAK Inhibitors in Dermatology: Clinical and Laboratory Monitoring. *Dermatol Ther (Heidelb)* **13**, 729-749 (2023).

60. Dal Buono, A.*, et al.* Sphingosine 1-Phosphate Modulation in Inflammatory Bowel Diseases: Keeping Lymphocytes Out of the Intestine. *Biomedicines* **10**(2022).

61. Naganuma, M.*, et al.* Efficacy of apheresis as maintenance therapy for patients with ulcerative colitis in an open-label prospective multicenter randomised controlled trial. *J Gastroenterol* **55**, 390-400 (2020).

62. Lai, Y.M.*, et al.* Adsorptive Granulocyte and Monocyte Apheresis in the Treatment of Ulcerative Colitis: The First Multicenter Study in China. *Gut Liver* **11**, 216-225 (2017).

63. Motoya, S.*, et al.* Safety and effectiveness of granulocyte and monocyte adsorptive apheresis in patients with inflammatory bowel disease in special situations: a multicentre cohort study. *BMC Gastroenterol* **19**, 196 (2019).

64. Uchino, M.*, et al.* Efficacy of Preoperative Oral Antibiotic Prophylaxis for the Prevention of Surgical Site Infections in Patients With Crohn Disease: A Randomized Controlled Trial. *Ann Surg* **269**, 420-426 (2019).

65. Gomollon, F. Surgery in ileocaecal Crohn's disease: one more option, sometimes the best? *Lancet Gastroenterol Hepatol* **2**, 768-769 (2017).

66. Townsend, C.M.*, et al.* Antibiotics for induction and maintenance of remission in Crohn's disease. *Cochrane Database Syst Rev* **2**, CD012730 (2019).

67. Nguyen, L.H.*, et al.* Antibiotic use and the development of inflammatory bowel disease: a national case-control study in Sweden. *Lancet Gastroenterol Hepatol* **5**, 986-995 (2020).

68. Balram, B.*, et al.* Risk Factors Associated with Clostridium difficile Infection in Inflammatory Bowel Disease: A Systematic Review and Meta-Analysis. *J Crohns Colitis* **13**, 27-38 (2019).

69. Yan, F.*, et al.* Colon-specific delivery of a probiotic-derived soluble protein ameliorates intestinal inflammation in mice through an EGFR-dependent mechanism. *J Clin Invest* **121**, 2242-2253 (2011).

70. Mardini, H.E. & Grigorian, A. Probiotics in inflammatory bowel disease: is it fair to lump them into a one size that fits all? *Inflamm Bowel Dis* **20**, e14 (2014).

71. Derwa, Y., Gracie, D.J., Hamlin, P.J. & Ford, A.C. Systematic review with meta-analysis: the efficacy of probiotics in inflammatory bowel disease. *Aliment Pharmacol Ther* **46**, 389-400 (2017).

72. Quraishi, M.N.*, et al.* Systematic review with meta-analysis: the efficacy of faecal microbiota transplantation for the treatment of recurrent and refractory Clostridium difficile infection. *Aliment Pharmacol Ther* **46**, 479-493 (2017).

73. Haifer, C., Leong, R.W. & Paramsothy, S. The role of faecal microbiota transplantation in the treatment of inflammatory bowel disease. *Curr Opin Pharmacol* **55**, 8-16 (2020).

74. Moayyedi, P.*, et al.* Fecal Microbiota Transplantation Induces Remission in Patients With Active Ulcerative Colitis in a Randomized Controlled Trial. *Gastroenterology* **149**, 102-109 e106 (2015).

75. Paramsothy, S.*, et al.* Faecal Microbiota Transplantation for Inflammatory Bowel Disease: A Systematic Review and Meta-analysis. *J Crohns Colitis* **11**, 1180-1199 (2017).

76. Fabrega, A. & Vila, J. Salmonella enterica serovar Typhimurium skills to succeed in the host: virulence and regulation. *Clin Microbiol Rev* **26**, 308-341 (2013).

77. Guo, S.*, et al.* Escherichia coli Nissle 1917 Protects Intestinal Barrier Function by Inhibiting NF-κB-Mediated Activation of the MLCK-P-MLC Signaling Pathway. *Mediators Inflamm* **2019**, 5796491 (2019).

78. Charbonneau, M.R., Isabella, V.M., Li, N. & Kurtz, C.B. Developing a new class of engineered live bacterial therapeutics to treat human diseases. *Nat Commun* **11**, 1738 (2020).

79. Lengfelder, I.*, et al.* Complex Bacterial Consortia Reprogram the Colitogenic Activity of Enterococcus faecalis in a Gnotobiotic Mouse Model of Chronic, Immune-Mediated Colitis. *Front Immunol* **10**, 1420 (2019).

80. Fedorak, R.N.*, et al.* Recombinant human interleukin 10 in the treatment of patients with mild to moderately active Crohn's disease. The Interleukin 10 Inflammatory Bowel Disease Cooperative Study Group. *Gastroenterology* **119**, 1473-1482 (2000).

81. Schreiber, S.*, et al.* Safety and efficacy of recombinant human interleukin 10 in chronic active Crohn's disease. Crohn's Disease IL-10 Cooperative Study Group. *Gastroenterology* **119**, 1461-1472 (2000).

82. Waeytens, A.*, et al.* Paracellular entry of interleukin-10 producing Lactococcus lactis in inflamed intestinal mucosa in mice. *Inflammatory Bowel Diseases* **14**, 471-479 (2008).

83. Steidler, L.*, et al.* Treatment of murine colitis by Lactococcus lactis secreting interleukin-10. *Science* **289**, 1352-1355 (2000).

84. Martín, R.*, et al.* Effects in the use of a genetically engineered strain of Lactococcus lactis delivering in situ IL-10 as a therapy to treat low-grade colon inflammation. *Hum Vaccin Immunother* **10**, 1611-1621 (2014).

85. Shen, H.*, et al.* Engineered microbial systems for advanced drug delivery. *Advanced Drug Delivery Reviews* **187**, 114364 (2022).

86. Borrero, J., Chen, Y., Dunny, G.M. & Kaznessis, Y.N. Modified lactic acid bacteria detect and inhibit multiresistant enterococci. *ACS Synth Biol* **4**, 299-306 (2015).

87. Keller, D.S., Windsor, A., Cohen, R. & Chand, M. Colorectal cancer in inflammatory bowel disease: review of the evidence. *Tech Coloproctol* **23**, 3-13 (2019).

88. Shah, S.C. & Itzkowitz, S.H. Colorectal Cancer in Inflammatory Bowel Disease: Mechanisms and Management. *Gastroenterology* **162**, 715-730 e713 (2022).

89. Frick, A.*, et al.* Overt Increase of Oxidative Stress and DNA Damage in Murine and Human Colitis and Colitis-Associated Neoplasia. *Mol Cancer Res* **16**, 634-642 (2018).

90. Itzkowitz, S.H. & Yio, X. Inflammation and cancer IV. Colorectal cancer in inflammatory bowel disease: the role of inflammation. *Am J Physiol Gastrointest Liver Physiol* **287**, G7-17 (2004).

91. Robles, A.I.*, et al.* Whole-Exome Sequencing Analyses of Inflammatory Bowel Disease-Associated Colorectal Cancers. *Gastroenterology* **150**, 931-943 (2016).

92. Beaugerie, L. & Itzkowitz, S.H. Cancers Complicating Inflammatory Bowel Disease. *N Engl J Med* **373**, 195 (2015).

93. Papadakis, K.A. & Targan, S.R. Role of cytokines in the pathogenesis of inflammatory bowel disease. *Annu Rev Med* **51**, 289-298 (2000).

94. Slebioda, T.J. & Kmiec, Z. Tumour necrosis factor superfamily members in the pathogenesis of inflammatory bowel disease. *Mediators Inflamm* **2014**, 325129 (2014).

95. Matsuda, R.*, et al.* Quantitive cytokine mRNA expression profiles in the colonic mucosa of patients with steroid naive ulcerative colitis during active and quiescent disease. *Inflamm Bowel Dis* **15**, 328-334 (2009).

96. Komatsu, M.*, et al.* Tumor necrosis factor-alpha in serum of patients with inflammatory bowel disease as measured by a highly sensitive immuno-PCR. *Clin Chem* **47**, 1297-1301 (2001).

97. Ma, T.Y.*, et al.* TNF-alpha-induced increase in intestinal epithelial tight junction permeability requires NF-kappa B activation. *Am J Physiol Gastrointest Liver Physiol* **286**, G367-376 (2004).

98. Abreu, M.T. Toll-like receptor signalling in the intestinal epithelium: how bacterial recognition shapes intestinal function. *Nat Rev Immunol* **10**, 131-144 (2010).

99. Goretsky, T.*, et al.* p53 mediates TNF-induced epithelial cell apoptosis in IBD. *Am J Pathol* **181**, 1306-1315 (2012).

100. Coccia, M.*, et al.* IL-1beta mediates chronic intestinal inflammation by promoting the accumulation of IL-17A secreting innate lymphoid cells and CD4(+) Th17 cells. *J Exp Med* **209**, 1595-1609 (2012).

101. Pearl, D.S.*, et al.* Cytokine mucosal expression in ulcerative colitis, the relationship between cytokine release and disease activity. *J Crohns Colitis* **7**, 481-489 (2013).

102. Bank, S.*, et al.* Polymorphisms in the Toll-Like Receptor and the IL-23/IL-17 Pathways Were Associated with Susceptibility to Inflammatory Bowel Disease in a Danish Cohort. *PLoS One* **10**, e0145302 (2015).

103. Ke, J.*, et al.* Role of NF-kappaB in TNF-alpha-induced COX-2 expression in synovial fibroblasts from human TMJ. *J Dent Res* **86**, 363-367 (2007).

104. McDaniel, D.K., Eden, K., Ringel, V.M. & Allen, I.C. Emerging Roles for Noncanonical NF-kappaB Signaling in the Modulation of Inflammatory Bowel Disease Pathobiology. *Inflamm Bowel Dis* **22**, 2265-2279 (2016).

105. Lu, Y., Li, X., Liu, S., Zhang, Y. & Zhang, D. Toll-like Receptors and Inflammatory Bowel Disease. *Front Immunol* **9**, 72 (2018).

106. Larsson, E.*, et al.* Analysis of gut microbial regulation of host gene expression along the length of the gut and regulation of gut microbial ecology through MyD88. *Gut* **61**, 1124-1131 (2012).

107. Rakoff-Nahoum, S., Paglino, J., Eslami-Varzaneh, F., Edberg, S. & Medzhitov, R. Recognition of commensal microflora by toll-like receptors is required for intestinal homeostasis. *Cell* **118**, 229-241 (2004).

108. Chow, J.C., Young, D.W., Golenbock, D.T., Christ, W.J. & Gusovsky, F. Toll-like receptor-4 mediates lipopolysaccharide-induced signal transduction. *J Biol Chem* **274**, 10689-10692 (1999).

109. Price, A.E.*, et al.* A Map of Toll-like Receptor Expression in the Intestinal Epithelium Reveals Distinct Spatial, Cell Type-Specific, and Temporal Patterns. *Immunity* **49**, 560-575 e566 (2018).

110. Vamadevan, A.S.*, et al.* Regulation of Toll-like receptor 4-associated MD-2 in intestinal epithelial cells: a comprehensive analysis. *Innate Immun* **16**, 93-103 (2010).

111. Abreu, M.T.*, et al.* TLR4 and MD-2 expression is regulated by immune-mediated signals in human intestinal epithelial cells. *J Biol Chem* **277**, 20431-20437 (2002).

112. Cario, E. & Podolsky, D.K. Differential alteration in intestinal epithelial cell expression of toll-like receptor 3 (TLR3) and TLR4 in inflammatory bowel disease. *Infect Immun* **68**, 7010-7017 (2000).

113. Guo, S.*, et al.* Lipopolysaccharide Regulation of Intestinal Tight Junction Permeability Is Mediated by TLR4 Signal Transduction Pathway Activation of FAK and MyD88. *J Immunol* **195**, 4999-5010 (2015).

114. Gewirtz, A.T.*, et al.* Salmonella typhimurium translocates flagellin across intestinal epithelia, inducing a proinflammatory response. *J Clin Invest* **107**, 99-109 (2001).

115. Rhee, S.H.*, et al.* Pathophysiological role of Toll-like receptor 5 engagement by bacterial flagellin in colonic inflammation. *Proc Natl Acad Sci U S A* **102**, 13610-13615 (2005).

116. Rodemann, J.F., Dubberke, E.R., Reske, K.A., Seo, D.H. & Stone, C.D. Incidence of Clostridium difficile infection in inflammatory bowel disease. *Clin Gastroenterol Hepatol* **5**, 339-344 (2007).

117. Navaneethan, U., Venkatesh, P.G. & Shen, B. Clostridium difficile infection and inflammatory bowel disease: understanding the evolving relationship. *World J Gastroenterol* **16**, 4892-4904 (2010).

118. Monaghan, T.M., Cockayne, A. & Mahida, Y.R. Pathogenesis of Clostridium difficile Infection and Its Potential Role in Inflammatory Bowel Disease. *Inflamm Bowel Dis* **21**, 1957-1966 (2015).

119. Bossuyt, P., Verhaegen, J., Van Assche, G., Rutgeerts, P. & Vermeire, S. Increasing incidence of Clostridium difficile-associated diarrhea in inflammatory bowel disease. *J Crohns Colitis* **3**, 4-7 (2009).

120. Ananthakrishnan, A.N., McGinley, E.L. & Binion, D.G. Excess hospitalisation burden associated with Clostridium difficile in patients with inflammatory bowel disease. *Gut* **57**, 205-210 (2008).

121. Gillespie, W.*, et al.* Clostridium difficile in Inflammatory Bowel Disease: A Retrospective Study. *Gastroenterol Res Pract* **2017**, 4803262 (2017).

122. Rahman, M.M. & McFadden, G. Modulation of tumor necrosis factor by microbial pathogens. *PLoS Pathog* **2**, e4 (2006).

123. Ferraretto, A.*, et al.* New methodological approach to induce a differentiation phenotype in Caco-2 cells prior to post-confluence stage. *Anticancer Res* **27**, 3919-3925 (2007).

124. Liévin-Le Moal, V. & Servin, A.L. Pathogenesis of human enterovirulent bacteria: lessons from cultured, fully differentiated human colon cancer cell lines. *Microbiol Mol Biol Rev* **77**, 380-439 (2013).

125. Mahler, M.*, et al.* Differential susceptibility of inbred mouse strains to dextran sulfate sodium-induced colitis. *Am J Physiol* **274**, G544-551 (1998).

126. Stanford, A.H.*, et al.* A direct comparison of mouse and human intestinal development using epithelial gene expression patterns. *Pediatr Res* **88**, 66-76 (2020).

127. Sato, T.*, et al.* Single Lgr5 stem cells build crypt-villus structures in vitro without a mesenchymal niche. *Nature* **459**, 262-265 (2009).

128. Zachos, N.C.*, et al.* Human Enteroids/Colonoids and Intestinal Organoids Functionally Recapitulate Normal Intestinal Physiology and Pathophysiology. *J Biol Chem* **291**, 3759-3766 (2016).

129. Santos, A.J.M., Lo, Y.H., Mah, A.T. & Kuo, C.J. The Intestinal Stem Cell Niche: Homeostasis and Adaptations. *Trends Cell Biol* **28**, 1062-1078 (2018).

130. Beumer, J.*, et al.* BMP gradient along the intestinal villus axis controls zonated enterocyte and goblet cell states. *Cell Rep* **38**, 110438 (2022).

131. He, X.C.*, et al.* BMP signaling inhibits intestinal stem cell self-renewal through suppression of Wnt-beta-catenin signaling. *Nat Genet* **36**, 1117-1121 (2004).

132. Reynolds, A.*, et al.* Canonical Wnt signals combined with suppressed TGFbeta/BMP pathways promote renewal of the native human colonic epithelium. *Gut* **63**, 610-621 (2014).

133. Spence, J.R.*, et al.* Directed differentiation of human pluripotent stem cells into intestinal tissue in vitro. *Nature* **470**, 105-109 (2011).

134. Michels, B.E.*, et al.* Pooled In Vitro and In Vivo CRISPR-Cas9 Screening Identifies Tumor Suppressors in Human Colon Organoids. *Cell Stem Cell* **26**, 782-792.e787 (2020).

135. Wan, C.*, et al.* Genome-scale CRISPR-Cas9 screen of Wnt/β-catenin signaling identifies therapeutic targets for colorectal cancer. *Sci Adv* **7**(2021).

136. Watanabe, S.*, et al.* Transplantation of intestinal organoids into a mouse model of colitis. *Nature Protocols* **17**, 649-671 (2022).

137. Moon, C., VanDussen, K.L., Miyoshi, H. & Stappenbeck, T.S. Development of a primary mouse intestinal epithelial cell monolayer culture system to evaluate factors that modulate IgA transcytosis. *Mucosal Immunol* **7**, 818-828 (2014).

138. Nozaki, K.*, et al.* Co-culture with intestinal epithelial organoids allows efficient expansion and motility analysis of intraepithelial lymphocytes. *J Gastroenterol* **51**, 206-213 (2016).

139. Beaurivage, C.*, et al.* Development of a human primary gut-on-a-chip to model inflammatory processes. *Sci Rep* **10**, 21475 (2020).

140. Liu, W. & Rodgers, G.P. Olfactomedin 4 expression and functions in innate immunity, inflammation, and cancer. *Cancer Metastasis Rev* **35**, 201-212 (2016).

141. Xu, H.*, et al.* Organoid technology in disease modelling, drug development, personalized treatment and regeneration medicine. *Exp Hematol Oncol* **7**, 30 (2018).

142. Munera, J.O. & Wells, J.M. Generation of Gastrointestinal Organoids from Human Pluripotent Stem Cells. *Methods Mol Biol* **1597**, 167-177 (2017).

143. Jee, J.*, et al.* Functional recovery by colon organoid transplantation in a mouse model of radiation proctitis. *Biomaterials* **275**, 120925 (2021).

144. Fatehullah, A., Tan, S.H. & Barker, N. Organoids as an in vitro model of human development and disease. *Nat Cell Biol* **18**, 246-254 (2016).

145. Puschhof, J.*, et al.* Intestinal organoid cocultures with microbes. *Nat Protoc* **16**, 4633-4649 (2021).

146. Almeqdadi, M., Mana, M.D., Roper, J. & Yilmaz, O.H. Gut organoids: mini-tissues in culture to study intestinal physiology and disease. *Am J Physiol Cell Physiol* **317**, C405-C419 (2019).

147. Langlands, A.J., Carroll, T.D., Chen, Y. & Nathke, I. Chir99021 and Valproic acid reduce the proliferative advantage of Apc mutant cells. *Cell Death Dis* **9**, 255 (2018).

148. Liu, Y.*, et al.* Technical standards of a foldable capsular vitreous body in terms of mechanical, optical, and biocompatible properties. *Artif Organs* **34**, 836-845 (2010).

149. O'Donnell, S. & O'Morain, C.A. Therapeutic benefits of budesonide in gastroenterology. *Ther Adv Chronic Dis* **1**, 177-186 (2010).

150. van der Flier, L.G., Haegebarth, A., Stange, D.E., van de Wetering, M. & Clevers, H. OLFM4 is a robust marker for stem cells in human intestine and marks a subset of colorectal cancer cells. *Gastroenterology* **137**, 15-17 (2009).

151. Neyazi, M.*, et al.* Overexpression of Cancer-Associated Stem Cell Gene OLFM4 in the Colonic Epithelium of Patients With Primary Sclerosing Cholangitis. *Inflamm Bowel Dis* **27**, 1316-1327 (2021).

152. Crawford, S.E., Ramani, S., Blutt, S.E. & Estes, M.K. Organoids to Dissect Gastrointestinal Virus-Host Interactions: What Have We Learned? *Viruses* **13**(2021).

153. Khare, V.*, et al.* Mesalamine and azathioprine modulate junctional complexes and restore epithelial barrier function in intestinal inflammation. *Scientific Reports* **9**, 2842 (2019).

154. Kalina, U.*, et al.* Enhanced production of IL-18 in butyrate-treated intestinal epithelium by stimulation of the proximal promoter region. *Eur J Immunol* **32**, 2635-2643 (2002).

155. Pages, F.*, et al.* Modulation of interleukin-18 expression in human colon carcinoma: consequences for tumor immune surveillance. *Int J Cancer* **84**, 326-330 (1999).

156. Zhou, Z., Cao, J., Liu, X. & Li, M. Evidence for the butyrate metabolism as key pathway improving ulcerative colitis in both pediatric and adult patients. *Bioengineered* **12**, 8309-8324 (2021).

157. Wu, X.*, et al.* Effects of the intestinal microbial metabolite butyrate on the development of colorectal cancer. *J Cancer* **9**, 2510-2517 (2018).

158. Facchin, S.*, et al.* Microbiota changes induced by microencapsulated sodium butyrate in patients with inflammatory bowel disease. *Neurogastroenterol Motil* **32**, e13914 (2020).

159. Levin, A.D., Wildenberg, M.E. & van den Brink, G.R. Mechanism of Action of Anti-TNF Therapy in Inflammatory Bowel Disease. *J Crohns Colitis* **10**, 989-997 (2016).

160. Braegger, C.P., Nicholls, S., Murch, S.H., Stephens, S. & MacDonald, T.T. Tumour necrosis factor alpha in stool as a marker of intestinal inflammation. *Lancet* **339**, 89-91 (1992).

161. Breese, E.J.*, et al.* Tumor necrosis factor alpha-producing cells in the intestinal mucosa of children with inflammatory bowel disease. *Gastroenterology* **106**, 1455-1466 (1994).

162. Murch, S.H., Lamkin, V.A., Savage, M.O., Walker-Smith, J.A. & MacDonald, T.T. Serum concentrations of tumour necrosis factor alpha in childhood chronic inflammatory bowel disease. *Gut* **32**, 913-917 (1991).

163. Derkx, B.*, et al.* Tumour-necrosis-factor antibody treatment in Crohn's disease. *Lancet* **342**, 173-174 (1993).

164. Bamias, G.*, et al.* Intestinal-specific TNFalpha overexpression induces Crohn's-like ileitis in mice. *PLoS One* **8**, e72594 (2013).

165. Papamichael, K., Vande Casteele, N., Ferrante, M., Gils, A. & Cheifetz, A.S. Therapeutic Drug Monitoring During Induction of Anti-Tumor Necrosis Factor Therapy in Inflammatory Bowel Disease: Defining a Therapeutic Drug Window. *Inflamm Bowel Dis* **23**, 1510-1515 (2017).

166. Guarner, F. & Malagelada, J.R. Gut flora in health and disease. *Lancet* **361**, 512-519 (2003).

167. Ghosh, S.S., Wang, J., Yannie, P.J. & Ghosh, S. Intestinal Barrier Dysfunction, LPS Translocation, and Disease Development. *J Endocr Soc* **4**, bvz039 (2020).

168. van der Bruggen, T., Nijenhuis, S., van Raaij, E., Verhoef, J. & van Asbeck, B.S. Lipopolysaccharide-induced tumor necrosis factor alpha production by human monocytes involves the raf-1/MEK1-MEK2/ERK1-ERK2 pathway. *Infect Immun* **67**, 3824-3829 (1999).

169. Alvarado, J., Taylor, P., Castillo, J.R. & Thomas, L.E. Interferon gamma bound to extracellular matrix changes the hyporesponsiveness to LPS in crypt but not villous intestinal epithelial cells. *Immunol Lett* **99**, 109-112 (2005).

170. Yang, J. & Yan, H. TLR5: beyond the recognition of flagellin. *Cell Mol Immunol* **14**, 1017-1019 (2017).

171. Akira, S., Uematsu, S. & Takeuchi, O. Pathogen recognition and innate immunity. *Cell* **124**, 783-801 (2006).

172. Pekkala, S.*, et al.* Toll-like receptor 5 in obesity: the role of gut microbiota and adipose tissue inflammation. *Obesity (Silver Spring)* **23**, 581-590 (2015).

173. Anas, A.A.*, et al.* Lung epithelial MyD88 drives early pulmonary clearance of Pseudomonas aeruginosa by a flagellin dependent mechanism. *Am J Physiol Lung Cell Mol Physiol* **311**, L219-228 (2016).

174. Descamps, D.*, et al.* Toll-like receptor 5 (TLR5), IL-1beta secretion, and asparagine endopeptidase are critical factors for alveolar macrophage phagocytosis and bacterial killing. *Proc Natl Acad Sci U S A* **109**, 1619-1624 (2012).

175. Issa, M., Ananthakrishnan, A.N. & Binion, D.G. Clostridium difficile and inflammatory bowel disease. *Inflamm Bowel Dis* **14**, 1432-1442 (2008).

176. Nguyen, T.L., Vieira-Silva, S., Liston, A. & Raes, J. How informative is the mouse for human gut microbiota research? *Dis Model Mech* **8**, 1-16 (2015).

177. Ehrhardt, K.*, et al.* Persistent Salmonella enterica Serovar Typhimurium Infection Induces Protease Expression During Intestinal Fibrosis. *Inflamm Bowel Dis* **25**, 1629-1643 (2019).

178. Li, C.*, et al.* Effects of different doses lipopolysaccharides on the mucosal barrier in mouse intestine. *Res Vet Sci* **133**, 75-84 (2020).

179. Castillo-Azofeifa, D.*, et al.* Atoh1(+) secretory progenitors possess renewal capacity independent of Lgr5(+) cells during colonic regeneration. *EMBO J* **38**(2019).

180. Harnack, C.*, et al.* R-spondin 3 promotes stem cell recovery and epithelial regeneration in the colon. *Nat Commun* **10**, 4368 (2019).

181. Lu, Y.C., Yeh, W.C. & Ohashi, P.S. LPS/TLR4 signal transduction pathway. *Cytokine* **42**, 145-151 (2008).

182. Grasa, Gonzalo, Martino & Murillo. The lipopolysaccharide from Escherichia coli O127: B8 induces inflammation and motility disturbances in rabbit ileum. *World Rabbit Science*, 185-191 (2017).

183. Markowitz, G.J.*, et al.* Inflammation-Dependent IL18 Signaling Restricts Hepatocellular Carcinoma Growth by Enhancing the Accumulation and Activity of Tumor-Infiltrating Lymphocytes. *Cancer Res* **76**, 2394-2405 (2016).

184. Kobayashi, S.*, et al.* Collagen type I-mediated mechanotransduction controls epithelial cell fate conversion during intestinal inflammation. *Inflamm Regen* **42**, 49 (2022).

185. Wu, D.D.*, et al.* Targeted epigenetic silencing of UCHL1 expression suppresses collagen-1 production in human lung epithelial cells. *Epigenetics* **18**, 2175522 (2023).

186. Hajam, I.A., Dar, P.A., Shahnawaz, I., Jaume, J.C. & Lee, J.H. Bacterial flagellin-a potent immunomodulatory agent. *Exp Mol Med* **49**, e373 (2017).

187. Gao, N., Kumar, A., Jyot, J. & Yu, F.S. Flagellin-induced corneal antimicrobial peptide production and wound repair involve a novel NF-kappaB-independent and EGFR-dependent pathway. *PLoS One* **5**, e9351 (2010).

188. Kinnebrew, M.A.*, et al.* Interleukin 23 production by intestinal CD103(+)CD11b(+) dendritic cells in response to bacterial flagellin enhances mucosal innate immune defense. *Immunity* **36**, 276-287 (2012).

189. Gordon, I.O., Agrawal, N., Goldblum, J.R., Fiocchi, C. & Rieder, F. Fibrosis in ulcerative colitis: mechanisms, features, and consequences of a neglected problem. *Inflamm Bowel Dis* **20**, 2198-2206 (2014).

190. Seicean, A., Moldovan-Pop, A. & Seicean, R. Ulcerative colitis worsened after Clostridium difficile infection: efficacy of infliximab. *World J Gastroenterol* **20**, 5135-5140 (2014).

191. Voth, D.E. & Ballard, J.D. Clostridium difficile toxins: mechanism of action and role in disease. *Clin Microbiol Rev* **18**, 247-263 (2005).

192. Ben-Horin, S., Kopylov, U. & Chowers, Y. Optimizing anti-TNF treatments in inflammatory bowel disease. *Autoimmun Rev* **13**, 24-30 (2014).

193. Kushnaryov, V.M.*, et al.* Cytotoxicity of Clostridium difficile toxin A for human colonic and pancreatic carcinoma cell lines. *Cancer Res* **52**, 5096-5099 (1992).

194. Mahida, Y.R.*, et al.* Effect of Clostridium difficile toxin A on human colonic lamina propria cells: early loss of macrophages followed by T-cell apoptosis. *Infect Immun* **66**, 5462-5469 (1998).

195. Ghorbaninejad, M.*, et al.* Contribution of NOTCH signaling pathway along with TNF-alpha in the intestinal inflammation of ulcerative colitis. *Gastroenterol Hepatol Bed Bench* **12**, S80-S86 (2019).

196. Roulis, M., Armaka, M., Manoloukos, M., Apostolaki, M. & Kollias, G. Intestinal epithelial cells as producers but not targets of chronic TNF suffice to cause murine Crohn-like pathology. *Proc Natl Acad Sci U S A* **108**, 5396-5401 (2011).

197. Jijon, H.B., Buret, A., Hirota, C.L., Hollenberg, M.D. & Beck, P.L. The EGF receptor and HER2 participate in TNF-alpha-dependent MAPK activation and IL-8 secretion in intestinal epithelial cells. *Mediators Inflamm* **2012**, 207398 (2012).

198. Duvallet, E., Semerano, L., Assier, E., Falgarone, G. & Boissier, M.C. Interleukin-23: a key cytokine in inflammatory diseases. *Ann Med* **43**, 503-511 (2011).

199. Schmidt, C.*, et al.* Expression of interleukin-12-related cytokine transcripts in inflammatory bowel disease: elevated interleukin-23p19 and interleukin-27p28 in Crohn's disease but not in ulcerative colitis. *Inflamm Bowel Dis* **11**, 16-23 (2005).

200. Lee, C.*, et al.* TNFalpha Induces LGR5+ Stem Cell Dysfunction In Patients With Crohn's Disease. *Cell Mol Gastroenterol Hepatol* **13**, 789-808 (2022).

201. Benoit, R.*, et al.* Pure endotoxin does not pass across the intestinal epithelium in vitro. *Shock* **10**, 43-48 (1998).

202. Sakai, J.*, et al.* Lipopolysaccharide-induced NF-kappaB nuclear translocation is primarily dependent on MyD88, but TNFalpha expression requires TRIF and MyD88. *Sci Rep* **7**, 1428 (2017).

203. Datta De, D., Datta, A., Bhattacharjya, S. & Roychoudhury, S. NF-kappaB mediated transcriptional repression of acid modifying hormone gastrin. *PLoS One* **8**, e73409 (2013).

204. Kordus, S.L., Thomas, A.K. & Lacy, D.B. Clostridioides difficile toxins: mechanisms of action and antitoxin therapeutics. *Nat Rev Microbiol* **20**, 285-298 (2022).

205. Lyerly, D.M., Saum, K.E., MacDonald, D.K. & Wilkins, T.D. Effects of Clostridium difficile toxins given intragastrically to animals. *Infect Immun* **47**, 349-352 (1985).

206. Papadakis, K.A. & Targan, S.R. Tumor necrosis factor: biology and therapeutic inhibitors. *Gastroenterology* **119**, 1148-1157 (2000).

207. Hayden, M.S. & Ghosh, S. Regulation of NF-kappaB by TNF family cytokines. *Semin Immunol* **26**, 253-266 (2014).

208. Sabio, G. & Davis, R.J. TNF and MAP kinase signalling pathways. *Semin Immunol* **26**, 237-245 (2014).

209. Sands, B.E. & Kaplan, G.G. The role of TNFalpha in ulcerative colitis. *J Clin Pharmacol* **47**, 930-941 (2007).

210. The Gene Ontology Resource: 20 years and still GOing strong. *Nucleic Acids Res* **47**, D330-d338 (2019).

211. Prieto-Pérez, R., Almoguera, B., Cabaleiro, T., Hakonarson, H. & Abad-Santos, F. Association between Genetic Polymorphisms and Response to Anti-TNFs in Patients with Inflammatory Bowel Disease. *Int J Mol Sci* **17**, 225 (2016).

212. Neurath, M.F. Cytokines in inflammatory bowel disease. *Nat Rev Immunol* **14**, 329-342 (2014).

213. Wang, D. & Dubois, R.N. The role of COX-2 in intestinal inflammation and colorectal cancer. *Oncogene* **29**, 781-788 (2010).

214. Pizarro, T.T., Arseneau, K.O., Bamias, G. & Cominelli, F. Mouse models for the study of Crohn's disease. *Trends Mol Med* **9**, 218-222 (2003).

215. Langrish, C.L.*, et al.* IL-23 drives a pathogenic T cell population that induces autoimmune inflammation. *J Exp Med* **201**, 233-240 (2005).

216. Mitsuyama, K. & Sata, M. Gut microflora: a new target for therapeutic approaches in inflammatory bowel disease. *Expert Opin Ther Targets* **12**, 301-312 (2008).

217. Wang, Y.H.*, et al.* [TNFalpha induced IL-8 production through p38 MAPK- NF-kB pathway in human hepatocellular carcinoma cells]. *Zhonghua Gan Zang Bing Za Zhi* **19**, 912-916 (2011).

218. Kazama, S.*, et al.* Immunohistochemical Expression of CD133 and LGR5 in Ulcerative Colitis-associated Colorectal Cancer and Dysplasia. *In Vivo* **33**, 1279-1284 (2019).

219. Boltin, D., Perets, T.T., Vilkin, A. & Niv, Y. Mucin function in inflammatory bowel disease: an update. *J Clin Gastroenterol* **47**, 106-111 (2013).

220. Shan, M.*, et al.* Mucus enhances gut homeostasis and oral tolerance by delivering immunoregulatory signals. *Science* **342**, 447-453 (2013).

221. Guo, X.Y., Liu, X.J. & Hao, J.Y. Gut microbiota in ulcerative colitis: insights on pathogenesis and treatment. *J Dig Dis* **21**, 147-159 (2020).

222. Caradonna, L.*, et al.* Enteric bacteria, lipopolysaccharides and related cytokines in inflammatory bowel disease: biological and clinical significance. *J Endotoxin Res* **6**, 205-214 (2000).

223. Stephens, M. & von der Weid, P.Y. Lipopolysaccharides modulate intestinal epithelial permeability and inflammation in a species-specific manner. *Gut Microbes* **11**, 421-432 (2020).

224. Corcoran, R.M.*, et al.* Association Between Ex Vivo Human Ulcerative Colitis Explant Protein Secretion Profiles and Disease Behaviour. *Dig Dis Sci* **67**, 5540-5550 (2022).

225. Katinios, G.*, et al.* Increased Colonic Epithelial Permeability and Mucosal Eosinophilia in Ulcerative Colitis in Remission Compared With Irritable Bowel Syndrome and Health. *Inflamm Bowel Dis* **26**, 974-984 (2020).

226. Lee, Y.P.*, et al.* Toll-like receptor 4 prevents AOM/DSS-induced colitis-associated colorectal cancer in Bacteroides fragilis gnotobiotic mice. *Hum Exp Toxicol* **40**, 622-633 (2021).

227. Palamides, P.*, et al.* A mouse model for ulcerative colitis based on NOD-scid IL2R gammanull mice reconstituted with peripheral blood mononuclear cells from affected individuals. *Dis Model Mech* **9**, 985-997 (2016).

228. Radulovic, K.*, et al.* The early activation marker CD69 regulates the expression of chemokines and CD4 T cell accumulation in intestine. *PLoS One* **8**, e65413 (2013).

229. Zhang, H.*, et al.* Therapeutic effects of triptolide via the inhibition of IL-1beta expression in a mouse model of ulcerative colitis. *Exp Ther Med* **12**, 1279-1286 (2016).

230. Wiercinska-Drapalo, A., Flisiak, R., Jaroszewicz, J. & Prokopowicz, D. Plasma interleukin-18 reflects severity of ulcerative colitis. *World J Gastroenterol* **11**, 605-608 (2005).

231. Wang, Y.*, et al.* A novel role for villin in intestinal epithelial cell survival and homeostasis. *J Biol Chem* **283**, 9454-9464 (2008).

232. Coskun, M.*, et al.* TNF-alpha-induced down-regulation of CDX2 suppresses MEP1A expression in colitis. *Biochim Biophys Acta* **1822**, 843-851 (2012).

233. Mohammadi, M., Hayatbakhsh, M.M., Zahedi, M.J., Jalalpour, M.R. & Pakgohar, A. Serum interleukin-23 levels in patients with ulcerative colitis. *Iran J Immunol* **8**, 183-188 (2011).

234. Hoesel, B. & Schmid, J.A. The complexity of NF-kappaB signaling in inflammation and cancer. *Mol Cancer* **12**, 86 (2013).

235. Smolinska, M.J., Page, T.H., Urbaniak, A.M., Mutch, B.E. & Horwood, N.J. Hck tyrosine kinase regulates TLR4-induced TNF and IL-6 production via AP-1. *J Immunol* **187**, 6043-6051 (2011).

236. Ko, H.M.*, et al.* The Role of TLR4 and Fyn Interaction on Lipopolysaccharide-Stimulated PAI-1 Expression in Astrocytes. *Mol Neurobiol* **52**, 8-25 (2015).

237. Stark, R.J.*, et al.* Endothelial nitric oxide synthase modulates Toll-like receptor 4-mediated IL-6 production and permeability via nitric oxide-independent signaling. *FASEB J* **32**, 945-956 (2018).

238. Daiber, A.*, et al.* New Therapeutic Implications of Endothelial Nitric Oxide Synthase (eNOS) Function/Dysfunction in Cardiovascular Disease. *Int J Mol Sci* **20**(2019).

239. Takahashi, S., Kapas, L., Fang, J. & Krueger, J.M. Somnogenic relationships between tumor necrosis factor and interleukin-1. *Am J Physiol* **276**, R1132-1140 (1999).

240. Fiedler, K., Kokai, E., Bresch, S. & Brunner, C. MyD88 is involved in myeloid as well as lymphoid hematopoiesis independent of the presence of a pathogen. *Am J Blood Res* **3**, 124-140 (2013).

241. Ikeda, H.*, et al.* Interaction of Toll-like receptors with bacterial components induces expression of CDX2 and MUC2 in rat biliary epithelium in vivo and in culture. *Lab Invest* **87**, 559-571 (2007).

242. Nomura, F.*, et al.* Cutting edge: endotoxin tolerance in mouse peritoneal macrophages correlates with down-regulation of surface toll-like receptor 4 expression. *J Immunol* **164**, 3476-3479 (2000).

243. Hausmann, M.*, et al.* Toll-like receptors 2 and 4 are up-regulated during intestinal inflammation. *Gastroenterology* **122**, 1987-2000 (2002).

244. Ding, X.*, et al.* TLR4 signaling induces TLR3 up-regulation in alveolar macrophages during acute lung injury. *Sci Rep* **7**, 34278 (2017).

245. Cavassani, K.A.*, et al.* TLR3 is an endogenous sensor of tissue necrosis during acute inflammatory events. *J Exp Med* **205**, 2609-2621 (2008).

246. Lu, N.*, et al.* Activation of the epidermal growth factor receptor in macrophages regulates cytokine production and experimental colitis. *J Immunol* **192**, 1013-1023 (2014).

247. Uronis, J.M.*, et al.* Modulation of the intestinal microbiota alters colitis-associated colorectal cancer susceptibility. *PLoS One* **4**, e6026 (2009).

248. Yesudhas, D., Gosu, V., Anwar, M.A. & Choi, S. Multiple roles of toll-like receptor 4 in colorectal cancer. *Front Immunol* **5**, 334 (2014).

249. Fukata, M.*, et al.* Cox-2 is regulated by Toll-like receptor-4 (TLR4) signaling: Role in proliferation and apoptosis in the intestine. *Gastroenterology* **131**, 862-877 (2006).

250. Roelofs, H.M., Te Morsche, R.H., van Heumen, B.W., Nagengast, F.M. & Peters, W.H. Over-expression of COX-2 mRNA in colorectal cancer. *BMC Gastroenterol* **14**, 1 (2014).

251. Kohno, H., Suzuki, R., Sugie, S. & Tanaka, T. Suppression of colitis-related mouse colon carcinogenesis by a COX-2 inhibitor and PPAR ligands. *BMC Cancer* **5**, 46 (2005).

252. Hardbower, D.M.*, et al.* EGFR regulates macrophage activation and function in bacterial infection. *J Clin Invest* **126**, 3296-3312 (2016).

253. Seshacharyulu, P.*, et al.* Targeting the EGFR signaling pathway in cancer therapy. *Expert Opin Ther Targets* **16**, 15-31 (2012).

254. Chattopadhyay, S.*, et al.* EGFR kinase activity is required for TLR4 signaling and the septic shock response. *EMBO Rep* **16**, 1535-1547 (2015).

255. De, S.*, et al.* Erlotinib protects against LPS-induced endotoxicity because TLR4 needs EGFR to signal. *Proc Natl Acad Sci U S A* **112**, 9680-9685 (2015).

256. Pagan, B.*, et al.* Erlotinib inhibits progression to dysplasia in a colitis-associated colon cancer model. *World J Gastroenterol* **17**, 4858-4866 (2011).

257. Piechota-Polanczyk, A. & Fichna, J. Review article: the role of oxidative stress in pathogenesis and treatment of inflammatory bowel diseases. *Naunyn Schmiedebergs Arch Pharmacol* **387**, 605-620 (2014).

258. Yasukawa, K., Tokuda, H., Tun, X., Utsumi, H. & Yamada, K. The detrimental effect of nitric oxide on tissue is associated with inflammatory events in the vascular endothelium and neutrophils in mice with dextran sodium sulfate-induced colitis. *Free Radic Res* **46**, 1427-1436 (2012).

259. Vargas-Roig, L.M., Gago, F.E., Tello, O., Aznar, J.C. & Ciocca, D.R. Heat shock protein expression and drug resistance in breast cancer patients treated with induction chemotherapy. *Int J Cancer* **79**, 468-475 (1998).

260. Ciancio, M.J. & Chang, E.B. Do heat shock proteins play any role in gut inflammation? *Inflamm Bowel Dis* **14 Suppl 2**, S102-103 (2008).

261. Ciocca, D.R. & Calderwood, S.K. Heat shock proteins in cancer: diagnostic, prognostic, predictive, and treatment implications. *Cell Stress Chaperones* **10**, 86-103 (2005).

262. Liu, L.*, et al.* Transduced protein transduction domain linked HSP27 protected LECs against UVB radiation-induced damage. *Exp Eye Res* **120**, 36-42 (2014).

263. Quintana, F.J. & Cohen, I.R. Heat shock proteins as endogenous adjuvants in sterile and septic inflammation. *J Immunol* **175**, 2777-2782 (2005).

264. Overstreet, A.M.*, et al.* The JAK inhibitor ruxolitinib reduces inflammation in an ILC3-independent model of innate immune colitis. *Mucosal Immunol* **11**, 1454-1465 (2018).

265. Funami, K., Matsumoto, M., Oshiumi, H., Inagaki, F. & Seya, T. Functional interfaces between TICAM-2/TRAM and TICAM-1/TRIF in TLR4 signaling. *Biochem Soc Trans* **45**, 929-935 (2017).

266. Fu, P.Y.*, et al.* New insight into BIRC3: A novel prognostic indicator and a potential therapeutic target for liver cancer. *J Cell Biochem* **120**, 6035-6045 (2019).

267. Liu, Y., Li, Z.H., Zhang, L. & Lu, S.B. ADAM8 promotes chondrosarcoma cell migration and invasion by activating the NF-kappaB/MMP-13 signaling axis. *Anticancer Drugs* **30**, e0790 (2019).

268. Marcos-Ramiro, B.*, et al.* RhoB controls endothelial barrier recovery by inhibiting Rac1 trafficking to the cell border. *J Cell Biol* **213**, 385-402 (2016).

269. Thion, M.S.*, et al.* Unraveling the Role of Huntingtin in Breast Cancer Metastasis. *J Natl Cancer Inst* **107**(2015).

270. Narizhneva, N.V.*, et al.* Thrombospondin-1 up-regulates expression of cell adhesion molecules and promotes monocyte binding to endothelium. *FASEB J* **19**, 1158-1160 (2005).

271. Zhang, Y., Liang, X., Bao, X., Xiao, W. & Chen, G. Toll-like receptor 4 (TLR4) inhibitors: Current research and prospective. *Eur J Med Chem* **235**, 114291 (2022).

272. Adhikari, A., Xu, M. & Chen, Z.J. Ubiquitin-mediated activation of TAK1 and IKK. *Oncogene* **26**, 3214-3226 (2007).

273. Cheng, A.*, et al.* Extractable and non-extractable polyphenols from blueberries modulate LPS-induced expression of iNOS and COX-2 in RAW264.7 macrophages via the NF-kappaB signalling pathway. *J Sci Food Agric* **96**, 3393-3400 (2016).

274. Mohyuddin, S.G.*, et al.* Effect of chitosan on blood profile, inflammatory cytokines by activating TLR4/NF-kappaB signaling pathway in intestine of heat stressed mice. *Sci Rep* **11**, 20608 (2021).

275. Gunnell, L.M.*, et al.* TAK1 regulates cartilage and joint development via the MAPK and BMP signaling pathways. *J Bone Miner Res* **25**, 1784-1797 (2010).

276. Ning, X.*, et al.* Synthesis and neuroprotective effect of E-3,4-dihydroxy styryl aralkyl ketones derivatives against oxidative stress and inflammation. *Bioorg Med Chem Lett* **23**, 3700-3703 (2013).

277. Chen, L.*, et al.* Discovery of caffeic acid phenethyl ester derivatives as novel myeloid differentiation protein 2 inhibitors for treatment of acute lung injury. *Eur J Med Chem* **143**, 361-375 (2018).

278. Lysakova-Devine, T.*, et al.* Viral inhibitory peptide of TLR4, a peptide derived from vaccinia protein A46, specifically inhibits TLR4 by directly targeting MyD88 adaptor-like and TRIF-related adaptor molecule. *J Immunol* **185**, 4261-4271 (2010).

279. Rakhesh, M., Cate, M., Vijay, R., Shrikant, A. & Shanjana, A. A TLR4-interacting peptide inhibits lipopolysaccharide-stimulated inflammatory responses, migration and invasion of colon cancer SW480 cells. *Oncoimmunology* **1**, 1495-1506 (2012).

280. Sugiyama, K., Muroi, M. & Tanamoto, K. A novel TLR4-binding peptide that inhibits LPS-induced activation of NF-kappaB and in vivo toxicity. *Eur J Pharmacol* **594**, 152-156 (2008).

281. Awasthi, S., Anbanandam, A. & Rodgers, K.K. Structure of a TLR4-interacting SPA4 peptide. *RSC Adv* **5**, 27431-27438 (2015).

282. Jones, G.R.*, et al.* Dynamics of Colon Monocyte and Macrophage Activation During Colitis. *Front Immunol* **9**, 2764 (2018).

283. Sumon, M.S.*, et al.* Growth performance, digestive enzyme activity and immune response of Macrobrachium rosenbergii fed with probiotic Clostridium butyricum incorporated diets. *Journal of King Saud University - Science* **30**, 21-28 (2018).

284. Romero-Lopez, J.P.*, et al.* Differential expression of TLR2 and TLR4 in alpha4beta7-positive leukocytes of patients with axial spondyloarthritis. *Rheumatology (Oxford)* **59**, 879-888 (2020).

285. Sato, T. & Clevers, H. Growing self-organizing mini-guts from a single intestinal stem cell: mechanism and applications. *Science* **340**, 1190-1194 (2013).

286. Sebert, M.*, et al.* Thrombin modifies growth, proliferation and apoptosis of human colon organoids: a protease-activated receptor 1- and protease-activated receptor 4-dependent mechanism. *Br J Pharmacol* **175**, 3656-3668 (2018).

287. Dotti, I.*, et al.* Alterations in the epithelial stem cell compartment could contribute to permanent changes in the mucosa of patients with ulcerative colitis. *Gut* **66**, 2069-2079 (2017).

288. Howell, K.J.*, et al.* DNA Methylation and Transcription Patterns in Intestinal Epithelial Cells From Pediatric Patients With Inflammatory Bowel Diseases Differentiate Disease Subtypes and Associate With Outcome. *Gastroenterology* **154**, 585-598 (2018).

289. Planell, N.*, et al.* Transcriptional analysis of the intestinal mucosa of patients with ulcerative colitis in remission reveals lasting epithelial cell alterations. *Gut* **62**, 967-976 (2013).

290. Obita, T., Ueda, T. & Imoto, T. Solution structure and activity of mouse lysozyme M. *Cell Mol Life Sci* **60**, 176-184 (2003).

291. Mitsuhashi, J., Mikami, T., Saigenji, K. & Okayasu, I. Significant correlation of morphological remodeling in ulcerative colitis with disease duration and between elevated p53 and p21 expression in rectal mucosa and neoplastic development. *Pathol Int* **55**, 113-121 (2005).

292. Zwiers, A.*, et al.* Increased expression of the tight junction molecule claudin-18 A1 in both experimental colitis and ulcerative colitis. *Inflamm Bowel Dis* **14**, 1652-1659 (2008).

293. Sentani, K.*, et al.* Expression of olfactomedin 4 and claudin-18 in serrated neoplasia of the colorectum: a characteristic pattern is associated with sessile serrated lesion. *Histopathology* **62**, 1018-1027 (2013).

294. Noben, M.*, et al.* Epithelial organoid cultures from patients with ulcerative colitis and Crohn's disease: a truly long-term model to study the molecular basis for inflammatory bowel disease? *Gut* **66**, 2193-2195 (2017).

295. Canto, E.*, et al.* TNF alpha production to TLR2 ligands in active IBD patients. *Clin Immunol* **119**, 156-165 (2006).

296. Tulkens, J.*, et al.* Increased levels of systemic LPS-positive bacterial extracellular vesicles in patients with intestinal barrier dysfunction. *Gut* **69**, 191-193 (2020).

297. Stecher, B.*, et al.* Salmonella enterica serovar typhimurium exploits inflammation to compete with the intestinal microbiota. *PLoS Biol* **5**, 2177-2189 (2007).

298. Jessen, D.L.*, et al.* Type III secretion needle proteins induce cell signaling and cytokine secretion via Toll-like receptors. *Infect Immun* **82**, 2300-2309 (2014).

299. Brož, P., Ohlson, M.B. & Monack, D.M. Innate immune response to Salmonella typhimurium, a model enteric pathogen. *Gut Microbes* **3**, 62 - 70 (2012).

300. Zhang, S.S.*, et al.* TLR4-IN-C34 Inhibits Lipopolysaccharide-Stimulated Inflammatory Responses via Downregulating TLR4/MyD88/NF-kappaB/NLRP3 Signaling Pathway and Reducing ROS Generation in BV2 Cells. *Inflammation* **45**, 838-850 (2022).

301. Jiang, K.*, et al.* Downregulation of TLR4 by miR-181a Provides Negative Feedback Regulation to Lipopolysaccharide-Induced Inflammation. *Front Pharmacol* **9**, 142 (2018).

302. Yashiro, M. Ulcerative colitis-associated colorectal cancer. *World J Gastroenterol* **20**, 16389-16397 (2014).

303. Shigaki, K.*, et al.* Immunohistochemical analysis of chromogranin A and p53 expressions in ulcerative colitis-associated neoplasia: neuroendocrine differentiation as an early event in the colitis-neoplasia sequence. *Hum Pathol* **44**, 2393-2399 (2013).

304. Ueda, Y., Ando, T., Nanjo, S., Ushijima, T. & Sugiyama, T. DNA methylation of microRNA-124a is a potential risk marker of colitis-associated cancer in patients with ulcerative colitis. *Dig Dis Sci* **59**, 2444-2451 (2014).

305. Zhuang, W.*, et al.* Clinical and Pathologic Complete Response to Gefitinib in a Patient with SqCLC Harboring EGFR p.E746_S752delinsV Mutation. *Onco Targets Ther* **14**, 4805-4808 (2021).

306. Hughes, R.*, et al.* Perivascular M2 Macrophages Stimulate Tumor Relapse after Chemotherapy. *Cancer Res* **75**, 3479-3491 (2015).

307. Tang, Y.*, et al.* Multiplex-invasive reaction-assisted qPCR for quantitatively detecting the abundance of EGFR exon 19 deletions in cfDNA. *Anal Methods* **12**, 3344-3350 (2020).

308. Li, Y.*, et al.* COX-2-PGE(2) Signaling Impairs Intestinal Epithelial Regeneration and Associates with TNF Inhibitor Responsiveness in Ulcerative Colitis. *EBioMedicine* **36**, 497-507 (2018).

309. Wells, J.M.*, et al.* Homeostasis of the gut barrier and potential biomarkers. *Am J Physiol Gastrointest Liver Physiol* **312**, G171-g193 (2017).

310. Levi-Galibov, O.*, et al.* Heat Shock Factor 1-dependent extracellular matrix remodeling mediates the transition from chronic intestinal inflammation to colon cancer. *Nat Commun* **11**, 6245 (2020).

311. Nagaraja, G.M.*, et al.* Silencing Hsp25/Hsp27 gene expression augments proteasome activity and increases CD8+ T-cell-mediated tumor killing and memory responses. *Cancer Prev Res (Phila)* **5**, 122-137 (2012).

312. Jolly, C. & Morimoto, R.I. Role of the heat shock response and molecular chaperones in oncogenesis and cell death. *J Natl Cancer Inst* **92**, 1564-1572 (2000).

313. Yan, J., Hedl, M. & Abraham, C. An inflammatory bowel disease-risk variant in INAVA decreases pattern recognition receptor-induced outcomes. *J Clin Invest* **127**, 2192-2205 (2017).

314. Hadisaputri, Y.*, et al.* TNFAIP3 overexpression is an independent factor for poor survival in esophageal squamous cell carcinoma. *International Journal of Oncology* **50**(2017).

315. Shaked, Y.*, et al.* Genetic heterogeneity of the vasculogenic phenotype parallels angiogenesis; Implications for cellular surrogate marker analysis of antiangiogenesis. *Cancer Cell* **7**, 101-111 (2005).

316. Yang, Q.W.*, et al.* Methylation-associated silencing of the thrombospondin-1 gene in human neuroblastoma. *Cancer Res* **63**, 6299-6310 (2003).

317. Aguilar, E.C.*, et al.* Butyrate impairs atherogenesis by reducing plaque inflammation and vulnerability and decreasing NFkappaB activation. *Nutr Metab Cardiovasc Dis* **24**, 606-613 (2014).

318. Ohira, H.*, et al.* Butyrate attenuates inflammation and lipolysis generated by the interaction of adipocytes and macrophages. *J Atheroscler Thromb* **20**, 425-442 (2013).

319. Awasthi, S., Brown, K., King, C., Awasthi, V. & Bondugula, R. A toll-like receptor-4-interacting surfactant protein-A-derived peptide suppresses tumor necrosis factor-alpha release from mouse JAWS II dendritic cells. *J Pharmacol Exp Ther* **336**, 672-681 (2011).

320. Ramani, V., Madhusoodhanan, R., Kosanke, S. & Awasthi, S. A TLR4-interacting SPA4 peptide inhibits LPS-induced lung inflammation. *Innate Immun* **19**, 596-610 (2013).

321. Shah, N.*, et al.* Role of toll-like receptor 4 in mediating multiorgan dysfunction in mice with acetaminophen induced acute liver failure. *Liver Transpl* **19**, 751-761 (2013).

Appendix

Appendix 1 - Detailed Materials & Methods for Proteome Arrays

Human Cytokine XL Proteome Array Kit (Catalogue Number ARY005B)

Preparation of Cell Lysates

Organoids were first washed with PBS, prior to being solubilised in lysis buffer. The cells were resuspended by thorough pipetting. The lysates were then rocked for 30 minutes at 4°C. The lysates were then transferred to a microcentrifuge and spun down at 14,000 g for 5 minutes. The supernatant was then transferred to a clean test tube and retained for quantification using a Nanodrop.

Reagent Preparation

The following reagents were then prepared:

Detection Antibody Cocktail

The Detection Antibody Cocktail was reconstituted in 100 µL of distilled water.

1X Wash Buffer

40 mL of 25X Wash Buffer Concentrate was added to 960 mL distilled water to prepare 1000 mL of 1X Wash Buffer.

Chemi Reagent Mix

Chemi Reagent 1 and 2 were mixed in equal volumes within 15 minutes of use, while protecting from light to preserve the signal. 1 mL of the resultant mixture were used per membrane.

1X Streptavidin-HRP

Immediately before use, Streptavidin-HRP was diluted in 1X Array Buffer 4.

Array Procedure

2 ml of Array Buffer 4 was added in each well of the provided 4-well plate. This serves as a blocking buffer. Each membrane was then placed in each well of the plate using tweezers. The membranes were then incubated for 1 hour on a rocking platform. During this blocking phase, the samples were prepared by adding 1 ml from each sample to 0.5 ml Array Buffer 4 in separate tubes. 15 ml of the reconstituted Human Cytokine Array Detection Antibody Cocktail was then added to each of these samples. These samples were then mixed and incubated at RT for 1 hour. Array Buffer 4 was then removed from the wells of the 4-well plate and the prepared sample/antibody mixtures were then added. The lid was then placed before incubating the plate overnight at 4^{o}C on a rocking platform.

The following day, each membrane was removed from the plate and placed into distinct plastic dishes with 20 ml 1X Wash Buffer, before being placed on a rocking platform for 10 minutes. This washing step was repeated a further 2 times. The wells of the plate were then rinsed with distilled water and dried thoroughly. In conjunction, the Streptavidin-HRP was diluted in Array Buffer 5 using the listed dilution factor on the vial. 2 ml of this diluted solution was then pipetted into each well of the 4-well plate. The washed membranes were then returned to the plate containing this diluted Streptavidin-HRP. The lid was then returned to the plate, which was then incubated for 30 minutes at RT on a rocking platform. Each array was then washed as described previously. These membranes were then removed from their separate wash containers and the excess Wash Buffer removed by blotting onto paper towels.

To image the arrays, the membranes were placed on a plastic sheet (i.e., cling film) with the identification number facing upwards. 1 ml of the prepared Chemi Reagent Mix was added evenly onto each membrane. An additional plastic sheet was placed on top of the membranes and smoothed to ensure removal of bubbles. This was left to incubate for 1 minute. They were then placed in the chemiluminescent imaging machine with the exposure set for 10 minutes. The resultant images were then assessed as outlined in the Data Analysis section.

Human NFκB Pathway Array Kit (Catalogue Number ARY029)

Preparation of Cell Lysates

Organoids were first washed with PBS, prior to being solubilised in lysis buffer. The cells were resuspended by thorough pipetting. The lysates were then rocked for 30 minutes at 4^{o}C. The lysates were then transferred to a microcentrifuge and spun down at 14,000 g for 5 minutes. The supernatant was then transferred to a clean test tube and retained for quantification using a Nanodrop.

Reagent Preparation

The following reagents were then prepared:

Detection Antibody Cocktail

The Detection Antibody Cocktail was reconstituted in 100 µL of distilled water.

1X Wash Buffer

40 mL of 25X Wash Buffer Concentrate was added to 960 mL distilled water to prepare 1000 mL of 1X Wash Buffer.

Chemi Reagent Mix

Chemi Reagent 1 and 2 were mixed in equal volumes within 15 minutes of use, while protecting from light to preserve the signal. 1 mL of the resultant mixture were used per membrane.

Array Buffer 3/6

Equal volumes of Array Buffers 3 and 6 were mixed fresh for each day of experimentation.

1X Streptavidin-HRP

Immediately before use, Streptavidin-HRP was diluted in 1X Array Buffer 3/6.

Array Procedure

2 ml of Array Buffer 3/6 (blocking buffer) was added to each well of the 4-well plate to be used. Membranes were then removed from their protective sheets and placed into each well of the plate using tweezers. The membranes were then incubated for 1 hour on a rocking platform shaker. While membranes were blocking, Array Buffer 1 was then added to samples a total volume of 1.5 ml. Once Array Buffer 3/6 was aspirated, these prepared samples were added to the plate and incubated on a rocking platform overnight at 4^{o}C.

The following day the membranes were removed and placed in separate dishes containing 20 ml 1X Wash Buffer for 10 minutes on a rocking platform. This was repeated an additional two times. Upon incubation, 15 µl reconstituted Detection Antibody Cocktail was diluted to 1.5 ml with Array Buffer 3/6 for each membrane. This was therefore upscaled to encompass all 6 membranes being tested. 1.5 ml solution was then added into each well of the 4-well plates. The membranes were then returned to the plates containing this diluted Detection Cocktail and covered. The plates were then incubated for 1 hour at RT on a rocking platform. The washing steps detailed earlier were then repeated.

Streptavidin-HRP was diluted in Array Buffer 3/6 using the listed dilution factor on the vial. 2 ml of this diluted solution was then pipetted into each well of the 4-well plate. The membranes were then returned to the plate containing the diluted Streptavidin-HRP. The lid was then replaced, and the plate then incubated for 30 minutes at RT on a rocking platform. The above washing steps were then repeated. The membranes were removed from their washing containers and the excess Wash Buffer removed by blotting onto paper towels.

To image the arrays, the membranes were placed on a plastic sheet with the identification number facing upwards. 1 ml of the prepared Chemi Reagent Mix was pipetted onto each membrane. An additional plastic sheet was placed on top of the membranes and smoothed to ensure even coverage and removal of bubbles. This was incubated for 1 minute. The membranes were then placed in the chemiluminescent imaging machine with the exposure set for 10 minutes. The resultant images were then assessed as detailed in the Data Analysis section.

Human Phospho-Kinase Array Kit (Catalogue Number ARY003C)

Preparation of Cell Lysates

Organoids were first washed with PBS, prior to being solubilised in lysis buffer. The cells were resuspended by thorough pipetting. The lysates were then rocked for 30 minutes at 4°C. The lysates were then transferred to a microcentrifuge and spun down at 14,000 g for 5 minutes. The supernatant was then transferred to a clean test tube and retained for quantification using a Nanodrop.

Reagent Preparation

The following reagents were then prepared:

Detection Antibody Cocktail A (red cap)

One vial of lyophilized biotinylated antibodies for use with Part A membranes. Detection Antibody Cocktail A was reconstituted in 100 µl distilled water.

Detection Antibody Cocktail B (blue cap)

One vial of lyophilized biotinylated antibodies to use with Part B membranes. Detection Antibody Cocktail B was reconstituted in 100 µl distilled water.

1X Array Buffer 2/3

2.0 mL of 5X Array Buffer 2 Concentrate was added to 8.0 mL of Array Buffer 3.

1X Wash Buffer

40 mL of 25X Wash Buffer Concentrate was added to 960 mL distilled water to prepare 1000 mL of 1X Wash Buffer.

Chemi Reagent Mix

Chemi Reagent 1 and 2 were mixed in equal volumes within

15 minutes of use, while protecting from light to preserve the signal. 1 mL of the resultant mixture were used per membrane.

1X Streptavidin-HRP

Immediately before use, Streptavidin-HRP was diluted in 1X Array Buffer 2/3.

Array Procedure

An 8-well plate was used due to the dual membrane set-up of this array. Both parts A and B were incubated in the same lysate preparation but distinct wells.

1 ml Array Buffer 1 was pipetted into each well of the 8-well plate, serving as a blocking buffer. Part A and Part B membranes were then placed into adjacent wells and incubated for 1 hour on a rocking platform.

During this blocking phase, the desired quantity of each sample was prepared by dilution with Array Buffer 1 – to a total volume of 2 ml. Array Buffer 1 was then aspirated from the plate and 1 ml of the samples were added to both Part A and Part B membranes. These were then incubated overnight at 4^{o}C on a rocking platform.

The following day, membranes were transferred to dishes containing 20 ml 1X Wash Buffer for 10 minutes on a rocking platform. This step was repeated for a total of 3 washes. 20 µl of reconstituted Detection Antibody Cocktail A was added to 1 ml Array buffer 2/3. 1 ml of this solution was then pipetted into each well of the 8-well plate. The Part A membranes were then removed from the washing containers and returned to the plate. This was then repeated with the reconstituted Detection Antibody Cocktail B for the Part B membranes. The plate was then incubated at RT for 2 hours on a rocking platform.

The washing process was then repeated with Part A and Part B membranes washed in separate containers. The Streptavidin-HRP was diluted in Array Buffer 2/3 before pipetting 1 ml into each well of the 8-well plate. Once the excess Wash Buffer had been drained from each membrane, they were returned to the plate containing the diluted Streptavidin-HRP and incubated at RT for 30 minutes on a rocking platform. The above wash steps were then repeated to remove excess Streptavidin-HRP.

For array imaging, the membranes were placed on a plastic sheet and coated with 1 ml of prepared Chemi Reagent Mix per membrane. All bubbles were removed by smoothing out with a plastic sheet placed on top of the membranes. The membranes were incubated for 1 minute at RT before being placed in the chemiluminescent imaging machine with the exposure set for 10 minutes. The resultant images were assessed as described in the Data Analysis section.

Data Analysis

The relative signal intensity of the exposed dots was quantified using ImageJ software. The values were then transferred to a Microsoft Excel spreadsheet and aligned with the relevant protein positions using the template provided. An average signal intensity was calculated from the duplicate spots. This was then corrected by subtracting the average background signal (of the negative control spots). The relative change in cytokine levels between samples were then determined by comparing corresponding signals on different arrays.

Appendix 2 – Proteome Array Membranes

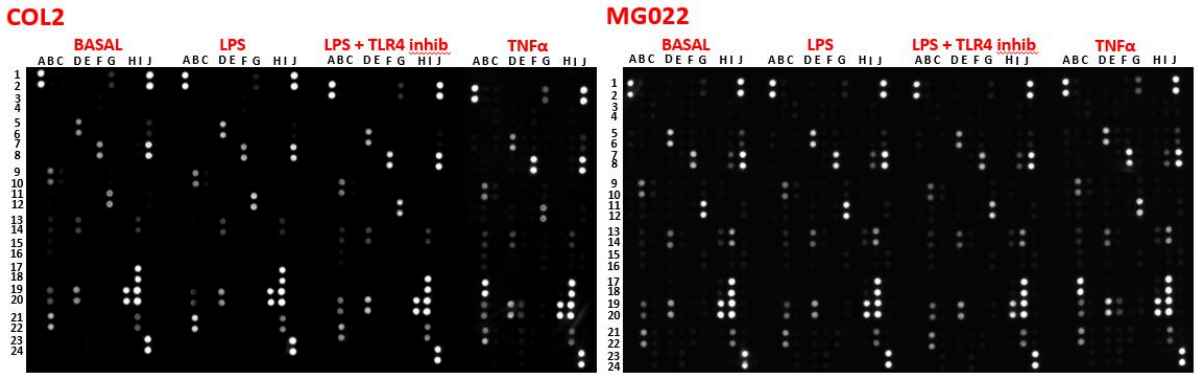

Figure A2.1: XL Cytokine Array membranes comparing healthy (left) and UC-derived (right) tissue responses to LPS exposure (+/- TLR4 inhibition) and TNFα, (Exposure time 1000 seconds).

Table A2.1: Human XL Cytokine Array coordinates correlating with each specific peptide of interest (part 1).

Coordinate	Analyte/Control	Entrez Gene ID	Alternate Nomenclature
A1, A2	Reference Spots	N/A	———
A3, A4	Adiponectin/Acrp30	11450	AdipoQ
A5, A6	Amphiregulin	11839	AR, SDGF
A7, A8	Angiopoietin-1	11600	Ang-1, Angpt1
A9, A10	Angiopoietin-2	11601	Ang-2, Angpt2
A11, A12	Angiopoietin-like 3	30924	ANGPT-L3
A13, A14	BAFF/BLyS/TNFSF13B	24099	CD257, TALL1, THANK, ZTNF4
A15, A16	C1q R1/CD93	17064	AA4 Antigen, C1q Rp, CD93
A17, A18	CCL2/JE/MCP-1	20296	MCAF
A19, A20	CCL3/CCL4/MIP-1α/β	20302/20303	———
A21, A22	CCL5/RANTES	20304	SISd
A23, A24	Reference Spots	N/A	———
B3, B4	CCL6/C10	20305	MRP-1
B5, B6	CCL11/Eotaxin	20292	———
B7, B8	CCL12/MCP-5	20293	———
B9, B10	CCL17/TARC	20295	———
B11, B12	CCL19/MIP-3β	24047	ELC
B13, B14	CCL20/MIP-3α	20297	exodus-1, LARC
B15, B16	CCL21/6Ckine	18829	exodus-2, SCYA21, SLC, TCA-4
B17, B18	CCL22/MDC	20299	ABCD-1, MDC, STCP-1

Table A2.2: Human XL Cytokine Array coordinates correlating with each specific peptide of interest (part 2).

Coordinate	Analyte/Control	Entrez Gene ID	Alternate Nomenclature
B19, B20	CD14	12475	———
B21, B22	CD40/TNFRSF5	21939	———
C3, C4	CD160	54215	Natural killer cell receptor BY55, NK1; NK28
C5, C6	Chemerin	71660	RARRES2, TIG-2
C7, C8	Chitinase 3-like 1	12654	CHI3L1, Cgp39, YKL40
C9, C10	Coagulation Factor III/Tissue Factor	14066	TF, CD142, Thromboplastin
C11, C12	Complement Component C5/C5a	15139	C5/C5a
C13, C14	Complement Factor D	11537	Adipsin, C3 convertase activator, Properdin factor D
C15, C16	C-Reactive Protein/CRP	12944	———
C17, C18	CX3CL1/Fractalkine	20312	FKN, Neurotactin
C19, C20	CXCL1/KC	14825	CINC-1; GRO alpha; KC; MGSA-alpha
C21, C22	CXCL2/MIP-2	20310	GROβ, GRO2, CINC-3
D1, D2	CXCL9/MIG	17329	CRG-10, CMK
D3, D4	CXCL10/IP-10	15945	CRG-2, C7
D5, D6	CXCL11/I-TAC	56066	H174, SCYB9B
D7, D8	CXCL13/BLC/BCA-1	55985	———
D9, D10	CXCL16	66102	SRPSOX
D11, D12	Cystatin C	13010	ARMD11, CST3, Gamma-trace

Table A2.3: Human XL Cytokine Array coordinates correlating with each specific peptide of interest (part 3).

Coordinate	Analyte/Control	Entrez Gene ID	Alternate Nomenclature
D13, D14	DKK-1	13380	Dickkopf-1
D15, D16	DPPIV/CD26	13482	Dpp4, Dipeptidyl-peptidase IV
D17, D18	EGF	13645	Epidermal Growth Factor
D19, D20	Endoglin/CD105	13805	ENG
D21, D22	Endostatin	12822	Col18a1
D23, D24	Fetuin A/AHSG	11625	AHSG, alpha-2-HS-glycoprotein
E1, E2	FGF acidic	14164	FGF-1
E3, E4	FGF-21	56636	———
E5, E6	Flt-3 Ligand	14256	Flt3lg
E7, E8	Gas 6	14456	Growth Arrest Specific
E9, E10	G-CSF	12985	Csf3
E11, E12	GDF-15	23886	MIC-1
E13, E14	GM-CSF	12981	Csf2
E15, E16	HGF	15234	Scatter Factor, SF, Hepatopoietin-A
E17, E18	ICAM-1/CD54	15894	———
E19, E20	IFN-γ	15978	IFNG
E21, E22	IGFBP-1	16006	———
E23, E24	IGFBP-2	16008	———
F1, F2	IGFBP-3	16009	———
F3, F4	IGFBP-5	16011	———
F5, F6	IGFBP-6	16012	———

Table A2.4: Human XL Cytokine Array coordinates correlating with each specific peptide of interest (part 4).

Coordinate	Analyte/Control	Entrez Gene ID	Alternate Nomenclature
F7, F8	IL-1α/IL-1F1	16175	———
F9, F10	IL-1β/IL-1F2	16176	———
F11, F12	IL-1ra/IL-1F3	16181	IL1RN
F13, F14	IL-2	16183	———
F15, F16	IL-3	16187	———
F17, F18	IL-4	16189	B cell-stimulatory factor-1
F19, F20	IL-5	16191	———
F21, F22	IL-6	16193	———
F23, F24	IL-7	16196	———
G1, G2	IL-10	16153	CSIF
G3, G4	IL-11	16156	———
G5, G6	IL-12 p40	16160	———
G7, G8	IL-13	16163	———
G9, G10	IL-15	16168	———
G11, G12	IL-17A	16171	———
G13, G14	IL-22	50929	IL-TIF
G15, G16	IL-23	83430	———
G17, G18	IL-27 p28	246779	———

Table A2.5: Human XL Cytokine Array coordinates correlating with each specific peptide of interest (part 5).

Coordinate	Analyte/Control	Entrez Gene ID	Alternate Nomenclature
G19, G20	IL-28A/B	330496/338374	———
G21, G22	IL-33	77125	NF HEV, DVS 27
G23, G24	LDL R	16835	low density lipoprotein receptor
H1, H2	Leptin	16846	OB
H3, H4	LIF	16878	———
H5, H6	Lipocalin-2/NGAL	16819	Siderocalin, 24p3
H7, H8	LIX	20311	CXCL5, GCP-2, ENA-78
H9, H10	M-CSF	12977	CSF-1
H11, H12	MMP-2	17390	Gelatinase A
H13, H14	MMP-3	17392	Stromelysin-1
H15, H16	MMP-9	17395	Clg4b, Gelatinase B, GELB
H17, H18	Myeloperoxidase	17523	MPO
H19, H20	Osteopontin (OPN)	20750	Eta-1, Spp1
H21, H22	Osteoprotegerin/TNFRSF11B	18383	OPG, Ocif
H23, H24	PD-ECGF/Thymidine phosphorylase	72962	dThdPase, ECGF1, Gliostatin, MEDPS1, MNGIE
I1, I2	PDGF-BB	18591	———
I3, I4	Pentraxin 2/SAP	20219	PTX2
I5, I6	Pentraxin 3/TSG-14	19288	PTX3
I7, I8	Periostin/OSF-2	50706	Fasciclin I-like, POSTN, TRIF52
I9, I10	Pref-1/DLK-1/FA1	13386	DLK1, pG2, ZOG

Table A2.6: Human XL Cytokine Array coordinates correlating with each specific peptide of interest (part 6).

Coordinate	Analyte/Control	Entrez Gene ID	Alternate Nomenclature
I11, I12	Proliferin	18811	MRP
I13, I14	Proprotein Convertase 9/PCSK9	100102	NARC-1
I15, I16	RAGE	11596	AGER
I17, I18	RBP4	19662	Retinol-Binding Protein 4
I19, I20	Reg3G	19695	PAP3
I21, I22	Resistin	57264	ADSF, FIZZ3
J1, J2	Reference Spots	N/A	———
J3, J4	E-Selectin/CD62E	20339	ELAM1, LECAM2, Sele
J5, J6	P-Selectin/CD62P	20344	GMP-140, LECAM3, Selep
J7, J8	Serpin E1/PAI-1	18787	Nexin, PLANH1
J9, J10	Serpin F1/PEDF	20317	EPC-1
J11, J12	Thrombopoietin	21832	Tpo, MGDF
J13, J14	TIM-1/KIM-1/HAVCR	171283	———
J15, J16	TNF-α	21926	TNFSF1A
J17, J18	VCAM-1/CD106	22329	———
J19, J20	VEGF	22339	VEGF-A, VPF
J21, J22	WISP-1/CCN4	22402	———
J23, J24	Negative Control	N/A	———

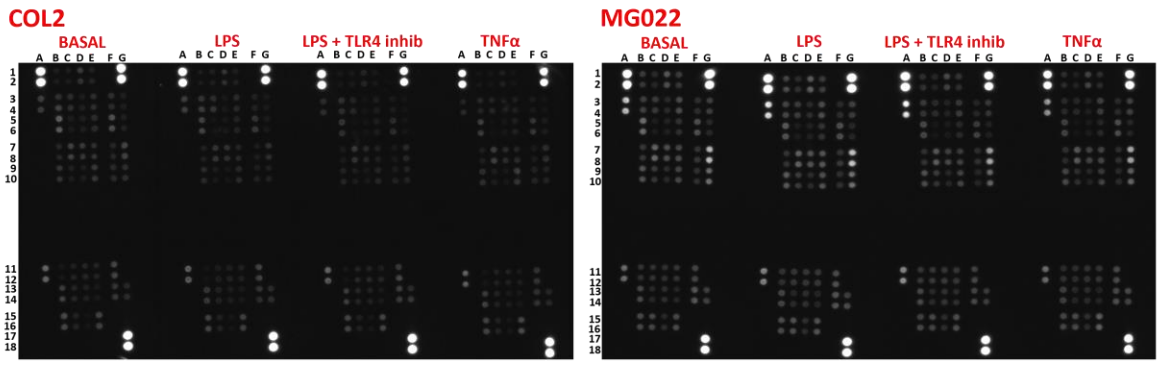

Figure A2.2: Phospho-Kinase Array membranes comparing healthy (left) and UC-derived (right) tissue responses to LPS exposure (+/- TLR4 inhibition) and TNFα, (Exposure time 1000 seconds).

Table A2.7: Phospho-Kinase Array coordinates correlating with each specific peptide of interest.

Membrane/ Coordinate	Target/Control	Phosphorylation Site	Membrane/ Coordinate	Target/Control	Phosphorylation Site
A-A1, A2	Reference Spot	——	A-E3, E4	p38α	T180/Y182
B-A11, A12	Akt 1/2/3	T308	A-E5, E6	PDGF Rβ	Y751
B-A13, A14	Akt 1/2/3	S473	A-E7, E8	PLC-γ1	Y783
B-A17, A18	Reference Spot	——	A-E9, E10	Src	Y419
A-B3, B4	CREB	S133	B-E11, E12	PYK2	Y402
A-B5, B6	EGF R	Y1086	B-E13, E14	RSK1/2	S221/S227
A-B7, B8	eNOS	S1177	B-E15, E16	RSK1/2/3	S380/S386/S377
A-B9, B10	ERK1/2	T202/Y204, T185/Y187	A-F3, F4	STAT2	(pY690)
B-B11, B12	Chk-2	T68	A-F5, F6	STAT5a/b	Y694/Y699
B-B13, B14	c-Jun	S63	A-F7, F8	WNK1	T60
A-C3, C4	Fgr	Y412	A-F9, F10	Yes	Y426
A-C5, C6	GSK-3α/β	S21/S9	B-F11, F12	STAT1	Y701
A-C7, C8	GSK-3β	S9	B-F13, F14	STAT3	Y705
A-C9, C10	HSP27	S78/S82	B-F15, F16	STAT3	S727
B-C11, C12	p53	S15	A-G1, G2	Reference Spot	——
B-C13, C14	p53	S46	A-G3, G4	β-Catenin	——
B-C15, C16	p53	S392	A-G9, G10	PBS (Negative Control)	——
A-D3, D4	JNK 1/2/3	T183/Y185, T221/Y223	B-G11, G12	STAT6	Y641
A-D5, D6	Lck	Y394	B-G13, G14	HSP60	——
A-D7, D8	Lyn	Y397	B-G17, G18	PBS (Negative Control)	——
A-D9, D10	MSK1/2	S376/S360			
B-D11, D12	p70 S6 Kinase	T389			
B-D13, D14	p70 S6 Kinase	T421/S424			
B-D15, D16	PRAS40	T246			

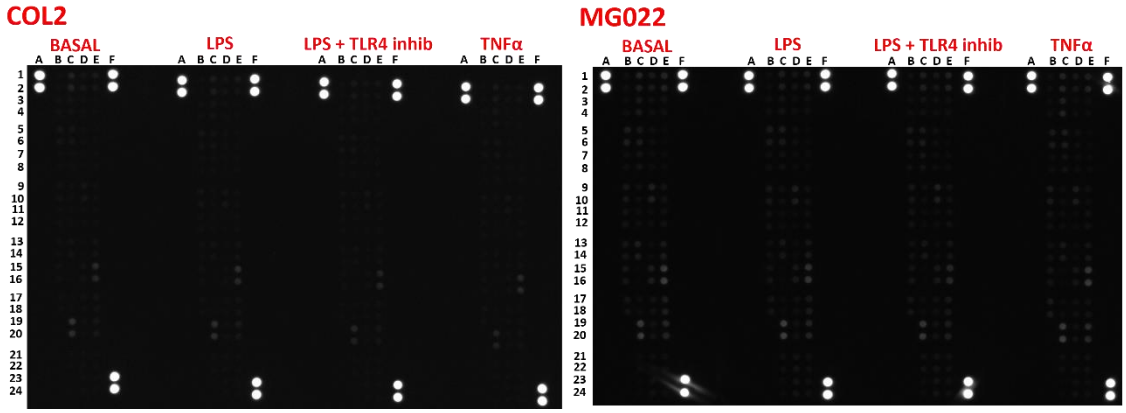

Figure A2.3: NFκB Array membranes comparing healthy (left) and UC-derived (right) tissue responses to LPS exposure (+/- TLR4 inhibition) and TNFα, (Exposure time 1000 seconds).

Table A2.8: NFκB Array coordinates correlating with each specific peptide of interest (part 1).

Coordinate	Target/Control	Entrez Gene ID	Alternate Nomenclature
A1, A2, A23, A24	Reference Spots	NA	RS
B1, B2	ASC	29108	PYCARD/CARD5
B3, B4	BCL10	8915	CLAP/CIPER/CARMEN/c-E10
B5, B6	CARD6	84674	CINCIN1
B7, B8	CD40/TNFRSF5	958	CDW40
B9, B10	cIAP1/BIRC2	329	———
B11, B12	cIAP2/BIRC3	330	———
B13, B14	FADD/MORT1	8772	GIG3
B15, B16	Fas/TNFRSF6/CD95	355	———
B17, B18	IκBα	4792	NFKBIA/MAD-3/NFKBI/IKBA
B19, B20	IκBε	4794	NFKBIE/IKBE
B21, B22	IKK1/IKKα/CHUK	1147	IKKA/IKBKA/TCF16
B23, B24	IKK2/IKKβ	3551	IKKB/NFKBIKB/IMD15
C1, C2	IKKγ/NEMO	8517	IKBKG/FIP3/IMD33
C3, C4	IL-1 RI	3554	CD121A/IL-1R-alpha
C5, C6	IL-17 RA	23765	CD217/CANDF5/CDw217
C7, C8	IL-18 Rα	8809	CD218a/IL18RA/IL1 RRP
C9, C10	IRAK1	3654	IRAK/pelle
C11, C12	IRF5	3663	SLEB10

Table A2.9: NFκB Array coordinates correlating with each specific peptide of interest (part 2).

Coordinate	Target/Control	Entrez Gene ID	Alternate Nomenclature
C13, C14	IRF8	3394	ICSBP/IMD32A
C15, C16	JNK1/2	5599/5601	SAPK1/MAPK8; SAPK1a/MAPK9
C17, C18	JNK2	5601	SAPK1a/MAPK9
C19, C20	LTBR/TNFRSF3	4055	CD18
C21, C22	Metadherin/AEG-1	92140	LYRIC/MTDH
C23, C24	MYD88	4615	———
D1, D2	NFκB1	4790	p50/p105
D3, D4	NFκB2	4791	p52/p100
D5, D6	NGF R/TNFRSF16	4804	CD271/p75NTR
D7, D8	p53	7157	———
D9, D10	p53 (pS46)	7157	———
D11, D12	RelA/p65	5970	NFKB3
D13, D14	RelA/p65 (pS529)	5970	NFKB4
D15, D16	c-Rel	5966	———
D17, D18	SHARPIN	81858	SIPL1
D19, D20	SOCS6	9306	CIS4/SSI4/SOCS4/STATI4
D21, D22	STAT1p91	6772	ISGF-3/STAT91
D23, D24	STAT1 (pY701)	6772	ISGF-3/STAT91

Table A2.10: NFκB Array coordinates correlating with each specific peptide of interest (part 3).

Coordinate	Target/Control	Entrez Gene ID	Alternate Nomenclature
E1, E2	STAT2	6773	P113/STAT113
E3, E4	STAT2 (pY690)	6773	P113/STAT113
E5, E6	STING/TMEM173	340061	———
E7, E8	TLR2	7097	TIL4/CD282
E9, E10	TNF RI/TNFRSF1A	7132	CD120a/TNFAR
E11, E12	TNF RII/TNFRSF1B	7133	CD120b/p75
E13, E14	TRAF2	7186	TRAP/TRAP3
E15, E16	TRAIL R1/DR4	8797	TNFRSF10A/CD261
E17, E18	TRAIL R2/DR5	8795	TNFRSF10B/CD262/KILLER/TRICK2
F1, F2	Reference Spots	NA	RS
F23, F24	Negative Control	NA	Controls (-)

Appendix 3 – Immunostaining Densitometry

Table A3.1: Densitometry values taken from immunohistochemistry images (Healthy v UC) using ImageJ.

	HEALTHY (COL2)		UC (MG022)	
IHC	**Mean**	**StDev**	**Mean**	**StDev**
BASAL CDX2	218.369	28.638	214.944	24.906
BASAL ECAD	195.942	38.183	189.872	35.438
BASAL MUC2	225.319	22.346	205.861	29.737
BASAL VIL	190.986	35.882	205.416	37.558
BASAL TLR4	196.842	38.299	164.166	31.128
BASAL MD2	170.968	42.843	183.345	22.157
BASAL NFKB	221.49	25.659	217.968	30.596
LPS CDX2	214.062	38.156	184.215	34.43
LPS ECAD	201.218	39.723	172.645	41.842
LPS MUC2	265.131	38.893	173.907	35.824
LPS VIL	195.135	41.094	227.611	36.682
LPS TLR4	189.078	42.285	210.968	37.698
LPS MD2	204.159	35.85	195.108	30.049
LPS NFKB	223.6	31.623	219.367	29.862
LPS + TLR4I CDX2	223.315	36.775	190.574	30.856
LPS + TLR4I ECAD	198.076	36.994	180.937	32.547
LPS + TLR4I MUC2	235.822	34.21	197.271	35.64
LPS + TLR4I VIL	207.763	27.244	195.253	20.137
LPS + TLR4I TLR4	192.363	30.013	170.166	31.128
LPS + TLR4I MD2	175.972	33.909	182.455	32.554
LPS + TLR4I NFKB	233.534	22.377	215.955	35.759

Table A3.2: Densitometry values taken from immunofluorescence images (Healthy v UC) using Image J.

	HEALTHY (COL2)		UC (MG022)	
IMMUNOFLUORESCENCE	**Mean**	**StDev**	**Mean**	**StDev**
BASAL CDX2	4.399	1.778	4.818	2.899
BASAL ECAD	8.038	3.292	8.196	4.181
BASAL MUC2	2.034	1.831	7.676	3.503
BASAL VIL	5.474	2.508	7.719	4.164
BASAL TLR4	5.921	2.516	1.285	0.996
BASAL MD2	3.625	1.305	4.579	2.278
BASAL NFKB				
LPS CDX2	4.244	2.659	3.554	1.721
LPS ECAD	7.974	3.388	5.495	2.488
LPS MUC2	7.606	3.679	15.403	5.109
LPS VIL	5.693	2.865	10.253	4.435
LPS TLR4	5.759	3.101	7.517	3.151
LPS MD2	4.848	2.281	6.577	2.909
LPS NFKB				

Table A3.3: Densitometry values of DAPI taken from immunohistochemistry images (Healthy v UC) using ImageJ.

IMMUNOFLUORESCENCE DAPI READINGS	HEALTHY (COL2)		UC (MG022)	
	Mean	StDev	Mean	StDev
TLR4/MUC2				
BASAL	7.617	2.73	8.868	4.303
LPS	7.293	3.081	9.283	5.331
VIL./TLR4				
BASAL	7.951	3.713	8.743	4.772
LPS	8.116	3.689	8.937	4.179
MD2/ECAD				
BASAL	7.232	4.416	7.845	3.862
LPS	7.682	4.473	8.198	4.103
VIL/CDX2				
BASAL	7.056	3.719	7.582	4.507
LPS	7.385	4.289	7.164	3.836

Appendix 4 – RNA-Sequencing Additional Data

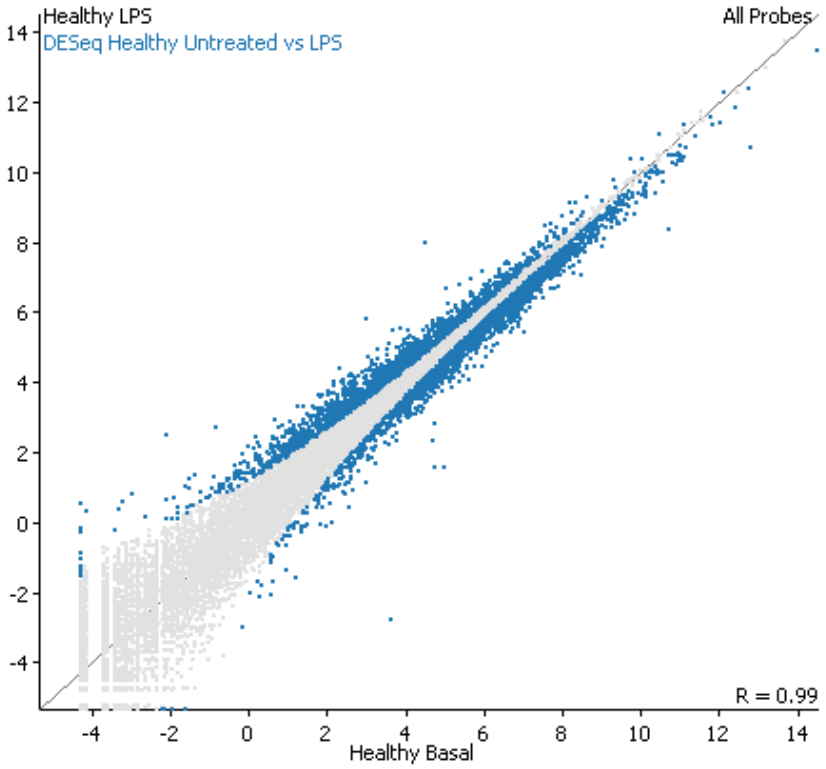

Figure A4.1: Scatter plot of normalised read counts from Healthy Untreated v LPS-treated DESeq data set.

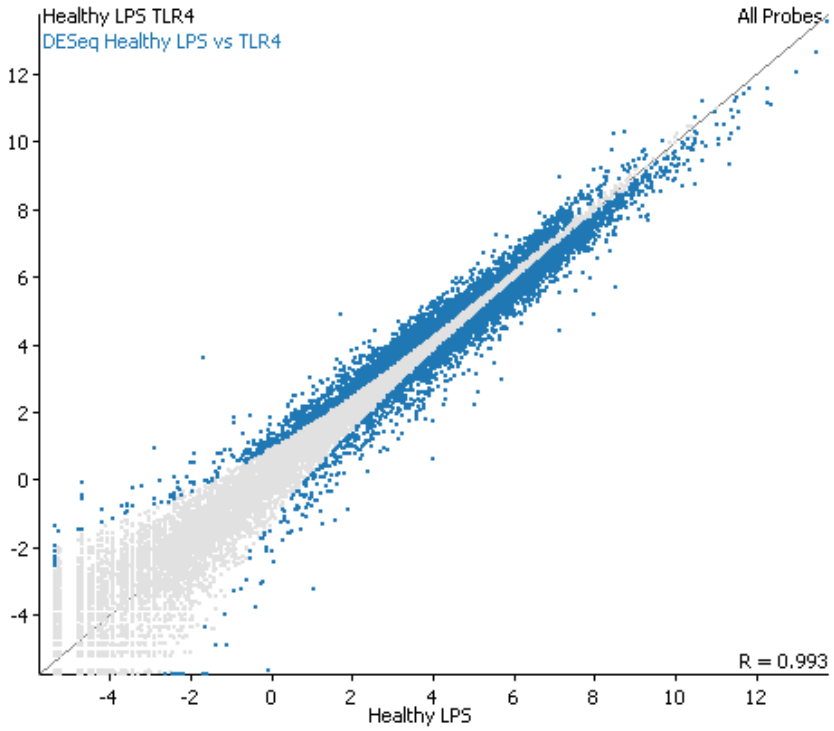

Figure A4.2: Scatter plot of normalised read counts from Healthy LPS-treated v LPS + TLR4 inhibition DESeq data

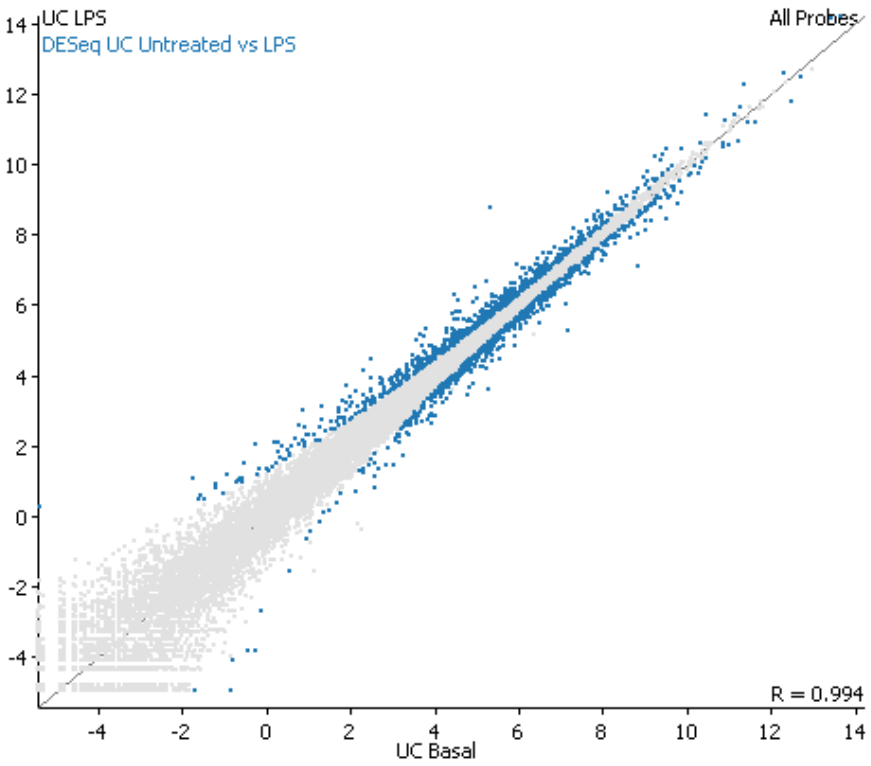

Figure A4.3: Scatter plot of normalised read counts from UC-derived organoids: Untreated v LPS-treated DESeq

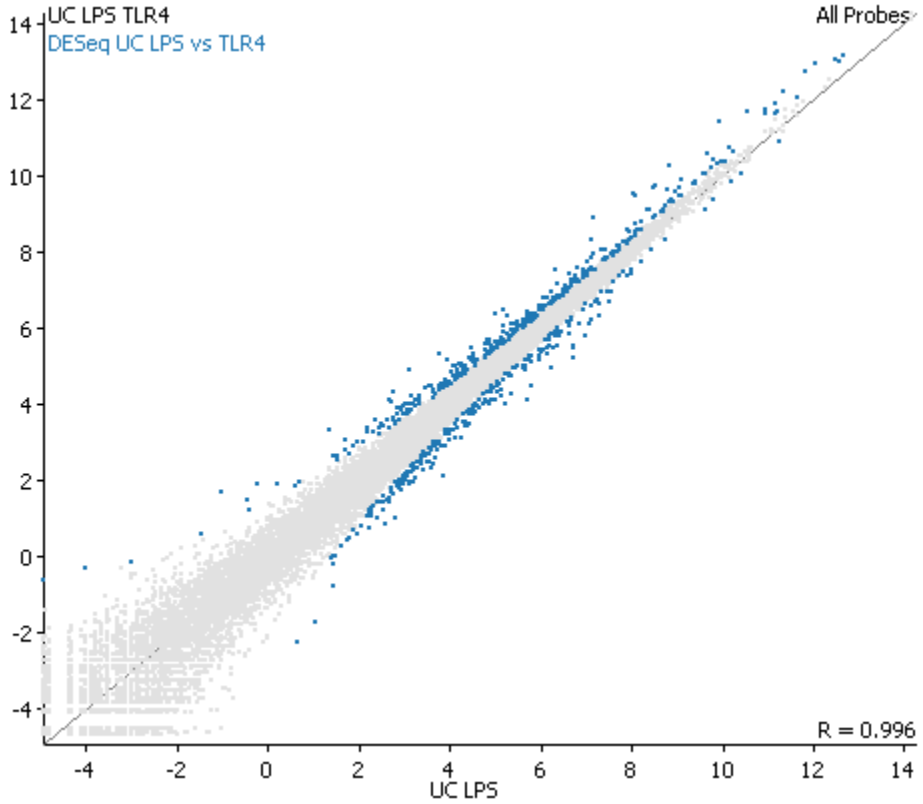

Figure A4.3: Scatter plot of normalised read counts from UC-derived organoids: LPS-treated v LPS + TLR4

Appendix 5a - Healthy Untreated v LPS DESeq GO Hits List

Gene	Expression change (Upreg/Downreg)	P-value (DESeq Healthy Untreated vs LPS)	Log2 Fold Change (DESeq Healthy Untreated vs LPS)
NOC2L	-	8.526491e-6	0.63675034
RNF223	-	3.463627e-4	-0.8811845
C1orf159	-	0.002247113	-0.6844478
AL390719.2	+	1.765023e-4	-0.94145167
SDF4	-	0.007529711	-0.2477713
ACAP3	-	5.960731e-4	-0.48531675
DVL1	-	2.9620546e-6	-0.53999484
CCNL2	-	1.053879e-12	-0.66984165
ATAD3A	+	2.9352308e-5	0.9280595
MIB2	+	3.1049944e-6	-0.64128023
SLC35E2B	-	3.4683742e-4	-0.39911562
CDK11A	-	1.9755596e-10	-0.9054158
AL031282.2	-	4.1489275e-7	-0.73152304
NADK	-	6.187686e-5	-0.39985436
GNB1	-	1.9386849e-5	-0.29619262
PRKCZ	+	1.2041031e-4	-0.4224671
TNFRSF14	+	2.0072186e-9	-0.6760035
PRDM16	+	0.0021482	-0.85928285
ARHGEF16	+	1.2764825e-6	-0.56726426
TPRG1L	+	1.397205e-5	-0.38233402
AL031847.2	-	0.00118937	0.3750843
RPL22	-	8.937101e-4	0.29293397
GPR153	-	1.4987044e-14	-0.8840705
NOL9	-	1.9961426e-6	0.8285084
ZBTB48	+	0.001315572	-0.6579538
PHF13	+	0.001776038	-0.4593128
DNAJC11	-	8.0378246e-5	0.44272348
VAMP3	+	1.2230706e-4	-0.31348094
TNFRSF9	-	1.2912224e-4	6.277747
PARK7	+	0.005560962	0.3091937
ERRFI1	-	7.4160874e-16	-0.5994155
GPR157	-	1.4101617e-5	-0.4830617
TMEM201	+	3.613798e-4	1.2784114
CLSTN1	-	1.8391685e-7	-0.385702
PGD	+	1.2343205e-5	0.42326862
DFFA	-	6.351606e-4	0.47652277

CASZ1	-	1.3132168e-4	-0.39560077
SRM	-	2.4257262e-5	1.1526082
MTOR	-	1.0128359e-6	0.50519264
FBXO2	-	1.5503899e-9	-0.9091131
FBXO44	+	0.001484147	-0.5896968
MTHFR	-	4.3986784e-16	-0.760349
CLCN6	+	2.2702922e-4	-0.5352888
KIAA2013	-	5.527625e-4	-0.3728188
PLOD1	+	0.005917298	-0.27795595
VPS13D	+	0.006007143	0.23704726
DHRS3	-	1.7704524e-6	-0.4981878
TMEM51-AS1	-	3.1047016e-11	-0.9034753
TMEM51	+	4.6872257e-4	-0.47362062
SLC25A34	+	0.008145689	-1.2061496
AL451042.2	+	0.002618164	-1.0050125
SZRD1	+	0.00355784	-0.24855602
NECAP2	+	3.5197897e-7	-0.5345367
ATP13A2	-	0.008807588	-0.547413
PADI2	-	1.2054505e-5	-0.3019844
RCC2	-	9.778779e-12	0.8534497
EMC1	-	6.67187e-5	0.5107549
AKR7A2	-	9.00674e-4	-0.32335094
CAPZB	-	0.001660729	-0.24798723
NBL1	+	3.3153105e-10	-0.5222904
MICOS10-NBL1	+	4.5959116e-4	-0.35460177
RNF186	-	1.810414e-4	-0.39061862
OTUD3	+	3.4167236e-4	-0.42644674
UBXN10	+	6.803959e-4	-0.6625499
CDA	+	1.1825763e-18	-0.8777824
PINK1	+	8.29256e-12	-0.59018004
ECE1	-	6.3490366e-11	-0.5021289
CDC42	+	0.006814993	-0.20478146
EPHB2	+	2.2383026e-13	1.0482167
KDM1A	+	6.134785e-4	0.39339498
HNRNPR	-	1.1471074e-8	0.56457835
ASAP3	-	0.002263396	-0.463764
ID3	-	5.8480746e-6	-0.67115194
GALE	-	2.8264945e-4	-0.38492006
HMGCL	-	8.221578e-8	-0.52595544
FUCA1	-	8.892802e-6	-0.34672827
PNRC2	+	2.133787e-4	-0.30657288
MYOM3	-	0.002407047	-0.68809694
IL22RA1	-	3.0564837e-10	-0.72589767
IFNLR1	-	6.1900665e-11	-0.67513585
STPG1	-	2.6855574e-7	-0.6455063
NIPAL3	+	0.002750568	-0.29094693

NCMAP	+	0.002772489	-0.54636127
MACO1	+	0.002054117	-0.34488493
LDLRAP1	+	3.9937368e-4	-0.40002927
STMN1	-	1.2917681e-13	1.3774337
ZNF593	+	6.937179e-4	1.5930817
CNKSR1	+	3.1588245e-6	-0.6402117
SH3BGRL3	+	0.002267034	-0.2915377
CRYBG2	-	4.1047933e-12	-0.68667364
DHDDS	+	1.9035575e-16	-0.7401627
HMGN2	+	8.711183e-5	0.5121222
RPS6KA1	+	0.00138285	-0.28004414
ARID1A	+	0.003766846	0.27698794
SFN	+	1.9985435e-5	-0.41450772
NUDC	+	1.1317028e-5	0.55238974
SLC9A1	-	8.3911425e-4	-0.32108632
WDTC1	+	6.249278e-10	-0.6318586
WASF2	-	1.6128723e-9	-0.4326289
AHDC1	-	0.009579689	-0.32087559
IFI6	-	2.8804544e-4	1.7075132
PPP1R8	+	0.003813299	0.42799497
RCC1	+	1.4770767e-6	0.6860031
SNHG3	+	0.003209226	0.25438395
SNHG12	-	0.005660356	-0.42167604
SERINC2	+	5.6501e-4	-0.6739594
LINC01226	+	2.1557023e-12	-1.1012418
TINAGL1	+	9.371805e-28	-0.9447764
KHDRBS1	+	0.009213872	0.24340998
TXLNA	+	0.007095654	0.2935329
TMEM234	-	0.001259132	-0.63454413
EIF3I	+	0.005144863	0.2848434
HDAC1	+	4.145858e-4	-0.28453484
FAM229A	-	6.2345853e-4	-0.98263407
BSDC1	-	3.1540697e-4	-0.37741023
RBBP4	+	2.2553644e-5	0.4175757
KIAA1522	+	4.6997993e-6	-0.40284574
RNF19B	-	0.001028438	-0.27612484
AZIN2	+	0.008185467	-0.68149424
PHC2	-	4.742444e-5	-0.4527886
ZMYM6	-	0.002394897	-0.38058373
SFPQ	-	2.2547913e-5	0.351192
ZMYM4	+	1.523478e-4	0.47030833
CLSPN	-	1.5419344e-15	1.8482858
AGO1	+	5.254583e-4	0.41160223
AGO3	+	2.1165685e-4	0.5728483
SH3D21	+	0	-1.5689144
AL591845.1	+	2.496286e-6	-1.0698295

STK40	-	2.9678364e-11	-0.7049089
DNALI1	+	0.006807386	0.89202887
GNL2	-	0.001077657	0.49259895
CDCA8	+	7.574092e-4	0.74533856
SF3A3	-	4.4976705e-6	0.77302945
UTP11	+	0.007803258	0.561774
AKIRIN1	+	0.004482783	-0.27667022
NDUFS5	+	5.005767e-4	0.44738582
MACF1	+	4.810945e-4	0.28063238
PABPC4	-	0.00757379	0.29655054
BMP8B	-	6.624547e-4	-0.44114387
MFSD2A	+	1.54145e-6	-0.6638587
PPT1	-	9.460805e-8	1.1962489
ZMPSTE24	+	0.002183784	0.318493
COL9A2	-	0.004052863	1.8042756
CTPS1	+	1.1005121e-6	1.1006873
PPIH	+	0.002208913	1.0951893
YBX1	+	1.4267206e-7	0.38154244
SLC2A1	-	4.004315e-19	-0.7359785
EBNA1BP2	-	1.2154792e-5	0.7327404
TMEM125	+	5.933358e-7	-0.6138065
C1orf210	-	1.6757398e-9	-0.61726147
CDC20	+	7.6825657e-10	1.242376
ELOVL1	-	3.029197e-15	-0.65445715
SZT2	+	3.9159704e-6	-0.50453097
HYI	-	0.00354016	-0.6975485
PTPRF	+	8.7878843e-10	-0.4978318
ST3GAL3	+	3.3022766e-4	1.7549461
DPH2	+	0.00101582	0.8183546
ATP6V0B	+	3.054696e-4	-0.39023423
TMEM53	-	0.005180738	-0.46826088
KIF2C	+	1.3581228e-4	1.079782
BEST4	-	0	-3.379076
HECTD3	-	3.2861865e-7	-0.41097948
TOE1	+	0.004171373	-0.6505565
TESK2	-	0.001736972	-0.5642618
MMACHC	+	3.843559e-4	1.0267452
AKR1A1	+	4.5609836e-6	-0.43542552
NASP	+	2.2463154e-9	0.7981784
GPBP1L1	-	8.3402504e-8	-0.4043997
MAST2	+	1.8705933e-8	-0.42808795
PIK3R3	-	0.008353354	0.30846685
TSPAN1	+	9.614094e-5	-0.2736002
CYP4X1	+	0.002211258	1.4298826
PDZK1IP1	-	8.000603e-4	1.0696603
FAF1	-	0.00114702	0.5041518

RNF11	+	2.6942887e-8	-0.46786028
OSBPL9	+	1.5006167e-6	-0.44145223
RAB3B	-	0	-1.4162688
ORC1	-	3.460961e-5	1.5175029
CPT2	+	3.932192e-4	-0.40642717
CZIB	-	0.008224639	-0.4996592
LRP8	-	3.6323522e-4	1.1381311
NDC1	-	6.2664446e-7	0.6742572
TMEM59	-	1.5232935e-6	-0.3742247
CYB5RL	-	0.001937639	1.2352875
MRPL37	+	0.006422453	0.37931556
ACOT11	+	0.007479132	-0.269202
TTC22	-	0.001922922	-0.3181466
DHCR24	-	1.5500964e-8	-0.38421774
USP24	-	2.125454e-5	0.40725765
JUN	-	1.7967123e-4	-0.31045273
AC105277.1	-	6.928423e-8	-0.96298236
HOOK1	+	8.301594e-8	0.5344494
NFIA	+	1.2525388e-12	0.7661998
DOCK7	-	0.002133859	0.33685932
ITGB3BP	-	8.367616e-4	1.3355526
PGM1	+	2.0153749e-8	-0.45025012
LEPR	+	1.0028851e-7	-0.9025827
SLC35D1	-	0.008188513	-0.21833442
SERBP1	-	1.0901958e-6	0.39108956
GADD45A	+	5.729779e-9	-0.5914909
GNG12	-	6.1693385e-12	-0.46474418
DEPDC1	-	1.4901108e-6	1.2345533
ZRANB2	-	5.856092e-4	-0.3723837
CRYZ	-	0.002350642	0.71641344
TYW3	+	3.1229006e-6	1.3454115
SLC44A5	-	0.001241201	0.9376857
ACADM	+	0.003804285	0.43937844
SAMD13	+	3.243544e-5	-0.8437011
GNG5	-	0.004503373	-0.28663975
AL359762.3	-	0.005188949	-0.29126683
SSX2IP	-	0.009512299	0.5037297
LPAR3	-	9.6343296e-14	-0.94458395
BCL10	-	0.006171701	-0.23004988
DDAH1	-	1.0373593e-4	0.30070424
ZNHIT6	-	8.307622e-5	0.8882336
CLCA4	+	1.4602485e-29	2.0913813
SH3GLB1	+	8.910123e-4	-0.26234493
HS2ST1	+	0.004119559	0.37163746
GBP1	-	4.8175032e-5	1.5854048
GBP2	-	2.853922e-10	-0.72351

LRRC8B	+	7.0459524e-4	0.45030382
AC093423.3	+	0.003619828	-0.6297903
LRRC8D	+	1.9317505e-15	-0.683354
ZNF644	-	3.490001e-5	0.45124975
CDC7	+	0.003446274	0.8286587
RPAP2	+	0.00135953	0.6889769
RPL5	+	1.6091686e-5	0.3520833
CCDC18-AS1	-	0.009106382	-0.49249026
BCAR3	-	3.148494e-6	-0.4657388
DNTTIP2	-	0.002602561	0.40159088
GCLM	-	0.001211724	0.39726526
F3	-	0.001908444	-0.43009967
TMEM56	+	2.3061962e-6	-0.39312878
TMEM56-RWDD3	+	0.006929361	-0.38878697
FRRS1	-	0.002486709	-0.36661735
AGL	+	0.001954327	0.31570494
AC118553.2	+	0.006143179	-0.21582606
MFSD14A	+	3.9375733e-5	-0.45028454
SASS6	-	0.003023017	0.9936573
CDC14A	+	0.005688812	-0.39491302
RNPC3	+	0.005046709	-0.5017695
PRMT6	+	0.001914498	0.8806771
VAV3	-	0.003046617	-0.26140568
HENMT1	-	0.002356213	0.73944426
WDR47	-	0.009517075	0.5129994
TMEM167B	+	4.864875e-5	-0.46640766
SCARNA2	+	4.3077026e-14	-0.63568014
AL356488.2	+	4.1908737e-14	-0.6357972
PSRC1	-	0.0025501	1.3042879
AMPD2	+	0.00190709	-0.53910923
GSTM4	+	3.0792257e-4	0.5450827
GSTM1	+	0.006165781	1.1702559
EPS8L3	-	7.888802e-8	-0.46868184
AHCYL1	+	8.0891605e-4	-0.26206928
AL160006.1	+	0.00362151	-0.69822043
DRAM2	-	5.8754213e-5	-0.40422606
CEPT1	+	0.003499775	-0.30675048
WDR77	-	0.004751881	0.49545598
ATP5PB	+	7.36269e-5	0.33394006
RAP1A	+	3.6887496e-4	-0.31322455
DDX20	+	8.67235e-5	0.7074954
WNT2B	+	2.579832e-4	-0.6246934
RHOC	-	9.145169e-13	-0.55912185
AL603832.3	-	9.996027e-12	-0.6015083
SLC16A1	-	6.0196723e-9	-0.4180347
RSBN1	-	0.001518236	-0.34171435

TRIM33	-	0.001796667	0.33015177
NRAS	-	0.00485131	-0.22295628
CSDE1	-	0.001597105	-0.23457545
IGSF3	-	3.0540767e-5	-0.36539125
TTF2	+	0.002392305	0.5730055
TENT5C	+	0.00522533	0.4070158
WDR3	+	2.101019e-5	0.87319994
HSD3B2	+	1.3128479e-5	-0.5022026
PHGDH	+	8.1250815e-17	1.2496755
HMGCS2	-	1.5027625e-22	-0.72952586
REG4	-	1.7515152e-8	-0.48911497
RNF115	-	0.006326326	0.573401
TXNIP	-	5.957054e-9	-0.42821267
PRKAB2	-	2.497741e-37	-1.0635508
AC242426.2	+	0.004023515	-0.31778005
FMO5	-	1.6149986e-12	-0.6674073
CHD1L	+	0.001651119	-0.34829473
HIST2H2BF	-	1.9147851e-17	1.6109693
HIST2H3D	-	1.899013e-4	1.2519555
HIST2H2BE	-	8.199584e-6	0.66096073
HIST2H2AC	+	5.8650575e-4	0.65346503
HIST2H2AB	-	1.3473492e-7	1.3772658
MTMR11	-	0	-1.166593
OTUD7B	-	0.009223921	-0.22183117
ANP32E	-	4.1259176e-4	0.5403271
MRPS21	+	0.004402627	0.39680216
ADAMTSL4-AS1	-	0.00169944	-0.90711594
MCL1	-	6.767097e-4	-0.23911954
CERS2	-	9.605469e-7	-0.389283
MINDY1	-	8.5870444e-4	-0.34958375
PRUNE1	+	0.005821485	-0.4294178
CDC42SE1	-	1.20160015e-8	-0.50022537
GABPB2	+	0.009431075	0.516159
ZNF687	+	0.001222874	-0.40565467
SELENBP1	-	3.088654e-7	-0.4493469
CGN	+	5.092605e-4	-0.25536072
RORC	-	8.158838e-13	-0.96413386
S100A10	-	1.303557e-4	-0.2636816
S100A6	-	1.8900763e-9	-0.41126046
S100A4	-	0.002249857	-0.46525502
S100A16	-	9.330082e-9	-0.45831007
S100A14	-	2.3552996e-15	-0.5680915
INTS3	+	0.009563851	-0.25451785
CRTC2	-	5.382007e-6	-0.65015453
IL6R	+	2.1907312e-4	-0.4270042
ADAR	-	2.6978092e-12	0.63024104

SHC1	-	5.2720562e-12	-0.625416
ZBTB7B	+	1.3448379e-16	-0.7004537
ADAM15	+	0.005117436	-0.3141253
EFNA1	+	7.008944e-26	-0.92524207
SLC50A1	+	5.904437e-17	-0.7086473
MUC1	-	2.64274e-5	1.2025073
THBS3	-	0.002343394	-0.7450801
CLK2	-	6.732585e-5	-0.55592406
HCN3	+	2.7048077e-12	-1.1206017
FDPS	+	9.327026e-23	-0.6778797
RIT1	-	0.003003378	-0.33658135
ARHGEF2	-	2.059725e-7	-0.44198453
MEX3A	-	0.009992437	1.9240676
PAQR6	-	0.001734471	-1.472741
CCT3	-	2.6245996e-8	0.54958385
MEF2D	-	1.9867184e-7	-0.51987773
IQGAP3	-	1.0223584e-12	1.406403
NAXE	+	0.009382038	0.39869592
GPATCH4	-	8.916295e-9	1.3990648
AL365181.2	-	0.005127322	-0.83394396
AL365181.3	-	0.003097351	-0.4146891
RRNAD1	+	0.009704583	-0.4326201
MRPL24	-	0.001087274	0.7592508
ARHGEF11	-	0.002061338	-0.2642664
KIRREL1	+	3.6587534e-4	0.5383615
IGSF9	-	1.0327996e-5	-0.4633033
PIGM	-	0.001338396	0.83114254
IGSF8	-	0.003009581	-0.32680705
PEA15	+	0.005752505	-0.3017991
COPA	-	5.7904434e-4	-0.26341984
F11R	-	4.0315074e-19	-0.6877985
AL591806.3	-	2.3137342e-18	-0.7188611
TSTD1	-	1.2506262e-5	-0.6209632
NIT1	+	1.3391077e-4	-0.46262482
C1orf226	+	1.5044039e-4	-0.41187388
UAP1	+	1.3459538e-9	-0.56361085
HSD17B7	+	2.8490813e-6	-0.6796342
NUF2	+	0.009434306	1.2081634
UCK2	+	8.009614e-6	0.63149893
GPA33	-	9.090482e-22	-0.6878382
POU2F1	+	1.3076111e-4	0.49403608
MPZL1	+	3.5409637e-5	-0.320909
DCAF6	+	1.460672e-6	-0.44936287
SFT2D2	+	1.4755074e-5	0.36215195
C1orf112	+	0.004194084	0.9864018
PRRC2C	+	7.8305886e-5	0.3488388

EEF1AKNMT	+	2.9332198e-6	0.81580484
PRDX6	+	3.0581745e-5	-0.33275563
DARS2	+	1.6717786e-4	0.55325735
CACYBP	+	2.53741e-6	0.7133072
RALGPS2	+	1.78851e-5	-0.382238
FAM20B	+	0.001822708	-0.29937083
ABL2	-	0.007760787	0.582852
SOAT1	+	0.001327149	0.4914137
TOR1AIP2	-	1.6631346e-13	-0.5123602
AL353708.3	-	0.003884185	-1.3001925
CEP350	+	0.002138519	0.2737025
QSOX1	+	5.133094e-25	-0.83144945
LHX4	+	0.005509765	-0.917514
ACBD6	-	0.002731612	0.8365138
IER5	+	5.4286545e-5	-0.46116278
GLUL	-	1.3255571e-7	-0.40025356
DHX9	+	1.3648335e-8	0.55689853
LAMC2	+	1.3792687e-17	0.71213764
TSEN15	+	0.001914852	0.8233446
TPR	-	0.004543831	0.2779781
ODR4	+	0.008750632	0.40338847
PTGS2	-	0.004092979	5.246848
UCHL5	-	0.00841171	0.3389084
RO60	+	6.37775e-4	0.35176843
CDC73	+	0.005750726	0.29154226
ASPM	-	1.0183859e-18	1.6085076
ZBTB41	-	0.001096143	0.36218393
DENND1B	-	0.00394578	-0.29003665
NEK7	+	0.004563767	-0.28791013
KIF14	-	1.0371842e-5	1.3042314
INAVA	+	5.1487907e-5	-0.36061835
KIF21B	-	4.4357573e-4	0.64236325
PHLDA3	-	0.00566846	-0.32153025
IPO9	+	4.6547273e-9	0.7526111
ELF3-AS1	-	3.6645159999999997e-005	-0.39798346
ELF3	+	3.5997323e-6	-0.33550242
AL691482.3	+	1.0502902e-7	-0.40448818
ARL8A	-	0.00389424	-0.39010718
ADIPOR1	-	2.4127948e-11	-0.57149297
BTG2	+	5.811157e-4	-0.4042611
ATP2B4	+	0.001502223	-0.29620337
SNRPE	+	2.2317823e-4	0.7744992
SOX13	+	6.093717e-6	-0.51641124
REN	-	5.9051513e-38	-1.1434271
GOLT1A	-	1.7956529e-6	-0.74281913

PPP1R15B	-	1.5395466e-5	-0.32458022
RBBP5	-	0.006067881	0.37938243
DSTYK	-	0.003756256	0.712738
CDK18	+	2.3594726e-5	-0.6494349
SLC45A3	-	4.7753947e-9	-0.63374394
NUCKS1	-	2.4148425e-4	0.31713232
CTSE	-	2.2242872e-11	0.8764102
IKBKE	+	5.3778547e-7	1.4774972
MAPKAPK2	+	9.4517236e-5	-0.34450355
C1orf116	-	9.872381e-4	-0.24261831
PFKFB2	+	5.6267254e-8	-0.5048538
YOD1	-	1.9457364e-21	-0.9070292
CD46	+	3.654946e-12	-0.47833145
MIR29B2CHG	-	2.3098255e-4	-0.51609045
PLXNA2	-	0.001267684	-0.2749031
LAMB3	-	0.005560167	-0.23293208
G0S2	+	1.7581558e-4	-0.48287395
IRF6	-	0.002266333	-0.2404021
UTP25	+	2.3277428e-4	1.0551666
SLC30A1	-	0.002961095	-0.25920454
INTS7	-	0.007291636	0.36169586
DTL	+	4.0330878e-10	1.8098904
ATF3	+	1.3642588e-6	0.47748294
FLVCR1	+	3.0382053e-4	-0.34139684
SMYD2	+	1.7610722e-4	0.8544933
PTPN14	-	0.002782018	0.7955951
CENPF	+	3.109945e-19	1.4704671
RRP15	+	2.1701084e-5	1.2495576
SLC30A10	-	8.3092464e-30	-1.0099664
EPRS	-	1.6651185e-5	0.38003063
BPNT1	-	6.16917e-4	-0.29082915
C1orf115	+	4.6738335e-11	-0.5333028
MARC2	+	0.009348873	-0.37749323
MARC1	+	0.002837381	1.0434881
BROX	+	0.00294384	-0.24877205
CAPN8	-	1.586391e-22	-0.7981146
CAPN2	+	2.3188399e-5	-0.28851026
CNIH4	+	0.001976094	-0.30761358
WDR26	-	4.9351584e-8	-0.44852126
H3F3A	+	2.1407734e-6	-0.41825092
ACBD3	-	0.009159487	-0.240255
PARP1	-	4.7405507e-16	0.92535204
ARF1	+	0.001051772	-0.27085245
GUK1	+	6.224134e-4	-0.39262885
TRIM11	-	4.349246e-4	-0.41270643
HIST3H2A	-	0.005633905	1.5302517

HIST3H2BB	+	1.9474214e-4	3.4961352
RHOU	+	9.985619e-7	-0.4584457
NUP133	-	7.3383264e-5	0.5895387
URB2	+	0.002893838	0.75360197
EXOC8	-	0.006311352	-0.34555963
TSNAX	+	0.002835651	0.46606433
TARBP1	-	0.002451341	0.6355585
TOMM20	-	1.6714501e-6	0.48103198
GGPS1	+	6.9264934e-5	-0.4538847
B3GALNT2	-	1.064126e-4	0.6170987
HEATR1	-	1.584505e-15	1.3127109
MTR	+	0.001555092	0.48391625
CHRM3	+	7.994032e-6	0.6395599
FH	-	0.002863095	0.341068
OPN3	-	3.3952942e-4	-0.35194114
EXO1	+	2.1912495e-4	1.6921049
ADSS	-	7.5887376e-4	0.46326807
DESI2	+	9.657982e-4	-0.3107376
HNRNPU	-	6.798776e-7	0.36385345
CNST	+	5.229041e-6	-0.49588215
CR589904.2	-	0.002230274	0.4756797
LYPD8	-	4.8640633e-11	0.60768646
SH3BP5L	-	1.2413219e-4	-0.50595224
ZNF692	-	0.002543418	-0.5753115
ADI1	-	0.005068228	0.30663297
MBOAT2	-	9.133699e-12	-1.0161862
ASAP2	+	7.349152e-5	-0.3255387
ITGB1BP1	-	0.002724529	0.557615
CPSF3	+	0.00583363	0.5015915
ADAM17	-	0.007255101	-0.31892473
RRM2	+	5.622023e-28	1.5443053
HPCAL1	+	4.2629513e-6	-0.56650996
ODC1	-	9.384424e-9	0.6301494
NOL10	-	7.3569434e-5	0.76715624
LPIN1	+	2.8518564e-15	-0.6513845
LRATD1	+	0.001267102	0.30222443
DDX1	+	0.001640093	0.33037344
LAPTM4A	-	0.007176373	-0.21871457
SDC1	-	0.003504412	-0.28692362
ITSN2	-	0.002009166	0.3113291
ADCY3	-	4.3691132e-5	0.8373243
ASXL2	-	0.002502827	0.30613166000000003
MAPRE3	+	1.9477235e-9	-0.63058025
TMEM214	+	3.7075864e-5	-0.38024524
OST4	-	2.2442851e-5	-0.42023408
SLC5A6	-	2.0335636e-5	0.85617024

CAD	+	1.7900025e-10	1.0932511
ZNF513	-	0.00581592	-0.49764103
PPM1G	-	6.3965047e-7	0.53154457
ZNF512	+	7.2109525e-4	0.9785644
GPN1	+	0.001534123	0.6454388
SLC4A1AP	+	0.001305546	0.6032063
FOSL2	+	2.1396072e-6	-0.34212288
WDR43	+	1.7969013e-9	1.0144429
YPEL5	+	1.5148596e-7	-0.58217525
LCLAT1	+	2.2292747e-6	0.96214193
BIRC6	+	0.002178381	0.2585746
TTC27	+	0.001203171	1.057607
LTBP1	+	3.4851091e-6	0.6426849
CRIM1	+	9.491051e-8	-0.42761266
FEZ2	-	0.001837783	-0.32765347
STRN	-	0.008872237	-0.22642311
CEBPZ	-	1.6679251e-6	0.6076562
HNRNPLL	-	0.005295187	0.40015757
SRSF7	-	0.003896536	0.34953207
DHX57	-	5.3088974e-5	1.2414005
MAP4K3	-	0.00371426	-0.33617175
TMEM178A	+	2.1154652e-5	-2.3874488
EML4	+	2.4852456e-10	0.5506887
THADA	-	3.5382564e-6	0.76050586
LRPPRC	-	8.782933e-15	0.7927493
PREPL	-	0.007516025	0.2912258
MCFD2	-	1.5930274e-8	-0.48348057
TTC7A	+	0.001293165	-0.3675467
CALM2	-	4.9164206e-5	-0.288754
EPCAM	+	6.166604e-11	-0.4183293
MSH2	+	9.303021e-7	0.8704533
FBXO11	-	0.001194923	-0.3095255
PSME4	-	5.4511876e-4	0.37844998
SPTBN1	+	9.931437e-12	0.44479442
RPS27A	+	1.5204021e-6	0.43432167
MTIF2	-	7.837366e-5	0.559469
CCDC88A	-	8.348844e-7	0.8976263
PNPT1	-	1.4338962e-5	1.029236
FAM161A	-	0.005528888	2.201129
CCT4	-	1.4188886e-7	0.5397093
B3GNT2	+	9.10843e-5	-0.37469962
EHBP1	+	0.002655286	0.7268019
SLC1A4	+	7.52933e-10	0.89394486
RAB1A	-	0.001054747	-0.25444436
SPRED2	-	6.830831e-5	-0.3633964
MEIS1	+	4.5712822e-4	-1.5162163

WDR92	-	0.006345035	1.1372725
PNO1	+	0.002179647	0.9448797
GFPT1	-	9.754924e-6	-0.3211598
AAK1	-	4.5368038e-6	0.37559947
ANXA4	+	1.000514e-4	0.31418854
MXD1	+	1.3e-43	-0.9204101
PCBP1	+	1.8331866e-5	-0.3235509
PAIP2B	-	0.009249773	0.6335998
RAB11FIP5	-	5.042752e-5	-0.41693935
SMYD5	+	0.002801576	0.99575365
CCT7	+	3.8021258e-7	0.48048365
ALMS1	+	0.004671291	0.5076146
MTHFD2	+	1.7922213e-5	0.46612298
INO80B-WBP1	+	0.001913179	-0.4696469
WBP1	+	0.001036586	-0.5236684
MOGS	-	9.544037e-4	-0.3795579
DQX1	-	9.456238e-5	-0.9283869
AUP1	-	0.00211525	-0.30947027
MRPL19	+	1.9805245e-4	0.46133542
KCMF1	+	5.6938832e-11	-0.52883554
TGOLN2	-	0.009712196	-0.18109153
RETSAT	-	6.3775707e-4	-0.25798276
CAPG	-	6.230055e-10	-0.588762
VAMP8	+	1.4009404e-6	-0.45057783
VAMP5	+	3.1641273e-5	-1.1294708
C2orf68	-	6.92981e-7	-0.6181697
POLR1A	-	4.8529823e-19	1.2558001
PTCD3	+	2.6791386e-4	0.48531297
MRPL35	+	0.008999965	0.31609944
KDM3A	+	6.9740805e-4	-0.30825368
CHMP3	-	0.006209998	0.24489343
RNF103	-	1.6613834e-11	-0.564258
RMND5A	+	1.4646826e-5	-0.37074122
EIF2AK3	-	0.002560799	-0.329478
STARD7	-	0.009984802	0.22048922
TMEM127	-	1.2121535e-7	-0.42849806
NCAPH	+	8.461218e-7	1.3286387
COX5B	+	0.008671575	-0.2421917
ACTR1B	-	5.9990716e-6	-0.4796296
EIF5B	+	2.0932683e-10	0.7090215
NPAS2	+	2.418373e-13	-0.6298878
TBC1D8	-	1.017039e-20	-1.1027604
RNF149	-	5.0403346e-6	-0.44255668
MAP4K4	+	0.002005626	0.4010145
IL1R1	+	3.7156357e-4	1.1107832
IL18R1	+	0.002924479	5.3732076

SLC9A2	+	3.5263055e-9	-0.45190382
MRPS9	+	0.00541199	0.5673653
FHL2	-	6.75448e-8	-0.4201832
NCK2	+	4.570551e-7	-0.4641031
SULT1C2	+	0.00435408	-0.9495475
RANBP2	+	6.482294e-6	0.41663447
SEPT10	-	1.6521097e-13	-0.6229777
SOWAHC	+	1.5718594e-7	-0.48932776
MALL	-	4.587074e-4	-0.33156407
BUB1	-	8.6828695e-15	1.7302421
ANAPC1	-	1.8347835e-5	0.7605875
TTL	+	2.4122305e-4	0.5066056
POLR1B	+	1.2109158e-9	1.272
SLC20A1	+	1.074426e-22	-0.7483611
CKAP2L	-	2.143693e-4	1.0364696
PSD4	+	1.1199581e-5	-0.3940317
PAX8-AS1	+	8.885558e-16	-0.58300966
DDX18	+	6.1093743e-7	0.75668436
INSIG2	+	1.4033607e-7	-0.5224284
EPB41L5	+	0.005658773	-0.28824577
TFCP2L1	-	0.008547865	0.23247197
NIFK	-	5.295254e-6	0.9823199
TSN	+	3.220172e-5	0.52976805
BIN1	-	0.005759936	0.39322436
MYO7B	+	8.100415e-14	-0.64049363
POLR2D	-	6.4397365e-4	0.47511733
UGGT1	+	9.495906e-8	0.4949549
ZRANB3	-	6.55672e-4	1.7014914
R3HDM1	+	2.5561228e-8	0.9079117
MCM6	-	9.6440664e-14	1.2621095
SPOPL	+	0.001179369	-0.3183801
RIF1	+	5.6255477e-8	0.59684193
PRPF40A	-	0.001539157	0.29311422
MARCH7	+	6.2715786e-5	-0.39775237
ITGB6	-	5.5576713e-11	-0.6134895
AC092153.1	-	3.9202383e-5	-0.604547
PSMD14	+	0.008402213	0.3281893
DPP4	-	2.5833655e-8	0.55602175
IFIH1	-	0.004426573	0.6748495
SLC38A11	-	0.001987066	1.3293784
GALNT3	-	4.8759325e-16	-0.5941499
B3GALT1	+	2.0971238e-4	0.52257633
STK39	-	1.7573317e-6	-0.40633947
CERS6	+	1.13416145e-5	0.35550362
NOSTRIN	+	5.1169474e-7	-0.5804593
DHRS9	+	3.798746e-10	-0.50883526

FASTKD1	-	7.933107e-4	0.4618772
SSB	+	3.184415e-7	0.6500164
METTL8	-	3.3768557e-4	0.89594513
DCAF17	+	1.2247103e-4	0.77408355
CYBRD1	+	0.001628928	0.25177354
ITGA6	+	0.008437059	-0.19063783
MAP3K20	+	1.9273193e-7	1.2110384
CDCA7	+	3.0301215e-12	1.2014947
CHRNA1	-	4.6178544e-4	-0.88731754
HAGLR	-	0.006084083	0.33521172
HNRNPA3	+	7.525952e-9	0.5076662
AGPS	+	1.7124244e-4	0.33470592
SESTD1	-	6.8163825e-4	-0.35846743
ITPRID2	+	2.3935897e-14	-0.5460987
DNAJC10	+	1.3101443e-7	0.56766707
NUP35	+	0.004374882	0.99295557
FSIP2	+	0.003955035	0.28256524
TFPI	-	8.953385e-6	-0.5420064
WDR75	+	0.003130749	0.5438571
SLC40A1	-	6.1452074e-4	-0.2495686
PMS1	+	0.003174832	0.69839597
NEMP2	-	0.003046824	1.1331667
STAT1	-	1.5767555e-4	0.4269072
MYO1B	+	2.3141176e-12	0.69916403
NABP1	+	9.844244e-5	-0.52571183
STK17B	-	0.001168137	-0.301835
SF3B1	-	0.003418245	-0.21828693
COQ10B	+	5.3261992e-5	-0.46672165
HSPD1	-	9.362164e-22	0.8764329
HSPE1	+	1.2160452e-13	0.98183227
HSPE1-MOB4	+	1.1872101e-5	0.601917
MARS2	+	0.002524543	0.77344394
SATB2-AS1	+	0.001429742	-0.59623945
C2orf69	+	0.009172238	0.43317884
SGO2	+	0.003200631	0.6034653
BZW1	+	0.003826128	-0.23207949
FAM126B	-	2.6883415e-4	-0.3132326
TRAK2	-	0.001230475	0.3231097
ALS2	-	0.009900251	0.45646447
NOP58	+	1.5830443e-9	1.0153496
FAM117B	+	0.002282052	-0.37548983
WDR12	-	1.0847541e-5	0.87731063
ABI2	+	0.005410667	0.55997145
RAPH1	-	4.355039e-6	-0.37564182
PARD3B	+	0.00535844	0.45905748
EEF1B2	+	0.005883476	0.2524658

FASTKD2	+	6.031528e-5	0.85256404
CCNYL1	+	4.9386796e-4	-0.3295088
RPE	+	0.001522047	0.4283527
LANCL1	-	1.4582594e-5	0.9666481
ATIC	+	1.0350386e-8	0.80062795
XRCC5	+	5.2534553e-5	0.3522524
RPL37A	+	0.002667728	0.25071508
ARPC2	+	1.7493172e-6	-0.34206808
PNKD	+	2.0078638e-11	-0.7014055
TMBIM1	-	3.5705289e-22	-0.64727086
CTDSP1	+	6.246262e-8	-0.5919028
VIL1	+	2.4550062e-14	-0.49891818
TTLL4	+	5.9849623e-4	-0.40902853
IHH	-	0.003375033	-0.60859656
NHEJ1	-	8.0468375e-8	-0.62985814
AC068946.1	-	7.467736e-10	-0.69174016
SLC23A3	-	1.9933881e-5	-0.90627855
CNPPD1	-	1.492885e-5	-0.44992095
RETREG2	+	6.77654e-5	-0.40096408
ZFAND2B	+	5.086275e-10	-0.8455304
ABCB6	-	1.1686661e-10	-0.8115502
AC068946.2	-	1.8606495e-9	-0.6594975
ATG9A	-	3.054832e-8	-0.57812244
ANKZF1	+	1.5500205e-10	-0.65803075
STK16	+	0.001325395	-0.4782891
TUBA4A	-	2.7967772e-7	-0.54498273
GMPPA	+	1.628478e-4	-0.4796665
SGPP2	+	0.002672907	-0.24280028
FARSB	-	2.082963e-8	0.7651969
ACSL3	+	1.9516179e-4	-0.28432995
SERPINE2	-	9.718609e-9	-0.48268545
CCL20	+	5.8491e-26	1.6698853
PID1	-	2.8183993e-5	0.8423431
GPR55	-	9.102176e-6	1.0426182
NCL	-	3.216673e-21	0.8761654
PTMA	+	1.6746395e-10	0.45602396
DIS3L2	+	8.582464e-4	0.712412
GIGYF2	+	0.002385989	0.2953184
KCNJ13	-	5.55727e-6	7.0797086
NGEF	-	2.1990712e-15	-0.94839627
ATG16L1	+	1.9401882e-4	-0.37975276
SCARNA6	+	0.004317313	-0.55452365
DGKD	+	0.008492231	-0.24812418
HJURP	-	2.0674526e-5	1.2762393
MLPH	+	1.6844879e-13	-0.7675282
RBM44	+	0.004707594	-1.1046852

SCLY	+	7.094364e-5	1.3519274
TRAF3IP1	+	7.8715786e-4	0.6850792
CAPN10	+	4.0455944e-7	-0.62347776
GPR35	+	1.1948738e-4	-0.40960473
HDLBP	-	0.0048314	-0.18926845
FARP2	+	0.009202432	-0.22076078
ATG4B	+	6.8318554e-12	-0.7638147
DTYMK	-	0.002274602	0.84685946
AC093642.2	+	0.001251991	-6.1681995
BHLHE40	+	5.823565e-19	-0.6180472
THUMPD3-AS1	-	6.3421226e-8	-0.8049129
SETD5	+	3.642585e-4	-0.31564206
ARPC4-TTLL3	+	0.004689614	-0.28700608
TTLL3	+	6.985262e-14	-1.1105751
CIDEC	-	2.4363096e-6	-1.384272
CRELD1	+	7.4163283e-4	-0.5745287
FANCD2	+	9.360069e-10	1.6033974
SEC13	-	2.3044875000000002e-009	-0.5841011
RAF1	-	6.17955e-5	-0.36675248
NUP210	-	0.002083025	0.9943168
HDAC11	+	4.146487e-5	-0.58393633
SLC6A6	+	3.5426902e-7	-0.6404522
NR2C2	+	5.495905e-5	-0.36621052
MRPS25	-	7.3234685e-4	0.5233009
SATB1	-	1.2766033e-4	-0.3941228
RAB5A	+	2.7183953e-4	-0.3383164
KAT2B	+	4.030311e-4	-0.36069763
THRB	-	1.043462e-5	-0.40326396
RARB	+	0.002419492	-0.8426163
TOP2B	-	2.1221413e-6	0.48135146
SLC4A7	-	2.1059395e-4	0.8152351
TGFBR2	+	9.27835e-4	0.34079722
OSBPL10	-	0.007571405	0.41960266
GLB1	-	1.0554346e-4	-0.33228824
CRTAP	+	2.3021708e-7	0.6933231
UBP1	-	8.022959e-5	0.37645772
CLASP2	-	0.001077789	0.43124726
EPM2AIP1	-	0.004711212	-0.39148295
LRRFIP2	-	1.1681847e-7	-0.45275384
CTDSPL	+	2.0725667e-4	0.42433506
VILL	+	1.7099715e-8	-0.46078035
PLCD1	-	9.022542e-4	-0.4673196
ACAA1	-	3.9061165e-6	-0.42931622
OXSR1	+	0.002094907	-0.26594368
XYLB	+	0.001588521	0.7280202

EXOG	+	0.008153151	1.0397102
WDR48	+	0.002915509	-0.35679978
CSRNP1	-	4.82887e-9	-0.72380596
RPSA	+	1.0340326e-8	0.4566256
ZNF620	+	0.007746833	1.035462
TRAK1	+	4.1178264e-6	-0.3779466
VIPR1	+	5.843152e-8	-0.5480725
NKTR	+	0.003876242	-0.2748133
HIGD1A	-	0.002291851	-0.21793781
ZNF662	+	0.00727217	2.055327
SNRK	+	0.001697783	-0.33102193
ZNF445	-	1.3731483e-4	0.63172257
KIF15	+	8.778874e-8	1.621069
ZDHHC3	-	0.006148354	-0.21422204
CDCP1	-	5.832233e-8	-0.38788283
LARS2	+	2.806049e-4	0.57036173
LIMD1	+	5.528784e-4	0.43721488
ALS2CL	-	1.47858e-40	-1.2581527
SCAP	-	4.392378e-5	-0.44394794
SMARCC1	-	1.5841701e-13	0.86186516
DHX30	+	4.9294706e-4	0.5370635
CDC25A	-	1.1286916e-6	1.1891236
PFKFB4	-	5.4319344e-6	-0.4484787
COL7A1	-	7.783026e-5	-1.4103669
SLC26A6	-	1.6544508e-18	-0.87291753
IP6K2	-	3.962477e-9	-0.5334506
PRKAR2A	-	1.2367067e-4	0.33844575
WDR6	+	8.176373e-9	-0.5436261
IMPDH2	-	1.3671886e-12	0.7547595
QARS	-	0.007093655	0.25046346
CCDC71	-	3.6637695e-4	-0.73776
RHOA	-	0.008370036	-0.18730652
MST1	-	4.0384566e-6	-0.8930527
GMPPB	-	3.1952815e-5	-0.44573537
IP6K1	-	0.007867648	-0.29032195
MST1R	-	5.2228017e-4	-0.35220703
RBM6	+	2.0371942e-8	-0.55020285
RBM5	+	5.9799495e-6	-0.44130024
SEMA3B	+	1.058806e-22	-1.0414625
NAA80	-	2.5740065e-4	-1.2004704
HYAL1	-	2.3024986e-6	-1.1405017
RASSF1	-	0.001355436	-0.5725738
TMEM115	-	0.004410867	-0.40838447
HEMK1	+	0.007935435	-0.48359495
MAPKAPK3	+	0.005499928	0.54181933
DCAF1	-	0.002460102	0.43205276

RAD54L2	+	0.003026717	0.43348256
PCBP4	-	5.194844e-5	-0.74282736
ABHD14A-ACY1	+	2.4673557e-9	-0.6941842
ACY1	+	2.2113905e-10	-0.7311489
TLR9	-	4.941861e-5	-2.6088018
NISCH	+	0.008807391	-0.31777486
PBRM1	-	2.589393e-4	0.35712597
GNL3	+	0.002493329	0.41638303
SPCS1	+	0.001233709	0.39594164
NEK4	-	0.001553656	0.4666919
PRKCD	+	7.219704e-10	-0.57107073
SELENOK	-	0.005112724	-0.44764924
APPL1	+	0.001218241	0.3438348
PDE12	+	0.002077347	0.3511418
ARF4	-	7.502892e-9	-0.4416984
PXK	+	3.4588455e-5	-0.6645422
PDHB	-	0.005935881	-0.31554297
PTPRG	+	3.9643844e-9	1.0058733
CADPS	-	0.008578371	0.42464072
MAGI1	-	2.482675e-5	-0.378829
LRIG1	-	8.916563e-4	1.0080037
KBTBD8	+	2.2685634e-4	1.1396492
TMF1	-	2.4698029e-5	-0.37562042
ARL6IP5	+	3.0564304e-9	-0.4391957
SHQ1	-	0.004462995	0.63222367
GXYLT2	+	0.009708926	0.7196359
ROBO1	-	9.151459e-8	0.85141623
GBE1	-	0.009186318	-0.28414786
PROS1	-	8.501026e-4	-0.39926025
ARL13B	+	0.002440497	1.0968736
MTRNR2L12	-	1.8014805e-7	-2.778164
CRYBG3	+	5.375579e-4	0.3821451
RIOX2	-	1.5883508e-5	1.0003687000000001
CLDND1	-	7.851345e-5	-0.48006967
CPOX	-	3.2968444e-4	0.6548686
DCBLD2	-	3.719705e-7	0.891881
FILIP1L	-	4.0525076e-4	0.7165278
TBC1D23	+	6.2103354e-5	-0.3804375
TOMM70	-	1.719292e-5	0.45503965
ADGRG7	+	3.677164e-5	0.8696712
CEP97	+	8.458512e-5	1.2444111
ALCAM	+	8.364352e-5	0.3988051
CBLB	-	2.9083883e-6	-0.4819143
CIP2A	-	3.0943214e-5	1.5144951
DZIP3	+	0.006655453	0.75658673
CD96	+	0.004629264	1.875828

ABHD10	+	3.3851806e-4	0.86510605
SLC35A5	+	0.008808901	0.35210192
SIDT1	+	0.002009115	-0.37878582
ZDHHC23	+	3.8579383e-4	0.59072775
QTRT2	+	0.005645182	0.5872094
AC093010.3	-	0.004104163	0.91747046
ZBTB20	-	1.7261447e-4	0.8699577
NR1I2	+	5.78794e-7	-0.5722724
LRRC58	-	4.517127e-12	0.8711097
POLQ	-	5.2367645e-6	1.2551087
FAM162A	+	4.304164e-6	-0.434323
PARP9	-	0.003197806	0.6480753
DTX3L	+	2.050986e-10	0.6200282
PARP14	+	2.1224991e-4	0.41820782
PDIA5	+	4.2350855e-4	-0.43757018
ADCY5	-	0.002673888	-0.7355831
HACD2	-	0.003158904	-0.21882428
MYLK	-	1.2599853e-4	-0.2834742
CCDC14	-	1.0128193e-8	-0.5560152
UMPS	+	0.002375171	0.50056696
ITGB5	-	9.741404e-11	-0.56962377
MCM2	+	5.44825e-13	1.5887258
ABTB1	+	2.0807939e-14	-1.2818451
MGLL	-	5.5464276e-11	-0.52274853
SEC61A1	+	2.0051434e-10	-0.44889283
RUVBL1	-	6.362459e-5	0.9040286
EEFSEC	+	0.004716162	0.858361
ACAD9	+	0.002598185	0.62571275
CNBP	-	5.917458e-6	-0.34722808
COPG1	+	0.001719952	-0.23424825
H1FX	-	1.7487913e-4	0.6513741
TMCC1	-	0.001148037	-0.32296422
MRPL3	-	2.1497786e-5	0.5914257
ACAD11	-	7.2624507e-6	-0.6891552
NPHP3-ACAD11	-	2.9343666e-4	-0.48965842
TOPBP1	-	2.3586479e-4	0.49184078
SRPRB	+	2.1118856e-4	0.6224344
SLCO2A1	-	9.1309287e-4	-0.33077595
PPP2R3A	+	7.918971e-4	-0.34783155
RNF7	+	0.002648088	-0.32646862
ATP1B3	+	1.6554832e-11	-0.49612218
GK5	-	0.002264682	-0.2822585
ATR	-	3.220437e-7	0.76228493
CHST2	+	0.002436905	1.0342914
PLOD2	-	4.924476e-23	-0.65180624
PLSCR4	-	0.004976655	-0.39217317

HLTF	-	7.899821e-9	0.94734055
TM4SF1	-	2.1747701e-10	-0.47136316
TM4SF4	+	0.005417149	-1.0517505
COMMD2	-	0.005773185	0.54912686
TSC22D2	+	6.326499e-9	-0.5286395
SERP1	-	1.1836188e-6	-0.39815563
EIF2A	+	0.00346619	-0.3246082
SIAH2	-	2.1766996e-4	-0.45804387
MBNL1-AS1	-	0.002125868	-0.6441822
P2RY1	+	1.077327e-4	0.58643174
GMPS	+	1.603019e-4	0.48611626
CCNL1	-	4.482911e-17	-0.78912175
RSRC1	+	0.008875161	0.5164097
GFM1	+	6.2784145e-10	0.8625709
RARRES1	-	1.9319692e-11	0.95802563
SMC4	+	1.1386037e-4	0.39123523
ARL14	+	0.001408251	-0.55371463
PPM1L	+	0.003168671	0.45713943
GOLIM4	-	6.872915e-4	0.2727709
MECOM	-	5.936921e-10	0.67122066
PHC3	-	0.004665378	0.266689
TNFSF10	-	1.3113924e-4	-0.4546958
ECT2	+	6.2980405e-5	0.47593874
ZMAT3	-	1.0868066e-8	0.644587
ACTL6A	+	1.0060751e-7	0.91887087
MRPL47	-	4.905281e-4	0.64243597
USP13	+	8.4532244e-4	1.4861417
ATP11B	+	1.2263143e-5	-0.3254104
LAMP3	-	0.003578021	1.3055098
B3GNT5	+	6.998985e-19	-0.6434842
AP2M1	+	0.001192088	-0.2512993
EIF4G1	+	0.005907905	0.20666471
FAM131A	+	0.001885608	-0.45437336
CLCN2	-	2.8252953e-5	-0.41561383
POLR2H	+	1.9429104e-5	-0.45422938
MAGEF1	-	3.019153e-4	0.73843884
LIPH	-	0.0057104	-0.22708946
IGF2BP2	-	2.512935e-10	-0.51886284
EIF4A2	+	4.0162626e-17	-0.59415936
RFC4	-	1.4636887e-4	1.1859243
ST6GAL1	+	4.248045e-7	0.5948335
BCL6	-	3.680713e-12	-0.88928056
CLDN1	-	0.003408768	0.53482896
OPA1	+	0.003230738	0.2798601
HES1	+	1.2249767e-9	-0.6909932
LSG1	-	5.495228e-4	0.48550278

APOD	-	0.008493234	-1.291162
MUC20-OT1	+	1.3184445e-13	-0.59294236
MUC20	+	1.1845275e-14	-0.6390041
TNK2	-	1.670557e-6	-0.673691
TFRC	-	1.3551745e-11	0.5791411
SLC51A	+	1.42e-43	-1.2696257
RNF168	-	9.800078e-5	-0.3439751
FBXO45	+	2.9862282e-4	0.5905833
NCBP2	-	4.991821e-4	-0.30753276
PIGZ	-	5.5431215e-12	-0.6152638
RUBCN	-	0.003871724	-0.33522776
LMLN	+	1.796392e-4	0.7705473
MYL5	+	0.003955387	-0.7699746
DGKQ	-	7.2442046e-5	-0.47938803
SLBP	-	0.001806513	0.4700565
TACC3	+	2.5313918e-9	1.1455057
MXD4	-	0.006252768	-0.38107643
TNIP2	-	0.00383541	-0.40482143
SH3BP2	+	2.2797048e-20	-0.8967228
ADD1	+	0.00696785	-0.20971291
NOP14	-	9.093576e-8	0.82214975
HTT	+	5.424278e-4	0.3017442
LYAR	-	3.3468004e-7	1.4630283
S100P	+	1.8169115e-10	-0.49589512
AFAP1	-	0.001474893	0.3110847
FGFBP1	-	2.6908346e-17	-0.7597637
QDPR	-	0.006491779	0.5622851
LAP3	+	0.001340002	0.5069904
NCAPG	+	1.8879386e-7	1.2102774
SEL1L3	-	2.5437772e-4	0.3165702
RBPJ	+	0.001744972	-0.3086656
TBC1D1	+	1.16010826e-10	-0.51313025
KLF3	+	2.4453896e-12	-0.4931664
FAM114A1	+	5.421192e-19	-0.64967114
SMIM14	-	0.00286125	-0.22825962
LIMCH1	+	6.2593445e-4	-0.36376396
TMEM33	+	2.7627018e-6	0.41107163
GUF1	+	0.002200496	0.45836014
GNPDA2	-	0.005772339	0.9473969
ATP10D	+	0.001557159	0.8414682
SLAIN2	+	0.005724965	-0.23873462
DCUN1D4	+	7.565198e-4	-0.38069203
DANCR	+	2.35133e-6	0.94293946
SCFD2	-	0.001072756	0.9225448
LNX1	-	2.954494e-4	-0.6194346
TMEM165	+	9.699552e-8	-0.45057464

CLOCK	-	0.009708619	0.2852467
KIAA1211	+	8.815418e-5	-0.42045426
PPAT	-	1.6860975e-5	1.0551394
PAICS	+	1.0093493e-17	0.96629995
SRP72	+	5.179359e-4	0.39249423
REST	+	1.1858713e-4	0.3871138
SULT1B1	-	1.9460958e-5	-0.31025302
UTP3	+	0.001732831	0.5184754
GRSF1	-	0.001070484	0.29995036
DCK	+	9.0453983e-4	0.6209012
SLC4A4	+	4.7022822e-15	1.006322
COX18	-	0.002720848	0.5788788
ANKRD17	-	0.001191382	0.27144957
CXCL8	+	4.450875e-8	2.1648498
CXCL1	+	7.341742e-8	1.6511569
CXCL3	-	6.013128e-6	1.517349
CXCL2	-	0.003674582	1.752992
EREG	+	1.713242e-12	1.2127404
AREG	+	0.004525667	0.32316902
G3BP2	-	3.2232545e-6	-0.37685755
NAAA	-	3.9994752e-13	-0.5977805
SDAD1	-	0.002251539	0.49031395
ART3	+	8.947779e-5	6.375013
SCARB2	-	8.650479e-4	-0.23734273
CCNI	-	4.0937663e-11	-0.45536074
CCNG2	+	2.793718e-4	-0.32189316
CNOT6L	-	0.001052204	-0.33529338
FRAS1	+	6.502676e-8	1.2200981
ANTXR2	-	2.411146e-6	-0.37337664
HNRNPD	-	8.149641e-9	0.56146103
ENOPH1	+	7.658972e-6	0.7567711
SCD5	-	0.002782575	0.8305322
SEC31A	-	0.003106953	-0.25495705
PLAC8	-	7.968119e-11	-0.6360308
GPAT3	+	0.001116962	-0.33683702
WDFY3	-	1.0473066e-5	0.4989333
PTPN13	+	0.003496504	0.447127
KLHL8	-	7.988592e-4	0.4571746
HSD17B11	-	0.003385242	-0.24287716
FAM13A	-	1.1462517e-33	-0.85327494
GPRIN3	-	1.04397026e-4	0.6349122
CCSER1	+	0.009503671	-0.40950075
SMARCAD1	+	1.9286708e-4	0.6350886
TSPAN5	-	2.442128e-12	-0.7657223
AC114811.2	+	6.9080346e-4	-1.243957
METAP1	+	0.003248638	0.32532674

ADH5	-	0.002856076	-0.31024364
MTTP	+	0.003674796	-0.4239905
DAPP1	+	8.2802115e-5	0.81491196
PPP3CA	-	1.11955975e-4	0.4281878
SLC39A8	-	3.3479805e-13	0.94875944
NFKB1	+	0.003238238	0.30639067
CENPE	-	7.5865006e-15	1.7613889
PPA2	-	0.002210674	0.38513854
GSTCD	+	0.002702021	0.58817506
NPNT	+	0.002755056	-0.2819713
CYP2U1	+	0.006623641	1.0819792
OSTC	+	2.3250857e-5	-0.47264898
EGF	+	8.9600224e-5	-0.6624823
AP1AR	+	6.0382627e-6	-0.48823133
ALPK1	+	0.001484113	-0.5230664
CAMK2D	-	3.5051497e-7	-0.40400502
SNHG8	+	0.003300704	0.55258910000000006
PRSS12	-	1.0477315e-4	-0.39218447
SEC24D	-	5.3904517e-19	-0.8060874
USP53	+	2.7339689e-5	-0.34792477
C4orf3	-	0.001629014	-0.25120983
MAD2L1	-	3.0247176e-7	1.4719052
EXOSC9	+	0.001705226	0.99395466
CCNA2	-	9.977536e-9	1.241577
SPATA5	+	0.002288157	0.92692584
ANKRD50	-	0.004201043	-0.3044784
INTU	+	0.001386829	0.9508728
HSPA4L	+	3.3164207e-11	1.051921
PLK4	+	2.5804444e-5	1.1673034
PGRMC2	-	5.917692e-4	-0.32409376
JADE1	+	0.004157169	0.9886396
NAA15	+	1.05272804e-7	0.616636
SETD7	-	1.0149824e-12	0.7072493
MAML3	-	1.3566704e-6	-0.6131133
SMARCA5	+	1.529604e-5	0.37513867
ABCE1	+	1.8547922e-11	0.9153566
OTUD4	-	0.00643106	0.29712448
LRBA	-	3.9748696e-4	0.30911690000000003
RPS3A	+	0.008718558	0.20774858
FAM160A1	+	0.003153222	-0.25664163
TMEM131L	+	0.0012987	1.6229798
PLRG1	-	0.005780256	0.39328703
GASK1B	-	6.1672044e-6	0.57912135
C4orf46	-	3.9765464e-6	1.7830685
PPID	-	0.005210333	0.43705592
NAF1	-	0.0031543	0.7688664

TMA16	+	0.001609726	1.1866393
MSMO1	+	1.8713494e-33	-0.7796615
DDX60	-	3.2972627e-9	0.9458741
PALLD	+	5.333654e-11	0.7803012
HPF1	-	0.00268579	1.0928813
AADAT	-	0.009721593	1.3837366
LINC01612	+	0.007704155	-0.74684584
TENM3	+	0.001054255	5.678354
IRF2	-	0.002095883	-0.33222255
CENPU	-	0.009603212	0.9285223
ACSL1	-	7.206832e-15	-0.5821624
CFAP97	-	8.74671e-4	0.50404805
SNX25	+	0.009062368	-0.29344913
TLR3	+	3.276289e-4	0.7723808
CYP4V2	+	0.002044919	0.4488468
FAT1	-	0.005833001	0.20552489
SDHA	+	0.005122985	-0.22472343
AC010442.1	-	4.3022126e-5	0.82707584
SLC9A3	-	1.8572167e-7	0.77964795
SLC9A3-AS1	+	5.7606205e-5	-0.8048931
TPPP	-	0.007796445	-0.362127
TRIP13	+	2.2928998e-5	1.8372954
NDUFS6	+	7.013812e-4	0.6012811
ICE1	+	0.001940909	0.41941532
NSUN2	-	1.9948493e-4	0.41021192
SRD5A1	+	0.00110391	0.4783772
SEMA5A	-	3.824914e-6	0.4146489
SNHG18	+	2.547994e-5	-0.6679194
ATPSCKMT	-	0.006562261	0.6699999
CCT5	+	1.8951802e-4	0.33713105
MARCH6	+	0.004566561	-0.22525688
DAP	-	1.3895251e-8	-0.43532592
RETREG1	-	0.005040816	-0.28228295
MYO10	-	1.5299326e-9	0.6012359
BRIX1	+	4.510792e-5	1.030631
LMBRD2	-	0.003586065	0.36022878
SKP2	+	1.1761173e-8	1.0245936
NADK2	-	2.6846605e-8	-0.5924964
CPLANE1	-	8.8569104e-5	0.8010101
NUP155	-	6.4934026e-12	1.080024
WDR70	+	0.001550945	0.75109476
OXCT1	-	4.4048636e-5	0.8141544
SELENOP	-	5.328505e-8	-0.45607963
ZNF131	+	0.006790999	0.52289754
HMGCS1	-	2.9022748e-10	-0.45271432
CCL28	-	3.734595e-15	0.9102467

MRPS30	+	5.1000266e-9	0.84240925
AC093297.2	+	0.005554636	1.0737725
ITGA2	+	1.3830793e-6	-0.47543553
GPX8	+	4.743362e-5	1.6142879
DHX29	-	0.007494837	0.33514145
MTREX	+	0.002626633	0.32963005
PLPP1	-	6.1700978e-18	-0.75101966
MAP3K1	+	0.001018915	0.47977817
SETD9	+	7.673867e-5	-0.6698928
MIER3	-	0.003345481	-0.24641356
DEPDC1B	-	1.837617e-4	1.089433
NDUFAF2	+	0.001704383	1.0725106
IPO11	+	2.8667403e-6	1.0255377
CWC27	+	0.00135255	0.7882041
CENPK	-	7.902178e-5	1.1973102
ERBIN	+	1.2596558e-5	-0.32308885
PIK3R1	+	0.007382438	0.26917115
CCNB1	+	2.1432248e-14	1.3880912
CENPH	+	0.001184191	1.6919904
BDP1	+	1.15584244e-10	0.7300052
MCCC2	+	2.1315022e-7	0.57751375
MRPS27	-	1.8384287e-4	0.5519974
TNPO1	+	7.061447e-5	0.3130207
UTP15	+	2.8293606e-4	1.0060228
ENC1	-	8.708581e-7	0.70353115
NSA2	+	0.002194788	0.4607118
FAM169A	-	1.0137459e-5	0.580354
GCNT4	-	4.956235e-4	-0.47467825
HMGCR	+	1.210194e-15	-0.57225907
F2RL1	+	1.2639423e-6	-0.372251
ZBED3	-	2.1308701e-4	0.75495887
WDR41	-	0.00378468	0.60763127
SCAMP1	+	0.005013479	-0.2983158
LHFPL2	-	0.003301518	-0.2295754
HOMER1	-	0.008065986	1.0310091
MTX3	-	0.001835105	0.80174977
DHFR	-	0.002222847	0.60517305
RPS23	-	7.375684e-9	0.52206516
POLR3G	+	0.003250148	1.1614949
ADGRV1	+	0.005166519	0.7032386
SLF1	+	0.0011321	0.960379
TTC37	-	0.001197345	0.34661308
RHOBTB3	+	1.8354847e-5	0.48227343
GLRX	-	4.71809e-8	-0.5256745
CAST	+	1.3783784e-4	-0.296429
ERAP1	-	0.008664053	0.25882196

ERAP2	+	2.8259772e-5	0.7646985
RGMB	+	3.1702606e-5	0.70138043
PAM	+	0.00176326	-0.24198094
PPIP5K2	+	1.3637685e-4	0.41584536
FER	+	0.005906146	0.4306819
PJA2	-	0.008977948	-0.21269163
WDR36	+	2.0685734e-8	0.93485534
STARD4	-	8.574515e-14	-0.606546
APC	+	0.002502668	0.29287222
REEP5	-	0.007724773	0.2734217
YTHDC2	+	4.205376e-6	0.67762214
FEM1C	-	1.656366e-5	-0.33942455
TICAM2	-	7.682633e-6	-0.8790747
ATG12	-	2.4423428e-4	-0.40041035
AP3S1	+	2.2738014e-10	-0.5127335
LVRN	+	0.009481995	-1.3477725
SEMA6A	-	1.2478664e-7	0.48000288
HSD17B4	+	6.291827e-4	0.28455448
SRFBP1	+	1.823861e-4	0.9289848
CSNK1G3	+	4.6713825e-4	-0.31851435
GRAMD2B	+	2.5582764e-17	-0.7043863
ALDH7A1	-	0.001600328	0.4255145
LMNB1	+	2.6721983e-22	1.2652476
MARCH3	-	3.075877e-4	-0.45546567
PRRC1	+	1.447312e-4	-0.31872055
LINC01184	-	1.6326514e-4	0.84331805
SLC12A2	+	0	1.21975
CDC42SE2	+	7.332239e-7	-0.3900633
P4HA2	-	2.495929e-23	-0.75036913
PDLIM4	+	4.5448982e-5	-0.77602065
SLC22A4	+	8.119828e-4	-0.6245609
SLC22A5	+	1.3361314e-6	-0.47314575
AC116366.3	+	2.4571575e-8	0.5913613
RAD50	+	2.8370991e-8	0.5700812
KIF3A	-	0.002687802	0.511967
SEPT8	-	4.7931617e-6	-0.4159482
SOWAHA	+	6.6980833e-6	-0.51730746
SHROOM1	-	4.556303e-7	-0.63776445
HSPA4	+	0.002887515	0.2708947
VDAC1	-	0.008578329	-0.19390461
TCF7	+	0.002215007	0.7754782
UBE2B	+	6.225431e-5	-0.43335173
JADE2	+	0.009626194	0.64171004
SAR1B	-	0.007214753	-0.22468516
SEC24A	+	6.567765e-13	-0.5754622
DDX46	+	4.4958288e-6	0.5111363

C5orf24	+	6.390084e-4	0.42021757
H2AFY	-	0.002780374	0.24416082
TGFBI	+	1.7365025e-13	0.6378553
SMAD5	+	2.8416158e-5	0.47061488
KLHL3	-	0.001025571	1.7218953
KIF20A	+	4.3159776e-5	1.2835175
FAM53C	+	0.001771763	-0.36392292
EGR1	+	2.6329413e-14	1.0300939
ETF1	-	0.003798443	0.28155112
HSPA9	-	2.5436532e-13	0.6638981
MATR3	+	0.002854903	0.2700907
SNHG4	+	7.076567e-5	1.104464
PURA	+	0.001018107	0.3344224
CYSTM1	+	4.2739784e-6	-0.38320598
HBEGF	-	8.804703e-4	-0.44421187
TAF7	-	0.007291963	-0.2714463
DIAPH1	-	6.793801e-4	-0.25238946
FCHSD1	-	3.295653e-6	-0.8012549
PCDH1	-	1.8888193e-17	-0.66343325
YIPF5	-	1.4643867e-4	-0.38880813
SH3RF2	+	0.002937936	0.31194675
LARS	-	5.1807615e-14	0.8677319
RBM27	+	0.001314353	0.36157072
TCERG1	+	0.00436497	0.3692398
SPINK1	-	4.6504005e-9	-1.2300357
SPINK5	+	0.004211213	0.42050573
PPARGC1B	+	1.5819223e-6	0.6835868
SLC6A7	+	2.144193e-7	-0.9878592
TCOF1	+	5.2162336e-10	1.1996703
CD74	-	8.476659e-6	0.6800349
NDST1	+	1.03263835e-10	-0.69887406
SMIM3	+	0.001518777	-0.38794664
GPX3	+	5.098501e-6	-0.9086423
TNIP1	-	7.049061e-13	-0.56187505
GM2A	+	0.006031662	0.38745108
G3BP1	+	8.5504416e-7	0.42369613
LARP1	+	2.8470168e-7	0.41110417
FAXDC2	-	1.8001702e-10	-1.0617313
GEMIN5	-	3.376489e-8	1.2622508
CYFIP2	+	3.1645488e-4	0.43551618
CCNJL	-	5.5792592e-5	-0.5237356
PTTG1	+	1.2839447e-4	1.118523
MIR3142HG	+	1.7073423e-4	4.459402
HMMR	+	4.9513196e-6	1.0204519
PANK3	-	1.8176908e-5	-0.29220015
SPDL1	+	5.855608e-4	1.0852656

NPM1	+	1.2907098e-13	0.6218239
UBTD2	-	0.001003396	-0.34473905
NEURL1B	+	8.822193e-28	-0.82470673
DUSP1	-	4.5942783e-9	-0.72925764
ERGIC1	+	1.2047895e-4	-0.294362
CREBRF	+	0.00255624	-0.46049392
STC2	-	2.0074984e-4	0.4826009
KIAA1191	-	1.9033502e-6	-0.40984204
ARL10	+	7.834934e-4	1.0212767
NOP16	-	0.001349933	0.8156837
CLTB	-	2.7515396e-4	-0.3571899
CDHR2	+	5.9612044e-5	-0.43787467
NSD1	+	7.1382233e-9	0.5866946
RAB24	-	1.6824768e-5	-0.69712746
MXD3	-	1.5564304e-4	-0.62992877
FAM193B	-	3.45802e-10	-0.84502774
TMED9	+	2.7030987e-7	-0.44370353
NHP2	-	4.8075333e-5	0.756383
PHYKPL	-	1.1257601e-5	-0.43189308
MGAT1	-	4.324172e-5	-0.42981312
BTNL8	+	1.07406464e-4	-0.36485597
BTNL3	+	4.4002835e-4	-0.3236855
TRIM41	+	0.005187375	-0.3807835
DUSP22	+	0.003944992	-0.55207103
GMDS	-	7.0158603e-7	0.4097135
SERPINB6	-	1.9900677e-5	-0.30877247
RIPK1	+	0.002594174	-0.30071118
SLC22A23	-	3.5411313e-7	-0.3988468
EEF1E1	-	0.003339734	0.82225144
PAK1IP1	+	0.001150302	0.9880287
NEDD9	-	6.981499e-5	-0.3081748
EDN1	+	0.005934173	0.6009894
NOL7	+	0.009757534	0.35271904
RANBP9	-	0.0010991	-0.33454147
ATXN1	-	7.2097763e-9	-0.53142774
KIF13A	-	5.9005653e-4	0.3468686
DEK	-	6.2431645e-5	-0.29263785
ID4	+	0.00119899	-0.64685047
ALDH5A1	+	9.467012e-5	0.81603646
TDP2	-	1.1346478e-9	-0.42443362
SLC17A4	+	0.006360499	-0.2833609
HIST1H3A	+	2.3848108e-5	1.1159053
HIST1H4A	+	6.4320266e-5	1.3490607
HIST1H4B	-	1.6354614e-4	0.49458715
HIST1H3B	-	2.4642889e-24	1.6271244
HIST1H2AB	-	1.354725e-9	1.8701768

HIST1H2BB	-	7.650667e-8	1.812989
HIST1H3C	+	9.1068796e-4	1.2198318
HIST1H4C	+	7.75454e-7	0.58993816
HIST1H2BC	-	1.9713364e-6	0.6578562
HIST1H1E	+	2.366835e-11	0.8712708
HIST1H2BE	+	1.1831907e-5	0.7869929
HIST1H4D	-	3.89846e-7	0.82190925
AL031777.3	-	1.8555312e-16	1.158461
HIST1H3D	-	3.7440138e-12	1.308455
HIST1H2AD	-	5.0608945e-10	1.2811413
HIST1H2BF	+	1.4308126e-16	1.6697083
HIST1H4E	+	2.505423e-9	0.6446837
HIST1H2BG	-	5.175679e-12	1.0614003
HIST1H2AE	+	1.5814722e-17	1.414429
HIST1H3E	+	1.3181413e-7	-0.8028142
HIST1H1D	-	8.9788155e-20	1.8523533
HIST1H3F	-	2.3890202e-12	1.4204404
HIST1H2BH	+	2.4529883e-9	0.92186946
HIST1H3G	-	2.3006454e-12	1.5062567
HIST1H2BI	+	1.2452387e-13	1.7498665
HIST1H4H	-	8.089643e-6	0.55140907
HIST1H2BJ	-	1.4970011e-5	0.7967058
HIST1H2AG	+	1.9349732e-6	0.71326673
HIST1H4I	+	1.3647268e-7	1.3703957
HIST1H2BK	-	0.007380849	0.39078367
HIST1H2AH	+	2.3034508e-16	1.7111008
HIST1H2BL	-	4.165492e-11	1.685435
HIST1H2AI	+	2.1536681e-10	1.4273914
HIST1H3H	+	6.3823613e-9	1.1319035
HIST1H2AJ	-	1.1601622e-6	1.5931798
HIST1H2BM	+	4.655514e-9	1.8974724
HIST1H2BN	+	1.4165283e-8	1.152458
HIST1H2AK	-	5.722248e-5	2.0817547
HIST1H2AL	+	5.1667324e-13	2.0166104
HIST1H1B	-	2.9881982e-35	1.6508265
HIST1H3I	-	2.2190168e-10	1.2106895
HIST1H4L	-	4.7062724e-7	1.2463088
HIST1H3J	-	4.0960676e-16	1.3512923
HIST1H2AM	-	3.4031338e-8	1.1216769
HIST1H2BO	+	4.5759905e-14	1.9569277
HLA-A	+	0.002949703	-0.2234005
PPP1R11	+	9.4923606e-5	-0.35276526
RNF39	-	0.001029321	-1.1683267
TRIM31	-	1.166552e-6	-0.37998965
TRIM10	-	0.002969523	-0.64243245
TRIM15	+	5.4652264e-5	-0.43803027

AL662795.2	-	0.006056394	0.7996943
HCG18	-	2.0299037e-4	0.5950662
HLA-E	+	0.005147162	-0.23962133
ABCF1	+	0.001691811	0.32742047
PPP1R10	-	0.008248793	-0.24901778
MDC1	-	5.66028e-4	0.6576979
TUBB	+	1.0162069e-8	0.4190786
FLOT1	-	3.3613848e-13	-0.6382521
DDR1	+	4.4353765e-8	-0.48153597
PSORS1C1	+	5.939035e-5	-0.6185575
TCF19	+	3.7498852e-5	0.78713053
MICA	+	9.5129997e-7	-0.6640141
DDX39B	-	2.973048e-6	-0.37246254
GPANK1	-	6.0654496e-5	-0.8346159
CSNK2B	+	0.007667173	-0.2893681
AL662899.2	+	0.001319048	-0.38142177
LY6G5B	+	1.6250064e-4	-1.081267
DDAH2	-	0.001587038	-0.344212
CLIC1	-	2.2869324e-6	-0.33479497
VARS	-	3.7847934e-7	0.60300344
NEU1	-	5.3955787e-19	-0.74638724
SLC44A4	-	6.338439e-7	-0.3492504
EHMT2-AS1	+	1.6956286e-4	-1.5626934
EHMT2	-	4.4977307e-4	0.696733
NELFE	-	0.00435075	-0.40297776
AL669918.1	-	0.002720088	0.6226741
TAP2	-	1.9870243e-4	0.6915166
RXRB	-	0.001025902	-0.4573012
SLC39A7	+	2.866255e-6	-0.3988163
RPS18	+	3.4752983e-8	0.41305098
B3GALT4	+	0.001098451	-0.6881776
RGL2	-	0.002488632	-0.6182137
ZBTB22	-	3.0707936e-6	-0.7757902
KIFC1	+	1.5485014e-8	1.2711655
PHF1	+	5.2389847e-13	-1.1102796
ZBTB9	+	0.003585661	1.1537734
ITPR3	+	0.001154332	-0.27086747
UQCC2	-	6.6808687e-4	0.76446325
LEMD2	-	4.6356938e-5	-0.44380978
NUDT3	-	5.700207e-6	0.6131456
ILRUN	-	9.255301e-7	-0.40873173
SNRPC	+	0.006094845	0.50520605
UHRF1BP1	+	3.924445e-6	0.7966557
PPARD	+	4.984964e-14	-0.66556233
RPL10A	+	8.0125174e-4	0.2784048
TEAD3	-	1.2401953e-8	-0.753796

FKBP5	-	0.002013072	0.5009259
MAPK14	+	0.005969788	-0.2589599
MAPK13	+	3.328935e-8	-0.41684353
Z84485.1	-	0.004493882	-1.6098521
BRPF3	+	0.0098312	-0.23467481
STK38	-	0.002382572	-0.26972094
CDKN1A	+	1.1337313e-9	-0.4493635
PPIL1	-	7.356234e-4	1.1095067
C6orf89	+	3.6282028e-4	-0.29498458
MTCH1	-	1.6737136e-9	-0.4983647
PIM1	+	1.0552247e-16	-0.630588
ZFAND3	+	1.1958459e-8	-0.49379203
BTBD9	-	0.008010026	-0.24933954
KCNK5	-	5.0602053e-14	-0.6608529
TFEB	-	4.3139778e-4	-0.62104774
BYSL	+	0.001868341	1.1161144
CCND3	-	1.4762224e-4	-0.3992439
C6orf132	-	2.0111404e-6	-0.38494933
TRERF1	-	2.6212126e-4	0.7776098
RPL7L1	+	0.001618338	0.36711878
PEX6	-	4.047263e-7	-0.7099393
KLHDC3	+	2.2475269e-4	-0.44045824
CUL7	-	3.8896027e-4	-0.5721018
KLC4	+	0.001309635	-0.3967749
PTK7	+	0.003815725	0.8669881
DNPH1	-	3.8457982e-4	0.79351525999999994
ZNF318	-	0.003653078	0.37428585
YIPF3	-	0.001448285	-0.3424638
XPO5	-	1.4268196e-7	0.9163549
GTPBP2	-	2.6898871e-17	-0.7356157
VEGFA	+	0	-1.0597419
C6orf223	+	2.2229163e-14	-0.65733427
AL109615.2	+	0.005701234	-0.92264014
MRPL14	-	0.002996742	-0.43892097
TMEM63B	+	5.9996474e-13	-0.64731544
HSP90AB1	+	6.390391e-4	0.26916
MEP1A	+	2.2790853e-16	-0.645159
TNFRSF21	-	3.245763e-17	-0.5888376
CD2AP	+	1.1675698e-5	-0.3079849
MMUT	-	0.008400699	-0.2764523
C6orf141	+	1.0477749e-4	-0.7699591
MCM3	-	1.3876381e-13	0.9825523
TRAM2	-	0.002944956	0.41393042
TMEM14A	+	0.009687361	0.583229
GSTA1	-	4.2192487e-4	1.5318984
ELOVL5	-	0.005515545	-0.25153688

AL033397.1	-	0.001323319	1.7249336
LRRC1	+	0.004153875	-0.22929266
BAG2	+	8.5100004e-7	1.1599988
LMBRD1	-	0.003487219	-0.28141895
SLC17A5	-	1.3835844e-6	-0.44144848
MYO6	+	3.892068e-4	-0.2691524
HMGN3	-	0.004755737	0.7316389
SH3BGRL2	+	0.008560476	-0.20406839
TTK	+	2.6201442e-6	1.4252898
PGM3	-	3.518426e-10	-0.6080523
ME1	-	3.7993587e-4	0.33279216
CYB5R4	+	0.005565198	0.40449408
LINC02535	-	0.002150075	-0.40579912
NT5E	+	2.2146638e-5	-0.33557805
SYNCRIP	-	7.842253e-6	0.39994213
ZNF292	+	0.001490889	-0.28229475
PNRC1	+	2.9481687e-5	-0.37902114
PM20D2	+	3.6328274e-6	0.78255665
UBE2J1	-	4.1506198e-4	-0.28938583
MDN1	-	1.6036105e-16	1.0999746
MANEA	+	0.004065465	0.72243124
FUT9	+	0.005646541	1.0249467
NDUFAF4	-	0.003140175	0.75879043
MMS22L	-	8.784917e-8	1.352151
PNISR	-	3.0961687e-8	-0.5507875
ASCC3	-	2.9779412e-9	0.60576487
PRDM1	+	1.2459351e-6	-0.6610948
CRYBG1	+	0.008100461	0.21126767
QRSL1	+	0.006902541	0.47064218
BEND3	-	0.007298735	0.6486371
SOBP	+	6.8355994e-6	-0.5506289
SNX3	-	0.001441268	-0.26945886
FOXO3	+	6.1049725e-8	-0.38564026
CD164	-	7.755157e-7	-0.33349383
MICAL1	-	6.3722636e-15	-0.777739
CDK19	-	2.2311523e-8	-0.5225811
GTF3C6	+	0.006222229	0.48381373
RPF2	+	9.2876704e-5	0.6974903
AL080317.1	+	0.001247954	0.9059878
REV3L	-	3.313036e-7	0.9336275
MARCKS	+	0.00948218	-0.19742575
RWDD1	+	0.001043328	0.5728586
MCM9	-	0.004432964	-0.3541113
ASF1A	+	0.004237409	0.79997045
SERINC1	-	1.9377336e-5	-0.3316192
PKIB	+	3.196544e-5	-0.33652428

SMPDL3A	+	3.8048124e-11	-0.5574836
TPD52L1	+	4.413803e-4	0.58616054
NCOA7	+	1.1203262e-7	0.77277184
EPB41L2	-	1.2633855e-4	0.32058048
ENPP3	+	6.5622219999999994e-014	-0.6530508
ENPP1	+	4.9687715e-6	-0.46215817
CCN2	-	6.510536e-5	-0.6586688
RPS12	+	8.791394e-12	0.57235247
SGK1	-	2.0207763e-6	-0.83126825
MYB	+	1.3901753e-8	0.68600833
MTFR2	-	0.002796052	1.6641096
BCLAF1	-	5.0429825e-4	0.32167515
TNFAIP3	+	5.554085e-10	0.8242366
PERP	-	2.3024161e-7	-0.35148364
HEBP2	+	2.900029e-4	-0.3198183
HECA	+	4.0185446e-12	-0.5621995
FUCA2	-	5.2986934e-4	0.39065352
PHACTR2	+	0.006757069	0.25911158
LTV1	+	0.005805362	0.6771787
UTRN	+	5.165925e-7	0.77788895
SHPRH	-	0.002926116	0.5884747
STXBP5	+	1.5320427e-4	0.3346669
SAMD5	+	4.4700437e-12	1.3153733
SASH1	+	0.006407185	0.70089823
TAB2	+	6.8580897e-7	-0.41625115
GINM1	+	1.5357882e-6	-0.5263838
NUP43	-	5.683633e-6	0.62563527
PCMT1	+	0.006660322	-0.29382157
AL355312.6	-	7.1999695e-10	-0.580141
LRP11	-	4.1904844e-11	-0.6028245
PLEKHG1	+	1.5240785e-5	0.6271764
MTHFD1L	+	8.29177e-9	1.3337818
FBXO5	-	3.206008e-5	1.4677556
CNKSR3	-	0.001262055	-0.32432485
SNX9	+	2.4227554e-4	-0.28536353
TMEM181	+	1.7089036e-5	-0.34474653
DYNLT1	-	0.002539535	-0.29177788
EZR	-	5.614452e-5	-0.26365027
RSPH3	-	0.002418461	-0.28146803
ACAT2	+	8.837798e-19	-0.6674144
AL162582.1	+	0.003022779	1.9377366
MAP3K4	+	0.001876214	0.5602192
RPS6KA2	-	0.007607368	0.5258439
RNASET2	-	0.008043028	0.33484372
PDGFA	-	5.449472e-6	0.6191567

PRKAR1B	-	2.6284874e-4	0.99635184
SUN1	+	3.3086042e-13	-0.5569202
GET4	+	1.240152e-4	-0.51425135
ADAP1	-	0.00299573	-0.32175836
COX19	-	8.39797e-5	-0.39940962
GPER1	+	0.001335174	-0.544613
ZFAND2A	-	2.1719907e-6	-0.76226145
MICALL2	-	7.406157e-19	-1.0320948
MAFK	+	2.2571369e-6	-0.5219195
TMEM184A	-	1.08886115e-5	-0.6374913
EIF3B	+	2.9946466e-5	0.39617923
GNA12	-	1.5073805e-5	-0.48709086
AP5Z1	+	0.005233592	-0.49042383
WIPI2	+	0.010063777	-0.28079775
AIMP2	+	0.00977782	0.5038334
EIF2AK1	-	3.1618617e-9	-0.50684625
RAC1	+	1.947017e-4	-0.25828925
KDELR2	-	1.9666859e-6	-0.34649816
PHF14	+	3.475302e-4	0.5453832
TMEM106B	+	3.704077e-7	0.5590655
SCIN	+	3.5880669e-6	-0.4425031
ARL4A	+	8.844586e-7	-0.55241305
BZW2	+	2.648916e-6	0.7972593
TSPAN13	+	2.7831125e-18	-0.62850493
AGR2	-	0.004097806	-0.22134049
AGR3	-	0.002901065	-0.34558707
SNX13	-	6.760468e-6	-0.3827008
TWISTNB	-	4.968722e-7	1.2526293
MACC1	-	7.1775845e-5	0.356451
ITGB8	+	1.0219728e-13	0.98617625
CDCA7L	-	8.6809337e-7	1.5608153
CYCS	-	1.03787694e-4	0.30908906
NFE2L3	+	0.002483225	-0.29137692
HNRNPA2B1	-	0.00269259	0.22411071
HOXA7	-	0.005679977	2.0099049
HOXA11	-	0.003483146	1.7365038
HOXA13	-	4.2246298e-5	0.41763803
TAX1BP1	+	0.007155563	-0.23036543
CREB5	+	8.007659e-5	2.3918548
PRR15	+	2.8943464e-7	-0.4551903
WIPF3	+	3.7232649e-6	-0.6160354
GGCT	-	1.936715e-9	0.9531999
AC005154.5	-	5.585208e-5	0.8927766
LSM5	-	0.003083527	0.6194062
NT5C3A	-	0.003602711	-0.32376367
ANLN	+	2.779299e-15	1.2702562

VPS41	-	3.2989883e-5	0.5038268
STK17A	+	3.0122035e-10	-0.635375
COA1	-	0.005424013	0.6533238
URGCP	-	0.00310457	-0.26683885
LINC00957	+	0.008228201	-1.0649978
DBNL	+	4.418133e-11	-0.593288
AC017116.1	+	0.007929594	-0.9572973
POLM	-	0.002560544	-0.5430077
POLD2	-	0.003764211	0.44308692
YKT6	+	1.2089198e-4	-0.345856
TMED4	-	7.970294e-6	-0.38756743
H2AFV	-	9.5008034e-4	0.38687465
PURB	-	2.3482087e-6	0.5690086
SNHG15	-	0.009157939	1.0094697
IGFBP3	-	1.4382785e-5	-0.38879508
UPP1	+	1.4263674e-4	-0.49678358
FIGNL1	-	4.7450543e-5	1.0297756
DDC	-	3.417006e-6	1.012459
COBL	-	4.0680172e-7	-0.43900773
SEC61G	-	0.009714034	-0.35048166
EGFR	+	0.003525695	-0.21624155
VOPP1	-	0.007574914	-0.31666782
CCT6A	+	6.885254e-8	0.5171097
SUMF2	+	2.2533814e-4	0.4182974
GUSB	-	5.6221456e-6	-0.40884218
BAZ1B	-	7.1765835e-6	0.42833212
BCL7B	-	2.1070016e-4	-0.45199677
MLXIPL	-	1.5732658e-38	-1.5146885
VPS37D	+	0.006921158	-1.5040678
STX1A	-	4.6869627e-7	-1.4306945
ABHD11	-	1.5792233e-7	-0.5602298
CLDN4	+	8.250353e-5	-0.6946936
CLIP2	+	5.444216e-9	-0.5733046
GTF2I	+	2.3938678e-6	0.6251117
CASTOR2	+	9.708951e-4	-0.80829525
POR	+	0.001503647	-0.3334823
TMEM120A	-	9.588686e-14	-0.7291906
PTPN12	+	1.8151595e-4	-0.36805487
APTR	-	7.276326e-4	-0.51346517
DMTF1	+	0.009734021	-0.3217756
ABCB1	-	0.001239515	-0.22810927
SRI	-	1.600624e-17	-0.63897395
GTPBP10	+	0.008554069	0.43002772
CLDN12	+	0.001621805	-0.26192996
CYP51A1	-	3.968118e-15	-0.5054437
AC000120.2	-	2.90962e-14	-0.49695793

CDK6	-	1.0071002e-6	0.5923197
BET1	-	5.7554105e-4	-0.6051154
PEG10	+	9.369083e-6	0.3756779
PPP1R9A	+	1.0151362e-10	0.8937435
PDK4	-	0.003372684	-0.61073077
ASNS	-	8.958177e-6	0.4996103
AC079781.5	-	6.582944e-6	0.5067515
BRI3	+	6.341711e-4	-0.436657
BAIAP2L1	-	3.6192246e-13	-0.5598959
TRRAP	+	1.9077605e-5	0.4183071
SMURF1	-	3.9506416e-5	-0.3766446
AC004922.1	+	3.5417982e-6	-0.36316702
ARPC1A	+	1.6327393e-8	-0.43986106
CYP3A5	-	0	-1.1632711
MCM7	-	4.8226007e-10	0.8197941
LAMTOR4	+	0.008505711	-0.370686
MAP11	-	2.6317024e-5	-0.58462757
STAG3L5P-PVRIG2P-PILRB	+	1.1788551e-9	-0.7424593
PILRB	+	1.585492e-8	-0.7417132
TSC22D4	-	1.9814428e-5	-0.54294074
SAP25	-	8.324802e-8	-1.6282761
AC069281.2	-	4.9967246e-19	-1.0221127
LRCH4	-	3.6935825e-17	-0.9447494
GNB2	+	4.3907836e-5	-0.44411898
GIGYF1	-	3.3864166e-5	-0.5878396
EPHB4	-	7.1553094e-4	0.41526002
AC254629.1	-	2.5057278e-13	-1.0129362
MUC12	+	4.1273934e-20	0.746126
MUC17	+	5.282617e-16	-0.5890277
AP1S1	+	0.004244577	-0.29775524
MOGAT3	-	1.7132209e-13	-1.0312877
PLOD3	-	0.00877084	-0.28945538
ZNHIT1	+	0.002002373	-0.38584092
NAPEPLD	-	7.730869e-10	0.56545585
ORC5	-	0.002901419	0.78453577
LHFPL3-AS2	-	0.004880541	-1.4602576
KMT2E-AS1	-	0.00596821	-1.1936432
PUS7	-	1.1330719e-5	0.9922335
HBP1	+	1.2883614e-6	-0.5174463
BCAP29	+	0.001866072	0.5319232
SLC26A3	-	6.0923185e-12	-0.4831521
LAMB1	-	3.2016078e-13	0.78594255
MET	+	0.003980149	-0.24258262
CFTR	+	2.7798965e-6	0.40085313
CADPS2	-	0.002085246	0.57577825

NDUFA5	-	2.0852529e-4	0.48502246
WASL	-	0.003108608	-0.21891545
ZNF800	-	4.08597e-4	-0.37822077
ARF5	+	8.359982e-4	-0.3750268
RBM28	-	3.4286686e-6	0.8300321
HILPDA	+	8.584626e-17	-0.88467276
CALU	+	1.6112776e-13	-0.6670384
UBE2H	-	1.16325815e-7	-0.4453911
CEP41	-	0.009231395	1.0860548
COPG2	-	0.008218306	0.48929977
PODXL	-	0.008456717	1.2819564
CHCHD3	-	3.2910483e-4	0.4419436
AKR1B1	-	0.002276303	1.6266278
NUP205	+	4.0764068e-9	0.74600285
KIAA1549	-	0.001373977	0.70251757
TBXAS1	+	0.004508191	0.5022775
MKRN1	-	4.0397417e-8	-0.4361873
MRPS33	-	2.1421899e-4	0.71160346
SSBP1	+	6.63791e-4	0.56979626
GSTK1	+	0.004676571	-0.25033137
TMEM139	+	5.4872116e-15	-0.8013843
ARHGEF5	+	3.0108233e-6	-0.5452185
CNTNAP2	+	2.4922406e-6	1.42696
PDIA4	-	0.002107169	-0.22123888
ZNF786	-	0.006320768	1.1189107
ATP6V0E2	+	0.006393712	0.70367676
REPIN1	+	0.00566256	0.31897333
AOC1	+	5.0009835e-6	-0.4277297
TMUB1	-	0.002123493	-0.44178927
ABCF2	-	8.9468256e-7	0.85234654
CHPF2	+	1.2656275e-6	-0.62643546
PRKAG2	-	0.006625755	-0.3378409
KMT2C	-	0.00857435	0.20232639
XRCC2	-	0.004536477	1.3132218
PAXIP1	-	0.006756195	0.521316
INSIG1	+	0	-0.95771307
RBM33	+	0.001840663	-0.30490923
AC021218.1	+	0.007762201	-0.2992991
NOM1	+	1.8497774e-5	0.83666605
NCAPG2	-	5.5744543e-14	1.6459775
ESYT2	-	4.088551e-4	-0.27708757
FBXO25	+	0.003996991	0.6855935
CLN8	+	9.216236e-4	-0.45047557
AGPAT5	+	1.5911127e-7	0.56360096
MFHAS1	-	4.861749e-7	0.5447586
PPP1R3B	-	5.8346063e-6	-0.43659163

FDFT1	+	3.8837957e-11	-0.48373592
CTSB	-	8.9761146e-5	-0.30624145
SLC7A2	+	2.6524282e-5	3.2955437
PCM1	+	4.278046e-5	0.39624
PSD3	-	0.001663694	0.34521714
SH2D4A	+	0.003338468	0.631677
LPL	+	9.067671e-8	1.4524419
FAM160B2	+	1.9138504e-7	-0.74942625
HR	-	3.1564052e-6	0.65402037
REEP4	-	0.005520471	-0.3814176
BMP1	+	6.586819e-4	-0.42101023
SLC39A14	+	4.894294e-7	-0.38611698
PDLIM2	+	3.0667114e-4	-0.57952654
BIN3	-	9.6103054e-4	-0.5281537
TNFRSF10D	-	8.452364e-4	-0.3884389
SLC25A37	+	0.005598626	0.6977988
DOCK5	+	4.15489e-6	-0.35106325
KCTD9	-	6.19334e-5	-0.3997408
CDCA2	+	1.08273605e-4	0.80483043
BNIP3L	+	1.4149498e-24	-0.76340747
DPYSL2	+	9.673628e-6	-0.35636416
PTK2B	+	1.6091597e-6	-0.4728228
ESCO2	+	3.8516845e-7	1.2123665
PBK	-	3.1996613e-5	1.2172529
ELP3	+	4.9656077e-4	0.640981
ZNF395	-	5.6630197e-6	-0.3617084
FBXO16	-	0.003969703	-0.3118392
FZD3	+	3.70167e-7	1.0973462
HMBOX1	+	0.001348314	-0.39791486
DUSP4	-	1.6355167e-4	0.5623784
GTF2E2	-	1.1140899e-6	-0.53357065
PPP2CB	-	3.0825306e-6	-0.3633946
MAK16	+	0.006762933	0.6417052
AC124067.4	-	0.004336502	0.8815452
ZNF703	+	2.9302893e-10	0.63867056
ERLIN2	+	0.006898479	0.30068567
TACC1	+	0.001915725	0.32830846
ADAM9	+	2.2015526e-4	-0.26057482
GINS4	+	0.001301942	1.1134521
AP3M2	+	8.928787e-5	1.4388485
IKBKB	+	0.010044124	-0.367789
POLB	+	0.002472056	0.94348305
HOOK3	+	8.6991634e-4	-0.39182454
PRKDC	-	0	1.4386722
MCM4	+	1.2760613999999999e-023	1.4282211

PCMTD1	-	1.8754038e-4	-0.34373087
RB1CC1	-	0.002689373	-0.2722099
LYPLA1	-	0.002813236	0.31708255
MRPL15	+	0.008018914	0.49770567
LYN	+	2.4696243e-5	0.55641764
UBXN2B	+	0.006953527	0.30434144
NSMAF	-	0.002931695	0.6049364
CHD7	+	6.1874033e-4	0.36466128
TTPA	-	0.002976744	1.1855339
PDE7A	-	0.002664667	0.93353105
RRS1	+	1.2474033e-4	1.084132
SNHG6	-	0.008276413	0.67465496
CSPP1	+	0.001035261	0.6404112
LACTB2	-	6.8420713e-4	0.57857096
RPL7	-	0.004458515	0.24330544
TMEM70	+	5.6402705e-8	-0.5477817
GDAP1	+	0.008152645	1.1581994
HNF4G	+	5.643107e-4	0.35043845
ZBTB10	+	0.002562046	0.40987754
ZNF704	-	0.00324055	0.34870738
PAG1	-	3.6248137e-5	-0.28594434
FABP5	+	1.858495e-11	1.3634571
IMPA1	-	1.898455e-4	-0.33966103
LRRCC1	+	1.3457277e-4	0.9397662
CA1	-	8.2868723e-7	0.39593896
CA2	+	3.3051063e-5	0.3075233
WWP1	+	1.6309822e-4	-0.36803374
NBN	-	7.0638277e-9	0.94413614
TMEM64	-	2.5146439e-5	1.1021134
OTUD6B	+	0.004529933	0.8228229
CDH17	-	2.5758857e-9	-0.4420416
GEM	-	0.002133203	-0.8185488
DPY19L4	+	2.3316234e-5	0.69367504
CCNE2	-	0.00187078	1.1934603
TP53INP1	-	5.9367458e-6	-0.478715
PLEKHF2	+	0.007659502	-0.31431425
PTDSS1	+	5.452026e-6	0.6021188
MTDH	+	0.001439315	0.25890917
POP1	+	3.953084e-4	0.93894213
VPS13B	+	1.459445e-4	0.4723763
SPAG1	+	3.0875375e-4	0.5571775
RNF19A	-	0.003316792	-0.24500288
YWHAZ	-	0.004706472	-0.18792826
ZNF706	-	0.003478564	-0.2999542
RRM2B	-	2.686641e-6	0.5374628
KLF10	-	0.001563475	-0.26775056

ATP6V1C1	+	6.4608414e-4	0.39620456
DCAF13	+	3.0820083e-5	0.87334865
OXR1	+	2.6929032e-5	-0.40625498
NUDCD1	-	0.002546157	0.7265052
KCNV1	-	0.001067078	1.6029143
SAMD12	-	1.00327285e-4	0.53303844
MAL2	+	8.403599e-8	-0.36613902
DSCC1	-	0.004132118	1.5177318
ZHX1	-	4.007215e-6	-0.41625294
ATAD2	-	0.001417936	0.4411432
FBXO32	-	2.274196e-4	-0.50150996
FER1L6	+	8.1870087e-7	-0.41331625
TMEM65	-	0.003014442	-0.37172619
NDUFB9	+	0.003163783	0.35680306
SQLE	+	1.8256038e-23	-0.6990143
WASHC5	-	4.237411e-6	0.5656133
LRATD2	-	5.865115e-5	0.49015936
CASC19	-	1.3425357e-10	0.9036175
MYC	+	8.012573e-6	0.8974071
PVT1	+	1.4680806e-5	1.5537117
EFR3A	+	7.728045e-6	0.5096454
NDRG1	-	1.3330352e-25	-0.67937565
PTK2	-	0.005438822	-0.25313514
PSCA	+	0.001193158	-1.0530775
GLI4	+	0.00772529	-0.6800015
TOP1MT	-	7.396074e-4	0.83859783
NAPRT	-	9.12298e-4	-0.5136055
NRBP2	-	2.1157653e-5	-0.7334818
EPPK1	-	1.34027e-7	0.60693383
MAF1	+	4.7516983e-4	-0.40526345
HGH1	+	0.006987778	0.63109356
MROH1	+	3.9957163e-6	-0.5796426
BOP1	-	9.402443e-6	0.9866559
HSF1	+	0.003944419	-0.3602354
DGAT1	-	2.3595403e-5	-0.44449255
SLC39A4	-	2.4851365e-8	-0.6192659
VPS28	-	5.218789e-6	-0.5773455
CYHR1	-	5.9300346e-5	-0.5651228
KIFC2	+	5.4948525e-11	-0.8663524
PPP1R16A	+	2.3827874e-4	-0.4566572
GPT	+	1.6391925e-4	-0.66009945
RECQL4	-	2.541074e-4	0.93704623
ZNF252P-AS1	+	0.00164913	-1.0795423
C8orf33	+	2.7806724e-21	-0.77295893
SMARCA2	+	3.9194006e-4	0.38083872
PUM3	-	2.1388331e-4	0.7105748

GLIS3	-	5.5056637e-10	0.8826527
SLC1A1	+	2.9320773e-4	-0.32833406
RIC1	+	3.2163665e-4	-0.39454398
ERMP1	-	2.0140411e-5	-0.36245084
IL33	+	1.0074195e-5	0.5992568
KDM4C	+	3.8572878e-5	-0.38773492
PTPRD	-	0.001836072	0.76685387
LURAP1L	+	8.0054524e-5	-0.48380926
NFIB	-	0.001002595	0.29489893
SNAPC3	+	0.0037307	-0.27741674
PSIP1	-	4.2241302e-4	0.737822
HAUS6	-	0.008906387	0.43957177
PLIN2	-	0.005422006	-0.22392511
ACER2	+	0.002875132	-0.258059
AL158206.1	+	0.008654144	-0.26045674
MLLT3	-	4.4461915e-5	-0.44570118
MTAP	+	3.92935e-8	0.93432343
C9orf72	-	0.004363351	-0.54489297
DNAJA1	+	2.937405e-8	0.54759234
SMU1	-	0.004415924	0.37332192
B4GALT1	-	3.2129853e-6	-0.35141614
CHMP5	+	2.2257361e-6	-0.43444878
NOL6	-	2.8140415e-4	0.8009466
PRSS3	+	1.3811213e-8	-0.55870444
UBE2R2	+	4.5760457e-12	-0.58281934
UBAP1	+	0.001014049	-0.31862828
FAM219A	-	3.982893e-7	-0.6217577
SIGMAR1	-	0.003100144	0.361516
FANCG	-	0.003895419	0.95532775
STOML2	-	0.006161696	0.36096248
FAM214B	-	1.3065443e-7	-0.6110362
TESK1	+	4.402559e-6	-0.59888333
CCDC107	+	0.007166149	-0.48292702
CA9	+	7.695478e-14	-0.77175224
GBA2	-	2.1627558e-8	-0.45964667
RGP1	+	2.9009638e-7	-0.41007924
TMEM8B	+	1.6597014e-4	-0.58536285
HRCT1	+	8.434118e-8	-1.2129467
GNE	-	4.8546106e-13	-0.5164312
MELK	+	1.7924805e-5	0.84944344
EBLN3P	+	1.8412381e-10	-0.6213722
POLR1E	+	0.001631156	1.0840951
TOMM5	-	0.003607398	0.53912836
SLC25A51	-	9.290359e-11	-0.8577218
ALDH1B1	+	3.077922e-6	0.90275633
AL358113.1	+	0.005296696	-0.2118891

TJP2	+	0.002903892	-0.22364973
ABHD17B	-	0.009845114	-0.37091842
GDA	+	4.6560493e-13	-0.5626816
ZFAND5	-	4.6204435e-4	-0.27753225
ALDH1A1	-	2.3040785e-7	0.4596396
TRPM6	-	1.0648227e-7	0.65602934
NMRK1	-	0.003242317	-0.48831537
OSTF1	+	1.350938e-4	-0.38554022
CEP78	+	5.118823e-13	1.209061
PSAT1	+	1.3470512e-14	0.8386428
TLE4	+	0.00268913	-0.39251447
SLC28A3	-	1.6669676e-4	2.7584145
NTRK2	+	3.8538725e-10	0.55897176
GOLM1	-	0.001108957	-0.22118796
CTSL	+	0.001124707	0.6519457
CKS2	+	3.781324e-5	0.9158035
IARS	-	3.3480177e-18	0.8698757
NOL8	-	0.004116743	0.6344288
CARD19	+	0.002029808	-0.57098037
WNK2	+	0.001082755	0.4961296
FAM120AOS	-	0.001998301	-0.32885587
FBP1	-	0.007837229	0.3784977
PTCH1	-	0.007266157	0.74159515
AL160269.1	-	4.8828058e-4	-0.37677252
SLC35D2	-	3.8389247e-5	-0.39266837
TDRD7	+	0.006476426	-0.29196694
NCBP1	+	0.001361044	0.4111651
ANP32B	+	2.4147618e-4	0.39495003
CORO2A	-	2.2552182e-5	-0.31448287
TEX10	-	0.009572511	0.60479575
MRPL50	-	0.007302729	0.58077806
ALDOB	-	3.5185504e-4	1.2479739
RNF20	+	2.8497612e-5	0.6530937
SMC2	+	4.990787e-13	1.3285664
SLC44A1	+	1.5263504e-5	-0.3290904
FKTN	+	4.3579807e-6	0.7867303
ZNF462	+	4.535889e-4	0.43428734
KLF4	-	2.884699e-12	-0.5585083
EPB41L4B	-	3.4649196e-15	-0.5375385
C9orf152	-	0.006360772	0.30464876
UGCG	+	1.5341559e-10	-0.54905194
HSDL2	+	0.001068285	0.34568423
SNX30	+	9.874362e-4	-0.30317825
BSPRY	+	0.009288604	-0.3630952
HDHD3	-	1.3886983e-10	-0.7170824
ALAD	-	1.564321e-8	-0.58722985

POLE3	-	0.009713366	0.47523227
KIF12	-	2.306688e-11	-1.1612072
AKNA	-	5.24761e-4	-0.50475883
WHRN	-	1.1872408e-7	-0.9654696
ATP6V1G1	+	0.001193031	-0.35261655
TLR4	+	0.007078902	0.45870927
CDK5RAP2	-	6.887876e-5	0.63496906
C5	-	0.00293602	2.0974886
GSN	+	3.5043584e-9	-0.49524787
RC3H2	-	0.009333293	0.23811837
DENND1A	-	6.817279e-5	-0.4158592
NEK6	+	2.9804244e-8	-0.45973924
SCAI	-	0.001131766	0.92842126
ZBTB43	+	3.4332974e-4	-0.43362057
ZBTB34	+	7.724246e-6	-0.52332044
RPL12	-	1.3421628e-6	0.3854073
FAM129B	-	9.553676e-7	-0.46466422
STXBP1	+	1.1788403e-4	-0.44212252
CDK9	+	4.157354e-10	-0.6508498
FPGS	+	0.003117555	-0.42215437
AL162586.1	+	0.0048289	-1.574055
AL157935.2	-	3.857366e-8	-0.50511944
ST6GALNAC6	-	1.8594626e-9	-0.56613505
ST6GALNAC4	-	3.7159186e-4	-0.65228033
PIP5KL1	-	4.0327315e-4	-1.521324
FAM102A	-	1.4307219e-11	-0.6322693
SLC25A25	+	1.5451649e-8	-0.58101946
SLC25A25-AS1	-	4.6523162e-8	-0.5639236
PTGES2	-	7.762368e-4	0.563976
LCN2	+	0	3.4657638
C9orf16	+	0.004683447	0.6022265
GOLGA2	-	4.8806046e-11	-0.5747249
ODF2	+	4.5729903e-4	0.67534995
SET	+	3.928378e-6	0.4010874
LRRC8A	+	1.6788743e-4	-0.42503935
NUP188	+	1.3189872e-8	0.77823025
SH3GLB2	-	3.1036277e-6	-0.5284776
MIGA2	+	7.972458e-8	-0.642412
CRAT	-	5.1794605e-6	-0.4923262
C9orf78	-	0.001425574	0.4740258
EXOSC2	+	4.0517648e-4	0.94814193
NUP214	+	4.562279e-5	0.5088264
DDX31	-	0.001032043	1.1220424
GTF3C4	+	3.6006977e-6	0.727895
RALGDS	-	1.7356452e-8	-0.7619442
AL162417.1	-	6.315764e-6	-0.7194205

SURF6	-	3.018239e-4	0.6065433
SURF4	-	6.8746136e-5	-0.30580977
REXO4	-	0.001804452	0.6095364
CACFD1	+	0.002311154	-0.43225548
RXRA	+	9.2957424e-7	-0.5252139
MRPS2	+	1.2958856e-4	0.98414063
QSOX2	-	1.35874e-5	1.1247569
INPP5E	-	0.001469995	-0.5965632
NOTCH1	-	0.002403215	0.5534946
AGPAT2	-	2.3402247e-7	-0.59935886
TMEM141	+	1.7857548e-5	-0.5066878
AL355987.3	+	1.8113836e-4	-0.60875094
CCDC183	+	4.80156e-40	-1.5683446
AL355987.4	+	1.933908e-37	-1.3445363
AL355987.2	+	2.6665984e-6	-0.63824975
RABL6	+	2.0692374e-5	-0.43121728
AJM1	+	1.471812e-4	-0.76097775
MAMDC4	+	4.7721708e-4	-0.6216299
EDF1	-	3.4464225e-5	-0.3649129
CLIC3	-	5.1436782e-5	-1.22866
ABCA2	-	0.001844562	-0.3802644
SAPCD2	-	4.6309594e-7	1.0218171
TPRN	-	4.7320503e-4	-0.39507064
NRARP	-	5.0426584e-6	0.5594998
EXD3	-	6.6749226e-7	-0.75640196
NOXA1	+	2.7679478e-6	-0.8560203
ENTPD8	-	1.2027622e-6	-0.80546194
ARRDC1	+	0.001962812	-0.45156276
ZMYND11	+	4.8099837e-6	0.5647175
GTPBP4	+	9.965969e-6	0.6462725
IDI1	-	3.386688e-6	-0.33181986
WDR37	+	1.7568718e-5	-0.5683617
PFKP	+	5.5040753e-11	-0.56885177
AL451164.2	+	0.006561623	-0.46174332
KLF6	-	7.072145e-35	-0.82459205
AKR1C3	+	0.004528894	-0.2227081
TUBAL3	-	0.002064673	-0.39890045
NET1	+	0.00124692	-0.24165286
TASOR2	+	3.2586217e-4	0.4181493
PFKFB3	+	7.512761e-4	-0.27299365
LINC02649	+	2.0339021e-4	-1.5359304
TAF3	+	6.8210263e-4	0.8096547
CELF2	+	4.3043343e-5	0.56671333
NUDT5	-	5.039628e-4	0.59017247
CDC123	+	6.174252e-5	0.6013658
OPTN	+	6.334302e-8	-0.46382117

MCM10	+	2.4106401e-7	1.756603
FAM107B	-	2.2513846e-4	-0.3649928
SUV39H2	+	0.00472178	0.84128594
NMT2	-	0.002426501	-0.39375427
MINDY3	-	0.006732868	-0.39628023
ARL5B	+	0.007385138	-0.24825607
MLLT10	+	0.004953348	0.5542606
PDSS1	+	0.003791209	0.62654763
ANKRD26	-	0.001733553	0.6044915
WAC	+	6.9736067e-4	-0.2665724
BAMBI	+	4.6795484e-4	-0.57453626
JCAD	-	0.005223198	5.1579247
MTPAP	-	6.887099e-4	0.69741094
PARD3	-	0.004359541	-0.28895015
CCNY	+	3.3551002e-22	-0.72556096
BMS1	+	0.001368242	0.4409432
ZNF487	+	0.001094425	-0.90662193
MARCH8	-	0.001185796	-0.43286264
GPRIN2	-	7.6486906e-8	-0.9398203
WASHC2A	+	2.610931e-5	0.6908954
SGMS1	-	0.003005936	0.4140807
A1CF	-	4.0305115e-10	-0.51460004
CSTF2T	-	0.004849184	0.6205819
ZWINT	-	3.198107e-9	1.1974989
IPMK	-	1.921404e-8	-0.4507592
TFAM	+	3.7330265e-6	0.67775863
SLC16A9	-	7.8332094e-5	-0.48625058
CCDC6	-	0.001007228	0.2721826
ANK3	-	0.0035716	-0.24836975
CDK1	+	4.910933e-7	1.1714851
RHOBTB1	-	3.571656e-8	-0.7760053
ARID5B	+	0.001660508	0.4661198
RTKN2	-	0.001283902	0.9676484
JMJD1C	-	0.003382439	-0.25247476
HERC4	-	2.5301758e-4	-0.34621194
DNA2	-	0.009562468	0.5817499
CCAR1	+	9.2862296e-10	0.68063956
DDX21	+	4.1525745e-16	0.8386844
HK1	+	0.001009779	-0.2729197
TSPAN15	+	0.006129882	-0.28841236
H2AFY2	+	0.008351562	0.847885
SAR1A	-	9.3455403e-4	-0.30614755
PPA1	-	7.7700555e-5	-0.35631353
EIF4EBP2	+	2.0368501e-5	-0.3264582
SGPL1	+	2.6371442e-6	-0.3746341
VSIR	-	0.004777887	-0.58299035

PSAP	-	1.2057498e-12	-0.47123653
DDIT4	+	1.0844756e-4	-0.35895324
MCU	+	0.005713562	-0.27098706
PLA2G12B	-	0.003994042	-0.78921175
P4HA1	-	3.30908e-40	-0.99442273
ECD	-	0.002514972	0.56253856
DNAJC9	-	1.0122632e-5	0.74283177
MRPS16	-	7.2408526e-5	0.47742304
SEC24C	+	4.5191136e-6	-0.37815294
ZSWIM8	+	5.183611e-18	-0.80233437
AC022400.10	+	0.006098078	-1.1148446
AC022400.7	-	0.001510228	-0.49146584
NDST2	-	0.001811585	-0.4795629
CAMK2G	-	2.7542922e-4	-0.38045144
PLAU	+	3.6125083e-4	1.4266986
VDAC2	+	2.550902e-4	-0.31648514
RPS24	+	0.002219941	0.26614362
PPIF	+	1.8044043e-4	0.5458174
ANXA11	-	1.7264634e-5	-0.31276354
PRXL2A	+	1.473038e-9	-0.4475016
TSPAN14	+	0.001809273	-0.28715208
CDHR1	+	1.3033577e-4	-0.496735
ADIRF	+	1.5737108e-8	-0.7105885
GLUD1	-	4.615593e-6	-0.39157087
MINPP1	+	3.9552677e-5	0.56789905
PAPSS2	+	2.6477394e-6	0.330947
STAMBPL1	+	2.4741137e-4	0.711169
FAS	+	0.003588232	0.3830576
LIPA	-	0.005143968	0.38844132
IFIT5	+	0.004784937	0.9728076
KIF20B	+	6.6100654e-9	1.0427608
IDE	-	1.238921e-8	0.607333
KIF11	+	1.6858668e-13	1.3858839
EXOC6	+	7.041298e-5	0.54224145
MYOF	-	0.007627891	0.20084158
CEP55	+	1.9011581e-9	1.2577362
FFAR4	+	8.75277e-4	0.2936105
NOC3L	-	5.8941103e-5	1.236474
HELLS	+	2.4197198e-16	1.6282064
CYP2C18	+	4.085782e-6	1.1022584
AL583836.1	+	0.002289306	0.8586857
ALDH18A1	-	1.0684789e-18	-0.63294184
ENTPD1-AS1	-	8.045747e-5	0.90020263
RRP12	-	0.001284534	0.81003124
PGAM1	+	2.1604194e-7	-0.4265498
ZFYVE27	+	1.7230888e-10	-0.86966133

SCD	+	6.069377e-17	-0.564832
OLMALINC	+	0.001762334	-0.4356232
SLF2	+	3.867471e-6	0.63211244
TWNK	+	6.0558114e-7	1.8526465
SFXN3	+	5.8446044e-8	-0.63610244
KAZALD1	+	0.002391586	-1.0262111
NPM3	-	9.7306276e-4	1.5865729
OGA	-	6.152605e-4	-0.29440096
PPRC1	+	1.49706375e-5	0.8586371
NOLC1	+	2.0566744e-20	1.2044814
GBF1	+	0.001048919	-0.2697071
ACTR1A	-	6.771496e-4	-0.307853
SFXN2	+	0.0090789	0.89137715
PDCD11	+	2.593262e-10	1.0173254
NEURL1	+	0.00970087	-0.83714175
SH3PXD2A	-	1.4314559e-10	-0.46394587
COL17A1	-	1.359015e-16	-0.54003567
GSTO2	+	0.00844203	0.81191397
MXI1	+	1.1485999e-15	-0.61811215
DUSP5	+	2.2934728e-13	-0.59517235
SHOC2	+	9.6902583e-4	-0.28105712
ADRA2A	+	8.114111e-4	0.92109674
ACSL5	+	5.8295243e-21	-0.7542217
TCF7L2	+	1.880427e-15	-0.5755601
PLEKHS1	+	2.0732316e-5	0.78562176
DCLRE1A	-	0.007629909	0.70258206
VWA2	+	4.4162302e-10	2.2651122
TRUB1	+	0.001971759	0.63543993
HSPA12A	-	0.003445003	0.65714324
SHTN1	-	1.6416592e-5	0.5926492
PDZD8	-	6.2375714e-4	0.2981465
EIF3A	-	4.2954198e-13	0.5752368
SFXN4	-	0.004291287	0.8312803
PRDX3	-	3.6077898e-5	0.4091981
TIAL1	-	1.4824084e-6	-0.4060005
INPP5F	+	0.005408444	-0.34876055
TACC2	+	0.005176276	0.2796543
PLEKHA1	+	8.0350316e-7	-0.3998121
ACADSB	+	6.24433e-4	0.6286094
FAM53B	-	1.6976702e-4	-0.3617689
ZRANB1	+	2.3364618e-4	-0.41041276
BCCIP	+	8.418335e-6	0.7619205
MKI67	-	0	1.6258383
PPP2R2D	+	1.5864804e-4	-0.44897836
PWWP2B	+	0.002658744	-0.48207954
INPP5A	+	1.0622914e-5	-0.5478404

ADAM8	-	1.7798055e-8	-1.0466049
ZNF511-PRAP1	+	9.506448e-6	-0.6378954
PRAP1	+	9.365987e-8	-0.8047313
BET1L	-	2.0885871e-12	-0.7669283
RIC8A	+	0.005026138	-0.30932027
PGGHG	+	4.205667e-7	-1.2097114
PKP3	+	0.001533237	-0.32416308
SIGIRR	-	1.2591613e-6	-0.6923047
ANO9	-	2.6237936e-15	-0.89332974
LMNTD2	-	2.7817767e-4	-0.97365564
AP006284.1	+	1.3355515e-7	-1.2560014
RASSF7	+	1.3891029e-6	-0.56190324
MIR210HG	-	1.4011788e-20	-1.1479428
CDHR5	-	2.4918966e-6	-0.42235985
EPS8L2	+	9.374682e-15	-0.74022096
PNPLA2	+	9.4725824e-11	-0.69058347
CRACR2B	+	0.003905632	-0.53629094
POLR2L	-	0.001460406	0.52708125
CHID1	-	4.5407785e-4	0.6134547
MUC5AC	+	2.2301003e-5	1.8098823
MOB2	-	1.8175192e-4	-0.62902784
SLC22A18	+	8.8210864e-4	-0.67857105
CARS	-	0.002190753	-0.2941836
NUP98	-	0.002445055	0.27509013
RHOG	-	7.391769e-4	-0.45973
RRM1	+	2.0058566e-11	0.86009073
TRIM22	+	9.7108196e-4	0.926074
FAM160A2	-	6.604969e-11	-0.6105879
TRIM3	-	5.1542245e-13	-0.8372661
ARFIP2	-	2.4980377e-6	-0.50302243
DNHD1	+	1.6779152e-10	-1.0426114
ILK	+	3.413766e-7	-0.5133963
TPP1	-	8.4538944e-4	-0.2716491
DCHS1	-	0.008876956	1.8210262
RPL27A	+	2.0165408e-4	0.31357515
TMEM41B	-	5.939222e-4	-0.31404966
IPO7	+	4.1943675e-9	0.5056747
ZNF143	+	0.006208134	-0.37251815
SBF2	-	5.3086373e-5	-0.39368942
ADM	+	1.2957172e-5	-0.55397373
MTRNR2L8	-	0.005434558	-5.6919336
CTR9	+	0.009228296	0.2897835
MICAL2	+	0.00135793	-0.2161953
FAR1	+	0.003737352	0.26000047
SPON1	+	1.809858e-15	0.57251817
RRAS2	-	0.009146479	-0.31348482

PDE3B	+	1.7299797e-4	0.55375844
CYP2R1	-	9.0885395e-4	-0.53072137
PLEKHA7	-	2.2677446e-5	-0.3679249
RPS13	-	5.5412584e-5	0.36386487
USH1C	-	0.001199381	-0.28482518
LDHA	+	2.730587e-8	-0.4037689
E2F8	-	7.94643e-4	1.0257695
NAV2	+	1.05489314e-13	1.900221
PRMT3	+	2.0018624e-4	1.1168092
ANO5	+	0.006052614	0.45403922
KIF18A	-	0.007190965	0.8361325
DNAJC24	+	0.002965909	0.88991123
AL035078.4	+	6.153153e-8	0.8586486
RCN1	+	1.3997083e-10	0.8138456
PRRG4	+	6.3932387e-10	-0.55225533
QSER1	+	5.375462e-6	0.50941354
AL049629.2	-	4.2308144e-15	-0.5967855
CD59	-	2.1442692e-19	-0.659037
FBXO3	-	0.005163314	-0.31581178
CAPRIN1	+	4.012349e-6	0.3558519
NAT10	+	5.8622747e-9	1.046706
EHF	+	1.5522105e-16	0.632345
APIP	-	0.001368718	0.36448556
CD44	+	1.4e-45	1.3042816
TRIM44	+	6.4472845e-9	0.7555439
TRAF6	-	0.009212893	-0.30957156
API5	+	0.002335138	0.27841613
AC068205.2	+	1.1960834e-6	-0.4386056
HSD17B12	+	1.3027419e-9	-0.4204619
SLC35C1	+	0.003024862	-0.3454466
CRY2	+	1.3873038e-5	-0.53854334
CREB3L1	+	7.4616907e-4	-0.41815385
CKAP5	-	9.768276e-10	0.64179987
LRP4	-	2.913424e-24	-0.81884867
MTCH2	-	7.0175587e-4	0.3249786
NUP160	-	3.0388781e-5	0.5851845
TNKS1BP1	-	0.004762607	-0.26239812
SSRP1	-	2.6461163e-13	0.84858423
SLC43A1	-	0.005287624	1.4176204
TMX2	+	3.880629e-4	0.4065012
FAM111B	+	5.534851e-14	1.5305213
FAM111A	+	2.2059797e-4	0.5731548
PATL1	-	3.1790894e-4	-0.32482877
MS4A12	+	3.7770585e-7	-0.76506937
CCDC86	+	0.004647974	0.79473215
PRPF19	-	1.445042e-7	0.7772285

TMEM109	+	0.003442158	0.55700094
TMEM132A	+	2.470102e-4	1.2353251
SYT7	-	8.6419786e-38	-1.0899413
DAGLA	+	0.007113468	0.876151
MYRF	+	3.3063232e-6	-0.5206079
FEN1	+	1.5961667e-10	1.276759
FADS2	+	1.4470666e-6	-0.37181208
FADS1	-	0.005009246	-0.2543581
INCENP	+	1.0401779e-4	0.6048238
ASRGL1	+	2.4369171e-9	1.4471107
LBHD1	-	0.002348057	-0.3622898
STX5	-	2.322018e-4	-0.5100451
PLAAT3	-	0.005925238	-0.44201156
STIP1	+	2.5545562e-5	0.39676753
PLCB3	+	1.88043e-9	-0.5561492
BAD	-	4.384354e-9	-0.73963284
CCDC88B	+	6.169215e-4	-0.7547662
EHD1	-	1.3148341e-4	-0.38984215
MIR194-2HG	-	2.5082636e-35	-1.21383
ATG2A	-	1.4010309e-4	-0.51118594
PPP2R5B	+	5.83853e-7	-0.589231
CDCA5	-	3.9968015e-7	1.4847277
TM7SF2	+	1.5505275e-5	-0.56611454
SYVN1	-	3.8470968e-4	-0.40551242
MRPL49	+	4.151231e-10	-0.6420293
POLA2	+	0.00267999	0.7588439
AP000944.4	-	0.00708403	-1.2071133
FRMD8	+	0.006827628	-0.3361343
NEAT1	+	0	-2.1074414
MALAT1	+	0	-0.9752185
SCYL1	+	0.005149589	-0.33966583
EHBP1L1	+	1.7221264e-8	-0.45821112
MAP3K11	-	1.1405278e-5	-0.4782269
SIPA1	+	7.2366954e-4	-0.5917287
RELA	-	1.656121e-4	-0.41915077
AP5B1	-	0.003321196	-0.3654218
CFL1	-	0.002223152	-0.2051941
MUS81	+	0.001162303	-0.41783643
EFEMP2	-	1.7443288e-8	-2.102902
C11orf68	-	0.002547329	-0.5712661
RAB1B	+	0.002143858	-0.31538996
SLC29A2	-	1.4953374e-6	-0.64452237
SPTBN2	-	2.554356e-4	0.78140086
PC	-	9.5077354e-7	-0.55489296
C11orf86	+	7.3211425e-4	-0.5250465
GRK2	+	4.3369614e-4	-0.35449323

SSH3	+	2.039408e-5	-0.5395234
POLD4	-	2.7125205e-15	-0.6876066
AP003419.1	-	5.1497902e-14	-0.66898686
AIP	+	0.009276146	-0.44812638
PITPNM1	-	1.07138556e-4	-0.4369836
UNC93B1	-	0.006460297	-0.45467326
ALDH3B1	+	0.002808494	-0.4350935
TCIRG1	+	4.2644097e-6	-0.57719594
C11orf24	-	7.899167e-6	-0.519327
CPT1A	-	5.6736952e-11	0.5333121
CCND1	+	7.234652e-6	0.44196555
DHCR7	-	7.0696476e-10	-0.5306978
NADSYN1	+	6.7723518e-6	-0.4173568
INPPL1	+	0.001309691	-0.34636918
CLPB	-	9.4534225e-6	0.8294644
ARAP1	-	4.1956798e-7	-0.55061316
ATG16L2	+	2.4083474e-12	-1.033275
P2RY2	+	2.529808e-6	-0.508333
AP002761.4	+	3.004132e-4	-0.41149643
PPME1	+	0.001743816	0.41132173
KCNE3	-	1.5152181e-10	0.92499113
NEU3	+	9.52165e-5	1.1943285
SLCO2B1	+	8.372841e-9	-0.59913373
ARRB1	-	1.4157146e-15	-0.63367975
AP001972.5	-	2.1980852e-5	-0.48813453
GDPD5	-	0.006613905	-0.8296561
MOGAT2	+	1.6872665e-13	-0.661355
TSKU	+	9.473199e-5	-0.48405892
AP003119.3	+	0.009454888	-0.81108654
B3GNT6	+	0.002907618	-0.56008756
CAPN5	+	1.0417167e-9	-0.49244303
MYO7A	+	0.005779201	-0.6995708
PAK1	-	4.7232263e-4	-0.2945814
AAMDC	+	0.008864937	-0.59109414
ALG8	-	3.1454652e-4	0.7363761
KCTD21	-	0.005285697	-0.348728
USP35	+	0.006727055	-0.61733395
GAB2	-	0.0038528	-0.33866304
NARS2	-	1.8982292e-4	0.86676013
DDIAS	+	1.4288299e-4	1.7790468
CREBZF	-	1.3907357e-6	-0.5161212
PICALM	-	4.7008097e-8	-0.406974
CTSC	-	1.179556e-4	0.43881914
CHORDC1	-	7.161138e-8	0.80914295
SMCO4	-	0.001352044	-0.45120433
C11orf54	+	2.5242698e-6	-0.39804575

PANX1	+	0.002760151	0.57099503
MRE11	-	5.359505e-5	0.9597359
ENDOD1	+	0.002046031	0.29055113
SESN3	-	2.8289644e-5	0.45782572
MTMR2	-	2.2972262e-10	0.8077121
BIRC3	+	3.6151844e-22	0.89634776
BIRC2	+	4.837497e-5	-0.3485987
TMEM123	-	0.010054944	-0.19928187
MSANTD4	-	5.167769e-4	1.0963775
CWF19L2	-	0.003453882	0.6780598
ATM	+	1.2496108e-6	0.8932417
POGLUT3	-	0.001965568	0.5017508
DDX10	+	1.9504538e-5	1.0412884
ZC3H12C	+	1.0773083e-16	1.5197729
PPP2R1B	-	0.003701506	-0.26966494
NXPE4	-	2.1499123e-4	-0.3116371
NXPE2	+	7.0636655e-20	-0.8425853
SIDT2	+	1.0806382e-5	-0.5046285
TAGLN	+	0.009692153	-1.2002435
PCSK7	-	0.001441329	-0.28592107
CEP164	+	0.001456478	0.6511678
TMPRSS4	+	0.002492831	-0.23032063
JAML	-	2.841375e-10	-1.2178209
MPZL3	-	1.2192695e-15	-0.7753196
MPZL2	-	1.1174361e-5	-0.38388687
ARCN1	+	0.001002914	-0.26599818
RPS25	-	2.0311284e-4	0.37496427
HMBS	+	0.007373101	0.60870343
H2AFX	-	9.036375e-4	0.6457647
C2CD2L	+	1.9197583e-22	-0.98882645
HINFP	+	1.05704275e-4	-0.54125965
NLRX1	+	0.002541323	-0.49447408
PDZD3	+	1.0616059e-32	-1.1089208
SC5D	+	1.7685128e-25	-0.7560694
SORL1	+	4.846578e-7	-0.34640226
UBASH3B	+	0.009084241	1.3590407
HSPA8	-	3.4550151e-22	0.7932694
SIAE	-	3.00196e-4	-0.27581486
NRGN	+	0.003250701	0.85712844
VSIG2	-	9.705602e-5	-0.42581978
ESAM	-	0.006183971	-0.4676305
EI24	+	1.0522677e-6	0.5265707
CHEK1	+	2.194624e-7	1.0197644
RPUSD4	-	0.003689947	0.73671156
SRPRA	-	0.009847649	-0.23265752
DCPS	+	0.00913197	0.6689193

GSEC	-	3.2346583e-5	-0.5835302
ST3GAL4	+	1.9505343e-30	-0.929186
BARX2	+	0.008881307	0.5321844
TMEM45B	+	5.847785e-13	-0.5246591
NFRKB	-	0.005233872	-0.3725057
APLP2	+	1.3341969e-6	-0.3338105
ST14	+	6.56246e-4	-0.32035694
NCAPD3	-	5.123228e-11	1.1339116
WNK1	+	1.0257608e-5	0.3467045
ERC1	+	5.5100216e-4	0.42124844
ADIPOR2	+	3.4302445e-7	-0.41678014
FKBP4	+	0.004381645	0.28243116
FOXM1	-	1.2473721e-11	1.1037416
CCND2	+	2.8355102e-29	0.82326096
AC008012.1	+	6.6018214e-7	0.47992557
RAD51AP1	+	1.8450229e-4	1.7461649
NDUFA9	+	0.008301	0.2916361
PLEKHG6	+	5.7904966e-8	-0.51832515
TNFRSF1A	-	1.3731365e-6	-0.41316378
SCNN1A	-	1.108e-42	-1.1170574
AC005840.1	+	8.5248606e-4	-0.37804657
VAMP1	-	0.001216098	-0.68540865
AC006064.5	+	4.332106e-6	-0.5065517
GAPDH	+	2.772291e-6	-0.34468785
NOP2	-	6.1142487e-6	0.8892784
AC006064.6	-	1.5650555e-7	0.46103144
CHD4	-	1.792571e-6	0.41636324
TPI1	+	1.5669876e-7	-0.37200344
ENO2	+	1.0062644e-31	-1.0170114
ATN1	+	0.005429947	-0.2972894
PHB2	-	0.002874587	-0.25162002
EMG1	+	0.001917909	0.56458616
M6PR	-	6.7834125e-4	0.4369077
A2M	-	0.002143215	-1.7561706
GABARAPL1	+	8.729132e-6	-0.77085364
STYK1	-	3.2785454e-5	-0.43329734
CDKN1B	+	1.9953959e-5	-0.4936294
GPRC5A	+	1.422789e-27	-0.7313349
GRIN2B	-	0.007962724	0.3753365
PLBD1	-	0.001399441	0.56661004
H2AFJ	+	0.007859005	-0.34346974
WBP11	-	0.005095682	0.3632333
EPS8	-	9.066378e-5	-0.28368983
MGST1	+	6.100643e-5	0.32002375
AC010197.2	-	3.8267136e-15	0.7178647
LDHB	-	1.3931903e-16	0.7328454

CMAS	+	3.5745442e-17	-0.5970864
ETNK1	+	0.004705026	-0.2251025
INTS13	-	0.00584462	0.43940976
TM7SF3	-	4.6633046e-5	0.38080484
ARNTL2	+	3.8381736e-4	0.51549613
MRPS35	+	3.0997646e-5	0.46320304
KLHL42	+	0.006829043	-0.28306752
IPO8	-	6.98094e-5	0.46238285
DDX11	+	2.107135e-9	-0.78193504
BICD1	+	0.006732122	0.88248134
DNM1L	+	0.003703693	0.3290472
PKP2	-	1.08735065e-8	0.48794365
KIF21A	-	6.311977e-5	0.5557147
SLC2A13	-	7.5183e-12	-0.65752184
PUS7L	-	3.1308007e-6	0.86578599999999994
SLC38A2	-	9.3176916e-26	-0.7198144
RPAP3	-	2.813932e-4	0.70710707
VDR	-	6.132619e-4	-0.2567504
ADCY6	-	1.6326114e-12	-0.57779455
CACNB3	+	0.003142763	-0.4711569
AC073610.2	-	4.409771e-4	-0.30836308
ARF3	-	3.3940224e-4	-0.263736
LMBR1L	-	2.8836657e-4	-0.55788684
TUBA1B	-	6.599835e-4	0.24801967
TROAP	+	0.009770492	0.9246402
RACGAP1	-	3.2810385e-7	0.82407737
METTL7A	+	1.2961985e-4	-0.30876288
SLC11A2	-	0.009757845	0.22629553
DAZAP2	+	0.001504786	-0.2367645
KRT80	-	7.779719e-5	-0.44121233
TNS2	+	0.002937304	-1.039983
SPRYD3	-	0.008615188	-0.35385782
ESPL1	+	1.0761032e-4	1.1492311
SP1	+	1.1062449e-4	-0.29530263
AC023509.1	+	0.001508595	-0.22696954
PCBP2	+	0.00784588	-0.18287611
CALCOCO1	-	5.1330947e-21	-1.028913
CBX5	-	7.432153e-12	0.6026803
HNRNPA1	+	1.1299638e-7	0.44501266
RDH5	+	0.008135567	-0.5396193
ORMDL2	+	0.009871754	-0.29889145
PYM1	-	1.215298e-5	-0.5180942
DGKA	+	2.8724772e-25	-0.8750696
AC034102.1	+	1.403636e-7	-0.39327303
RPS26	+	1.8332894e-5	0.4370278
ERBB3	+	1.16909265e-23	-0.6878186

AC034102.3	+	1.8803467e-4	0.5997864
PA2G4	+	7.9707047e-10	0.6514922
RPL41	+	4.1316024e-11	0.7858593
ESYT1	+	1.7552826e-5	0.4129014
SMARCC2	-	0.002624243	-0.261537
CS	-	8.000845e-6	0.36083806
PAN2	-	0.001863776	-0.4670907
TIMELESS	-	1.3188228e-11	1.2703173
RBMS2	+	4.0579107e-5	-0.42669633
BAZ2A	-	0.004247218	-0.22313575
STAT6	-	7.149174e-10	-0.51245016
LRP1	+	4.501331e-6	-0.42435783
NDUFA4L2	-	2.7911955e-8	-0.62378323
DDIT3	-	5.8777528e-6	-0.9319992
MBD6	+	0.00621875	-0.29899263
DCTN2	-	1.618116e-5	-0.3765674
PIP4K2C	+	5.691506e-4	-0.32362106
OS9	+	1.4522246e-5	-0.31910068
CDK4	-	4.6555035e-9	1.1623352
AC025165.3	+	2.3192704e-4	0.9766778
TSFM	+	2.1148146e-4	0.9809461
CTDSP2	-	7.950532e-28	-0.7607008
LRIG3	-	3.752561e-6	0.764332
PPM1H	-	1.2120731e-6	1.01705
XPOT	+	4.4629826e-7	0.60593116
LLPH	-	0.003344197	0.516305
DYRK2	+	8.283572e-8	-0.40954927
NUP107	+	5.4914586e-4	0.6512559
SLC35E3	+	0.008958455	0.7270736
MDM2	+	0.003800489	0.25557342
LYZ	+	0.009898034	0.16738527
CCT2	+	3.5410515e-9	0.59935874
PTPRB	-	1.2819739e-5	-0.40742612
PTPRR	-	1.9651366e-12	-0.61580765
TSPAN8	-	2.5659322e-6	-0.32054836
ZFC3H1	-	0.007306681	-0.25953493
TMEM19	+	0.002428618	0.46507862
TRHDE	+	3.5947323e-5	-0.6542744
NAP1L1	-	7.1614297e-13	0.6816619
E2F7	-	3.5529607e-4	1.3868138
LIN7A	-	0.00251165	-1.082135
C12orf29	+	0.004634458	0.6589537
TMTC3	+	4.7566064e-4	0.40799278
KITLG	-	4.2743628000000003e-007	0.6345805
DUSP6	-	6.499354e-26	-0.76541054

POC1B	-	0.002241922	-0.36554465
BTG1	-	9.988343e-13	-0.5581428
MRPL42	+	4.362021e-9	0.74236304
VEZT	+	0.003531478	-0.2706282
METAP2	+	2.6762387e-5	0.59160566
NTN4	-	2.3269159e-7	1.1864978
SNRPF	+	3.551412e-5	1.0348547
NEDD1	+	0.002306936	0.58485335
TMPO	+	1.8886985e-9	0.5844023
UTP20	+	1.5145764e-12	1.3418146
ARL1	-	0.006146329	-0.25575677
MYBPC1	+	0.001446865	-0.7382791
DRAM1	+	1.6659325e-6	0.62898475
PARPBP	+	5.256623e-4	1.108207
HELLPAR	+	1.2333147e-4	2.3973422
NT5DC3	-	9.851836e-7	0.70444447
HSP90B1	+	9.3487883e-4	-0.252523
NFYB	-	0.009163786	0.57929736
TXNRD1	+	0.002279547	-0.21374838
C12orf45	+	1.7850631e-8	1.4666952
APPL2	-	1.8507586e-7	-0.4040001
C12orf75	+	7.56799e-4	-0.27011207
TCP11L2	+	6.0906267e-9	-0.78577167
TMEM263	+	5.036414e-5	-0.44643617
CRY1	-	3.2260205e-4	-0.5185703
CORO1C	-	1.9481991e-5	-0.3450588
SSH1	-	6.8577e-4	0.47620818
ALKBH2	-	0.00495769	1.4558506
UNG	+	9.538546e-4	0.56985253
KCTD10	-	7.299711e-4	-0.33454704
MMAB	-	1.8113444e-4	-0.4930389
MVK	+	9.640535e-5	-0.55800056
ANAPC7	-	0.002703772	0.49860534
TCTN1	+	0.009105974	0.96631277
SH2B3	+	2.3259506e-12	-0.5782533
MAPKAPK5-AS1	-	0.00105829	-0.6400085
ERP29	+	0.001228141	0.30474567
TRAFD1	+	2.4020419e-5	-0.5676765
AC004086.1	-	0.008830478	0.23199058
PTPN11	+	1.8396106e-5	0.36468825
AC004551.1	+	1.9815536e-5	-0.33041456
DDX54	-	1.6312236e-4	0.5794668
TPCN1	+	1.2806634e-10	-0.639057
PLBD2	+	1.1825829e-12	0.7772023
RBM19	-	6.6229637e-4	0.6661298
TBX3	-	0.002010315	-0.24587886

WSB2	-	5.958304e-22	-0.71241015
VSIG10	-	3.2047882e-12	-0.5270313
TAOK3	-	0.007412778	-0.23870334
SUDS3	+	0.001709133	-0.2921793
PRKAB1	+	7.161373e-5	-0.45728067
CIT	-	2.9532905e-9	1.4713299
RPLP0	-	0.003820564	-0.2044018
PXN	-	1.2902996e-6	-0.40021265
TRIAP1	-	5.509915e-5	1.2318056
SRSF9	-	3.830736e-7	-0.4477229
RNF10	+	2.2875386e-13	-0.5659613
MLEC	+	8.9686015e-5	0.2979587
HNF1A	+	6.084211e-4	-0.5536166
P2RX4	+	1.8400959e-10	-0.61975896
CAMKK2	-	2.3978257e-4	-0.34546348
ANAPC5	-	2.0329226e-4	0.43684465
ORAI1	+	0.00411447	0.8084935
RHOF	-	3.7687006e-14	-0.61384547
LINC01089	-	2.5818375e-13	-1.4273608
MLXIP	+	0.002505349	-0.23910975
KNTC1	+	0.001890241	0.67219007
DENR	+	0.00550536	0.32469267
HIP1R	+	5.3882627e-7	-0.62159353
VPS37B	-	0.00683975	-0.28530917
PITPNM2	-	1.3203802e-6	-0.62535065
MPHOSPH9	-	3.5231013e-5	0.8793769
DDX55	+	0.004690536	0.7648536
NCOR2	-	0.003720144	-0.26553082
SCARB1	-	1.7475467e-11	-0.65516895
UBC	-	4.313433e-11	-0.49124077
DHX37	-	0.004198511	0.64269024
AACS	+	1.4473523e-4	-0.32642278
STX2	-	0.002933246	1.1023865
RAN	+	9.2556554e-8	0.49400723
ULK1	+	6.9365566e-16	-1.1102195
AC131009.4	+	0.007593463	-1.2454896
PUS1	+	0.002790771	0.8517589
EP400	+	7.4894074e-4	0.37723088
NOC4L	+	0.001924098	1.1351905
PGAM5	+	2.7610158e-5	0.59017336
ANKLE2	-	0.004659569	-0.24468933
GOLGA3	-	6.9204026e-7	-0.40473938
CHFR	-	0.006992546	-0.34424233
ZNF891	-	0.001067062	1.3354908
PSPC1	-	0.003998782	0.489473
ZMYM5	-	1.3748878e-4	-0.5901859

XPO4	-	1.1245656e-8	0.9577088
SKA3	-	0.003432655	0.8365996
SACS	-	0.00146127	1.1665882
MIPEP	-	2.0794068e-5	0.7734342
AL359736.1	+	9.977311e-6	-0.6101754
SPATA13	+	8.9476416e-8	-0.50612116
PARP4	-	0.003356819	-0.22555743
CENPJ	-	1.8904236e-4	-0.66965187
USP12	-	0.008600479	-0.2529956
GTF3A	+	3.6015696e-4	0.54952556
CDX2	-	3.7528003e-9	-0.5513212
SLC7A1	-	2.3398167e-4	0.35349753
HMGB1	-	1.8034111e-4	0.33151215
HSPH1	-	1.5580371e-19	0.9087638
FRY	+	4.6882324e-4	-0.30751798
BRCA2	+	1.0496441e-9	1.346389
RFC3	+	1.7432241e-6	1.4521787
SMAD9	-	2.685154e-4	-0.8766469
UFM1	+	0.001060732	-0.32017505
SLC25A15	+	8.569574e-4	0.9742087
KBTBD6	-	0.006380387	0.98940593
VWA8	-	2.3776762e-5	0.6268141
AKAP11	+	2.9232554e-9	0.6841742
TSC22D1	-	2.152961e-6	-0.33503494
TPT1	-	5.9745886e-4	-0.22443709
TPT1-AS1	+	7.8619475e-4	-0.5262498
ZC3H13	-	5.7569573e-6	0.5815483
LRCH1	+	0.002624558	-0.32003734
ESD	-	3.3646094e-4	0.44484285
RB1	+	0.007686961	0.31351578
RCBTB1	-	9.078202e-5	1.1155417
RNASEH2B	+	0.00985369	0.76537967
CKAP2	+	1.6735145e-5	0.8549592
SUGT1	+	5.7171617e-4	0.3889363
OLFM4	+	2.7450135e-33	0.92437005
DIAPH3	-	1.0867121e-6	1.4851301
DACH1	-	1.8684546e-4	0.748555
KLF5	+	2.3823761e-4	-0.24733555
TBC1D4	-	1.534521e-4	0.4579413
AL137782.1	+	7.2540867e-13	-0.6377833
LMO7	+	6.428818e-14	-0.5604558
FBXL3	-	1.5623783e-7	-0.46114483
MYCBP2	-	1.8696851e-14	0.8717531
NDFIP2	+	6.835027e-5	-0.32262078
SPRY2	-	1.5698737e-7	-0.4845559
MBNL2	+	0.002865062	-0.2800291

IPO5	+	3.6743327e-20	1.0624012
FARP1	+	0.003381084	0.29320815
STK24	-	1.020594e-8	-0.4091949
SLC15A1	-	1.5436322e-4	-0.3585214
DOCK9	-	0.003613148	0.29875207
UBAC2	+	2.5513192e-4	-0.3631759
TPP2	+	1.3881489e-6	0.6729923
BIVM	+	0.001610979	0.5909411
ERCC5	+	0.002948473	-0.28204393
ARGLU1	-	1.5228542e-7	-0.48731247
IRS2	-	3.8941027e-11	-0.69770414
NAXD	+	1.8373238e-4	-0.45355436
ARHGEF7	+	0.0092282	-0.28452522
CUL4A	+	1.1749872e-4	0.43711153
TFDP1	+	4.911707e-7	0.5432757
RASA3	-	1.6866958e-4	-0.9893405
UPF3A	+	0.002393745	0.6141022
CHAMP1	+	0.003208606	0.55097115
AL355075.4	-	3.2858837e-12	-0.60606164
RPPH1	-	3.334665e-12	-0.6060505
TEP1	-	1.6327761e-17	-0.6633949
APEX1	+	3.131204e-7	0.63668686
PIP4P1	-	7.017985e-11	-0.7723645
PNP	+	6.251954e-5	-0.40000615
ANG	+	2.4257377e-11	-0.93684006
RNASE4	+	2.4269104e-19	-0.837854
AL163636.2	+	1.9845976e-20	-0.85854536
TMEM253	+	0.003491964	-0.50667775
SUPT16H	-	2.2877409e-13	0.8134836
CHD8	-	8.242863e-4	0.3368056
DAD1	-	1.2857128e-4	-0.36297312
ABHD4	+	6.503749e-8	-0.58092123
OXA1L	+	1.1831778e-4	0.47874466
MMP14	+	3.5589663e-4	-0.36127973
LRP10	+	7.3763654e-6	-0.38972288
PRMT5	-	0.007494926	0.41790667
AJUBA	-	2.9036159e-5	0.59057355
ACIN1	-	0.00260926	-0.24919929
AP1G2	-	2.5328587e-8	-0.538226
DCAF11	+	0.003630434	-0.27927664
REC8	+	3.0237756e-4	-1.1150509
IPO4	-	7.452649e-6	0.95869726
AL136295.4	-	0.001953607	0.5025713
DHRS1	-	0.004226517	-0.38364896
CIDEB	-	8.655743e-4	-0.69937015
ADCY4	-	2.7345692e-7	-1.550712

RIPK3	-	0.008753107	-0.38821262
NFATC4	+	3.6759313e-9	-2.1343093
NYNRIN	+	5.8253616e-5	-0.6842457
KHNYN	+	3.0162905e-20	-0.6616003
ARHGAP5	+	2.2173584e-10	-0.4593535
EGLN3	-	1.0409052e-37	-0.84186894
FAM177A1	+	0.001193491	-0.28997597
NFKBIA	-	0.007394155	-0.24255367
FOXA1	-	6.324332e-4	0.40411925
SEC23A	-	1.2364812e-5	-0.3331291
PNN	+	0.006776799	-0.2665538
TOGARAM1	+	0.001533324	0.53312093
FANCM	+	1.738346e-4	1.2106235
KLHDC2	+	1.516878e-8	-0.65612984
SOS2	-	7.539472e-6	-0.40769902
NIN	-	1.7405453e-5	0.48832873
TMX1	+	0.001785062	0.3703641
NID2	-	3.3356197e-4	0.71879154
ERO1A	-	4.4074637e-13	-0.47688913
GNPNAT1	-	0.002267584	0.2718741
DDHD1	-	0.001073392	0.7856812
WDHD1	-	3.0400977e-6	1.3471717
SOCS4	+	0.005393704	0.33166423
LGALS3	+	1.9355143e-4	-0.23586482
DLGAP5	-	3.7270662e-10	1.5546085
KIAA0586	+	5.4767897e-5	0.8469543
PCNX4	+	5.833185e-4	0.47624436
PPM1A	+	2.5151181e-5	-0.329155
HIF1A	+	4.2236648e-11	0.5635474
AL137129.1	+	0.009029478	0.6134439
SYNE2	+	3.071709e-13	0.67808235
MTHFD1	+	8.69183e-21	1.1979923
AKAP5	+	0.003177802	0.7135466
GPX2	-	5.703185e-23	0.80868113
MAX	-	3.5801932e-7	-0.5467274
GPHN	+	2.2513137e-4	0.78554654
EIF2S1	+	2.6994527e-4	0.42336747
PLEK2	-	2.463487e-10	-0.68739647
TMEM229B	-	2.0817975e-5	-0.6563255
PLEKHH1	+	0.0033718	-0.25931472
ARG2	+	7.556978e-30	-1.1674253
ERH	-	0.002054391	0.43755707
SUSD6	+	3.422975e-6	-0.43241102
SRSF5	+	4.5564724e-13	-0.65353024
SYNJ2BP	-	5.318176e-4	0.3300354
PCNX1	+	6.677815e-4	0.39686298

SIPA1L1	+	6.1845775e-8	0.62160957
ZFYVE1	-	4.826115e-6	-0.5438639
RBM25	+	0.003213984	0.30250883
PSEN1	+	0.003778218	-0.22928584
PNMA1	-	4.2041562e-10	-0.5181078
ELMSAN1	-	1.5207623e-6	-0.3941006
NPC2	-	0.008028092	-0.2241329
YLPM1	+	5.243448e-8	0.6446781
DLST	+	3.3924315e-4	-0.30947608
TMED10	-	0.002330125	-0.22001529
ERG28	-	1.0539451e-16	-0.72961557
AHSA1	+	0.009302199	0.30222264
TTC8	+	0.007547922	0.80167276
FOXN3	-	3.2417237e-16	-0.6863649
TC2N	-	9.063717e-4	-0.26620308
TRIP11	-	0.001333868	0.33743742
CPSF2	+	1.8203133e-6	0.49100226
GOLGA5	+	0.005949864	-0.3154329
UBR7	+	6.705436e-4	0.55784297
SERPINA1	-	2.4444153e-4	-0.47866637
CLMN	-	1.04568666e-10	-0.47663078
SNHG10	-	4.5874097e-7	-0.558297
SCARNA13	-	1.4930929e-7	-0.5870347
AK7	+	0.001016509	-0.5664409
BCL11B	-	0.001061846	0.78517264
WARS	-	3.5427227e-11	0.9250757
PPP2R5C	+	4.9572423e-6	-0.38824397
DYNC1H1	+	6.698216e-17	0.5869084
HSP90AA1	-	1.291279e-17	0.6578829
ANKRD9	-	3.4953178e-12	-0.6514275
AMN	+	1.5125948e-10	-0.8995691
TNFAIP2	+	7.3531154e-14	2.2705972
EIF5	+	1.6287784e-5	-0.33510673
CKB	-	1.3578543e-12	-0.66305447
TRMT61A	+	0.008548068	0.95695144
KLC1	+	0.003776109	-0.279405
PPP1R13B	-	0.001164872	-0.33376652
INF2	+	0.005490954	-0.27689204
CYFIP1	-	0.00621442	-0.21140711
AC124312.3	+	4.1825208e-4	-1.2070876
HERC2	-	5.0884894e-11	0.69088393
FAN1	+	0.001936633	0.5655654
MTMR10	-	3.3119527e-6	-0.48884496
ARHGAP11A	+	5.6403433e-14	1.3618507
LPCAT4	-	1.4305304e-15	-0.780085
AQR	-	1.5479053e-4	0.45171094

ZNF770	-	0.006330812	0.31415617
FAM98B	+	4.182932e-6	0.82715994
THBS1	+	1.2345042e-18	0.7362137
FSIP1	-	0.004226971	1.6702561
EIF2AK4	+	4.8065383e-4	0.5074491
BMF	-	0.001093672	-0.73816764
BUB1B	+	1.2244336e-10	1.4596981
CCDC9B	-	0.005981382	-0.9215762
DISP2	+	6.995034e-4	-0.5551502
KNSTRN	+	0.004905451	0.5695717
IVD	+	3.5572692e-4	0.5614352
BAHD1	+	0.001152294	-0.3524932
KNL1	+	8.754137e-10	1.0757322
RAD51-AS1	-	6.6832994e-4	-0.91823226
ZFYVE19	+	8.2768365e-6	-0.5918051
SPINT1	+	1.04900025e-14	-0.61190623
CHP1	+	1.1406243e-10	-0.44804713
AC087721.2	+	4.2417567e-5	0.65916
NUSAP1	+	2.8527035e-8	1.1287097
MGA	+	1.3877405e-10	0.7533856
MAPKBP1	+	1.5784786e-7	-0.66145325
JMJD7-PLA2G4B	+	4.5607638e-4	-0.6265157
PLA2G4B	+	0.001654514	-0.80005705
PLA2G4F	-	6.5291544e-12	-0.80262387
TMEM87A	-	1.1295867e-6	-0.443741
ZNF106	-	0.001740505	0.28821394
SNAP23	+	0.005847661	-0.27412975
TTBK2	-	0.006994401	0.6729899
CCNDBP1	+	4.0191016e-4	-0.42306823
TUBGCP4	+	2.683583e-4	0.54528844
TP53BP1	-	0.001250545	0.494052
SERF2	+	0.007746123	-0.22858533
WDR76	+	0.003153123	0.7976996
EIF3J	+	0.002977758	0.35826224
SPG11	-	5.736199e-4	0.3046135
SORD	+	6.015001e-8	0.6480694
DUOXA2	+	5.3055084e-4	-0.6295699
DUOXA1	-	5.803085e-5	-0.8234028
SLC28A2	+	0.009935315	0.23911674
C15orf48	+	0.009723708	-0.20939997
SLC30A4	-	0.007133769	0.42308742
DUT	+	9.0035086e-5	0.83426994
EID1	+	0.002488844	0.47308353
DMXL2	-	0.001045535	0.3031788
TMOD2	+	2.8170552e-4	0.9992553
LEO1	-	1.60274e-4	0.60955215

MAPK6	+	7.718257e-9	-0.49501288
MYO5C	-	9.067847e-6	0.42570367
MYO5A	-	0.006851221	5.0694294
FAM214A	-	0.001052011	-0.44537675
WDR72	-	0.00166236	5.5458155
CCPG1	-	1.0357927e-4	0.39832616
DNAAF4-CCPG1	-	1.2021351e-4	0.41789997
CGNL1	+	0.004833841	-0.8891794
MYZAP	+	2.170691e-22	-0.8697942
GCOM1	+	1.4830977e-32	-0.98476577
MINDY2	+	0.003131566	-0.31204167
CCNB2	+	1.5836344e-4	0.8953321
MYO1E	-	0.002864619	-0.2301585
FAM81A	+	5.576326e-4	0.8069888
GCNT3	+	2.290114e-7	-0.39406872
BNIP2	-	0.001951318	-0.4140918
ANXA2	-	6.074338e-4	-0.26686436
VPS13C	-	1.754441e-10	0.5755639
C2CD4A	+	3.657223e-4	1.625529
TLN2	+	0.001178203	0.3166129
CA12	-	1.4062947e-17	-0.56104165
LINC02568	+	0.005514942	-0.7336639
HERC1	-	0.00687028	0.26834008
DAPK2	-	3.9632272e-14	-0.8925577
AC087632.1	-	7.072653e-4	0.72507219999999994
PCLAF	-	3.5849916e-6	1.1815542
HACD3	+	8.895871e-5	0.42989677
SLC24A1	+	0.004761548	0.8750286
RPL4	-	2.9966337e-4	0.25534943
ZWILCH	+	4.3798796e-6	0.98404986
SMAD6	+	0.003170332	0.87886035
CLN6	-	8.3172505e-5	0.7201783
ANP32A	-	0.008291587	0.2736555
PAQR5	+	3.5579061e-12	-0.5444604
AC027237.1	+	7.4360764e-6	0.9328466
TLE3	-	1.7225058e-6	-0.45344043
UACA	-	6.156032e-8	-0.41244164
PARP6	-	0.002275001	-0.41549578
NEO1	+	4.849423e-7	0.45937324
CD276	+	2.5365094e-7	-0.5069721
ARID3B	+	1.0078135e-7	-0.94250405
CLK3	+	3.037779e-8	-0.5623937
ULK3	-	0.008450313	-0.39007044
FAM219B	-	0.005087557	-0.37949646
COX5A	-	0.004925179	0.26123387
RPP25	-	0.008580838	0.81337065

NEIL1	+	1.4043757e-4	-0.70972407
MAN2C1	-	1.7011058e-7	-0.64131904
SNX33	+	7.4956e-5	-0.41155455
ETFA	-	0.001133997	-0.26113203
RCN2	+	0.002541494	0.47097507
MORF4L1	+	9.27189e-5	-0.31754732
ARNT2	+	4.6737085e-4	1.7176023
ABHD17C	+	0.003710605	-0.2405821
CEMIP	+	5.236103e-7	0.6881855
STARD5	-	0.009058077	-0.3771572
AC245033.4	-	0.002402459	0.30876857
RPS17	-	3.767447e-5	0.34289476
AC245033.1	-	6.141326e-5	0.3387761
ZNF592	+	0.005410371	-0.26660398
AEN	+	5.219907e-4	0.7178555
ISG20	+	1.8056742e-5	-0.7552209
MFGE8	-	7.69941e-5	-0.4184895
ABHD2	+	0.002005638	-0.21817462
FANCI	+	1.3189073e-12	1.3391793
POLG	-	2.9294225e-4	-0.35777882
TICRR	+	5.773408e-6	1.293074
PLIN1	-	5.8833033e-5	-1.0431557
IDH2	-	1.6040813e-4	0.382276
SEMA4B	+	8.296071e-9	-0.55038583
CIB1	-	4.7772126e-19	-0.7370763
GDPGP1	+	1.7556366e-4	-0.5237705
AC091167.2	+	1.1160792e-5	-0.44768453
NGRN	+	1.0900831e-6	-0.45072123
BLM	+	4.412504e-6	1.6168725
FURIN	+	0.001643218	-0.31564876
PRC1	-	3.5812499e-12	1.1101973
AC068831.7	-	2.0062632e-7	0.7428981
LINC01578	+	9.170076e-6	-0.50346196
AC013394.1	+	1.3297172e-4	-0.45424488
CHD2	+	1.1597401e-6	-0.4095078
SYNM	+	4.076285e-5	1.6375649
LYSMD4	-	0.00563431	-0.6455001
CHSY1	-	0.001917563	0.56722736
SELENOS	-	0.00529114	-0.2623343
SNRNP25	+	0.004680235	0.7093407
RHBDF1	-	1.0683575e-5	-0.6388332
LUC7L	-	0.003385957	-0.38803154
FAM234A	+	1.0012666e-5	-0.46613902
Z69667.1	+	1.5554863e-11	-1.5505285
ARHGDIG	+	8.918611e-10	-1.3169476
PDIA2	+	9.779724e-12	-2.1149628

CHTF18	+	1.7945669e-4	1.2401949
BAIAP3	+	0.001079209	-0.7806024
JPT2	+	1.8805217e-7	-0.42338204
MAPK8IP3	+	6.2020853e-13	-0.8442002
EME2	+	6.3039315e-6	-0.6562342
SPSB3	-	0.008495119	-0.5248547
HAGH	-	1.12000256e-4	-0.5683412
RPS2	-	4.1404373e-8	0.44177115
BRICD5	-	2.8559866e-6	-1.0558947
PGP	-	3.153996e-4	-0.46432456
E4F1	+	4.458077e-8	-0.87088376
DNASE1L2	+	0.001587844	-1.5742704
CCNF	+	4.7674308e-5	0.9230704
TEDC2	+	0.008586481	1.9792817
PDPK1	+	0.001251687	-0.2875248
ERVK13-1	-	4.6928616e-12	-0.7918251
KCTD5	+	8.229792e-7	-0.5159338
SRRM2	+	6.993485e-14	-0.50776035
AC092117.1	+	0.009738578	-1.3149946
ZG16B	+	1.8598213e-10	0.94535689999999994
PKMYT1	-	0.009159349	0.9176251
BICDL2	-	8.333193e-5	-0.44889778
IL32	+	1.2117453e-9	0.65480584
TRAP1	-	3.691725e-11	1.0465114
TFAP4	-	0.006616313	1.2712698
AC020663.4	-	0.008834987	-0.6780756
ABAT	+	3.284378e-6	0.7282046
PMM2	+	0.002856411	-0.32628655
AC022167.2	+	0.001626172	-0.48701257
CARHSP1	-	1.4781992e-6	-0.52274674
RMI2	+	2.5057208e-4	1.3036114
LITAF	-	2.1220015e-9	-0.4471438
RSL1D1	-	1.2676217e-12	0.90594405
GSPT1	-	2.0955058e-6	0.41386777
PDXDC1	+	3.577217e-4	-0.26494822
RRN3	-	1.8729457e-7	0.7755321
ABCC1	+	0.006129093	0.35149497
SMG1	-	0.006234911	0.21360923
SYT17	+	3.0079807e-4	-0.65634525
TMC5	+	1.0371979e-5	-0.40445703
GDE1	-	8.391867e-10	-0.46935704
KNOP1	-	0.002871406	0.5345023
GPRC5B	-	0.009519308	1.1817534
THUMPD1	-	0.003494404	0.37479937
TMEM159	+	1.474235e-7	-0.5717941
ANKS4B	+	4.151218e-6	-0.43882763

AC092338.1	-	4.7248133e-4	-0.39599788
USP31	-	1.847319e-11	1.1098255
EARS2	-	0.003019238	0.6976957
UBFD1	+	0.002325254	0.42948693
PLK1	+	3.0930926e-7	1.0638813
ARHGAP17	-	1.5486483e-5	-0.37891665
AQP8	+	2.8091115e-6	0.9889904
IL4R	+	2.4610242e-7	-0.5533938
NUPR1	-	9.2896744e-7	-1.3083981
TUFM	-	0.001993593	0.31167606
QPRT	+	1.0972959e-20	-0.8185923
ZG16	+	1.6275155e-18	-1.1110219
KIF22	+	3.384937e-4	0.8172922
AC009133.1	-	6.3643895e-8	-0.91854364
SEZ6L2	-	0.004538916	-0.349466
TMEM219	+	1.4241628e-4	-0.4441354
TAOK2	+	0.005866944	-0.29818386
HIRIP3	-	6.0863455e-4	1.1158319
AC093512.2	+	8.577077e-4	-0.5870818
ALDOA	+	0.001632797	-0.57953215
PPP4C	+	0.001371411	-0.3388387
YPEL3	-	6.7415154e-22	-1.2898113
GDPD3	-	2.4461054e-4	-0.5511992
MAPK3	-	5.014104e-12	-0.6576829
TBC1D10B	-	0.004040337	-0.32025027
DCTPP1	-	0.003946148	0.440485
FBRS	+	1.5296023e-4	-0.3949818
AC135048.1	+	7.271541e-5	-0.7411855
ORAI3	+	6.2041073e-7	-0.7342769
HSD3B7	+	3.1300253e-5	1.1162901
STX4	+	0.001194986	-0.39696828
AC135050.2	-	0.008103017	-0.44516087
BCKDK	+	2.2200864e-5	-0.59875053
PRSS8	-	8.8338164e-4	-0.6989533
C16orf58	-	9.238405e-4	-0.47329783
SHCBP1	-	1.5781382e-4	1.1228657
GPT2	+	1.1912977e-5	-0.50604343
NETO2	-	0.005255493	0.35737547
ITFG1	-	9.931022e-4	-0.2805403
SIAH1	-	3.8015674e-4	-0.46537277
AC026470.1	-	4.8819147e-6	-0.40955654
HEATR3	+	0.00196064	0.5459147
TOX3	-	8.8685885e-4	-0.33538368
LPCAT2	+	0.003849446	-0.30747926
AMFR	-	6.752206e-5	-0.33478424
NUDT21	-	1.93834e-7	0.6222514

OGFOD1	+	1.0388987e-4	0.7322318
MT2A	+	4.081473e-5	3.7998128
MT1E	+	2.908828e-6	2.8289318
MT1G	-	3.544855e-4	2.46475
NUP93	+	9.817592e-5	0.7941555
HERPUD1	+	3.0626677e-6	-0.43134242
CX3CL1	+	4.9789464e-6	1.9708177
POLR2C	+	0.009119899	-0.33159116
DOK4	-	3.1685017e-12	-0.6258198
ADGRG1	+	1.4116065e-4	0.540668
MMP15	+	6.754633e-4	-0.3430341
GOT2	-	4.66551e-5	0.42501324
CA7	+	0	-3.2110689
PDP2	+	0.006124366	-0.2952332
CES2	+	6.5992487e-9	-0.4138513
AC009084.1	+	0.00248373	-0.35247526
TRADD	-	1.080773e-4	-0.64019287
HSF4	+	2.8034407e-4	-1.3402714
ELMO3	+	4.1132187e-4	-0.42633438
ATP6V0D1	-	0.002124977	-0.30399576
CENPT	-	0.001609034	-0.5212223
EDC4	+	1.2031066e-5	-0.50767624
AC040162.3	+	0.002283143	-0.5231308
PSKH1	+	0.002418663	-0.4449772
AC020978.5	-	0.001847371	-0.40873033
ESRP2	-	3.3959837e-4	-0.36150122
SMPD3	-	1.8420831e-8	-0.60040885
AC099521.2	-	1.7563646e-6	-1.3333851
CDH3	+	0.005866655	-0.2804527
HAS3	+	6.9435e-32	-1.291672
UTP4	+	5.0197857e-5	0.83052236
AC026464.4	+	0.005892608	-0.2979084
VPS4A	+	0.001084043	-0.30738258
NOB1	-	4.8346666e-4	0.6982722
AC009022.1	-	3.7708836e-13	-0.98491615
PDPR	+	1.7117864e-5	0.6923928
AARS	-	4.0590257e-6	-0.34796283
DDX19A	+	0.005428137	0.5499815
SF3B3	+	4.1783628e-7	0.45894462
MARVELD3	+	3.3154793e-4	-0.29048723
PHLPP2	-	0.00510952	-0.20756234
IST1	+	1.3753456e-6	-0.40795407
ZNF821	-	0.003605701	-0.86489165
ZFHX3	-	1.1231507e-4	0.6700611
MLKL	-	0.001994443	0.75876945
FA2H	-	3.4108375e-8	-0.5585603

WDR59	-	1.06007516e-4	-0.48498523
ZNRF1	+	7.9543755e-4	-0.46652892
LDHD	-	3.7656802e-5	-0.6278924
BCAR1	-	3.3629716e-5	-0.45979708
AC009163.2	-	1.4730149e-5	-0.45369574
CHST5	-	1.9325619e-6	-0.4745805
GABARAPL2	+	7.0395004e-6	-0.45001867
KARS	-	9.815396e-6	0.51260597
MON1B	+	0.005643091	-0.28190893
CENPN	+	1.0210372e-4	0.9978405
AC092718.3	-	0.008862301	1.1195827
GAN	+	9.354313e-7	-0.46336994
CMIP	+	7.50605e-16	-0.7044866
HSD17B2	+	1.2463407e-4	-0.30048284
ATP2C2	+	6.1887107e-4	0.3938144
MEAK7	-	6.909703e-7	-0.5637755
COTL1	-	3.846468e-4	0.4058339
GINS2	-	2.2309926e-8	2.0556848
IRF8	+	4.0258057e-4	0.6869316
MAP1LC3B	+	4.2659866e-7	-0.45807183
SLC7A5	-	0.001167384	0.4383834
CYBA	-	0.006590295	0.34966338
MVD	-	3.2248114e-13	-0.7431248
SNAI3-AS1	+	6.6040957e-6	-0.70130324
CDT1	+	3.418825e-5	1.2046256
APRT	-	0.008166835	0.5078929
TRAPPC2L	+	0.006154913	0.6941886
ANKRD11	-	0.005899836	0.24923642
RPL13	+	0.00785188	0.26259103
CHMP1A	-	3.6272904e-5	-0.44373617
CDK10	+	0.001035197	-0.4993885
FANCA	-	3.7156653e-6	1.1194736
SPIRE2	+	2.805719e-7	-0.60050577
GEMIN4	-	0.002588082	0.7199311
CRK	-	0.006683724	-0.21583122
MYO1C	-	3.686949e-7	-0.42763898
SLC43A2	-	5.7553494e-4	1.2954539
MIR22HG	-	7.365469e-38	-1.3353236
RPA1	+	3.53668e-4	0.47066075
TSR1	-	4.8818407e-7	0.84741765
MNT	-	7.734706e-8	-0.65948665
METTL16	-	3.611639e-4	0.7858103
CLUH	-	4.274952e-5	0.5267537
SPATA22	-	2.029735e-4	-1.6331769
TRPV3	-	5.114694e-19	-1.2043749
AC027796.3	-	0.004075421	-0.38640147

AC027796.4	-	0.004365291	-1.2245551
HASPIN	+	0.002554497	1.2874042
ANKFY1	-	7.9830934e-4	0.36201307
MYBBP1A	-	0.004226307	0.5350994
PELP1	-	2.4035799e-5	0.7475516
ARRB2	+	0.004689719	-0.41998675
MINK1	+	5.5599832e-14	-0.5896333
CAMTA2	-	9.8644625e-5	-0.42606413
C1QBP	-	2.237235e-12	0.87637264
DHX33	-	1.257139e-4	0.8046225
DERL2	-	0.005372831	-0.38843307
TXNDC17	+	0.006449833	-0.27859232
MED31	-	0.004916704	-0.61092925
SLC16A13	+	1.4416517e-7	-0.93584865
ACADVL	+	1.4359486e-11	-0.5136658
DVL2	-	5.142746e-7	-0.6479178
GABARAP	-	1.0233864e-5	-0.42924443
AC120057.2	-	1.9530662e-5	-0.4279767
AC003688.1	-	8.977445e-6	-0.5263708
CLDN7	-	4.644663e-16	-0.6262229
KCTD11	+	1.39394505e-8	-0.7869269
TNK1	+	5.0412385e-5	-0.57287246
TMEM256-PLSCR3	-	3.5536822e-4	-0.6020116
TMEM256	-	1.431314e-8	-0.7672668
SENP3-EIF4A1	+	6.0955074e-7	0.4119709
EIF4A1	+	1.4868806e-5	0.33000395
CD68	+	2.0871578e-15	-0.75716954
TP53	-	1.0232996e-13	1.4135436
CYB5D1	+	1.4565686e-4	0.91258276
AC104581.4	+	6.908754e-5	0.9911757
AC129492.1	-	1.4379046e-4	-0.6577851
VAMP2	-	4.6124763e-4	-0.4980327
BORCS6	-	0.00111635	-0.57700855
AURKB	-	1.7778493e-5	1.4489112
CTC1	-	5.390894e-4	-0.46596938
PFAS	+	4.752868e-8	1.5975709
NDEL1	+	1.2682039e-4	-0.41063568
MYH10	-	3.4555036e-11	0.84768194
SCO1	-	0.001189942	0.3934854
AC015908.6	-	3.117569e-10	-0.6611377
TMEM238L	-	4.450906e-11	-0.67591774
ELAC2	-	2.632114e-4	0.4779162
ADORA2B	+	7.291512e-4	-0.3455834
UBB	+	1.10352785e-5	-0.31273642
LRRC75A	-	0.003670925	-0.2572385
MPRIP	+	2.314112e-5	-0.31295246

FLCN	-	5.015321e-4	-0.3902128
COPS3	-	0.001410279	0.53336173
TOM1L2	-	1.4658061e-12	-0.6590704
ALKBH5	+	0.003888167	-0.2538875
FLII	-	2.5112377e-7	-0.42430955
MIEF2	+	0.007759233	-0.6048493
MAPK7	+	1.9820462e-5	-0.6121277
RNF112	+	0.001033838	-2.1696315
ALDH3A2	+	9.871599e-5	0.3391734
ALDH3A1	-	0.001393546	2.7087722
MTRNR2L1	+	5.917451e-4	-1.1693791
WSB1	+	1.077394e-21	-0.8089741
TMEM97	+	3.6631952e-16	-0.712583
IFT20	-	0.006676885	-0.58658326
TNFAIP1	+	0.00121167	-0.3464636
PIGS	-	2.2352113e-8	-0.53419805
ALDOC	-	1.929042e-12	-0.56520224
SPAG5	-	2.211502e-7	1.0417875
SUPT6H	+	1.6262966e-4	0.35879728
TRAF4	+	1.0293548e-7	-0.5900754
MYO18A	-	4.2740433e-9	-0.47914425
TIAF1	-	9.436388e-6	-0.50372493
TP53I13	+	4.285673e-4	-0.5723156
SSH2	-	0.005903059	-0.2543454
ATAD5	+	0.001167701	1.0024863
NF1	+	0.0023177	0.2667073
RAB11FIP4	+	2.713637e-4	-0.33034298
UTP6	-	0.008989795	0.43637875
MYO1D	-	1.9623509e-14	-0.48981547
RFFL	-	1.7073841e-8	-0.45759955
AC004223.3	-	2.2832553e-4	-0.4205734
RAD51D	-	1.1117184e-4	1.3252183
NLE1	-	4.1460132e-4	1.5952827
SLFN5	+	3.1610788e-4	0.6801287
SLFN13	-	3.1987316e-4	0.83392435
AP2B1	+	1.2288838e-11	0.565044
TAF15	+	1.7471051e-10	0.6867788
MMP28	-	1.7778092e-8	-0.53231764
CCL15	-	0.009014589	-0.4181016
PIGW	+	0.007896597	0.902964
DHRS11	+	1.0384455e-4	-0.36083975
AATF	+	2.8939587e-5	0.6621763
SRCIN1	-	0.001760154	-0.89601946
MLLT6	+	7.3675864e-7	-0.4863989
CWC25	-	3.492787e-4	-0.529428
RPL23	-	3.08278e-4	0.31806594

LASP1	+	4.2922213e-7	-0.35494676
RPL19	+	0.005960586	0.21528795
MED1	-	2.1137354e-4	0.38977483
PPP1R1B	+	0.002896112	0.269306
STARD3	+	2.025453e-4	-0.50989914
ERBB2	+	2.888777e-4	-0.33519605
MIEN1	-	0.004196387	-0.3666148
GRB7	+	1.3561148e-12	-1.064595
ORMDL3	-	4.6899095e-13	-0.7350864
PSMD3	+	0.004277768	-0.25958797
NR1D1	-	6.845148e-4	-0.49627975
MSL1	+	1.0717439e-12	-0.59861314
RAPGEFL1	+	1.9081362e-19	-0.8574127
RARA-AS1	-	0.005310013	-0.99321204
TOP2A	-	2.5922767e-27	1.4232298
IGFBP4	+	1.727804e-19	-0.87812513
TNS4	-	7.2498823e-4	-0.47692645
KRT12	-	1.2371844e-6	-0.870478
KRT20	-	9.5227995e-4	-0.2241416
KRT15	-	2.7015414e-5	-0.65583706
AC125257.1	-	0.0045572	0.7752838
KLHL11	-	3.2990916e-5	0.7539061
ACLY	-	7.876348e-8	-0.38374934
C17orf113	-	0.005173675	-1.2105693
KAT2A	-	0.003660881	0.6343147
AC099811.2	-	0.001458211	-0.31214574
RAB5C	-	0.003498813	-0.25738376
STAT5A	+	1.628919e-5	1.5310409
CAVIN1	-	0.002092159	0.38528323
ATP6V0A1	+	2.4648928e-4	-0.33517104
COASY	+	5.239424e-8	-0.5126016
MLX	+	3.46617e-8	-0.48256806
RETREG3	-	4.8863946e-4	-0.30587545
PLEKHH3	-	3.9932313e-8	-0.90797687
EZH1	-	9.403357e-17	-0.95593363
PSME3	+	0.00178179	0.3350359
RUNDC1	+	0.001018692	-0.36877048
VAT1	-	1.3317823e-4	-0.3076285
BRCA1	-	4.6342428e-9	1.2772933
NBR1	+	2.2976298e-4	-0.32333204
DUSP3	-	0.001274702	-0.2726597
HDAC5	-	5.843045e-5	-0.8513887
ATXN7L3	-	4.8594218e-4	-0.34408042
DBF4B	+	5.0756475e-4	2.0739946
EFTUD2	-	0.0097438	0.2873633
KIF18B	-	8.543066e-5	1.2233688

PLCD3	-	0.005127253	-0.25999093
ACBD4	+	4.437763e-8	-0.80069196
ARHGAP27	-	1.515885e-16	-0.74834013
PLEKHM1	-	4.4811236e-6	-0.48282585
LINC02210-CRHR1	+	0.009122859	-0.67326933
KANSL1	-	3.3146785e-7	-0.44501135
WNT3	-	0.002129355	-1.2228593
AC005670.3	-	0.005784639	0.7547256
NPEPPS	+	3.8583053e-7	-0.40080494
KPNB1	+	3.9618943e-5	0.324508
AC003665.1	-	8.241359e-12	-0.92228097
SCRN2	-	0.005609484	-0.54835325
SP6	-	2.4537754e-11	-0.678477
PNPO	+	0.003141341	0.47996232
AC018521.1	+	1.7805407e-8	-0.65268403
AC018521.2	-	0.005208291	-1.1559333
CDK5RAP3	+	4.958635e-15	-0.8337003
NFE2L1	+	1.006038e-8	-0.4036609
HOXB3	-	0.008048415	-0.44983715
HOXB9	-	4.1221466e-9	0.73300153
HOXB13	-	0.005698194	0.32706288
ATP5MC1	+	0.00269591	0.4775173
PHB	-	3.9316868e-7	0.5543084
TMEM92	+	0.005928943	-0.4029442
ACSF2	+	1.0227904e-37	-1.2387968
ABCC3	+	6.47132e-11	-0.48498914
LUC7L3	+	0.006079823	-0.2655806
ANKRD40CL	-	0.004910789	-0.3924804
TOB1	-	1.4608268e-11	-0.4925468
SPAG9	-	1.40677505e-8	-0.45300257
NME1	+	4.0841797e-10	1.2381783
NME1-NME2	+	5.666543e-7	0.5142723
NME2	+	1.8761777e-5	0.44714424
UTP18	+	0.003484013	0.5608069
COX11	-	0.004414388	0.48322392
STXBP4	+	4.9240363e-5	0.8631786
DGKE	+	9.778763e-7	-0.6403546
TRIM25	-	1.461578e-14	-0.5797101
SCPEP1	+	2.3779739e-4	-0.4327488
MRPS23	-	0.001746833	0.7003746
AC015813.2	-	2.626557e-5	0.389638
SRSF1	-	1.0817205e-6	0.4126483
MTMR4	-	1.5718474e-4	-0.37311116
RAD51C	+	7.1700284e-5	1.6845684
TRIM37	-	3.4210112e-7	0.8144645
SKA2	-	6.8808935e-5	0.7416468

PRR11	+	5.8408386e-7	1.2495416
YPEL2	+	3.3831811e-6	-0.6303076
CA4	+	6.129264e-29	1.1527762
BRIP1	-	9.8165016e-5	1.2889663
INTS2	-	8.238139e-6	0.7712445
FTSJ3	-	9.6692785e-4	0.49758148
TEX2	-	1.9723987e-4	0.4523787
DDX5	-	1.6043476e-4	-0.2947099
AXIN2	-	0.002685894	0.52876395
CACNG4	+	0.004992958	-1.3530698
NOL11	+	1.4465288e-4	0.6455659
BPTF	+	4.8637006e-4	0.32142946
KPNA2	+	3.04089e-12	0.8240016
WIPI1	-	2.634472e-5	-0.56469303
MAP2K6	+	3.2214037e-11	1.1904109
CDC42EP4	-	2.1283892e-4	-0.33836508
GPRC5C	+	0.00624013	-0.35835442
SLC9A3R1	+	1.25380675e-5	-0.36894277
OTOP2	+	0.004585591	-2.0638597
HID1	-	2.3182902e-7	-0.7320274
GGA3	-	3.8045354e-9	-0.61983275
MRPS7	+	0.00190702	0.49879506
TMEM94	+	2.5531764e-12	-0.70151734
LLGL2	+	0.010024125	-0.5324725
MYO15B	+	1.9484469e-18	-0.7967409
SMIM5	+	0.007382672	-0.4533015
WBP2	-	2.5253383e-10	-0.6279465
TEN1-CDK3	+	5.744683e-10	-0.9369097
TEN1	+	1.2776804e-4	-0.7371311
CDK3	+	4.416662e-8	-1.2814656
UBALD2	+	3.6307003e-5	-0.65517855
SNHG16	+	8.3418114e-13	1.0164161
ST6GALNAC1	-	4.999729e-5	0.3958735
SNHG20	+	3.5025674e-5	1.4568315
SEC14L1	+	6.989195e-6	-0.44162685
SCARNA16	+	5.4144784e-5	1.8782222
TMC6	-	7.0467254e-4	-0.5644899
BIRC5	+	1.2444141e-6	1.1209241
DNAH17	-	0.006875693	5.063155
CYTH1	-	1.18346856e-4	-0.394781
AC022966.1	-	3.965899e-5	0.7103906
TIMP2	-	1.5171622e-5	-0.43342894
LGALS3BP	-	0.008024476	-0.24993221
CBX2	+	1.8896024e-4	1.5109506
AC124319.1	+	5.088225e-4	0.28056982
AATK	-	1.0554097e-6	-1.3705561

AC110285.2	-	0.00614349	-1.3632771
BAHCC1	+	2.3170191e-4	-0.8951186
NPLOC4	-	5.046019e-15	-0.62118787
CCDC137	+	0.007616016	-0.412452
HGS	+	1.3653797e-11	-0.72102314
MRPL12	+	0.001458537	0.5003466
P4HB	-	0.00115944	-0.2175716
ARHGDIA	-	0.002471133	-0.3026549
AC145207.5	-	0.00331519	0.85022736
ALYREF	-	4.3187512e-4	0.66327965
PCYT2	-	4.2269926e-7	-0.5644141
SIRT7	-	1.1600948e-12	-0.72331655
MAFG	-	2.3373654e-7	-0.5799111
RFNG	-	3.2948577e-5	-0.7061588
SLC16A3	+	0.001921995	-0.6107282
CSNK1D	-	2.2113427e-7	-0.42495868
SECTM1	-	0.004632074	-0.41798493
NARF	+	0.001025563	-0.42695493
WDR45B	-	2.2740353e-6	-0.42284143
TBCD	+	1.7990474e-6	0.6956408
THOC1	-	0.00134773	0.8153069
TYMS	+	1.0515134e-12	1.3904042
YES1	-	0.005776018	-0.21493196
NDC80	+	4.608436e-5	1.434897
LPIN2	-	1.5082914e-13	-0.604883
MYL12A	+	4.746234e-5	-0.30899373
MYL12B	+	8.056845e-4	-0.25654063
MTCL1	+	3.0593903e-6	0.70972174
TWSG1	+	0.001369784	-0.32371822
RALBP1	+	3.0777996e-4	-0.30490547
NAPG	+	6.0456307e-7	-0.46267405
SPIRE1	-	4.2730944e-6	-0.5157415
SEH1L	+	7.488366e-5	0.578064
SNRPD1	+	1.2715602e-5	0.8810258
ABHD3	-	1.9109082e-7	-0.39997375
MIB1	+	1.394018e-5	-0.36554888
GATA6-AS1	-	0.001202784	-0.8408548
RIOK3	+	6.097214e-14	-0.5398049
RMC1	+	2.3197294e-4	-0.44840893
NPC1	-	1.57881e-15	-0.68406254
LAMA3	+	1.301666e-4	0.30875203
IMPACT	+	2.6434005e-4	0.58253103
DSC2	-	1.9524308e-4	-0.2477287
DSG2	+	2.666963e-6	-0.3286301
B4GALT6	-	9.3135063e-4	1.0269555
INO80C	-	3.4586399e-6	-0.72896737

SLC39A6	-	6.77701e-4	0.6304719
MOCOS	+	1.3875842e-4	0.5387177
EPG5	-	1.3758488e-7	-0.52935153
ATP5F1A	-	4.15834e-4	0.26940036
HAUS1	+	0.003209817	1.0052658
PIAS2	-	1.9655826e-4	0.5711998
CTIF	+	1.6521566e-4	-0.62408996
SMAD7	-	1.6500751e-6	-0.6634188
SNHG22	+	4.936283e-6	-0.52893496
SCARNA17	+	1.6325106e-7	-0.73832995
MBD1	-	5.488684e-4	-0.37293357
SKA1	+	4.4506356e-7	1.9442327
ME2	+	2.2717284e-6	0.66587025
C18orf54	+	0.00153889	1.3448641
CCDC68	-	2.1233396e-5	-0.39390072
WDR7	+	6.3439606e-6	0.75537443
NARS	-	1.2827808e-12	0.6167924
LMAN1	-	1.3589803e-12	-0.53449804
PMAIP1	+	0.005693525	0.94588023
RNF152	-	3.2296657e-4	-0.26925552
SERPINB5	+	8.515302e-8	0.5776389
TIMM21	+	0.003884853	0.7077957
ATP9B	+	0.005086043	0.53015655
PLPP2	-	2.3946182e-5	-0.52852964
SHC2	-	0.005569315	-1.8543104
MISP	+	4.2566628e-4	-0.27456334
TMEM259	-	3.2518103e-6	-0.526094
ABCA7	+	1.7691664e-9	-0.7282705
AC004151.1	+	1.9830668e-4	-0.6105588
GPX4	+	3.5301408e-11	-0.7197867
STK11	+	2.3248982e-4	-0.40968305
CIRBP	+	4.4860293e-9	-0.57625437
GAMT	-	0.001394095	1.809443
CSNK1G2	+	1.0620411e-5	-0.57413274
MKNK2	-	3.9932575e-13	-0.67232853
MOB3A	-	0.009902836	-0.3203404
IZUMO4	+	9.797498e-4	-1.449251
PLEKHJ1	-	3.071635e-4	-0.35553288
SPPL2B	+	1.9027597e-5	-0.5987125
TIMM13	-	8.0714e-5	0.7791905
LMNB2	-	2.393133e-11	0.80713457
GADD45B	+	1.8837545e-5	-0.87710416
AC006538.1	+	7.173688e-4	0.64013493
TLE5	-	4.3146964e-4	-0.36360422
GNA11	+	0.001271092	-0.29454547
NFIC	+	1.0484123e-6	1.0519955

MFSD12	-	0.005838722	0.5198239
TJP3	+	6.123972e-13	-0.6342607
DAPK3	-	0.00374082	-0.42990354
EEF2	-	0.008106966	-0.21788384
MAP2K2	-	2.4549113e-10	-0.59473217
AC016586.1	-	5.1973032e-8	-0.6890043
STAP2	-	0.004708493	-0.3136992
SH3GL1	-	7.592719e-5	-0.43452325
CHAF1A	+	1.0375519e-5	0.91536784
UBXN6	-	8.719171e-6	-0.55743015
PLIN3	-	1.7443476e-8	-0.6079565
UHRF1	+	3.5808284e-7	1.572282
SAFB	+	0.00258889	0.31924254
RFX2	-	2.8176542e-4	-0.9744835
SLC25A23	-	9.8305924e-21	-0.7674715
CRB3	+	9.679489e-6	-0.52996653
AC010503.4	+	2.4809367e-6	-0.5955983
TNFSF9	+	5.036317e-7	-0.61582464
GPR108	-	6.1053876e-4	-0.39967752
TRIP10	+	2.5489227e-5	-0.44366437
SH2D3A	-	7.870869e-6	-0.572977
INSR	-	4.1934126e-4	-0.28244025
AC008878.3	+	1.22803485e-5	-0.41990936
ARHGEF18	+	6.7812653e-6	-0.41102943
MCOLN1	+	6.3382316e-4	-0.55289364
AC008763.2	+	9.910818e-7	-0.500555
STXBP2	+	1.2559265e-8	-0.5199769
MAP2K7	+	2.8172135e-4	-0.42706046
CD320	-	0.002235112	0.6302006
ANGPTL4	+	8.638615e-10	-0.81347615
RAB11B	+	0.001135596	-0.37140638
HNRNPM	+	2.1207388e-16	0.78478146
ZNF121	-	1.4917493e-4	0.5411605
PPAN	+	0.005059593	0.6878502
DNMT1	-	1.8396982e-17	1.1138241
ICAM1	+	2.3830496e-6	2.6622655
CDKN2D	-	0.004359997	-0.68824106
ILF3	+	6.53828e-4	0.31858143
DNM2	+	4.428124e-23	-0.7500129
YIPF2	-	0.0026818	-0.41068307
LDLR	+	1.328664e-30	-0.79253906
SPC24	-	0.002469838	1.1586715
DOCK6	-	2.4338806e-6	-0.5254919
EPOR	-	1.5930729e-6	-1.399342
RGL3	-	1.5743524e-14	-0.9654574
AC010422.8	-	0.002366965	-0.39087075

DHPS	-	1.3840118e-5	-0.6480327
HOOK2	-	2.0593369e-10	-0.66698736
THSD8	+	0.001184403	1.0926367
RNASEH2A	+	9.2658936e-4	1.0648478
FARSA	-	0.007963938	0.41409227
GADD45GIP1	-	2.1586176e-5	1.0091
STX10	-	2.980033e-6	-0.67578447
CCDC130	+	0.001887398	-0.5231079
AC020916.1	-	2.4524716e-14	-1.1732731
ASF1B	-	3.5097182e-4	0.92675066
DNAJB1	-	0.008670006	0.21876867
CYP4F12	+	7.3518424e-7	-0.47728306
UCA1	+	0	-1.0996739
FAM32A	+	0.003364099	-0.29321653
EPS15L1	-	5.4182013e-4	-0.39366284
SLC35E1	-	0.002024017	-0.29160082
MYO9B	+	6.3244614e-9	-0.5410735
OCEL1	+	2.0054104e-6	-0.6850535
NR2F6	-	8.45423e-11	-0.68263936
AC010646.1	-	4.4217126e-5	-0.7105459
MRPL34	+	0.008248712	0.39349434
DDA1	+	1.94124e-4	-0.42550594
ANO8	-	0.002454033	-0.56173116
ARRDC2	+	1.3832639e-4	-0.64037514
MAST3	+	4.8449033e-7	-0.50761205
AC008397.2	-	3.677149e-22	-1.2701576
AC005759.1	-	2.0885144e-36	-1.9431119
AC008397.1	-	2.048212e-5	-0.6314292
JUND	-	4.7745387e-5	-0.40825626
LSM4	-	3.4032715e-4	-0.374265
PGPEP1	+	6.672042e-4	-0.28563768
GDF15	+	1.6630227e-12	0.8504271
COPE	-	0.008215526	-0.33191368
AC092279.1	+	0.003653253	0.7671436
ZNF507	+	0.001913528	0.49583828
PDCD5	+	0.007576477	0.6304591
RHPN2	-	2.0078383e-4	-0.30712414
CEBPG	+	1.21542515e-4	-0.2900333
KIAA0355	+	0.001923974	-0.4647205
UBA2	+	0.008864952	0.28873345
AC020907.6	+	2.8228326e-13	-0.51823676
FXYD3	+	1.8785703e-14	-0.5481587
LGI4	-	4.496632e-6	-1.5577253
LSR	+	0.001245502	-0.32458627
AD000090.1	+	1.862261e-39	-6.3746963
HAUS5	+	0.005830473	1.43197

WDR62	+	7.431531e-5	1.4109287
ZNF146	+	2.036395e-6	0.6584971
SPINT2	+	8.380614e-17	-0.5902874
AC011479.1	+	3.2075393e-14	-0.6186315
C19orf33	+	0.008209927	-0.38197523
KCNK6	+	0.003786976	-0.32598883
ACTN4	+	0.007554835	-0.20612174
CAPN12	-	5.567893e-9	-1.725826
LGALS4	-	2.5775746e-8	-0.3797076
AC104534.1	+	0.00833317	-0.5117619
SIRT2	-	8.1067154e-4	-0.41516933
MRPS12	+	0.006526087	0.6059481
ZFP36	+	0.007405405	-0.26035362
FBL	-	2.974857e-10	0.88602257
PSMC4	+	0.005435598	0.31326213
ZNF780B	-	0.001070629	0.7757055
AKT2	-	0.001861723	-0.35125393
LTBP4	+	3.0526146e-6	-0.7084281
ITPKC	+	0.001326146	-0.43030357
MIA-RAB4B	+	4.5625764e-8	-0.67681766
RAB4B	+	2.3863533e-10	-0.73437303
RAB4B-EGLN2	+	1.2052543e-4	-0.39406696
CYP2S1	+	7.4196054e-9	-0.54744345
CEACAM7	-	1.1256985e-11	-0.48620906
CEACAM5	+	1.8832942e-7	0.35679933
CEACAM6	+	0.002184832	-0.20584813
CEACAM3	+	8.015554e-4	-2.327261
RABAC1	-	6.1527686e-4	-0.50604576
AC010616.2	-	0.001653515	-0.5669174
DEDD2	-	0.003060096	-0.4596445
GSK3A	-	0.004254095	-0.30568084
ERF	-	0.001407565	-0.43253914
CIC	+	0.002720101	-0.3405646
CEACAM1	-	1.9935094e-22	-0.7000753
CD177	+	3.0234343e-15	3.2565653
IRGQ	-	1.3853115e-4	0.44019732
KCNN4	-	2.3213565e-6	-0.76934916
AC092072.1	+	0.007850898	-0.84020054
ZNF224	+	0.007797731	-0.45311347
PVR	+	0.007406312	-0.29363889
BCL3	+	2.84282e-4	-0.4265901
CBLC	+	1.3564974e-4	-0.44702896
NECTIN2	+	0.003457703	-0.29828504
TOMM40	+	2.3247983e-6	0.72805345
CLASRP	+	8.321276e-10	-0.8578836
CD3EAP	+	0.003815164	1.239787

RTN2	-	2.2821747e-4	-0.9438566
VASP	+	5.6925546e-6	-0.39536855
OPA3	-	6.986969e-5	-0.4990015
EML2	-	0.0070718	-0.31729025
GIPR	+	9.208632e-11	-1.0788567
ARHGAP35	+	1.7418019e-5	-0.29792377
SAE1	+	0.009414865	0.30417374
SELENOW	+	2.8455094e-12	-0.5876904
LIG1	-	4.971315e-4	0.7379925
KDELR1	-	1.770897e-4	-0.2976517
AC008403.1	+	0.006665631	-0.51248586
CYTH2	+	3.8267583e-24	-0.8707651
LMTK3	-	7.9561386e-4	-0.64136326
SULT2B1	+	1.1780826e-6	-1.1779865
FAM83E	-	0.003392617	-0.33633637
PPP1R15A	+	4.13898e-4	-0.40061504
BAX	+	0.006789938	0.3567655
RUVBL2	+	0.004649817	0.45063785
TRPM4	+	6.325659e-4	-0.37541875
RPL13A	+	0.00285902	0.22087212
RPS11	+	0.005488429	0.21358639
PRRG2	+	0.005269278	-0.56850976
RRAS	-	8.7492996e-10	-0.8468504
PRMT1	+	7.4886857e-4	0.49789786
MED25	+	0.002961568	-0.3653082
PTOV1	+	3.3711412e-4	-0.45057014
PNKP	-	0.002846672	-0.46386173
AKT1S1	-	0.007490029	-0.3134838
TBC1D17	+	7.48512e-4	-0.5211954
NR1H2	+	7.429394e-4	-0.4018127
AC020909.2	+	1.4182842e-12	-1.8627521
SPIB	+	0	-2.3927653
EMC10	+	0.009359481	0.26398718
C19orf48	-	6.901569e-4	0.8512985
KLK1	-	7.984563e-16	-0.76336414
SPACA6	+	0.002299379	-0.90648204
ZNF480	+	0.008286036	0.57685846
ZNF320	-	0.0090899	-0.59139144
MYADM	+	1.6408772e-5	-0.67059606
TMC4	-	8.1490164e-8	-0.5741563
MBOAT7	-	3.5285487e-4	-0.36653996
TSEN34	+	0.002146818	-0.4418112
LENG8	+	1.2168031e-28	-1.0721982
AC011476.2	-	0.004053294	-0.56189215
RDH13	-	4.141241e-9	-0.65644634
EPS8L1	+	2.8422833e-12	-0.7434736

AC010327.1	-	1.02035905e-7	-0.41525018
TMEM86B	-	0.004090518	-1.035719
PPP6R1	-	4.8819897e-4	-0.3497109
HSPBP1	-	6.501796e-5	1.0453513
TMEM150B	-	0.006555765	-0.5867942
COX6B2	-	0.001872936	-1.1241348
AC005261.2	+	9.107414e-5	0.814069
ZNF776	+	0.005576775	-0.6013931
ZNF587B	+	0.004131572	0.8156066
ZNF274	+	2.596892e-6	-0.6355936
CHMP2A	-	0.01000425	-0.25497755
MZF1	-	1.2313304e-5	-0.6570284
NRSN2-AS1	-	1.3429177e-6	-0.69809043
NRSN2	+	0.006238491	-0.5198859
TRIB3	+	2.1011125e-24	-0.9104111
RBCK1	+	6.1750787e-26	-1.0266968
TBC1D20	-	1.5597115e-9	-0.600541
CSNK2A1	-	3.1841334e-6	-0.37810737
SLC52A3	-	2.4907916e-9	-0.7388397
SDCBP2	-	1.04887177e-16	-0.69376475
AL136531.2	-	3.6601483e-10	-0.6591642
FKBP1A	-	0.005161457	0.2561228
STK35	+	7.153068e-6	-0.39998537
NOP56	+	5.177447e-10	0.920065
IDH3B	-	0.007447823	0.3347859
ITPA	+	3.3324485e-4	0.79527926
ATRN	+	1.8556738e-6	0.64887595
C20orf27	-	0.004057404	0.9471561
CDC25B	+	9.831608e-4	0.42181075
MAVS	+	0.006025023	0.21481879
PCNA	-	7.999863e-10	0.7578736
GPCPD1	-	1.10594585e-4	-0.5312242
TRMT6	-	0.009428076	0.68365526
MCM8	+	6.5641194e-7	1.212996
AL035461.3	+	6.0075134e-5	0.5996308
FERMT1	-	1.1995391e-4	0.37054443
TMX4	-	9.7246637e-4	0.47597113
PLCB4	+	1.906449e-10	0.58469135
SLX4IP	+	0.001619952	0.6491933
JAG1	-	1.2819721e-6	0.3715594
ESF1	-	3.1185375e-6	0.9735692
SEC23B	+	0.007404023	0.2691894
RIN2	+	4.276224e-6	-0.37953863
RALGAPA2	-	0.003168654	0.23401766
XRN2	+	2.6951685e-7	0.6321153
APMAP	-	0.004525119	0.30906767

ENTPD6	+	3.0890698e-7	-0.45104432
ABHD12	-	9.8967785e-6	-0.42619163
GINS1	+	4.0155207e-4	0.94353306
ID1	+	1.0162285e-21	-1.026605
BCL2L1	-	3.5941408e-12	-0.5876117
TPX2	+	1.2657695e-12	1.0834827
TM9SF4	+	0.002086033	-0.27257672
NOL4L	-	8.221874e-4	-0.2689567
CHMP4B	+	1.4139456e-9	-0.46061927
AHCY	-	2.7459537e-10	0.76487565
TP53INP2	+	3.6731179e-13	-0.5960149
GGT7	-	1.2449717e-11	-0.91288614
ACSS2	+	9.089434e-31	-0.8096371
TRPC4AP	-	2.3877678e-7	-0.47705397
EDEM2	-	0.003469343	-0.37262908
MMP24	+	0.009685719	-0.73882604
CEP250	+	0.004044365	0.42437977
SPAG4	+	4.1467554e-9	-0.98098904
PHF20	+	4.677388e-4	0.5217137
MYL9	+	0.005458072	1.4980531
SOGA1	-	0.003975689	0.5343248
TLDC2	+	0.008790302	-0.44534135
SAMHD1	-	2.6252365e-4	0.8862361
RPN2	+	2.0851212e-5	-0.30460066
BLCAP	-	5.02695e-10	-0.4887554
VSTM2L	+	0.00863229	-0.7386264
RPRD1B	+	1.4642515e-4	-0.44219938
FAM83D	+	0.001169004	0.8541012
PLCG1	+	5.9170433e-4	-0.38852984
LPIN3	+	5.0656437e-20	-0.8994175
CHD6	-	0.002553019	0.68089217
Z98752.3	+	1.6637185e-5	-0.5797513
SGK2	+	3.036572e-9	-0.45780012
MYBL2	+	5.46029e-4	0.6218302
HNF4A	+	0.001253819	-0.21676022
HNF4A-AS1	-	0.001131255	-2.7781641
SERINC3	-	0.003768815	-0.22956584
TOMM34	-	1.12320035e-4	0.7527521
PI3	+	0	2.8374958
UBE2C	+	5.7602995e-7	1.6650862
AL162458.1	-	1.222468e-4	-1.0206269
NCOA5	-	0.00552892	0.40979263
SLC35C2	-	0.001282798	-0.4745133
ZMYND8	-	0.003940865	-0.26014692
CSE1L	+	8.834196e-8	0.57294756
STAU1	-	9.3983545e-12	-0.52907485

DDX27	+	1.7085069e-4	0.52374846
ZFAS1	+	0.005623851	-0.34872577
RNF114	+	0.009626197	-0.24543397
TMEM189-UBE2V1	-	0.009582212	-0.20488656
TMEM189	-	2.1166817e-7	-0.5629268
KCNG1	-	0.001339162	-0.73256624
NFATC2	-	0.003604334	1.9742471
ATP9A	-	5.9198597e-25	-0.7341625
ZNF217	-	4.5232024e-8	-0.45194876
FAM210B	+	4.3201926e-5	0.66102296
AURKA	-	8.493024e-6	0.7986065
CSTF1	+	0.001821441	0.49113578
BMP7	-	5.299788e-4	0.65265524
MTRNR2L3	-	1.1072774e-4	-2.3790371
PCK1	+	0	-2.329672
GNAS	+	0.00551224	-0.1987374
NELFCD	+	2.8605407e-4	0.5132661
CTSZ	-	3.1506486e-6	-0.3472456
OSBPL2	+	2.4917537e-9	-0.55847025
SLCO4A1	+	8.925054e-16	-0.86296487
ARFGAP1	+	5.255708e-10	-0.8224536
PTK6	-	8.223007e-20	-0.8335192
GMEB2	-	0.00126294	-0.52531856
DNAJC5	+	3.6598252e-7	-0.4535295
UCKL1	-	5.828846e-6	-0.64896834
FP236383.2	-	0.007347519	-5.62778
AF127577.4	-	6.0648676e-5	-0.6598697
CXADR	+	3.6314965e-8	-0.40613413
APP	-	0.009235575	-0.1752503
CCT8	-	2.908306e-7	0.5318136
BACH1	+	2.0905628e-4	-0.34870088
TIAM1	-	2.9178438e-4	0.8301947
MIS18A	-	0.002201987	1.0995072
URB1	-	3.907581e-8	0.9765958
AP000295.1	+	2.9446567e-11	-0.5739425
IL10RB	+	1.4915732e-12	-0.635319
IFNAR1	+	0.003617006	-0.25621048
IFNGR2	+	6.975982e-8	-0.46536425
GART	-	2.372348e-6	0.5969894
MRPS6	+	5.213557e-12	-0.57749844
SLC5A3	+	0.006358459	-0.1994664
AP000317.2	+	6.293401e-4	-0.52053165
RCAN1	-	0.002336252	-0.25673708
CHAF1B	+	0.001351649	0.94919175
HLCS	-	0.001405705	0.4902752
PSMG1	-	1.9187371e-5	1.0853908

FAM3B	+	0.003588816	-0.9623005
MX1	+	0.005778931	-0.72657835
TMPRSS2	-	1.9108416e-8	-0.37995708
C2CD2	-	0.003075263	0.5828392
ABCG1	+	1.3303925e-24	-0.99034196
TFF3	-	6.123716e-7	-0.48298252
TFF2	-	0.001676168	-0.47910735
TFF1	-	2.3285222e-6	-0.45414692
RRP1B	+	3.5586296e-9	0.9847303
PDXK	+	6.8449514e-4	-0.28650445
RRP1	+	0.003498004	0.7873782
UBE2G2	-	0.002807752	0.42348439
PTTG1IP	-	3.0275374e-15	-0.5331446
POFUT2	-	1.8090219e-18	-1.1103492
COL6A1	+	2.9016608e-5	-1.0238502
LSS	-	3.376238e-11	-0.6126359
DIP2A	+	9.86616e-4	-0.3524177
PRMT2	+	0.004533011	-0.28187934
HDHD5	-	0.001928758	0.6608607
CECR2	+	4.1082496e-10	-1.0779728
BCL2L13	+	9.3228286e-11	-0.634208
MICAL3	-	5.355676e-7	-0.37343976
AC016026.1	-	1.7027225e-5	-0.44077
AC016027.1	-	0.001961672	-0.71248996
PEX26	+	9.132298e-15	-0.52909046
SLC25A1	-	2.1208855e-8	-0.52079964
HIRA	-	6.064166e-4	0.44181973
C22orf39	-	8.175429e-4	0.42347607
CDC45	+	0.00483334	1.2494987
RANBP1	+	1.9059774e-9	1.0410913
RTN4R	-	0.003720394	-0.6040392
MED15	+	2.5016746e-7	-0.50132877
AIFM3	+	0.002068183	-0.57895005
TOP3B	-	0.006471064	-0.5054865
GUCD1	-	5.4470427e-28	-0.8570153
SNRPD3	+	0.007222399	0.29020542
GRK3	+	6.252952e-4	0.43658456
XBP1	-	3.2318292e-6	-0.36635965
ZNRF3	+	3.355046e-6	1.0483086
NIPSNAP1	-	0.006091305	-0.28815302
AC004997.1	-	0.007052301	-0.52183646
TBC1D10A	-	1.113048e-4	-0.5381418
SEC14L2	+	9.2760235e-9	-0.77264553
GAL3ST1	-	4.126187e-9	-0.84680825
TCN2	+	2.5491811e-12	-1.0842032
PIK3IP1	-	0.006633032	-0.55493027

PATZ1	-	0.008090706	0.7320416
SLC5A1	+	2.2891165e-8	0.94356394
RTCB	-	0.009623712	-0.23973715
ISX	+	9.4711686e-7	-0.4026075
TOM1	+	6.8095886e-8	-0.667422
HMOX1	+	1.4373803e-5	-0.53979194
MCM5	+	0.008610149	0.48129573
FOXRED2	-	1.0771776e-4	1.4439689
MPST	+	7.80867e-9	-0.57783914
CDC42EP1	+	2.682654e-7	0.8042132
LGALS2	-	7.6987945e-8	1.8073299
GGA1	+	0.008064704	-0.3368988
LGALS1	+	9.353608e-8	-0.79538935
TRIOBP	+	1.4375753e-4	-0.4106687
MICALL1	+	7.343438e-4	-0.43454024
KDELR3	+	0.002595814	-0.46355537
DDX17	-	5.588972e-4	-0.25107673
TOMM22	+	0.007025312	0.36880675
JOSD1	-	2.9038463e-13	-0.5654422
GTPBP1	+	2.7315078e-13	-0.71135134
SUN2	-	1.355577e-11	-0.6374827
APOBEC3C	+	4.0555676e-8	-0.47984353
RPL3	-	0.008168168	0.1975263
ATF4	+	5.4496877e-7	-0.36053938
FAM83F	+	2.1363269e-7	-0.4507191
TNRC6B	+	2.2224438e-6	0.4531935
ADSL	+	1.7663271e-5	0.8464568
AL022238.4	+	4.100819e-10	-0.658376
SGSM3	+	4.4636222e-15	-0.8609825
XPNPEP3	+	2.295415e-4	0.5382226
ZC3H7B	+	0.001788624	0.37860775
TEF	+	8.384539e-17	-0.91308314
ACO2	+	3.1810737e-4	-0.30010173
PMM1	-	3.1609483e-24	-1.3664005
XRCC6	+	0.009786379	0.2235257
SNU13	-	0.001799006	0.4755734
C22orf46	+	7.535432e-4	0.7739344
SREBF2	+	1.4857204e-9	-0.4603394
NAGA	-	0.008499695	-0.29620263
PHETA2	+	3.4350003e-4	-1.0529453
CYB5R3	-	2.6796115e-4	-0.36639783
ARFGAP3	-	2.692287e-10	-0.5982022
PACSIN2	-	0.00943697	-0.20199837
TSPO	+	0.003646145	-0.3725304
PNPLA3	+	5.4880874e-15	-0.95938563
SAMM50	+	0.002499149	0.44648454

SHISAL1	-	0.00321162	3.2642918
KIAA0930	-	2.4548356e-4	-0.35504034
ATXN10	+	0.006104006	0.33886304
PPARA	+	5.9422325e-7	-0.36005515
TTC38	+	3.2297516e-4	-0.3025973
GTSE1	+	1.0528586e-6	1.4952825
GRAMD4	+	0.001370719	-0.40261433
CERK	-	0.007005057	-0.4220291
TBC1D22A	+	0.004642934	-0.34532136
TUBGCP6	-	0.003041421	-0.42166668
CPT1B	-	1.9803734e-7	-0.85376114
CHKB-CPT1B	-	7.591959e-12	-0.7922063
CHKB	-	3.0134234e-7	-0.70071554
MT-ND2	+	1.8580456e-20	0.631389
MT-CO1	+	1.0167823e-7	-0.36263716
MT-ATP8	+	1.0185454e-17	0.61896384
MT-ATP6	+	3.1178554e-14	0.5817015
MT-ND3	+	2.60978e-40	0.9224574
MT-ND4L	+	0.005684407	0.18725486
MT-ND4	+	0.005482932	0.19615729
MT-ND6	-	4.5659404e-17	0.79284
MT-CYB	+	0.00144605	0.22547081
PLCXD1	+	6.503477e-10	-0.7270331
AKAP17A	+	1.868002e-5	-0.506137
PRKX	-	9.369206e-4	0.63575137
STS	+	1.5133198e-5	0.518041
MID1	-	5.344676e-5	0.54276776
PRPS2	+	2.5856745e-5	0.5814287
TMSB4X	+	0.00465976	-0.22022998
OFD1	+	0.001295356	-0.42948323
RBBP7	-	1.5468395e-4	0.42836007
PHKA2	-	3.9999905e-34	-0.89621425
MAP7D2	-	0.001333125	0.88948184
MBTPS2	+	6.106982e-5	0.74687254
PRDX4	+	0.003930315	0.4360091
SAT1	+	2.549302e-13	-0.61312
POLA1	+	5.1508406e-9	1.4125934
GK	+	4.889937e-4	-0.49029183
SYTL5	+	6.248129e-4	-0.51053363
CXorf38	-	5.864787e-5	-0.5269408
DDX3X	+	0.001198853	-0.24721377
MAOB	-	4.470763e-9	0.75474143
MIR222HG	-	1.779156e-4	-0.6872216
SLC9A7	-	0.001729159	0.699799
CDK16	+	7.9435995e-5	-0.400099
ARAF	+	0.006382531	-0.32067698

SLC38A5	-	7.660848e-5	1.0983866
EBP	+	8.076277e-15	-0.6354966
AF196969.1	+	2.2980535e-12	-0.66176057
WDR13	+	4.303728e-4	-0.4469153
SUV39H1	+	3.069936e-4	1.4348125
HDAC6	+	2.5723267e-8	-0.6426916
PQBP1	+	0.003055053	-0.40504676
TIMM17B	-	0.002650454	-0.58358765
SLC35A2	-	0.001271134	-0.37012592
OTUD5	-	0.004506121	-0.34996605
CCDC120	+	2.2843973e-11	-0.8542949
WDR45	-	0.00131864	-0.6079133
CLCN5	+	0.001143277	0.54071665
KDM5C	-	0.001511591	-0.29367152
SMC1A	-	1.5768295e-6	0.45729446
HUWE1	-	5.615051e-8	0.45346037
GNL3L	+	2.3326536e-6	0.54463524
APEX2	+	0.003743173	-0.43825647
PAGE2B	+	0.009549912	-5.502455
MTRNR2L10	-	1.4864036e-4	-1.7360389
SPIN4	-	0.004747423	-0.41621333
LAS1L	-	1.2730251e-4	1.0233287
HEPH	+	3.3332675e-8	-0.4170816
YIPF6	+	0.001523458	-0.29963407
EFNB1	+	4.124297e-4	-0.3321534
IGBP1	+	1.3058946e-6	-0.5038485
KIF4A	+	8.079358e-8	1.316654
FOXO4	+	7.60366e-9	-0.81529737
AL590764.2	-	0.004207742	-0.30625248
OGT	+	8.192061e-6	-0.37517092
ERCC6L	-	2.7509133e-5	1.438542
XIST	-	5.251081e-15	4.607124
ATRX	-	4.9661817e-6	0.46028647
PGK1	+	1.8765884e-5	-0.29621106
BRWD3	-	3.2942107e-6	-0.4051717
HMGN5	-	0.009944852	1.0845363
DIAPH2	+	6.354134e-4	-0.29934174
SRPX2	+	6.7824484e-9	-0.8099367
SYTL4	-	2.7221452e-8	-0.55829716
NOX1	-	1.7032466e-5	0.55741554
RPL36A	+	1.857719e-8	0.58718634
RPL36A-HNRNPH2	+	8.827786e-5	0.388036
MORF4L2	-	4.1408748e-5	-0.36120525
RADX	+	0.001368015	-0.9495349
RNF128	+	1.1215324e-4	-0.30433458
TBC1D8B	+	4.010592e-5	-0.4197441

MORC4	-	6.719652e-4	0.5224659
CLDN2	+	5.7e-44	1.8362545
PRPS1	+	5.458025e-4	1.0135698
PSMD10	-	0.006404508	-0.34600046
TMEM164	+	2.2805188e-4	-0.31674972
AMOT	-	0.001998223	0.44069177
PLS3	+	9.429835e-7	0.7284145
DANT2	-	0.00152132	0.9732454
SLC6A14	+	8.361789e-6	0.57846326
KLHL13	-	2.6713104e-5	0.8694665
IL13RA1	+	0.00363043	-0.269405
PGRMC1	+	3.4100235e-6	-0.36364335
UBE2A	+	0.009498351	-0.24730812
NKRF	-	0.001593463	0.7363656
UPF3B	-	0.005427199	0.569917
STAG2	+	3.8952154e-11	-0.5052883
XPNPEP2	+	3.1389302e-9	-0.64332974
ZDHHC9	-	8.289454e-8	-0.49732286
UTP14A	+	4.7797515e-5	0.98580885
ELF4	-	1.11432186e-4	-0.3523248
AIFM1	-	1.7711716e-6	0.59037244
RAP2C	-	0.007045541	-0.28048044
MBNL3	-	1.4410631e-7	0.68735766
GPC4	-	6.9673854e-4	0.5551629
RTL8C	+	4.0070707e-4	-0.4882864
SMIM10L2B	-	1.8553538e-4	-1.0268897
HTATSF1	+	0.005311679	0.30180576
RBMX	-	2.591091e-7	0.5255982
TMEM185A	-	7.0316053e-4	-0.77002305
HMGB3	+	6.9340353e-4	0.6190252
VMA21	+	1.2822225e-5	0.653257
GABRE	-	1.5669694e-26	-1.2820233
NSDHL	+	1.027478e-6	-0.54115635
SLC6A8	+	1.398048e-26	-0.96193635
FLNA	-	2.7708943e-14	1.0401176
DNASE1L1	-	5.8408106e-5	-0.5726539
TAZ	+	0.001186759	-0.6010774
ATP6AP1	+	2.8034627e-5	-0.3950445
GDI1	+	2.5549726e-15	-0.7137057
FAM50A	+	0.006218713	-0.31174484
PLXNA3	+	1.9932191e-13	-0.7573008
UBL4A	-	0.008895709	-0.33925188
SLC10A3	-	8.3612234e-5	-0.69085145
FAM3A	-	1.092168e-6	-0.69105273
G6PD	-	0.001466053	0.42470714
DKC1	+	1.963529e-11	1.0852023

BRCC3	+	2.8795932e-4	0.4327121
VBP1	+	0.006467061	0.40772802
USP9Y	+	2.4430687e-4	0.4839188
DDX3Y	+	9.4189454e-7	-0.5237322

Appendix 5b - UC Untreated v LPS DESeq GO Hits List

Gene	Expression change (Upreg/Downreg)	P-value (DESeq UC Untreated vs LPS)	Log2 Fold Change (DESeq UC Untreated vs LPS)
CPTP	+	0.001021866	-0.45570332
CCNL2	-	3.0710921e-6	0.5013549
TNFRSF14	+	6.4495974e-4	0.36469272
KCNAB2	+	9.7977765e-18	0.914092
TNFRSF25	-	6.0469203e-4	1.2052348
KLHL21	-	2.4489868e-8	0.9819713
DNAJC11	-	4.522483e-4	-0.41924822
ERRFI1	-	3.4356098e-11	0.5591307
MIR34AHG	-	3.200105e-5	1.0386186
PGD	+	0.002046965	-0.28701624
MTHFR	-	2.5547852e-6	-0.4842962
VPS13D	+	5.4962136e-4	-0.29185197
ATP13A2	-	1.6548258e-5	-0.44037476
PADI1	+	7.9218526e-14	2.1268482
ARHGEF10L	+	0.001940552	-0.33771423
AKR7A3	-	0.002041905	-0.40433106
RNF186	-	0.00222804	0.37641314
MUL1	-	8.3802897e-4	-0.48432928
EIF4G3	-	2.2762064e-4	-0.3223075
LINC01355	-	0.002429056	1.2946936
E2F2	-	0.002589288	-0.43138412
RPL11	+	0.002706527	-0.25516245
CLIC4	+	1.6365778e-4	0.3317952
RSRP1	-	1.7718698e-29	1.1791393
LDLRAP1	+	0.001613429	-0.38439697
SFN	+	1.2138997e-5	-0.41069993
AHDC1	-	4.937703e-4	0.42084715
EYA3	-	6.8047106e-5	0.43994233
SESN2	+	1.5318856e-10	-0.8059524
SNHG3	+	8.863959e-7	-0.45981935
TINAGL1	+	2.1184485e-5	0.39279842
COL16A1	-	0.002849032	1.6678997
SMIM12	-	9.829075e-4	-0.42417654
GJB3	+	1.8881498e-7	-0.94023097
SFPQ	-	0.001857452	-0.29240033
THRAP3	+	6.663267e-9	-0.513713
SH3D21	+	2.4380822e-6	0.45863664
AL591845.1	+	0.001113497	0.6065534

ZC3H12A	+	5.021319e-28	1.4874555
MFSD2A	+	0.001706072	-0.39453098
RLF	+	1.2201089e-4	0.42985728
COL9A2	-	5.368044e-7	2.7785945
GUCA2A	-	9.491245e-9	-1.0948614
SLC2A1	-	6.959413e-7	0.44045988
C1orf210	-	0.001666314	-0.3097099
KDM4A	+	1.502989e-5	-0.41216198
AL451062.3	+	0.001514859	-0.37772715
SLC6A9	-	0.001612603	-0.42912936
BEST4	-	4.6217005e-4	-1.0354289
HECTD3	-	3.0785316e-4	-0.3241348
ZSWIM5	-	0.002340441	-0.4852951
PIK3R3	-	3.7632693e-5	-0.5330588
PDZK1IP1	-	3.1032976e-19	1.8481253
FOXD2	+	9.610107e-4	-0.44638067
SLC5A9	+	1.6248494e-5	0.9715742
RAB3B	-	4.4641556e-4	0.28784996
TMEM59	-	3.1546954e-4	0.29838982
ACOT11	+	1.7975514e-4	-0.4186769
DHCR24	-	1.0317738e-5	-0.3461217
PCSK9	+	2.920894e-7	-0.5168936
PLPP3	-	6.422909e-6	0.71562153
JUN	-	7.0356595e-4	0.28418583
LEPR	+	1.782129e-5	0.58727175
WDR78	-	2.9559376e-6	-0.8351029
MIER1	+	1.3054855e-4	-0.34779024
GADD45A	+	2.0603837e-4	0.36951843
SRSF11	+	6.51284e-6	0.45616862
FUBP1	-	8.903114e-6	0.49713984
DNAJB4	+	5.3519328e-11	1.4954853
CTBS	-	0.001224144	0.40119168
MCOLN2	-	6.781022e-4	-0.5000294
DDAH1	-	1.6507933e-6	-0.4012025
CLCA1	+	1.5151408e-6	-0.721265
GBP1	-	0.001117016	1.0823895
GBP2	-	2.1773348e-10	0.62693626
CCDC18-AS1	-	4.066585e-6	0.810414
F3	-	5.4694543e-12	0.7511836
AGL	+	2.4087181e-5	-0.45887512
PRPF38B	+	2.8140834e-4	0.4528492
AHCYL1	+	4.3427877e-4	0.27081862
DRAM2	-	1.5090101e-6	0.50150263
CEPT1	+	5.2526416e-6	0.5025876
DENND2D	-	1.4104381e-4	0.40492007
BCL2L15	-	6.404781e-8	-0.529507

ATP1A1	+	8.321665e-14	-0.5275699
TENT5C	+	2.5121885e-11	0.732888
PHGDH	+	0.001064421	0.3659785
HMGCS2	-	1.183856e-4	-0.28271067
SEC22B	-	3.0017676e-5	0.4889286
TXNIP	-	5.824008e-39	0.91355515
PRKAB2	-	3.8988444e-11	0.65540683
HIST2H2BE	-	0.001477253	0.4070047
MTMR11	-	2.3113335e-16	0.64362884
ECM1	+	9.718508e-8	1.4458326
CTSS	-	5.540125e-4	0.31782144
AL590133.2	+	6.9375517e-4	-6.335709
CGN	+	0.00114207	-0.26338834
TUFT1	+	1.9829265e-4	0.38531676
RORC	-	2.8843694e-9	0.64814436
S100A10	-	1.1421028e-4	-0.3209867
S100A14	-	1.5388975e-4	-0.29972836
RPS27	+	3.5257151e-4	-0.33138186
EFNA1	+	2.8438724e-21	0.7908262
SLC50A1	+	9.49471e-4	0.30920702
MUC1	-	5.001867e-5	-0.8450921
KHDC4	-	1.09538945e-7	0.70295334
MEF2D	-	0.002169525	0.33693194
ETV3	-	0.001177913	0.32806963
IGSF9	-	0.002259013	0.32539773
UCK2	+	4.1378576e-6	-0.63454276
DCAF6	+	0.00278976	-0.2830226
ATP1B1	+	1.3013574e-4	0.28594032
VAMP4	-	0.001561603	0.58493793
QSOX1	+	0.002343677	0.26051646
IER5	+	2.0985075e-5	0.4588114
LAMC2	+	4.57862e-16	0.65263706
SMG7	+	0.002051348	0.25944194
IVNS1ABP	-	1.6146587e-5	0.42933148
CSRP1	-	4.760991e-6	-0.4679307
NAV1	+	3.893658e-6	-0.62887174
ELF3-AS1	-	8.287399e-7	-0.6486728
PPFIA4	+	2.7749365e-5	0.8825796
BTG2	+	6.314725e-4	0.35116696
ATP2B4	+	2.021183e-7	0.53895134
BLACAT1	-	0.001511629	0.84459025
CTSE	-	1.3071335e-14	1.438726
IKBKE	+	7.231649e-4	0.8784611
PIGR	-	2.0703879e-13	0.5149617
C1orf116	-	1.995862e-5	-0.3824878
YOD1	-	6.9084956e-5	0.43468863

CD46	+	1.0904409e-8	0.4523878
MIR29B2CHG	-	4.527675e-5	0.508842
LAMB3	-	4.127251e-12	0.6259207
G0S2	+	1.5791426e-16	0.7063152
IRF6	-	7.648699e-7	0.3696815
SLC30A1	-	1.5584465e-12	0.59039277
ATF3	+	2.705977e-9	0.61732876
FLVCR1	+	5.0500256e-4	-0.4074139
SLC30A10	-	5.7969777e-5	-0.50998
COQ8A	+	6.541546e-6	0.53317034
SIPA1L2	-	9.926214e-5	-0.47725844
IRF2BP2	-	3.4431005e-6	0.37448895
CNST	+	3.0733473e-4	0.4088577
CR589904.2	-	3.4540832e-12	0.82530683
LYPD8	-	2.7243755e-24	0.8836389
ZNF692	-	0.002699095	0.6660991
FAM110C	-	0.001703231	0.32687238
ID2	+	1.2983754e-4	-0.6414239
RRM2	+	5.334939e-6	0.5703646
ROCK2	-	3.31276e-11	-0.6295636
NBAS	-	9.37919e-4	0.35234493
PUM2	-	8.761109e-5	0.3465423
RHOB	+	2.72606e-7	-0.5521814
PRKD3	-	5.516158e-4	0.4210274
QPCT	+	1.1449374e-13	0.8798535
HNRNPLL	-	5.7011406e-4	0.47829828
GALM	+	2.4103822e-6	-0.53569597
MAP4K3	-	3.6124626e-4	0.38770106
TMEM178A	+	0.001835536	1.2425373
MCFD2	-	8.73701e-5	0.35730225
EPCAM	+	6.172537e-4	0.2604235
SPTBN1	+	2.3738367e-6	-0.3389897
REL	+	3.0621544e-7	0.49966553
AC010733.2	+	2.4930769e-5	0.53531
PELI1	-	8.4142994e-5	0.39957258
SERTAD2	-	1.6781803e-9	0.5189672
AAK1	-	2.0369498e-7	-0.4573065
ANXA4	+	5.772736e-4	-0.2990739
MXD1	+	1.683371e-8	0.44075248
TIA1	-	7.510558e-5	0.50090325
TEX261	-	0.001670712	-0.38159057
DCTN1	-	4.212129e-5	-0.3937077
TMSB10	+	7.200452e-4	-0.28269303
MAT2A	+	3.3817957e-10	-0.6233641
ST3GAL5	-	7.4863783e-4	1.6567507
KDM3A	+	1.2388054e-15	0.70105755

RNF103	-	6.9229005e-5	0.34609738
RMND5A	+	1.7150745e-5	0.36220098
KRCC1	-	1.06265914e-4	-0.47049046
FABP1	-	5.289609e-4	-0.6923309
GPAT2	-	0.003054517	1.2404927
TMEM131	-	0.001291539	-0.2828492
CREG2	-	6.909811e-5	1.1737647
FHL2	-	4.4653547e-4	0.2806324
SULT1C2	+	1.5715366e-22	1.1758639
MALL	-	3.1149764e-5	-0.3762257
TMEM87B	+	0.001401001	-0.27483943
ZC3H6	+	2.1574018e-5	0.5298376
SLC20A1	+	5.657079e-4	-0.26531488
IL1A	-	1.8232977e-9	2.31276
IL1B	-	2.2882004e-6	2.027469
PSD4	+	7.042952e-6	-0.46507776
STEAP3	+	6.4442675e-6	-0.7184964
DBI	+	3.3963403e-5	-0.44431707
UGGT1	+	7.0605206e-4	-0.31588992
C2orf27A	+	8.736696e-6	0.629537
DARS	-	1.5906061e-4	0.36840352
HNMT	+	6.342941e-5	-0.5873059
LY75-CD302	-	1.9413965e-4	-0.3581366
LY75	-	1.9460064e-4	-0.33843714
PDK1	+	2.2483038e-9	0.5609304
MAP3K20	+	0.001984021	0.56063545
CDCA7	+	3.3505145e-7	0.9319373
SP3	-	2.876511e-4	0.32180429
SESTD1	-	9.473956e-6	0.4772353
ITPRID2	+	0.001426546	0.24890392
FSIP2	+	2.6772053e-5	-0.5899632
ITGAV	+	2.6364485e-6	0.3837691
TFPI	-	0.001025911	1.2830106
SLC40A1	-	1.433276e-39	0.96575624
C2orf88	+	5.5749267e-9	-1.0817398
STK17B	-	0.002430394	0.28591606
SF3B1	-	1.02004925e-7	0.46983695
MARS2	+	0.001856204	-0.84803706
SATB2	-	4.420014e-21	-0.75665784
CLK1	-	0	1.8305583
TRAK2	-	5.562237e-9	-0.63459605
FZD7	+	3.29626e-4	0.56709707
CCNYL1	+	3.9715148e-4	-0.43311116
IDH1	-	1.5380147e-8	-0.4311545
LANCL1	-	0.001826637	0.50239515
RPL37A	+	0.002218744	-0.28103408

IGFBP2	+	7.883965e-7	0.44989318
VIL1	+	1.4802007e-5	-0.30351567
IHH	-	8.6233136e-4	0.3426789
NHEJ1	-	8.574732e-11	0.6261266
AC068946.1	-	9.989046e-11	0.6192
ANKZF1	+	6.1623666e-8	0.5794915
GMPPA	+	9.084321e-5	0.56469893
CHPF	-	7.507629e-11	0.7493043
SERPINE2	-	5.297565e-11	0.5887298
IRS1	-	0.002304185	-0.40040958
RHBDD1	+	9.386054e-4	0.40115172
CCL20	+	1.4099091e-33	1.5311254
PID1	-	8.869964e-9	-1.7458625
C2orf72	+	5.6878733e-4	-0.39359316
MLPH	+	8.677941e-9	0.6120466
RBM44	+	4.983162e-4	1.6611351
BHLHE40	+	4.8220654e-9	0.43670788
THUMPD3-AS1	-	1.9998339e-4	0.5979475
ARPC4	+	0.001597592	-0.27993605
TTLL3	+	1.1301033e-10	0.91873014
JAGN1	+	2.4508435e-4	-0.5152059
IL17RE	+	4.149977e-4	-0.40181154
VHL	+	0.001162733	-0.35547784
IRAK2	+	0.001177064	0.610355
TSEN2	+	1.403301e-4	-0.77335966
ACVR2B	+	5.0534345e-6	0.7884604
WDR48	+	1.6853313e-6	0.63133544
NKTR	+	2.4264632e-4	0.38539943
ALS2CL	-	1.0527107e-8	0.58480746
TMA7	+	0.002384492	-0.5057683
UQCRC1	-	5.277647e-4	-0.3126212
WDR6	+	7.541907e-4	-0.41398746
LAMB2	-	7.10752e-5	-0.6147812
TCTA	+	4.0107872e-4	-0.68047655
ALAS1	+	0.001222	-0.29270658
ARF4	-	9.0351336e-5	0.33304703
FLNB	+	3.5297615e-4	-0.26917404
PXK	+	0.00100738	0.48596993
TMF1	-	4.2388408e-4	0.34309852
PPP4R2	+	7.564655e-4	0.31988448
PROS1	-	2.2482674e-4	-0.6619259
DHFR2	-	0.002889591	-0.9132093
CLDND1	-	3.735736e-7	0.6293988
NFKBIZ	+	2.8296903e-26	1.4369951
BBX	+	3.5427487e-4	0.50107986
AC112128.1	-	0.002201694	0.42632028

SPICE1	-	9.44844e-4	0.45680475
USF3	-	3.2497155e-5	-0.3835502
TMEM39A	-	3.4964232e-9	0.8397984
HGD	-	1.6912223e-4	0.41263494
POLQ	-	0.002288307	0.7479586
MYLK	-	0.001102421	-0.26399827
CCDC14	-	0.00224906	0.35990047
MUC13	-	4.0623205e-4	0.2718943
TMCC1	-	8.6918124e-4	0.32393372
PPP2R3A	+	3.355428e-8	-0.7131431
NCK1	+	1.6977308e-4	0.5337522
SLC25A36	+	9.897918e-8	0.57270414
XRN1	-	1.7837537e-4	0.34261104
U2SURP	+	0.001489871	-0.34233746
AC107021.2	-	6.533355e-5	0.91663355
PLSCR4	-	0.002306969	-0.50918525
HPS3	+	0.002414708	0.41464263
TM4SF1	-	3.7444953e-4	0.27009904
PFN2	-	7.822954e-5	0.47185943
SERP1	-	1.7414172e-6	0.42335603
MBNL1	+	0.002798543	-0.2520133
TIPARP	+	3.7321857e-13	0.7456068
CCNL1	-	2.2519503e-14	0.77941537
SMC4	+	6.536365e-5	0.41085458
ARL14	+	6.1712327e-4	-0.48739403
GOLIM4	-	3.91973e-5	-0.41416895
MECOM	-	3.2673874e-5	-0.4675007
LRRC31	-	1.5580856e-5	-0.6557021
FNDC3B	+	0.001690971	0.25685683
ZMAT3	-	8.148026e-6	0.53105605
FXR1	+	7.022866e-4	0.3760891
KLHL24	+	9.7848264e-5	0.46126688
YEATS2	+	7.556447e-7	0.47550148
EIF4G1	+	4.486465e-4	-0.26806372
EPHB3	+	1.01956054e-7	1.162782
IGF2BP2	-	0.001109453	0.2814469
EIF4A2	+	6.361388e-8	0.45966524
BCL6	-	5.474048e-4	0.4559781
LPP	+	2.4929075e-4	-0.27303556
BDH1	-	0.001034756	-0.3788879
ATP5ME	-	0.001542684	-0.41178736
LETM1	-	8.756287e-9	-0.5428262
HTT	+	7.201291e-4	-0.29498923
PSAPL1	-	1.2665615e-12	1.7776302
SH3TC1	+	4.5131237e-5	0.6605779
FGFBP1	-	6.909827e-5	-0.33258513

PROM1	-	4.521149e-4	-0.34662202
MED28	+	4.1818962e-4	0.40199587
LCORL	-	4.5264664e-4	0.5206214
ADGRA3	-	0.003070778	-0.3284024
PPARGC1A	-	1.164968e-15	-1.0439974
ZCCHC4	+	2.5078323e-4	0.72520363
RBPJ	+	8.7161624e-7	0.46537933
KLF3	+	8.5712045e-8	-0.40053624
ATP8A1	-	4.880193e-11	-0.75743777
LRRC66	-	4.1976094e-4	-0.657091
KIT	+	0.002175006	-0.3038496
TMEM165	+	1.6910263e-4	0.34761286
KIAA1211	+	2.5115974e-4	-0.37324437
UGT2B17	-	2.5113581e-20	-1.3507329
UGT2B15	-	0.001076943	-1.3310261
SULT1B1	-	0.001079495	-0.26828334
SLC4A4	+	6.497141e-12	-0.71944517
RASSF6	-	1.265886e-6	0.40128234
CXCL8	+	1.151877e-6	1.1598135
CCNG2	+	6.0052134e-6	0.39643756
CNOT6L	-	2.4243171999999997e-007	0.5149979
BMP2K	+	5.1352305e-9	-0.5274799
ANTXR2	-	2.4226162e-4	0.3196453
RASGEF1B	-	1.101636e-7	1.0705289
ABCG2	-	8.132351e-5	0.39526886
FAM13A	-	2.761536e-12	0.5169721
ATOH1	+	0.001143014	-1.440956
TSPAN5	-	0.001139777	0.4665076
AC114811.2	+	5.422972e-5	2.1445563
ADH1C	-	3.638978e-17	-1.2100596
DAPP1	+	1.660368e-8	1.0511047
ARHGEF38	+	0.001084185	0.47453117
HADH	+	0.002519377	-0.29216358
OSTC	+	0.002272717	0.35678092
EGF	+	1.6942693e-8	0.85025364
PRSS12	-	3.7343625e-6	-0.42856812
SEC24D	-	4.2618427e-7	0.4416263
NDNF	-	0.002194597	0.2955982
HSPA4L	+	1.768463e-8	0.7622514
SLC7A11	-	1.2591671e-8	-0.5487611
SETD7	-	0.001656832	0.30988312
SMAD1	+	9.004969e-4	-0.43333805
TMEM144	+	2.054531e-4	0.46795958
DDX60	-	0.002083639	0.46047056
DDX60L	-	0.001923579	0.3013367

CEP44	+	8.8906137e-4	0.6096143
ACSL1	-	3.2531537e-4	-0.2761376
ANKRD37	+	2.940372e-7	0.70971906
TLR3	+	1.0283593e-6	0.6355063
AC010442.1	-	5.4220457e-8	-1.0457629
SLC9A3	-	8.177256e-17	-1.1666917
NDUFS6	+	4.7879826e-6	-0.7772132
SEMA5A	-	3.365417e-13	-0.93613255
CMBL	-	1.0645767e-5	-0.41015896
MARCH6	+	2.9145053e-4	0.29199994
DAB2	-	0.001798082	-0.3638636
PTGER4	+	5.582718e-5	0.58963346
SELENOP	-	4.7110646e-8	0.5642276
CCL28	-	1.1209698e-4	0.45821443
NNT	+	2.4070198e-6	-0.41705614
GPBP1	+	7.5808915e-5	0.38333672
TRIM23	-	0.001482414	0.6073581
SLC30A5	+	1.9607537e-4	0.4065488
HEXB	+	0.001993255	0.27681348
IQGAP2	+	1.6379627e-9	-0.58370787
ZBED3	-	6.543818e-11	-1.1713984
SCAMP1	+	0.001528026	0.3215959
TMEM161B-AS1	+	1.08229735e-7	0.6734841
ARRDC3	-	1.7936941e-37	1.216084
RGMB	+	1.0992484e-7	0.79503965
SLCO4C1	-	1.556386e-9	-0.9621975
FEM1C	-	1.5939545e-9	0.5456761
TICAM2	-	8.3983736e-4	0.7544643
ZNF608	-	3.2146403e-4	-0.45580208
GRAMD2B	+	4.671779e-5	0.3564054
PRRC1	+	1.2921977e-4	0.33064815
FNIP1	-	0.002111861	0.3143743
SLC22A4	+	9.942651e-4	-0.98096097
IRF1	-	6.001429e-6	0.5953549
LEAP2	+	3.534089e-5	0.88791245
SEC24A	+	1.5216395e-5	0.37305477
PURA	+	8.064418e-6	0.4269351
IGIP	+	4.6092406e-4	0.58705366
HBEGF	-	1.0630145e-8	-0.65750694
SH3RF2	+	0.002375773	-0.3246854
SPINK1	-	3.9360393e-6	1.4917482
SPINK5	+	4.0374417e-4	-0.50416696
AC021078.1	-	1.6640354e-4	0.32156628
PPARGC1B	+	1.9947551e-7	-0.664348
SLC26A2	+	0	-1.7422694
CDX1	+	1.1909228e-5	-0.427927

CD74	-	1.1065717e-4	0.744429
NDST1	+	3.721077e-5	-0.48175853
SLC36A1	+	2.0238318e-8	-0.679781
FAXDC2	-	1.8862456e-8	0.9510925
CNOT8	+	5.1189685e-4	0.352736
CYFIP2	+	2.56456e-4	-0.5949572
MIR3142HG	+	2.4207306e-5	6.6642137
PANK3	-	0.002976958	-0.22881186
STK10	-	9.71556e-5	-0.6382257
UBTD2	-	4.3910154e-4	-0.37258378
CREBRF	+	5.280833e-4	0.45288858
CLTB	-	7.169699e-5	-0.3816127
CDHR2	+	1.8856501e-10	0.71608233
RAB24	-	0.001039787	0.5379999
FAM193B	-	9.642911e-5	0.60548985
N4BP3	+	7.921734e-4	0.53647214
CLK4	-	0.002044613	0.59960765
SQSTM1	+	4.825594e-12	0.6090434
FOXQ1	+	4.4718277e-6	0.81984985
ECI2	-	9.1205386e-4	-0.47628805
SSR1	-	0.001805562	0.24929799
TXNDC5	-	4.4900415e-5	0.3837261
BLOC1S5-TXNDC5	-	3.7326008e-5	0.38903695
ADTRP	-	1.3050967e-4	0.42385805
SOX4	+	9.138238e-6	0.46124357
CARMIL1	+	0.001369567	-0.28596976
TRIM38	+	0.001554452	0.43285802
HIST1H2BC	-	4.0810867e-4	0.41664582
HIST1H1E	+	1.3900033e-8	-0.639505
HIST1H2BD	+	2.8846334e-4	0.32923335
BTN3A2	+	9.1523555e-4	0.86039776
BTN3A1	+	1.5864742e-11	1.3806454
BTN3A3	+	1.2834767e-4	1.2902458
HLA-F	+	1.4177684e-8	0.7918028
HLA-A	+	1.956373e-13	0.5878677
RNF39	-	2.5085694e-11	1.2039648
PPP1R10	-	3.5759464e-9	-0.6079027
FLOT1	-	1.3245913e-4	-0.35228667
IER3	-	3.5034704e-5	0.47838566
PSORS1C1	+	3.7178463e-6	0.83004194
POU5F1	-	0.001268898	0.67185986
PSORS1C3	-	8.9882646e-4	1.2118794
HLA-C	-	6.729986e-6	0.36256567
HLA-B	-	4.4765945e-22	0.7942031
HCP5	+	0.001422422	0.5215928

DDX39B	-	0.001617978	0.268121
C6orf47	-	0.002694529	-0.46738753
HSPA1A	+	0.001858028	0.47485197
HSPA1B	+	3.0596115e-28	0.95358884
AL671762.1	+	0.001959143	0.43090007
AL645922.1	+	5.6925453e-10	0.9362198
CFB	+	3.5026065e-10	0.91852736
TNXB	-	0.001576854	1.3929944
TAP1	-	5.397809e-7	0.5082326
BRD2	+	2.1075786e-4	0.29167724
TAPBP	-	5.705047e-5	0.38564286
MAPK14	+	0.002606305	0.26996166
C6orf222	-	7.655473e-26	1.3636136
PIM1	+	1.1784096e-7	0.43293336
NFYA	+	0.001344238	0.40524903
C6orf132	-	8.195166e-4	-0.2842972
KLC4	+	8.587204e-4	-0.38685182
ABCC10	+	2.6554175e-4	-0.5405361
GTPBP2	-	0.002984892	0.289385
VEGFA	+	5.3747294e-24	0.739431
AL109615.2	+	7.7497703e-4	1.2038502
HSP90AB1	+	5.4788774e-7	0.42274854
NFKBIE	-	2.1524374e-4	0.67289597
CLIC5	-	0.001340339	0.30353323
TNFRSF21	-	1.9965191e-7	0.3896703
AL033397.1	-	3.1723492e-4	1.9615929
AL135905.1	-	0.002326372	-1.2748139
TMEM30A	-	4.2755955e-6	0.3711465
AL359715.1	+	0.002891174	0.8901026
TENT5A	-	4.4383322e-10	0.62009466
DOP1A	+	6.7827405e-6	-0.5359795
PGM3	-	4.0361872e-10	0.61659503
ZNF292	+	5.947575e-9	0.557535
PNRC1	+	9.110175e-12	0.6373925
MAP3K7	-	2.4242232e-4	0.45132956
PNISR	-	8.35094e-9	0.5926724
PRDM1	+	0.00143573	0.4388586
CD24	-	2.654914e-8	-0.45886153
FOXO3	+	5.876359e-13	0.54421496
MAN1A1	-	2.033377e-4	-0.40630987
SMPDL3A	+	8.321049e-4	0.30233696
ECHDC1	-	5.5275264e-4	-0.41878965
AKAP7	+	4.616092e-11	0.7697205
MED23	-	0.001488786	0.36214933
ENPP3	+	1.9168718e-7	0.516281
SGK1	-	0.001393376	-0.6438147

TNFAIP3	+	2.8149884e-22	1.1309117
ARFGEF3	+	0.001445205	-0.27563402
NHSL1	-	8.7631886e-21	-0.7489604
REPS1	-	0.001001668	-0.43877023
ABRACL	+	0.002485392	-0.42032763
PHACTR2	+	1.2296747e-4	-0.39386243
AL355312.6	-	0.001614869	0.3035734
LRP11	-	2.70079e-4	0.3354465
ACAT2	+	2.1274984e-9	-0.55008364
IGF2R	+	5.0970556e-12	-0.5267793
FRMD1	-	1.2825314e-5	1.1375688
WDR27	-	0.002693948	0.5030993
MICALL2	-	3.8905063e-7	0.6058113
IQCE	+	5.981292e-4	-0.40715057
ARL4A	+	1.1435713e-4	-0.44836956
TSPAN13	+	1.4349916e-17	0.6572085
AGR2	-	6.9253123e-4	0.26979604
RAPGEF5	-	1.0543047e-4	0.4216697
NFE2L3	+	9.815013e-4	0.30637205
HOXA6	-	0.001942262	1.5027682
WIPF3	+	4.8114464e-7	0.45540074
EPDR1	+	0.003026142	0.74705064
YAE1	+	2.728313e-4	-0.83436203
IGFBP3	-	3.0725658e-7	0.880116
TNS3	-	4.3312208e-11	-0.69926435
GRB10	-	8.637289e-4	0.4154376
ASL	+	4.3704192e-4	-0.37642983
BCL7B	-	1.6435234e-4	-0.501552
CCDC146	+	0.002000483	0.6617711
STEAP2	+	0.001253476	0.47850665
CLDN12	+	1.9123188e-4	0.32418638
AKAP9	+	3.0824734e-4	-0.3614007
HEPACAM2	-	4.993807e-4	-0.993324
CASD1	+	2.871765e-5	-0.4514327
PEG10	+	1.3193088e-33	-1.0973909
TRRAP	+	5.3312207e-5	-0.38544405
SMURF1	-	1.0733955e-4	0.328564
AC004922.1	+	9.135015e-4	-0.26687694
ARPC1B	+	1.6446945e-8	-0.51508236
CYP3A5	-	4.0493653e-9	0.47790504
CYP3A4	-	3.2281794e-6	1.5135796
AZGP1	-	2.7122447e-9	0.9605754
AGFG2	+	0.001526783	-0.42607576
SAP25	-	5.2728985e-5	1.3901391
SRRT	+	0.002101398	-0.38257104
MUC12	+	1.034576e-17	-0.79692507

MUC17	+	7.9103727e-19	0.73361444
MOGAT3	-	3.8988102e-4	0.4516906
NAPEPLD	-	5.578191e-4	0.40952885
NAMPT	-	4.567712e-4	0.37153098
HBP1	+	4.2476863e-4	0.37042564
SLC26A3	-	1.2443359e-14	-0.57729006
DNAJB9	+	7.7135956e-5	0.5747797
CFTR	+	4.263413e-14	-0.72542757
AC000123.3	-	0.001009984	0.63664174
HILPDA	+	2.986702e-29	1.1804582
AC010655.2	+	0.001793618	0.76237446
CALU	+	7.618892e-9	0.559291
AHCYL2	+	2.037729e-4	0.2769168
AKR1B10	+	1.1308013e-4	0.29452774
CYREN	-	0.001900349	-0.5815905
TMEM140	+	4.4206722e-4	0.9862669
CREB3L2	-	4.2226652e-4	0.27512854
TBXAS1	+	0.002065206	0.5348337
KIAA1147	-	5.577457e-8	0.54128575
SLC4A2	+	1.9149118e-4	-0.5393952
AC021218.1	+	5.2902027e-4	-0.39048687
PTPRN2	-	1.0263161e-7	0.5657245
KBTBD11	+	2.882815e-6	-0.45020118
PPP1R3B	-	2.3387866e-11	0.6329873
CTSB	-	3.5045797e-4	0.31742454
MTUS1	-	2.9978115e-4	-0.31314066
HR	-	6.252236e-4	-0.68784755
SORBS3	+	2.0977125e-6	-0.7628144
TNFRSF10B	-	4.6134896e-10	0.5897953
TNFRSF10C	+	2.4743952e-4	1.1930398
SLC25A37	+	4.164286e-5	0.82719636
DOCK5	+	7.239297e-6	-0.35502297
GNRH1	-	9.2526537e-4	1.6938021
PPP2R2A	+	2.033697e-6	0.4495321
DPYSL2	+	3.1889242e-4	-0.32799277
KIF13B	-	0.002763316	-0.23535171
GTF2E2	-	0.001863767	0.36273673
RAB11FIP1	-	0.00236353	0.2261818
PLPP5	-	0.001219168	0.60440826
NSD3	-	7.0350216e-4	0.32625484
TACC1	+	2.995399e-6	-0.5299894
SLC20A2	-	3.0834086e-5	-0.41819188
FNTA	+	1.0444223e-4	0.48505792
PRKDC	-	0.001971515	-0.28349155
SDR16C5	-	7.2434e-10	1.1082575
CA8	-	0.001678758	1.1892486

ASPH	-	5.143519e-6	0.36890572
RDH10	+	2.9389541e-5	0.4073575
TMEM70	+	2.6682399e-8	0.48879337
PAG1	-	5.984348e-4	0.25046682
CA13	+	7.023949e-4	-0.5372143
CA1	-	0	-1.9086468
CA2	+	5.473757e-20	-0.782315
INTS8	+	7.4212917e-4	0.3854241
TP53INP1	-	1.4929671e-4	0.4449748
SPAG1	+	0.002288313	-0.44594094
RNF19A	-	1.2218491e-7	0.4807381
AP003469.4	-	0.001603762	0.79803413
ZNF706	-	4.3499703e-4	0.3758208
KLF10	-	7.938183e-4	0.28171903
OXR1	+	2.1009424e-4	0.3806513
RAD21	-	0.002480102	0.25966537
EXT1	-	3.1776022e-4	-0.33956173
ATAD2	-	1.3394632e-4	0.59329444
FBXO32	-	1.4795658e-5	0.5039452
FER1L6	+	4.505369e-5	-0.54730797
NDUFB9	+	2.9506593e-5	-0.4592553
MTSS1	-	6.9462473e-4	0.56426173
NDRG1	-	8.496319e-7	0.35025382
AC083843.3	-	5.09382e-7	1.1469907
FAM83H	-	1.2417452e-4	-0.39874214
EPPK1	-	2.9380834e-25	-1.0133972
PLEC	-	5.487455e-6	-0.3969053
SLC39A4	-	0.001540028	0.3542744
ZNF252P-AS1	+	3.0044072e-7	1.8583459
C8orf33	+	0.002207086	-0.2623944
RFX3	-	1.10955654e-4	0.55273753
SLC1A1	+	0.00218301	0.2871311
PLPP6	+	9.646091e-5	-0.7453389
ERMP1	-	5.814501e-4	0.28116667
ZDHHC21	-	0.002002377	-0.38267627
AL158206.1	+	4.1689863e-4	0.44498727
CDKN2B	-	6.6209686e-6	-0.5032051
DNAJA1	+	1.5161974e-11	0.77123517
BAG1	-	1.5065658e-6	-0.5483774
PRSS3	+	0.00138433	-0.36260876
UNC13B	+	2.6559355e-5	-0.41036123
TLN1	-	3.0270546e-6	-0.41974953
RGP1	+	2.7611179e-5	-0.34733355
HRCT1	+	4.947564e-5	-0.906665
GNE	-	3.3948118e-14	-0.5872215
EBLN3P	+	8.902604e-15	0.7730864

SHB	-	4.7353894e-4	-0.5150399
PTAR1	-	0.001945167	0.3102595
GDA	+	3.9320497e-17	0.78916234
TRPM6	-	8.2844135e-35	-1.6571991
PCSK5	+	2.1082456e-6	-0.42333397
UBQLN1	-	2.705646e-5	0.37743667
CKS2	+	0.002158776	0.63928604
SYK	+	3.4653753e-5	-0.4228453
NFIL3	-	3.811208e-6	0.5053938
CORO2A	-	1.7889063e-8	-0.4358371
ALDOB	-	3.7841403e-4	1.535701
ABCA1	-	6.0804127e-6	-0.9697255
UGCG	+	6.0877708e-5	0.39853662
ALAD	-	7.254286e-4	-0.3674261
TNFSF15	-	1.2707159e-8	-1.0478419
ZBTB34	+	0.002648953	0.37091467
FAM129B	-	0.001417268	-0.2902975
SLC25A25	+	4.9493354e-7	0.4945138
LCN2	+	0	3.429006
SPTAN1	+	6.160004e-8	-0.4112938
TOR1A	-	0.002637021	-0.53085965
HMCN2	+	9.735404e-9	-0.79607666
ASS1	+	1.2313788e-7	-0.4641563
ABO	-	1.8052579e-4	-0.48250777
PHPT1	+	9.129612e-6	0.5764599
MAMDC4	+	1.2460555e-4	0.6828318
TUBB4B	+	6.546895e-4	-0.32114828
NRARP	-	9.407226e-4	-0.3624726
AKR1C1	+	6.9667117e-15	0.89005685
AKR1C2	-	1.850494e-11	1.0601383
AKR1C3	+	2.4046046e-11	0.5837611
ASB13	-	0.001120959	-0.4608649
PFKFB3	+	2.3404387e-28	0.9090885
LINC02649	+	4.862123e-5	0.9035811
RSU1	-	0.002728286	-0.34403372
TMEM236	+	4.6106265e-7	-1.0561665
MRC1	+	0.003074241	-3.0366712
ARL5B	+	5.3781775e-9	0.5676637
NEBL	-	3.5533816e-5	0.43657193
WAC-AS1	-	1.1675016e-4	-0.709983
MAP3K8	+	1.0176807e-4	0.82686794
AL117339.5	+	9.263459e-6	1.3533592
WASHC2C	+	6.888795e-5	-0.7580994
CDK1	+	6.807173e-4	0.7161311
AIFM2	-	0.001138455	-0.38133606
PSAP	-	6.0779555e-5	0.29630002

DNAJB12	-	0.001217236	-0.44686416
P4HA1	-	6.511796e-19	0.7471849
FUT11	+	7.347993e-11	0.63721969999999994
CDHR1	+	2.1434796e-6	-0.45599186
ATAD1	-	1.0750249e-5	0.44015977
PPP1R3C	-	4.3e-44	1.557838
TNKS2	+	3.0416724e-5	0.41197363
MYOF	-	7.168112e-6	-0.3595495
FFAR4	+	7.361986e-11	-0.7590038
PLCE1	+	5.9378517e-6	-0.36641973
SORBS1	-	5.923078e-7	0.6480361
DNMBP	-	1.247164e-5	0.36230364
SCD	+	1.795826e-4	-0.2545926
OGA	-	0.002141021	0.3031119
NFKB2	+	2.0098261e-7	0.6763281
MXI1	+	5.9863603e-5	0.3100461
SMNDC1	-	1.6610372e-4	0.48970687
DUSP5	+	1.1476306e-20	0.7825918
FGFR2	-	8.967676e-5	0.49510688
TACC2	+	0.001378234	-0.31373483
CLRN3	-	0.001138268	-0.3598582
ADAM8	-	3.5511693e-25	1.3051387
ANO9	-	3.646273e-8	0.5525522
RASSF7	+	1.32131545e-5	0.48216042
MUC2	+	2.3306772e-9	-0.58718073
MUC5B	+	1.4596831e-7	0.7385734
KCNQ1OT1	-	1.7906021e-4	0.36808798
PHLDA2	-	0.001383252	0.42125735
TRIM22	+	1.411055e-7	1.5631486
DNHD1	+	0.002293554	0.46165046
ZNF143	+	6.002058e-4	0.46455783
WEE1	+	2.613639e-6	0.6845763
ADM	+	2.983e-42	1.4087197
MICAL2	+	1.8704051e-4	-0.27236947
NUCB2	+	0.001109114	0.5133738
NCR3LG1	+	2.8398078e-6	-0.57865214
ABTB2	-	0.002245653	0.36825308
PRR5L	+	9.194699e-14	-0.81809133
TTC17	+	0.001726348	0.32751873
ARHGAP1	-	0.00300046	-0.33588812
DDB2	+	1.15635856e-7	0.814233
ACP2	-	2.3558374e-4	-0.69441646
DTX4	+	1.9622441e-4	-0.3321314
MS4A12	+	9.194914e-4	-0.38565624
SYT7	-	0.001783599	0.30236486
AP003108.5	-	3.8671304e-4	1.5270679

FADS2	+	2.3190132e-9	-0.5224126
FADS1	-	2.9801683e-7	-0.4797014
SCGB2A1	+	3.722048e-4	2.123952
HNRNPUL2-BSCL2	-	7.945123e-4	-0.3134026
HNRNPUL2	-	0.002091465	-0.2854766
WDR74	-	1.7439606e-4	-0.41219252
AP000721.1	+	0.0021144	-0.49632612
AP001453.5	+	0.002633766	-0.42384255
PLCB3	+	4.9243565e-4	-0.32908532
MIR194-2HG	-	0.001371003	0.38027668
ARL2-SNX15	+	2.7693154e-8	-0.72378856
SNX15	+	2.0896651e-7	-0.72434425
TM7SF2	+	1.4671314e-10	-0.8185433
CAPN1	+	7.5102615e-4	-0.37089476
NEAT1	+	3.0571e-41	0.92710257
MALAT1	+	2.3468972e-16	0.7098478
CFL1	-	0.002868279	-0.2288009
EFEMP2	-	5.2618456e-5	1.19151
BRMS1	-	3.4429654e-4	-0.8222828
DPP3	+	3.4087006e-5	-0.51781017
PC	-	5.3312697e-6	-0.52339536
C11orf86	+	0.001806928	-0.5104646
PPME1	+	0.001840092	0.39251775
ARRB1	-	7.803605e-8	-0.47761476
AP001972.5	-	4.8114195e-8	-0.7163402
PAK1	-	1.011412e-4	0.33090314
KCTD14	-	6.580754e-9	0.6996369
CREBZF	-	6.849913e-11	0.7052062
SYTL2	-	8.233848e-8	-0.464415
PRSS23	+	1.0487871e-4	0.31125757
FZD4	-	2.85626e-4	-0.7397752
CHORDC1	-	1.1231004e-7	0.99614745
SCARNA9	+	3.0259675e-4	0.64208144
TAF1D	-	3.433903e-10	0.7237298
SRSF8	+	0.001100517	-0.49276188
BIRC3	+	2.39E-06	1.5850106
BIRC2	+	1.1688521e-6	0.4716982
TMEM123	-	3.7347647e-8	0.46730122
ACAT1	+	0.001216645	-0.47353783
EXPH5	-	0.001247122	-0.36767268
ZC3H12C	+	4.7694e-7	0.8466895
DLAT	+	0.001052408	-0.3123424
IL18	-	0.001532493	-0.74135625
NXPE1	-	3.549959e-8	0.47930658
NXPE4	-	5.1467612e-8	-0.4764941

NXPE2	+	0.002116212	-0.35086417
SIK3	-	2.4412537e-5	-0.66214514
MPZL3	-	9.656393e-12	0.65441877
MPZL2	-	5.6775425e-5	0.33497915
ARCN1	+	1.0546136e-4	0.31567585
C2CD2L	+	4.4244883e-4	0.38053238
USP2	-	5.439158e-11	-1.2575766
TRIM29	-	1.9978928e-5	0.6801949
HSPA8	-	1.7492522e-19	0.7671301
SRPRA	-	5.1348197e-5	0.36227143
GSEC	-	1.0980648e-6	0.7652571
ST3GAL4	+	4.5869154e-5	0.33656856
FKBP4	+	3.7493734e-5	0.40048072
CRACR2A	-	2.8635845e-5	-0.8335583
PTMS	+	1.1156366e-9	-0.6065057
ENO2	+	3.26146e-23	0.8492548
LPCAT3	-	1.1166794e-6	-0.5687186
C1RL	-	2.2170699e-4	-0.55616903
CDKN1B	+	7.3467054e-5	0.4144371
AC008115.3	+	4.679841e-4	1.719546
MGST1	+	8.076821e-4	0.3005083
GOLT1B	+	5.337887e-6	0.7354264
ETNK1	+	4.061568e-6	0.3930839
ITPR2	-	0.001468828	-0.38466755
STK38L	+	7.8811124e-4	0.38358262
PKP2	-	4.5990783e-10	-0.5419424
SLC38A1	-	1.9668607e-5	-0.33316585
SLC38A2	-	1.3235794e-11	-0.5439331
SLC38A4	-	3.6830083e-5	-0.9558964
CCNT1	-	7.3665564e-5	0.40432605
TUBA1C	+	3.2530952e-8	-0.49826515
AC008147.2	-	1.9204937e-4	0.80828273
METTL7A	+	1.5818551e-7	-0.4270362
SLC11A2	-	6.781811e-9	0.47138742
LETMD1	+	7.76568e-5	0.41483837
NR4A1	+	0.001413198	0.6491425
KRT7	+	0.001612788	0.7069142
KRT8	-	8.751564e-9	-0.46531087
KRT18	+	3.8069476e-5	-0.35113162
PYM1	-	4.6241318e-4	-0.4478062
DGKA	+	1.0036207e-4	0.33630973
RPS26	+	1.7587466e-7	-0.5401015
RPL41	+	3.5072843e-19	-1.0674362
ESYT1	+	0.001133299	-0.33995643
MYL6B	+	0.00148156	-0.40302742
ANKRD52	-	6.51381e-6	-0.4507843

PAN2	-	9.845754e-4	0.48093778
RBMS2	+	8.205439e-5	-0.40529186
PTGES3	-	1.5608732e-4	0.3123688
MYO1A	-	1.9781266e-5	-0.33212197
NEMP1	-	2.060332e-4	0.75053847
LRP1	+	2.7492514e-4	-0.35174873
NDUFA4L2	-	0.002191578	0.51759017
SRGAP1	+	9.139491e-5	-0.45461795
XPOT	+	3.900554e-5	0.41397652
RASSF3	+	6.033641e-4	-0.29997492
LYZ	+	2.8604796e-7	0.37148666
PTPRR	-	6.415743e-11	0.57764375
TBC1D15	+	2.8499594e-4	0.59473115
PHLDA1	-	8.384608e-7	0.476674
KITLG	-	4.8532317e-4	-0.55622154
DUSP6	-	5.069222e-10	0.4606763
POC1B-GALNT4	-	0.001106847	-0.29090652
GALNT4	-	5.6711637e-4	-0.3020864
ATP2B1	-	1.6632567e-8	-0.5448732
BTG1	-	4.4752363e-5	0.33366632
FGD6	-	5.714202e-7	0.47293293
ARL1	-	8.696859e-6	0.41997275
CKAP4	-	7.801102e-4	0.32767025
TMEM263	+	2.917078e-8	0.61659014
SSH1	-	0.00147972	-0.40955067
ACACB	+	2.1233373e-5	-0.62739134
KCTD10	-	5.9626554e-4	-0.3620338
MMAB	-	7.101128e-4	-0.4438887
MVK	+	8.6241047e-4	-0.448644
PLBD2	+	9.803923e-4	-0.45550266
TBX3	-	2.2655785e-8	0.5431854
VSIG10	-	7.274581e-6	-0.36624163
PEBP1	+	4.0452713e-7	-0.4452141
DYNLL1	+	5.2226114e-4	0.35872325
MLXIP	+	4.2552088e-4	-0.32504028
RSRC2	-	2.8742643e-6	0.54099536
UBC	-	1.4332631e-4	0.28667253
AACS	+	2.963524e-7	-0.45253652
ULK1	+	1.5217168e-4	0.42860997
AC131009.4	+	3.2855365e-5	1.5237403
ZNF84	+	0.001550908	0.5834958
ZMYM2	+	2.0649827e-4	0.3586713
ATP12A	+	4.0984004e-11	0.8790549
NUP58	+	2.9660914e-6	0.45547387
USP12	-	2.6063808e-5	0.39254215
SLC46A3	-	1.107563e-5	-0.6476804

HSPH1	-	1.0498408e-15	1.0161028
FRY	+	8.752167e-10	0.67896587
SMIM2-AS1	+	0.001444449	-0.49833876
COG3	+	7.058251e-4	0.33436868
ITM2B	+	0.001783837	0.2522936
INTS6	-	3.7100253e-5	0.42138138
OLFM4	+	3.0050867e-8	0.65238744
KLF5	+	1.1446359e-6	-0.36074615
SLITRK6	-	9.98977e-8	1.836846
MBNL2	+	1.8072866e-7	0.46602923
EFNB2	-	0.001126065	-0.250051
ARGLU1	-	8.583317e-6	0.46304995
ANKRD10	-	0.001350725	0.35386062
GRTP1	-	0.001927376	-0.40048358
AL355075.4	-	4.0354615e-4	-0.2998694
RPPH1	-	4.001409e-4	-0.2999949
RNASE4	+	3.542773e-4	0.320264
AL163636.2	+	1.8837913e-4	0.3350309
RNASE1	-	0.002241253	0.53811765
ABHD4	+	3.1452507e-4	0.42492417
PPP1R3E	-	8.93104e-9	1.304453
PCK2	+	0.00293878	-0.32456034
NFATC4	+	0.001247981	0.76390165
NYNRIN	+	0.001084439	-0.48274374
ARHGAP5	+	0.001908772	0.256402
EGLN3	-	2.6091996e-6	0.3247694
NFKBIA	-	2.4939932e-11	0.65850973
FOXA1	-	2.8268027e-4	-0.4916576
PRPF39	+	0.001042642	0.5067232
MGAT2	+	1.5532716e-4	-0.41012335
PYGL	-	0.001229517	-0.39217615
ERO1A	-	1.5690066000000001e-027	0.8245975
GCH1	-	2.550698e-4	-0.49316472
SOCS4	+	0.002450031	-0.40295583
MAPK1IP1L	+	0.001546263	-0.288516
ATG14	-	5.5265444e-4	0.56372476
SYNE2	+	1.817455e-5	-0.4027613
PLEKHG3	+	8.192811e-4	0.32446995
GPX2	-	3.150256e-8	0.49605235
FUT8	+	6.912794e-5	0.4835592
ZFP36L1	-	2.3767144e-16	0.8170803
SRSF5	+	3.234789e-6	-0.47764537
TTC9	+	5.252534e-12	0.9312587
RBM25	+	8.145373e-5	0.42285213
PNMA1	-	4.934443e-7	-0.6001361

TMED10	-	9.594897e-4	0.26492327
JDP2	+	1.4435558e-4	-0.63808423
CIPC	+	1.02224e-4	-0.44258362
AL162171.1	-	8.622609e-5	-0.59088415
CALM1	+	7.388117e-4	-0.26991358
CCDC88C	-	3.2056567e-5	-0.3938877
RIN3	+	0.002281371	-0.6475015
ITPK1	-	9.217981e-5	-0.39398855
CLMN	-	0.001166146	-0.23247401
BCL11B	-	4.858105e-4	-0.68321514
DYNC1H1	+	5.921362e-7	-0.36734837
HSP90AA1	-	3.5345415e-8	0.53892803
TNFAIP2	+	2.4618248e-5	1.3488663
EIF5	+	9.1302996e-7	-0.43945417
NIPA1	+	1.0588863e-8	0.56417835
SNHG14	+	0.001343143	0.4496081
HERC2	-	3.4250132e-9	-0.5960178
FMN1	-	1.0253927e-5	-0.44754568
SPRED1	+	0.002721451	0.260778
THBS1	+	2.1061149e-5	-0.35946628
BMF	-	5.1758684e-7	0.87836105
PHGR1	+	0.001157293	-0.32327005
GCHFR	+	1.741957e-4	-1.071849
CHAC1	+	2.3696879e-7	-0.89111215
INO80	-	0.001573449	-0.4058799
ITPKA	+	5.8540295e-6	-0.62582195
LTK	-	4.891675e-4	-1.3253363
TMEM87A	-	4.592033e-5	0.39306378
TMEM62	+	0.001391706	-0.47846556
ZSCAN29	-	0.001926129	-0.47683415
PATL2	-	0.001045278	1.2915775
B2M	+	1.3688191e-14	0.56955326
SORD	+	9.165355e-5	0.4986875
DUOX2	-	4.9191802e-27	0.91610044
DUOXA2	+	5.147369e-25	1.0727342
DUOX1	+	2.24605e-5	0.89453036
C15orf48	+	0.001478243	-0.29761595
AC025580.2	+	9.7012933e-4	0.5076055
SEMA6D	+	1.4920056e-5	-1.4414519
TRPM7	-	5.9899787e-4	-0.31661564
AP4E1	+	1.1222481e-4	-0.5112456
TCF12	+	9.544514e-4	0.3218321
CGNL1	+	8.2116737e-4	0.655111
GCNT3	+	1.9709587e-9	-0.4519364
VPS13C	-	0.002718261	-0.30987793
TLN2	+	5.5990192e-8	-0.50508875

CA12	-	0.001361342	-0.21947327
SPG21	-	3.5590028e-7	0.5050267
SLC51B	+	2.8533705e-5	-0.59308434
SMAD3	+	2.3948557e-8	0.47210145
FEM1B	+	9.815315e-4	0.29442644
PML	+	3.8325135e-5	0.6492798
CLK3	+	3.922548e-5	0.41449565
CSK	+	0.001767714	-0.37767312
SCAMP5	+	3.3180788e-6	-1.0509659
FBXO22	+	0.002363917	0.43368924
IDH3A	+	0.001171776	-0.30249718
DNAJA4	+	3.2765195e-9	0.594179
TMED3	+	8.5363653e-4	0.4071664
ISG20	+	4.9088633e-4	0.45496577
MFGE8	-	0.003009546	0.51734585
ANPEP	-	3.7149742e-4	-0.3176572
AC091167.2	+	1.4465237e-5	0.41783485
NGRN	+	8.556362e-6	0.3969947
ARRDC4	+	1.1002398e-10	0.5239731
AC015660.1	-	1.1000268e-5	0.6750949
LRRK1	+	0.001424363	-0.43465775
PDIA2	+	5.807429e-4	0.5666675
FBXL16	-	5.721827e-5	0.97548395
UNKL	-	1.2949966e-4	0.9823013
MAPK8IP3	+	9.376426e-4	0.37581643
FAHD1	+	4.8135113e-4	-0.44948658
NDUFB10	+	7.19326e-5	-0.5219063
NOXO1	-	0.002272285	0.5829882
SLC9A3R2	+	0.002012776	0.49918476
NTHL1	-	9.348741e-5	1.0148991
ZG16B	+	8.173357e-10	0.9166091
PRSS22	-	0.002689625	0.5948601
IL32	+	3.7517657e-6	0.49406627
DNASE1	+	9.853918e-6	0.727912
ADCY9	-	0.002762126	-0.42990366
HMOX2	+	3.233149e-5	-0.5254466
ABAT	+	5.816496e-4	-0.6173288
CPPED1	-	6.1613995e-5	-0.5265515
MARF1	-	4.2045394e-6	0.40052345
ITPRIPL2	+	3.7003279e-6	-0.44662255
TMEM159	+	3.7112914e-6	0.46350488
ERN2	-	1.2208334e-5	-0.52306956
CHP2	+	3.886739e-15	-0.7073692
PRKCB	+	2.4303785e-4	-6.397152
APOBR	+	1.6940273e-8	-0.77403253
NUPR1	-	9.7349885e-26	1.2531737

SULT1A1	-	0.001029319	-0.4803894
ZG16	+	1.03169494e-19	-1.0723453
SEZ6L2	-	4.6398508e-4	0.4493563
SEPHS2	-	8.440317e-9	-0.55579257
SETD1A	+	0.00131627	-0.5746381
FUS	+	0.002966061	-0.2663559
PYCARD	-	6.8404697e-6	-0.90139896
C16orf58	-	0.001780734	0.3678966
ITFG1	-	1.6256075e-4	0.36188856
AC007906.2	-	1.0267509e-7	-1.3979826
RBL2	+	0.001545553	0.3290204
CPNE2	+	1.782602e-5	-0.58066905
CIAPIN1	-	0.001060122	-0.54542506
USB1	+	6.8710005e-4	-0.5821186
CA7	+	2.3038768e-10	-1.5032126
PDP2	+	0.002433876	-0.3088915
CIAO2B	-	0.002181646	-0.41032335
AC074143.1	+	6.963728e-4	0.59563226
HSD11B2	+	1.620934e-11	-0.9823885
ATP6V0D1	-	0.001439433	-0.36225134
PSKH1	+	6.193642e-5	-0.58222765
SLC7A6	+	1.19220485e-5	-0.8751022
CYB5B	+	0.00101423	-0.2829862
PDPR	+	4.7979665e-9	-1.0358617
EXOSC6	-	0.002834085	-0.4580604
PHLPP2	-	7.110404e-16	-0.6551201
GABARAPL2	+	3.7340427e-4	0.37515274
TERF2IP	+	1.2046462e-6	0.64074975
AC009148.1	-	2.555164e-5	2.1109204
OSGIN1	+	2.2227936e-5	0.7244737
COX4I1	+	4.200892e-5	-0.35542828
SLC7A5	-	2.1977843e-4	-0.40060675
SNAI3-AS1	+	3.6970133e-4	-0.7591305
MIR22HG	-	2.4661066e-8	-0.67873293
RPA1	+	0.00255927	0.3718134
OVCA2	+	0.002743878	-0.5052741
CLUH	-	0.001811075	-0.365201
ANKFY1	-	0.002883986	-0.32573223
AC118754.1	+	2.1692183e-7	0.645808
GGT6	-	2.0671761e-5	-0.5138481
ARRB2	+	5.809773e-4	-0.56202984
PFN1	-	5.298899e-6	-0.39973804
KIF1C	+	0.002729343	-0.25286585
WSCD1	+	0.001080781	-0.32128745
FGF11	+	2.5413434e-5	0.893302
AC113189.4	+	2.7215365e-5	0.8905016

CD68	+	3.7291982e-5	0.42787984
NDEL1	+	0.002352144	0.32326955
AC015908.6	-	0.002244613	-0.33326808
TMEM238L	-	8.8998064e-4	-0.36366454
TOM1L2	-	0.001407656	-0.3329857
ALDH3A2	+	2.4188415e-5	0.38378897
ALDH3A1	-	2.6848886e-6	1.6470262
SPECC1	+	6.064394e-6	-0.45864135
WSB1	+	7.708036e-6	0.3884864
SUPT6H	+	2.5457153e-4	-0.367936
TMIGD1	-	5.5460832e-6	-1.3152723
ZNF207	+	4.7721518e-5	0.3450321
CISD3	+	0.002763675	-0.37499857
LINC00672	+	0.001672961	-1.5232831
GRB7	+	7.5468406e-6	0.6803186
MSL1	+	4.5103127e-10	0.55196476
KRT12	-	2.2223482e-8	1.0993028
KRT19	-	4.5695525e-4	-0.31896082
EIF1	+	1.5735794e-4	0.29023272
ACLY	-	1.2896589e-6	-0.36017352
CAVIN1	-	3.049861e-9	-0.80442667
COASY	+	0.001754986	-0.330888
EZH1	-	3.4467146e-5	0.47345528
RPL27	+	5.473797e-5	-0.3393992
GPATCH8	-	0.002208608	0.29598978
HEXIM1	+	0.002702824	-0.3010643
KANSL1	-	1.0311071e-4	0.3274653
CDK5RAP3	+	2.6508857e-5	0.4880996
AC004477.1	-	0.001438103	1.9987756
ITGA3	+	0.001443041	-0.31619456
TMEM92	+	4.8811472e-4	0.44457808
ACSF2	+	0.002840803	0.28582627
AC005921.3	+	0.001904419	1.2570493
ANKRD40CL	-	4.514344e-4	-0.46984777
DGKE	+	3.7929065e-5	0.5156031
SRSF1	-	0.00290118	0.2781312
YPEL2	+	3.1877978e-6	0.5399136
VMP1	+	1.0275632e-7	0.45061466
CA4	+	6.945163e-17	0.88731325
KCNH6	+	1.2525813e-4	1.3855233
DCAF7	+	0.002223366	0.24835306
CCDC47	-	0.002720436	-0.30919734
DDX42	+	0.001679338	-0.33510822
ERN1	-	1.0253137e-6	0.5293869
RAB37	+	0.00125696	-1.159685
SLC9A3R1	+	0.001477388	-0.25768554

ARMC7	+	6.011503e-4	-0.68068355
MYO15B	+	6.1304286e-7	0.48079535
EVPL	-	0.00192918	-0.35210532
JMJD6	-	1.6420657e-6	0.6263604
TIMP2	-	1.4773126e-5	0.4976792
CANT1	-	2.8128116e-4	-0.28513575
ENGASE	+	5.8800593e-4	0.45774463
AC027601.6	-	0.001505322	1.0001998
PCYT2	-	9.44384e-4	-0.32620892
MAFG	-	0.001616882	0.36358553
PYCR1	-	1.7951248e-4	0.44340667
FASN	-	5.419198e-8	-0.5191489
AC132872.3	+	9.792252e-4	-3.2566967
AC132872.4	+	0.00304308	-2.4892895
SPIRE1	-	8.561541e-6	0.51725185
RIOK3	+	2.9854061e-6	0.36699244
LAMA3	+	4.683158e-5	0.435832
DSC2	-	6.486534e-6	-0.34485194
GAREM1	-	0.001251304	-0.3424889
ZBTB7C	-	5.6061666e-9	-0.6330027
ACAA2	-	3.0464113e-7	-0.5095994
LMAN1	-	4.8880344e-9	0.46905476
PMAIP1	+	6.7178007e-7	1.2341281
RNF152	-	3.172725e-4	-0.3033754
ZCCHC2	+	2.2574315e-5	0.44272998
SERPINB8	+	5.9647045e-5	-0.7739868
RTTN	-	0.001097033	0.6591305
MISP	+	2.8562368e-4	-0.3175775
MIDN	+	0.002268161	-0.31267777
CIRBP	+	3.172043e-4	-0.35371995
PLEKHJ1	-	0.001132014	-0.34979534
AC005954.1	-	0.00246822	0.6814862
GTF2F1	-	3.6996423e-4	-0.42796192
TNFSF9	+	1.3373168e-5	0.58105975
PNPLA6	+	2.9083143e-4	-0.40282905
ANGPTL4	+	1.2263264e-15	0.88016313
ZNF440	+	0.001300122	0.4311395
TRIR	-	9.0115314e-8	-0.5847417
JUNB	+	2.213053e-10	0.6726062
AC020916.1	-	3.4240114e-5	0.69445854
ADGRE5	+	2.9377054e-5	-0.4172954
GIPC1	-	2.3279667e-6	-0.43557224
DNAJB1	-	3.1723595e-9	0.55472517
CYP4F2	-	6.595646e-4	0.5458742
NR2F6	-	0.00285631	-0.30512983
DDA1	+	3.1942345e-4	-0.47643325

B3GNT3	+	0.001708426	-0.3126138
ARRDC2	+	0.002328514	0.5958348
MAST3	+	7.687798e-4	-0.37178802
AC005759.1	-	0.001990212	0.3776856
GDF15	+	3.9346412e-10	0.6224302
UPF1	+	0.00175728	0.3016917
CEBPA	-	3.0344914e-5	-0.41543633
COX6B1	+	4.381405e-5	-0.38990557
AC011479.4	-	0.001255273	-4.0578575
ECH1	-	1.809239e-5	0.5667767
FCGBP	-	3.2273328e-10	-0.64895266
AXL	+	1.2758415e-8	1.3520492
CEACAM7	-	5.370631e-7	0.37803409
CEACAM6	+	4.387123e-4	0.25987935
DEDD2	-	5.4376107e-4	0.52806497
MEGF8	+	2.477295e-4	-0.48155862
CD177	+	5.3454344e-30	1.9721793
ETHE1	-	9.552816e-8	-0.5928902
ZNF575	+	3.8483492e-7	-1.4774879
IRGQ	-	3.474821e-4	-0.452625
PLAUR	-	0.001235098	0.4747816
KCNN4	-	1.4109602e-7	0.7259994
AC008755.1	-	2.9859208e-7	-0.6171652
BBC3	-	2.2637103e-6	0.8089645
SPHK2	+	3.122837e-6	-0.8110681
GYS1	-	0.001192744	-0.42171457
RPS11	+	7.960595e-4	-0.29516852
MYH14	+	4.734369e-5	-0.32981727
SPIB	+	1.1193895e-9	-1.5536604
ZNF841	-	8.02276e-5	0.7841926
ZNF160	-	2.6413173e-4	0.48924902
ZNF525	+	2.2726388e-4	0.7765333
LENG8	+	1.9168185e-7	0.54425263
LENG9	-	0.00162518	-0.82703716
CSNK2A1	-	8.67465e-6	0.35562167
SRXN1	-	3.0600137e-4	0.41962457
AL121758.1	-	1.8789488e-4	0.43781668
FKBP1A	-	0.001136361	-0.3085004
FASTKD5	-	3.1557828e-4	-0.5736149
CENPB	-	2.9835917e-4	-0.4399675
AP5S1	+	7.25435e-5	-0.97522944
MAVS	+	2.763812e-7	-0.4106297
FERMT1	-	1.5198356e-5	-0.38315418
BMP2	+	3.7035483e-5	0.44059363
BTBD3	+	1.4680749e-5	-0.38808066
RRBP1	-	1.1734771e-5	-0.35856447

FOXA2	-	2.0540905e-5	0.60694575
ACSS1	-	9.2322014e-5	-0.5839725
ID1	+	1.02654834e-4	-0.4758775
BCL2L1	-	4.777302e-7	-0.50237864
ACTL10	+	0.001460837	-1.6017385
TP53INP2	+	9.663553e-4	-0.3034248
SPAG4	+	2.0571689e-4	0.5509007
RBM39	-	2.743352e-10	0.5612793
NDRG3	-	9.968188e-4	-0.47092587
ZHX3	-	2.0013063e-4	-0.47261488
AL031681.2	+	0.001531324	-0.5097917
HNF4A	+	9.346512e-5	-0.29322997
PI3	+	1.564023e-23	1.8109926
NCOA5	-	2.3129967e-4	-0.6962202
PARD6B	+	0.001809671	0.31740776
KCNG1	-	0.002458353	0.42489848
BMP7	-	1.342179e-12	0.88486624
SLCO4A1	+	4.58946e-5	0.52681607
EEF1A2	-	1.3680379e-9	1.7845818
NRIP1	-	8.776806e-6	-0.4337704
CXADR	+	1.6970896e-5	0.34242147
IFNGR2	+	1.0064434e-5	0.37666526
ETS2	+	3.0894548e-4	0.3175991
B3GALT5	+	2.8294428e-7	0.38070363
BACE2	+	2.0200938e-5	0.40178525
ABCG1	+	2.591184e-8	0.5517762
TFF3	-	1.5530226e-6	0.3913459
TFF2	-	3.168241e-8	0.9617881
TFF1	-	0.002522028	0.28031498
PDE9A	+	3.7012353e-7	-0.7204101
POFUT2	-	8.496e-6	0.5474729
LSS	-	1.2503263e-12	-0.6688714
PCNT	+	2.0108624e-4	-0.50509244
IL17RA	+	5.1552095e-5	-0.56775147
PI4KA	-	0.001236071	-0.3572866
CRKL	+	0.001365034	0.2603599
PPIL2	+	0.002882134	-0.39397874
CCDC117	+	8.810868e-5	0.55847305
GAS2L1	+	3.6440734e-4	-0.78660196
TCN2	+	9.445256e-4	0.4239827
TUG1	+	8.764074e-4	0.31544068
LIMK2	+	1.4901136e-4	-0.46044824
PIK3IP1	-	1.4094762e-5	0.6593691
SLC5A1	+	4.8085816e-17	0.740463
ISX	+	3.0974944e-16	-0.7840576
MYH9	-	4.985257e-7	-0.37331715

KCTD17	+	5.552318e-4	-0.7104597
LGALS2	-	6.0148124e-4	0.93755895
MICALL1	+	0.001014936	-0.49065268
MAFF	+	1.9721053e-7	0.62079847
KDELR3	+	7.119348e-15	1.1348472
DDX17	-	0.00114031	0.25175557
GTPBP1	+	0.001485541	0.33099198
CBX6	-	3.1761215e-7	-0.4764103
PDGFB	-	2.8087674e-9	1.3922445
MGAT3	+	1.5164843e-4	0.6624901
EP300	+	0.001824361	-0.25226015
POLDIP3	-	0.001743227	0.35366538
Z93241.1	+	6.0318504e-4	-2.291233
ARFGAP3	-	8.686504e-6	0.43253562
RTL6	-	2.3016795e-4	-0.4985993
GRAMD4	+	4.9019884e-4	-0.3936477
PIM3	+	1.3394996e-5	0.5088587
MT-ND1	+	9.71e-43	-1.0345094
MT-ND2	+	7.4188336e-33	-0.93376184
MT-CO1	+	4.937222e-4	0.26218316
MT-ATP8	+	3.2321937e-24	-0.81457067
MT-ATP6	+	6.1835387e-10	-0.47891378
MT-ND3	+	1.6704118e-35	-0.9446437
MT-ND4L	+	8.834162e-5	-0.32603133
PLCXD1	+	1.5695406e-4	-0.42066917
AKAP17A	+	1.4164046e-5	0.5401828
ACE2	-	3.92139e-6	0.5887516
AC097625.2	-	1.0815082e-5	0.58378327
REPS2	+	4.2526623e-5	-0.5418806
PHKA2	-	2.9487148e-6	0.36291054
SAT1	+	3.3566463e-5	0.39293477
BCOR	-	0.002034554	0.35860115
MAOA	+	2.8683264e-11	-0.5544223
MAOB	-	0.001218827	-0.47836775
MIR222HG	-	8.193358e-6	1.0660772
RBM3	+	2.6093681e-5	-0.41181132
CCDC120	+	1.15721174e-4	-0.6157682
HUWE1	-	7.905162e-4	-0.25026056
FAAH2	+	2.0753065e-4	0.90933025
HEPH	+	0.001288286	0.22913976
YIPF6	+	9.901888e-4	0.31484398
AL590764.2	-	7.578112e-15	0.7118588
IL2RG	-	6.2548634e-16	0.6744259
GJB1	+	0.001900515	-0.34047484
OGT	+	2.0185474e-4	0.3271633
SRPX2	+	0.002443808	0.45884204

NOX1	-	0.001655126	-0.31603536
TSC22D3	-	5.785716e-4	0.40656477
PSMD10	-	1.9235114e-5	0.5227031
ACSL4	-	2.4794592e-6	-0.5186952
PLS3	+	0.002195005	0.6078974
LINC01285	+	0.00138813	1.9233848
PGRMC1	+	1.0061873e-6	0.39418426
SLC25A5	+	8.229374e-5	-0.28591725
ZDHHC9	-	0.001965754	0.2820453
ELF4	-	9.5275993e-4	-0.3278178
AIFM1	-	1.7580489e-5	-0.5137814
MBNL3	-	4.0483449e-4	-0.44239214
GABRE	-	1.3065112e-17	1.038292
HCFC1	-	0.002020248	-0.3392818
IRAK1	-	4.073098e-8	-0.5694259
UTY	-	5.575807e-4	0.45887175